UNIVERSIDAD COMPLUTENSE DE MADRID

FACULTAD DE FARMACIA

TESIS DOCTORAL

Papel del miR-143-3p, miR-155-5p, miR-15a-5p y miR-199a-3p como mediadores clave de la apoptosis, la resistencia a insulina y la inflamación vascular en la aterosclerosis

The role of miR-143-3p, miR-155-5p, miR-15a-5p, and miR-199a-3p as key mediators in apoptosis, insulin resistance, and vascular inflammation in atherosclerosis

MEMORIA PARA OPTAR AL GRADO DE DOCTORA

PRESENTADA POR

Paula González López

DIRIGIDA POR

Almudena Gómez Hernández
Óscar Escribano Illanes

UNIVERSIDAD COMPLUTENSE DE MADRID

FACULTAD DE FARMACIA

PROGRAMA DE DOCTORADO BIOQUÍMICA, BIOLOGÍA MOLECULAR Y BIOMEDICINA

TESIS DOCTORAL

Papel del miR-143-3p, miR-155-5p, miR-15a-5p y miR-199a-3p como mediadores clave de la apoptosis, la resistencia a insulina y la inflamación vascular en la aterosclerosis

The role of miR-143-3p, miR-155-5p, miR-15a-5p, and miR-199a-3p as key mediators in apoptosis, insulin resistance, and vascular inflammation in atherosclerosis

MEMORIA PARA OPTAR AL GRADO DE DOCTORA

PRESENTADA POR

Paula González López

DIRECTORES

Almudena Gómez Hernández y Óscar Escribano Illanes

A mi familia

"...Ya sé que es el final,
no habrá segunda parte,
y no sé cómo hacer para borrarte.
Para empezar (diré que es el final).
Miedo de volver a los infiernos,
miedo a que me tengas miedo,
a tenerte que olvidar.
Miedo de quererte sin quererlo,
de encontrarte de repente,
de no verte nunca más..."

-Miedo, M-Clan

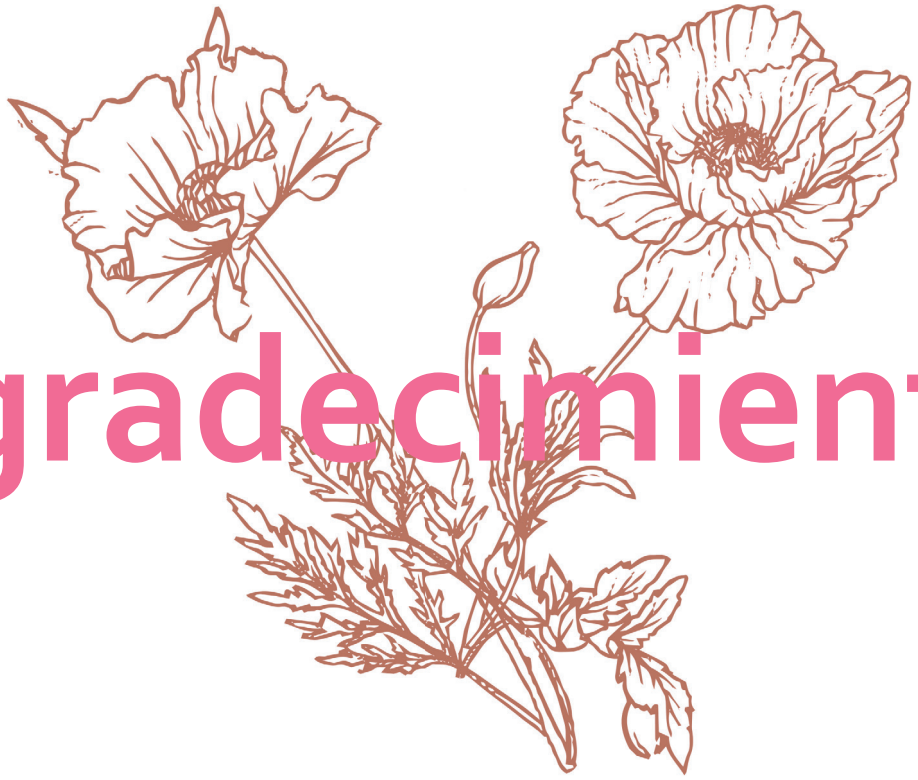

Agradecimientos

AGRADECIMIENTOS

Solo se me ocurre antes de empezar, gracias por los días que vendrán, y es que Gracias viene del latín *gratia* y significa la honra y alabanza que sin más se tributa a otro. Y empiezo así, porque los que aparecen aquí (y si me he olvidado de alguien, lo siento) han puesto su grano de arena para sacar esta tesis adelante de manera altruista, y decir gracias sabe a poco, pero quedará patente para los que lo lean. Ahora bien, aviso a navegantes, no os enfadéis si mi agradecimiento es escueto, o pueda parecer insuficiente, si estáis aquí, verdaderamente no tengo palabras para agradeceros la ayuda.

Empezar con mis directores **Almudena y Óscar**, gracias por vuestra guía y apoyo en este trabajo, vuestra rigurosidad en todo momento y ayudarme a ser perfeccionista. Seguir con mis compañeros de laboratorio. **Carla**, gracias por la ayuda en los primeros momentos. Sobre todo, gracias a los compañeros de la temporada 2023, **Alba**, la loca del autoclave, el deporte, tan increíblemente echada para delante, aunque seas técnico y Swifitie, se te quiere, gracias por agarrarme fuerte la mano siempre que lo he necesitado. **Marta**, la mujer más válida que ha llegado al Lab 6, la suerte que hemos tenido de conocerte no lo sabe nadie, gracias por ser una nube de pegatina, farola de serpentina, que quita el sufrimiento y las penas del pensamiento. **Rubén**, contigo empezó todo, con ese café solo en el despacho, gracias por preguntar, por implicarte y por quitarme el miedo a caer en los infiernos (aunque tú si te caíste), disfruta de Suecia, ya sabes que tienes nivel para eso y mucho más. **Víctor**, el estudiante que nos alegraba el café y los tiempos de espera con sus trucos, gracias por hacer magia cambiando espadas por rosas. **Javi**, tú que parecía que venías de antes de miles de años luz, pero no, el murciano más madrileño/valenciano, siento que al principio tuviese miedo de fiarme de ti, y, sobre todo, gracias por ser como dinamita en una fuga de gas, y ayudarme a respirar. Y si he hablado del papi, no podía faltar la mami, **Paula G** (mi tocaya), la mejor dragona del mundo, gracias por crecer muchas flores sin ningún control por los callejones que pisas, tirar pa´lante y quitar las penas. Gracias por hacer que cualquier día sea fin de semana, igual que en las vacaciones de verano.

Continuar con mi laboratorio de acogida, el "Lab 15" (AP, AGU, PBD), gracias, **Almudena Porras** por escoger a las maravillosas personas que lo componen. **Cris**, la química que siempre supo hacer más que tampones, reina de las inmunos y la histología, mi compi de rock, reggaetón, agostos en el departamento (vaciando campanas de xileno), audios cuestionables por Salamanca, y de sentirnos viejas cuando nadie conoce a Álex Ubago, gracias por ser la de verdad, una ilusión por amiga y soñar más despierta que dormida. **Nerea**, la bioquímica más amable y altruista (menos bioquímica), la que es celíaca y no se enfada por ponerle un regalo en harina, la que empezó la tesis siendo postdoc, la que es una suerte llamarla amiga, la octava maravilla de Carabanchel, gracias a cultivos por unirnos y a ti por ser como un vino tinto y, sobre todo, por ser siempre el timón en mi deriva. **Mateo**, nuestra Esperanza Gracia particular, la persona con el mejor humor del departamento, el que siempre está dispuesto a servir, gracias por quererte comer de un boca'o el mundo, dibujar sonrisas en mi cara y ayudarme a mantener pulsos con mi oscuridad. **Minerva**, la que tiene tantas capas como las cebollas, y cada una es más especial que la anterior, me quedo tranquila sabiendo que los eyeliners de colores y los pendientes se quedan en buenas manos, gracias por señalar el siguiente escalón, y estar en el tejado esperando a que llegue yo. **Jaime**, gracias por ser un sol, siempre amable y con buenas palabras. **María R**, mi compañera de despacho, la de los cruasanes plancha, las naranjas (D.E.P), las paellas, los gatetes (Roger for presidente) y las reuniones, gracias por estar en las noches más oscuras, en las carreteras crudas, en los golpes de la vida, por no olvidarme, por no olvidarte. **María F**, la embajadora oficial de Bimba y Lola, una de las personas más genuinas que he conocido (y conoceré), gracias por ser el mundo patas arriba, el llanto, la carcajada, y los empujones a la alambrada. **Inés**, la física, la persona más graciosa directa e indirectamente, la que bebe rubia la cerveza, que tu cabeza nunca deje de alzar el vuelo, gracias por ser una estrella y alejar las pesadillas dejando en un agujero flores amarillas. **Paula L**, el mejor comodín para amigos de mierda, la tranquilidad hecha persona, gracias por haberte encontrado, por ser como una planta que nace a la sombra de la sierra y enseñarme que es mejor flotar a caminar como un muerto. **Juan**, (Porrhígado), el loboferoz de las barbacoas, gracias por ser un tren llamado huracán, y demostrar que la vida es un cigarro que no se debe apagar. Gracias por ser mis adoptantes y mis héroes del sábado.

Seguir con el laboratorio 21, **Charles**, nunca olvidaré que fuiste la primera persona en darme una oportunidad, mi compañero de charlas en cultivos, gracias por ser mi amigo, por hacer la mejor tarta de Guinness del mundo, marcar el paso, romper el hielo, y demostrar que la vida en un minuto no pasa tan deprisa, haciéndonos, por si acaso, disfrutar a todos los que te conocemos. **Bei**, la persona más amable, madura y genial que conozco, mi compañera de "fikas", penas, alegrías (siempre en el Kladdkakan) y tatuajes de última hora, gracias por nunca dejarme sola, incluirme y siempre dejarme pasear por las huellas que dejan tus zapatos, sonrío por tener esta amistad contigo. **Pat**, la mejor farmacéutica, brindo por las coincidencias y días croquetas que empezaron nuestra amistad, gracias por volar, y vivir porque no te hace falta valor, y dejarme vivir volando junto a ti. **Gema y Elena**, las mamis del 21, gracias por siempre ayudarme, por nunca decirme que no, y por enseñarme cada vez que lo he necesitado. Y los niños que se quedan, el 21 está en buenas manos con todos vosotros. Gracias por todos los momentos que pasamos.

No me olvido del resto de estudiantes, postdocs, e IPs del departamento, en especial a **ACME**, creo que nadie se va a cansar de decirte que eres un soplo de aire fresco, gracias por ser un bohemio de la vida que no tiene nada que ver con los bigotes señoriales que se pasean por Jerez. **Paloma** gracias por siempre tener una sonrisa y un consejo para mí. **Lola**, gracias por tu positividad y alegría. **Carlos Guillén**, gracias por ser distinto, por volver a volver, no ser lo mismo que ayer, por demostrar que se puede perder la vista, pero nunca la mirada. **Carmen Álvarez** gracias por aguantar mi mano y ser cuando lo he necesitado un consejo de sabios. Y en general, al resto de personas que están o han pasado por el Departamento de Bioquímica y Biología molecular, muchas gracias por todo.

A toda la gente del IRyCIS por darme la oportunidad de empezar en ciencia, pero sobre todo a mis profesoras **Gemma** y **Aleja**, gracias por enseñarme a ser una gran compañera y que los desayunos son sagrados, y a **Diego Gómez-Coronado Cáceres**, gracias por enseñarme todo lo que sé. Gracias por enseñarme que no había que echar raíces en un sitio, que el mejor día es en el que el alma tiene hambre y sed, a no olvidar lo aprendido, y que, si me rodeo de buenos, también lo pareceré.

And I am not forgetting about the floor 8 from the Bioclinicum in Sweeden. **Anton**, I honestly have no words to explain how much you helped me in 3 months, thank you for giving me the chance to work with you and being the best mentor a person can ask for, for bringing back my love for doing science and riding high through all of that sorrow. **Osman** and **Vladimir**, the best and most humble postdocs ever, thank you for the talks, the advices and the company in the bus rides, thank you for being like a place of hope and no pain. **Katja**, my table neighbor and an amazing person, thank you for teaching me that I can't be perfect. **Shiying** and **Yinda**, my lab (team) mates, thank you for always being there to help me and teaching me any time I needed to learn something new, nice work we did, you're gonna go far. **Linda**, the nicest person, always there to help, thank you for making the lab a place that we could call home. **Patricia**, my closest friend, my coffee mate, I will always be grateful for the fellowship, for gifting me with your friendship muito obrigada, porque olho ao meu lado e aí está você, aquele que tem que estar. **Gera**, como agradecerte todo, no hay palabras, gracias por hacerme asumir que rendirse no es una opción, no pierdas tu sentido de justicia nunca. **Aida**, **Julia** and **Effy**, it was incredible meeting you girls, I was lucky to share department and Midsommar with you, gracias porque con vosotras dicen que tengo nuevas amigas. And last but not least Thank you so much to **Peder Olofsson**, for showing me that being humble is the way to success, and always treating me so nicely.

Continuar con los de siempre, los que nunca faltan, los que están: mi familia. **Papá**, gracias por enseñarme lo que siempre me ha acompañado esta vida, la música; por la ayuda, por regalarme tu carácter, por ser siempre mi chófer y guía, la pregunta del millón y sobre todo por ser sorprendente, tu que desde muy crío te saliste del renglón, por darte prisa en enseñarme la lección. **Mamá**, mi (supuesta) gallega, la matriarca, la persona más fiel y con el corazón más grande y puro que conozco, gracias por darme dos culturas, por hacerme sentir orgullosa de que me llamen meiga, por siempre darme la mano, pero dejándome equivocarme cuando tocaba, espero algún día llegar a ser tan buena como tu moitas grazas por enseñarme a ter unha voz que non podan silenciar, a sacar da miña gorxa, voces novas, co vento en contra, a voltar sempre ao camino, e berrar forte que eston viva.

Abu, la persona más divina que conozco, la que siempre me acompaña en todo con los ojos cerrados, la que cae (y no tira) las cosas, la reina de los laísmos, la razón por la que amo las telenovelas, eurovisión y las películas de cine de barrio, y la persona más importante de mi vida, muchas gracias por ser el sol cuando amanece, y por enseñarme a ser libre. Mi **tía Yoli**, la persona a la que acudo cuando tengo problemas, la que me ha regalado al primo más pesado del mundo, y también al que más quiero, gracias a ti, a **Aure** (aunque me saques de mis casillas y uses ahin o fíte) y a **Mu**, por estar y ser siempre mis chicas cocodrilo y el marcapasos que me anima el corazón. Mi **tio Alfonso**, el fiestero, la cordialidad hecha persona, el que me da los mejores consejos y que me enseña (aunque me cueste hacerle caso) las mejores maneras de resolver conflictos, gracias por dejarme claro que siempre puedo contar contigo y que en esta vida no hay luz sin oscuridad. **Bea**, **Fer** y **Luci**, gracias por siempre estar ahí y pensar lo mejor para mí, pero, sobre todo, gracias por enseñarme que a veces, las palabras que no existen me pueden salvar.

Gracias a ti, **Nacho**, seguramente la persona más internacional que conozco, gracias por compartir tus días conmigo, por acompañarme en mis locuras, aunque eso implique casi caernos por precipicios, o atascar el coche en la nieve; gracias por siempre ayudarme, por echarme la bronca cuando lo he necesitado y ser la mano que tira de mi cuando me caigo, gracias porque se te nota en la voz que dentro eres de colores, porque te sobra el valor que le falta a mis noches, por encontrarte entre tantas flores, por cogerme la mano y decirme que solo no comprendes la vida, por ser capaz de nadar en el mar más profundo y como un superhéroe, salvarme de mi mundo.

A **Anita**, mi hermana, la que me acompaña desde los 4 años, ¡brindo por las amistades de dos dígitos!, agradezco a la vida por juntarnos, y te agradezco haber estado siempre ahí, a pie de cañón, en las buenas, las malas y las peores; por ser arte, porque si quieres puedes quedarte toda la vida conmigo, que yo seré feliz; gracias por cuidarme mucho hoy, y algo más mañana, porque no me conformo con nada desde que te he conocido. Nada me hace más feliz que la portada de mi tesis este hecha por ti.

A mis amigos de la carrera: **Javi**, **Adri**, **Raúl** y **Fran**, gracias por los cafés, los vídeos en directo de cigüeñas y ayudarme a superar la carrera. A mis amigos del master: **Chamo**, amigo, el que llega a Galicia y se le pega el acento, o piensa que la capital de CyL, es León, mi confidente, probablemente la persona a la que peor le caigan los franceses y con la peor mala suerte (o no), gracias por tener el corazón alicata'o hasta el techo, por llenar de porvenir los bolsillos del mandil y colgar un recuerdo de cada azulejo, que la luna te siga sabiendo a poco. **Rubén**, la única persona que con 25 años puede tirarse dos meses saliendo de fiesta todos los findes, que lleva revistas de national geographic para no dormirse en el coche, al que se le cae la escalera de casa y aún así no falla, gracias por dejarte llevar, arrancarte sin más, por ir despacito pero normal, por nunca estar descolorio'. **María**, mi viguesa favorita, la reina de los faros, la que más aguanta a Chamo, aunque odie a sus gatos, la tía más guay, la que siempre nos abre las puertas de su casa y con la que mejor se viaja, gracias por hacer que los sueños viajen con el viento. **Montse**, gracias por estar, por demostrarme que mola comerse el mundo y que la única verdad es que solo hay un modo, dejar que el tiempo lo cure todo. Gracias también a **Laura**, **Álvaro**, **Jorge** y los demás, por hacerme el master (aunque lo truncase el Covid), las cenas y las quedadas tan divertidas.

Por último, gracias a mis reinas del cotilleo, a las dueñas del veneno, a mis diosas de Atenas, **Emma**, mi *make up addict*, la única persona loca del crossfit a la que quiero en mi vida, mi alma gemela, el mejor *eyeliner* de España, gracias por ser como una roca, una rosa en un callejón y siempre luchar conmigo. **Fede**, mi compañero de bachatas y reggaetón en las calles de Grecia y de realities en los aviones, gracias por tener sonrisas de hierro de esas que disipan las brumas. Y **David**, la persona que ama las tartas de queso tanto como yo, el biosanitario más amable y calmado que conozco, gracias por enseñarme que yendo despacio nunca aprendes a frenar.

Pero, sobre todo, gracias a todos una vez más, por darle pinceladas de color a la gris realidad del doctorado.

"...Vaite de aí, rexoubeiro,
rexoubar á túa casa,
se na miña casa hai fume,
na túa queima que abrasa..."

-Figa, Tanxugueiras

Index

CONTENT INDEX

FIGURES AND TABLES INDEX

ABBREVIATIONS INDEX

3' UTR. 3' untranslated region

95% CI. 95% confident interval

ABCA1. ATP-binding cassette subfamily A member 1

ACA. Advanced carotid atherosclerosis

AKT. Protein kinase B

Ang II. Angiotensin II

APCs. Antigen-presenting cells

ApoB. Apolipoprotein B

ApoE$^{-/-}$. Apolipoprotein E deficient

A.U.C. Area under the curve

α-SMA. alpha- Smooth muscle actin

BCR. B-cell receptor

BMI. Body mass index

BSA. Bovine serum albumin

BW. Body weight

CAs. Control aortas

cDNA. Complementary DNA

CDS. Messenger RNA coding region

COX-2. Cyclooxygenase-2

CSFs. Colony stimulating factors

CT. Cycle threshold

CTCF. Corrected total cell fluorescence

CVDs. Cardiovascular diseases

DCs. Dendritic cells

DGCR8. DiGeorge syndrome critical region gene 8

DLS. Dynamic light scattering

DMSO. Dimethyl sulfoxide

DP1. Prostaglandin D2 receptor 1

dsRNA. Double-stranded RNA

ECM. Extracellular matrix

ECs. Endothelial cells

eNOS. Endothelial nitric oxide synthase

ERK1/2. Extracellular signal-regulated kinase 1 / 2

EVs. Extracellular vesicles

Exo-miRNAs. Exosomal microRNAs

FAs. Fibroatheromas

FBS. Foetal bovine serum

FELASA. Federation of European Laboratory Animal Science Associations

GLUT4. Glucose transporter type 4

GM130. Golgi subfamily A member 2

GPx. Glutathione peroxidase

GW182. Trinucleotide repeat containing adaptor 6A

gWAT. Gonadal white adipose tissue

H_3. Histone 3

H&E. Hematoxylin and eosin

HFD. High fat diet

H-L. High-low limit

HuBL. B6.129S7-Ldlrtm1Her/J mice on C57BL/6J background and Human APOB100-tg Ldlrtm1Her

HUVECs. Human umbilical vein endothelial cells

i.p. Intraperitoneally

ICAM-1. Intercellular adhesion molecule-1

IF. Immunofluorescence

IFNγ. Interferon gamma

IGF. Insulin-like growth factor

IGF-IIR. Insulin-like growth factor-II receptor

IGF-IR. Insulin-like growth factor-I receptor

IHC. Immunohistochemistry

IKK. Inhibitor of nuclear factor kappa B. Subunits alpha, beta and gamma (IKKα/β/γ)

IL. Interleukin

IL-1R. Interleukin-1 family receptor

IPH. Intraplaque hemorrhage

IR. Insulin receptor

IRS. Insulin receptor substrate

iWAT. Inguinal white adipose tissue

IκB. Nuclear factor-kappa B inhibitor

IκBα. Nuclear factor-kappa B inhibitor alpha

JAK. Janus kinase

KLFs. Krüppel-like factors

***LDLr*$^{-/-}$.** Low-density lipoprotein receptor deficient

LDLs. Low-density lipoproteins

LOX-1. Lectin-like oxidized low-density lipoprotein receptor 1

LRNC. Lipid-rich necrotic core

MAPK. Mitogen-activated protein kinase

MCP-1. Monocyte chemoattractant protein-1

miRNA. MicroRNA

MMP. Matrix metalloprotease

mRNA. Messenger RNA

mTOR. mammalian target of rapamycin

mTORC2. mammalian target of rapamycin complex 2

NADPH. Nicotinamide adenine dinucleotide phosphate

NAFLD. Non-alcoholic fatty liver disease

NEMO. Nuclear factor-kappa B essential modulator

NETs. Neutrophil extracellular traps

NF-κB. Nuclear factor kappa B

NIK. Nuclear factor kappa B inducing kinase

NO. Nitric oxide

NOX. Nicotinamide adenine dinucleotide phosphate oxidases

Nrf2. Nuclear factor erythroid 2-related factor 2

O.C.T. Tissue-Tek® optimal cutting temperature compound

ORO. Oil Red O

Ox-LDLs. Oxidized low-density lipoproteins

p85α. phosphoinositide 3-kinase regulatory subunit p85 alpha

PBS. Phosphate buffered saline

PCSK9. Proprotein convertase subtilisin/kexin type 9

PD-1. Programmed cell death protein 1

PDK1. 3-phosphoinositide-dependent protein kinase-1

PI3K. Phosphoinositide 3-kinase

PIP3. Phosphoinositide -3,4,5-triphosphate

pre-miRNA. miRNA precursor

pri-miRNAs. Primary microRNAs

qPCR. Quantitative polymerase chain reaction

RIPK1. Receptor-interacting serine/threonine-protein kinase 1

RISC. miRNA-induced silencing complex

ROC. Receiver operating characteristic analysis curve

ROS. Reactive oxygen species

RQ. Relative quantification

RT. Reverse transcription

S473. Serine 473

SAH. S-adenosylhomocysteine

SAHH. S-adenosylhomocysteine hydrolase

Sens %. Sensitivity

SOD. Superoxide dismutase

Spec %. Specifity

ssRNA. Single-stranded RNA

STAT. Signal transducer and activator of transcription

STD. Standard-type diet

T308. Threonine 308

TAB2. Transforming growth factor-beta activated kinase 1 binding protein 2

TAK1. Transforming growth factor-beta activated kinase 1

TBS. Tris-buffered saline

TCR. T-cell receptor

TF. Tissue factor

Tfh. Follicular helper T cells

TGF. Transforming growth factor

TGF-β. Transforming growth factor-beta

Th. T helper T cells

TNAP. Tissue non-specific alkaline phosphatase

TNFR. Tumor necrosis factor receptor

TNFα. Tumor necrosis factor alpha

TRADD. Tumor necrosis factor receptor type1 associated death domain protein

TRAF. Tumor necrosis factor receptor-associated factor

Treg. Regulatory T cells

TTBS. Tween®20-Tris-buffered saline

VCAM-1. Vascular cell adhesion molecule-1

VEGF. Vascular endothelial growth factor

VSMCs. Vascular smooth muscle cells

WT. Wild-type

“Lástima de astillas en los dedos,
de nudos marineros,
que no me dejan ir,
todos somos víctimas del miedo,
del vértigo a la inmesidad de la
existencia”

-La inmensidad, La M.O.D.A.

1. Resumen

1. RESUMEN

Introducción. La aterosclerosis es una enfermedad inflamatoria crónica que afecta a las arterias de mediano y gran calibre de diferentes lechos vasculares y que se caracteriza por el engrosamiento de la capa íntima y media con pérdida de la elasticidad. Su lesión básica es la placa de ateroma compuesta fundamentalmente de lípidos, tejido fibroso y células inflamatorias, y pasa por diferentes estadios (1).

El proceso aterosclerótico comienza con una disfunción endotelial que cursa con el desacoplamiento de la enzima óxido nítrico sintasa endotelial por distintas causas como la pérdida de glicocálix o el estrés de cizallamiento que genera la corriente sanguínea sobre el endotelio. Estos procesos inducen la inflamación, el estrés oxidativo del endotelio, y la activación del endotelio vascular, que aumenta la permeabilidad y favorece la entrada de lipoproteínas de baja densidad (LDLs) o monocitos, que en condiciones fisiológicas no entrarían a la pared vascular (1–8). Los monocitos una vez se encuentran en el ambiente inflamatorio típico de la enfermedad aterosclerótica se diferencian a macrófagos que van a captar las LDL modificadas transformándose en células espumosas, que liberan moléculas proinflamatorias (9–11). Además de macrófagos, en las lesiones ateroscleróticas hay presencia de otras células inmunes como: células T proinflamatorias ($CD8^+$ o Th1) (12,13), y antiinflamatorias Treg (14); y células B2 (proateroscleróticas) y B1 (antiateroscleróticas), así como anticuerpos IgM protectores (15), o IgG e IgEs que promueven la enfermedad (16,17).

El otro tipo celular residente de las arterias son las células del músculo liso vascular (VSMCs), que también tienen un papel importante en la progresión de la aterosclerosis. En condiciones fisiológicas, las VSMCs tienen un fenotipo contráctil para mantener el tono vascular, pero en el contexto aterosclerótico, éstas adquieren un fenotipo sintético, con una mayor capacidad de migración y proliferación; un fenotipo osteoclástico; fibroblástico; o fenotipo similar a los macrófagos, pudiendo captar LDL modificadas y dando lugar a las células espumosas (18,19). Además de efectos específicos del tipo celular y de la capa vascular, hay vías que están alteradas como la vía de la insulina y de los factores de crecimiento similares a insulina (20–24); o la vía inflamatoria del factor nuclear-kappa B (NF-κB) (25–30).

Por otro lado, los microRNAs (miRNAs) son pequeñas moléculas de RNA no codificante que regulan negativamente la expresión de sus genes diana mediante la supresión de la traducción o la degradación directa del RNA mensajero (mRNAs). Se descubrieron en 1994, y puesto que son capaces de modular la expresión de distintos genes, se han visto alterados en diversas enfermedades como el cáncer, el Alzheimer, o la aterosclerosis (31–36).

Es por ello que, teniendo en cuenta estos antecedentes nos planteamos la siguiente hipótesis y objetivos:

Hipótesis: Durante el proceso aterosclerótico ocurre la alteración de distintos miRNAs que van a promover o intentar paliar el progreso de la enfermedad mediante la modulación de dianas específica.

Objetivos: Por lo tanto, nuestro objetivo principal fue estudiar la desregulación de diferentes miRNAs durante la progresión de la aterosclerosis:

1. Identificar posibles miRNAs involucrados en la aterosclerosis experimental y humana.

2. Estudiar el papel de la desregulación de miR-143-3p y su diana IGF-IIR en la inestabilidad de la placa aterosclerótica.

3. Analizar la implicación de miR-155-5p y sus dianas AKT, eNOS y p85α en la progresión de la aterosclerosis y la resistencia vascular a la insulina.

4. Investigar el papel de los miR-15a-5p y miR-199a-3p y sus dianas IKKs, NF-κB p65, mTOR y LOX-1 en la progresión de la aterosclerosis, principalmente en la inflamación y en la formación de células espumosas.

5. Confirmar si los miR-143-3p, miR-155-5p, miR-15a-5p y miR-199a-3p también se encuentran alterados en las carótidas y en las células inmunes de un modelo de ratón transgénico para el gen humano *APOB100* que desarrolla aterosclerosis.

6. Identificar si los miRNAs seleccionados pueden ser utilizados como biomarcadores no invasivos para la aterosclerosis avanzada.

Metodología y resultados: Para abordar la mayor parte de los objetivos se utilizó un modelo de ratón deficiente de la apolipoproteína E (*ApoE*$^{-/-}$) al que se alimentó con una dieta estándar o alta en grasas durante 8 y 18 semanas tras el destete, y tres grupos de muestras vasculares humanas: arterias control (CAs, sin aterosclerosis), arterias de sujetos que tenían lesiones iniciales o fibroateromas (FAs), y carótidas de pacientes que presentaban una lesión aterosclerótica carotídea avanzada (ACA).

1. Identificación de posibles miRNAs involucrados en aterosclerosis. En primer lugar, se realizó un estudio in silico en GEO Database y PubMed, para seleccionar los miRNAs que podrían modular la enfermedad aterosclerótica y finalmente fueron seleccionados 24 genes candidatos. Para comprobar si estaban alterados en los ratones, se extrajeron los miRNAs de las aortas completas de los ratones tras 8 y 18 semanas en dieta; se obtuvieron los DNAs complementarios por retrotranscripción, y se calculó la expresión relativa de los miRNAs seleccionados por RT-qPCR. De los 24 miRNAs candidatos, 3 presentaban niveles alterados en las aortas de los ratones tras 8 semanas de dieta, y 11 presentaban niveles alterados en las aortas de los ratones tras 18 semanas en dieta alta en grasa. Estos 11 miRNAs se analizaron también en las muestras humanas encontrándose 6 de estos miRNAs alterados cuando había una aterosclerosis avanzada. De ellos, los niveles de miR-143-3p, miR-155 5p, miR-15a-5p y miR-199a-3p estaban alterados en el mismo sentido tanto en las muestras de ratón como en las humanas.

2. Estudio del papel de miR-143-3p y su diana IGF-IIR en la inestabilidad de la placa aterosclerótica. Los niveles de miR-143-3p se encontraron disminuidos en la aorta del ratón *ApoE*$^{-/-}$ tras 18 semanas con dieta rica en grasas, y en la carótida de los pacientes con ACA por RT-qPCR.

A continuación, se realizó un estudio *in silico* en distintas bases de datos de interacción de miRNA-mRNA para seleccionar dianas de interés. Se decidió estudiar el receptor del factor de crecimiento similar a insulina de tipo II (IGF-IIR), diana confirmada del miR-143-3p. Primero se extrajeron proteínas de la arteria de los ratones *ApoE*$^{-/-}$ de 18 semanas de dieta, y mediante *Western blot*, se observó un aumento de la expresión de IGF-IIR sin alcanzar la significación estadística. Sin embargo, en experimentos *in vitro* realizados en dos líneas celulares vasculares: células endoteliales de la vena del cordón umbilical humano (HUVECs) y VSMCs de ratón, se obtuvo una disminución del IGF-IIR cuando las células eran transfectadas con miméticos del miR-143-3p. Además, también confirmamos como la apoptosis celular de estas líneas, medida como la actividad de la proteína caspasa-3 por *Western blot,* disminuía tras aumentar la expresión del miR-143-3p.

3. Implicación de miR-155-5p y sus dianas AKT, eNOS y p85α en la progresión de la aterosclerosis y la resistencia vascular a la insulina. Los niveles de miR-155-5p se encontraron aumentados en la arteria de ratones *ApoE*$^{-/-}$ tras 18 semanas con dieta rica en grasas y en las carótidas de los pacientes con ACA.

Como en el objetivo anterior, también aquí se realizó un estudio in silico en bases de datos de interacción miRNA-mRNA. En este caso se decidió estudiar la relación con su diana confirmada AKT. La expresión de AKT se encontró disminuida en los ratones *ApoE*$^{-/-}$ tras 18 semanas de dieta con respecto a los animales wild type mediante *Western blot* y en el grupo ACA por inmunohistoquímica

(IHQ). Además, se confirmó que en HUVECs y en VSMCs se producía una disminución de AKT si se transfectaban las células con un mimético del miR-155-5p. Debido a que AKT es una proteína clave en la vía de respuesta a la insulina, se analizó si la respuesta a insulina estaba disminuida tras aumentar el miR-155-5p en la línea de VSMCs, obteniendo una menor actividad de AKT, medida como la fosforilación en el residuo serina 473 en respuesta a insulina.

Además, también se estudió la expresión del miR-155-5p por RT-qPCR en los pacientes con ACA en función del índice de masa corporal (IMC) y la expresión de AKT por IHQ. Se obtuvo un aumento del miRNA y una disminución en la expresión de AKT proporcional al IMC. También se analizó la expresión del miR 155-5p en función de otras características clínicas y observamos que la expresión relativa de este miRNA aumentaba en pacientes con diabetes y ACA, o si el paciente era sintomático.

4. Estudio del papel de los miR-15a-5p y miR-199a-3p y sus dianas IKKs, NF-κB p65, mTOR y LOX-1 en la progresión de la aterosclerosis, principalmente en la inflamación y en la formación de células espumosas. Los niveles de miR-15a-5p y miR-199a-3p estaban disminuidos en la aorta de ratones *ApoE*$^{-/-}$ tras 18 semanas de dieta rica en grasas, y en las carótidas del grupo de pacientes ACA.

En este caso, tras la búsqueda in silico de potenciales dianas, se eligieron proteínas pertenecientes a la vía de NF-κB. IKKα e IKKβ como posibles dianas del miR-15a-5p e IKKβ y p65 como posibles dianas del miR-199a-3p. IKKα, IKKβ y p65 se encontraban aumentadas por *Western blot* o IHQ en la aorta de los ratones *ApoE*$^{-/-}$ tras 18 semanas de dieta grasa, y en las carótidas del grupo de pacientes con ACA. También en HUVECs y VSMCs, se obtuvo una disminución de las dianas cuando las células eran transfectadas con miméticos de miR-15a-5p y miR-199a-3p. Además, se pudo confirmar la relación de miR-15a-5p con IKKα e IKKβ, y de miR-199a-3p con IKKβ mediante ensayos luciferasa en la línea celular HEK293. Se obtuvo una bajada en la actividad de NF-κB e inflamación en HUVECs y VSMCs al aumentar el miR-15a-5p y en HUVECs también con el miR-199a-3p, medido como la fosforilación de IKKα/β por Western blot en HUVECs y VSMCs, y la translocación de p65 al núcleo por inmunofluorescencia (IF) en HUVECs.

Por otro lado, en las bases de datos de interacción miRNA-mRNA también aparecía el receptor de la lipoproteína de baja densidad oxidada tipo lectina 1 (LOX-1) como una posible diana del miR-15a-5p. Se estudió la expresión de LOX-1 en la aorta de los ratones *ApoE*$^{-/-}$ y en humanos por IF e IHQ, encontrándose aumentada. También se obtuvo una disminución de la proteína al incrementar los niveles de miR-15a-5p mediante transfección de miméticos en VSMCs. Y finalmente, al tratar las células con LDL oxidadas y realizar la tinción con Oil Red O, se obtuvo una disminución de la acumulación lipídica si se inducía la sobreexpresión del miR-15a-5p o del miR-199a 3p.

5. Confirmar si los miR-143-3p, miR-155-5p, miR-15a-5p y miR-199a-3p también se encuentran alterados en las carótidas y en las células inmunes de un modelo de aterosclerosis en un ratón transgénico para el gen humano *APOB100*. Debido a que el estudio de los miRNAs se realizó en la arteria aorta del ratón *ApoE*$^{-/-}$, y en las muestras vasculares humanas comparábamos aorta y carótida; confirmamos las alteraciones en miR-143-3p, miR-155-5p, miR-15a-5p y miR-199a-3p en otro modelo de aterosclerosis en ratón, a nivel vascular tanto en las arterias como en las carótidas y en las células inmunes. Para poder abordar este objetivo, realicé una estancia de tres meses en el laboratorio de Anton Gisterå, en el Instituto de Investigación Karolinska de Estocolmo (Suecia), un laboratorio especializado en el estudio de la inmunología en el proceso aterosclerótico.

Se utilizó el modelo HuBL, que es un ratón que contiene el transgén de la apolipoproteína B100 humana y desarrolla lesiones ateroscleróticas y una dislipemia muy similar al humano. En este caso se aislaron los miRNAs de las carótidas comunes, la bifurcación carótida, y células $CD3^+$ (células T) y $CD3^-$ (células B, células T inmaduras, y otras células inmunes) del bazo de ratones hembra de 11 y 46

semanas para estudiar la alteración de los miRNAs en la aterosclerosis inicial (donde hay lesiones en la bifurcación carótida y no en las carótidas comunes), y avanzada (donde hay lesiones ateroscleróticas tanto en la bifurcación carótida como en las carótidas comunes). A nivel vascular, pudimos confirmar que los niveles de miR-143-3p se encontraban disminuidos y los niveles de miR-155-5p aumentados en la aterosclerosis carotídea inicial y avanzada; mientras que los niveles de miR-15a-5p y miR-199a-3p se encontraban disminuidos en la aterosclerosis carotídea inicial. Además, la expresión del miR-143-3p aumentó tanto en las células $CD3^+$ como en las $CD3^-$ en la aterosclerosis avanzada; el miR-199a-3p solo se detectó en células $CD3^-$ donde también estaba aumentado; y los niveles de miR-155-5p y miR-15a-5p se encontraron aumentados en las células $CD3^+$ en comparación con las $CD3^-$ en la aterosclerosis carotídea inicial.

6. **Confirmar si miR-143-3p, miR-155-5p, miR-15a-5p y miR-199a-3p pueden ser potenciales biomarcadores de la enfermedad aterosclerótica avanzada en humanos.** Se utilizó el plasma de pacientes con aterosclerosis carotídea avanzada y sujetos sin aterosclerosis, de los que se precipitaron las vesículas extracelulares y se aislaron los miRNAs. Además, se confirmó mediante *Western blot* de marcadores de exosomas y por dispersión de luz dinámica (DLS), que el pellet de las vesículas extracelulares obtenido estaba enriquecido en exosomas.

Se aislaron miRNAs de las vesículas extracelulares y se estudió la expresión relativa de miR-143-3p, miR-155-5p, miR-15a-5p y miR-199a-3p por RT-qPCR. Se obtuvo una disminución significativa de la expresión del miR-143-3p y un aumento significativo de la expresión de los miR-15a-5p y miR-199a-3p, en el plasma de pacientes con una aterosclerosis carotidea avanzada, mientras que no se observaron cambios significativos en los niveles de miR-155-5p. Para confirmar que estos miRNAs podrían ser potenciales biomarcadores de la enfermedad, se realizó un análisis de curva operativa del receptor (ROC), y se confirmaron el miR-143-3p y el miR-15a-5p como potenciales biomarcadores de la aterosclerosis carotídea avanzada, y al miR-199a-3p solo en combinación con el miR-15a-5p.

Conclusiones:

En base a los estudios realizados y los resultados obtenidos en la presente tesis doctoral, podemos llegar a las siguientes conclusiones:

1. La disminución de miR-143-3p induce un aumento en la expresión de IGF-IIR que promueve la apoptosis de las células vasculares y la inestabilidad de las placas de ateroma.

2. Niveles elevados de miR-155-5p inducen resistencia a la insulina vascular en la aterosclerosis experimental y humana mediante la inhibición de la expresión de AKT.

3. La disminución de miR-15a-5p y miR-199a-3p induce la sobreexpresión de IKKα, IKKβ, p65 y LOX-1, favoreciendo la inflamación vascular y la captación de lípidos durante la progresión de la aterosclerosis.

4. La disminución de miR-15a-5p y miR-199a-3p se observa en la aterosclerosis carotidea experimental temprana, así como el aumento de miR-155-5p y la disminución de miR-143-3p, se observa tanto en la aterosclerosis carotídea temprana como avanzada.

5. miR-143-3p, miR-15a-5p y la combinación de miR-15a-5p y miR-199a-3p son potenciales biomarcadores no invasivos de aterosclerosis carotídea avanzada en humanos.

Nuestros resultados muestran que los niveles alterados de los miR-143-3p (i), miR-155-5p (ii), miR-15a-5p (iii,iv) y miR-199a-3p (iii,iv) en lesiones vasculares están involucrados en la progresión de la aterosclerosis experimental y humana promoviendo: (i) apoptosis de células endoteliales y del músculo liso vascular e inestabilidad de la placa, (ii) resistencia a la insulina vascular, (iii) inflamación y (iv) captación de lípidos en las células del músculo liso vascular. Esta investigación contribuye a una comprensión integral de la participación de ciertos miRNAs en la progresión de la aterosclerosis y, además, se propone al miR-143-3p y miR-15a-5p como potenciales biomarcadores no invasivos de aterosclerosis avanzada.

"¿Cómo van a silenciar al jilguero o al
canario?
Si no hay cárcel ni tumba para el canto
libertario"

-Fiesta Pagana, Mägo de Oz

1. Abstract

1. ABSTRACT

Introduction. Atherosclerosis is a chronic inflammatory disease that affects medium- and large-sized arteries of different vascular beds and is characterized by thickening of the intima and media layer with loss of elasticity. Its basic lesion is the atheromatous plaque, which is mainly composed of lipids, fibrous tissue, and inflammatory cells, and goes through different stages (1).

The atherosclerotic process begins with endothelial dysfunction, resulting in the uncoupling of endothelial nitric oxide synthase due to various causes such as the loss of the glycocalyx or the shear stress generated by blood flow on the endothelium. These processes induce inflammation and oxidative stress of the endothelium, thereby "activating" these cells, allowing the entry of low-density lipoproteins (LDLs) or monocytes, which under physiological conditions do not enter the vascular wall (1–8). Once in the inflammatory environment typical of atherosclerotic disease, monocytes differentiate into macrophages that capture modified LDLs, transforming into foam cells that release pro-inflammatory molecules (9–11). In addition to macrophages, atherosclerotic lesions contain other immune cells such as proinflammatory T cells ($CD8^+$ or Th1) (12,13), anti-inflammatory Treg (14), and B2 (pro-atherosclerotic) and B1 (anti-atherosclerotic) cells, as well as protective IgM antibodies (15) or IgG and IgE antibodies that promote the disease (16,17).

The other resident cell type in the arteries is vascular smooth muscle cells (VSMCs), which also play a significant role in the progression of atherosclerosis. Under physiological conditions, VSMCs have a contractile phenotype to maintain vascular tone. However, in the atherosclerotic process, they acquire a synthetic phenotype with increased migration and proliferation capabilities, an osteoclastic-, fibroblastic-, or macrophage-like phenotype, allowing them to capture modified LDLs and give rise to foam cells (18,19). In addition to cell type-specific effects and vascular layer-specific effects, there are altered pathways such as the insulin and insulin-like growth factor pathways (20–24) and the inflammatory nuclear factor-kappa B (NF-κB) pathway (25–30).

On the other hand, microRNAs (miRNAs) are small non-coding RNA molecules that negatively regulate the expression of their target genes by suppressing translation or directly degrading messenger RNA (mRNA). They were discovered in 1994, and since they can modulate the expression of various genes, they have been found to be altered in various diseases such as cancer, Alzheimer's, or atherosclerosis (31–36).

Considering these background findings, we have formulated the following hypothesis and objectives.

Hypothesis: During the atherosclerotic process, various miRNA alterations occur, promoting or attempting to mitigate disease progression through the modulation of specific targets.

Objectives: The overall objective is to study the alteration of selected miRNAs in murine and human atherosclerosis. The specific objectives are as follows:

1. Identify potential miRNAs involved in experimental and human atherosclerosis.

2. Study the role of miR-143-3p dysregulation and its target IGF-IIR in the atherosclerotic plaque instability.

3. Analyze the involvement of miR-155-5p and its targets AKT, eNOS, p85α in the progression of atherosclerosis and vascular insulin resistance.

4. Investigate the role of miR-15a-5p and miR-199a-3p and their targets IKKs, NF-κB p65, mTOR and LOX-1 in the progression of atherosclerosis, mainly in inflammation and in the formation of foam cells.

5. Confirm if miR-143-3p, miR-155-5p, miR-15a-5p and miR-199a-3p are also altered in the carotids and immune cells from a mouse model of atherosclerosis transgenic for the human *APOB100* gene.

6. Identify if the selected miRNAs can be used as non-invasive biomarkers for advanced atherosclerosis.

Methodology and Results: To address the general objective, we used an apolipoprotein E-deficient mouse model (*ApoE*$^{-/-}$) fed with either a standard diet or a high fat diet for 8- and 18-weeks post-weaning. Additionally, three groups of human vascular samples were included: control arteries (CAs, without atherosclerosis), arteries from patients with early lesions or fibroatheromas (FAs), and carotid arteries from patients with advanced carotid atherosclerotic (ACA) lesions.

1. Identification of potential miRNAs involved in atherosclerosis. First, an *in silico* search was conducted using the GEO Database and PubMed to select miRNAs that might modulate atherosclerosis progression. A total of 24 candidates were selected. To confirm if these miRNAs were altered in mice, miRNAs were isolated from the whole aortas of mice after 8- and 18-weeks on diet. Complementary DNAs were obtained through reverse transcription, and the relative expression of the selected miRNAs was calculated using RT-qPCR. Out of the 24 candidate miRNAs, 3 had altered levels in the aortas of mice after 8 weeks on a high-fat diet, and 11 had altered levels in the aortas of mice after 18 weeks on a high-fat diet. These 11 miRNAs were also analyzed in human samples, and 6 of them were found to be altered in the presence of advanced atherosclerosis. Among them, miR-143-3p, miR-155-5p, miR-15a-5p, and miR-199a-3p showed consistent alterations in both mouse and human samples.

2. Study of the role of miR-143-3p and its target IGF-IIR in atherosclerotic plaque instability. miR-143-3p levels were found to be decreased in the aortas of *ApoE*$^{-/-}$ mice after 18 weeks on a high-fat diet and in the carotids of patients with ACA, as measured by RT-qPCR.

An *in silico* study was conducted in various miRNA-mRNA interaction databases to select interesting targets. The insulin-like growth factor type II receptor (IGF-IIR), a confirmed target of miR-143-3p, was chosen for further investigation. Protein extraction from the arteries of *ApoE*$^{-/-}$ mice after 18 weeks on the diet showed an increase in IGF-IIR expression, although it did not reach statistical significance. However, *in vitro* experiments conducted in two vascular cell lines, human umbilical vein endothelial cells (HUVECs) and mouse VSMCs, revealed a decrease in IGF-IIR when cells were transfected with miR-143-3p mimetics. Additionally, the cellular apoptosis of these lines, measured as caspase-3 protein activity through Western blot, decreased following increased miR-143-3p expression.

3. Implication of miR-155-5p and its targets AKT, eNOS, and p85α in atherosclerosis progression and vascular insulin resistance. miR-155-5p levels were found to be increased in the arteries of *ApoE*$^{-/-}$ mice after 18 weeks on a high-fat diet and in the carotids of patients with ACA.

A similar *in silico* study was conducted to investigate miRNA-mRNA interactions, and the relationship with its confirmed target AKT was chosen for further analysis. AKT expression was found to be decreased in *ApoE*$^{-/-}$ mice after 18 weeks on a high-fat diet compared to wild-type animals, as shown through Western blot analysis. The ACA group also exhibited reduced AKT expression, confirmed by immunohistochemistry (IHC). It was further demonstrated that in HUVECs and VSMCs, AKT decreased upon transfection with miR-155-5p mimics. Due to AKT's key role in the insulin response pathway, the study examined whether insulin response was impaired after increased miR-155-5p expression in the VSMC line, resulting in decreased AKT activity as measured by serine 473 phosphorylation in response to insulin.

Additionally, miR-155-5p expression was analyzed by RT-qPCR in ACA patients based on body mass index (BMI) and AKT expression by IHC. It was observed that miR-155-5p levels increased proportionally with BMI. The expression of miR-155-5p was also analyzed based on other clinical characteristics and we observed that the relative expression of this miRNA increased in patients with diabetes and ACA, or if the patient was symptomatic.

4. Study of the role of miR-15a-5p and miR-199a-3p and their targets IKKs, NF-κB p65, mTOR, and LOX-1 in atherosclerosis progression, especially in inflammation and foam cell formation. miR-15a-5p and miR-199a-3p levels were decreased in the aortas of *ApoE*$^{-/-}$ mice after 18 weeks on a high-fat diet and in the carotids of the ACA patient group.

Following *in silico* analysis to identify potential targets, proteins belonging to the NF-κB pathway were selected. IKKα and IKKβ were considered potential targets of miR-15a-5p, while IKKβ and p65 were potential targets of miR-199a-3p. Western blot and IHC revealed increased expression of IKKα, IKKβ, and p65 in the aortas of *ApoE*$^{-/-}$ mice after 18 weeks on the high-fat diet and in the carotids of the ACA patient group. Furthermore, in HUVECs and VSMCs, targets showed decreased expression when cells were transfected with miR-15a-5p and miR-199a-3p mimetics. The relationship between miR-15a-5p and IKKα and IKKβ, as well as miR-199a-3p and IKKβ, was confirmed through luciferase assays in the HEK293 cell line. Increasing miR-15a-5p and miR-199a-3p led to reduced NF-κB activity and inflammation in HUVECs and VSMCs, as demonstrated by the phosphorylation of IKKα/β through Western blot in HUVECs and VSMCs, and p65 translocation to the nucleus through immunofluorescence in HUVECs.

Additionally, the lectin-like oxidized low-density lipoprotein receptor 1 (LOX-1) was identified as a potential target of miR-15a-5p in miRNA-mRNA interaction databases. LOX-1 expression was studied in the aortas of *ApoE*$^{-/-}$ mice and in humans through immunofluorescence and IHC, revealing increased LOX-1 levels. When VSMCs were transfected with miR-15a-5p or miR-199a-3p mimetics and treated with oxidized LDL, lipid accumulation decreased, as indicated by Oil Red O staining.

5. Confirmation of miR-143-3p, miR-155-5p, miR-15a-5p, and miR-199a-3p alterations in carotid arteries and immune cells in a transgenic mouse model for human *APOB100* gene. Since the miRNA study was conducted in the aortic artery of *ApoE*$^{-/-}$ mice, and the human vascular samples compared aortic and carotid arteries, we confirmed alterations in miR-143-3p, miR-155-5p, miR-15a-5p, and miR-199a-3p in another mice model of atherosclerosis, at both vascular levels (arteries and carotids) and in immune cells. To address this objective, I conducted a three-month research stay in Anton Gisterå's laboratory at the Karolinska Institute in Stockholm, Sweden, a specialized lab in the study of immunology in the atherosclerotic process.

We used the HuBL model, a mouse containing the transgene of human apolipoprotein B100, which develops atherosclerotic lesions and dyslipidemia very similar to humans. In this case, we isolated miRNAs from common carotids, carotid bifurcations, and $CD3^+$ cells (T cells) and $CD3^-$ cells (B cells, immature T cells, and other immune cells) from the spleen of female mice at 11 and 46 weeks to study miRNA alterations in early atherosclerosis (with lesions in the carotid bifurcation and not in common carotids) and advanced atherosclerosis (with atherosclerotic lesions in both the carotid bifurcation and common carotids). At the vascular level, we confirmed that miR-143-3p levels were decreased and miR-155-5p levels were increased in both early and advanced carotid atherosclerosis. In contrast, miR-15a-5p and miR-199a-3p levels were decreased in early carotid atherosclerosis. Furthermore, miR-143-3p expression increased in both $CD3^+$ and $CD3^-$ cells in advanced atherosclerosis. miR-199a-3p was detected only in $CD3^-$ cells, where it was also increased. miR-155-5p and miR-15a-5p levels were elevated in $CD3^+$ cells compared to $CD3^-$ cells in early carotid atherosclerosis.

6. **Confirmation of miR-143-3p, miR-155-5p, miR-15a-5p, and miR-199a-3p as potential biomarkers for advanced atherosclerotic disease in humans.** Plasma samples from patients with advanced carotid atherosclerosis and individuals without atherosclerosis were used. Extracellular vesicles were precipitated from the plasma, and miRNAs were isolated. It was confirmed through Western blot analysis of exosome markers and dynamic light scattering (DLS) that the obtained extracellular vesicle pellet was enriched in exosomes.

miRNAs were extracted from extracellular vesicles, and the relative expression of miR-143-3p, miR-155-5p, miR-15a-5p, and miR-199a-3p was studied using RT-qPCR. A significant decrease in miR-143-3p expression and a significant increase in miR-15a-5p and miR-199a-3p expression were observed in the plasma of patients with advanced carotid atherosclerosis. However, there were no significant changes in miR 155-5p levels. To confirm the potential of these miRNAs as biomarkers for the disease, ROC curve analysis was performed, confirming miR-143-3p and miR-15a-5p as potential biomarkers for advanced carotid atherosclerosis, and miR-199a-3p in combination with miR-15a-5p.

Conclusions:

Based on the studies carried out and the results obtained in this doctoral thesis, we can reach the following conclusions:

1. The downregulation of miR-143-3p promotes vascular cell apoptosis and plaque instability by targeting IGF-IIR.

2. Increased levels of miR-155-5p induces vascular insulin resistance in experimental and human atherosclerosis by targeting AKT.

3. The decrease in miR-15a-5p and miR-199a-3p induces the upregulation of IKKα, IKKβ, p65 and LOX-1 favouring inflammation and lipid uptake in atherosclerosis.

4. The downregulation of miR-15a-5p and miR-199a-3p occurs in early experimental atherosclerosis, while increased miR-155-5p and decreased miR-143-3p is observed in both early and advanced carotid atherosclerosis.

5. miR-143-3p, miR-15a-5p and the combination of miR-15a-5p and miR-199a-3p are potential non-invasive biomarkers of human advanced carotid atherosclerosis.

Our results demonstrate that altered levels of miR-143-3p (i), miR-155-5p (ii), miR-15a-5p (iii,iv), and miR-199a-3p (iii,iv) in vascular lesions are involved in the progression of experimental and human atherosclerosis, promoting: (i) apoptosis of endothelial and vascular smooth muscle cells and plaque instability, (ii) vascular insulin resistance, (iii) inflammation, and (iv) lipid uptake in vascular smooth muscle cells. This research contributes to a comprehensive understanding of the involvement of specific miRNAs in atherosclerosis progression and suggests miR-143-3p and miR-15a-5p as potential non-invasive biomarkers for advanced atherosclerosis.

"...No sé que fue de aquel rumor,
que nos vio crecer,
siendo la carne del león.
Mírame, soy feliz, tu juego me ha,
dejado así.
Engañar, seducir,
ponerme guapo para ti,
no sé dónde quedo el rumor,
pagó la jaula al domador"

-Un día en el mundo, Vestusta Morla

2. Introduction

2. INTRODUCTION

Cardiovascular diseases (CVDs) are the main cause of death in Western countries (1) being atherosclerosis the most fatal CVD in developed and undeveloped countries (2). The main issue with this disease is that it curses with a relatively long asymptomatic period that can go back to infant days, until clinical complications occur later in life (2). Atherosclerosis is a disease of large and medium-sized muscular arteries characterised by inflammation and dysfunction of the lining of the involved blood vessels and the build-up of cholesterol, lipids, and cellular debris. This results in the formation of a plaque, obstruction of blood flow and diminished oxygen supply to target organs (3).

2.1 Atherosclerosis: from physiology to pathology

2.1.1 Function and structure of the vascular wall

Prior to understanding the atherosclerotic process, it is necessary to understand the basics of vascular histology and physiology. The vessel wall consists of three main layers: the intima, media, and adventitia with different compositions and functions (Figure I).

Intima: It is the inner layer in close contact with the blood. The intima begins as a thin layer of endothelial cells (ECs) in newborns. During aging, this layer becomes more complex and consists of several layers (3). The endothelium remains the inner layer covering the subendothelial layer, consisting of connective tissue conforming the extracellular matrix (ECM), a few vascular smooth muscle cells (VSMCs), and dendritic cells (3). Finally, there is a separation between the intima and media layer: the internal elastic membrane (lamina) which is composed of a fenestrated layer of elastic fibers (3).

Media: It is the medium layer of arteries and veins and consists of layers of VSMCs with elastic and collagen fibers between them, making it the thickest layer under non-pathological conditions. The VSMCs have two main functions in the media: contraction to preserve vascular tone and secrete molecules to maintain the ECM. The first function is more evident in small or medium arteries, whereas the second one is more important in larger arteries (4).

Adventitia: It is the outer layer of arteries and the most heterogeneous. It consists of an ECM matrix with fibroblasts (the main cell type), immune cells, nerves, and small blood vessels that conforms the *vasa vasorum*. This *vasa vasorum* provides nutrients and removes waste from larger veins and arteries. At first, the adventitia received less recognition than the other layers; however, it has recently gained popularity. The cells in this layer are able to capture stimuli coming from cells of both the vascular wall and adjacent tissues; in fact, they can act as the first "injury sensing tissue" in the vascular wall (5).

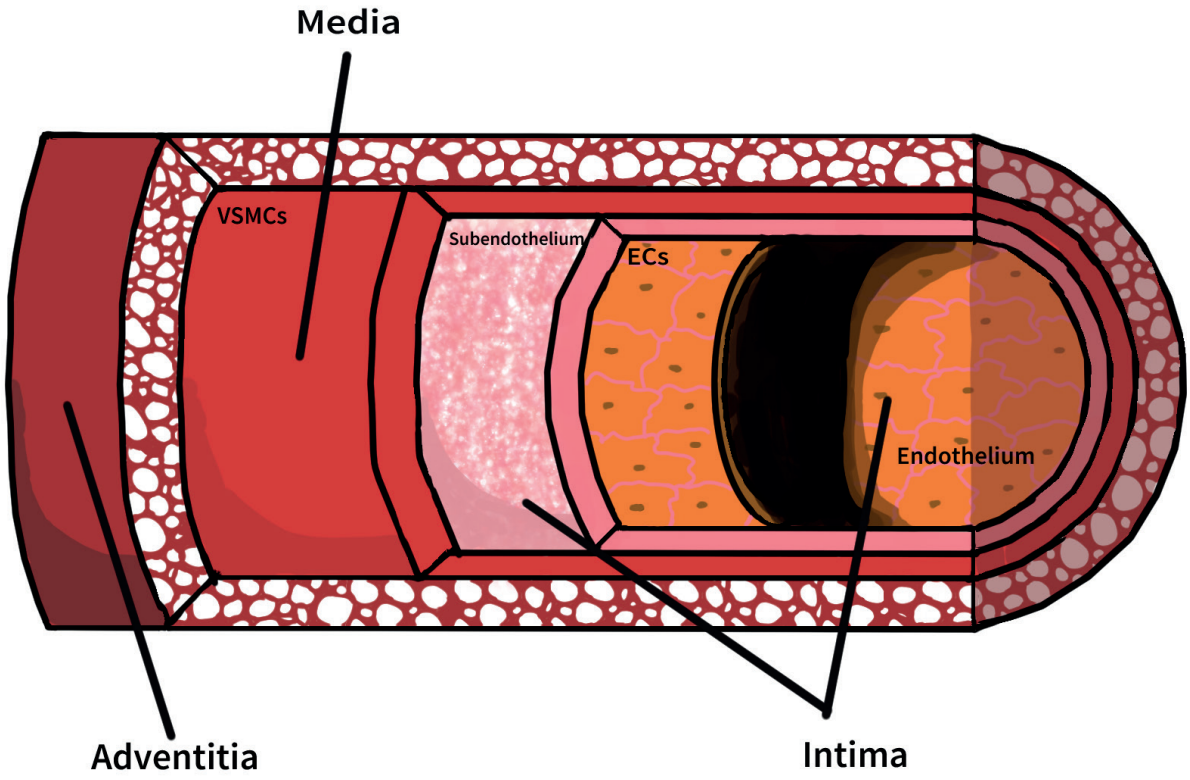

Figure I. Morphology of a blood vessel. This image shows the three main layers of the vessel wall: adventitia; media; and intima, which is formed by the subendothelium and the endothelium. ECs= endothelial cells; VSMCs= vascular smooth muscle cells. © Paula González

2.1.2 Endothelial function and dysfunction

As previously stated, the endothelium is a monolayer of cells in close contact with the blood that it is part of the intima layer. However, even though it is thin, it is crucial for maintaining homeostasis of the vascular wall and for the appearance and development of various CVDs.

Endothelial cells are influenced by two hemodynamic forces: cyclical strain, caused by the extension and distension of the vessel diameter, and shear stress, defined as the tension generated by blood flow, and it is the reason why ECs are aligned parallel to it (37,38). Shear stress is defined by the mean flow ratio, which depends on cyclical strain and bending of the vascular wall (disturbed blood flow areas), viscosity, which depends on the speed of the blood flow, and the physical characteristics of the blood (38,39). Because ECs are in close contact with this force, either high or low shear stress stimulates changes in the ECs signalling pathway; therefore, mechanical stimuli on factors that affect vascular homeostasis and other cell types, such as VSMCs (39,40) (Figure II).

A healthy endothelium is capable of integrating many signals and multiple factors that control vascular tone, cell adhesion, proliferation of VSMCs, and vascular permeability (6). The endothelium produces molecules that relax the vascular tone, such as nitric oxide (NO) and prostacyclin, or contract the vascular wall, such as angiotensin II (Ang II) (6,41). NO is produced by endothelial nitric oxide synthase (eNOS) in response to different stimuli, such as shear stress, and maintains quiescence of the vascular wall, decreasing inflammation, thrombosis, and cell proliferation; thus, it is used to measure endothelial function (6). Other factor that controls endothelial function are the vascular endothelial growth factors (VEGFs), that modulate endothelial permeability to cells and agents, the formation of the endothelial monolayer; as well as being an angiogenic and vasoactive factors (42) (Figure II).

When the endothelium gets activated (also known as endothelial dysfunction) under certain conditions (e.g. inflammation, shear stress, oxidative stress…), it stops being quiescent and enters a "defensive" mode characterized by the expression of cell-surface adhesion molecules (e.g. the vascular cell adhesion molecule (VCAM-1) or the monocyte chemoattractant protein-1 (MCP-1)) that recruits inflammatory cells, that enters the subendothelial space; and switches NO production by eNOS to reactive oxygen species (ROS), known as eNOS uncoupling (6–8). ROS are secondary messengers under physiological conditions, but when there are more ROS than those that are capable of being buffered by endothelial antioxidant molecules, oxidative stress occurs, leading to inflammation and endothelial damage (14) (Figure II).

Shear stress is one of the main causes of endothelial activation. In fact, there are areas in the arteries that are more prone to vascular injuries, and they are disturbed blood flow areas that promote eNOS uncoupling and inflammatory pathways (8). The change in endothelial permeability also permits the entrance of low-density lipoproteins (LDLs) into the vascular intima, that in conjunction with the oxidative conditions due to eNOS uncoupling, oxidize LDLs to form oxidized LDLs (Ox-LDLs) that accumulate in the intima, forming atherosclerotic plaques (43). In addition, shear stress also diminishes molecules such as Krüppel-like factors 2 and 4 (KLF2 and KLF4) and the nuclear factor erythroid-derived 2-related factor 2 (Nrf2), which are mechanosensitive mediators that diminish endothelial dysfunction and oxidative stress (43) (Figure II).

Therefore, activation of the endothelium, entrance of LDLs, and recruitment of monocytes into the subendothelial space are the first steps in atherosclerotic progression.

Lastly, glycocalyx, a sugar-enriched layer produced by endothelial cells that appears in the apical wall, formed mostly by glycosylated proteins and proteoglycans, which bind to the endothelial cell membrane and are crucial for its permeability. This matrix modulates the entrance of factors not only by their size but also by their charge (electrostatic barrier) because it is negatively charged; therefore, it acts as a barrier that prevents negative charged molecules or cells (e.g., erythrocytes or bacteria) from entering the vascular wall (44) (Figure II).

The glycocalyx also communicates mechanical signals generated by shear stress to the ECs and the ECM because its main components, syndecans and glypicans, are bound to the endothelial membrane in areas where they can communicate mechanical changes to cytoskeletal proteins, among others. Syndecans like syndecan-1 is implicated in phenotype and inflammation modulation, and glypicans, like glypican-1, are related to eNOS phosphorylation and NO production. There are also glycosaminoglycans, such as hyaluronic acid, salicylic acid, and heparan sulphate, that bind to syndecans and glypicans to form the glycocalyx. Other molecules such as matrix metalloproteases (MMPs), adhesion molecules such as CD44, or integrins conform this matrix (45,46).

In healthy conditions, the glycocalyx has a specific width (that differs between veins, capillaries, and arteries) and is constantly changing. But in the atherosclerotic process, the accumulation of LDLs in the subendothelial space increases ROS production, MMPs, leukocyte adhesion molecules, and inflammation in the endothelium, this affects the presence of antioxidant enzymes and the composition of the glycocalyx leading to its "shedding" (44–46). When the glycocalyx is degraded, the permeability of the endothelium decreases, more LDLs enter, inflammation and oxidative stress increase, and atherosclerosis progresses (Figure II).

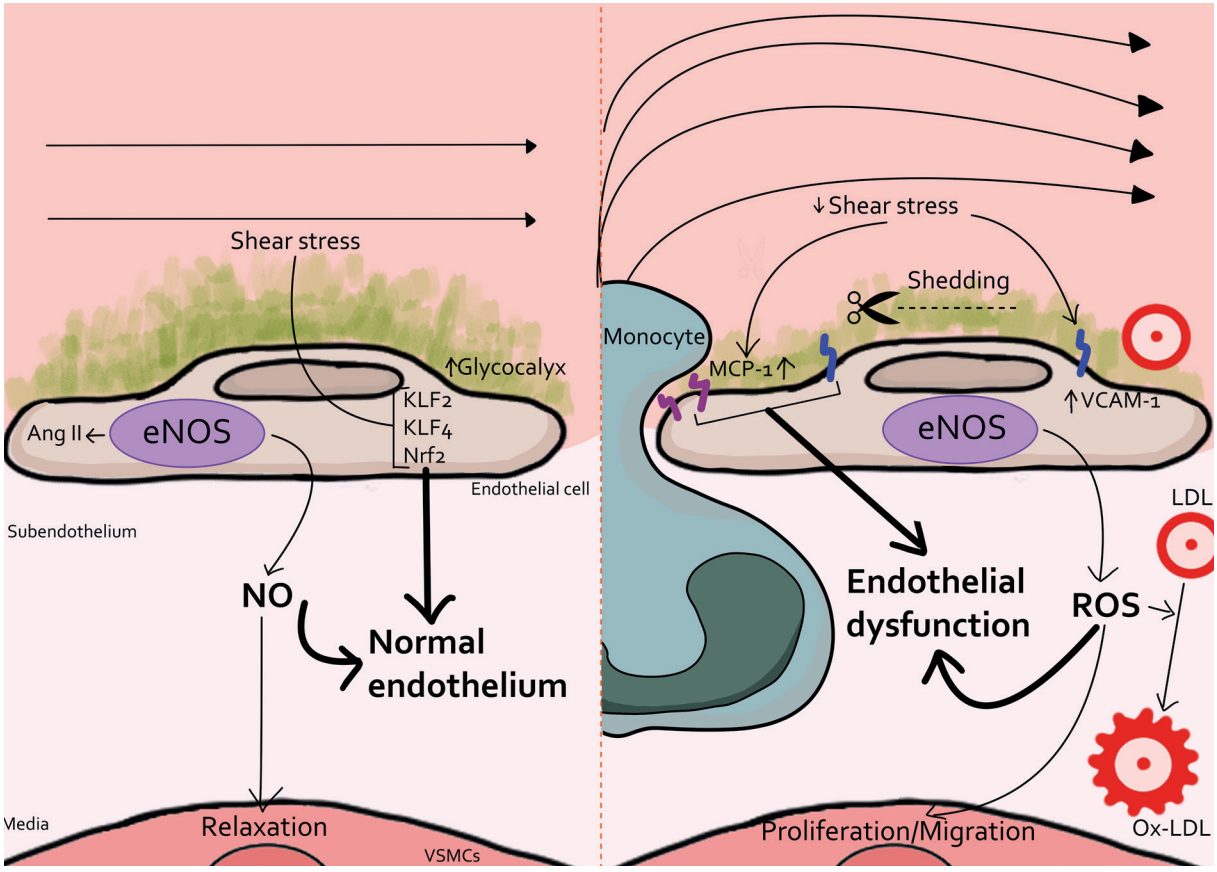

Figure II. Mechanisms of endothelial activation. This picture represents an endothelium under physiological conditions (left), with a physiological shear stress caused by the laminar efflux of the blood; eNOS producing NO for the correct relaxation of the vessel, and Ang II for the contraction; the production of KLF2-4 and Nrf2 promoted by shear stress; and a normal glycocalyx that prevents from the infiltration of molecules and inflammatory cells. On the contrary, the right side of the illustration represents an activated endothelial cell, where there is a turbulent blood flow that decreases shear stress inducing the shedding of the glycocalyx and the expression of adhesion molecules like MCP-1 or VCAM-1, that allows the infiltration of monocytes and LDLs in the vascular wall; and eNOS uncoupling increasing ROS production; moreover the LDLs with the ROS are going to produce Ox-LDLs and this oxidative environment is going to affect the VSMCs that are going to proliferate and migrate from the media. NO= nitric oxide; eNOS= endothelial NO synthase; Ang-II= angiotensin II; KLF 2-4= Krüppel-like factor 2 and 4; Nrf2= nuclear factor erythroid-derived 2-related factor 2; ROS= reactive oxygen species; LDL= low-density lipoprotein; Ox-LDL= oxidized low-density lipoproteins; MCP-1= monocyte chemoattractant protein-1; VCAM-1= vascular adhesion molecule-1; VSMCs= vascular smooth muscle cells. © Paula González.

2.1.3 Inflammation in the atherosclerotic progression

Atherosclerosis has been defined in recent years as a chronic inflammatory disease (47) while, traditionally atherosclerosis has been regarded as a disease driven by LDLs accumulation in the vascular subendothelium (47,48). This subclinical inflammation attracts cells from the innate and adaptive immune responses to the atherosclerotic plaque (47), and the signalling pathways mediated by these immune cells are altered during atherosclerotic progression (48).

2.1.3.1 Innate or adaptive immune responses, and inflammation in the promotion of atherosclerosis

There are different innate and adaptive immune response cell types, all of which have different functions and effects on atherosclerosis. The innate immune response has two components, humoral and cellular (49). The humoral arm of the innate response is led by molecules, such as pentraxins (for example, C reactive protein, pentaxin 3), collectines (e.g. A surfactant protein), or ficolins, these molecules are like "pre-antibodies" that activate the complement and regulate inflammation (50), and antibodies. The cellular arm of the innate response is formed by mononuclear and polymorphonuclear

phagocytes, which are macrophages and dendritic cells, which are both derived from monocytes and present antigens to T cells from the adaptive immune system; the polymorphonuclear phagocytes are neutrophils, basophils, and eosinophils, which also present antigens to the adaptive immune system (49).

We begin by explaining the role of macrophages in atherosclerosis. These cells are pivotal for the development of atherosclerosis. First, there is an endothelial dysfunction and a pathogenic accumulation of LDLs (enriched in cholesterol and containing apolipoprotein B (ApoB)) in the vascular wall, where they are susceptible to modifications such as oxidation. Increased oxidative stress and inflammation in the endothelium lead to the recruitment of monocytes by cells with chemoattractant molecules such as MCP-1 or chemokine ligands 3, 4, and 5 (9).

Monocytes then enter the vascular wall and try to clear LDLs that accumulate in the vascular wall. They transform into macrophages that clear LDL under normal conditions by their LDL receptor (LDLr); however, in hypercholesterolemic conditions, there are not only increased monocytes (9), but the macrophage-LDLr decreases and they begin to take up Ox-LDL by their scavenger receptors (for example, CD36, lectin-like Ox-LDL receptor-1 (*OLR-1* or LOX 1)) switching to a foam cell phenotype (10), but macrophages can have other phenotypes. Classically, macrophages have been classified as M1 (pro-inflammatory) related to T helper (Th) type-1 (Th1) T-cells, which are usually localized in the shoulder (high inflammation and apoptosis) area of the plaques, and M2 (anti-inflammatory) macrophages related to Th2 T-cells, these cells are usually localized in the adventitia and in stable plaques (11) (Figure III).

Dendritic cells (DCs) are potent antigen-presenting cells; therefore, like macrophages, they serve as a bridge between the innate and adaptive immune responses. The role played by antigen-presenting cells (APCs) in atherosclerosis is still under discussion, but just like macrophages, DCs uptake LDLs, turning into foam cells, increasing ROS and inflammation, and presenting antigens to T cells, promoting their proliferation in the plaque, and they also promote tumor necrosis factor alpha (TNFα) and interferon gamma (IFNγ) in antigen activated T cells (51). Nonetheless, the exact role of DCs in atherosclerosis remains to be elucidated (Figure III).

The last innate response cells are neutrophils, basophils, and eosinophils. Neutrophils are known to present antigens to T cells and form pro-inflammatory neutrophil extracellular traps (NETs), these NETs are stimulated by cholesterol crystals, Ox-LDLs, and various chemokines (52). Interestingly, when the formation of NETs is inhibited, plaque size is reduced in mice (53) because the formation of NETs is associated with an increase in pro-inflammatory macrophages that promote the disease (52). The influence of basophils and eosinophils on atherosclerosis is not well known; eosinophils are greater in size than neutrophils and are mostly involved in allergic responses presenting antigens to Th2 cells. They can form pro-inflammatory eosinophil extracellular traps, but how they affect atherosclerosis remains unknown. Basophils are smaller than eosinophils and are involved in allergenic responses, like the other cells they can form extracellular traps, but how they affect atherosclerosis is unknown (54) (Figure III).

The adaptive immune response is carried out by lymphocytes that can be B cells (B lymphocytes) and T cells (T lymphocytes). B cells are important for humoral and adaptive immunity, since they oversee free antibodies in the circulation and have the B-cell receptor (BCR) to recognize antigens (55). There are two main types of B cells: B1 cells, which are divided into B1a, B1b, and B2 cells, with different effects and functions. There are four types of antibodies: IgM, IgG, IgE, and IgA.

IgMs have a low affinity to antigens and can be found in the blood as well as in atherosclerotic injuries, because they have been proven to identify oxidation-specific motifs that are found in Ox-LDLs (and other structures) with an anti-atherosclerotic effect (15). IgGs are the most prevalent immunoglobulins in the blood and have a high antigen neutralizing capacity; however, IgGs have also been found in mouse plaques, promoting atherosclerosis (16). IgEs are the lowest expressed in the blood and participate in allergenic responses, however, mice lacking IgEs showed protection against atherosclerosis and obesity by reducing foam cell formation (17). Lastly, IgAs are very prevalent in mucosal surfaces and the blood and participate in allergic responses; however, how these antibodies may affect atherosclerosis remains unclear (56) (Figure III).

For the different types of B cells, we have the B1-cell type, which is divided into B1a and B1b if they are $CD5^+$ or $CD5^-$, respectively. They secrete IgM into the blood and interact with T cells. These cells have been well described in mice, but their existence in humans is still under discussion. Follicular B cells, which are B2 cells and make up for most circulating B cells, produce antibodies after a second encounter with an antigen, leading to an antigen specific T-cell response. Another type of B2 cells are the marginal zone ones that derive from the bone marrow, and to finish, we have the regulatory B cells that induce immunosuppressive regulatory T cells (Treg) (55). Specifically speaking about atherosclerosis, B1 cells are atheroprotective by secreting IgMs, whereas B2 cells are considered atherogenic by secreting IgGs that activate T cells and increase inflammation (57) (Figure III).

Finally, we introduce the T cells. Beginning with T cells expressing CD4 or $CD4^+$ T cells, they can differentiate into Th and Treg subtypes, each with different effects on atherosclerosis. Th cells have different subtypes: Th1, Th2, Th9, Th17, Th22, and follicular helper (Tfh) cells with different functions and effects on disease progression (37) (Figure III).

Th1 cells secrete pro-inflammatory IFNγ and TNFα, promoting atherosclerosis development and chronic inflammation (12). Th2 cells produce interleukin-4 (IL)-4 to counteract the IFNγ produced by Th1 cells; therefore, we believe that they would protect against atherosclerosis. However, even though these cells seem to be protective against the malady in humans, this association is not so clear (59). Th9 cells produce IL-9 and are associated with increased inflammation and atherosclerosis (60). Th17 cells produce IL-17, but their effect on the disease is controversial; some studies describe that Th17 cells protect against the disease, while others defend it as a promoter (61). Th22 cells produce IL-22, which induces inflammation and atherosclerosis in apolipoprotein E deficient ($ApoE^{-/-}$) mice (62). Tfh are closely related to B cells in germinal centres and to an increase in atherosclerosis in different mouse models (63). Treg cells have been shown to be protective against atherosclerosis, since these cells are inversely correlated with the size of the injury (14) (Figure III).

The other T cell type is CD8 or $CD8^+$ T cells. When activated, these cells secrete TNFα and IFNγ to increase inflammation and apoptosis. In the context of atherosclerosis, $CD8^+$ T cells are more abundant than $CD4^+$ cells in human and mouse injuries, where they aggravate atherosclerotic lesion formation by controlling macrophage accumulation in the vessel walls (13).

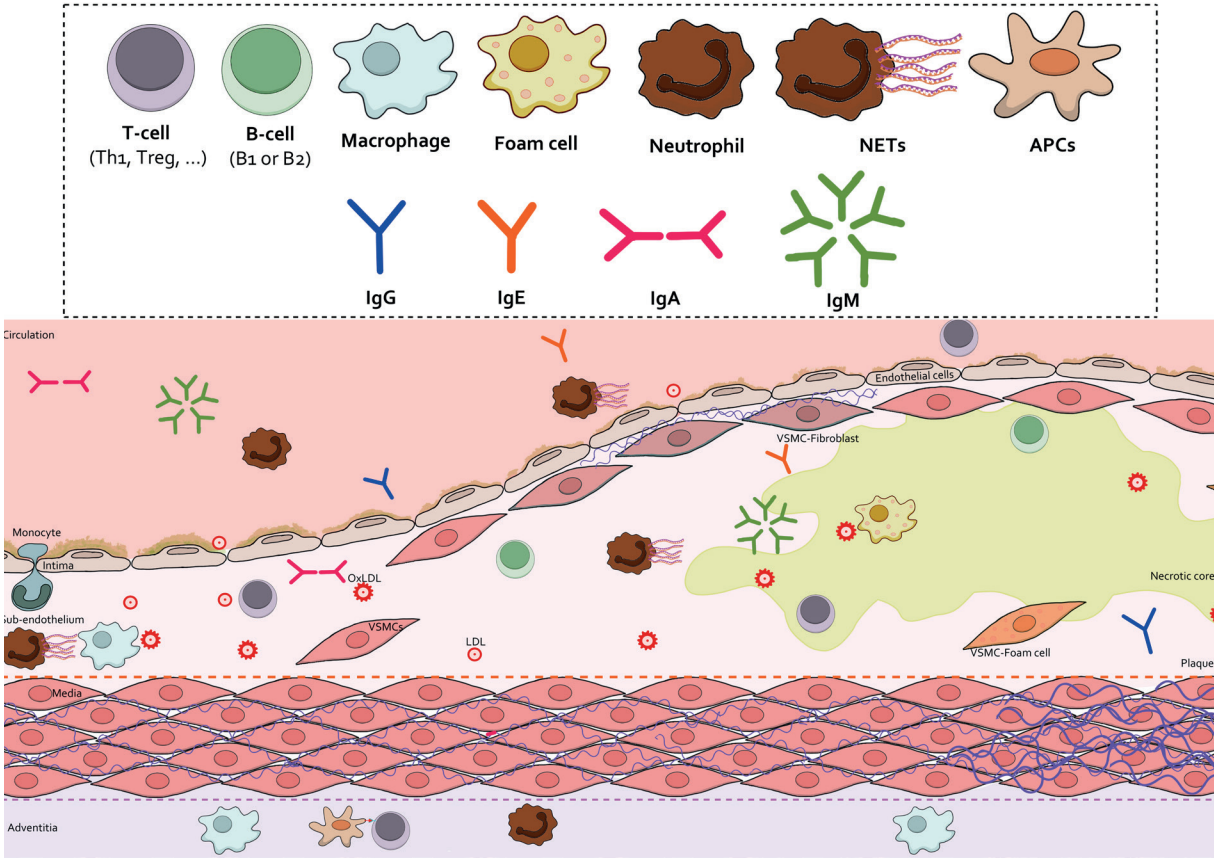

Figure III. Immune cells in atherosclerosis. This illustration shows the different immune cells that can be involved in atherosclerosis. There are T cells (purple cells) than can be pro-atherogenic like Th1 or anti-atherogenic like Th2; B cells (green) that can be B1 or anti-atherogenic and B2 or pro-atherogenic; APCs; macrophages; monocytes; foam cells; and neutrophils that can form the pro-atherogenic NETs. The different antibodies are also represented, IgGs (blue), IgEs (orange), IgAs (pink) and IgEs (green). They all participate in atherosclerosis by protecting against or promoting the disease progression depending on the environment inside the vascular wall. Ig= immunoglobulin; VSMC= vascular smooth muscle cell; NET= neutrophil extracellular traps; APC= antigen presentation cells; Ox-LDL= oxidized low-density lipoproteins. © Paula González.

2.1.3.2 Pro- and anti-Inflammatory molecules in atherosclerosis development

Maintaining homeostasis in the vascular wall is important for maintaining health; however, during atherosclerosis progression, different molecules promote inflammation and oxidative stress, leading to endothelial dysfunction, cell apoptosis, and plaque rupture. Among these molecules are ROS and cytokines.

As previously stated, NO is produced by eNOS in the endothelium and is important for optimal vasculature functioning (Chapter 2.1.2). However, when there are oxidative stress and higher ROS production, there is a lower NO bioavailability and eNOS uncoupling, contributing to the major ROS presence. The main sources of ROS in the vascular wall that are altered during atherosclerosis, are the nicotinamide adenine dinucleotide phosphate (NADPH) oxidases (NOX), with three main isoforms in the vascular wall: NOX1, in VSMCs; NOX2 in endothelial cells; and NOX4 in both cell types. NOX1 and NOX2 have been proven to promote atherosclerosis, while NOX4 is consider atheroprotective (64); the xanthine oxidases that are important in the production of ROS in the endothelium under physiological conditions, but during atherosclerosis they are accumulated in the plaque increasing ROS, oxidative stress and monocyte infiltration (65); also the mitochondria is an important ROS production site in cells, as well as a ROS controlling site. Most of the antioxidant enzymes are located in

the mitochondria, like superoxide dismutase (SOD) 1 and 2 (there is also a cytoplasmic isoform: SOD_3); the catalase, and the glutathione peroxidase (GPx). The effect of decreased SOD in atherosclerosis is context dependent, but decreased catalase and GPx activities are related to an increase in atherosclerosis (64).

ROS production directly increases oxidative stress, leading to atherosclerosis; moreover, ROS also increase inflammation. ROS are capable of activating the $NLRP_3$-inflammasome and increasing inflammatory chemokines such as IL-1β and IL-18 to promote atherosclerosis in *ApoE*$^{-/-}$ mice (66), as well as other cytokines like IL-6 or TNFα to increase inflammation (67).

Cytokines are used to define "one term for a group of protein-cell regulators, variously called lymphokines, monokines, interleukins, interferons, which are produced by a wide variety of cells in the body, play an important role in many physiological responses, are involved in the pathophysiology of a range of diseases, and have therapeutic potential" (68). Cytokines are organised in different classes: ILs, TNFs, IFNs, colony stimulating factors (CSFs), transforming growth factors (TGFs) and chemokines. They are important regulators of inflammation and immunity (69).

IFNs, all the ILs except the IL-1 family and CSFs act through the Janus kinase (JAK)-signal transducer and activator of transcription (STAT) pathway; TNFs, the IL-1 family act through the nuclear factor kappa B (NF-κB) and the mitogen-activated protein kinases (MAPK) pathways; and the TGFs act through the Smads pathway (69).

The IL-1 family has 11 members, highlighting IL-1α, IL-1β, IL-33 and IL-18. These cytokines act as ligands to specific receptors (IL-1Rs) there are 10 types with an extracellular part that recognize the ILs and an intracellular part that has a toll-like receptor domain, that when active leads to the activation of the NF-κB domain (70) (Figure IV). IL-1α is a proinflammatory chemokine that has been proven to be increased in human and mouse atherosclerosis (25). IL-1β and IL-18 are also proinflammatory, their secretion is promoted by the $NLRP_3$ inflammasome and its increased in human and experimental atherosclerosis where they increase IFNγ (71,72). IL-33 has proven to be (in contrast with the other IL-1 family cytokines) atheroprotective, IL-33 has shown to decrease IFNγ and Th1 cells while increasing Th2 in atherosclerosis (73).

IL-2, IL-6, IL-10, IL-17, or IL-21 are other interleukins that participate in atherosclerosis. IL 2 and IL-10 are part of the anti-inflammatory cytokines and are considered protective against atherosclerosis by increasing the population of Treg and decreasing LDLs, respectively (74,75). On the contrary, IL-6, IL-17 and IL-21 are part of the pro-inflammatory cytokines and contribute to atherosclerosis development. IL-6 is increased in atherosclerotic injuries and promotes the disease by activating the NF-κB and $STAT_3$ pathways (76,77); IL-10 and IL-21 are also increased in mouse and human atherosclerosis and promote the disease by increasing macrophage activation, IFNγ and plaque instability (78,79) (Figure IV).

Then we have the CSF, for example the granulocyte-monocyte-CSF is pro-atherosclerotic by stimulating intima cells proliferation as well as the production of IFNγ in Th1 cells (80); the granulocyte-CSF also promotes atherosclerosis by increasing ROS production and macrophage activation (81,82); another CSF would be the macrophages CSF, that is also increased in human and mouse atherosclerosis and promotes the disease by augmenting the monocyte infiltration in the injury and foam cell formation (83,84).

TGFs like TGF-beta (TGF-β) has a dual role in the vascular wall. TGF-β increase inflammation in endothelial cells by increasing chemokines like MCP-1, or Intercellular adhesion molecule I (ICAM-1); but in VSMCs the effect is the contrary, those cytokines are decreased and has an anti-inflammatory

effect, however the global effect of the molecule seems to be pro-atherogenic (85). TNFs like TNFα is also important for the inflammatory promotion of atherosclerosis, in fact when TNFα is increased in the endothelium activating NF-κB and NLRP3 inflammasome increasing IL-1β and therefore, the disease progresses (86,87). IFNs like IFNγ is increased during atherosclerosis and leads to the differentiation of pro atherosclerotic T cells like Th1 (78) (Figure IV).

Lastly, chemokines or chemoattractant molecules are also implicated in the inflammatory-atherosclerotic progression. MCP-1 is increased in atherosclerosis, this chemokine is expressed in damaged tissues and increases monocyte and T-cell infiltration leading to the progression of the malady (88). ICAM-1 is also important for macrophage recruitment leading to atherosclerosis development, and when it is decreased, there is a smaller injury and NF-κB activity (89). The vascular cell adhesion molecule-1 (VCAM-1) is poorly expressed in the endothelium under physiological conditions, but when there is inflammation, the expression increases, leading to LDL transcytosis through the vascular wall and a higher lipidic plaque (87).

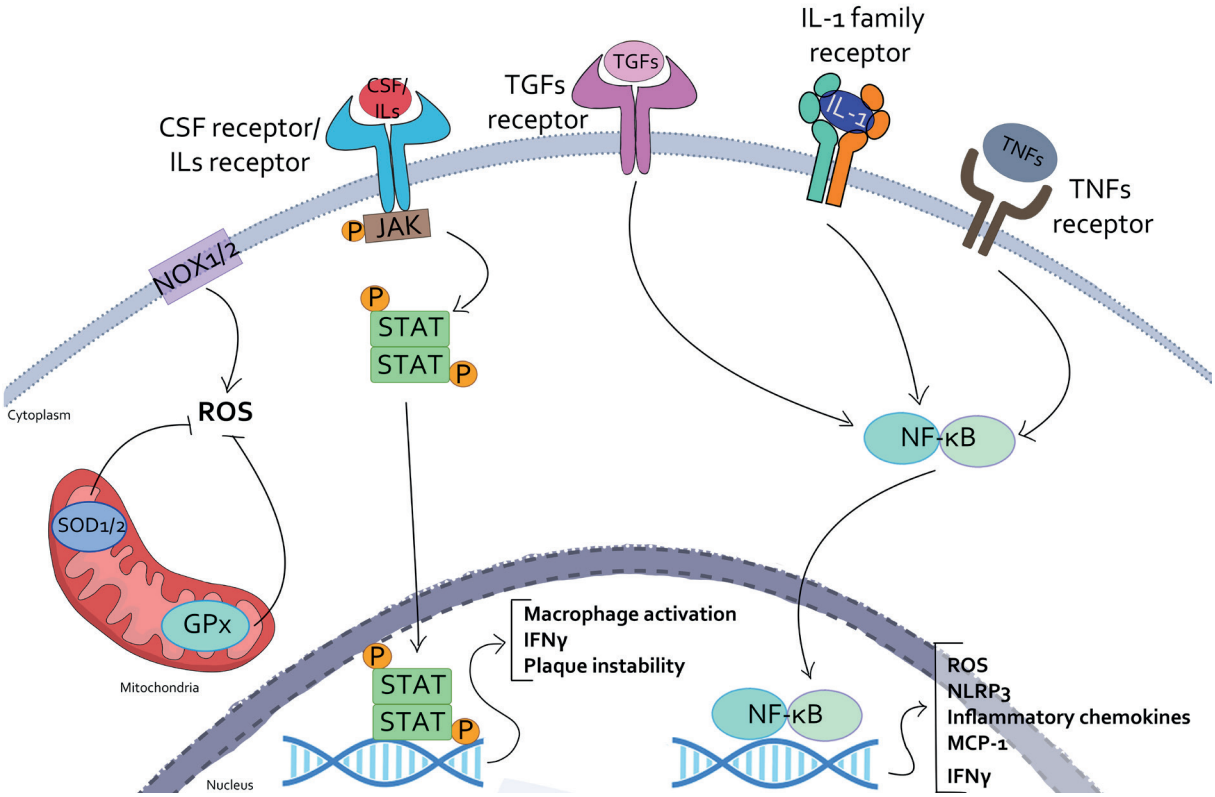

Figure IV. Inflammatory molecules in atherosclerosis. During atherosclerosis development and progression there are many molecules that promote inflammatory pathways and genes. We have enzymes like NOX1 or 2 that increase ROS inside the cells, however, there are also cellular mechanisms to decrease ROS production, these are antioxidant enzymes like SOD 1 or 2 or GPx, both in the mitochondria. Other chemokines like ILs (e.g., IL-6, IL-2, IL-10, IL-21…) or CSFs get to their receptors, these receptors activate the JAK/STAT pathway, and STAT is a transcription factor that when active, promotes the translation of pro-inflammatory genes like IFNγ, or genes that promote plaque instability and macrophage activation. There are other chemokines like TGFs, the IL 1 family proteins or TNFs, that also bind with their specific receptors from the cell membrane to promote pathways that can activate, among others, the NF-κB pathway, once active this transcription factor also promotes the expression of genes that increase ROS, the NLRP3 inflammasome, inflammatory chemokines like IL-6, IL-21, IFNγ; or chemoattractant molecules like MCP-1. NOX= NADPH oxidases; SOD= superoxide dismutase; GPx= glutathione peroxidase; ROS= reactive oxygen species; ILs= interleukins; CSFs= colony stimulating factors; JAK= Janus kinase; STAT= signal transducers and activators of transcription; IFNγ= interferon gamma; TGFs= transforming growth factors; TNFs= tumor necrosis factors; NF-κB = nuclear factor kappa B; NLRP3= nucleotide-binding domain, leucine-rich containing family, pyrin domain-containing-3; MCP-1= monocyte chemoattractant protein-1. © Paula González.

2.1.4 Vascular smooth muscle cells: proliferation, apoptosis and phenotype switching in atherosclerosis

VSMCs are the main component in the media layer of the arteries. Under physiological conditions VSMCs have a contractile phenotype with a low rate of proliferation, but when there is an alteration in homeostasis, they adopt a "synthetic" phenotype characterized by high proliferation, migration, and production of ECM. In addition, the contractile phenotype of the VSMCs amongst large or small vessels is different to modulate the systemic and/or blood flow to organs (18). VSMCs content and structure also changes with age and sex, for example, adult women have a thicker media than adult men (90), but interestingly, male VSMCs proliferate more than females (91) and respond better to signals like NO (18).

Proliferation of VSMCs drives atherosclerosis progression, in fact, they account for approximately 70 % of the cells that constitute the atherosclerotic plaque (92). There are different explanations for this increase in proliferation, for example Ox-LDLs induce Nrf2 in atherosclerosis, even though is an antioxidant molecule, is related to LOX-1 increasing this synthetic phenotype of VSMCs (92). Also the NO produced by the endothelium affects the proliferation of VSMCs, uncoupled eNOS, and decreased NO increases the proliferation of VSMCs (93,94). However, the proliferation of VSMCs and thicker media has been related to stable plaques (95).

VSMCs not only proliferate in atherosclerosis, but they also migrate from media to intima. In health, the ECM in which the VSMCs are embedded protects against this phenotype switching, but when altered it allows not only the proliferative phenotype, but also the migration of the cells to the intima. The inflammatory environment of the disease may change the composition of the ECM from laminin and collagen-4 to syndecan-4 and collagen-1 (96) leading to this VSMCs phenotype switching and migration. When they migrate and under specific conditions, the VSMCs can adopt a macrophage-, osteoblast- or mesenchymal-like phenotype (19).

VSMCs are one of the main sources of foam cells in atherosclerosis, the mechanisms underlying this switch remain poorly understood, however these cells can uptake Ox-LDL leading to this phenotype. Lately some studies are trying to give light into this question, the P2RY12/P2Y12 receptor, originally identified in platelets, to induce their aggregation and thromboembolism, promotes VSMCs-foam cell formation by decreasing cholesterol efflux and lipolysis as well as autophagy in those cells (97); c-FOS is also important in this regard, mitochondrial ROS increase c-FOS in VSMCs driving an increase in LOX-1 expression and VSMCs-foam cells (98); other works give the smooth muscle 22α a protective role against VSMCs-foam cell formation by regulating the liver X receptor translocation to the nucleus and cholesterol efflux accumulation in the cells (99).

Under specific stimuli, the VSMCs lose their smooth-muscle specific markers and change to osteoblast-like cells (19). In an *in vitro* scale this transformation is induced with β-glycerophosphate and *in vivo* can be induced with an adenine and high phosphorus diet, and the mechanism by which the VSMCs turn to an osteoblast phenotype may involve mitochondrial dysfunction, when these cells turn osteoblastic they create a pro-calcification environment leading to the calcification of the plaque (100); recently S adenosylhomocysteine (SAH) hydrolase (SAHH), a risk factor of CVDs, has been related to plaque calcification, SAHH inhibition accumulates SAH in the vascular wall decreasing AMPK and increasing VSMC-osteoblast like cells (101).

Other phenotypes that VSMCs can adapt are mesenchymal and myofibroblast-like. Inhibiting the TGF-β pathway in VSMCs from *ApoE*$^{-/-}$ mice under a HFD turns them into a mesenchymal-like phenotype that can differentiate into other macrophages-, osteoblast-, or adipocyte-like cells promoting atherosclerosis (102). When VSMCs turn to myofibroblast like cells they are part of the vascular remodelling of the media ECM by secreting collagen type-1, recent works propose the

prostaglandin D2 receptor 1 (DP1) as a modulator of this switch. When DP1 is decreased, there is angiotensin II-media thickening, and VSMCs transformation to myofibroblast (103).

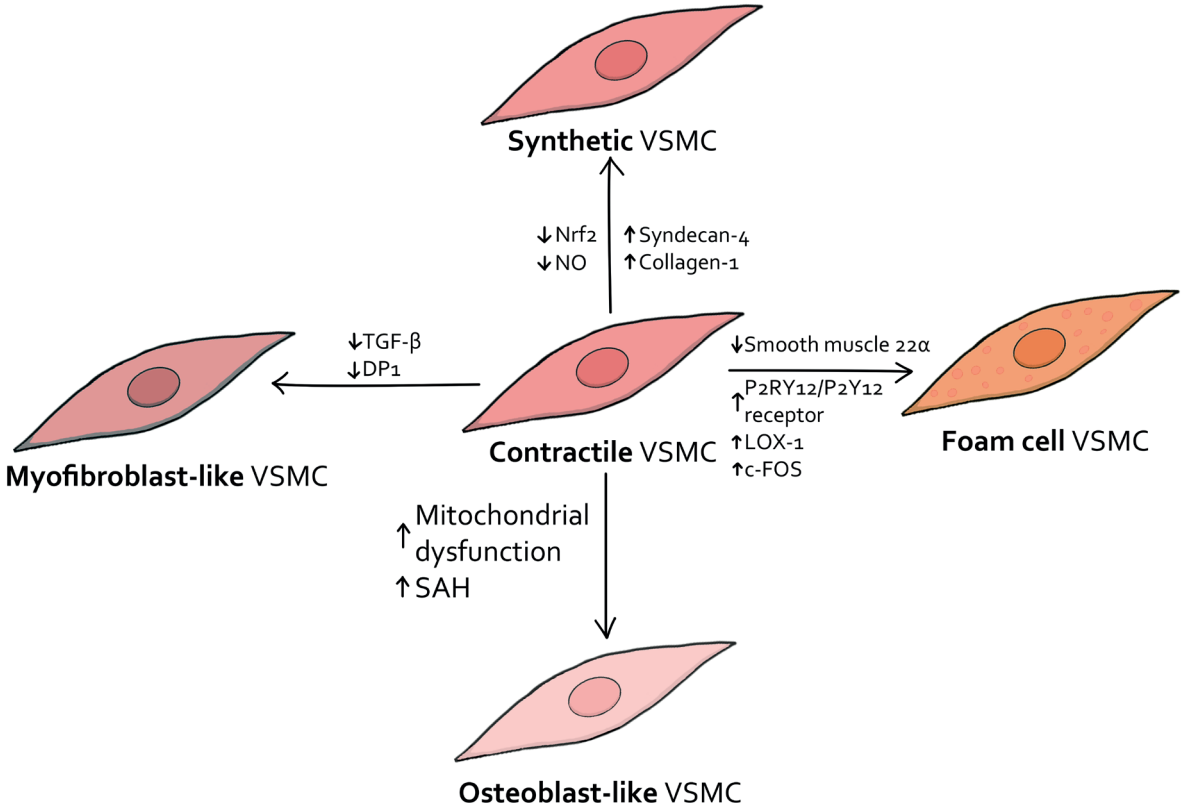

Figure V. VSMCs phenotypes. This figure represents the different VSMCs phenotypes in atherosclerosis, the contractile, synthetic, foam cell, osteoblast, and myofibroblast-like and different possible mechanism by which this switching occurs. SAH= S-adenosylhomocysteine; Nrf2= nuclear factor erythroid 2-related factor 2; NO= nitric oxide; LOX-1= lectin-like oxidized low-density lipoprotein receptor 1; TGF-β= transforming growth factor- beta; DP-1= prostaglandin D2 receptor 1; VSMC= vascular smooth muscle cell. © Paula González.

Finally, in the most advanced stages of the disease, apoptosis is increased in the VSMCs leading to plaque instability and rupture, but the underlying cause of this apoptosis is unknown, lately, the proprotein convertase subtilisin/kexin type 9 that has shown to promote senescence and apoptosis in mice, and has also been detected in human atherosclerosis giving it a potential relevance in the apoptosis-driven plaque rupture (104).

2.1.5 Plaque rupture and thrombosis

When there is an advanced atherosclerotic plaque, we can observe two outcomes that define two types: unstable, if plaques break leading to thrombosis or stable plaques, that are protected from rupture.

The stable plaques are mostly characterized by a thick fibrous cap made of ECM populated of myofibroblast-like cells that mainly come from VSMCs, this myofibroblast transition is led by platelet-derived growth factor, increasing this protective smooth muscle cells and the fibrous cap (105) (Figure VI).

One of the main associations between atherosclerosis and vascular symptomatology is the change from the stable to unstable plaque type, but there is a very big handicap to study it and it is the lack of animal models to use and compare with human subjects.

The unstable plaque also known as vulnerable, "high-risk" and "thrombosis prone" is characterized by a thin fibrous cap and a lipid-rich necrotic core (LRNC). This rupture occurs in the 75 % of patients with atherosclerosis, and most of these ruptures happens in the inflammatory shoulder area, where the fibrous cap meets the endothelium (106,107) (Figure VI). In addition, in the plaque areas we can also observe calcification and intraplaque hemorrhage (IPH), but the presence of these last two have been controversial, since it is hard to associate them to symptomatology, however, more recently, the presence of both intraplaque haemorrhage and calcification has also been proposed as risk factors for stroke and carotid heart disease (108).

Sadly, the mechanisms of plaque instability remain unknown, some authors propose VSMCs apoptosis thinning the fibrous cap, as well as neoangiogenesis, this process is promoted by the hypoxia conditions that occur in the plaque. This new vasculature arises from the adventitia *vasa vasorum*, these vessels in the plaque and IPH can promote plaque instability in an indirect way, by increasing inflammation and the LRNC in vulnerable plaques (109). Another new possible explanation of plaque instability is the presence of cholesterol crystals in the plaque, these crystals increase inflammation and stress, and also are proven to weaken the thin fibrous cap in these plaques (110). In this regard, the content of foam cells (pro-inflammatory and pro-oxidative) is important to enrich the LRNC, when these cells die, they release their cellular content to the plaque contributing to the before mentioned enrichment, in vulnerable plaques (111). Other pro-inflammatory immune cells like $CD4^+$ $CD28^{null}$ T cells are increased in unstable plaques, these cells are cytotoxic and produce IFNγ, that can contribute to plaque rupture; in addition, advanced plaques from patients with acute coronary syndrome, show that Tregs (that are mostly considered protective in the context of atherosclerosis) are decreased in the unstable plaques (112,113).

Like plaque instability, the mechanisms of calcium accumulation in the plaques are still unknown. Recently the tissue non-specific alkaline phosphatase (TNAP) has emerged as a possible modulator. The inhibition of TNAP decreased the calcification in human VSMCs and mice atherosclerosis, in the last one it also ameliorated dyslipidaemia and plasma cholesterol levels (114).

To finish, when the plaque ruptures, this exposes vascular or LRNC components to the blood, amongst these components is the tissue factor (TF) from macrophages and VSMCs that activates the coagulation cascade, the complement and the recruitment of platelets in the vascular damaged area, and leads to the formation of blood thrombus and the symptomatology of different CVDs (115,116) (Figure VI). In fact, since 1999, it is known that inhibition of TF reduces thrombosis in vulnerable plaques (117).

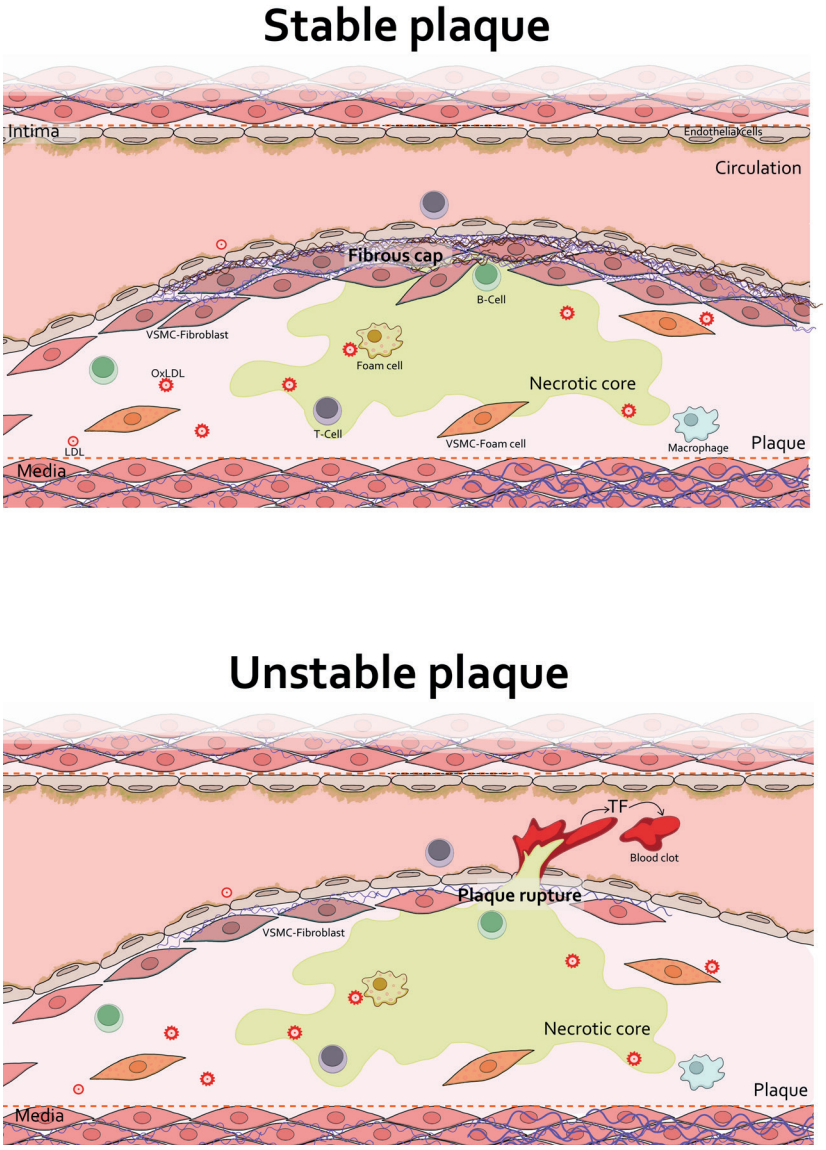

Figure VI. Stable vs. unstable plaque. This illustration shows a stable plaque (upper panel) with a thick fibrous cap made from fibroblast-like VSMCs and ECM; and an unstable plaque (lower panel) with a plaque rupture that exposes the LRNC and the TF to the blood stream creating a blood clot. VSMC= vascular smooth muscle cell; LRNC= lipid-rich necrotic core; TF= tissue factor; LDL= low-density lipoprotein; Ox-LDL= oxidized low-density lipoproteins; VSMCs= vascular smooth muscle cells. © Paula González.

2.1.6 Animal models of atherosclerosis

The need to study the mechanisms underlying atherosclerosis prompted the development of animal models to answer all the ongoing questions about the disease progression. In 1908 Ignatowski described the effects of a high fat diet in atherosclerosis progression in rabbits (118). Rabbits continued to be crucial in atherosclerosis investigation until 1950s, permitting the discovery of the main cell types in atherosclerosis lesions, how dietary cholesterol entered the vessel wall by the LDLs, and how important is inflammation for the disease progression (119).

In recent years, murine models are dominating atherosclerosis investigation, but that does not mean that there is no investigation in other species like zebrafish, hamsters, pigs, nonhuman primates, or chickens. But, although human atherosclerosis occurs since childhood, animals tend to be fairly protected against atherosclerosis development increasing the need to generate protocols

to accelerate the development of the disease, one of the most effective is to feed the animals with "atherogenic" diets, these are high fat diets (HFD) that mimic human diets, one of the most used one is the Western diet (119).

As previously stated, zebrafishes have been used to study atherosclerosis by giving them a HFD, this model is nice to study the fatty streak offset in living organisms, but they do not develop advanced injuries (120). The pig has also been used to study the malady, its cardiovascular system is very similar to humans, which is an advantage, and develop atherosclerosis if given a HFD, but there is a lack of antibodies that detect pig proteins and cell markers, minimizing the investigation to mostly histological measurements, which is a disadvantage (121). Guinea pigs and hamsters have similar lipid handling as humans, but there is no consistency between studies (119). Nonhuman primates develop injuries that are very similar to humans when fed a HFD, but there are a lot of ethical considerations for the use of primates, which limits the use of these species in atherosclerosis investigation (122).

Since 1990, the mouse became the main animal model to study atherosclerosis, the principal genetic background of mouse models of atherosclerosis is the C57BL/6J because can be considered "susceptible" to atherosclerosis progression, but usually this background is combined with genetic engineering to promote atherosclerosis progression (119). *ApoE*$^{-/-}$ mice strain is one of the most used models of atherosclerosis and was first described in 1992. *ApoE* is a ligand for receptors that clean chylomicrons and very low density lipoproteins, by this deficiency, mice are hypercholesterolemic and develop atherosclerosis spontaneously, but the disease can also be accelerated by feeding the mice with a HFD (123). The second most used mouse strain to develop atherosclerosis is the LDL receptor deficient (*Ldlr*$^{-/-}$) model that also has hypercholesterolemia, and develops atherosclerosis, but slower than in the *ApoE*$^{-/-}$ mice, unless a HFD is used, because the lipid profile in *Ldlr*$^{-/-}$ mice is less affected than in the *ApoE*$^{-/-}$ mice (124,125).

Recently, new mouse models of advanced atherosclerosis have been arising. The proprotein convertase subtilisin/kexin type 9 (PCSK9), is expressed in the liver and binds to the LDLr, (PCSK9 inhibitors are a new therapy against CVDs in humans) the injection of adenovirus containing gain of function of human D374Y-PCSK9 fed a Western diet increases hypercholesterolemia and atherosclerosis in the mice (126). The last models are mouse strains with humanized lipoproteins profiles like the human *APOB* transgenic mice, a strain containing the human *APOB* and the *Ldlr*$^{-/-}$ develops severe hypercholesterolemia and atherosclerosis (127). But even if the animal models of atherosclerosis are getting better, there is still a long way to go, by now, human remains the best and more accurate model for human atherosclerosis investigation.

2.2 Signalling pathways in atherosclerosis

2.2.1 Insulin signalling pathway and resistance

The insulin hormone was discovered one hundred years ago, in 1921, and since its discovery a lot of advances have occurred to affirm that this hormone is secreted by pancreatic β-cells in response to increased glucose levels in the blood to be internalized in tissues (128). Nowadays, one of the crucial points of investigation is the interaction between insulin or insulin-like growth factors (IGFs) and their specific receptors, because insulin insulin receptor (IR) interaction regulates glucose utilization in human tissues and the disruption of this utilization leads to the development of insulin resistance and diseases like type-two diabetes (129).

To further understand how insulin signalling impairing affects health and disease, we first must explain the insulin receptor characteristics and the pathway that begins when the hormone binds to the receptor.

The IR is part of a tyrosine kinase receptors subfamily that includes the IR and the IGFs receptors. The structure is of a tetramer made of the combination of two α/β subunits, that come from the same precursor. Both α subunits are extracellular, and therefore, insulin binds to them. Once insulin is fused, the β subunits activate their tyrosine-kinase activity and phosphorylate one-another beginning the intracellular insulin signalling pathway (130). When the IR is active, it phosphorylates the insulin receptor substrates (IRSs), that recruit different mediators and can activate different signalling pathways, but we are going to focus on the protein kinase B (AKT) (Figure VII).

Active-IRSs recruit the phosphoinositide 3-kinase (PI3K), this protein phosphorylates the phosphoinositide-4,5-biphosphate from the cell plasma membrane into phosphoinositide 3,4,5-triphosphate (PIP_3). PIP_3 is a secondary mediator that activates serine/threonine kinases like 3-phosphoinositide-dependent protein kinase-1 (PDK1) that mediates the first phosphorylation of AKT in the threonine 308 (T_{308}) residue to separate this protein from the membrane, only when free the mammalian target of rapamycin complex 2 (mTORC2) is able to phosphorylate the residue serine 473 (S_{473}) to fully activate AKT (20). AKT is a key node in the insulin responsive pathway, because when active, it has more than a hundred substrates, implicated in different biological functions, therefore mediating most if not all the physiological and metabolic functions of insulin, like fatty acid synthesis (SREBP-1 pathway), cell proliferation (mTORC1 pathway), or glucose uptake (increase in glucose transporter type 4 ($GLUT_4$) translocation) (21). That is one of the reasons by which insulin resistance is linked to a decrease of active AKT (Figure VII).

Then we have the IGFs, there are two types the IGF-I and the IGF-II, each bind to the IGF-I receptor (IGF-IR), and the IGF-II can also bind to the IGF-II receptor (IGF-IIR). The most study out of the IGFs is the IGF-I that is mostly produced by the liver and regulates bone and muscle growth, as well as regulate the growth of pancreatic islets (22). And like insulin, IGF-I and IGF-II bind to their IGF-IR in the tissue and is able to activate multiple pathways, having the PI3K/AKT among them (23,24) (Figure VII).

More specifically, IGF-II is crucial during embryonic development and after birth the levels in plasma decrease, however even though in adult mice IGF-II is almost undetectable in humans, this IGF isoform is the most expressed one in adults (24). At first, the binding of IGF-II to its specific receptor, the IGF-IIR (also known as manose-6-phosphate receptor) was considered a regulation union that led to IGF-II clearance through the lysosome in cells, or the inactivation of the protein if bound in the plasma (131). This was because this IGF-IIR is a single transmembrane glycoprotein and no intrinsic activity was given to it after the union of IGF-II, but in 1990, Okamoto T. *et al.* proved that the union between IGF-II and its receptor generated a conformational change in IGF-IIR from lysosomal vesicles and plasma membranes that activates G-proteins (132). In recent years IGF-IIR activity has been tightly related to cardiomyocytes apoptosis (131,133) (Figure VII).

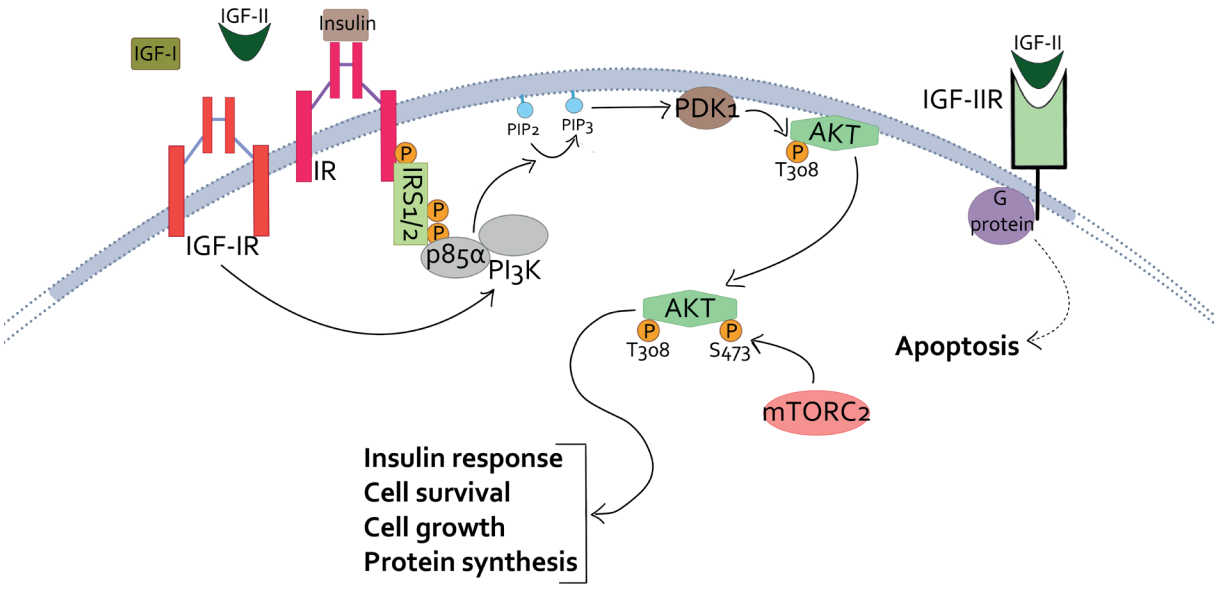

Figure VII. PI3K/AKT and IGF-IIR signalling pathways. This graph represents AKT activation by insulin and IGF-I. First, insulin gets to the insulin receptor (IR) activating its tyrosine-kinase activity and recruiting the insulin receptor substrates activating the recruitment of p85α, this transforms the PIP2 in PIP3, which activates the PDK1 to modulate the first phosphorylation of AKT in T308. This mono phosphorylated AKT cleaves from the cell membrane into the cytoplasm where mTORC2 phosphorylates AKT S473 to fully activate the kinase and promote insulin response, cell survival and growth and protein synthesis. Then the IGF-IR is also able to activate the PI3K to begin this signalling pathway. Lastly, this illustration also shows the IGF-IIR that has a G protein activity and modulates cell apoptosis when active. The dashed line represents an unknown or unconfirmed effect, while the continuous line represents a known or confirmed effect. AKT= protein kinase B; IR= insulin receptor; PI3K= phosphoinositide 3-kinase; p85α = phosphoinositide 3-kinase regulatory subunit p85 alpha; PIP2= phosphoinositide-4,5-biphosphate; PIP3= phosphoinositide-3,4,5-triphosphate; PDK1= 3-phosphoinositide-dependent protein kinase-1; T308= threonine 308; S473= serine 473; mTORC2= mammalian target of rapamycin complex 2; IGF-IR= insulin-like growth factor-I receptor; IGF-IIR= insulin–like growth factor-II receptor. © Paula González.

Insulin resistance is defined as a state of reduced responsiveness of insulin-targeting tissues to physiological levels of insulin (134). There are three tissue types that are crucial for insulin signalling and resistance: liver, that regulates glucose production in the body; white adipose tissues, that modulate lipid synthesis; and the skeletal muscle, the main tissue of insulin-driven glucose consumption (134). Insulin resistance in the skeletal muscle is characterized by a decrease in GLUT4 expression and activity, as well as a decrease in the activation of the IR/PI3K/AKT pathway, in all cases the activation is measured by the phosphorylation of the protein, for example a decrease in the phosphorylation of the S473 from AKT means an inactivation of the pathway and a lack of insulin responsiveness (135). Same thing happens in the liver, where a decrease in the PI3K/AKT pathway activation is related to insulin resistance, an increase in gluconeogenesis and a decrease in glycogen synthesis (136). Also, in the white adipose tissue, insulin resistance is related to a decrease in the PI3K/AKT pathway and a decrease in phospho S473, in fact, in this case, is related to an increase in lipid deposition, and apoptosis of the white adipocytes (137) (Figure VIII).

Obese patients can have a subclinical inflammation in the white adipose tissue that can lead to insulin resistance (not all obese patients develop insulin resistance, even though it is a risk factor), however, to develop whole body insulin resistance, you also need it in the liver and with this, comes the comorbidities like type-2 diabetes, non-alcoholic fatty liver disease (NAFLD) or CVDs (138,139). All of them are part of what is called metabolic syndrome, not only that, but insulin resistance in both diabetic and non-diabetic patients is a well-known risk factor for CVDs, and hyperinsulinemia is also linked to atherosclerosis progression (140). In addition, we know that the IGF-IR protects against apoptosis in VSMCs, and therefore against atherosclerotic progression and plaque rupture (141), and that the PI3K/AKT pathway is increased in macrophages and VSMCs driven the progression of the

disease by increasing cell proliferation (142,143). But how insulin resistance begins in the vascular tissue and is linked to atherosclerosis remains unknown (Figure VIII).

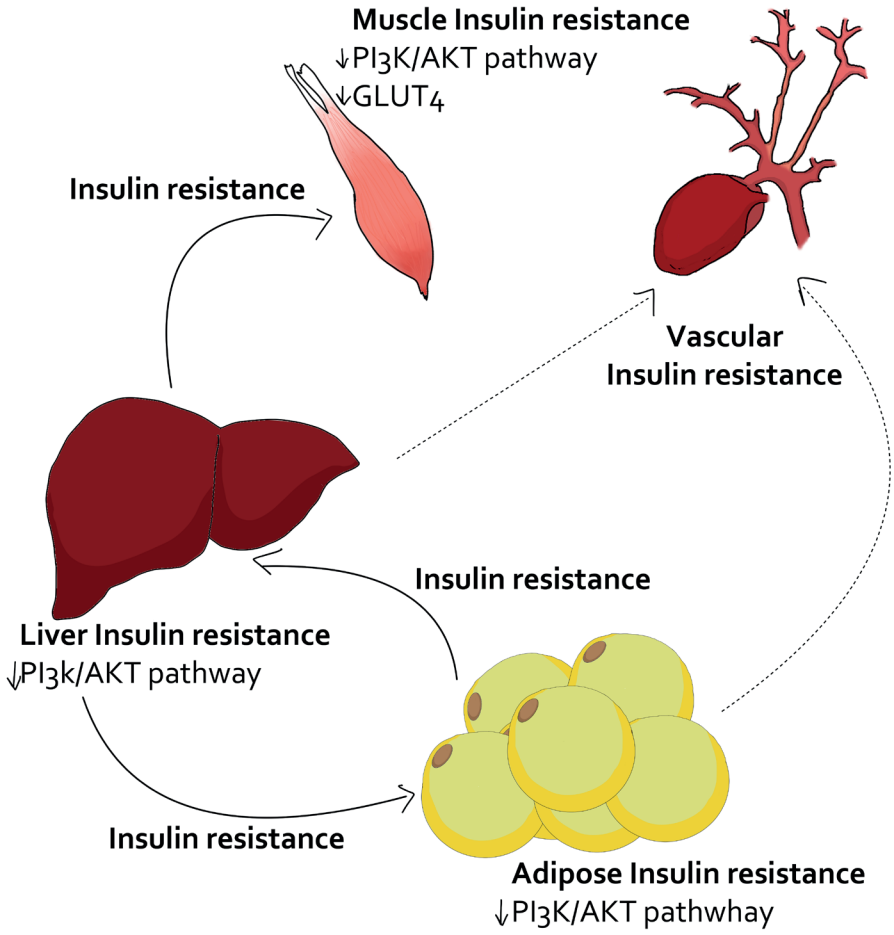

Figure VIII. Systemic insulin resistance communication. Insulin resistance in the adipose tissue can be related to a decrease in the PI3K/AKT pathway and can get to the liver (also decreasing that pathway) to promote whole body insulin resistance, increasing this in the white adipose tissue, or starting this in the muscle where GLUT4 and the PI3K/AKT pathway will decrease. But, as represented by the dashed line, how adipose and liver insulin resistance is leased to the vascular tissue and atherosclerosis remains unknown. PI3K= phosphoinositide 3-kinase; GLUT4= glucose transporter type 4. © Paula González.

2.2.2 Nuclear factor-κB pathway

The nuclear-factor kappa B (NF-κB) is a family of dimeric proteins that modulate inflammatory responses; and cellular proliferation, survival, and differentiation in mostly all multicellular organisms, by integrating specific signals like TNFs or ILs. The family is composed by five monomers: p65/RelA, RelB, cRel, p50 and p52, they share a common amino-terminal REL homology domain, RHD, and form homo or heterodimers to differentially bind the DNA to regulate the transcription of specific sets of genes. The activation of the dimers is at the same time, regulated by two pathways: the canonical and the non-canonical (26,27).

The canonical pathway, also known as NEMO-dependent is fast and transient and mostly led by the p65/RelA-p50 heterodimer of NF-κB. Without any activator, the p65-p50 heterodimer is sequestered in the cytoplasm by the NF-κB inhibitors (IκBs) like IκB alpha (IκBα). To detach the IκBα-NF-κB union, the IκBα needs to be phosphorylated by the IκB kinases (IKKs), which is the main event in the canonical pathway. There are different IKKs but the most important one in this pathway is the subunit IKKbeta (IKKβ, also known as IKK2) that forms a complex with the subunit IKKalpha (IKKα, also known as IKK1

or CHUK) and IKKgamma (IKKγ also known as NF-κB essential modulator, NEMO) (28). But to have a better image of this pathway lets go to the beginning. Different signals can activate specific receptors and the NF-κB response like pattern-recognition receptors; T- and B-cell receptors (TCR and BCR, respectively); and inflammatory cytokines receptors such as TNFs receptors (TNFRs), IL-6R, IL-1βR, etc. (28).

Damaged tissue releases TNFα to activate the TNFR to recruit the TNFR-1 associated death-domain protein (TRADD), that is then going to interact with the E3 ubiquitinase cIAP, and the TNFR-associated factor 2 (TRAF2) and 5 (TRAF5). This cIAP-TRAF2-5 complex is a recruiting signal to the receptor-interacting serine/threonine-protein kinase 1 (RIPK1), for its ubiquitination. The ubiquitinated RIPK1, recruits the TGF-β-activated kinase 1 (TAK1) to also be ubiquitinated. Ubiquitinated TAK1 forms a complex with the TAK1 binding protein 2 (TAB2) and frees itself from the receptor. The TAB2-TAK1 complex promotes the auto-phosphorylation of TAK1 activating the protein. Active TAK1 phosphorylates the IKK complex, once phosphorylated the IKKα/β/γ phosphorylates the IκBα, which is a signalling of ubiquitination that degrades the protein, to free the p65-p50 NF-κB dimer (that is also phosphorylated) and allow its translocation from the cytoplasm to the nucleus to promote the expression of proinflammatory cytokines. The other possible activators like IL-1β, or antigens recognized by the TCR or BCR also activates a signalling pathway that converges in the TAB2-TAK1 complex formation and TAK1 autophosphorylation, to activate the IKKα/β/γ complex and free the NF-κB dimer from IκBα, to promote the expression of a specific set of genes (28) (Figure IX).

The non-canonical pathway also known as NEMO-independent pathway is led by the p52-RelB heterodimer, even though in some cell types p65 may also be involved. In contrast with the canonical pathway, the activation of the non-canonical one is slow and persistent, but like the canonical, one of the main inductors is the TNFs family. One molecule from the family like TNFα gets to the TNFR and recruits the proteins TRAF2-3 and the E3 ubiquitinase cIAP to ubiquitinate TRAF3 to signal the accumulation of the NF-κB inducing kinase (NIK) in the cytoplasm. NIK will then phosphorylate IKKα, the main IKK modulator of this pathway that dimerize with another molecule of IKKα and NIK. This IKKα-NIK complex will phosphorylate the heterodimer formed by p100-RelB, this phosphorylation serves as a ubiquitination signal of the p100 monomer to be processed by the proteasome to conform p52-RelB heterodimer that will translocate to the nucleus to modulate specific sets of genes that at first were thought to only be related to B-cell maturation and lymphoid organ development, but now an aberrant activation of the non-canonical pathway is confirmed to contribute to the pathogenesis of inflammatory diseases (144) (Figure IX).

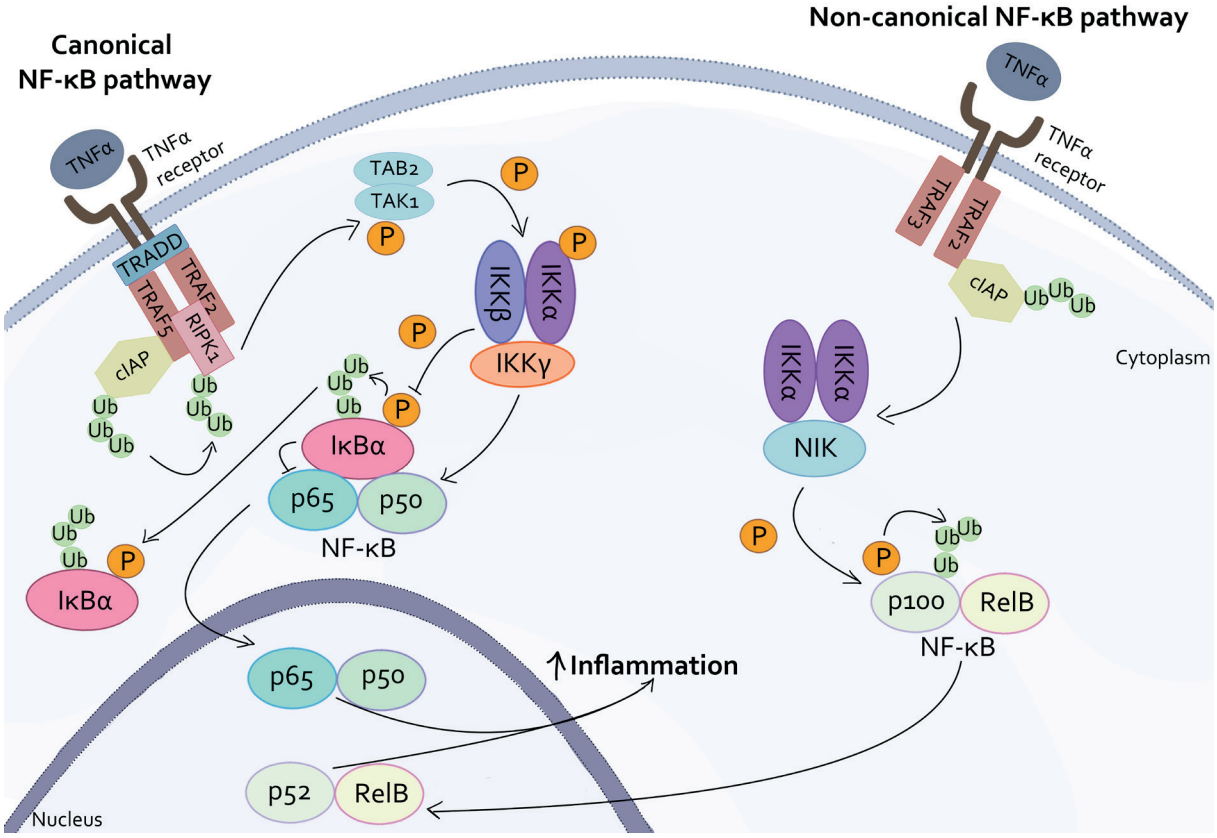

Figure IX. NF-κB canonical and non-canonical pathway. This graph shows the NF-κB canonical pathway, with the TNFα getting to its receptor to recruit the death-domain protein associated to the TNFR1 (TRADD), the factor associated to the TNFα receptor 2 and 5 (TRAF2 and 5) and the E3 ubiquitinase cIAP; this ubiquitinates (Ub) the receptor-interacting serine/threonine-protein kinase 1 (RIPK1) and calls the TGF-β-activated kinase 1 (TAK1) and the TAK1 binding protein 2 (TAB2) to autophosphorylate TAK1 and signal the complexing of the inhibitors of nuclear factor-kappa B (NF-κB) (IκB) kinases (IKKs) alpha (IKKα), beta (IKKβ) and gamma (IKKγ). The IKK complex phosphorylates the IκBα to free the NF-κB dimer from it, to enter the nucleus and increase gene expression. In the non-canonical pathway TNFα gets to its receptor to recruit TRAF2 and 3, and cIAP to increase the NF-κB inducing kinase (NIK) that forms a complex with two monomers of IKKα to phosphorylate the NF-κB dimer conform by p100 and RelB, this ubiquitinates p100 to form p52-RelB dimer that enters the nucleus to increase gene expression. © Paula González.

Taking into account that the NF-κB pathway is one of the main regulators of inflammation in cells and that atherosclerosis is defined as an inflammatory disease, study how dysregulations in the pathway are related to the disease may be interesting. RIPK1 has been proven to be overexpressed in experimental and human early-atherosclerotic injuries and the treatment with RIPK1 anti-sense in mice, macrophages and endothelial cells decreases NF-κB activation, improving atherosclerosis (25). As previously stated, VSMCs are crucial for atherosclerosis development, and NF-κB activation by TNFα has been proven to increase the expression of adhesion molecules like VCAM-1 in these cells, which facilitates the invasion of monocytes and leucocytes to promote the progression of the disease (145). Other studies has shown that under an inflammatory stimuli like lipopolysaccharide, human umbilical vein endothelial cells (HUVECs) increase ICAM-1, VCAM-1, MMP9 and cyclooxygenase-2 (COX-2) via the NF-κB pathway (29). In addition an overexpression in the NF-κB pathway in infiltrating macrophages in atherosclerotic plaques, increase pro-inflammatory genes like *Ccl2* (encoding for MCP-1) or *Il6*, and adhesion molecules like VCAM-1 *in vitro,* and *in vivo* to promote atherosclerotic progression in mice (30,146).

2.3 microRNAs from their synthesis to their effects

2.3.1 Biosynthesis, function, and biology of microRNAs

microRNAs (miRNAs) are small non-coding RNAs for about 19 to 24 nucleotides long, that do not translate into protein, but modulate the expression of them by binding to their messenger RNA (mRNA), serving as a signal for silencing or degradation of the mRNA (31). The first ever discovered miRNA was Lin-4 in *C. elegans* in 1993 where they discovered that a small transcript for the Lin-4 gene had complementary sequences in the 3´untranslated region of the mRNA for Lin-14, regulating the translation of Lin-14 by an antisense-RNA-RNA interaction (147). From that year to nowadays a lot has been discovered about miRNAs biology.

Animal miRNAs are encoded as individual miRNA genes (monocistronic), as miRNA clusters (polycistronic), or in introns of protein-coding genes (intronic) (32). The first step in the biosynthesis of miRNAs happens in the nucleus and consists in the processing of the primary miRNAs (pri-miRNAs) that has a hairpin shape, by the microprocessor complex. This complex is formed by the RNAse III Drosha and the double-stranded RNA (dsRNA)-binding protein, DiGeorge syndrome critical region gene 8 (DGCR8). This pri-miRNA is usually over several kilobases long with a 5´cap and a poly(A) tail (like a usual mRNA) transcribed from the DNA by an RNA polymerase II. Once transcribed the hairpin structure is crucial for the recognition of the pri-miRNA by the microprocessor complex, the average shape of the pri-miRNA consist of a stem with three helical turns with dsRNA segments that are surrounded by two single-stranded RNA (ssRNA) segments at the end (the basal segments on one side and the terminal loop at the other. The part where the ssRNA and dsRNA are conjoined is called SD junction, and is the part that is recognize by DGCR8, in addition with a methylation of the pri-miRNA by the methyltransferase like 3. Once DGCR8 is linked to the SD junction, recruits Drosha that transiently interacts with the pri-miRNA (about 33 bp long) SD junction to catalyse the processing of the hairpin structure into two products: the miRNA precursor (pre-miRNA) that is about 70 nucleotides long with the terminal loop, and a 11bp long part with the basal segments (148,149) (Figure X).

Then the pre-miRNAs are exported to the cytoplasm by the nuclear exportin-5 to be processed by the RNAse III Dicer. Like it happened for the pri-miRNA, the hairpin shape that the pre-miRNA still has, is crucial for the correct recognition and processing of Dicer, this is called the "loop-counting rule" and explains that Dicer recognises the 3´and 5´ends of the pre-miRNA and measures a fixed distance to cleave to the hairpin that is determined by its distance relative to the nearby loop structure. When optimal (2nt), Dicer secures the catalytic centre to achieve precise processing of the pre-miRNA (150) to cut the hood and liberate a 22-24 nucleotides long RNA duplex (32). Later the duplex is recognized by the protein Argonaute in a process that needs from the heat shock proteins 70 and 90, to form the miRNA-induced silencing complex (RISC), one of the strands will be selected by Argonaute while the other will be degraded. RISC is not only conformed by Argonaute and the selected miRNA strand, but also the effector protein trinucleotide repeat containing adaptor 6A (GW182). The GW182 proteins act as molecular scaffolds to bridge Argonaute proteins the specific mRNA which the miRNA is going to bind to (151) (Figure X).

The selection of the duplex by Argonaute is important if the 3´side of the pre-miRNA is selected, we call it 3p strand; and if the 5´side is selected, 5p strand. In most cases there is one strand that is predominantly selected, receiving the name of "miR" or "guide" strand, while the less selected one is called "miR*" or "passenger" strand (151). The selection of one or the other is important since their sequences are complementary, therefore having potentially different targets and effects. This is because the recognition of a specific mRNA target is driven by a region called seed region between the 2-8 first nucleotides from the miRNA sequence (common for all the miRNAs from a specific family) being the best union if all the nucleotides are recognized and losing affinity if some of the nucleotides from the extremes are not complementary (152). In addition, the localization in the mRNA where the

complementary sequence is recognized is also important for the translational-repressor effect that the miRNA is going to have. If the miRNA binds to the mRNA in the coding region (CDS) efficiently represses translation of the protein but the mRNA remains intact, while binding to the 3´untranslated region (3´UTR) efficiently triggers mRNA degradation (153). In contrast to what happens between CDS and 3´UTR, the union of the miRNA in the 5´UTR of the mRNA seems to stabilize both molecules increasing the translation of the mRNA (154) (Figure X).

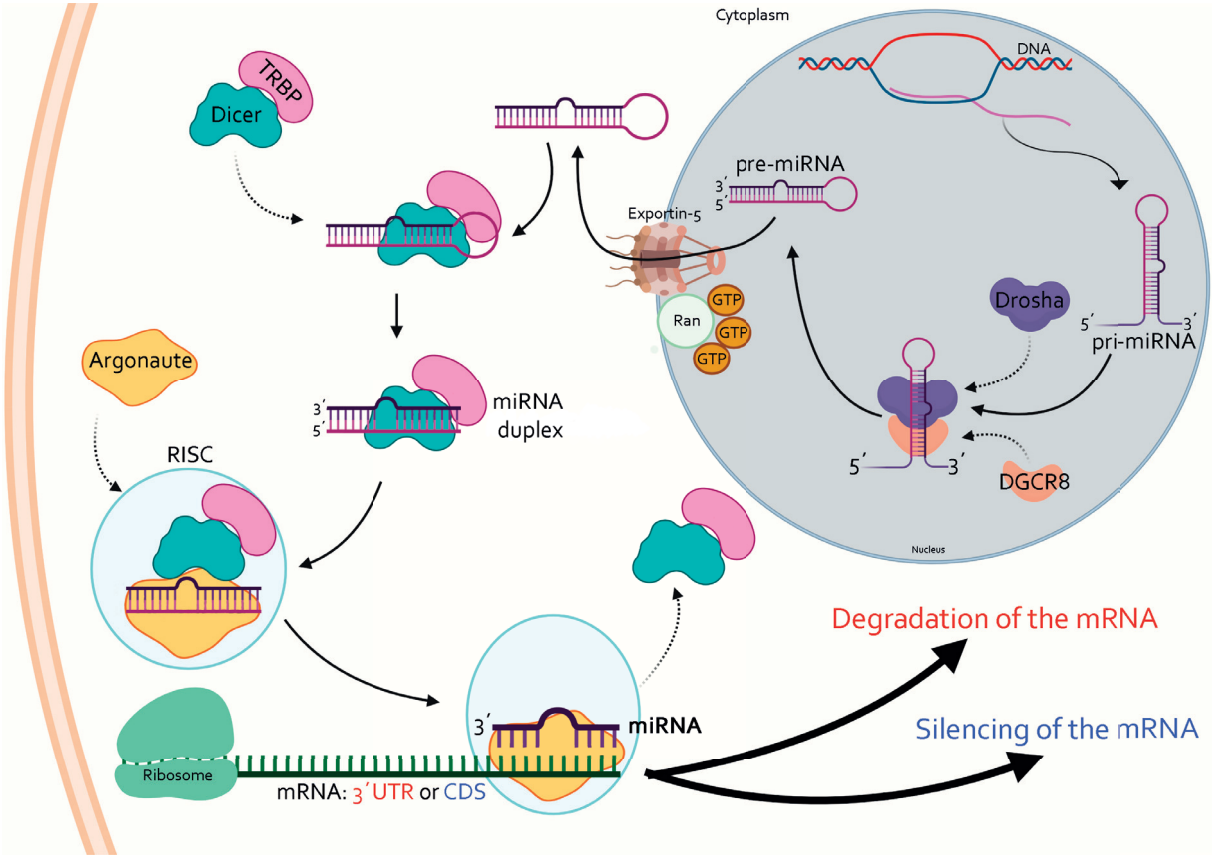

Figure X. Biosynthesis of miRNAs. This image shows the biology and synthesis of miRNAs. It begins in the nucleus as a pri-miRNA that is processed by Drosha and DGCR8 to form the pre-miRNA that travels to the cytoplasm where TRBP and Dicer cut the hairpin structure to give raise to the miRNA duplex. The miRNA duplex is recognized by Argonaute to conform the RISC to select the miRNA strand and guide it to the target mRNA. Once fused with the target mRNA, it will lead to its degradation (red) if the target sequence is in the 3´UTR, or its silencing (blue) if the target sequence is in the CDS of the miRNA. miRNA= microRNA; GTP= guanosine triphosphate; UTR= untranslated region; CDS= coding sequence; DGCR8= DiGeorge syndrome critical region 8; RISC= miRNA induced silencing complex; pri-miRNA= primary miRNA; pre-miRNA= miRNA precursor; mRNA= messenger RNA. Ilustration created with Biorender. © Paula González.

Lastly, miRNAs have been confirmed to be driven in the plasma inside of exosomes, serving as molecular communicators between different cell types both in healthy conditions and in diseases, one of them being atherosclerosis (155). For example, the miR-23a-3p is increased in the extracellular vesicles from atherosclerotic mice and can promote endothelial inflammation and dysfunction by targeting Dusp5 and maintaining the phosphorylation of extracellular signal-regulated kinase 1/2 (ERK1/2) in vitro (156).

2.3.2 microRNAs and atherosclerosis

Since miRNAs are negative regulators of the expression of proteins, their dysregulation has been involved in the development and progression of different diseases. The expression of miRNAs has, in fact, been proven to be altered in metabolic diseases like obesity (157), NAFLD (158) or diabetes (159); as well as other diseases like Alzheimer (35), cancer (34) or CVDs like atherosclerosis.

miRNA dysregulation has been observed in different parts of the atherosclerotic process. miR-217, a miRNA that is linked to aging is also involved in atherosclerosis progression, when miR-217 is increased in the endothelium, promoting endothelial dysfunction by decreasing the vascular endothelial growth factor receptor, an inhibitor of eNOS expression (36). miR-345-3p expression decreases in HUVECs treated with Ox-LDLs, increasing its target TRAF6, the NF-κB pathway, inflammation and apoptosis (160) (Figure XI).

miR-93, miR-145 and miR-128-3p modulate VSMCs switching from a healthy phenotype to a synthetic proliferative and migratory phenotype. miR-93 increases in the VSMCs of rats after a carotid artery injury *in vivo*, increasing their migration and proliferation by targeting mitofusin 2 and the Raf-extracellular signal-regulated kinases 1/2 pathway to increase neointima formation (161). miR-145 is also important for maintaining the contractile phenotype in healthy VSMCs by increasing genes involved in contraction or alpha-smooth muscle actin (α-SMA) while decreasing genes that promote the synthetic phenotype like Krüppel-like factor 4/5. Indeed, during atherosclerosis progression there is a decrease in miR-145 expression (162). miR-128-3p is decreased in the carotids of mice with stenosis, promoting the proliferative and migratory phenotype acting on its direct target Krüppel-like factor 4. In this case, this target modulates the methylation in the DNA of the key VSMCs differentiation marker myosin heavy chain 11 increasing the proliferation of the cells and the media layer from arteries (163). In addition, miRNAs are also able to modulate plaque calcification. miR-125b was decreased in the calcified aortas of *ApoE*$^{-/-}$ mice, in addition in vitro assays with VSMCs confirmed that a decrease in miR-125b increases the osteoblast transcription factor SP7 (direct target) promoting the osteogenic transdifferentiation of VSMCs and the calcification of the atherosclerotic injury (164). miR-200b-3p is upregulated in the plasma of patients with atherosclerosis and in macrophages treated with Ox-LDLs, this miRNA has the cholesterol transporter ATP binding cassette subfamily A member 1 (ABCA1) as a confirmed target, so when increased this miRNA promotes lipid deposition and foam cells formation in macrophages by decreasing the cholesterol efflux, promoting atherosclerosis (165) (Figure XI).

Assessing the dysregulation of miRNAs during different parts of the atherosclerotic pathway and modulating or reversing that dysregulation can, therefore, be a potential clinical target for atherosclerotic diseases.

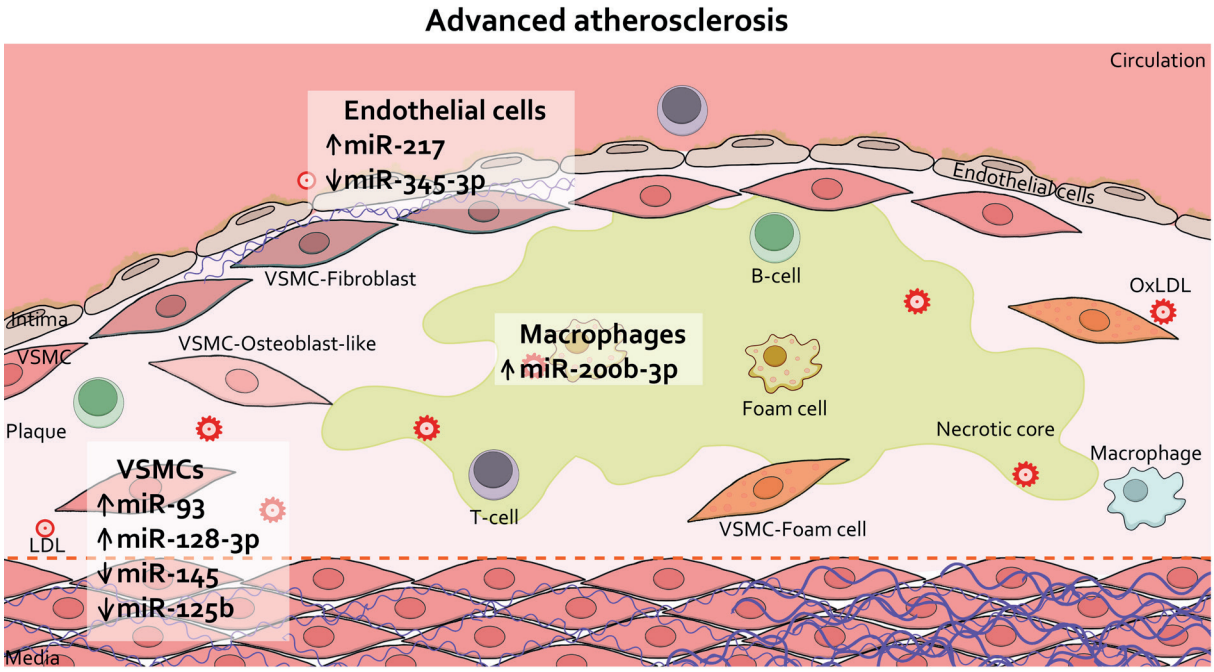

Figure XI. miRNA dysregulation during atherosclerosis. This illustration shows some of the miRNA dysregulations that occur during atherosclerosis progression. In endothelial cells there is an upregulation of miR-217 and a decrease in miR-345-3p. In VSMCs, there is an increase in miR-93 and miR-128-3p; and a decrease in miR-145 and miR-125b modulating the phenotype switch in these cell types. In macrophages Ox-LDL increases miR-200b-3p. VSMCs= vascular smooth muscle cell; LDL= low-density lipoprotein; Ox-LDL= oxidized low-density liporproteins. © Paula González.

“Voy aprendiendo el oficio,
olvidando el porvenir,
me quejo sólo de vicio,
maneras de vivir”

-Maneras de vivir, Leño

3. Aims

3. AIMS

Atherosclerosis is a long-term dynamic disease. The first injuries may appear during childhood and can be asymptomatic until the death of an individual. During this time, different processes occur, one of which is the dysregulation in the expression of different miRNAs. We hypothesized that this dysregulation alters specific targets to promote or protect against the progression of atherosclerosis. Therefore, our **main aim** was to study the dysregulation of different miRNAs during atherosclerosis progression.

To achieve this main aim, we established the following specific aims:

1. Identify potential miRNAs involved in experimental and human atherosclerosis.

2. Study the role of miR-143-3p dysregulation and its target IGF-IIR in the atherosclerotic plaque instability.

3. Analyze the involvement of miR-155-5p and its targets AKT, eNOS, p85α in the progression of atherosclerosis and vascular insulin resistance.

4. Investigate the role of miR-15a-5p and miR-199a-3p and their targets IKK, NF-κB p65, mTOR and LOX-1 in the progression of atherosclerosis, mainly in inflammation and in the formation of foam cells.

5. Confirm if miR-143-3p, miR-155-5p, miR-15a-5p and miR-199a-3p are also altered in the carotids and immune cells from a mouse model of atherosclerosis transgenic for the human *APOB100* gene.

6. Identify if the selected miRNAs can be used as non-invasive biomarkers for advanced atherosclerosis.

“Creo en los fantasmas terribles,
de algún extraño lugar,
y en mis tonterías para,
hacer tu risa estallar.
En un mundo descomunal,
siento tu fragilidad ”

-Lucha de gigantes, Nacha Pop

4. Material and Methods

4. MATERIAL AND METHODS

4.1 Human samples

4.1.1 Characterization of the human cohort

Two cohorts of patients were included in this study. In the first of them, human aortas were consecutively collected from deceased organ donors from 2010 to 2013 under the authorization of the French Biomedicine Agency (PFS 09-007). After macroscopic examination, aortas were classified into two groups according to the Stary classification (166): control aortas (CAs (without atherosclerosis), n=7) and aortas with fibrolipidic initial plaques (FAs (fibroatheromas), n=7). A small portion of the tissue from each sample was fixed in 4% paraformaldehyde for histological and immunochemical assessments. For the CA samples, it was practically and virtually impossible to separate and process the tunica intima independently. For these samples, the adventitia was carefully removed, and only the results obtained from the tunica media are presented. There were no significant differences in terms of age and gender. The study conformed to the principles outlined in the Declaration of Helsinki.

The second cohort included patients with advanced carotid atherosclerosis (ACA). Forty atherosclerotic plaques from patients with a carotid stenosis higher than 70% undergoing carotid endarterectomy at IIS-Fundación Jiménez Díaz (Table 2). The plaques showed an increase in inflammatory cells (Stary stages V–VI), whereas the adjacent areas were mainly composed of VSMCs and lipid deposits (Stary stage III) (166,167). In the same study, plasma was collected from 29 patients to obtain extracellular vesicles and quantify miRNAs (Table 4). The study was approved by the Hospital's Ethics Committee (IIS-Fundación Jiménez Díaz) with reference number PI1442016 according to the institutional and Good Clinical Practice guidelines, which were performed in accordance with the Declaration of Helsinki. All the participants provided written informed consent.

4.1.2 microRNA isolation from paraffin-embedded vascular samples

The miRNA content of paraffin-embedded carotids and aortas was extracted using the RNeasy FFPE kit (Qiagen, Germany). All extractions were performed according to the manufacturer's protocol using 1-2 sections of 20 µm thick per sample. All centrifugations in this protocol were performed at room temperature, unless otherwise specified.

Firstly, 1 or 2 sections of 20 µm each were introduced into a 1.5 mL tube (excess paraffin was removed from the tissues) and 160 µL of deparaffinization solution (Qiagen, Germany) was added. To correctly deparaffinate the samples, we mixed thoroughly for at least 30 seconds using a vortex until the tissue precipitated at the bottom of the tube, followed by a 30 second pulse at maximum speed at the centrifuge to separate the paraffin, which must be in an aqueous phase, from the tissue that will be at the bottom of the tube.

Afterwards, 150 µL of the PKD buffer was added and the tube was incubated for 3 minutes at 56 °C, then vortexed until the phases were homogenous, before centrifugation at 11,000 x g for 1 minute. Next, 10 µL of proteinase K was added, mixed softly by pipetting and the sample was incubated at 56 ºC followed by an 80 ºC incubation both for 15 minutes with regular vortexing.

At least 150 µL of the inferior phase containing the nucleic acids was recovered and incubated on ice for 3 minutes before a 15-minutes, 20,000 x g centrifugation. The supernatant was transferred to another 2 mL tube (the pellet has leftover tissues and DNA, so we need to be careful not to disrupt the pellet). We added 1/10 of the volume of DNase booster buffer and 10 µL of DNase I stock solution, we gave the mix a short spin in the centrifuge and then we incubated the mix for 15 minutes at room

temperature. To adjust the joint conditions in the mix, we added 320 µL of RBC buffer, and then 1,120 µL of 100% ethanol was mixed with the vortex after each step (a precipitate may appear, but this does not affect the extraction).

We added all the volume of each sample to a filter cartridge inside a 2 mL collection tube and to add 700 µL at a time and centrifuged for 15 s at ≥ 8,000 x g until all the volume had passed through the cartridge, discharging the eluted volume after every centrifugation. To wash the cartridge 500 µL of RPE buffer was added followed by a 15-seconds centrifugation at ≥ 8, 000 x g, and this step was repeated. To fully dry the cartridge, we added it to another 2 mL collection tube and centrifuged it at maximum speed for 10 minutes with the lid open. Finally, to elute the miRNAs and tRNA, 25 µL of RNAse free water was added to the cartridges and a 2-minutes centrifugation at maximum speed was carried out, and the elute contained the RNAs, that were storage at -80 ºC until processing them.

4.1.3 Histological techniques

4.1.3.1 Hematoxylin and eosin staining

Paraffin-embedded human carotid arteries and aortas were stained with hematoxylin and eosin (H&E) purchased from PanReac Appli-Chem ITW Reagents. First, the sections were deparaffinized using xylene, followed by hydration by a 3-minute incubation in 100 %, 96 %, 70 % ethanol, and distilled water. Then, the samples were incubated with Mayer´s hematoxylin for 10 minutes; excess staining was removed with successive washings with tap water and one last 5 minutes wash with distilled water before contrasting with a 1 to 5 minutes incubation with alcoholic eosin. Finally, the samples were dehydrated by a 3-minutes incubation in distilled water, 70 %, 96 %, 100 % and three 5 minutes incubations in xylene before being mounted with DPX mounting medium (255,254.1610, PanReac Appli-Chem ITW Reagent, Sigma-Aldrich, USA).

4.1.3.2 Masson´s trichrome staining

Paraffin-embedded human carotids were stained with Masson´s trichrome purchased from Sigma Aldrich and counterstained with Weigert´s ferric hematoxylin following the manufacturer's protocol. The samples were deparaffinized using xylene, followed by a 3-minutes incubation in 100 %, 96 %, 90 %, and 70 % ethanol, and distilled water. The tissue was fixed in 10 % formalin for 2 minutes and washed with distilled water for 3 minutes. The nuclei were stained with Weigert´s ferric hematoxylin for 5 minutes, and excess staining was removed with tap water, followed by a 30 second wash in 1 % acetic acid. Then, the samples were incubated with the first stain: azophloxin for 10 minutes, with another wash in 1 % acetic acid for 30 seconds; then, followed by an incubation with the second stain: orange phosphotungstic acid for 1 minute with another wash in 1 % acetic acid for 30 seconds. Lastly, the samples were incubated with the third stain: green light SF for 2 minutes with another wash in 1% acetic acid for 30 seconds. Finally, the samples were dehydrated and washed three times with xylene before being mounted with DPX mounting medium (255,254.1610, PanReac Appli-Chem ITW Reagent, Sigma-Aldrich, USA).

4.1.3.3 Immunohistochemistry and Immunofluorescence of human vascular tissues

Paraffin-embedded human vascular samples were cut into 5 µm sections, and AKT, IKKα, IKKβ, p65 and LOX-1 were detected using immunoperoxidase with rabbit anti-AKT (#9272, Cell Signaling Technology Inc. ®, USA), anti-IKKα (sc-7606, Santa Cruz Biotechnology, USA), anti-IKKβ (#2678, Cell Signaling Technology, Inc.®, USA), anti p65 (#PA1-186; Invitrogen, USA) and anti-LOX-1 (#PA5-102452, Invitrogen, USA) polyclonal antibodies (Table IV).

The samples were deparaffinized using two 5-minutes incubations in xylene and hydrated by a 3-minutes incubation in 100 %, 96 %, and 70 % ethanol, and distilled water. To inactivate endogenous peroxidase, the samples were incubated for 30 minutes in a H_2O_2 3 %: methanol solution at a 1:1 dilution. To increase antigen retrieval, for the immunohistochemistry, the sections were boiled for a maximum of 40 minutes in 100 mM citrate at pH 6. For the anti-IKKα antibody, an additional 5-minutes incubation with 0.5 % Tween® 20 in distilled water was added. Next, the samples were incubated for 1 hour at room temperature in blocking buffer consisting of 4 % BSA and 6 % serum in phosphate-buffered saline (PBS) 1X, followed by overnight incubation at 4 °C with the specific primary antibody. Primary antibodies were prepared in a 4 % BSA and 1 % normal serum solution in PBS 1X. When we used peroxidase-conjugated secondary antibodies (anti-AKT and anti-p65 antibodies), the slides were incubated with peroxidase substrate DAB (416424, Palex, Spain) for 30 minutes. For the IKKα and LOX-1, an incubation of 30 minutes with Vectastain Elite ABC-HRP Kit (416411, Palex, Spain) at room temperature was carried out after the secondary antibody incubation and before the DAB incubation. The sections were counterstained with hematoxylin, dehydrated, and mounted in DPX mounting medium (255,254.1610, PanReac Appli-Chem ITW Reagent, Sigma-Aldrich, USA). In each experiment, negative controls without primary antibody were included to check for nonspecific staining.

For the immunofluorescence, the slides were dehydrated as previously described and permeabilized with 0.2 % Triton in PBS 1X. Then, the slides were blocked with 4 % BSA and 6 % serum in PBS 1X before incubating with anti-LOX-1 (1:200) and α-SMA (1:1000) (Table IV) primary antibodies at the same time at 4 ºC overnight. The next day, the slides were incubated with Alexa fluor™ 488 anti-Rabbit for anti-LOX-1, since the α-SMA antibody is already conjugated with a secondary antibody. For counterstaining, the samples were incubated with DAPI at a 1:10,000 dilution for 10 minutes before mounting with Fluoromount™ Aqueous Mounting Medium (F4680, Sigma-Aldrich, USA).

4.2 Animal procedures

4.2.1 Description of the Apolipoprotein E knockout (*ApoE*$^{-/-}$) mouse model

For this thesis, we used the *ApoE*$^{-/-}$ mouse model, a well-known atherosclerotic model that develops atherosclerotic lesions similar to those in humans, both spontaneously and after being fed a high-fat diet (HFD) (123). In the present study, male mice of this model were compared with male C57Bl/6 wild-type (WT) mice.

The WT mice were fed a standard diet ([STD] 5.3 % of the kcal was provided by fat, Rod18 H, LASvendi, Germany) for 8 or 18 weeks, whereas the *ApoE*$^{-/-}$ mice were separated into two groups: one was fed the STD and the other a HFD (60.3 % of the kcal was provided by fat, TD. 06414, Envigo, USA) for 8 or 18 weeks before sacrifice.

Table I. Composition of the diets used in this study.

	STD %kcal from	HFD %kcal from
Protein	18.9	18.3
Carbohydrate	75.8	21.4
Fat	5.3	60.3

WT and *ApoE*$^{-/-}$ mice were maintained under standard light (12 h light/dark cycles), temperature (23.3 ºC), and humidity (65.1 %) conditions, and *ad libitum* diet from weaning up to sacrifice (Figure XII).

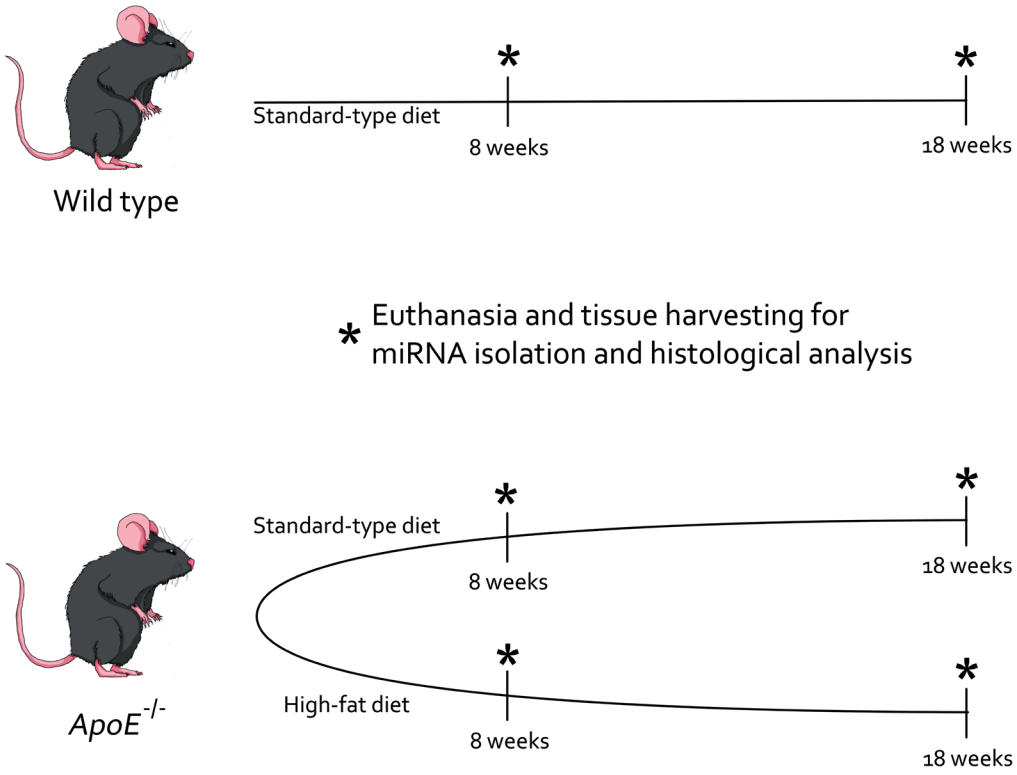

Figure XII. Graphical scheme of the *ApoE*$^{-/-}$ mouse model. This illustration shows the two wild type groups fed a standard type-diet for 8 and 18 weeks before euthanasia (up), and the four groups of the *ApoE*$^{-/-}$ model; two fed a standard type-diet and two a high-fat diet for 8 and 18 weeks. The asterisk represents the time where the mice were euthanized, where the different tissues were harvested for miRNA isolation and histological analysis. *ApoE*$^{-/-}$= apolipoprotein E deficient mice.

4.2.2 Description of the HuBL mouse model

Female B6.129S7-*Ldlr*tm1Her/J (Jax strain 002207) mice on C57BL/6J background and Human *APOB100*-tg *Ldlr*tm1Her (HuBL) mice backcrossed to C57BL/6J for 10 generations were used (168). The latter strain carries the full-length human *APOB100* gene, in which codon 2153 has been converted from Gln to Leu to prevent the formation of *apoB48*, thus generating only *apoB100*.

For this work, the mice were fed a standard chow diet (2018 Teklad Global 18 % Protein Rodent Diet, Envigo, USA) and water *ad libitum*, and maintained in the same light, humidity, and heat conditions previously mentioned (Chapter 4.2.1) from their weaning up to their sacrifice at 11 or 46 weeks. All experiments were performed according to institutional guidelines and were approved by the Stockholm Regional Board for Animal Ethics (Figure XIII).

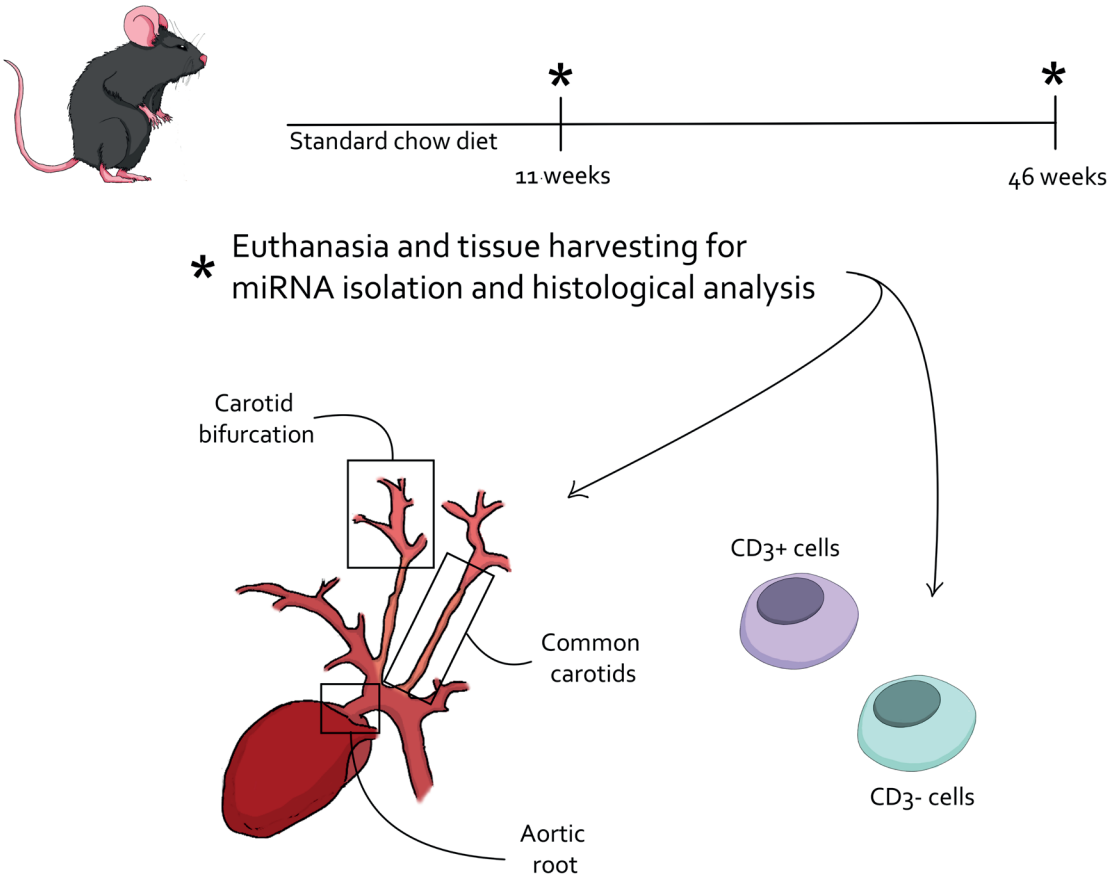

Figure XIII. Graphical scheme of the HuBL mouse model. This illustration shows the two HuBL groups fed a standard chow diet for 11- and 46-weeks before euthanasia. The asterisk represents the time where the mice were euthanized, where the different tissues were harvested for miRNA isolation and histological analysis, in this case, the illustration also shows schemes of the tissues collected like the carotids, the aortic root and the $CD3^+$ and $CD3^-$ splenocytes isolated from the mice spleen. HuBL= low-density lipoprotein receptor knock-out mice transgenic for the human *apolipoprotein B 100* gene.

4.2.3 *In vivo* techniques and experiments

4.2.3.1 Sacrifice of the mice

After 8 or 18 weeks of feeding the corresponding diet, the animals were sacrificed after fasting for 16 h. All animal experiments were conducted in accordance with the accepted standards of animal use approved by the Complutense University of Madrid Ethics Committee, Autonomic Community of Madrid (PROEX188/88) and the guidelines from Directive 2010/63/EU of the European Parliament on the protection of animals used for scientific purposes. The microbiological and health status of the mice were controlled by the Federation of European Laboratory Animal Science Associations (FELASA) criteria and showed no pathogenic infection.

For euthanasia, the mice were anesthetized with Ketamine (Ketalar® [Pfizer, USA]) and Xylazine (Rompun® [Bayer, Germany]) intraperitoneal injection on a 50:5 dose per Kg. The aorta was harvested and stored at -80 °C, while the aortic root was washed with saline, included in the Tissue-Tek® O.C.T. (VWR BDH Chemicals®, USA) and then stored at -80 ºC for further analysis. Blood was extracted from the jugular vein and mixed with 0.4 % p/v Citrate on a 1:10 dilution (Merck, USA), then the plasma was

recovered after a 1200 x g centrifugation of 15 minutes at 4 ºC for subsequent analysis. Before injection, the animals were weighed, and plasma glucose was measured using an Accu-Chek® glucometer (Aviva, Roche, Switzerland).

The HuBL mice were euthanized by a CO_2 overdose inside a chamber, and afterwards blood was collected by cardiac puncture in EDTA-coated tubes and the vasculature was perfused with sterile PBS, and the different tissues were collected. The carotid arteries and the spleen were dissected and put in RNAlater storage reagent (AM720, Thermo Fisher, USA) for later RNA isolation. The heart was dissected and preserved in optimal cutting temperature compound for immunohistochemistry. The proximal part of the aortic root was sectioned using the Thermo Fisher CryoStar NX50 cryostat and stained with hematoxylin and Oil Red O.

4.2.3.2 In vivo insulin signaling studies

To study the vascular insulin signaling in physiological conditions, in vivo insulin signaling assays were performed. 16-hours fasted mice were intraperitoneally (i.p.) injected with 1 U/kg BW of insulin glulisine (Apidra SoloStar, France) or an equivalent volume of 0.9 % p/v saline solution (n= 5 per group). After 10 minutes, mice were sacrificed, and harvested tissues were immediately frozen in liquid nitrogen. Insulin signaling was assessed by Western blot against phospho-AKT (Ser473) (Table IV) in tissue homogenates.

4.2.3.3 CD3+ cell sorting

Single-cell suspensions were prepared from spleens and $CD3^+$ cells were isolated by negative selection with antibodies against CD11b, CD16/32, CD45R, and Ter-119 following the manufacturer's protocol (Dynabeads untouched mouse T cells kit, Invitrogen™, Thermo Fisher Scientific, USA).

4.2.4 Molecular biology techniques

4.2.4.1 miRNA and total RNA isolation from the mice

The miRNA content in the aortas, carotids and $CD3$ cells from the spleen was extracted using the mirVana™ miRNA Isolation Kit (Invitrogen™, Thermo Fisher Scientific, USA). All extractions were performed according to the manufacturer's protocol. All centrifugations were performed at 4 °C and 10,000 x g.

The aorta was crushed in liquid nitrogen until it was powdered for miRNA extraction, while the carotids and cells were directly crushed in the Lysis/Binding buffer with a Qiagen Tissue Lyser. To carry out the protocol, the aortas was weighed around 22 mg; for the carotids and $CD3^+$ cells around 10 mg weight was assessed, and 30 mg for the $CD3^-$ cells. Here we explain the volumes for the aorta (22 mg). First, we added 10 volumes of lysis/binding buffer for each gram of tissue (220 µL); 1/10 volumes of miRNA homogenate additive were added (22 µL) later, followed by a 10-minute incubation on ice. Then, we added the same amount of acid-phenol: chloroform as the lysis/binding buffer (220 µL), the result was centrifuged for 5 minutes, after which there were two phases. For the extraction of miRNAs and total RNA, we recovered the upper phase (approximately 200 µL).

Now we added 1/3 of 100 % ethanol and passed the mixture through a filter cartridge (AM10051G, Thermo Fisher Scientific, USA) and centrifuged for 15 seconds. The cartridge contained total RNA and the eluted portion of miRNAs. To isolate the miRNAs, 2/3 of 100 % ethanol was added to the eluent with the miRNAs and passed through another filter cartridge inside a collection tube, followed by centrifugation at 10, 000 x g for 15 seconds at 4 °C. The miRNAs were then stuck in the cartridge and the eluent was discarded.

To isolate total RNA and miRNAs from the cartridges, the filter must be washed. A first wash consisting of 700 µL of wash solution 1 was carried out followed by a 10 second centrifugation. Another two washings with 500 µL of wash solution 2/3 were performed each, followed by a 10 second centrifugation. Lastly, 100 µL of RNAse-free water was added to each cartridge (for total RNA or miRNA isolation) and passed through a 1.5 mL tube for another 10 seconds of centrifugation. The resulting eluent contained miRNAs or total RNA from each sample and was stored at -80 °C.

The miRNA sample concentration was determined using NanoDropTM 2000 and NanoDrop 2000/2000c Operating Software (Thermo Scientific, USA).

4.2.4.2 Protein extraction from the mouse aorta

The mouse aorta was crushed in liquid nitrogen using a mortar until the tissue became a powder. Then, the powder was added to a 1.5 mL tube with 200 µL of lysis buffer (50 mM HEPES (BP310-500, Fisher, USA) [pH 7.4], 1 % Triton X-100, 50 mM sodium pyrophosphate, 0.1 M sodium fluoride, 10 mM EDTA, 10 mM sodium orthovanadate, 10 µg/mL aprotinin, 10 µg/mL leupeptin, and 2 mM PMSF) and was homogenized by syringing at least 40 times/sample with a 25G 5 mL syringe. The homogenate was centrifuged for 15 minutes at 13.500 x g and 4 °C. After centrifugation, the supernatant containing the proteins was collected for Western blot and stored at -80 ºC.

4.2.5 Histological techniques

4.2.5.1 Oil Red O staining of aortic roots

Aortic root samples were included in Tissue-Tek® optimal cutting temperature (O.C.T.) compound (Sakura Finetek, Japan) and later frozen in liquid nitrogen. The O.C.T. embedded aortic root samples from the experimental model were cut into 5 µm sections using a cryostat (CM1510 S; Leica, Germany). Cut sections were stained with Oil Red O and hematoxylin to assess the lipid depots. The individual lesion areas in the aortic root were determined by averaging the maximal values. Stock Oil Red O (Sigma-Aldrich, USA) solution was prepared with 3 mg/mL Oil Red O in 99 % isopropanol. The stock solution was diluted at a 3:2 ratio in ultrapure water.

Frozen cryosections were air dried at room temperature and then fixed in 10 % formalin for 10 minutes, followed by a quick wash in 60 % isopropanol; afterwards, the samples were stained with the Oil Red O stock (filtered before use) for 30 minutes; another quick wash with 60 % isopropanol was carried out followed by another 5 minutes wash with distilled water, after which excess coloring was removed from the samples, a 5 to 10 minutes counterstained with Carazzi´s hematoxylin (255298.1610, PanReac Appli-Chem ITW Reagent, Sigma-Aldrich, USA); excess hematoxylin was removed with a 5 minutes water wash, and the sections were mounted with aqueous mounting medium for imaging (Vector Labs, Palex, Spain).

Images were acquired using an inverted Eclipse TE300 microscope coupled with a Digital Sight DS-U2 camera (Nikon, Japan). Quantification of Oil Red O staining in aortic roots was performed using IP Win32 v4.5 software (Acromag, USA). Finally, % stenosis, % lesion area/total area, and % lipid deposition/total area was analyzed using the ImageJ software.

4.2.5.2 En Face analysis of the whole aorta

Atherosclerotic lesions were quantified using *en face* analysis of the entire aorta. For en face preparations, the aorta was opened longitudinally while still attached to the heart and major branching arteries in the body. The aorta from the heart to the iliac bifurcation was then removed and pinned on a white wax surface in a dissecting pan using stainless steel pins 0.2 mm in diameter.

After overnight fixation with 4 % paraformaldehyde and rinsing with PBS, the aortas were stained for 6 minutes in a filtered solution containing 0.5 % Oil Red O.35 % ethanol, and 50 % acetone, and then unstained in 80 % ethanol. The Oil Red O-stained aortas were photographed using an inverted Eclipse TE300 microscope coupled to a Digital Sight DS-U2 camera (Nikon, Japan), and the atherosclerotic lesions were quantified using IP Win32 v4.5 software (Acromag, USA).

4.2.5.3 Immunohistochemistry and Immunofluorescence of the aortic root

Frozen cryosections were air dried at room temperature, fixed in pure acetone for 10 minutes, rinsed with PBS 1X for 5 minutes, incubated for 30 minutes with 3 % H_2O_2: methanol in a 1:1 dilution to inactivate the endogen peroxidase, and rinsed with PBS 1X for 5 minutes. Afterwards, the samples were incubated for 1 hour at room temperature in a humid chamber with blocking solution (4 % BSA and 6 % goat serum in PBS 1X) and rinsed with PBS 1X before adding the primary antibody.

The anti-IKKβ (#2684, Cell Signalling Technology®, Table IV) antibody was prepared in 4 % BSA and 1 % goat serum in PBS 1X solution, and the samples were incubated overnight at 4 °C in a humid chamber. The primary antibody was removed after another wash with PBS 1X, and the secondary rabbit peroxidase antibody was prepared in 4 % BSA in PBS 1X solution at 1:200 dilution and incubated for 1 hour. The slides were then rinsed and incubated with the peroxidase substrate DAB (416424, Palex, Spain) for 2 minutes before stopping the reaction with distilled water. Finally, the sections were counterstained with Carazzi's hematoxylin for 2 minutes, rinsed with water, and mounted using an aqueous mounting medium for imaging (Vector Laboratories, Palex, Spain).

The images of sections were acquired, and the staining was quantified in the 100x images, using the IP Win32 v4.5 software (Acromag, USA).

For the single immunofluorescence, the slides were fixed in acetone as previously stated. After fixing, the sections were incubated with Avidin/biotin blocking kit (SP-2001, Vector Labs, USA) for 30 minutes before blocking with 5 % normal horse serum in PBS 1X for another 30 minutes. Then the primary antibody was added at the correct dilution, anti-CD4 or anti-CD8 (1:100) (Table IV) and incubated at 4 ºC overnight. Afterwards, the sections were incubated for 1 hour at room temperature and protected from light with the secondary antibody DyLight/Alexa 594 anti-Rat (1:200, SA5-1008, Invitrogen, USA) and then mounted with Fluorescent Mounting Medium (#S 3023, Dako, Denmark).

For the double immunofluorescence for anti-CD4 and anti-CD3, first we performed the incubation with the primary and secondary antibodies for anti-CD4 as previously described Then, the slides were blocked again with 5 % normal goat serum in PBS 1X, and incubated with the anti-CD3 antibody (AF3628, R&D System, USA), at a 1:300 dilution for 1 hour at room temperature, followed by the corresponding secondary antibody DyLight®/Alexa 488 anti-Rabbit (ab96899, Abcam, USA) for another hour, before incubating with DAPI (1:1,000) for 20 minutes. Finally, the slides were mounted with Fluorescent Mounting Medium (#S 3023, Dako, Denmark).

The pictures for the CD4, CD8 and CD3 immunofluorescences were taken with a Nikon Instruments Fully-Automated A1 Confocal Laser Microscope and the NIS image acquiring Software (Nikon, Japan).

However, for the double immunofluorescence of p65/CD31, p65/α-SMA, and LOX-1/α-SMA (Table IV), the protocol was different. After fixing, the samples were permeabilized with 0.2 % Triton in PBS 1X before blocking with 4 % BSA and 6 % serum in PBS 1X. The primary antibodies were added in pairs as follows: anti-p65 and anti CD31; anti-p65 and anti-α-SMA; and anti-LOX-1 and anti-α-SMA, at the dilutions specified in the Table IV. In the double immunofluorescences of p65 or LOX-1 with α-SMA, the secondary antibodies used were Alexa Fluor 488 anti-Rabbit against anti-p65 and anti-LOX-1. In the double immunofluorescence p65 and CD31, the secondary antibodies used were Alexa Fluor™ 594

anti-Rabbit against anti-p65 and Alexa Fluor™ 488 anti-Goat against anti CD31. The incubation with the secondary antibodies were for 1 hour. Finally, the samples were counterstained with DAPI for 10 minutes before mounting with Fluoromount™ Aqueous Mounting Medium (F4680, Sigma, USA).

4.3 *In vitro* experimentation

4.3.1 Cell culture conditions

4.3.1.1 Human umbilical vein endothelial cells (HUVECs)

HUVECs were purchased from PromoCell (Germany). They were grown in MCDB-131 culture medium (Life Technologies, USA) enriched with L-glutamine 2 mM (Gibco™, Fisher Scientific, USA), foetal bovine serum (FBS) 7.5 % v/v (Gibco™, Fisher Scientific, USA), Penicillin/Streptomycin 100 U/mL (Gibco™, Fisher Scientific, USA) and endothelial growth factor 1X (R&D systems®, USA) and 0.2 % v/v MycoZap™ Plus-CL (VZA-2012, Lonza, Switzerland). Cells were received at passage 2 and grown until passage 8. All the cells were grown at 37°C in a humidified incubator with 5 % CO_2 (Fisher Scientific, USA).

4.3.1.2 Vascular smooth muscle cells (VSMCs)

The generation of immortalized WT VSMCs lines has been previously described (169). Cell lines were cultured to subconfluence (70–80 %) with DMEM/high glucose (DMEM, SH30022.1, Cytiva) medium supplemented with 10 % v/v FBS (Gibco™, Fisher Scientific, USA), 100 U/mL Penicillin/Streptomycin (Gibco™, Fisher Scientific, USA), 2 % v/v HEPES pH 7.4 (BP310-500, Fisher Scientific, USA) and 0.2 % v/v MycoZap™ Plus-CL (Lonza, Switzerland). All cells were grown to 80 % confluence at 37 °C in a humidified incubator with 5 % CO_2 (Fisher Scientific, USA).

4.3.2 Cell culture maintenance

4.3.2.1 Cell passage

For the correct maintenance of the cells, they were grown until 80 % confluence before passage. The cells were washed with PBS 1X before adding 0.25 % trypsin-EDTA (Gibco™, Fisher Scientific, USA) for a quick 2-minutes incubation, and trypsin was inactivated by adding FBS medium, followed by a centrifugation at 1,200 rpm for 5-minutes to remove trypsin. The cell pellet was then resuspended in FBS medium and transferred to a new culture plate at the desired dilution.

4.3.2.2 Cell freezing and thawing

For the correct freezing of the cells, they need to be in a medium with an anti-freezing component to prevent the formation of crystals that can damage the cells, this is the dimethyl sulfoxide (DMSO). In addition, they need to be in a recipient that allows slow freezing of -1 ºC every minute. "Mr. Frosty™", a plastic recipient filled with 2-propanol, permits slow freezing.

To freeze the cells, the culture medium was removed, and the cells were washed with PBS 1X. Then, the cells were lifted with 0.25 % trypsin-EDTA and centrifuged to remove the medium. Afterwards, the pellet containing the cells was resuspended in freezing medium (FBS with 20 % v/v of DMSO) that was collected in cryotubes (10018-754, VWR®, USA) and put in the "Mr. Frosty™", for its freezing in an ultra-freezer. Frozen cells can be stored at -80 °C for months; however, for longer time periods it is better to store them in a liquid nitrogen tank. To thaw the cells, they are tempered in a bath, the freezing medium is removed by centrifugation, and they are passed to the maintenance medium with FBS as fast as possible.

4.3.3 Molecular biology techniques

4.3.3.1 miRNA isolation from cultured cells

The miRNA content of the cells was extracted using the mirVana™ miRNA Isolation Kit (Invitrogen™, Thermo Fisher Scientific, USA). The protocol is explained in more detail in the 4.2.4.1 section. However, there are some specifications for isolation in cell cultures.

After the 72-hours transfection with INTERFERin® or 48 hours with RNAiMAX reagent, the cells were washed with PBS 1X. First, 300 µL of lysis/binding buffer were added to each well and the cells were raised using a plastic scraper (3010, Costar ®, Corning Inc., USA). Then 30 µL of miRNA homogenate additive was added, followed by a 10-minutes incubation on ice. Then 300 µL of acid-phenol: chloroform was added and mixed until it became cloudy, and then centrifuged for 5 minutes, after which there were two phases; if not, this step was repeated. For the extraction of miRNAs and total RNA, we recovered the upper phase (approximately 300 µL) and measured the volume.

4.3.3.2 Transfection with miRNA precursors

The mimics of miR-155-5p, miR-143-3p, miR-15a-5p, and miR-199a-3p were purchased from Sigma-Aldrich. Approximately 5 × 104 HUVECs and 2.5 × 104 VSMCs were seeded in P60 culture plates (353002, Falcon™, Thermo Fisher Scientific, USA) and transfected with 10 nM MISSION® miRNA mimic hsa-miR-143-3p or hsa-miR-15a-5p (HMI0221 or HMI0256, Sigma Aldrich, USA); 20 nM hsa-miR-155-5p (HMI0254, Sigma Aldrich, USA); and 100 nM hsa-miR-199a-3p (HMI0340, Sigma Aldrich, USA).

The miRNA mimics were transfected using 4-6 µL of the siRNA transfection reagent INTERFERin® (#409-10, Polyplus Transfection®, France) following the manufacturer's protocol.

The cells were seeded 24 hours before transfection, and the medium was substituted with 1 mL FBS-medium at the beginning of the experiment. First, the mixtures of miRNA mimic and INTERFERin® were performed in a medium without FBS until a final volume of 100 µL/condition, this mix was incubated for 10-30 minutes and added dropwise to the cells. After 6 hours of incubation at 37 ºC another 1 mL of FBS-medium was added to each condition. miRNA levels in transfected cells were assessed 72 hours after transfection and protein downregulation was analyzed 96 hours after transfection.

For the transfection of 20 nM miR-15a-5p and 100 nM miR-199a-3p into VSMCs, Lipofectamine™ RNAiMAX (13778500, Thermo Fisher, USA) was used following the manufacturer's protocol.

We performed inverse transfection to transfect the mimics with RNAiMAX. For a final volume of 1 × 105 cells in 1mL of FBS-medium, we first prepared a mixture of mimic and Opti MEM™ (Gibco™, Fisher Scientific, USA), and a mixture of RNAiMAX and Opti-MEM™, both to a final volume of 100 µL/condition and allowed to sit for 5 minutes at room temperature. Next, we mixed the mimic and RNAiMAX in Opti-MEM™ at a 1:1 dilution to obtain 200 µL of mix/condition, and the mixture was incubated for at least 20 minutes to allow RNAiMAX to introduce the mimics and form small vesicles. During this 20-minutes incubation, the cells were lifted with trypsin and counted to make a dilution of 1 × 105 cells/mL of medium. Once the incubation was finished, the mix of mimic, RNAiMAX, was added drop by drop to the P60, followed by the 1 mL of suspended cells at the right concentration. miRNA expression and protein downregulation were analyzed 48 hours after transfection.

After transfection, cells were stimulated with different molecules to assess the biological effects of miRNA overexpression.

4.3.3.2.1 Insulin stimulation of the cells

After the 96-hour transfection with INTERFERin®, the cells were deprived with DMEM without FBS for 6 hours and in the last 10 minutes 100 nM insulin was added in the presence or absence of mimic-miR-155-5p overexpression. Next, the proteins were isolated, and insulin resistance was assessed by measuring AKT phosphorylation levels of the serine 473 (S473) residue (Table IV).

4.3.3.2.2 Thapsigargin stimulation of the cells

To study the effect of miR-143-3p on apoptosis, HUVECs were transfected for 96 hours with the miRNA mimic. The transfection medium was replaced with MCDB-131 medium without FBS to deprive the HUVECs for 6 hours with or without the miRNA mimic. For the VSMCs, there was a 2-hour deprivation in FBS-free DMEM medium followed by a 2-hour treatment with thapsigargin (100 nM, Santa Cruz Biotechnology, USA). The proteins were then isolated and used to study apoptosis by measuring the amount of cleaved caspase-3 using β-actin as loading control.

4.3.3.2.3 Tumor necrosis factor alpha (TNFα) stimulation of the cells

To assess the effect of miR-15a-5p and miR-199a-3p on the NF-κB pathway, HUVECs and VSMCs were transfected with mimic-miR-15a-5p and/or mimic-miR-199a-3p. They were deprived of FBS for 1 hour and were transfected with the mimics for 96 hours (HUVECs) or 48 hours (VSMCs) and then stimulated with 10 ng/mL TNFα (Sigma-Aldrich, USA) for 10 minutes. The proteins were isolated, and we analyzed the phosphorylation of IKKα/β and the levels of IκBα as well as p65 levels and its phosphorylation by Western blot.

4.3.3.2.4 Oxidized low density lipoprotein (Ox-LDL) stimulation of the cells

To estimate whether miR-15a-5p and miR-199a-3p may be affecting LDL uptake in VSMCs. 3.5 x 103 cells were seeded in 96-well culture plates (FB012931, Fisherbrand™, Fisher, USA) for a 48-hours transfection with the mimics. For the last 24 hours, VSMCs were treated with 100 µg/mL Ox-LDLs from human plasma (L34357, Thermo Fisher Scientific, USA) in the presence or absence of the mimics. The lipid content of the cells after 24-hour incubation was analyzed by quantifying Oil Red O staining.

4.3.4 Protein isolation from cultured cells

Once the in vitro experiments were completed, cells were washed with PBS 1X. First, 60 µL Lysis buffer (50 mM Tris, 150 mM NaCl, 1 % v/v Triton X-100, 10 mM sodium orthovanadate, 10 µg/ml aprotinin, 10 µg/ml leupeptin, and 2 mM PMSF, pH 8) was added to each well, and the cells were raised using a plastic scraper. After recovering the lysis buffer with the cells in a 1.5 mL tube, the cells were vortexed at least 10 times for 10 seconds each, followed by centrifugation to concentrate the cells and membranes in a pellet. The pellet was then sonicated for 4 pulses of 60 amplitude and 0.5 Â s each with a sonicator (VC 100 Sonics & Materials Inc, USA). To allow all the membranes to break and release proteins in the buffer, the cells were incubated on ice for a minimum of 30 minutes before centrifugation at 13,500 x g for 15-minutes at 4 °C. After centrifugation, the proteins were in the supernatant, and the leftover membranes were in the pellet. Finally, the supernatant was used to quantify protein concentration using the Bradford method.

4.3.5 Nuclear fractionation and extraction of proteins

HUVECs were maintained in MCDB-131 medium without FBS for 1 hour, then stimulated with TNFα (10 ng/mL) for 10 minutes. The cells were then scraped and homogenized in buffer A (10 mM HEPES (pH 7.8), 15 mM KCl, 2 mM $MgCl_2$, 0.1 mM EDTA, 1 mM dithiothreitol (DTT), and 1 mM phenylmethylsulphonyl fluoride) and syringed with an insulin syringe at least 40 times to mechanically break the cellular membrane. After 10 minutes on ice, the cell homogenates were pelleted and resuspended in two volumes of buffer. Subsequently, 3 M KCl was added dropwise to reach a 0.39 M KCl concentration. Nuclei were extracted from the cells after incubation for 1 hour at 4 °C followed by centrifugation at 12,000 x g for another 1 hour. The supernatants were then dialyzed in buffer C (50 mM HEPES (pH 7.8), 50 mM KCl, 0.1 mM EDTA, 1 mM DTT, and 1 mM phenylmethylsulphonyl fluoride with 10 % (v/v) glycerol). The samples were then cleared by centrifugation and sonicated using a VC 100 sonicator (Sonics & Materials Inc., USA) to break the nuclear membrane. Protein concentration in the cytoplasm and nuclei was measured. Then, we analyzed the levels and phosphorylation of IκBα, IKKα and IKKβ in cytosolic fractions by Western blot as described above. We measured p65 in the nuclear and cytosol fractions by Western blot. We used β-actin and histone H_3 as control for total protein in cytosolic and nuclear fractions, respectively.

4.3.6 Immunofluorescence of p65

The coverslips were pretreated with 0.2 % gelatin for 30 minutes at room temperature and rinsed twice with PBS 1X in a 24-well culture plate, after which 15 × 103 HUVECs were seeded for transfection. After the 96 hours-transfection with mimic-miR-15a-5p and/or mimic-miR-199a-3p followed by 1 hour of deprivation and stimulation with 10 ng/mL TNFα, the cells were rinsed twice with PBS 1X and fixed with 4 % paraformaldehyde (252931.1214, PanReac AppliChem, ITW Reagents, USA) for 20 minutes, rinsed twice with PBS 1X again and permeabilized with Triton X-100 0.5 % and SDS 0.1 % for 5 minutes each. Next, the cells were blocked with PBS 1X-4 % BSA (A6588,0100, PanReac AppliChem, ITW Reagents, USA) and 1.5 % normal goat serum (1000C, Invitrogen, USA) for 30 minutes at room temperature, and then the p65-NF-κB primary antibody was diluted at 1:200 in the blocking buffer and incubated at 4 °C overnight.

After the primary antibody incubation, the cells were rinsed three times with PBS 1X, and were then incubated with the secondary antibody 555 goat anti-rabbit (A32732, Invitrogen, USA) diluted at 1:500 and DAPI (A4099, Sigma Aldrich, Germany) at 1:1,000 in the blocking buffer, for 1 hour at room temperature. Finally, the cells were rinsed twice with PBS 1X and once with distilled water, and the coverslips were mounted with ProLong™ Gold Antifade Reagent Mounting Medium (P36930, Invitrogen, USA) and inverted onto glass slides. The colocalization of p65/DAPI and DAPI/p65 was calculated using the JaCoP plugin from the Image J-win64 Software to calculate M1, M2, and Pearson's coefficients.

4.3.7 Oil Red O staining from cultured cells

After 100 µg/mL Ox-LDL treatment for the last 24 hours of the 48-hours transfection with the miR-15a-5p and miR-199a-3p mimics, the cells were carefully washed twice with PBS 1X and placed on ice. To fix the cells, they were incubated for 20 minutes in 10 % formalin (5701; Fisher Scientific, USA). Formalin was washed three times with PBS 1X, and the rest of the protocol was performed at room temperature. The cells were quickly washed with 65 % isopropanol before the 15-minutes incubation with the Oil Red O stock solution and washed again with 65 % isopropanol. Finally, the cells were washed with distilled water to remove excess coloring before taking pictures of the 96-well to the microscope.

To prepare the Oil Red O stock solution, we weighted 0.5 g of Oil Red O in 100 mL of 99 % isopropanol and then we added 40 mL of water. We let it be for 10-15 minutes before filtering the stock, after which it was stable for 1-2 hours.

4.3.8 Dual Luciferase assay to confirm possible targets from miR-15a-5p and miR-199a-3p

For reporter assays, a region of wild-type 3'-untranslated region (3'UTR) from IKBKB (miR-15a-5p), the 3UTR from mutated IKBKB (miR-15a-5p), the wild-type 3'UTR from IKBKB (miR-199a-3p), the 3'UTR from mutated IKBKB (miR-199a-3p), the wild-type 3'UTR from CHUK (miR-15a-5p), the 3'UTR from mutated CHUK (miR-15a-5p), the wild-type 3'UTR from RELA (miR-199a-3p) and the 3'UTR from mutated RELA (miR-199a-3p) were constructed annealing the following primers:

3'UTR-IKBKB (miR-15a-5p) F: 5'-TCGAGACTGACCTCTTTTTATTTCACTGCTG CTATATTAAAAGGAGTATGC-3' and 3'UTR-IKBKB (miR-15a-5p) R: 5'-GGCCGCA TACTCCTTTTAATATAGCAGCAGTGAAATAA AAAGAGGTCAGTC-3'; 3'UTR-IKBKB (miR-15a-5p) mutated. F: 5'-TCGAGACTGACCTCTTTTTATTTCACCCCTTTGCTATTAAA AGGAGTATGC -3' and 3'UTR- IKBKB (miR-15a-5p) mutated. R: 5'-GGCCGC ATACTCCTTTTAATAGCAAAGGGGTGAAATAAAAAGAGGTCAGTC-3'

3'UTR-IKBKB (miR-199a-3p) F: 5'-TCGAGACTGACCGCCTTGTCTGCACACTGGAGG TCCTCCATTTAT TAAAAGGAGTATGC-3' and 3'UTR-IKBKB (miR-199a-3p) R: 5'-GGCCGCATACTCCTTTTAATAAATGGAGGACCTCCAGTGTGCAGACAAGGCGGTCAGTC-3'; and 3'UTR-IKBKB (miR-199a-3p) mutated F: 5'-TCGAGACTGACCGGC GCCTTGTCTGCGAGGACCATATTAAAAGGAGTATGC-3' and 3'UTR-IKBKB (miR-199a-3p) mutated R: 5'-GGCCGCATACTCCTTTTAATATGGTCCTCGCAGACAAGGCGCC GGTCAGTC-3'.

3'UTR-CHUK (miR-15a-5p) F: 5'-TCGAGACTGACGAATATTCCTTTATTTTGCTGCT TATTAAAAGGAGTATGC-3' and 3'UTR-CHUK (miR-15a-5p) R: 5'-GGCCGCATA CTCCTTTTAATAAGCAGCAAAATAAAGGAATATTCGTCAGTC-3'; and 3'UTR-CHUK (miR-15a-5p) mutated F: 5'-TCGAGACTGACGAATATTCCTTTATTTCTGTAAGTAT TAAAAGGAGTATGC-3' and 3'UTR-CHUK (miR-15a-5p) mutated R: 5'-GGCCGCATACT CCTTTTAATACTTACAGAAATAAAGGAATATTCGTCAGTC-3'.

CDS-RELA (miR-199a-3p) F: 5'-TCGAGACTGACAGGTGACAGTGCGGGACC CATCAGTATTAAAAGGAGTATGC-3' and 3'UTR-RELA (miR-199a-3p) R: 5'-GGCCGCATACTCCTTTTAATACTGATGGGTCCCGC ACTGTCACCTGTCAGTC-3'; and 3'UTR-RELA (miR-199a-3p) mutated F: 5'-TCGAGACTGACAGGTGACAGTGCGG GACCAGGCCATATTAAAAGGAGTATGC -3' and 3'UTR-RELA (miR-199a-3p) mutated R: 5'-GGCCGCATACTCCTTTTAATATGGCCTGGTCCCGCACTGTCACCTGTCAGTC-3'.

Annealing was conducted by incubating both oligos for 4 minutes at 95 °C and for 10 minutes at 70 °C in annealing buffer (100 mM potassium acetate, 30 mM HEPES, pH 7.4, and 2-mM magnesium acetate). Oligos were then phosphorylated and cloned into the psiCHECK2 vector from Promega digested with XhoI and NotI.

Thirty thousand HEK293 cells were plated in DMEM containing 10 % FBS. Twenty-four hours later, cells were transfected with the psiCHECK2 vectors either with mimic-miR control, mimic-miR-15a-5p or mimic-miR-199a-5p using Lipofectamine™ RNAiMAX (13778500, Thermo Fisher, USA) following the manufacturer's instructions. The luciferase reporter assay was performed 72 hours after transfection using the Dual-Glo luciferase kit (Promega, Madison, WI, USA).

4.4 Exosome precipitation and analysis

4.4.1 Exosome precipitation from plasma

To precipitate the exosomes from the plasma samples, the mirVana™ total exosome RNA and protein isolation kit (from plasma) (4478545, Thermo Fisher Scientific, Waltham, MA, USA) was used following the manufacturer's protocol.

First, the plasma was clarified with one centrifugation at 2,000 x g for 20 minutes and a second centrifugation at 10,000 x g for the same amount of time; in both cases, the supernatant was collected, and the pellet was discharged. When the plasma was ready, 0.5 volumes of PBS 1X and 0.2 volumes of the Exosome Precipitation Reagent (from plasma) (4484451, Thermo Fisher Scientific, USA) were added until the sample became cloudy, and the mixture was incubated for 30 minutes on ice, followed by centrifugation at 10,000 x g for 30 minutes at room temperature. 50 µL of PBS 1X was added to the pellet and incubated overnight at 4 °C to soften it before resuspension. The pellet containing the extracellular vesicles was used to extract miRNAs. To confirm that the pellet was enriched with exosomes, diffuse light scattering analysis and Western blot were performed.

4.4.2 Molecular biology techniques

4.4.2.1 miRNA isolation from exosomes

The miRNA content of the exosomes was extracted using the mirVana™ Total exosome RNA and Protein Isolation Kit (from plasma) (Invitrogen™, Thermo Fisher Scientific, USA). The protocol is very similar to mirVana™, as explained in more detail in 4.2.4.1 section. However, there are some specifications for their isolation from exosomes.

We began by adding PBS 1X until a final volume of 200 µL, since we had the exosomes in 50 µL of PBS 1X, we added 150 µL. Then we added a volume of 2 X denaturing solution (200 µL) and allowed it to sit for 5 minutes on ice. After incubation, another volume of acid-phenol-chloroform was added (400 µL). Up until this point, the protocol is the same as mirVana™ previously explained in section 4.2.4.1.

4.4.2.2 Protein isolation

After extraction of the exosomes, the pellet containing the extracellular vesicles was resuspended in 50 µL of PBS 1X. This suspension can be directly used for the analysis of superficial and internal proteins.

4.4.2.3 Dynamic light scattering (DLS)

The resuspension of exosomes in 50 µL of PBS 1X, used for protein isolation, was also used for DLS to study the size of the exosomal particles in the pellet. Five measurements of each sample were performed using the DLS system Malvern Z sizer NS.

4.5 Molecular biology techniques commonly used in all samples

4.5.1 Reverse transcription (RT) and quantitative polymerase chain reaction (qPCR)

Complementary DNA (cDNA) for mRNA analysis was synthesized using the high-capacity cDNA reverse transcription kit for mRNAs; and using the TaqMan® advanced miRNA cDNA synthesis kit for miRNAs. Quantitative polymerase chain reaction (qPCR) was performed using cDNA as the template and TaqMan® Fast Advanced Master Mix (Thermo Scientific, USA). Genes were detected using TaqMan® probes (Thermo Scientific, USA) for miRNAs and mRNAs (Table III). All probes for the miRNAs detected both the mouse and human target genes. The RT-qPCR experiments were performed using an ABI Prism 7900HT Thermal Cycler and the QuantStudio™ 7 Pro Real-Time PCR System (Applied Biosystems, USA). The following protocol was used: enzyme activation at 95 °C for 20 seconds, followed by 40 cycles at 95 °C for 1 second to denature and 20 seconds 60 °C to anneal/extend.

The relative abundance of miRNA and mRNA targets, normalized with the endogenous gene and relative to the control, was calculated as follow: Relative Quantification (RQ) = $2^{-\Delta\Delta Ct}$; ΔCt (cycle threshold) = Ct (miRNA target) – Ct (endogenous gene); ΔΔCt = [ΔCt (for any sample) – ΔCt (for the control)]. Amplification of miR-191-5p (tissues and cells) or miR 16 5p (exosomes) was used as an internal control for all samples.

4.5.2 Bradford assays for the quantification of protein concentration

Aorta, cell, and exosome protein lysates were quantified using the Bradford protein assay, a colorimetric method. The assay was performed in 96-well plates. First, a calibration curve from 1 to 5 µg/µL of Quick Start Bovine Serum Albumin (BSA) standard (#5000206, Bio-Rad, USA) was performed, and then 1 µL of the sample lysate was added in triplicate. The calibration curve and lysates were added to distilled water until a final volume of 50 µL. Bradford stain (#5000006, Bio-Rad, USA) was prepared on a 1/5 dilution as specified by the manufacturer and then 200 µL was added to each well containing BSA or lysate. The plaque was incubated away from light for 5-minutes and then read at 595 nm using a BioTek® PowerWave XS (Agilent Technologies, USA) reader and the Agilent BioTek Gene5 software v3.12 (Agilent Technologies, USA).

4.5.3 Western blot analysis

Proteins from cell lysates (20–40 µg) and tissue samples (60 µg) were prepared in 4 X sample buffer (2 % SDS; 1M tris pH 6,8; 10 % glycerol, and 4 % β-mercaptoethanol in distilled water) and boiled in a thermoblock at 95 °C for 5 minutes prior to electrophoresis.

For electrophoresis, proteins were separated on a 10 % or 10–20 % gradient acrylamide gel with a 4 % acrylamide concentration fraction. Before loading the samples, the gels were placed in the tetracell and the space between them was filled with running buffer 1X (Tris 250 mM, Glycine 2.5 M, 1 % w/v SDS for running buffer 10 X) for electrophoresis. Then, the different wells were washed using a syringe and running buffer 1X and then the samples were loaded. First, the running speed was set to a fixed 100 volts with a variable amperage and watts until the samples reached the separating gel, at which point the voltage was raised to 120 volts until the end.

After electrophoresis, the proteins inside the gels were transferred to a 0.45 µM pore PVDF membrane (Merck, Germany) for 1 hour and 30 minutes or 2 hours at 110V, on ice in transfer buffer (124 mM Tris and 1 M Glycine in 20% metanol). The PVDF membranes were blocked by agitation at a low speed with a blocking buffer consisting of 5 % w/v milk (00017658, Dismadel S.L., Spain) and 3 % w/v BSA

fraction (pH=7.0) for Western blot (A6588,0100, PanReac, AppliChem, ITW reagents, USA) in Tween®20-Tris-buffered saline (TTBS, Tris 100 mM, NaCl 1.5 M and 0.2 % v/v of 10 % v/v Tween®20 (142312.1611, PanReac, AppliChem, ITW reagents, USA)) for 1 hour at room temperature. The remaining blocking buffer was washed thrice with three 10-minutes fast speed washes with TTBS before adding the primary antibodies.

The primary antibodies used are shown in Table IV, and all of them were diluted in TTBS, incubated overnight with agitation at 4 °C, and washed by three 10-minutes fast speed washes with TTBS before incubation with secondary antibodies (Table IV). Rabbit and mouse primary antibodies were detected using horseradish peroxidase-conjugated anti-rabbit IgG (NA931V; 1:4000 in TTBS) and anti-mouse IgG secondary antibodies (NA934V; 1:5000 in TTBS) (GE Healthcare, UK), respectively. Secondary antibodies were prepared in TTBS with 1 % w/v BSA (rabbit) or 1 % w/v milk (mouse) and incubated for 1 hour at room temperature with low-speed agitation.

To visualize the bands, the membranes were incubated in the dark using SuperSignal™ West Pico PLUS Chemiluminescent Substrate (34580, Thermo Fisher Scientific®, USA) and VWR® Life Science imager gel and documentation analysis system v.4.3.9. and VWR® imager software v.1.8.2. (VWRTM, Avantor, USA). The loading was normalized with β-actin.

When it was possible, phospho-proteins and their total expression were detected in the same gel using a Stripping Buffer (1 M Tris 6.8 pH, 10 % w/v SDS up to 100 mL of distilled H_2O, for every 25 mL of this buffer, 174 µL of β-mercaptoethanol was added) for 20 minutes, blocking the membrane again before incubation with the next antibody.

4.6 Bioinformatical analysis

4.6.1 *In silico* search for miRNA and targets

The miRNAs analyzed in the study were identified by an exhaustive search for key words (miRNAs, atherosclerosis, and inflammation, NF-κB) in different publications in PubMed and the GEO database from NCBI. Once the miRNAs of interest were selected, the interaction between them and their mRNA targets was evaluated using miRNA-Target Interaction databases such as TargetScan, miRWalk, miRDB, and miRTarBase (at their latest online versions). The data collected from these databases were analyzed, and only those targets that appeared in two or more databases were considered possible targets. Hybridization experiments were performed using the multiple alignment tool in ClustalW v2. 0.12 (Desmond D. Higgins, EMBL, Ireland) to identify the possible area of interaction between the miRNA and mRNA if it did not appear in the previously mentioned databases.

4.6.2 Statistical analysis

4.6.2.1 Quantification of Western blot images

Band densitometry of the Western blot images was performed using ImageJ Software (v1.52a, National Institute of Health, USA). First, the image type was changed from RGB to 8-byte. Then, the rectangle tool was used to select the first band with the selected first lane tool (or Ctrl+1), and the rest of the bands were selected individually with the selected tool (or Ctrl+2). The measurement tool was used to measure the area of each band (or Ctrl+3). The values were then copied and pasted on an Excel spreadsheet to calculate the mean, standard deviation, and standard error of each group.

4.6.2.2 Quantification of Oil Red O stains and immunohistochemistry

The immunohistochemistry and Oil Red O staining images were quantified using the "count and measure objects" tool in the Image-Pro Plus software IPWin (v4.5, Media Cybernetics, USA) (IPWin v4.5 software). The color considered positive staining for the same protein was manually selected, and the value corresponding to the sum of all stained areas was obtained. The results are expressed as the percentage of stained area with respect to the total area analyzed in each sample.

ImageJ software was also used to quantify the Oil Red O staining images of the VSMCs. All images were open as a stack and converted to an 8-gray scale. Then, a common threshold was set for all images using the adjusted threshold tool. To analyze the positive staining, the measurements were set to area, integrated density, and adjusted threshold. Finally, the measurement tool in the analysis menu was used to quantify positive staining in all images at the same time.

4.6.2.3 Quantification of the immunofluorescence of p65

To quantify the corrected total cell fluorescence (CTCF) intensity of p65 in the different images, the ImageJ Software (v1.52a, National Institute of Health, USA) was used. First, the measurements need to be set to area, integrated density, minimum and maximum gray values, and mean gray value.

Now we select the cell of interest using the free form selection tool and measure; to calculate the CTCF we need to measure the background, so from each cell (minimum of three maxima of five cells from each image) we did 3 background measurements with the circle tool. Once the measurement was completed, all the data were copied and pasted to another Excel sheet. The corrected total cell fluorescence was calculated using the following formula:

$$CTCF = Integrated\ density - (Area\ of\ selected\ cell \times [\bar{x}\ fluorescence\ of\ background\ readings])$$

The JaCoP plugin from ImageJ software was used to measure the colocalization of p65 and DAPI. The images of p65 and DAPI were opened, the image type was changed to 8-byte and then a blue (DAPI) or red (p65) filter was added. Then, each image was added to the JaCop plugin to perform this analysis: Pearson's, M1, and M2 coefficients; Coste's automatic threshold; and cytofluorogram and click on analysis, at which point the threshold selected by the plugin may need to be changed, and the image is re-analyzed. Finally, the Pearson's, M1, and M2 coefficients were copied in an Excel sheet to calculate the mean, standard deviation, and error of the coefficients in each condition.

4.6.2.4 Graphpad Prism for statistical analysis and the design of graphs

The data from the experimental groups were analyzed using GraphPad Prism v8.2.1 software (GraphPad Software, USA). The minimum "n" for statistical analysis of the in vitro experiments was 3. In the case of mouse and human samples, the minimum sample size for each group was 4.

Normality tests were performed to confirm that the data followed a normal distribution. Statistical significance of the differences between groups that had a Gaussian distribution was assessed by Student's t-test when comparing two groups, or by ANOVA tests followed by a Bonferroni or Tukey post-hoc test when comparing more than two groups. If the variables did not have a Gaussian distribution, the differences between the two groups were studied with a Mann-Whitney test, or with a Kruskal-Wallis's test followed by Dunn's post-hoc test when comparing more than two groups. Correlations between variables were assessed using two-tailed Spearman's or Pearson's r correlation analysis. The exact p value is indicated in each figure when it reached statistical significance ($p < 0.05$). Receiver Operating Characteristic (ROC) analysis was performed to test the diagnostic accuracy of the evaluated miRNAs.

4.6.2.5 *Cytoscape and InteractiVenn*

The Cytoscape v.3.8.2. on Java 11.0.6. by AdoptOpenJDK (Germany) was used to represent the proposed targets of each miRNA and the regulatory axis during atherosclerosis progression.

The online site http://www.interactivenn.net/ was used to generate the Venn diagram with the target results of each database.

4.6.2.6 *CLIPStudio*

The CLIPStudio v. 2.2.2 was used to create all the images from this thesis. All the rights and fair use of the images are reserved to Paula González, as the creator of the of them.

4.7 Materials

4.7.1 Reagents used in cell culture

Insulin is soluble in ultrapure water at concentration of 1 mM. For these experiments, the working concentration was 100 nM.

Thapsigargin is a sesquiterpene lactone extracted from the plant Thapsia garganica that inhibits endoplasmic reticulum Ca2+/ATPase-generating stress. Soluble in DMSO to a 1 mM stock solution. For these experiments, the working concentration was 100 nM.

TNFα is a proinflammatory cytokine, soluble in ultrapure water to a concentration of 10 µg/mL. For the experiments, the working concentration was 10 ng/mL.

Ox-LDLs were purchased from Thermo Fisher at a 2.5 mg/mL concentration. For the experiments, the working concentration was 100 µg/mL.

4.7.2 Table of kits used

Table II. Kits used in this thesis

Name	Manufacturer	Reference
RNeasy FFPE kit	Qiagen	73504
mirVana™ miRNA Isolation Kit	Invitrogen™	AM1560
TaqMan™ Advanced miRNA cDNA Synthesis Kit	Invitrogen™	A28007
mirVana™ Total exosome RNA and protein isolation kit	Invitrogen™	4478545
Total Exosome Isolation Kit (from plasma)	Invitrogen™	4484450

4.7.3 Table of miRNA and genes probes

All probes used were TaqMan®miRNA and TaqMan®genes assays.

Table III. TaqMan® Probes used in this work.

Origin	miRNA/genes	Reference
Mus musculus	**mmu-let-7d-5p**	mmu478439_mir
Mus musculus	**mmu-miR-15b-5p**	mmu482957_mir
Mus musculus	**mmu-miR-22-3p**	mmu480104_mir
Mus musculus	**mmu-miR-26b-5p**	mmu482965_mir
Mus musculus	**mmu-miR-27b-3p**	mmu478270_mir
Mus musculus	**mmu-miR-34a-5p**	mmu481304_mir
Mus musculus	**mmu-miR-122-5p**	mmu480899_mir
Mus musculus	**mmu-miR-146b-5p**	mmu478513_mir
Mus musculus	**mmu-miR-149-5p**	mmu480946_mir
Mus musculus	**mmu-miR-375-3p**	mmu481141_mir
Mus musculus	**mmu-miR-191-5p**	mmu481584_mir
Mus musculus	**mmu-miR-9-5p**	mmu481285_mir
Mus musculus	**mmu-miR-15a-5p**	mmu482962_mir
Mus musculus	**mmu-miR-16-5p**	mmu482960_mir
Homo sapiens	**hsa-miR-199a-3p**	477961_mir
Mus musculus	**mmu-miR-218-5p**	mmu481001_mir
Homo sapiens	**hsa-miR-301a-3p**	477815_mir
Homo sapiens	**hsa-let-7c-5p**	478577_mir
Homo sapiens	**hsa-let-7g-5p**	478580_mir
Homo sapiens	**hsa-let-7i-5p**	478375_mir
Homo sapiens	**hsa-miR-143-3p**	477912_mir
Homo sapiens	**hsa-miR-145-5p**	477916_mir
Mus musculus	**mmu-miR-155-5p**	mmu480953_mir
Mus musculus	**mmu-miR-221-5p**	mmu481659_mir
Mus musculus	**mmu-miR-223-3p**	mmu481007_mir
Mus musculus	***Hprt***	Mm03024075_m1
Mus musculus	***Foxp3***	Mm00475162_m1
Mus musculus	***Ifng***	Mm01168134_m1
Mus musculus	***Il21***	Mm00517640_m1
Mus musculus	***Pdcd1***	Mm01285676_m1
Mus musculus	***Vcam1***	Mm01320970_m1
Mus musculus	***Il1β***	Mm00434228_m1
Mus musculus	***Ccl2***	Mm00441242_m1

4.7.4 Table of antibodies

Table IV. Primary and secondary antibodies used in this study.

Antibody	Dilution	Supplier	Reference	Technique
AKT	1:1000	Cell Signalling Technology ®	#9272	WB
	1:200			IHC
β-Actin	1:5000	Sigma Aldrich	A5441	WB
Cleaved Caspase 3 (D175)	1:1000	Cell Signalling Technology ®	#9661	WB
eNOS	1:1000	Merck Milipore	#07-520	WB
IGF-IIR (H-300)	1:1000	Santa Cruz Biotechnology	sc-25462	WB
IKKα (B-8)	1:250	Santa Cruz Biotechnology	sc-7606	WB
	1:25			IIHC-P
IKKβ	1:1000	Cell Signalling Technology ®	#2678	WB
	1:50			IHC-P
IKKβ	1:200	Proteintech ®	15649-1-AP	OCT-IHC
IκBα (L35A5)	1:2000	Cell Signalling Technology ®	#4814	WB
NF-κB p65	1:2000	Invitrogen	#PA1-186	WB
	1:200			IF
	1:300			IHC/IF
p85α	1:1000	Abcam	Ab191606	WB
p-AKT (S473) (193H12)	1:1000	Cell Signalling Technology ®	#4058	WB
anti-CD3 antibody [SP7]	1:300	Abcam	Ab16669	IF
anti-CD4	1:100	BD Biosystems	553647	IF
anti-CD8	1:100	BD Biosystems	553027	IF
LOX-1	1:1000	Invitrogen	#PA5-102452	WB
	1:100			IHC-P/IF
Anti-Actin, α-Smooth Muscle - Cy3™ antibody, Mouse monoclonal	1:1000	Sigma	C6198	IF
Mouse/Rat CD31/PECAM-1 Antibody	1:200	R&D System	AF3628	IF
DAPI	1:1000	Thermo Fisher Scientific	62248	IF
p-IKKα/β (Ser176/180)	1:1000	Cell Signalling Technology ®	#2697	WB
555 Goat Anti-Rabbit	1:500	Invitrogen	A32732	IF
Horse Anti-Rabbit IgG (H+L), Biotinylated	1:200	Vector Laboratories (Palex)	BA-1100-1.5	IHC-P
Goat Anti-Rabbit IgG (H+L), Horseradish Peroxidase (HRP) Conjugate, affinity purified	1:3000	Invitrogen	A16096	WB
	1:200			IHC
Horse Anti-Mouse IgG (H+L), Biotinylated	1:200	Vector Laboratories (Palex)	BA-2001	IHC-P
Donkey Anti-Rat IgG (H+L) (DyLight® 594) cross-absorbed	1:200	Abcam	SA5-1008	IF
Goat Anti-Rabbit IgG (H+L) (DyLight® 488) preadsorbed	1:200	Abcam	Ab96899	IF
Alexa Fluor™ 594 Donkey anti-Rabbit IgG (H+L)	1:200	Thermo Scientific	A21207	IF
Alexa Fluor™ 488 Donkey anti-Rabbit IgG (H+L)	1:200	Thermo Scientific	A21206	IF
Alexa Fluor™ 488 Donkey anti-Goat IgG (H+L)	1:200	Thermo Scientific	A11055	IF
ECLTM Anti-Mouse IgG, Horseradish Peroxidase linked whole antibody (from sheep)	1:5000	Sigma Aldrich	NA931V	WB

"Donde el deseo viaja en ascensores,
un agujero queda para mi,
que me dejo la vida en sus rincones,
pongamos que hablo de Madrid"

-Pongamos que hablo de Madrid,
Joaquín Sabina

5- Results

5. RESULTS

5.1. Characterization of mouse and human atherosclerosis

To carry out this work, we have used a classical model of atherosclerosis as *ApoE*$^{-/-}$ mice under HFD for 8 or 18 weeks (Chapter 4.2.1). Firstly, we confirmed that *ApoE*$^{-/-}$ mice had a significant increase in body weight in addition to hypercholesterolemia and hypertriglyceridemia (Table 1, ‡), being significantly higher in *ApoE*$^{-/-}$ fed with HFD for 18 weeks.

Table 1. Table representing the data corresponding to the body weight (BW), gonadal white adipose tissue (gWAT)/BW and inguinal white adipose tissue (iWAT)/BW ratios; cholesterol, triglycerides, and glucose levels in the blood of the 8 and 18-week experimental groups.

	8 wks						18 wks					
	WT STD	*ApoE*$^{-/-}$ STD	*ApoE*$^{-/-}$ HFD	WT STD vs. *ApoE*$^{-/-}$ STD	WT STD vs. *ApoE*$^{-/-}$ HFD	*ApoE*$^{-/-}$ STD vs. *ApoE*$^{-/-}$ HFD	WT STD	*ApoE*$^{-/-}$ STD	*ApoE*$^{-/-}$ HFD	WT STD vs. *ApoE*$^{-/-}$ STD	WT STD vs. *ApoE*$^{-/-}$ HFD	*ApoE*$^{-/-}$ STD vs. *ApoE*$^{-/-}$ HFD
BW (g) ‡	25.9 ± 0.34	25 ± 0.45	29 ± 0.42	p=n.s.	**p<0.0001**	**p<0.0001**	28.6 ± 0.32	29.3 ± 0.41	34.3 ± 1.02	p=n.s.	**p<0.0001**	**p=0.0017**
gWAT (mg)/ BW (g) ‡	8.2 ± 0.71	5.4 ± 1.0	20.6 ± 3.23	p=n.s.	**p=0.0012**	**p=0.005**	5.9 ± 0.91	5.3 ± 0.48	38.2 ± 4.01	p=n.s.	**p<0.0001**	**p<0.0001**
iWAT (mg)/ BW (g) ‡	4.9 ± 0.66	5.0 ± 0.36	17.1 ± 3.47	p=n.s.	**p=0.0024**	**p=0.057**	3.7 ± 0.54	6.1 ± 0.59	21.2 ± 3.13	p=n.s.	**p=0.008**	**p=0.090**
Cholesterol (mg/dL) ‡	96.4 ± 6.5	188.9 ± 16.8	209.8 ± 2.1	**p=0.001**	**p<0.0001**	p=n.s.	117.5 ± 3.9	201.9 ± 8.3	234.0 ± 6.5	**p<0.0001**	**p<0.0001**	**p=0.063**
Triglycerides (mg/mL) ‡	49.2 ± 4.9	84.8 ± 9.5	88.5 ± 6.7	p=n.s.	**p=0.065**	p=n.s.	30.7 ± 3.1	72.8 ± 8.1	86.4 ± 5.4	**p=0.024**	**p=0.029**	p=n.s.
Blood glucose (mg/ dL) ‡	376.1 ± 11.75	227.6 ± 12.96	427 ± 24.23	**p<0.0001**	p=n.s.	**p<0.0001**	279.8 ± 9.49	216.3 ± 6.04	339.2 ± 13.58	p=n.s.	p=n.s.	**p<0.0001**

‡ Results shared with PhD. Thesis from Andrea Raposo López-Pastor (Result section 4.2.1 and 4.2.2).

After that, we analyzed vascular damage by Oil Red O (ORO) staining of aortic roots (Figure 1A). A significant increase in lipid depot, lesion area and % of stenosis was noted in aortic roots from *ApoE*$^{-/-}$-fed a HFD for 18 weeks in comparison with the other groups (Figure 1B). Similarly, *en face* analysis of ORO-stained whole aorta showed a significant increase in the lesion area in *ApoE*$^{-/-}$ HFD vs. WT STD and *ApoE*$^{-/-}$STD mice after 18 weeks of diet (Figure 2).

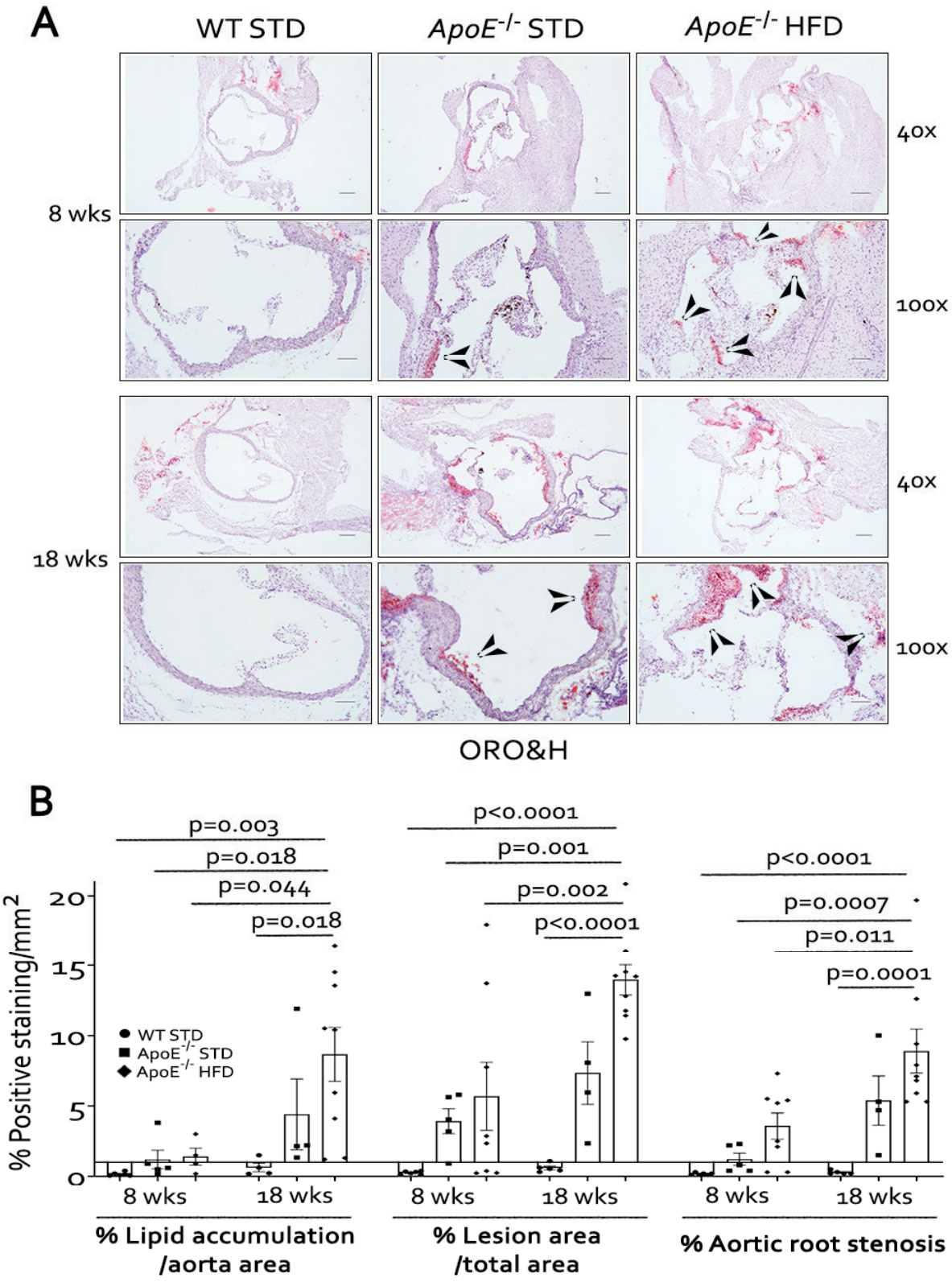

Figure 1. Histological characterization of experimental atherosclerosis. (A) Representative images of the Oil Red O staining of the aortic roots from the six groups of the experimental mouse model of atherosclerosis. Magnification 40x (scale bar= 200 µm); magnification 100x (scale bar= 100 µm). Black arrows point out the lipid depots in the aortic roots. **(B)** Quantification of the percentage of lipid accumulation, lesion area and stenosis of aortic root from the mouse model. WT= wild-type; STD= standard type diet; *ApoE*$^{-/-}$= apolipoprotein E deficient mice; HFD= high-fat diet; wks= weeks; ORO= Oil Red O; H= hematoxylin. WT STD 8 weeks (n=5); *ApoE*$^{-/-}$ STD 8 weeks (n=5); *ApoE*$^{-/-}$ HFD 8 weeks (n=7); WT STD 18 weeks (n=5); *ApoE*$^{-/-}$ STD 18 weeks (n=4); *ApoE*$^{-/-}$ HFD 18 weeks (n=9).

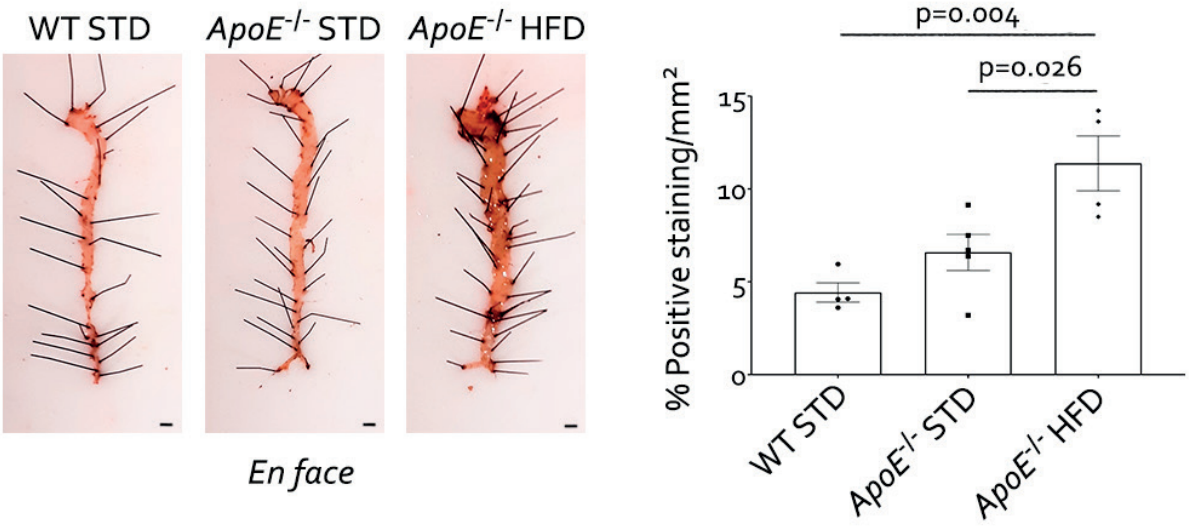

Figure 2. Histological characterization of experimental atherosclerosis. *En face* staining of aortas from male WT mice fed a standard diet, male *ApoE*$^{-/-}$ mice fed a STD, and male *ApoE*$^{-/-}$ mice fed a HFD for 18 weeks. Scale bar=100 µm. WT= wild-type; STD= standard type diet; *ApoE*$^{-/-}$= apolipoprotein E deficient mice; HFD= high fat diet. WT STD (n=4); *ApoE*$^{-/-}$ STD (n=5); *ApoE*$^{-/-}$ HFD (n=4).

On the other hand, the human vascular samples were also characterized to assess the plaque type. Firstly, different clinical parameters were studied in the ACA patients like age, biological sex, body mass index (BMI), diabetes, hypertension, coronary artery disease, and smoking habits (Table 2).

Table 2. Clinical characteristics of patients bearing advanced carotid atherosclerosis (ACA).

	ACA Patients (Carotid Plaque) (n=14)
Age, years	70 ± 7
Biological sex (male/female), %	71.4 % / 28.6 %
BMI (Kg/m²)	29.2 ± 6.3
Diabetes mellitus, %	42.9 %
Hypertension, %	85.7 %
Coronary artery disease, %	100 %
Current smoking, %	37.7 %

Secondly, we performed H&E and Masson's trichrome stainings, and we could differentiate regions as media in samples from CAs and FAs; and media, fibrous and shoulders in samples from ACA (Figure 3). Histological analysis revealed that complicated plaques from ACA contained an intraplaque haemorrhage and/or a certain degree of calcification. The non complicated regions were composed of fibrous thickening with a variable content of VSMCs (Figure 3).

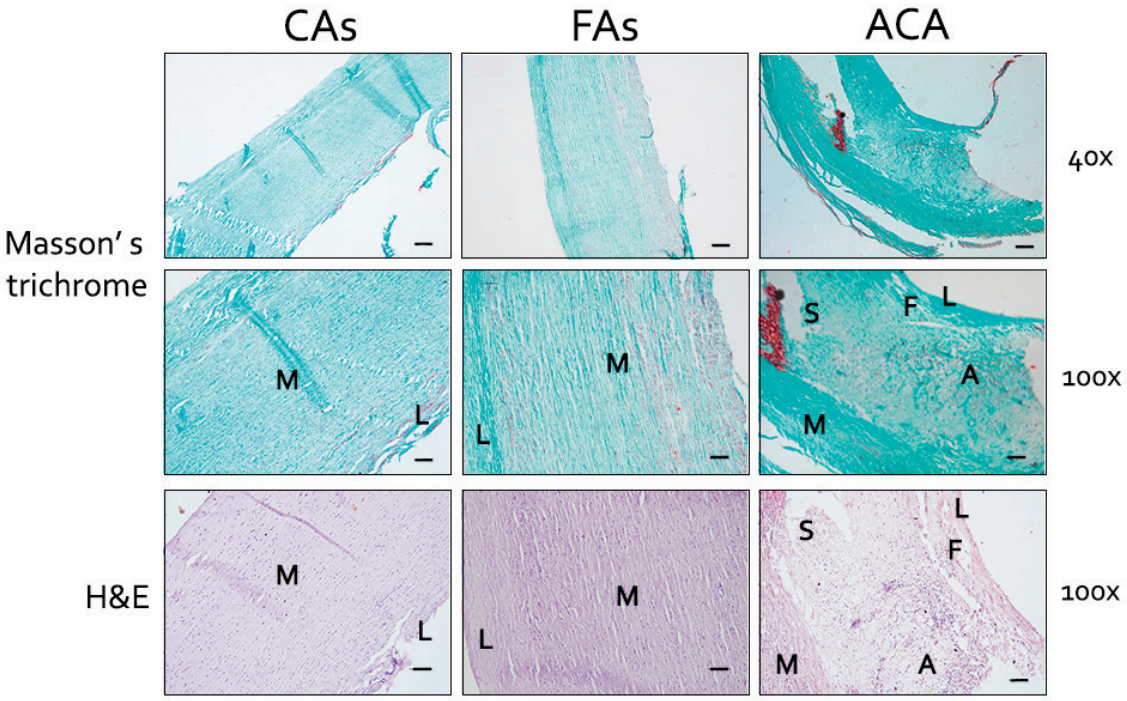

Figure 3. Histological characterization of human atherosclerosis. Representative images of Masson's trichrome and hematoxylin and eosin staining from the aorta of control subjects (CAs), subjects with initial lesions or fibroatheroma (FAs), and the carotid artery from patients with advanced carotid atherosclerosis (ACA). Magnification 40x (scale bar = 200 µm) and 100x (scale bar = 100 µm). CAs= control aortas; FAs= fibroatheroma; ACA= advanced carotid atherosclerotic plaque; M=media; F=fibrous; S=shoulder; A=atheroma; L=lumen; H&E = hematoxylin and eosin.

5.2. miRNAs profile in experimental and human atherosclerosis

To elucidate the potential miRNAs that could be involved in the progression of atherosclerosis, we performed an *in silico* study in PubMed using the following keywords: *miRNAs* and *atherosclerosis*, *miRNAs* and *NAFLD*, and *miRNAs* and *inflammation*. In addition, we searched the GEO Database to confirm whether some of the miRNAs found in PubMed, have been reported as possible modulators of the disease in other murine or human studies.

As a result, we concluded that twenty-four miRNAs of interest were separated into three groups: miRNAs that could be potential modulators of NAFLD (let-7d-5p, miR-15b-5p, miR-22-3p, miR-26b-5p, miR-27b-3p, miR-34a-5p, miR-122-5p, miR-146b-5p, miR-149-5p, and miR-375-5p), miRNAs that could be promoters of atherosclerosis (let-7c-5p, let-7g-5p, let-7i-5p, miR-143-3p, miR-145-5p, miR-155-5p, miR-221-5p, and miR-223-3p), and miRNAs that could regulate the NF-κB pathway (miR-9-5p, miR-15a-5p, miR-16-5p, miR-199a-3p, miR-218-5p, miR-223-3p, and miR-301a-3p).

The expression of these miRNAs was studied in the aortas of mice fed 8 and 18 weeks of diet using RT-qPCR. After 8-weeks of HFD, there were changes in the expression of only three miRNAs: miR-149-5p, miR-155-5p, and miR-223-3p (Figure 4A, p values in Table 3). However, after 18 weeks of HFD the expression of 11 miRNAs was significantly altered: let-7c-5p, let-7d-5p, let-7i-5p, miR-9-5p, miR-15a-5p, miR-16-5p, miR-122-5p, miR-143-3p, miR-149-5p, miR-155-5p, and miR-199a-3p (Figure 4B, p values in Table 3).

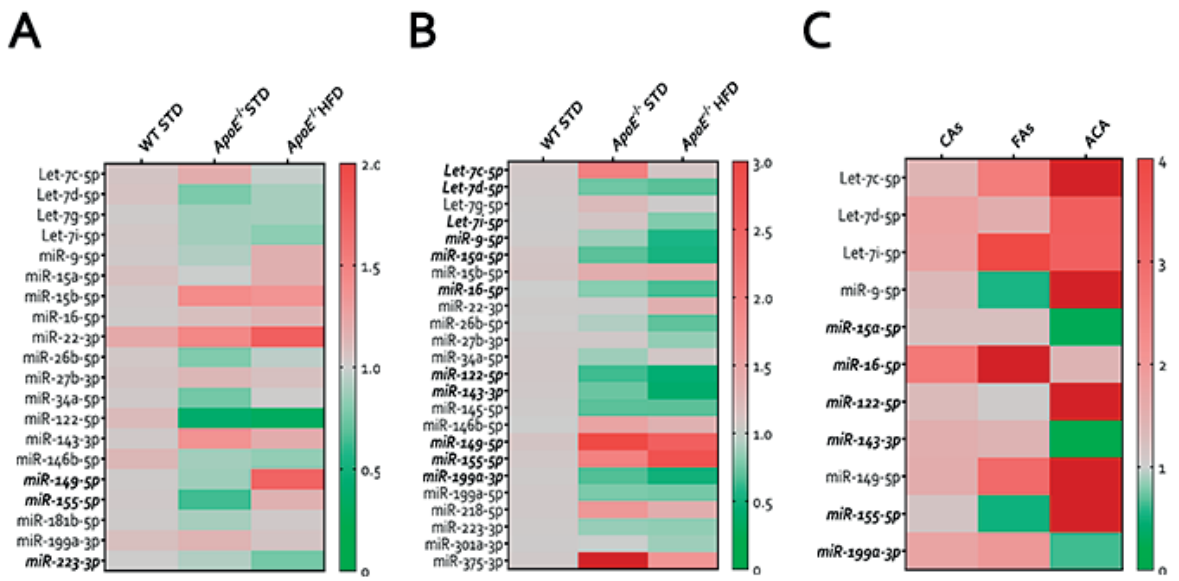

Figure 4. Heatmaps of miRNAs studied in experimental and human atherosclerosis. Using RT-qPCR, we analyzed 20 (in the 8 weeks groups) and 24 (in the 18 weeks groups) miRNAs in thoracic aorta arteries from WT, *ApoE*$^{-/-}$ STD, and *ApoE*$^{-/-}$ HFD at 8 **(A)** and 18 **(B)** weeks of diet, respectively, and 11 miRNAs that were altered the most in the mouse model were studied in human samples **(C)**. Using the mean values of RQ (0-3) for each group, we generated three heatmaps using GraphPad Prism v8. The p values are listed in Table 3. WT= wild-type; STD= standard type diet; *ApoE*$^{-/-}$ = apolipoprotein E deficient mice; HFD= high-fat diet; CAs= control aortas; FAs= fibroatheroma; ACA= advanced carotid atherosclerosis. WT STD 8 weeks (n=5); *ApoE*$^{-/-}$ STD 8 weeks (n=5); *ApoE*$^{-/-}$ HFD 8 weeks (n=7); WT STD 18 weeks (n=5); *ApoE*$^{-/-}$ STD 18 weeks (n=4); *ApoE*$^{-/-}$ HFD 18 weeks (n=9); CAs (n=7); FAs (n=7); ACA (n=14).

To confirm whether the levels of the studied miRNAs in the murine model might be clinically relevant in human atherosclerosis, these miRNAs were selected for analysis in the aorta of the CAs and FAs, and the carotid of the ACA group using RT qPCR. From the 11 miRNAs selected, six were altered in ACA patients: miR-15a-5p, miR-16-5p, miR-122-5p, miR-143-3p, miR-155-5p, and miR-199a-3p (Figure 4C, p values in Table 3).

Succeeding the screening of the firstly selected twenty-four miRNAs in the aorta of our experimental model and patients (Table 3), four miRNAs were selected for further analysis because they had the same pattern of significant alteration in our experimental model and human atherosclerosis. The miRNAs selected were the following: miR-143-3p, miR-155-5p, miR-15a-5p, and miR-199a-3p. In addition, considering that most of the significant histological and molecular changes happened after 18 weeks of diet, we decided to continue the investigation only in these groups.

Table 3. miRNAs were studied using an experimental atherosclerosis model and human atherosclerosis samples. The upregulation or downregulation of statistically significant alterations is marked in bold.

miRNAs	8 weeks-fed mouse model		18 weeks-fed mice model		Human samples	
	Alteration	p value	Alteration	p value	Alteration	p value
Let-7c-5p	None (WT vs. *ApoE*$^{-/-}$ STD)	>0.999	**Upregulation (WT vs. *ApoE*$^{-/-}$ STD)**	**0.035**	Upregulation (CAs vs. ACA)	0.230
	None (WT vs. *ApoE*$^{-/-}$ HFD)	>0.999	**Downregulation (ApoE$^{-/-}$ STD vs. *ApoE*$^{-/-}$ HFD)**	**0.030**	Upregulation (FAs vs. ACA)	0.332
Let-7d-5p	None (WT vs. *ApoE*$^{-/-}$ STD)	0.616	None (WT vs. *ApoE*$^{-/-}$ STD)	0.081	Upregulation (CAs vs. ACA)	0.753
	None (WT vs. *ApoE*$^{-/-}$ HFD)	>0.999	**Downregulation (WT vs. *ApoE*$^{-/-}$ HFD)**	**0.027**	Upregulation (FAs vs. ACA)	0.641
Let-7g-5p	None (WT vs. *ApoE*$^{-/-}$ STD)	>0.999	None (WT vs. *ApoE*$^{-/-}$ STD)	0.570		
	None (WT vs. *ApoE*$^{-/-}$ HFD)	>0.999	None (WT vs. *ApoE*$^{-/-}$ HFD)	>0.999		
Let-7i-5p	None (WT vs. *ApoE*$^{-/-}$ STD)	>0.999	None (WT vs. *ApoE*$^{-/-}$ STD)	>0.999	Upregulation (CAs vs. ACA)	>0.999
	None (WT vs. *ApoE*$^{-/-}$ HFD)	0.450	**Downregulation (*ApoE*$^{-/-}$ STD vs. *ApoE*$^{-/-}$ HFD)**	**0.021**	Downregulation (FAs vs. ACA)	>0.999
miR-9-5p	None (WT vs. *ApoE*$^{-/-}$ STD)	0.941	None (WT vs. *ApoE*$^{-/-}$ STD)	0.719	Undetermined data for all samples	
	None (WT vs. *ApoE*$^{-/-}$ HFD)	0.829	Downregulation (WT vs. *ApoE*$^{-/-}$ HFD)	0.057	Undetermined data for all samples	
miR-15b-5p	None (WT vs. *ApoE*$^{-/-}$ STD)	0.561	None (WT vs. *ApoE*$^{-/-}$ STD)	>0.999		
	None (WT vs. *ApoE*$^{-/-}$ HFD)	0.640	None (WT vs. *ApoE*$^{-/-}$ HFD)	>0.999		
miR-16-5p	None (WT vs. *ApoE*$^{-/-}$ STD)	0.944	None (WT vs. *ApoE*$^{-/-}$ STD)	0.300	Upregulation (CAs vs. ACA)	0.333
	None (WT vs. *ApoE*$^{-/-}$ HFD)	0.817	**Downregulation (WT vs. *ApoE*$^{-/-}$ HFD)**	**0.027**	**Downregulation (FAs vs. ACA)**	**0.014**
miR-22-3p	Upregulation (WT vs. *ApoE*$^{-/-}$ STD)	>0.999	None (WT vs. *ApoE*$^{-/-}$ STD)	>0.999		
	Upregulation (WT vs. *ApoE*$^{-/-}$ HFD)	0.355	Upregulation (WT vs. *ApoE*$^{-/-}$ HFD)	0.697		
miR-26b-5p	Downregulation (WT vs. *ApoE*$^{-/-}$ STD)	0.728	None (WT vs. *ApoE*$^{-/-}$ STD)	>0.999	None (CAs vs. ACA)	>0.999
	None (WT vs. *ApoE*$^{-/-}$ HFD)	>0.999	Downregulation (WT vs. *ApoE*$^{-/-}$ HFD)	0.056	None (FAs vs. ACA)	>0.999
miR-27b-3p	None (WT vs. *ApoE*$^{-/-}$ STD)	>0.999	None (WT vs. *ApoE*$^{-/-}$ STD)	>0.999		
	None (WT vs. *ApoE*$^{-/-}$ HFD)	>0.999	Downregulation (WT vs. *ApoE*$^{-/-}$ HFD)	>0.999		
miR-34a-5p	Downregulation (WT vs. *ApoE*$^{-/-}$ STD)	0.459	Downregulation (WT vs. *ApoE*$^{-/-}$ STD)	>0.999		
	None (WT vs. *ApoE*$^{-/-}$ HFD)	>0.999	None (WT vs. *ApoE*$^{-/-}$ HFD)	>0.999		
miR-122-5p	**Downregulation (WT vs. *ApoE*$^{-/-}$ STD)**	**0.009**	Downregulation (WT vs. *ApoE*$^{-/-}$ STD)	0.080	**Upregulation (CAs vs. ACA)**	**0.014**
	Downregulation (WT vs. *ApoE*$^{-/-}$ HFD)	**0.002**	**Downregulation (WT vs. *ApoE*$^{-/-}$ HFD)**	**0.010**	**Upregulation (FAs vs. ACA)**	**0.027**
miR-145-5p			Downregulation (WT vs. *ApoE*$^{-/-}$ STD)	0.274		
			Downregulation (WT vs. *ApoE*$^{-/-}$ HFD)	0.248		
miR-146b-5p	Downregulation (WT vs. *ApoE*$^{-/-}$ STD)	>0.999	Upregulation (WT vs. *ApoE*$^{-/-}$ STD)	0.255		
	Downregulation (WT vs. *ApoE*$^{-/-}$ HFD)	>0.999	Upregulation (WT vs. *ApoE*$^{-/-}$ HFD)	0.784		
miR-149-5p	None (WT vs. *ApoE*$^{-/-}$ STD)	>0.999	**Upregulation (WT vs. *ApoE*$^{-/-}$ STD)**	**0.015**	Upregulation (CAs vs. ACA)	0.317
	Upregulation (*ApoE*$^{-/-}$ STD vs. *ApoE*$^{-/-}$ HFD)	**0.043**	Upregulation (WT vs. *ApoE*$^{-/-}$ HFD)	0.057	Undetermined data for FAs	
miR-218-5p			Upregulation (WT vs. *ApoE*$^{-/-}$ STD)	0.243		
			Upregulation (WT vs. *ApoE*$^{-/-}$ HFD)	0.976		
miR-223-3p	None (WT vs. *ApoE*$^{-/-}$ STD)	>0.999	Downregulation (WT vs. *ApoE*$^{-/-}$ STD)	0.600		
	Downregulation (WT vs. *ApoE*$^{-/-}$ HFD)	**0.022**	Downregulation (WT vs. *ApoE*$^{-/-}$ HFD)	0.460		
miR-301a-3p			None (WT vs. *ApoE*$^{-/-}$ STD)	>0.999		
			Downregulation (WT vs. ApoE$^{-/-}$ HFD)	0.625		
miR-375-3p			Upregulation (WT vs. *ApoE*$^{-/-}$ STD)	0.079		
			Upregulation (WT vs. *ApoE*$^{-/-}$ HFD)	>0.999		

5.3. Study of the role of miR-143-3p dysregulation and its target IGF-IIR in atherosclerotic plaque instability

5.3.1. miR-143-3p is downregulated in human and experimental atherosclerosis

As previously explained, miR-143-3p was downregulated in the aorta of *ApoE*$^{-/-}$ mice fed a HFD for 18 weeks (Figure 5A) and in carotid plaques from patients with advanced atherosclerosis (Figure 6). We wanted to link this alteration with the severity of the disease, by comparing the percentages of lipid accumulation, lesion area and stenosis in the aortic roots and the expression of this miRNA. Our results showed that the expression of miR-143-3p was inversely correlated with the percentage of lipid deposition (Figure 5B) and lesion area in the root (Figure 5C) in a statistically significant manner.

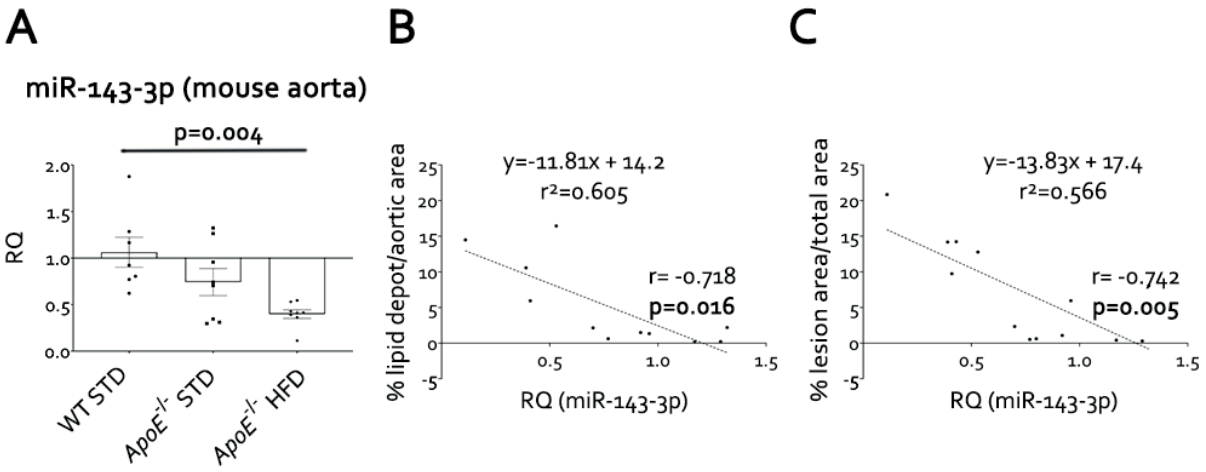

Figure 5. miR-143-3p is downregulated in aorta from the experimental atherosclerosis model and correlates with the disease progression. (A) The expression of miR-143-3p was quantified by RT-qPCR in the aorta of the 18-weeks fed mice. By Spearman's correlation, we set different correlation between miR-143-3p and % lipid depot/ aortic area **(B)**, and % lesion area/total area **(C)**. WT= wild-type; STD= standard type diet; *ApoE*$^{-/-}$ = apolipoprotein E deficient mice; HFD= high-fat diet; RQ = relative quantification. WT STD (n = 7); *ApoE*$^{-/-}$ STD (n = 8); *ApoE*$^{-/-}$ HFD (n = 8).

The next step was to determine a possible target that may promote disease progression. *In silico* analyses were performed using different miRNA-target interaction databases to select among all possible genes. First, we searched the list of possible targets from TargetScan, miRDB, and miRWalk databases (Figure 7A), and only targets with a potential role in atherosclerosis that appeared in at least two databases were considered. Finally, these targets were also searched in miRTarBase, a database for confirmed miRNA-target interactions, to identify some of them as actual targets.

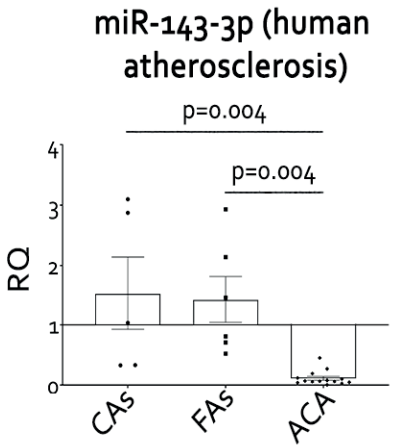

Figure 6. miR-143-3p is downregulated in human advanced atherosclerosis. The expression of miR -143-3p was studied by RT-qPCR in the samples of control, initial atherosclerosis, and advanced atherosclerosis patients. CAs= control aortas; FAs= fibroatheroma; ACA= advanced carotid atherosclerosis; RQ = relative quantification. CAs (n = 5); FAs (n = 6); ACA (n = 14).

From all the possible targets, we chose to study the insulin-like growth factor type-2 (IGF II) receptor (IGF IIR) (Figure 7B). Not only this is a confirmed target of miR-143-3p, but previous results from our group have also demonstrated that overexpression of this protein is related to an increase in apoptosis (Figure 7C) and also, its expression was significantly higher in the shoulder regions of carotid plaque from ACA patients, being a vulnerable region of plaque rupture (141).

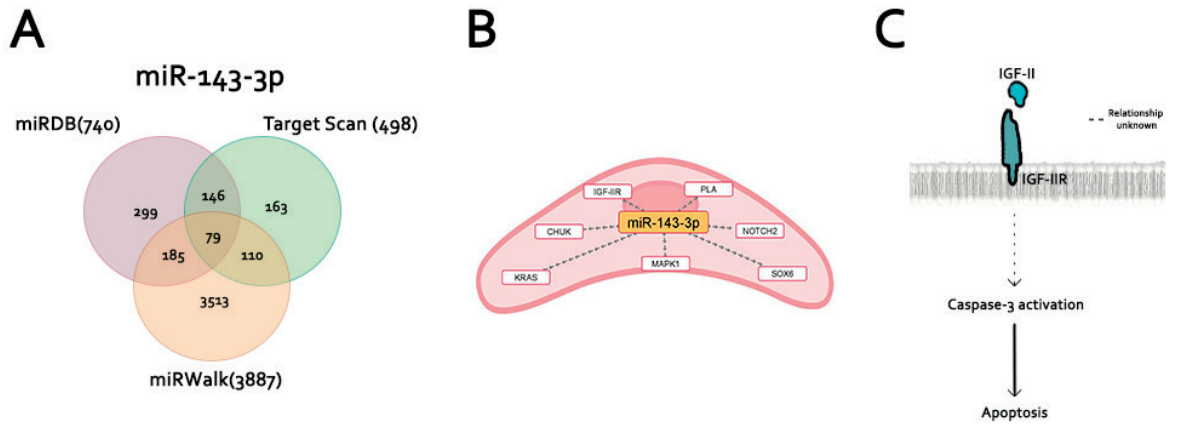

Figure 7. *In silico* search for possible targets of miR-143-3p. We performed a search in different miRNA-target databases to choose potential pro-atherosclerotic proteins modulated by miR-143-3p, with those results we performed **(A)** Venn diagram representing different results obtained from miR-143-3p in databases, such as miRDB, TargetScan, and miRWalk. **(B)** Graphics showing possible targets of miR-143-3p. **(C)** Graphical scheme of possible modulation of atherosclerosis by IGF IIR. The dotted line represents an unknown interaction between IGF IIR and caspase-3 activation. IGF-II = insulin-like growth factor type II; IGF-IIR = IGF-II receptor.

5.3.2. The expression of IGF-IIR is increased in the plasma and aorta of the mice

IGF-IIR can be in the membrane of cells or soluble in plasma binding IGF-II. The expression of this protein was measured by Western blot in whole aorta lysates and plasma samples from the 18-weeks groups. Firstly, we studied IGF-IIR in the aorta of mice, its expression seems to be increased in the HFD-fed group without reaching statistical significance (Figure 8A). Moreover, the expression of IGF-IIR was significantly higher in the plasma of *ApoE*$^{-/-}$ mice fed a HFD (Figure 8B); therefore, we also analysed the expression of IGF-II, finding that this protein was significantly decreased in the plasma of these mice (Figure 8B).

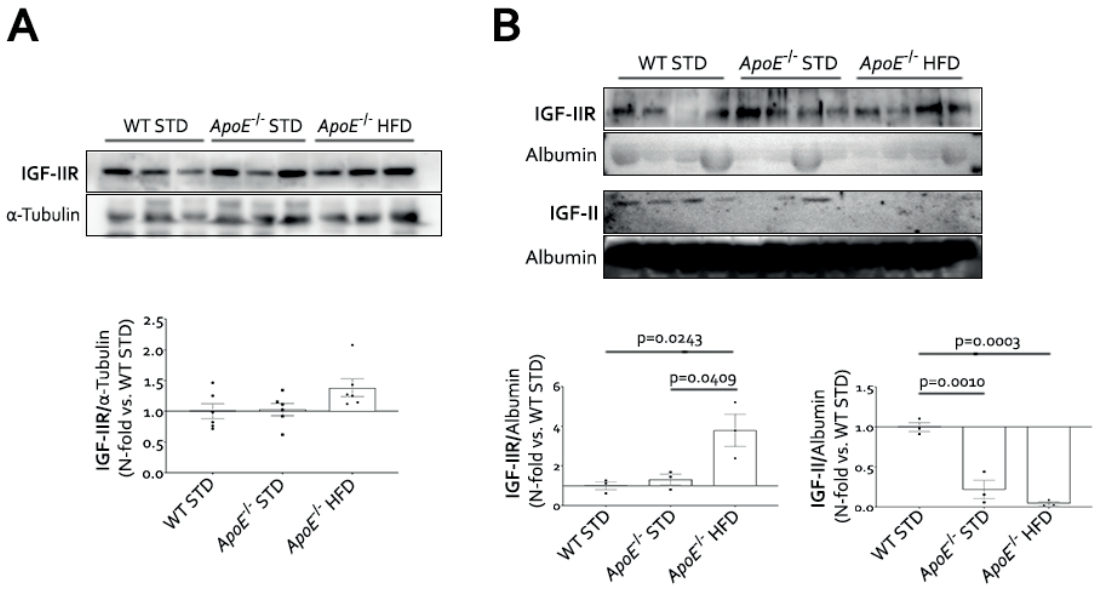

Figure 8. IGF-IIR and IGF-II levels in the aorta and plasma of the mouse model of atherosclerosis. Representative images and quantification of the Western blots of IGF-IIR in the aorta **(A)** and plasma **(B)** of the mouse model; the levels of IGF-II were also assessed by Western blot (B) in the plasma of the mouse model. IGF-IIR = insulin like growth factor type 2 receptor. WT= wild-type; STD= standard type diet; *ApoE*$^{-/-}$= apolipoprotein E deficient mice; HFD= high-fat diet; IGF-IIR = insulin-like growth factor type II receptor. WT STD 18 wks (n = 6); *ApoE*$^{-/-}$ STD 18 wks (n = 6); *ApoE*$^{-/-}$ HFD 18 wks (n = 6).

5.3.3. miR-143-3p protects against apoptosis in HUVECs and VSMCs

Since miR-143-3p was downregulated and its target, IGF-IIR, was overexpressed in human and experimental atherosclerosis (Figure 6, 5A and 8, respectively), we were interested in deciphering the protective role of this miRNA in the atherosclerotic process and for this reason we planned to perform *in vitro* experiments with endothelial (HUVECs) and vascular smooth muscle cell lines (VSMCs). We began by promoting the expression of the miRNA using a specific miRNA mimic, which are non-natural double-stranded miRNA-like RNA fragments that bind the target of the miRNA at issue. The effect of the mimic in promoting the expression of miR-143-3p was assessed by RT-qPCR in HUVECs (Figure 9A) and VSMCs (Figure 10A). In both cases, transfection with the mimic significantly increased the miR-143-3p levels.

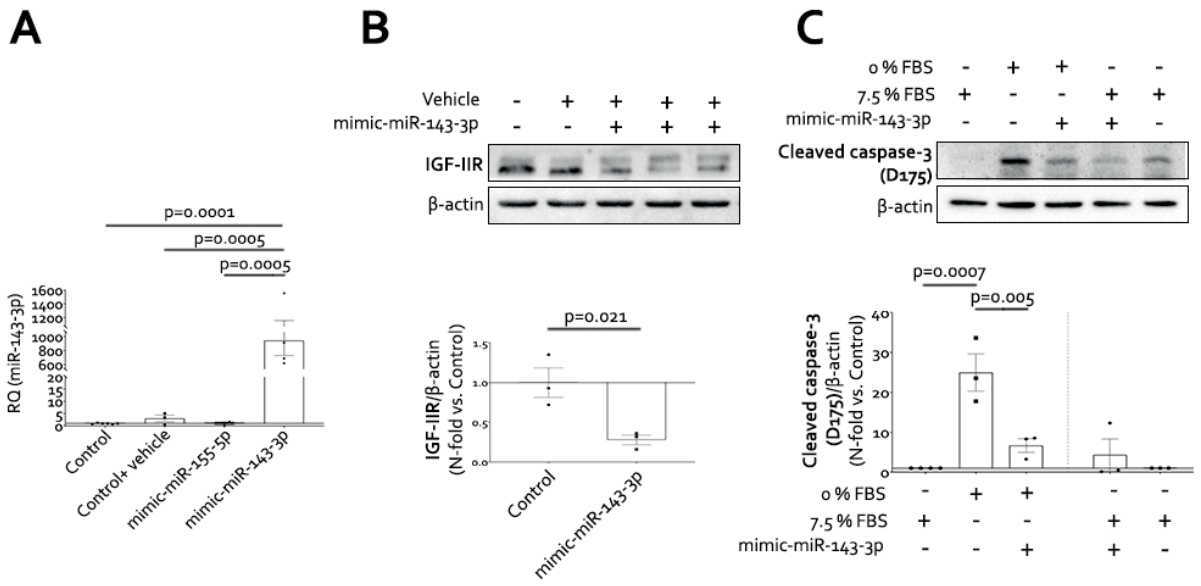

Figure 9. miR-143-3p downregulates IGF-IIR in HUVECs, protecting against apoptosis. Overexpression of miR-143-3p was assessed by RT-qPCR in HUVECs **(A)**, and the effect on its confirmed target IGF-IIR was studied by Western blot **(B)**. HUVECs were subjected to a 6-hour FBS deprivation to induce apoptosis in the presence or absence of mimic-miR-143-3p, and apoptosis was measured by cleaved caspase-3 Western blot **(C)**. RQ= relative quantification; IGF-IIR= insulin-like growth factor type II receptor; D= aspartate; FBS= foetal bovine serum. All the *in vitro* experiments were performed at least in triplicate.

The repressive effect of the miRNA mimic on IGF-IIR was quantified by Western blot in HUVECs (Figure 9B) and VSMCs (Figure 10B), which showed a significant decrease in expression in both cases. To confirm the protective upshot of miR-143-3p in both cell types, we induced apoptosis in the presence or absence of the mimic. Apoptosis was prompted by a 6-hours deprivation of FBS in HUVECs and by a 2-hour deprivation of FBS followed by a 2-hour incubation with thapsigargin in VSMCs. Apoptosis was determined by Western blot for the cleaved form of caspase-3 and our results showed a significant decrease of cleaved caspase-3 in HUVECs (Figure 9C) and VSMCs (Figure 10C) when the expression of miR-143-3p was induced in comparison with the control under pro-apoptotic conditions.

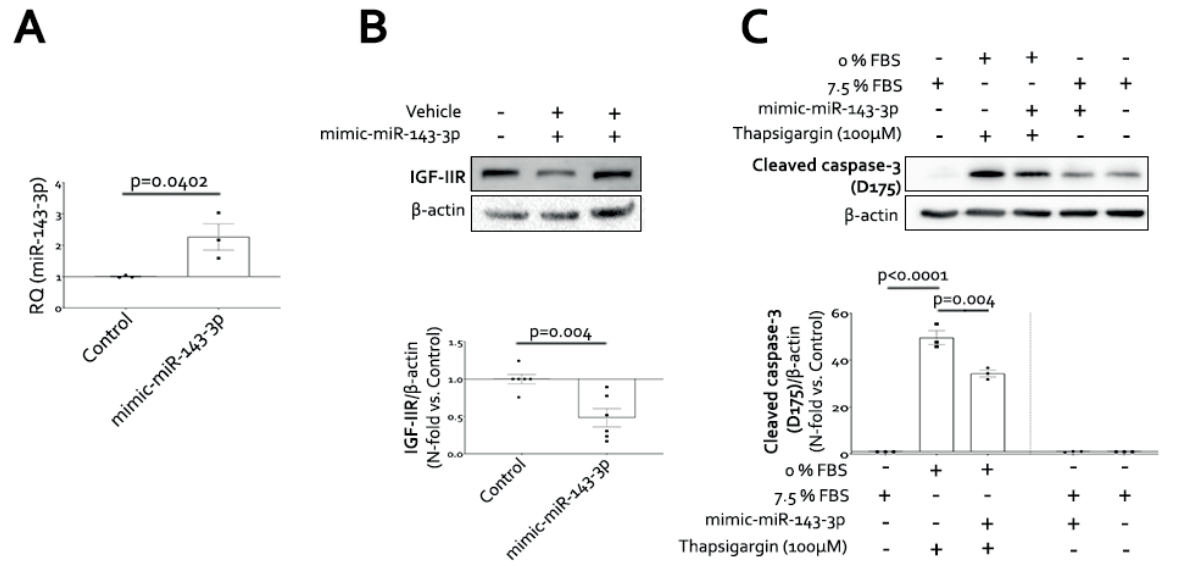

Figure 10. miR-143-3p downregulates IGF-IIR in VSMCs, protecting against apoptosis. Overexpression of miR-143-3p in VSMCs was assessed by RT-qPCR **(A)**, and the effect on its confirmed target IGF-IIR was studied by Western blot **(B)**. VSMCs were subjected to a 6-hour FBS deprivation followed by a 2-hour incubation with thapsigargin to induce apoptosis in the presence or absence of mimic-miR-143-3p, and apoptosis was measured by cleaved caspase-3 Western blot **(C)**. RQ= relative quantification; IGF-IIR= insulin-like growth factor type II receptor; D= aspartate; FBS= foetal bovine serum. All the *in vitro* experiments were performed at least in triplicate.

5.4. Analysis of the involvement of miR-155-5p and its targets AKT, eNOS, and p85α in the progression of atherosclerosis and vascular insulin resistance

5.4.1. miR-155-5p is overexpressed in human and experimental atherosclerosis

miR-155-5p was overexpressed in the aortas of the 18-weeks mice (Figure 11A) and the ACA patients (Figure 12). In the same way we did for the miR-143-3p, we also correlated the levels of miR-155-5p with the severity of the disease by a Spearman's correlation analysis. So, we obtained a signifi cant and positive correlation between miR-155-5p levels and the percentage of aortic root stenosis (Figure 11B) or lesion area (Figure 11C).

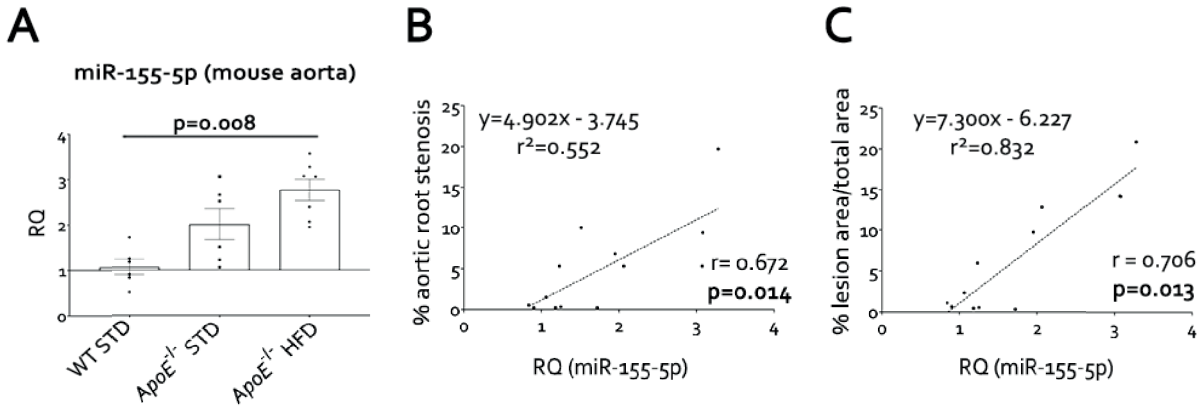

Figure 11. miR-155-5p is overexpressed in mouse atherosclerosis. (A) The expression of miR-155-5p was quantified by RT-qPCR in the aorta of the 18-weeks fed mice. By Spearman's correlation, we set different correlations between miR-155-5p and % aortic root stenosis **(B)**, and % lesion area /total area **(C)**. WT= wild-type; STD= standard type diet; *ApoE*$^{-/-}$= apolipoprotein E deficient mice; HFD= high-fat diet; RQ= relative quantification. WT STD (n=6); *ApoE*$^{-/-}$ STD (n=6); *ApoE*$^{-/-}$ HFD (n=7).

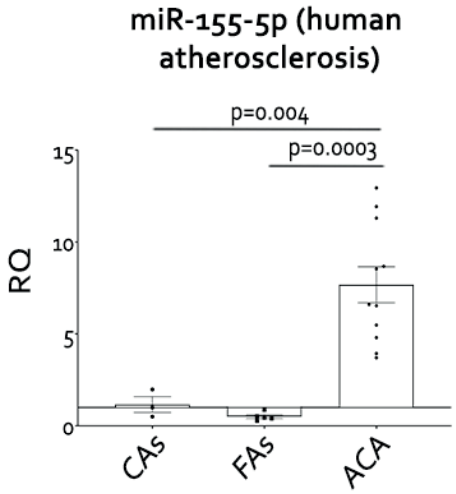

Figure 12. miR-155-5p is overexpressed in human advanced atherosclerosis. The expression of miR-155-5p was studied by RT-qPCR in the samples of control, initial atherosclerosis, and advanced atherosclerosis patients. CAs= control aortas; FAs= fibroatheroma; ACA= advanced carotid atherosclerotic plaque. CAs (n=3); FAs (n=5) and ACA (n=11).

After that, we performed an *in silico* search of miRNA-target interaction databases (Figure 13A), and the possible targets that appeared in at least two of them were confirmed as targets by a search in miRTarBase (Figure 13B). From all the possible and confirmed targets for miR-155-5p, AKT was the most interesting for us. This protein is crucial in the insulin signalling pathway (Figure 13C); moreover, it also phosphorylates multiple proteins that participate in many other pathways.

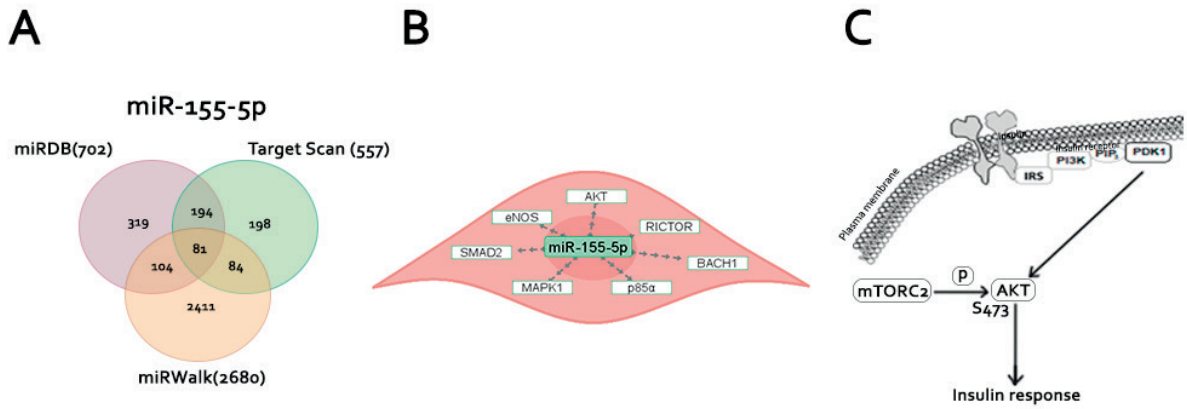

Figure 13. *In silico* search for possible targets of miR-155-5p. We performed a search in different miRNA-target databases to choose potential proteins involved in atherosclerosis and insulin resistance and modulated by miR 155-5p. With those results, we performed **(A)** Venn diagram representing different results obtained from miR-155-5p in databases, such as miRDB, TargetScan, and miRWalk. **(B)** Graph showing possible miR-155-5p targets. **(C)** Graphical scheme of possible modulation of atherosclerosis by AKT through the insulin response. AKT= protein kinase B; S= serine; T= threonine; mTORC2= mammalian target of rapamycin complex 2.

5.4.2. Analysis of AKT levels and activation in experimental atherosclerosis

Once AKT was selected as the target of miR-155-5p in this study, we first assessed AKT protein levels in aorta of mice after 18-weeks of diet by Western blot. After this period, the expression was significantly decreased in the *ApoE*$^{-/-}$ mice fed a STD and HFD compared with the control (Figure 14A), even though the expression was slightly lower in the HFD group than in the STD group.

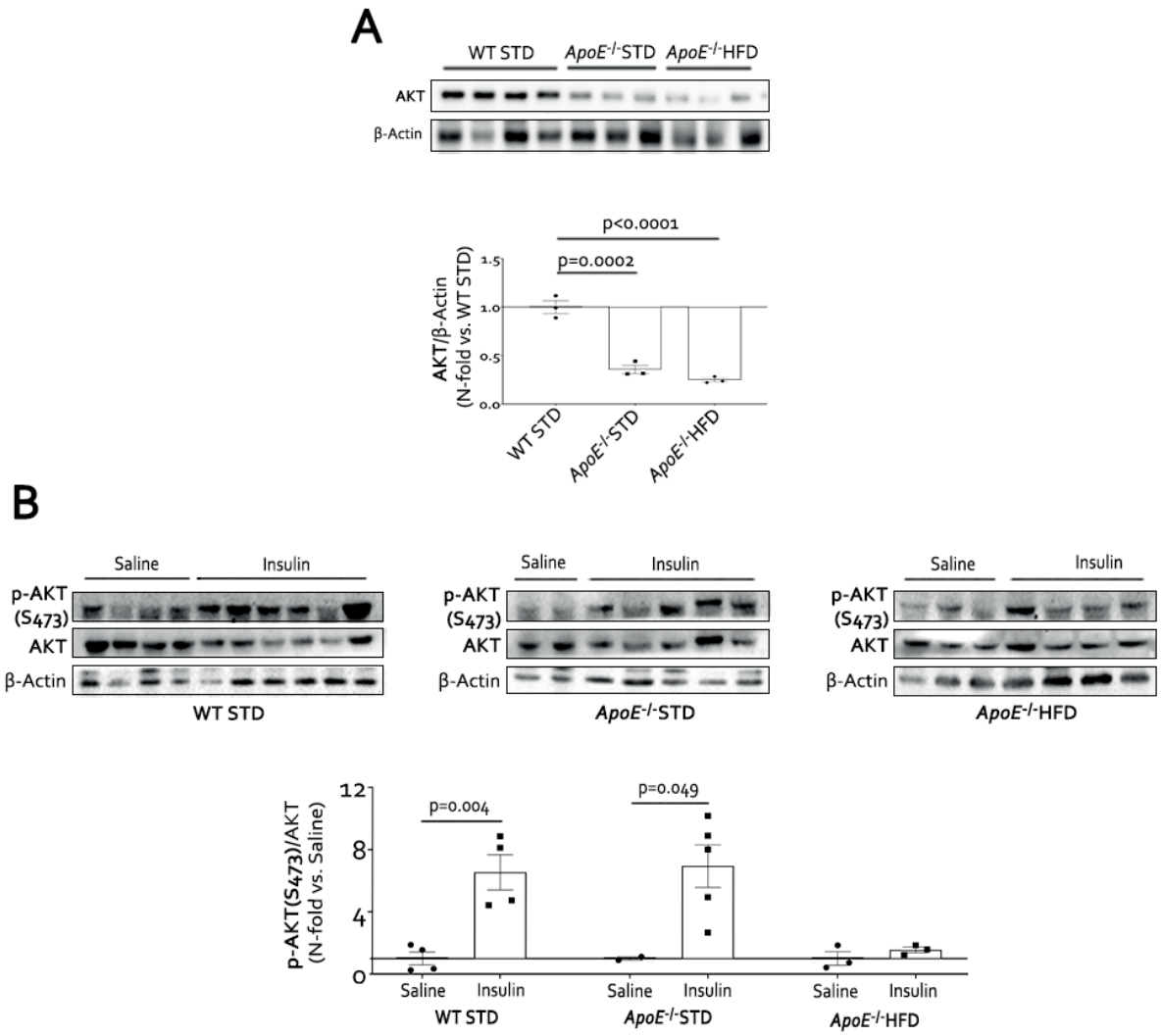

Figure 14. Analysis of AKT expression and insulin signalling in the aorta from the experimental model of atherosclerosis. **(A)** Representative Western blot images of the expression of AKT (upper) and their quantification (lower) in murine aorta samples. **(B)** Representative Western blot images of AKT phosphorylation in Ser473 (upper) and their quantification (lower) in aortas from mice subjected to *in vivo* insulin signalling studies. WT= wild-type; STD= standard type diet; A*poE*$^{-/-}$= apolipoprptein E deficient mice; HFD= high-fat diet; S=serine; AKT = protein kinase B. WT STD 18 wks (n = 4); A*poE*$^{-/-}$ STD 18 wks (n = 3); A*poE* $^{-/-}$ HFD 18 wks (n = 3). In vivo signalling experiments: WT STD 18 wks saline (n = 4); WT STD 18 wks insulin (n = 6); A*poE*$^{-/-}$ STD 18 wks saline (n = 2); A*poE*$^{-/-}$ STD 18 wks insulin (n = 5); A*poE*$^{-/-}$ HFD 18 wks saline (n = 3); A*poE*$^{-/-}$ HFD 18 wks insulin (n = 4).

AKT activation is essential in the target tissue for a proper response to insulin. To evaluate this response in the aortic tissue of our groups of mice, we performed *in vivo* insulin signalling. To do this, we intraperitoneally injected insulin or saline (as a control) into the mice 10 minutes before sacrifice, and then the aorta was harvested. By Western blot, the activation of AKT was analyzed, measuring the phosphorylation of its serine 473 residue (S473) in the aortas of the different WT, *ApoE*$^{-/-}$ STD and *ApoE*$^{-/-}$ HFD groups that were treated with saline or insulin. (Figure 14B). We found a significant increase in S473 phosphorylation induced by insulin administration in the WT and *ApoE*$^{-/-}$ STD groups. However, this increase was lost in the HFD group, confirming vascular insulin resistance (Figure 14B).

5.4.3. AKT is decreased in human atherosclerosis

AKT levels were also measured in paraffin-embedded aortic and carotid tissues from human samples (Figure 15A). Similar results to those obtained in the experimental model were found in human samples. So, AKT protein levels were significantly decreased in the ACA patients in relation to FAs samples (Figure 15B). Therefore, to confirm whether the levels of miR-155-5p and AKT were related in these patients, we performed Spearman's correlation analysis (Figure 15C). In the carotid of patients with atherosclerosis, miR-155-5p levels significantly and negatively correlated with the expression of AKT.

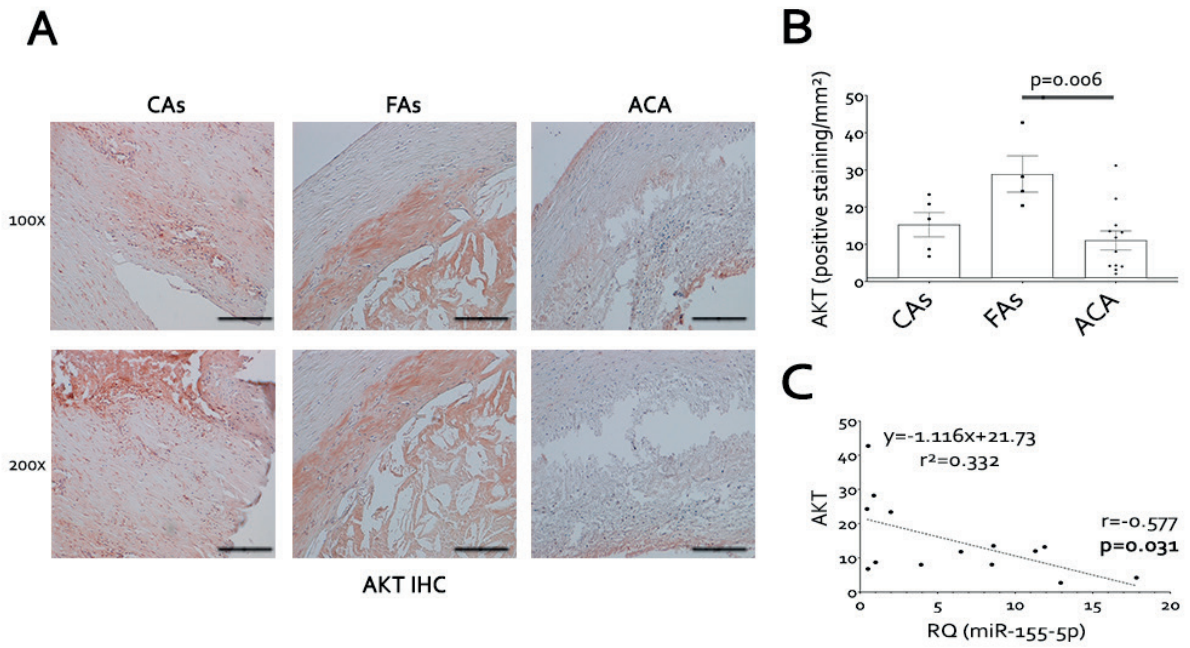

Figure 15. AKT expression decreases with the progression of atherosclerosis and is correlated with miR-155-5p expression in human plaques. Representative images of AKT levels measured by immunohistochemistry in the aorta and carotid human samples **(A)** and their quantification **(B)** expressed as % positive staining/mm2. Magnification 100× (scale bar = 100 µm); magnification 200× (scale bar = 50 µm). **(C)** Scatter plot and Spearman's r correlation analysis between the expression of miR-155-5p and AKT expression in human samples. CAs= control aorta; FAs= fibroatheroma; ACA= advanced carotid atherosclerotic plaque; IHC= immunohistochemistry; RQ = relative quantification; AKT = protein kinase B. CAs (n = 5); FAs (n = 4); ACA (n = 12). miR-155-5p-AKT correlation (n=14).

5.4.4. The levels of miR-155-5p and AKT are related to obesity

We also wanted to confirm whether the levels of miR-155-5p might be altered as the BMI augmented. We classified the patients according to their body mass index following the criteria established by the World Health Organization (lean BMI=18.5-24.9, overweight BMI=25.0-29.9, and obese BMI>30.0). We observed a significant increase in miR-155-5p expression (Figure 16A), as well as a progressive decrease in AKT (Figure 17A and B), as the BMI increased. This was supported by a significant and positive correlation between the BMI and miR-155-5p levels (Figure 16B) and a significant and inverse correlation between the BMI and AKT levels (Figure 17C).

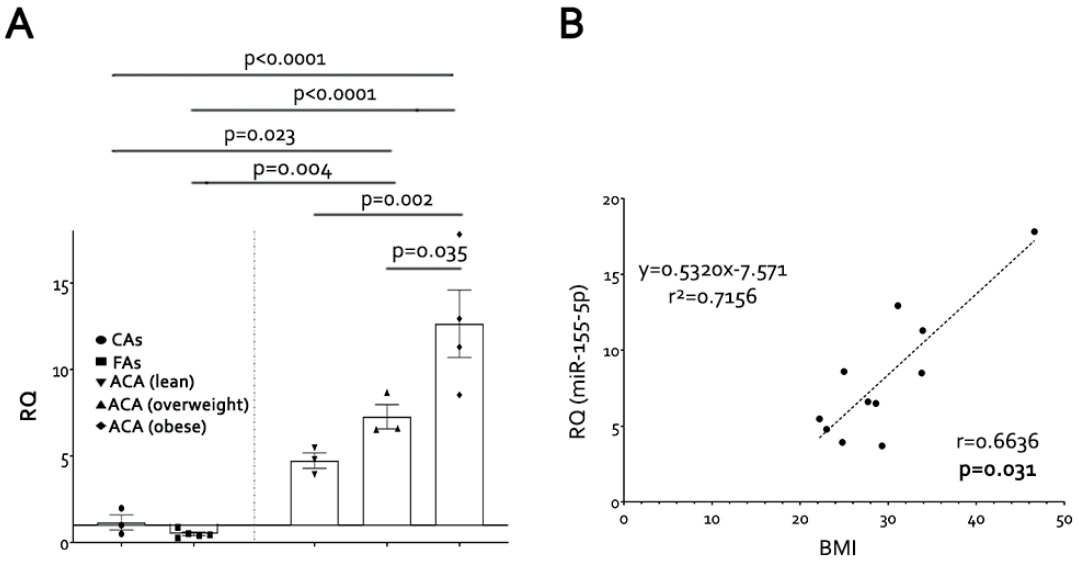

Figure 16. The expression of miR-155-5p is correlated with the BMI in human samples. (A) Expression levels of miR-155-5p in human carotid samples of patients stratified according to the BMI. miR-155-5p expression was quantified using RT-qPCR **(B).** Scatter plots and Spearman's r correlations between the BMI and miR-155-5p expression. CAs= control aorta; FAs= fibroatheroma; ACA= advanced carotid atherosclerosis; RQ = relative quantification; BMI= body mass index. miR-155-5p RT-qPCR: CAs (n = 3); FAs (n = 5); ACA (lean) (n = 3); ACA (overweight) (n = 3); ACA (obese) (n = 4). Correlation between miR-155-5p and BMI (n = 11).

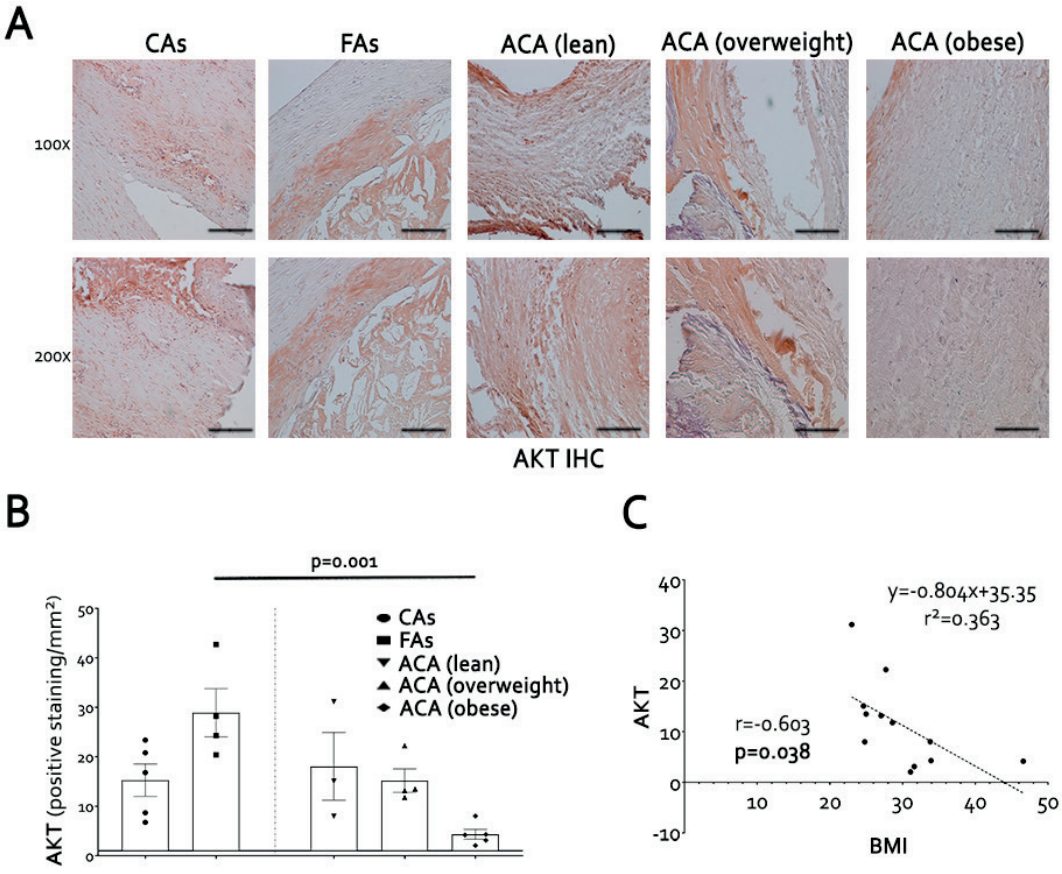

Figure 17. The expression of AKT is correlated with the BMI in human samples. Representative images of AKT immunohistochemistry **(A)** and their quantification **(B)** in human samples from patients stratified according to the BMI. Magnification 100× (scale bar = 100 µm); magnification 200× (scale bar = 50 µm). **(C)** Scatter plots and Spearman's r correlations between the BMI and AKT expression. AKT levels and BMI. CAs= control aorta; FAs= fibroatheroma; ACA= advanced carotid atherosclerosis; RQ = relative quantification; AKT = protein kinase B; IHC=immunohistochemistry. CAs (n = 5); FAs (n = 4); ACA (lean) (n = 3); ACA (overweight) (n = 4); ACA (obese) (n = 5). Correlation between AKT and BMI (n = 12).

5.4.5. miR-155-5p levels and its relationship with diabetes and instability of carotid plaques

The levels of miR-155-5p in the vascular tissues of the patients were also studied and compared to other clinical characteristics that we had access to, for example, if the patients were diabetic or not, and if a patient was asymptomatic or symptomatic.

First, we separated the patients with advanced carotid atherosclerosis into diabetic and non-diabetic, and in this case, the levels of miR-155-5p were statistically higher in the diabetic patients than in the other groups (Figure 18A). Secondly, we divided the ACA patients whether they had an asymptomatic or symptomatic atherosclerosis, also in this case, miR-155-5p was overexpressed in the symptomatic patients in comparison with the rest (Figure 18B), and the asymptomatic patients also had a higher expression of this miRNA when compared to FAs subjects (Figure 18B).

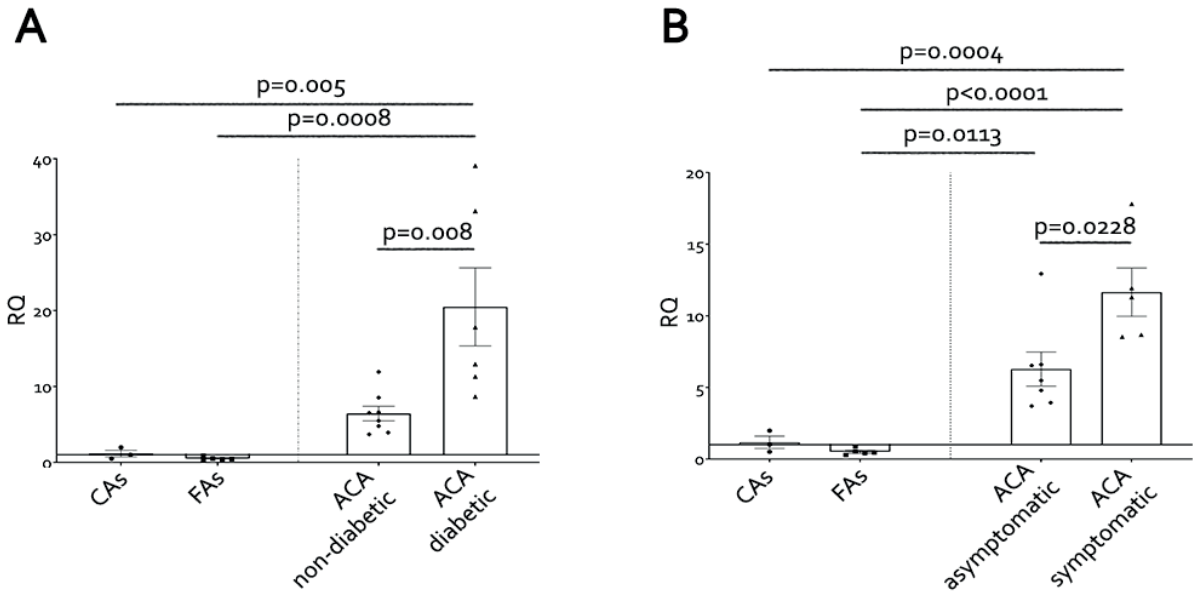

Figure 18. The expression of miR-155-5p is related with different clinical characteristics. (A) ACA patients were divided into diabetic and non-diabetic, and the expression of miR-155-5p was assessed by RT-qPCR. **(B)** ACA patients were divided into symptomatic and asymptomatic and the expression of miR-155-5p was studied by RT-qPCR. CAs= control aorta; FAs= fibroatheroma; ACA= advanced carotid atherosclerosis; RQ = relative quantification. CAs (n=3); FAs (n=5); ACA (non-diabetic (n=8)); ACA (diabetic (n=6)); ACA (asymptomatic (n=7)); ACA (symptomatic (n=5)).

5.4.6. miR-155-5p modulates the levels of AKT and eNOS in HUVECs

After the *in silico* search for confirmed or potential targets for miR-155-5p, not only AKT appeared to be an interesting target, but on a cellular scale, we also wanted to confirm whether this miRNA was able to downregulate eNOS.

We began by confirming the induction of miR-155-5p in the cells by RT-qPCR (Figure 19), the cells were transfected with mimic-miR-155-5p, and the RT-qPCR showed a significant increase in the miRNA levels in comparison with the control, vehicle, and cells transfected with mimic-miR-143-3p (Figure 19).

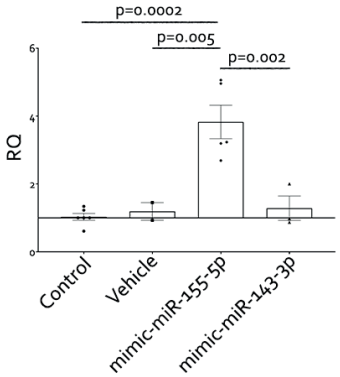

Figure 19. The levels of miR 155-5p were increased by the mimic transfection. The cells were transfected with mimic-miR-155-5p, and the induction was assessed by RT-qPCR. RQ = relative quantification. All the *in vitro* experiments were performed at least in triplicate.

When the overexpression of miR-155-5p was confirmed, we studied the effect of this induction on the chosen targets, AKT (Figure 20A) and eNOS (Figure 20B); in both cases, the expression of both proteins was decreased by the mimic-miR-155-5p.

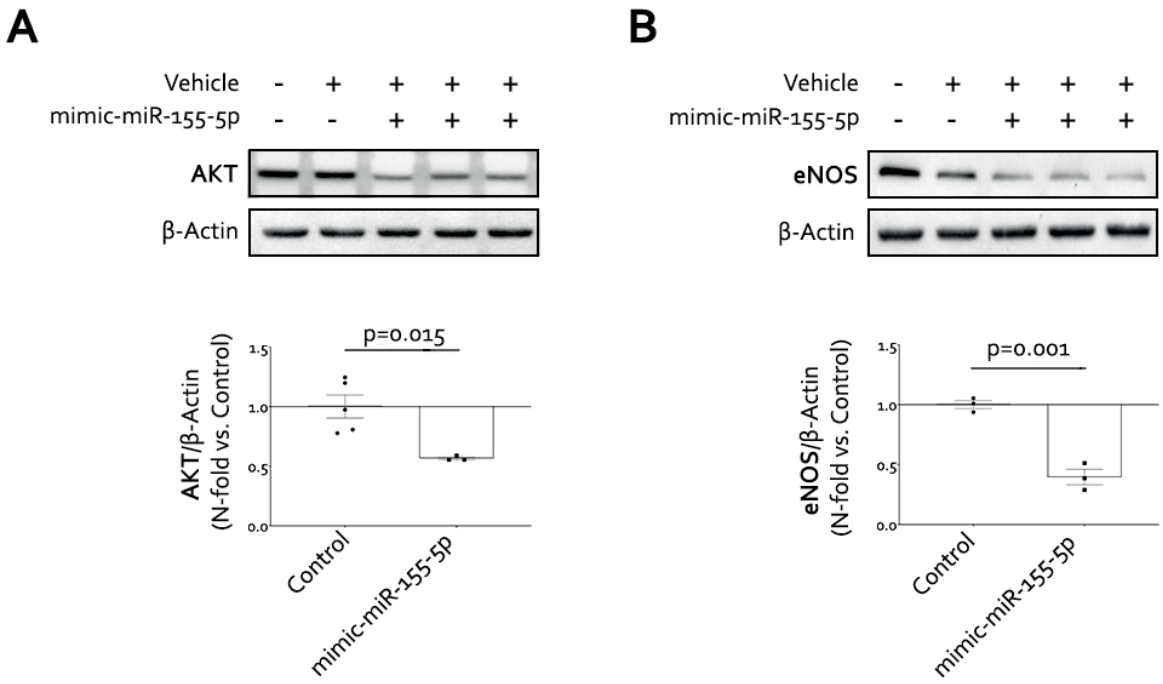

Figure 20. miR-155-5p modulates the expression of AKT and eNOS in HUVECs. HUVECs were transfected with mimic-miR-155-5p and its effect on AKT **(A)** and eNOS **(B)** expression was analysed by Western blot. AKT= protein kinase B; eNOS= endothelial nitric oxide synthase. All the *in vitro* experiments were performed at least in triplicate.

5.4.7. miR-155-5p modulates p85α, AKT, and insulin resistance in VSMCs

In VSMCs, the studied targets of miR-155-5p were AKT and p85α, both proteins had been previously confirmed by other authors and they are part of insulin signalling pathway. Therefore, we transfected the VSMCs with the mimic-miR-155-5p. After transfection, we first evaluated the effect of miR-155-5p on selected targets in VSMCs by Western blot. In both cases, miR-155-5p overexpression significantly decreased the expression of AKT (Figure 21A) and p85α (Figure 21B) in VSMCs.

AKT is a protein that requires two phosphorylations to be fully active: one in the residue T308 and the second in the S473; when the last phosphorylation occurs, is when the protein is fully active. To determine the effect of miR-155-5p on insulin-mediated AKT activation, we stimulated VSMCs with insulin (100 nM) for 10 minutes in the presence or absence of mimic-miR-155-5p and measured the phosphorylation of S473 in AKT by Western blot. In fact, VSMCs overexpressing miR-155-5p showed a significant reduction in AKT phosphorylation in S473 after insulin stimulation (Figure 21C).

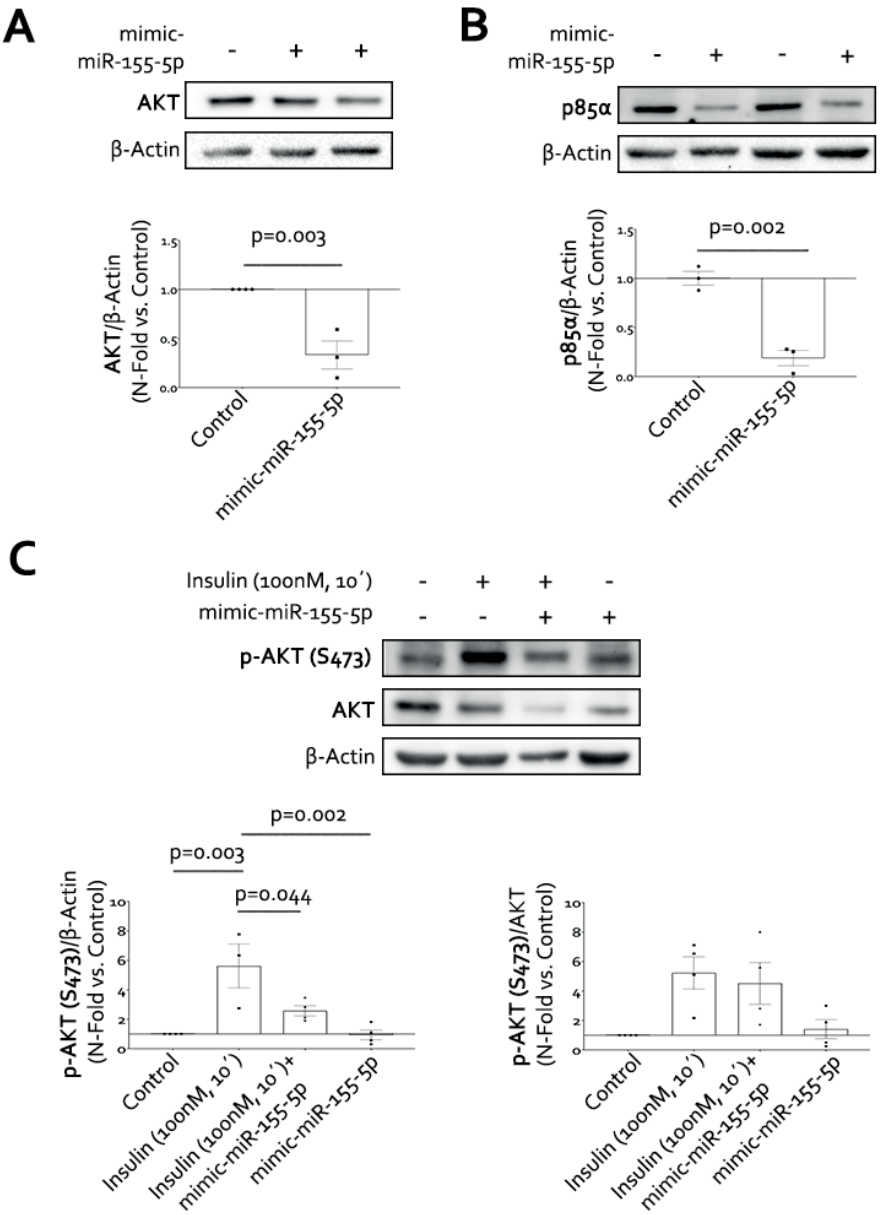

Figure 21. miR-155-5p modulates targets from the insulin pathway, such as p85α and AKT, thereby regulating insulin resistance in VSMCs. Representative Western blot images of the expression of AKT **(A)** and p85α **(B)** and their quantification in transfected VSMCs. **(C)** Representative Western blot images of AKT phosphorylation in response to insulin stimulation in transfected VSMCs and their quantification. VSMCs were deprived of FBS for 6h and then stimulated with 100 nM insulin for 10 minutes, and the activation of AKT by insulin was measured by the phosphorylation on S473. AKT= protein kinase B; S= serine; p85α= phosphoinositide 3-kinase regulatory subunit p85 alpha. All the *in vitro* experiments were performed at least in triplicate.

5.5. Role of miR-15a-5p and miR-199a-3p in the progression of atherosclerosis

5.5.1. miR-15a-5p and miR-199a-3p are decreased in experimental and human atherosclerosis

The expression of miR-15a-5p and miR-199a-3p was analysed in whole aorta lysates from the 18-weeks mice groups and paraffin-embedded aortic tissue from the patients by RT-qPCR. miR-15a-5p expression was decreased in the aorta from *ApoE*$^{-/-}$ HFD group (Figure 22A), and the same was observed in the ACA patients in comparison with subjects CAs and FAs (Figure 23A). When comparing atherosclerosis progression in the mice and miR-15a-5p expression, there was a significant and inverse correlation between miR-15a-5p levels and the percentage of lipid deposition (Figure 22B) and lesion area (Figure 22C).

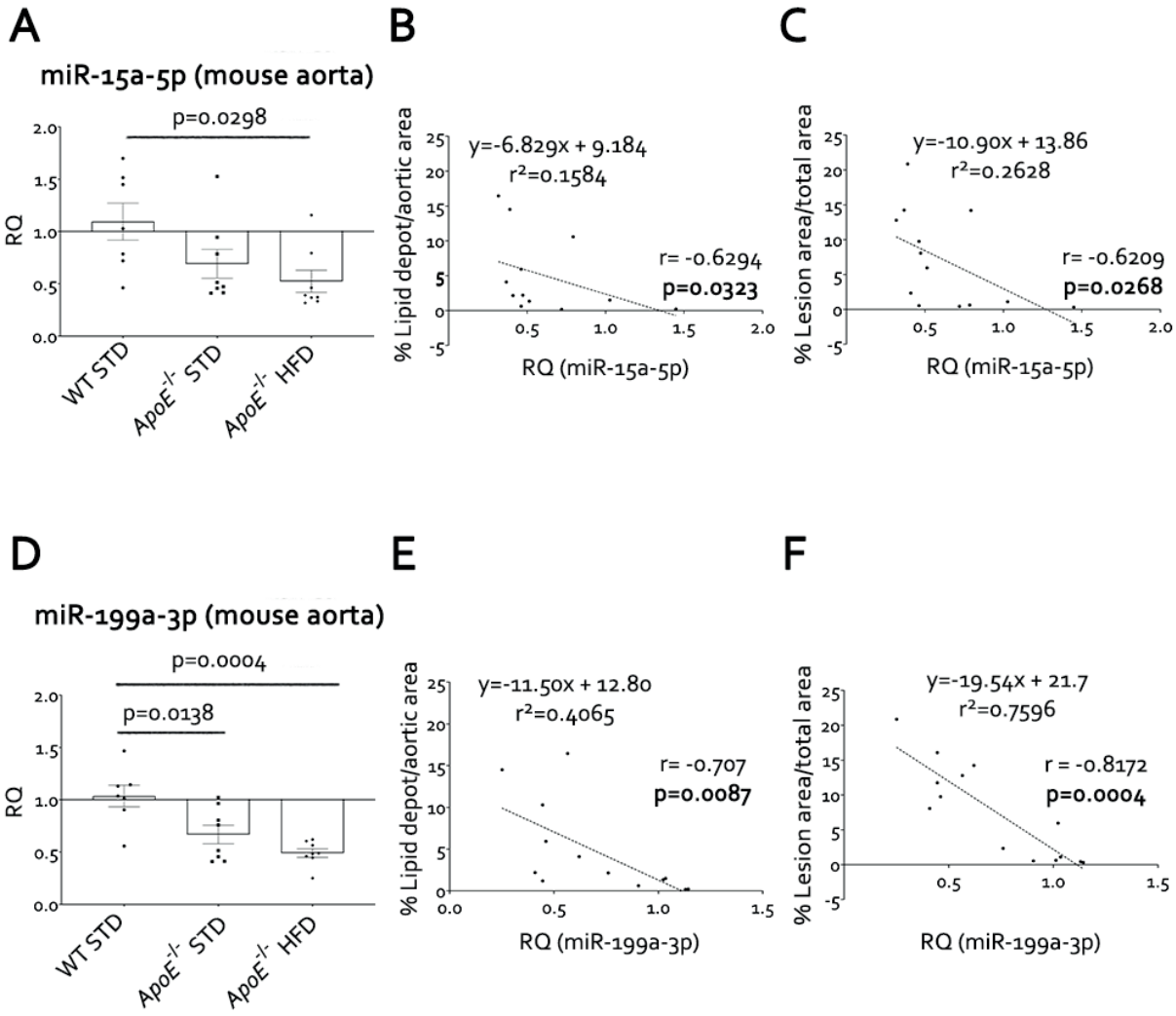

Figure 22. miR-15a-5p and miR-199a-3p are downregulated in the experimental model of atherosclerosis. The expression of miR-15a-5p **(A)** and miR-199a-3p **(D)** was quantified by RT-qPCR in the aorta of the 18-weeks fed mice. By Spearman's correlation, we set different correlations between miR-15a-5p and % lipid deposition/aortic area **(B)**, and % lesion area/total area **(C)** and miR-199a-3p and % lipid deposition/aortic area **(E)** and % lesion area/total area **(F)**. WT= wild-type; STD= standard type diet; *ApoE*$^{-/-}$= apolipoprotein E deficient mice; HFD= high-fat diet; RQ = relative quantification. WT STD (n=7); *ApoE*$^{-/-}$ STD (n=8); *ApoE*$^{-/-}$ HFD (n=8). Correlation between miR-15a-5p and atherosclerosis (n=14). Correlation between miR-199a-3p and atherosclerosis (n=14).

The expression of miR-199a-3p was also significantly downregulated in the *ApoE*$^{-/-}$ HFD group compared to the WT STD, but also in the *ApoE*$^{-/-}$ STD group compared to the WT STD (Figure 22D). However, this miRNA was only decreased in human advanced atherosclerosis samples, compared with subjects with FAs (Figure 23B). In addition, the expression of miR-199a-3p in mice was significantly correlated with the percentages of lipid deposition/aortic area (Figure 22E) and lesion area/total area (Figure 22F) in the aortic root as happened with miR-15a-5p.

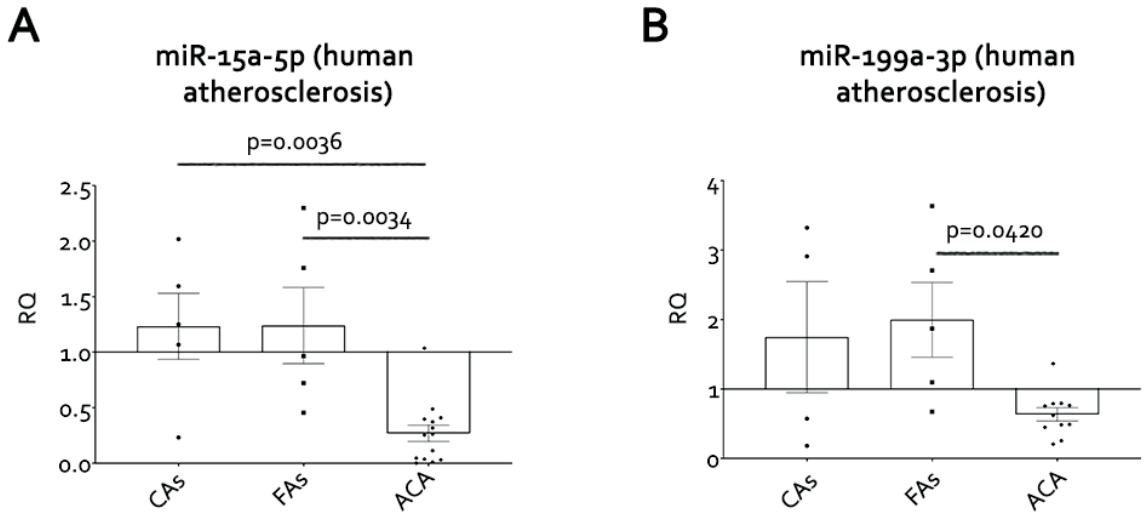

Figure 23. miR-15a-5p and miR-199a-3p are downregulated in human atherosclerosis. The expression of miR-15a-5p **(A)** and miR-199a-3p **(B)** was quantified by RT-qPCR in aorta from subjects without atherosclerosis, and subjects with initial atherosclerosis and in carotid from patients with advanced atherosclerosis. CAs= control aortas; FAs= fibroatheroma; ACA= advanced carotid atherosclerosis; RQ= relative quantification. CAs (n=5); FAs (n=5); ACA (n=14).

After that, we were interested in finding potential targets of both miRNAs. In the case of miR-15a-5p, we chose to study four possible targets, IKKα and IKKβ, which are catalytic subunits of IKK complex and induce the activation of NF-κB pathway, as well as LOX-1 and mTOR (Figure 24A, B and E). And for miR-199a-3p, searching for possible targets in miRNA target interaction databases resulted in the selection of IKKβ and p65, both components of the NF-κB pathway as well as mTOR (Figure 24 C-E).

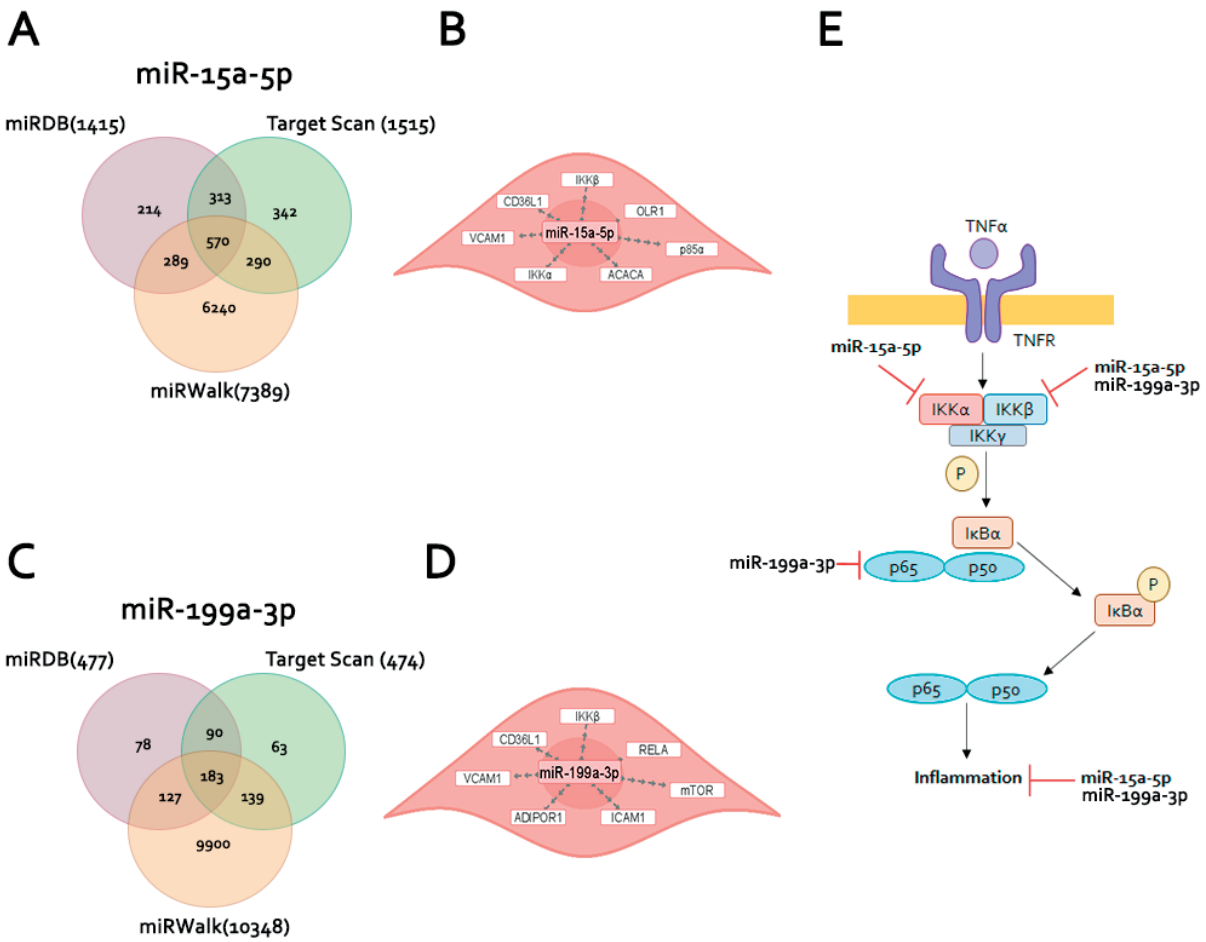

Figure 24. *In silico* search for possible targets of miR-15a-5p and miR-199a-3p. We performed a search in different miRNA-target databases to choose potential pro-atherosclerotic proteins modulated by miR-15a-5p and miR-199a-3p, with those results we performed a Venn diagram representing different results obtained from miR-15a-5p **(A)** and miR-199a-3p **(C)** in databases, such as miRDB, TargetScan, and miRWalk. Graphics showing possible miR-15a-5p **(B)** and miR-199a-3p **(D)** targets. **(E)** Graphical scheme of NF-κB pathway and its modulation by miR-15a-5p or/and miR-199a-3p. IKK= inhibitor of nuclear factor kappa B. Subunits alpha, beta and gamma (IKKα/β/γ); IκBα =nuclear factor-kappa B inhibitor alpha.

5.5.2. IKKα, IKKβ and p65 are increased in the aorta of *ApoE*$^{-/-}$ mice

To assess the expression of our selected possible targets, IKKα (miR-15a-5p), IKKβ (miR-15a-5p and miR-199a-3p), and p65 (miR-199a-3p), we homogenized the aortas of the different groups in a buffer to isolate the total proteins that were studied by Western blot (Figure 25A).

The expression of IKKα was increased in the *ApoE*$^{-/-}$ group fed a HFD, compared with the WT STD group (Figure 25A and B); p65 was also increased in the HFD group compared with the *ApoE*$^{-/-}$ STD and WT STD groups (Figure 25A and B). This increase of p65 was confirmed by immunofluorescence of p65 in the aortic roots showing that the protein was increased in endothelial cells (Figure 27) and VSMCs (Figure 28) from *ApoE*$^{-/-}$ HFD. In addition, the levels of IκBα, inhibitory subunit of the NF-κB, were also found to be lower in aorta from *ApoE*$^{-/-}$ HFD than in the control group (Figure 25B).

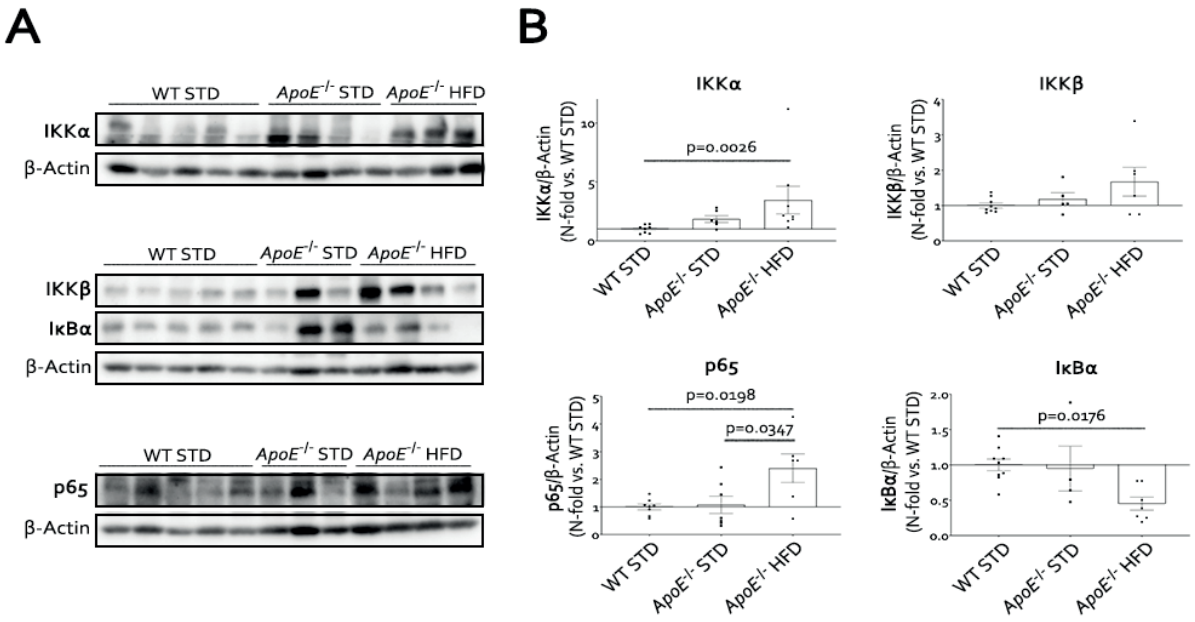

Figure 25. The expression of IKKα, IKKβ and p65 is upregulated in the aorta from *ApoE*$^{-/-}$ mice by HFD. (A) Representative Western blot images from the aorta of the three groups. **(B)** Measurement of the levels of IKKα, IKKβ, IκBα and p65 by Western blot in the aorta of the experimental groups. IKKα= inhibitor of nuclear factor-kappa B kinase subunit alpha; IKKβ= inhibitor of nuclear factor-kappa B kinase subunit beta; IκBα= nuclear factor kappa-B kinase inhibitor alpha; WT= wild-type; STD= Standard type diet; *ApoE*$^{-/-}$= apolipoprotein E deficient mice; HFD= high-fat diet. WT STD (n=9); *ApoE*$^{-/-}$ STD (4-6); *ApoE*$^{-/-}$ HFD (n=6-8).

Since IKKβ showed a tendency to be increased in the aorta of the HFD group by Western blot, but without statistical significance (Figure 25B), we performed an IHC against IKKβ in the aortic root of all the mouse groups (Figure 26A), confirming that IKKβ was increased in the *ApoE*$^{-/-}$ HFD group (Figure 26B).

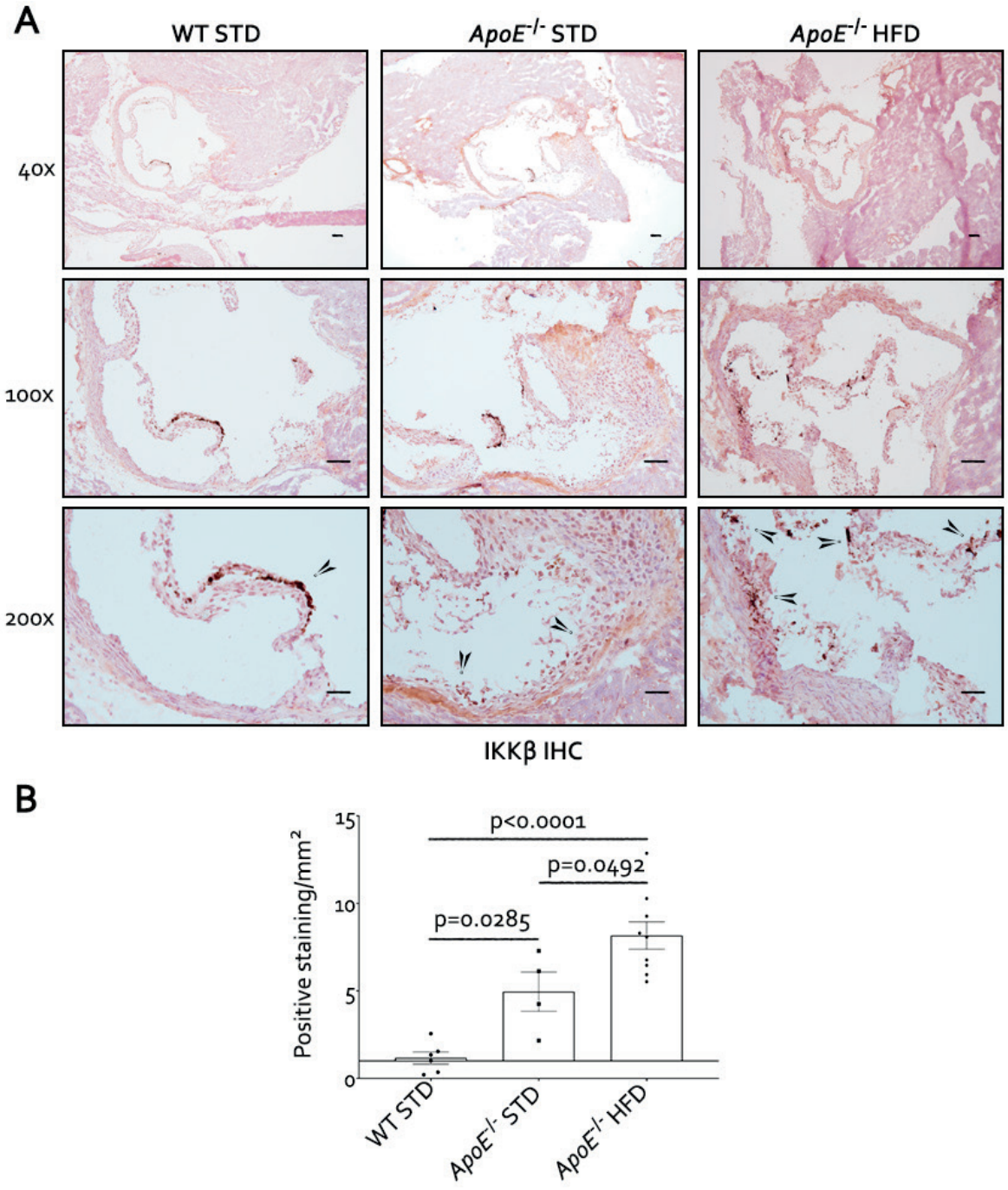

Figure 26. The expression of IKKβ was increased in the aortic root from *ApoE*$^{-/-}$ mice. Representative images **(A)** and quantification **(B)** from the immunohistochemistry of IKKβ in the aortic root of the experimental groups. Magnification 100x (scale bar=100 µm); magnification 200x (scale bar=50 µm). IKKα= Inhibitor of kappa-B kinase subunit alpha; IKKβ= inhibitor of nuclear factor-kappa B kinase subunit beta; WT= wild-type; STD= standard type diet; *ApoE*$^{-/-}$ = apolipoprotein E deficient mice; HFD= High-fat diet; IHC= Immunohistochemistry. WT STD (n=6); *ApoE*$^{-/-}$ STD (4); *ApoE*$^{-/-}$ HFD (n=9).

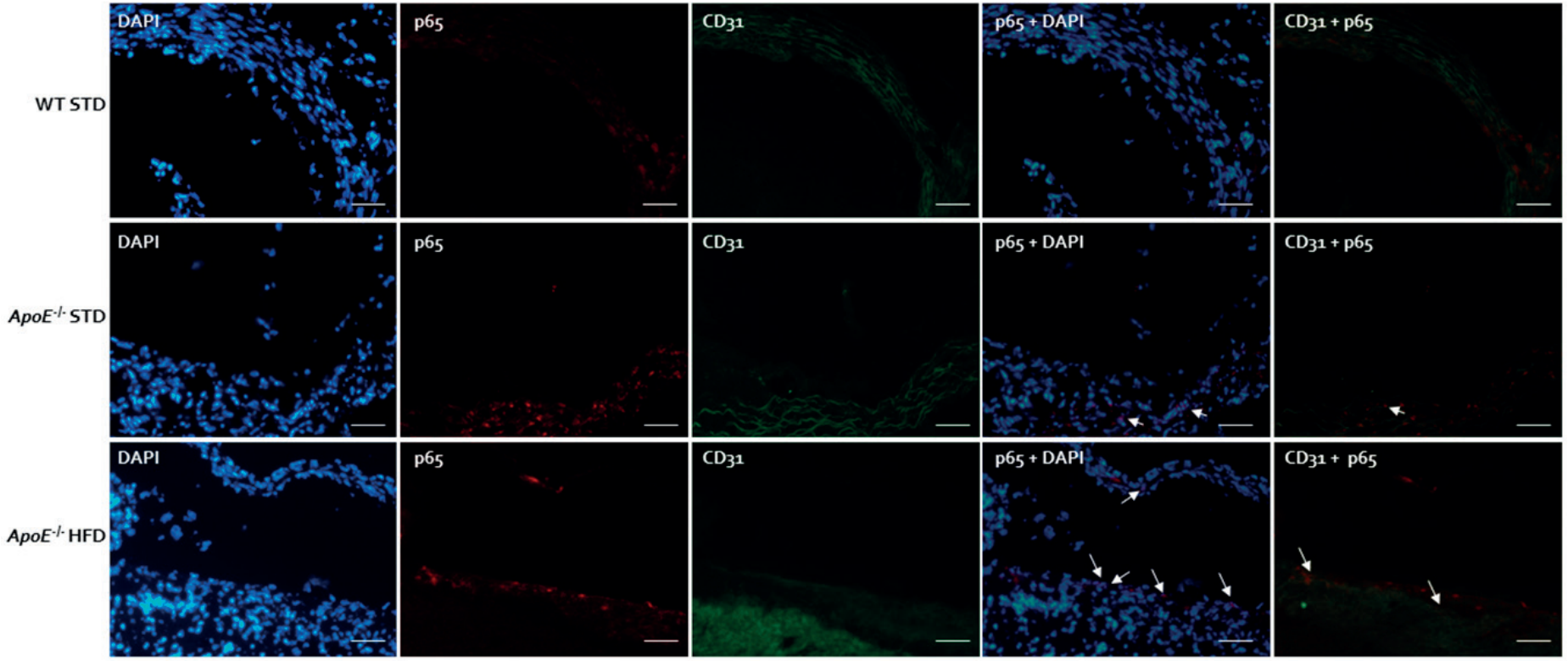

Figure 27. Active p65 levels in endothelial cells from aortic roots in the experimental model of atherosclerosis. In aortic roots from WT STD 18 wks, *ApoE*$^{-/-}$ STD 18 wks and *ApoE*$^{-/-}$ HFD 18 wks, we analyzed the colocalization of p65 (red) and nuclei (blue) to detect active p65 (p65 merged with DAPI). Moreover, we also colocalized p65 with CD31 (green) to detect endothelial cells that express p65 (p65 merged with CD31). Magnification 200x, scale bar = 50 µm. WT= wild-type; STD= standard type diet; *ApoE*$^{-/-}$= apolipoprotein E deficient mice; HFD= High-fat diet. WT STD (n=6); *ApoE*$^{-/-}$ STD (n=4); *ApoE*$^{-/-}$ HFD (n=9).

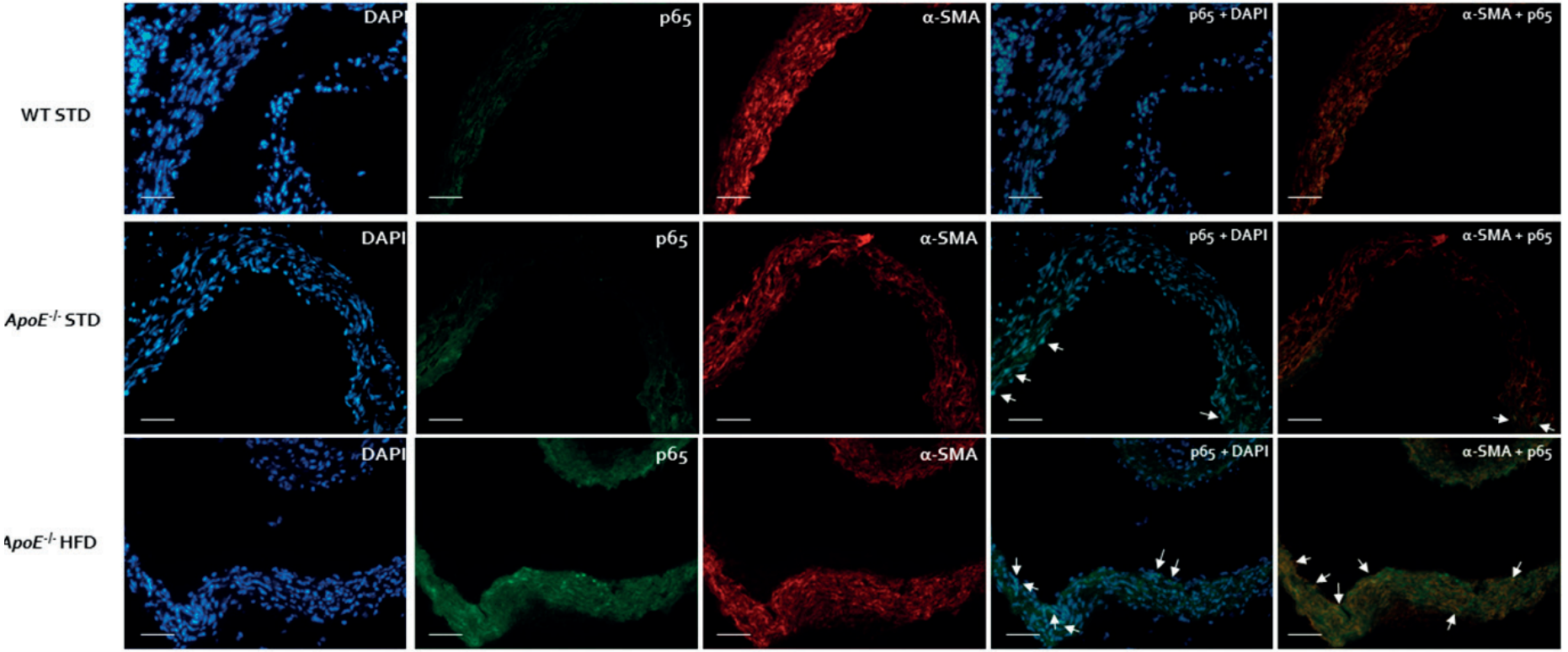

Figure 28. Active p65 levels in vascular smooth muscle cells from aortic roots in the experimental model of atherosclerosis. In aortic roots from WT STD 18 wks, *ApoE*$^{-/-}$ STD 18 wks and *ApoE* $^{-/-}$ HFD 18 wks, we analyzed the colocalization of p65 (green) and nuclei (blue) to detect active p65 (p65 merged with nuclei). Moreover, we also colocalized p65 with α-SMA to detect VSMCs that express p65 (p65 merged with α-SMA). Magnification 200x, scale bar = 50 µm. WT= wild-type; STD= standard type diet; *ApoE*$^{-/-}$= apolipoprotein E deficient mice; α-SMA= alpha-smooth muscle actin; HFD= High-fat diet. WT STD (n=6); *ApoE*$^{-/-}$ STD (n=4); *ApoE*$^{-/-}$ HFD (n=9).

5.5.3. The expression of IKKα, IKKβ and p65 is increased in human advanced atherosclerosis

When we confirmed that the expression of our selected targets was increased in the aorta from the mouse model, the next step was to study their expression in our human samples.

First, we performed IHC against IKKα in CAs, FAs, and ACA (Figure 29A), that showed an increased expression in the ACA compared with the control groups (Figure 29B). This protein is a possible target for miR-15a-5p, so we correlated the expression of both by a Spearman's correlation that confirmed that these molecules were related (Figure 29C).

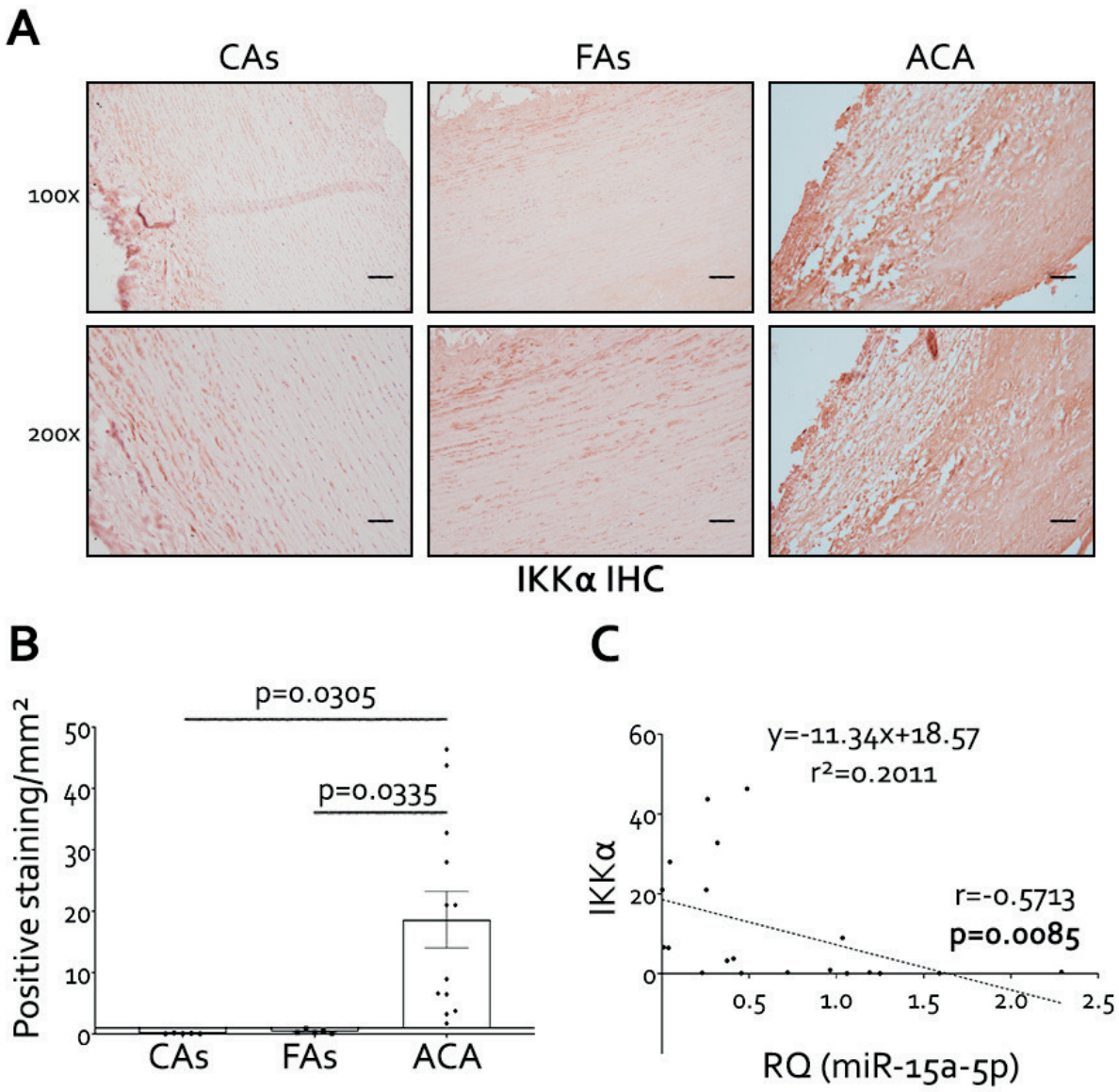

Figure 29. The expression of IKKα is upregulated in carotid plaques from patients with advanced atherosclerosis. (A) Representative images from the IHC of IKKα. Magnification 100x (scale bar = 100 μm); magnification 200x (scale bar = 50 μm). The expression of IKKα **(B)** was measured and the relation with miR-15a-5p expression (C) was tested by a Spearman's correlation. IKKα= inhibitor of nuclear factor kappa-B kinase subunit alpha; CAs= control aortas; FAs= fibroatheromas; ACA= advanced carotid atherosclerosis; RQ= relative quantification; IHC= immunohistochemistry. CAs (n=5); FAs (n=5); ACA (n=12). Correlation between miR-15a-5p and IKKα (n=12).

Then we performed IHC against IKKβ in our samples from human subjects (Figure 30A). IKKβ was also overexpressed in the ACA patients compared with the controls (Figure 30B). We also correlated the expression of miR-15a-5p and miR-199a-3p with this protein, but only the miR-15a-5p was correlated

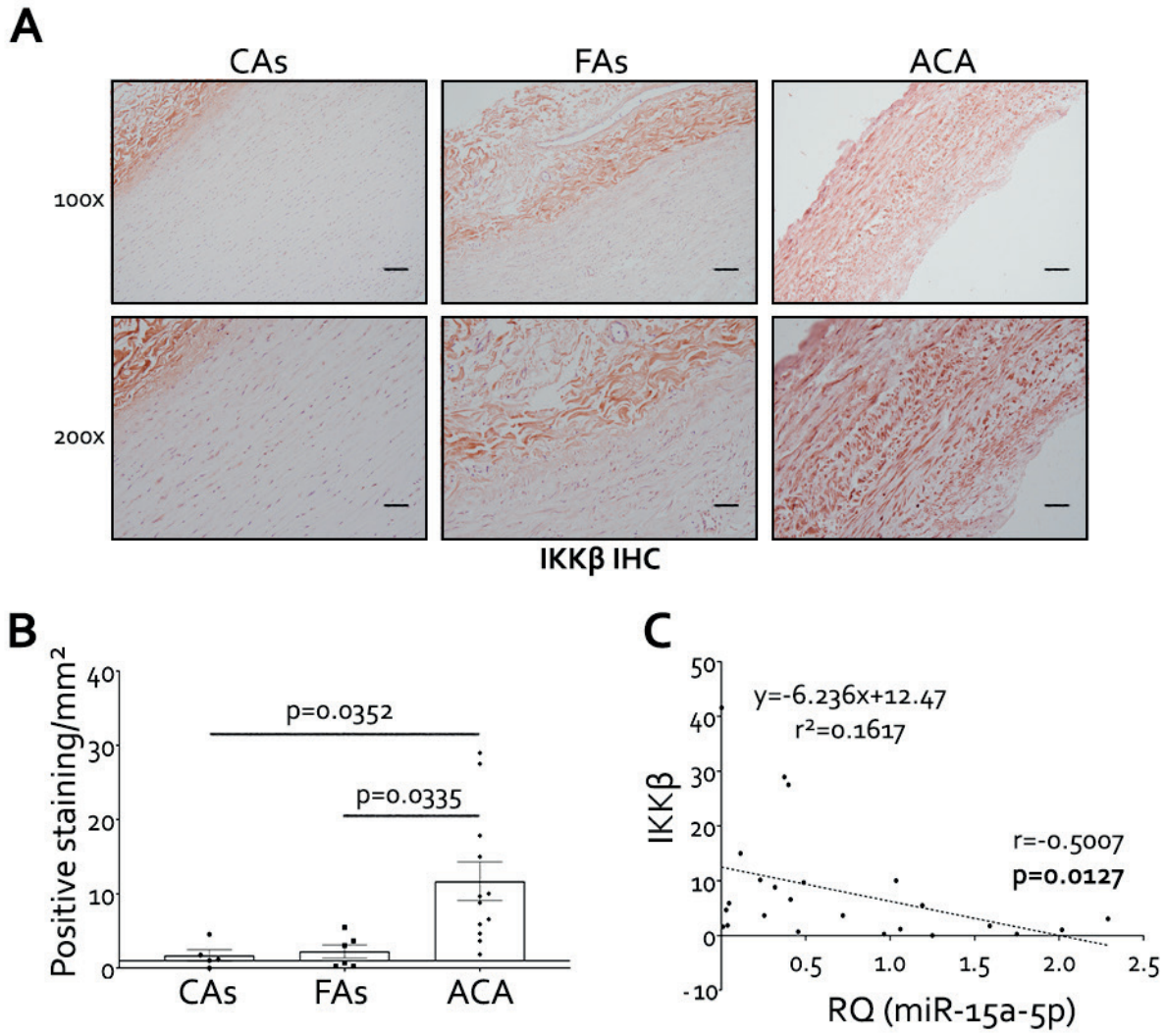

Figure 30. The expression of IKKβ is upregulated in carotid plaques from patients with advanced atherosclerosis. (A) Representative images from the immunohistochemistry of IKKβ. Magnification 100x (scale bar=100 μm); magnification 200x (scale bar=50 μm). The expression of IKKα **(B)** was measured and the relation with miR-15a-5p expression **(C)** was tested by a Spearman´s correlation. IKKβ= inhibitor of nuclear factor kappa-B kinase subunit beta; CAs= control aortas; FAs= fibroatheromas; ACA= advanced carotid atherosclerosis; RQ= relative quantification; IHC= immunohistochemistry. CAs (n=5); FAs (n=5); ACA (n=12). Correlation between miR-15a 5p and IKKβ (n=12).

Lastly, we did IHC against p65 in human vascular samples (Figure 31A). The levels of p65 were increased in the ACA patients compared with the controls (Figure 31B). Finally, we also correlated the expression of miR-15a-5p and miR-199a-3p with this protein, but only the miR-15a-5p levels negatively correlated with p65 in human atherosclerosis (Figure 31C).

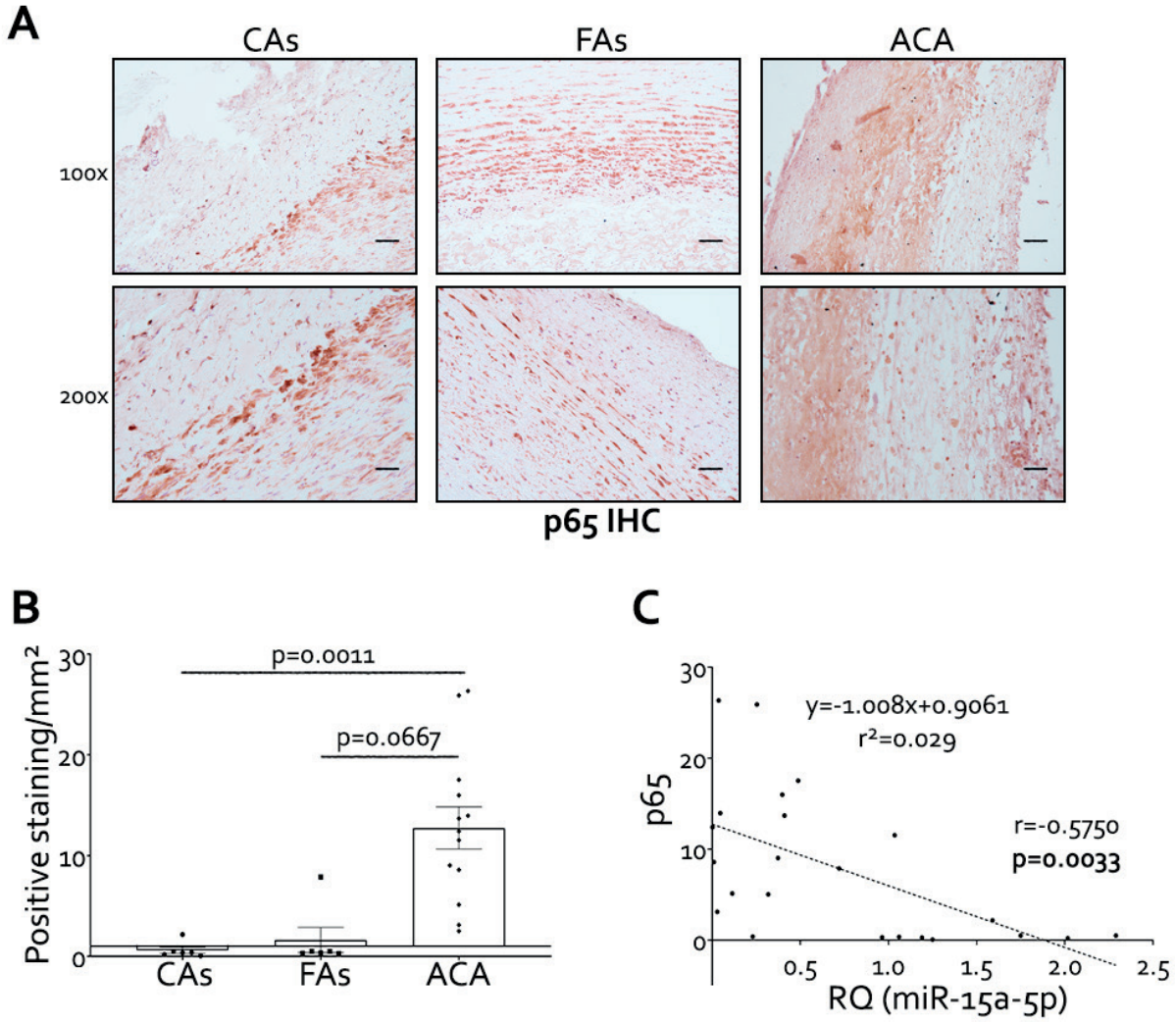

Figure 31. The expression of p65 is upregulated in carotid plaques from patients with advanced atherosclerosis. (A) Representative images from the immunohistochemistry of p65. Magnification 100x (scale bar=100 μm); magnification 200x (scale bar=50 μm). The expression of p65 **(B)** was measured and the relation with miR-15a-5p expression **(C)** was tested by a Spearman's correlation. CAs= control aortas; FAs= fibroatheromas; ACA= advanced carotid atherosclerosis; RQ= relative quantification; IHC= immunohistochemistry. CAs (n=5); FAs (n=5); ACA (n=12). Correlation between miR-15a-5p and p65 (n=12).

5.5.4. miR-15a-5p and miR-199a-3p modulate the expression of different inflammatory and proliferative targets in vascular cells

The next steps in our work were to study how miR-15a-5p affects the selected targets involved in NF-κB pathway in vascular cells. We began by inducing the expression of miR-15a-5p transfecting a mimic-miR-15a-5p in HUVECs (Figure 32A). Then, we analyzed the effect on the selected targets by Western blot (Figure 32B). After the induction of miR-15a-5p we obtained a significant decrease in the expression of IKKα, IKKβ and p65 (Figure 32C), nevertheless, we think the reduction in p65 expression was due to an indirect effect of the miRNA. In addition, we did not observe any change in IκBα levels (Figure 32C).

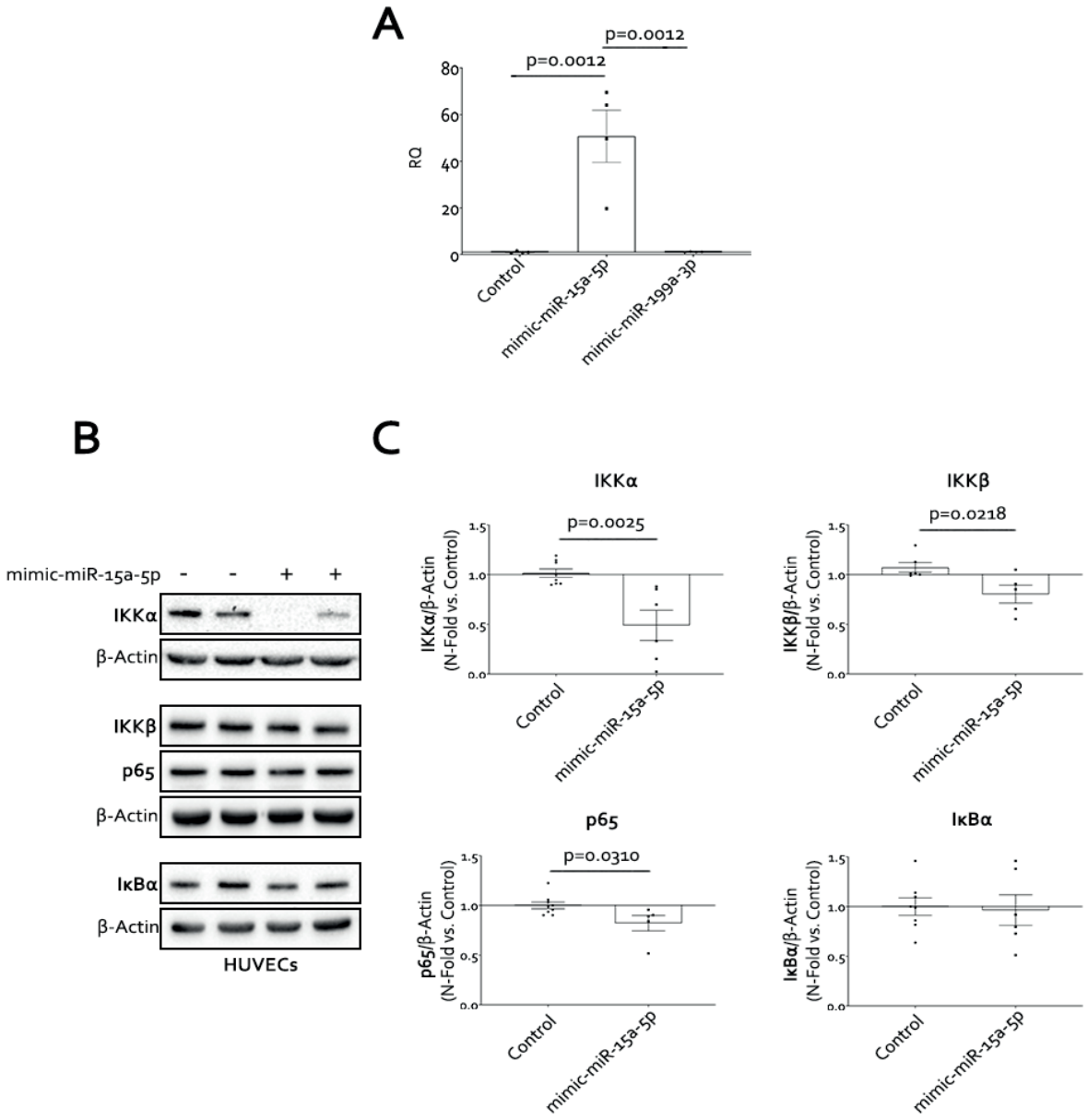

Figure 32. miR-15a-5p overexpression reduced IKKα, IKKβ and p65 levels in endothelial cells. HUVECs were transfected with mimic-miR-15a-5p for 72h. The increase in miRNA expression was measured by RT-qPCR **(A)**. The silencing effect miR-15a-5p has on their targets IKKα (**C**, upper-left) and IKKβ (**C**, upper-right), as well as p65 (**C**, lower-left) and IκBα (**C**, lower-right), was analysed by Western blot 96h after transfection **(B)**. IKKα= inhibitor of nuclear factor kappa-B kinase subunit alpha; IKKβ= inhibitor of nuclear factor kappa-B kinase subunit beta; IκBα= nuclear factor kappa-B kinase inhibitor alpha; HUVECs = Human umbilical vein endothelial cells; RQ= relative quantification. All the *in vitro* experiments were performed at least in triplicate.

In addition, we also evaluated whether miR-15a-5p overexpression might reduce the same protein targets in VSMCs. First, we performed an RT-qPCR to confirm the increase in miR-15a-5p expression by the mimics in VSMCs (Figure 33A). Afterwards, we confirmed that miR-15a-5p overexpression decreased the expression of our selected targets (Figure 33B-C). We achieved a significant decrease of IKKβ, and p65 (Figure 33B) amongst other possible targets like mTOR (Figure 33C), important for the VSMCs phenotype-switching.

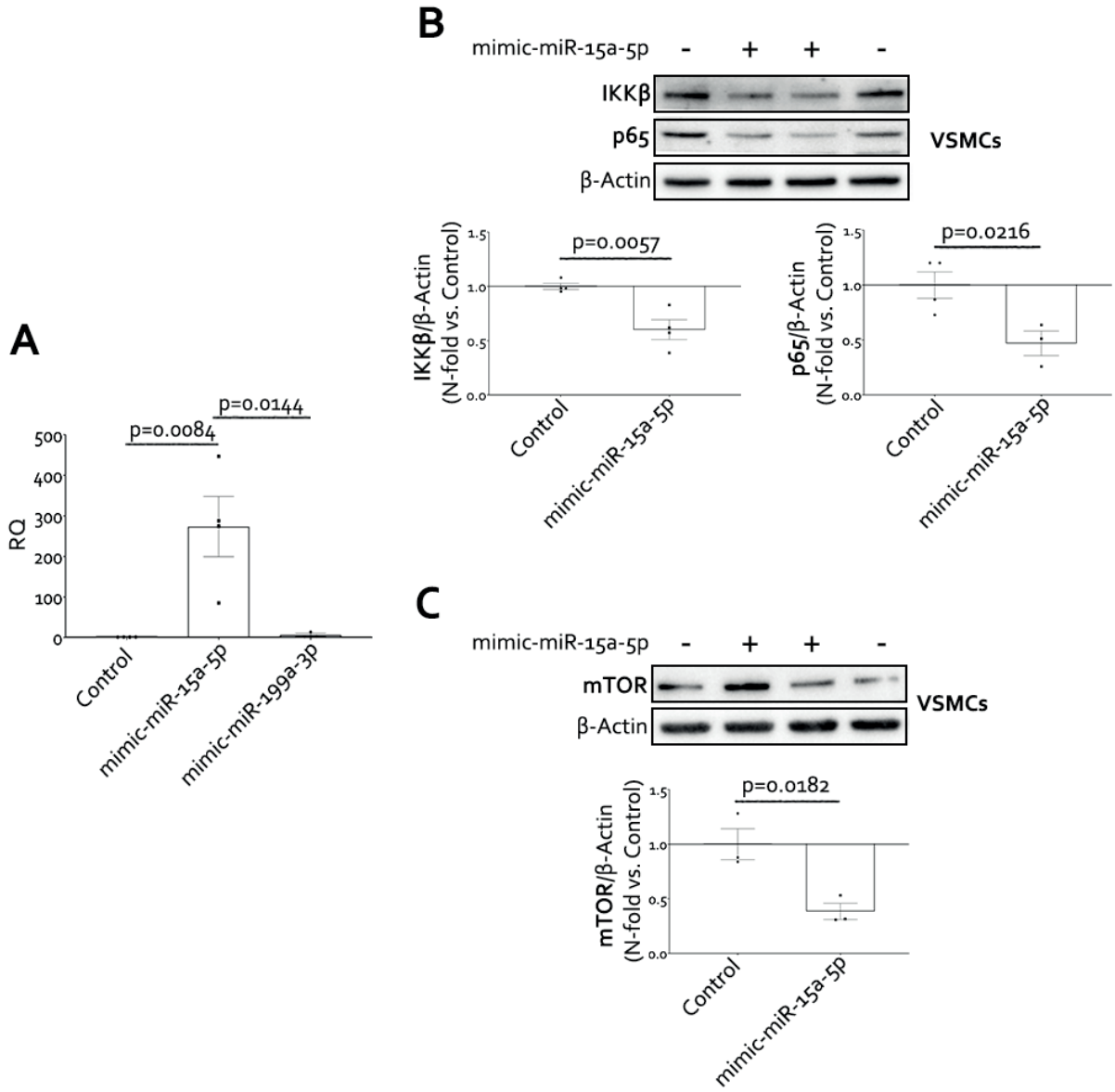

Figure 33. miR-15a-5p overexpression reduced IKKβ, p65, and mTOR expression in VSMCs. VSMCs were transfected with mimic-miR-15a-5p for 48h. The increase in miRNA expression was measured by RT-qPCR **(A)**. The silencing effect of miR-15a-3p for 48h has on their targets IKKβ (**B**, upper-left), p65 (**B**, upper-right), and mTOR **(C)**, was analysed by Western blot **(B-C)**. IKKβ= inhibitor of nuclear factor kappa-B kinase subunit beta; mTOR= mammalian target of rapamycin; VSMCs= vascular smooth muscle cells; RQ= relative quantification. All the *in vitro* experiments were performed in triplicate.

Next, we wanted to confirm that miR-199a-3p was also capable of doing the same observed in miR-15a-5p, we induced miR-199a-3p overexpression using mimic-miRNAs (Figure 34A). Then, the expression of the selected targets, IKKβ and p65, were studied by Western blot (Figure 34B). In HUVECs, there was a significant decrease in these proteins in the presence of the mimic-miR-199a-3p (Figure 34C). Surprisingly, there was also a significant decrease in the expression of IκBα, but this must be a secondary effect of the miRNA overexpression.

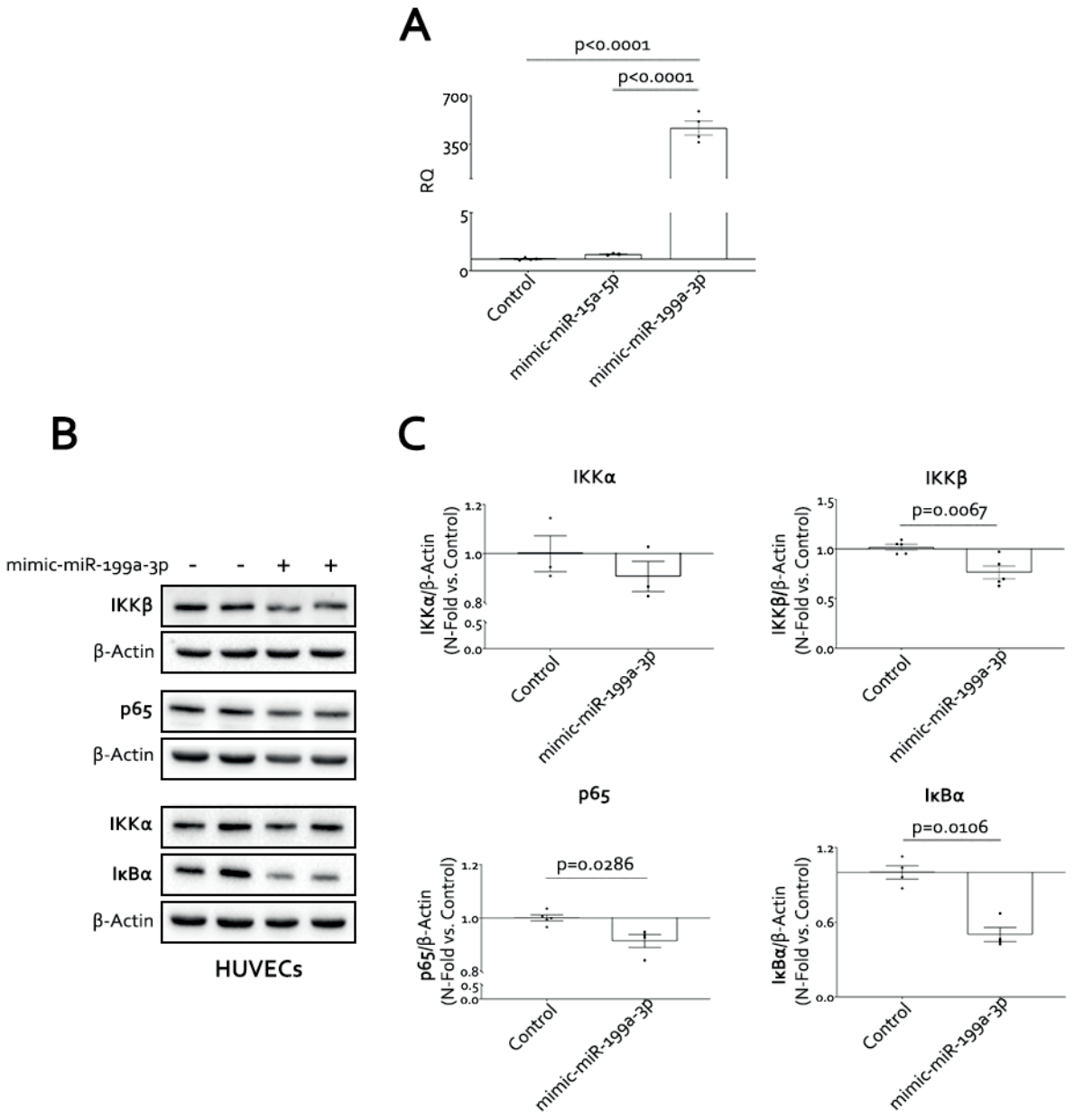

Figure 34. miR-199a-3p overexpression reduced IKKβ, p65 and IκBα expression in endothelial cells. (A) HUVECs were transfected with mimic-miR-199a-3p for 72h. The increase in miRNA expression was measured by RT-qPCR. **(B)** The silencing effect of miR-199a-3p for 96h on their targets IKKα (**C**, upper-left) and IKKβ (**C**, upper right), p65 (**C**, lower left) and IκBα (**C**, lower right), was analysed by Western blot. IKKα= inhibitor of nuclear factor kappa-B kinase subunit alpha; IKKβ= inhibitor of nuclear factor kappa-B kinase subunit beta; IκBα= nuclear factor kappa-B kinase inhibitor alpha; HUVECs = Human umbilical vein endothelial cells; RQ= relative quantification. All the *in vitro* experiments were performed at least in triplicate.

The induction of miR-199a-3p was also done in VSMCs and assessed by RT-qPCR confirming that the mimic increased the expression of the miRNA (Figure 35A). We also studied the expression of the selected targets: mTOR, IKKβ and p65 after the induction of miR-199a-3p obtaining a decrease in IKKβ and mTOR expression, but not in p65 (Figure 35B).

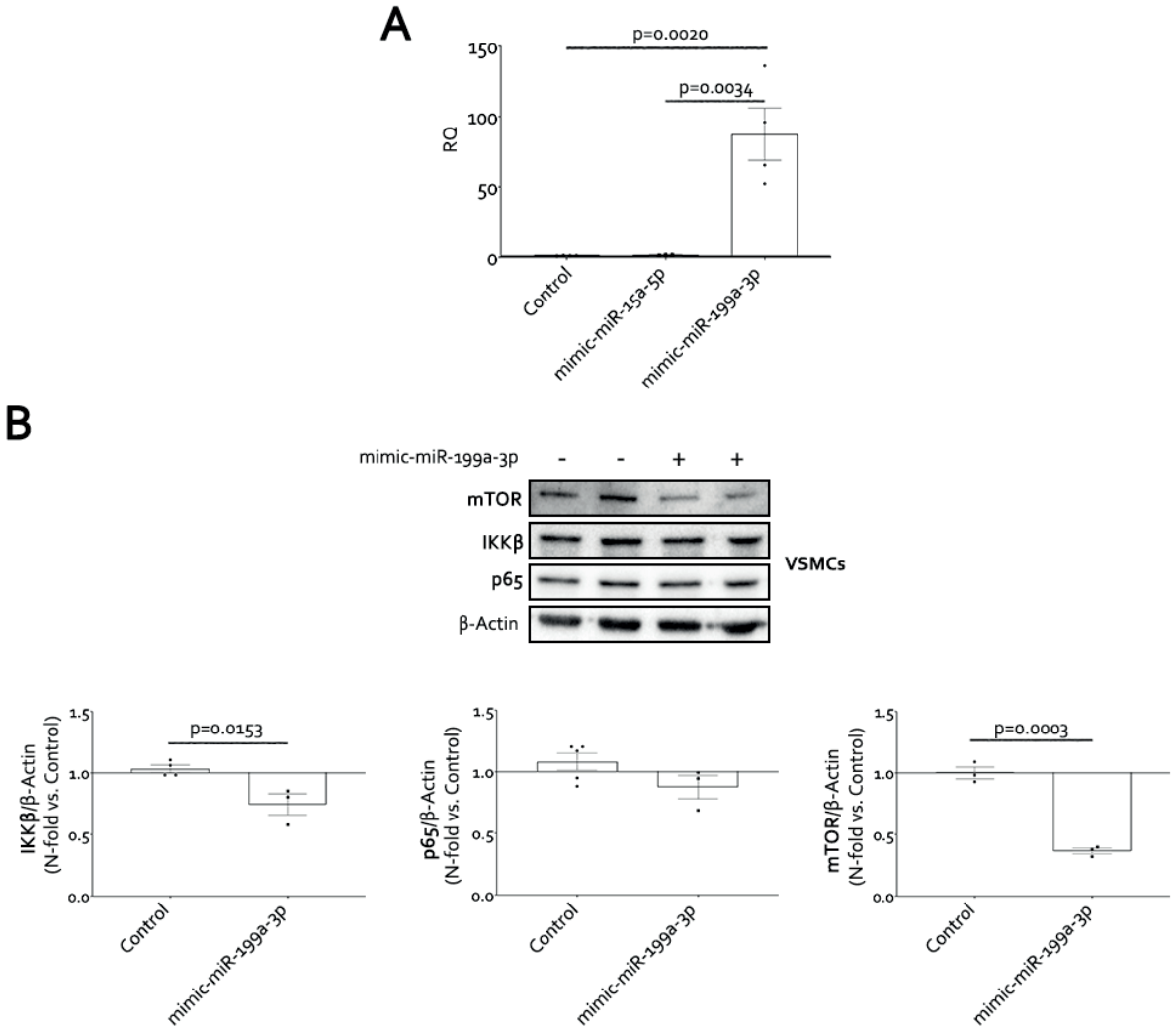

Figure 35. miR-199a-3p overexpression reduced IKKβ and mTOR expression in VSMCs. (A) VSMCs were transfected with mimic-miR-199a-3p for 48h. The increase in miRNA expression was measured by RT-qPCR. **(B)** The silencing effect of miR-199a-3p for 96 hours on their targets IKKβ (left), p65 (middle), and mTOR (right), was analysed by Western blot. IKKβ= inhibitor of nuclear factor kappa-B kinase subunit beta; mTOR= mammalian target of rapamycin; VSMCs= vascular smooth muscle cells; RQ = relative quantification. All the *in vitro* experiments were performed in triplicate.

5.5.5. miR-15a-5p and miR-199a-3p impair IKKα/β activation decreasing inflammation in vascular cells

IKKα/β are catalytic subunits of IKK complex and they are activated when they are phosphorylated. Then, they phosphorylate IκBα, inhibitory subunit of NF-κB, allowing the dimmer to enter the nucleus where it acts as a transcription factor. First, we did a time-course stimulation with TNFα for 10 to 40 minutes in HUVECs, to decide the correct time of treatment. We studied the phosphorylation of IKKα/β (Figure 36A) and p65 (Figure 36B) and IκBα protein levels (Figure 36C) by Western blot and decided that the treatment with TNFα for 10 minutes was the optimal time to obtain NF-κB activation (Figure 36A-C). To confirm that after this time p65 was translocated to the nucleus (and therefore, active) we performed a cellular sub-fractioning and p65 protein levels in the cytoplasmic and nuclear fractions were measured by Western Blot (Figure 36D). So, we might observe that TNFα for 10 minutes induced an increase of p65 protein levels in the nucleus and a decrease of p65 in the cytoplasm (Figure 36D) indicating the translocation and activation of p65 NF-κB.

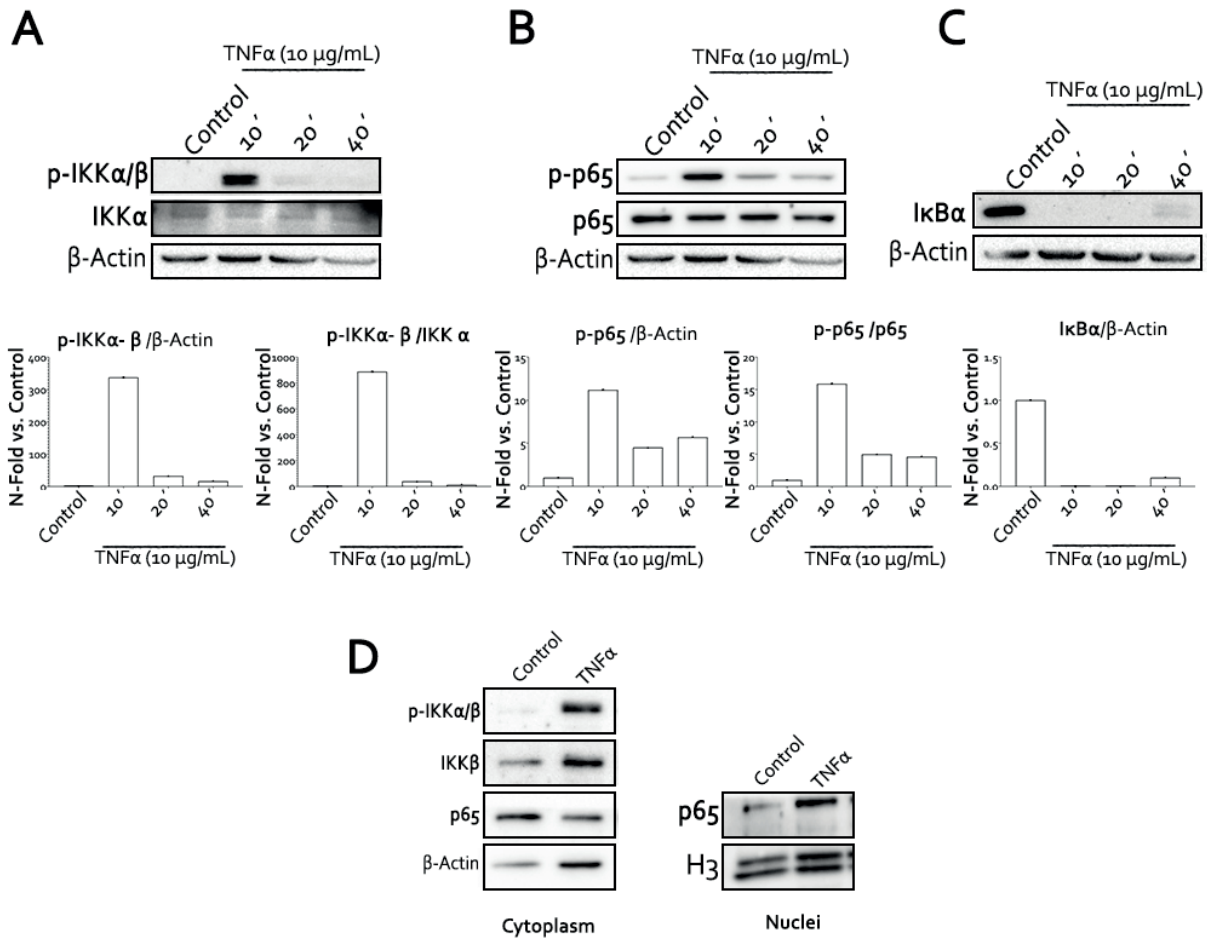

Figure 36. Effect of TNFα in NF-κB pathway in HUVECs. To establish the correct time of stimulation with TNFα a time course was done, and the activation of the pathway was assessed by Western blot of p-IKKα/β **(A)**, p-p65 **(B)** and IκBα **(C)** at 10, 20 and 40 minutes of stimulation with TNFα (10 µg/mL). The same proteins were studied by Western blot after a cellular sub-fractioning of cytoplasm and nuclei **(D)** to confirm p65 translocation to the nucleus. IKKα= inhibitor of nuclear factor kappa-B kinase subunit alpha; IKKβ= inhibitor of nuclear factor kappa-B kinase subunit beta; IκBα= nuclear factor kappa-B kinase inhibitor alpha; TNFα= tumor necrosis factor alpha; ´ = minutes; H3= histone 3.

To assess that miR-15a-5p was affecting not only the expression of IKKα/β but also its activity, we stimulated HUVECs with TNFα for 10 minutes in the presence or absence of the mimic-miR-15a-5p and the effect was assessed by Western blot (Figure 37A). When there was an overexpression of miR-15a-5p, there was a decrease in IKKα/β phosphorylation induced by TNFα, this decrease was led by the decrease of total IKKβ in the presence of the miRNA (Figure 37B).

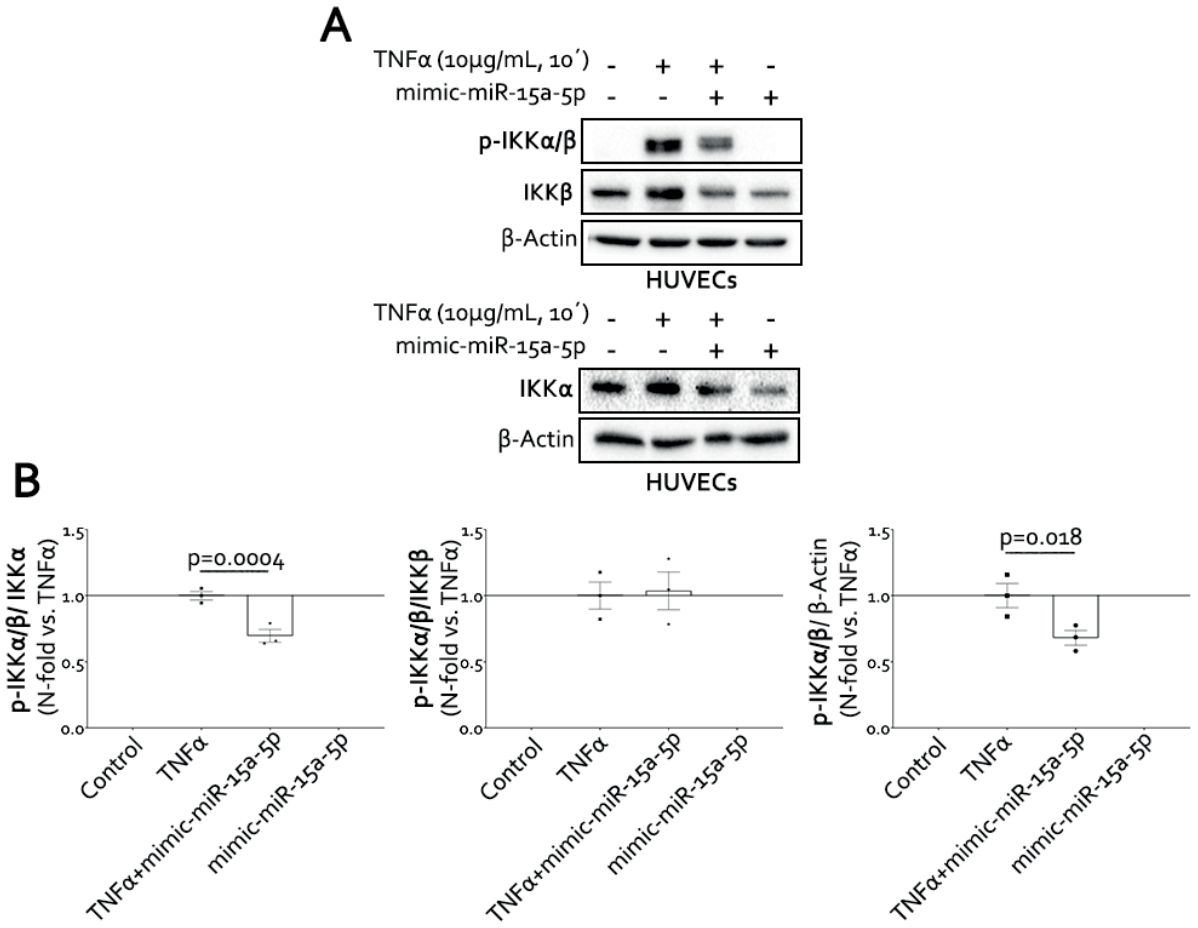

Figure 37. miR-15a-5p affects the activity of IKK complex in HUVECs. HUVECs were treated with TNFα (10μg/mL) for 10 minutes after the transfection with mimic-miR-15a-5p. The protein levels of their targets were measured by Western blot **(A)** and their quantifications represented by different graphics **(B).** miR-15a-5p overexpression reduced the phosphorylation of IKKα/β induced by TNFα. IKKα= inhibitor of nuclear factor kappa-B kinase subunit alpha; IKKβ= inhibitor of nuclear factor kappa-B kinase subunit beta; IκBα = nuclear factor kappa-B kinase inhibitor alpha; TNFα= tumor necrosis factor alpha; ´ = minutes; HUVECs= human umbilical vein endothelial cells. All the *in vitro* experiments were performed at least in triplicate.

The same experiment was performed but overexpressing miR-199a-3p with or without TNFα stimulation (Figure 38A), obtaining the same result. There was a decrease in IKKα/β activation induced by TNFα when miR-199a-3p is overexpressed, and this effect was mostly due to the decrease of IKKβ (Figure 38B).

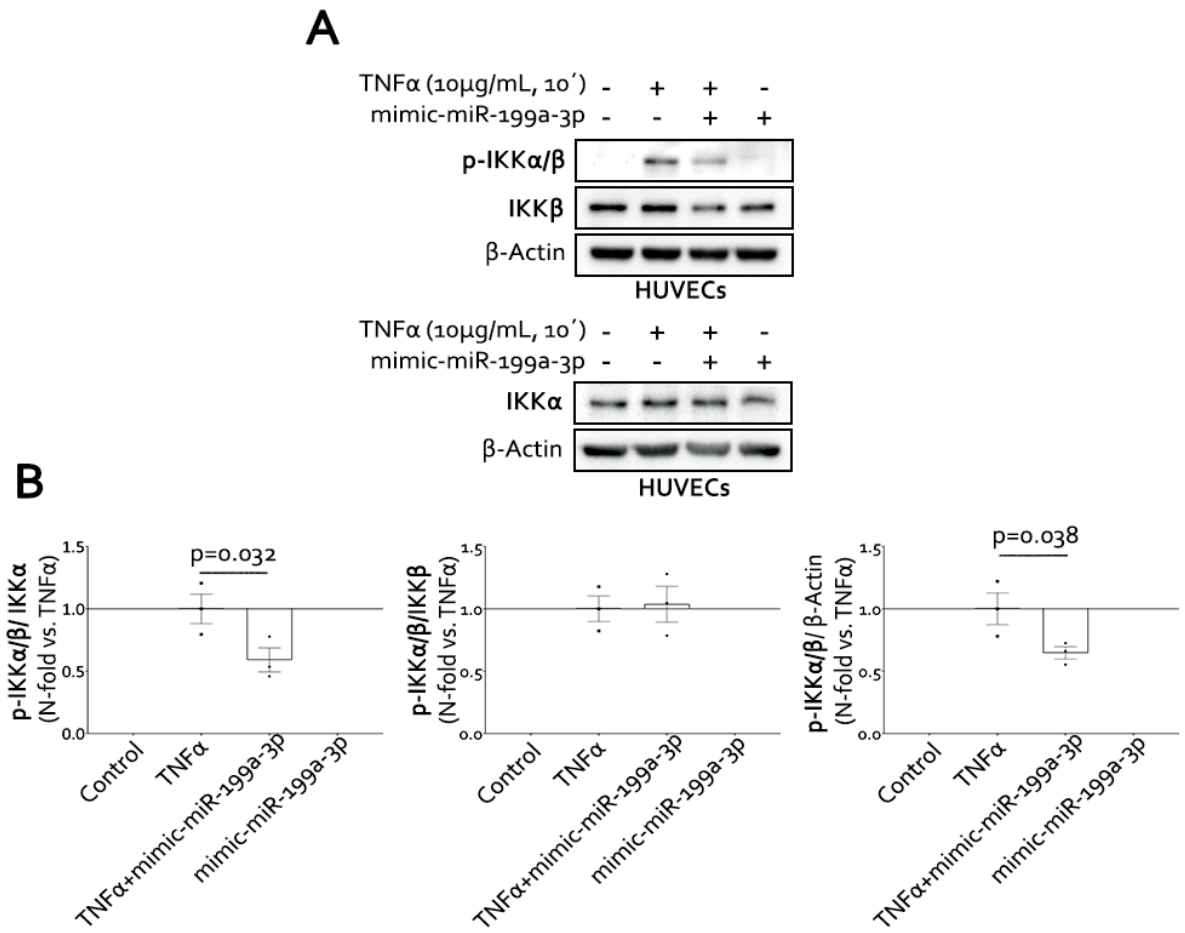

Figure 38. miR-199a-3p affects the activity of IKK complex in HUVECs. HUVECs were treated with TNFα (10 µg/mL) for 10 minutes after the transfection with mimic-miR-199a-3p. The protein levels of their targets were measured by Western blot **(A)** and their quantifications represented by different graphics **(B)**. miR-199a-3p overexpression reduced the phosphorylation of IKKα/β induced by TNFα. IKKα = inhibitor of nuclear factor kappa-B kinase subunit alpha; IKKβ= inhibitor of nuclear factor kappa-B kinase subunit beta; IκBα= nuclear factor kappa-B kinase inhibitor alpha; TNFα= tumor necrosis factor alpha; ´= minutes; HUVECs= human umbilical vein endothelial cells. All the *in vitro* experiments were performed at least in triplicate.

NF-κB is active when translocated to the nucleus, therefore, we performed an immunofluorescence against p65 in HUVECs transfected with one miRNAs in the presence or absence of TNFα (Figure 39). To quantify the activity of this transcription factor each p65 picture was superposed with the DAPI image (nuclei) and the co-localization between each other was assessed with the M1 and M2 Mander's coefficients (Figure 40A-B) as well as the Pearson's correlation (Figure 39C). The M1 coefficient indicates the amount of p65 that colocalize with DAPI and it is in the nuclei, the M2 shows the amount of DAPI that colocalize with p65, and the Pearson's coefficient relates the M1 and M2 coefficient (values between 0 to 1 scale, being 1 the maximum correlation).

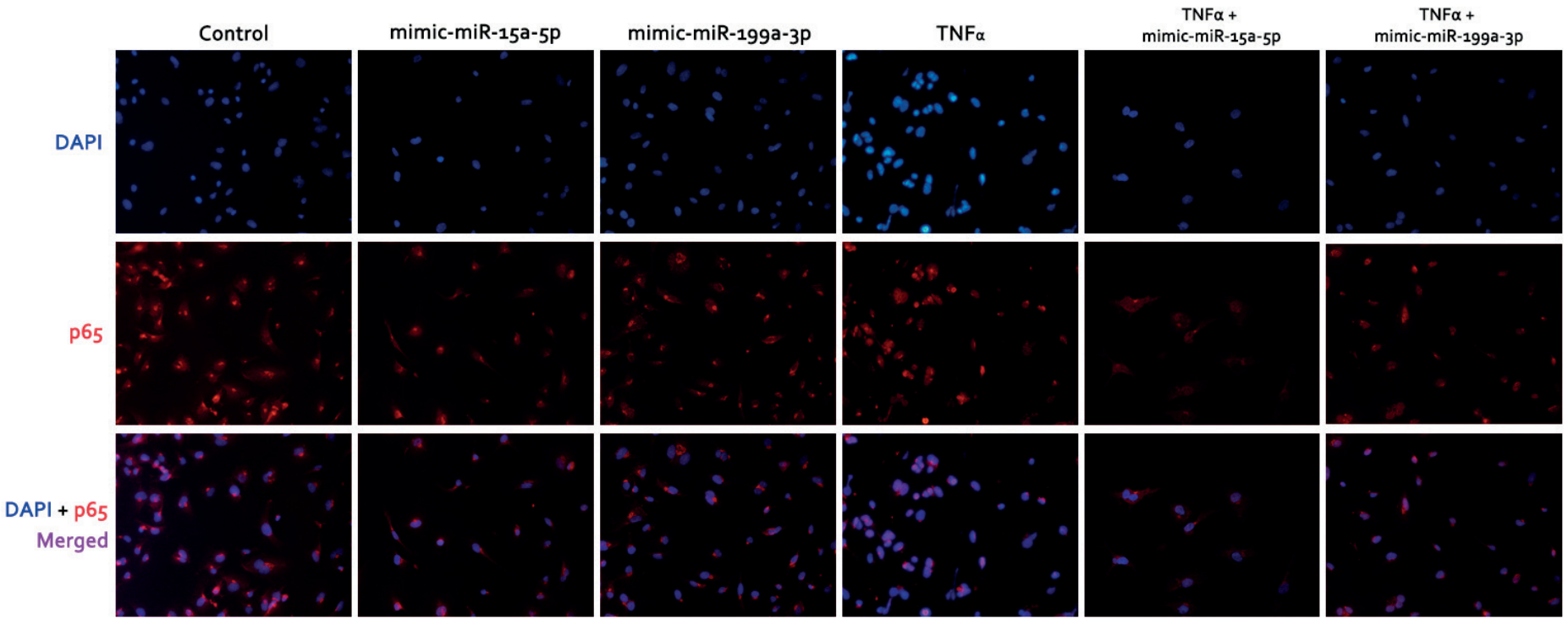

Figure 39. miR-15a-5p and miR-199a-3p reduced the translocation of p65 in endothelial cells. HUVECs were stimulated with TNFα with or without mimic-miR-15a-5p, mimic miR 199a-3p, and the activation of p65 was measured by immunofluorescence. Representative images from the immunofluorescence of p65 (red) contrasted with DAPI (blue) and merged (purple). TNFα= Tumor necrosis factor alpha; HUVECs = human umbilical vein endothelial cells. All the *in vitro* experiments were performed at least in triplicate.

There was an increase in the M1 coefficient when the cells were stimulated with TNFα in absence of the mimic-miRNAs when compared with the control; and if the cells were stimulated with TNFα in presence of the mimic miR-199a 3p compared with the cells that only had an overexpression of the miRNA. However, TNFα had no effect in this coefficient in the presence of mimic-miR-15a-5p when compared with its specific control, but it was decreased when compared with the cells that were stimulated with TNFα with or without mimic-miR-199a-3p (Figure 40A).

The M2 coefficient was only increased in the cells stimulated with TNFα in the presence of the mimic-miR-15a-5p when compared to its control and cells that were stimulated with this molecule in the presence of mimic-miR-199a-3p. But the M2 coefficient was decreased if the cells were stimulated with TNFα in the presence of mimic-199a-3p when compared with cells stimulated with TNFα without any mimic (Figure 40B).

The Pearson's coefficient was increased in the cells stimulated with TNFα in the absence of mimics and in the presence of mimic-miR-199a-3p when compared to its control, respectively (Figure 40C). This coefficient showed no changes if the cells were stimulated with TNFα in the presence of mimic-miR-15a-5p if compared with cells without TNFα stimulation but was decreased compared with cells stimulated with this molecule without mimics (Figure 40C).

In summary there was an induction of p65 translocation when the cells were stimulated with TNFα without the overexpression of both miRNAs, but this induction was impaired by miR-15a-5p overexpression. However, the increase of miR-199a-3p by itself was not able to impair the translocation of NF-κB to the nucleus, nonetheless it seemed lower than the cells stimulated only with TNFα.

Lastly, we also quantified the fluorescence of p65 using the corrected total cell fluorescence (CTCF), this showed a decrease in p65 expression if miR-15a-5p or miR-199a-3p were induced (Figure 40D).

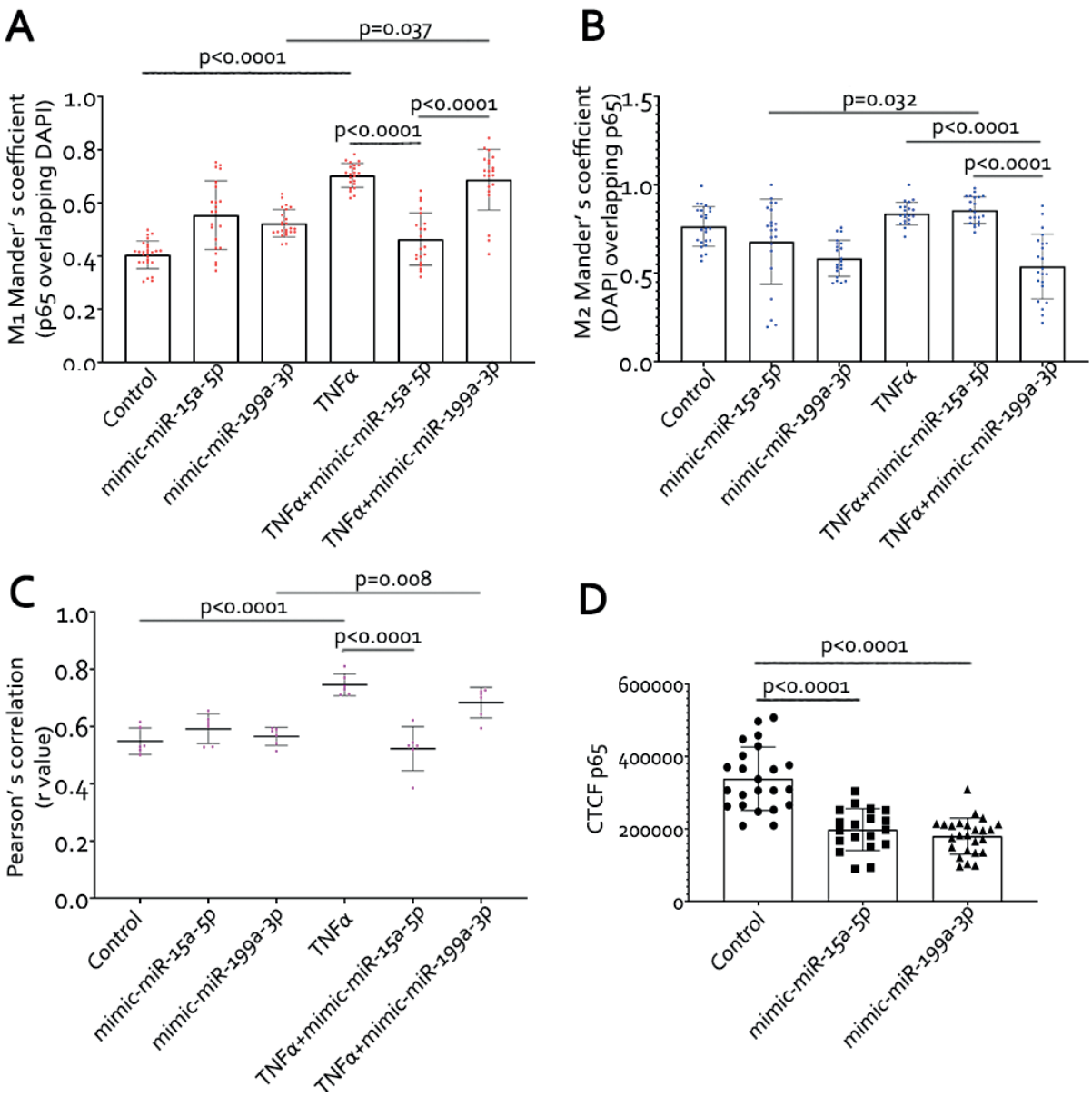

Figure 40. miR-15a-5p and miR-199a-3p reduced the activation of p65 in endothelial cells. HUVECs were stimulated with TNFα with or without mimic-miR-15a-5p or mimic-miR-199a-3p and the activation of p65 was measured by immunofluorescence. Since p65 is active in the nucleus, the JaCoP plugin from Fiji was used to quantify the colocalization of p65 and DAPI by three values: the M1 **(A)** and M2 **(B)** Mander's coefficient, and the Pearson's correlation **(C)** of each picture. In all cases, the closer the value is to 1, indicated more colocalization. **(D)** The intensity of fluorescence of p65 was measured in all the conditions. TNFα= tumor necrosis factor alpha; CTCF= corrected total cell fluorescence. To quantify the co-localization, ten pictures were taken for each condition and analyzed as an individual point. All the *in vitro* experiments were repeated at least in triplicate.

Since IKKβ and p65 were decreased by the induction of miR-15a-5p in VSMCs (Figure 33B) as well as in HUVECs (Figure 32C) but not by inducing miR-199a-3p (Figure 35B), and after confirming that in these last cell type IKK signalling was impaired by miR-15a-5p. We wanted to confirm if this miRNA was also impairing the activation of the NF-κB pathway in presence of specific activators also in VSMCs.

VSMCs were stimulated with TNFα for 10 minutes with or without miR-15a-5p induction by mimic-miRNA. The activation of the NF-κB pathway was assessed by Western blot of IKKα/β phosphorylation (Figure 41A). In VSMCs, miR-15a-5p overexpression significantly decreased IKKα/β activation induced by TNFα (Figure 41B) and increased the levels of IκBα (Figure 41B).

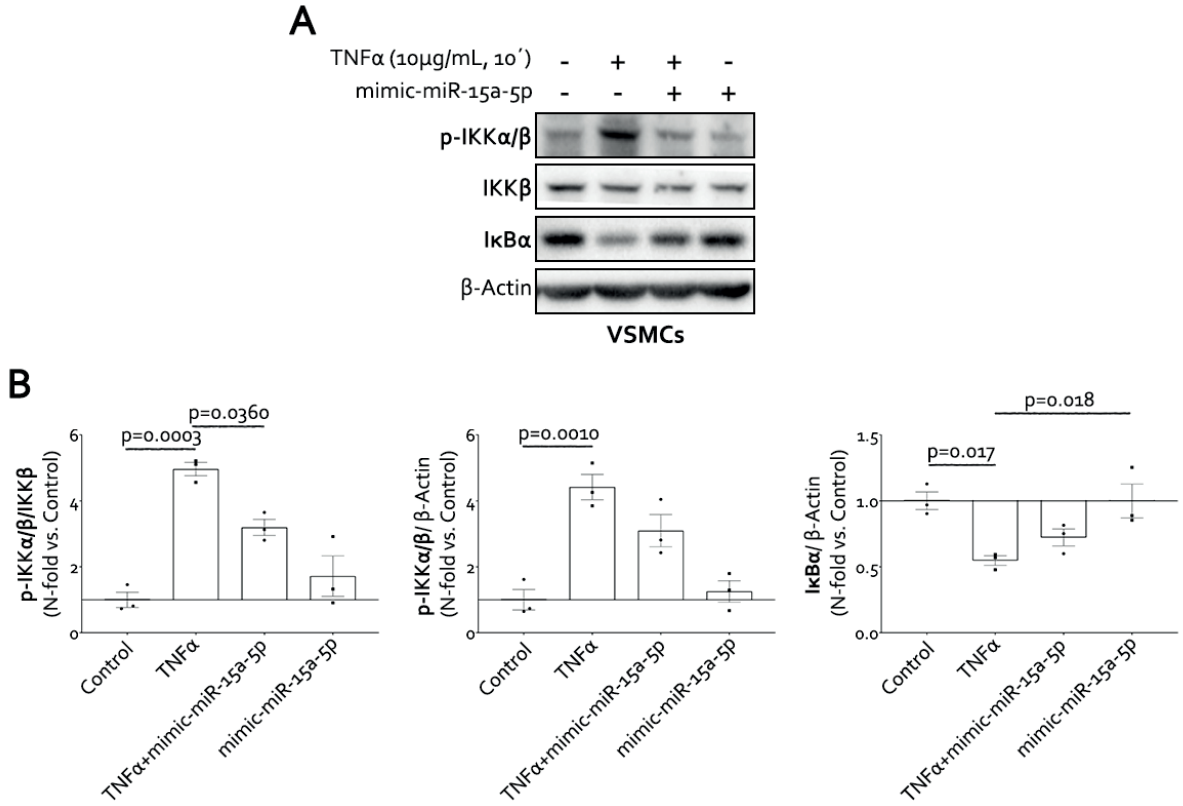

Figure 41. miR-15a-5p affects the activity of IKK complex in VSMCs. Cells were treated with TNFα (10 μg/mL) for 10 minutes after the transfection with mimic-miR-15a-5p. The protein levels of their targets were measured by Western blot **(A)** and their quantifications represented by different graphics **(B)**. IKKα = Inhibitor of nuclear factor kappa-B kinase subunit alpha; IKKβ= inhibitor of nuclear factor kappa-B kinase subunit beta; IκBα= nuclear factor kappa-B kinase inhibitor alpha; TNFα= tumor necrosis factor alpha; ´= minutes; VSMCs = vascular smooth muscle cells. All the *in vitro* experiments were performed at least in triplicate.

5.5.6. IKBKB and CHUK are confirmed targets of miR-15a-5p and IKBKB of miR-199a-3p

We performed experiments based on luciferase constructs to demonstrate the direct interaction of miR-15a-5p and miR-199a-3p with the 3´UTRs of p65, IKKβ and IKKα mRNAs (Figure 42). Our results demonstrate a direct and specific interaction of miR-15a-5p with the 3´UTR of IKBKB (IKKβ) and CHUK (IKKα) mRNAs and miR-199a-3p with the 3´UTR of IKBKB (IKKβ) mRNA. However, we did not find any change regarding the interaction of miR-199a-3p with the 3´UTR of RELA (p65) mRNA.

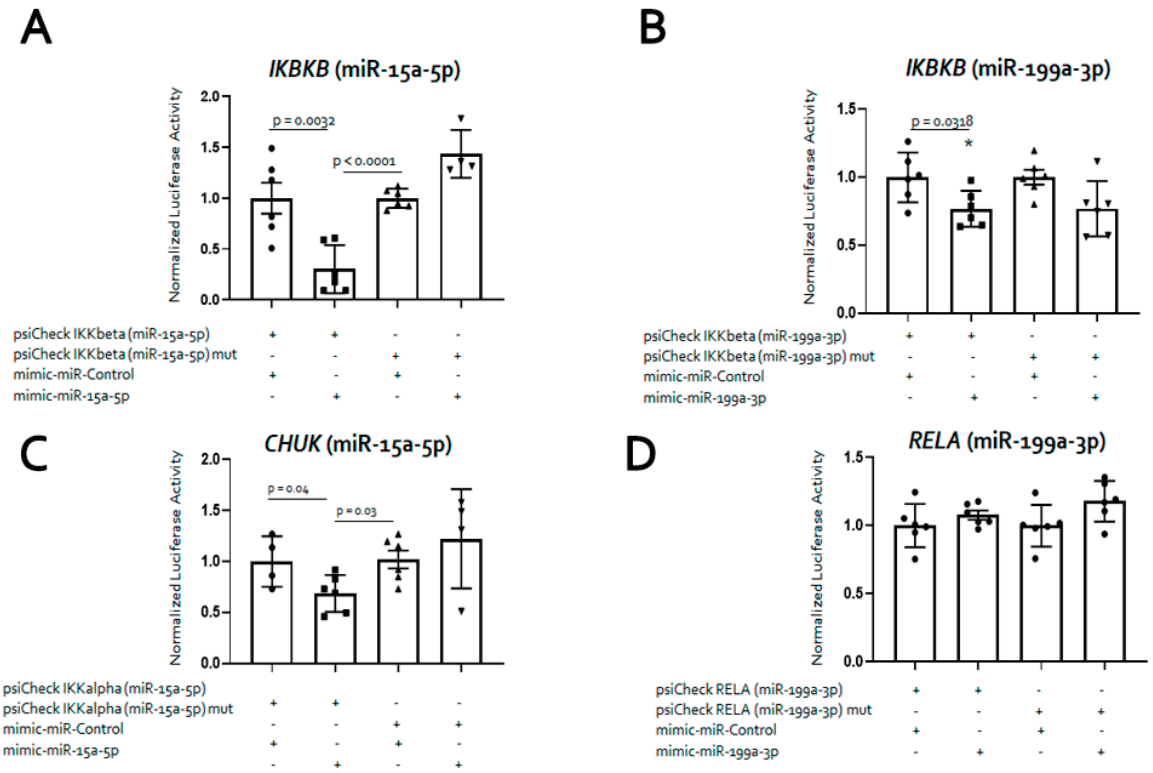

Figure 42. Regulation of IKBKB, CHUK and RELA expression by the interaction of miR-15a-5p or miR-199a-3p with its 3' UTR sequence. Shown is the normalized Renilla luciferase activity in HEK293 cells transfected with the different constructs. **(A)** HEK293 cells were co-transfected with the psiCHECK IKKbeta (miR-15a-5p) and psiCHECK IKKbeta (miR-15a-5p) mutated plasmids together with mimic-miR control or mimic-miR-15a-5p. **(B)** HEK293 cells were co-transfected with the psiCHECK IKKbeta (miR-199a-3p) and psiCHECK IKKbeta (miR-199a-3p) mutated plasmids together with mimic-miR control or mimic-miR-199a-3p. **(C)** HEK293 cells were co-transfected with the psiCHECK IKKalpha (miR-15a-5p) and psiCHECK IKKalpha (miR-15a-5p) mutated plasmids together with mimic-miR control or mimic-miR-15a-5p. **(D)** HEK293 cells were co-transfected with the psiCHECK RELA (miR-199a-3p) and psiCHECK RELA (miR-199a-3p) mutated plasmids together with mimic-miR control or mimic-miR-199a-3p. In all cases, Renilla luciferase activity was normalized to firefly luciferase activity. *CHUK* (IKKα); *IKBKB* (IKKβ); *RELA* (p65). All the *in vitro* experiments were performed at least in triplicate.

5.5.7. Role of miR-15a-5p and miR-199a-3p in the foaming of VSMCs

Among the possible targets that appeared in the miRNA-target databases for miR-15a-5p and miR-199a-3p that modulate ox-LDL uptake were lectin-like oxidized low density lipoprotein receptor 1 (*OLR1* (gene) or LOX-1 (protein)) for miR-15a-5p or CD36 for miR-199a-3p. The ox-LDL uptake is important in VSMCs, because when they capture these molecules, they switch to a foam cell phenotype. First, we performed an immunofluorescence for LOX-1 and α-SMA to confirm that LOX-1 was expressed by VSMCs from the media layer. Confirming LOX-1 staining in aortic roots from *ApoE* $^{-/-}$ HFD, where the levels of miR-15a-5p were lower (Figure 43A and 22A, respectively). In this sense, *in vitro* experiments demonstrated that miR-15a-5p overexpression significantly reduced LOX 1 protein levels in VSMCs (Figure 43B).

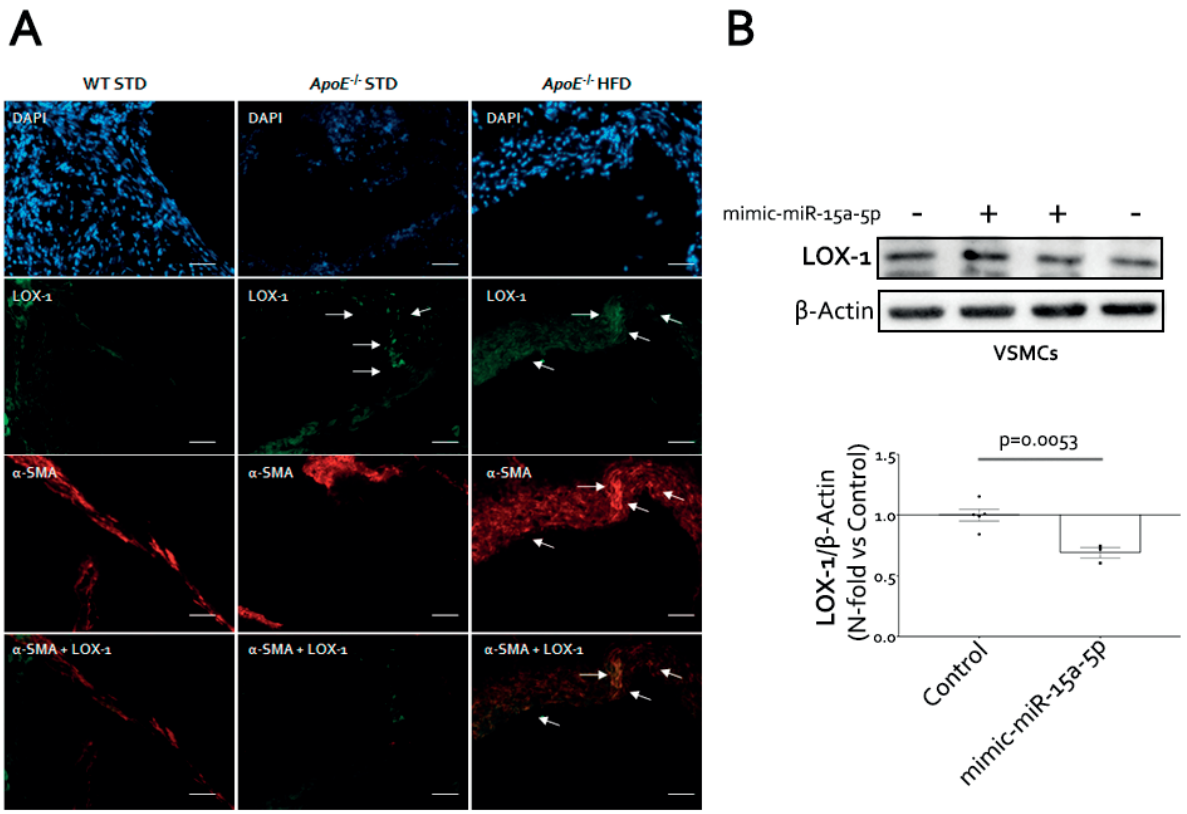

Figure 43. Role of LOX-1 in the progression of experimental atherosclerosis. (A) Double immunofluorescence of LOX-1 (green) and α-SMA (red) in aortic roots from WT STD 18 wks, *ApoE*$^{-/-}$ STD 18 wks and *ApoE*$^{-/-}$ HFD 18 wks. Magnification 200x, scale bar = 50 μm. **(B)** VSMCs were transfected with mimic-miR-15a-5p for 48 hours and we measured LOX-1 protein levels by Western-blot. WT = wild-type; STD = standard-type diet; HFD= high fat diet; *ApoE*$^{-/-}$= apolipoprotein E deficient; LOX-1 = lectin-like oxidized low-density lipoprotein receptor-1. All the *in vitro* experiments were performed at least in triplicate.

To confirm that the protein was also expressed in human atherosclerosis, we performed an IHC against LOX 1 (Figure 44A). Observing that patients with advanced carotid atherosclerosis and lower miR-15a-5p levels had a significant increase of LOX-1 protein levels (Figure 44A). Moreover, we also performed a double immunofluorescence of LOX-1 and α-SMA, and we found that LOX-1 was expressed by VSMCs in human plaques (Figure 44B).

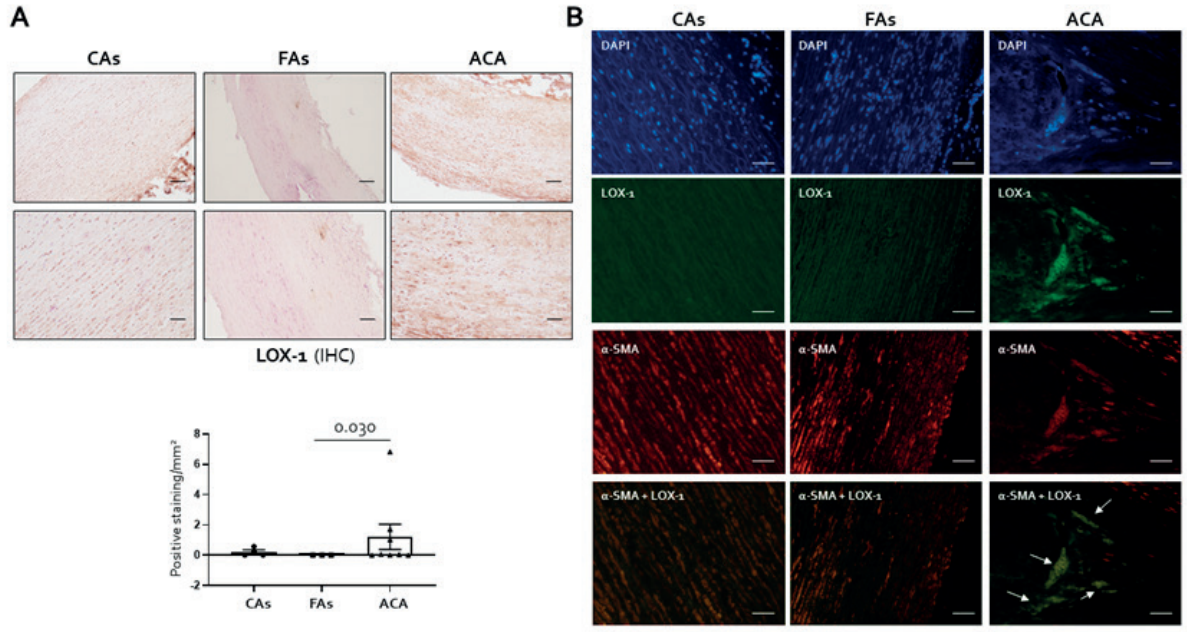

Figure 44. Role of LOX-1 in the progression of human atherosclerosis. (A) We studied LOX-1 protein levels in aorta from CAs, FAs and in carotid from ACA patients by immunohistochemistry with LOX-1 antibodies. The quantification is expressed as positive staining/mm2. Upper images (magnification 100x, scale bar = 100 µm), lower images (magnification 200x, scale bar = 50 µm). **(B)** Double immunofluorescence of LOX-1 (green) and α-SMA (red) in vascular samples of CAs, FAs and ACA. Magnification 200x, scale bar = 50 µm. CAs= control aortas; FAs= fibroatheromas; ACA= advanced carotid atherosclerosis; LOX-1= lectin-like oxidized low-density lipoprotein receptor-1; IHC= immunohistochemistry. CAs (n=4); FAs (n=3); ACA (n=8).

Finally, we studied whether the overexpression of miR-15a-5p or miR-199a-3p might have a protector role in foaming of VSMCs. For that, VSMCs were treated with 100 µg/mL of ox LDL in presence or not of mimic-miR-15a-5p or mimic-miR-199a-3p, and lipid content was quantified by an ORO staining (Figure 45A). Our results show that miR-15a-5p or miR 199a-3p overexpression reduced ox-LDL uptake by VSMCs (Figure 45A and B).

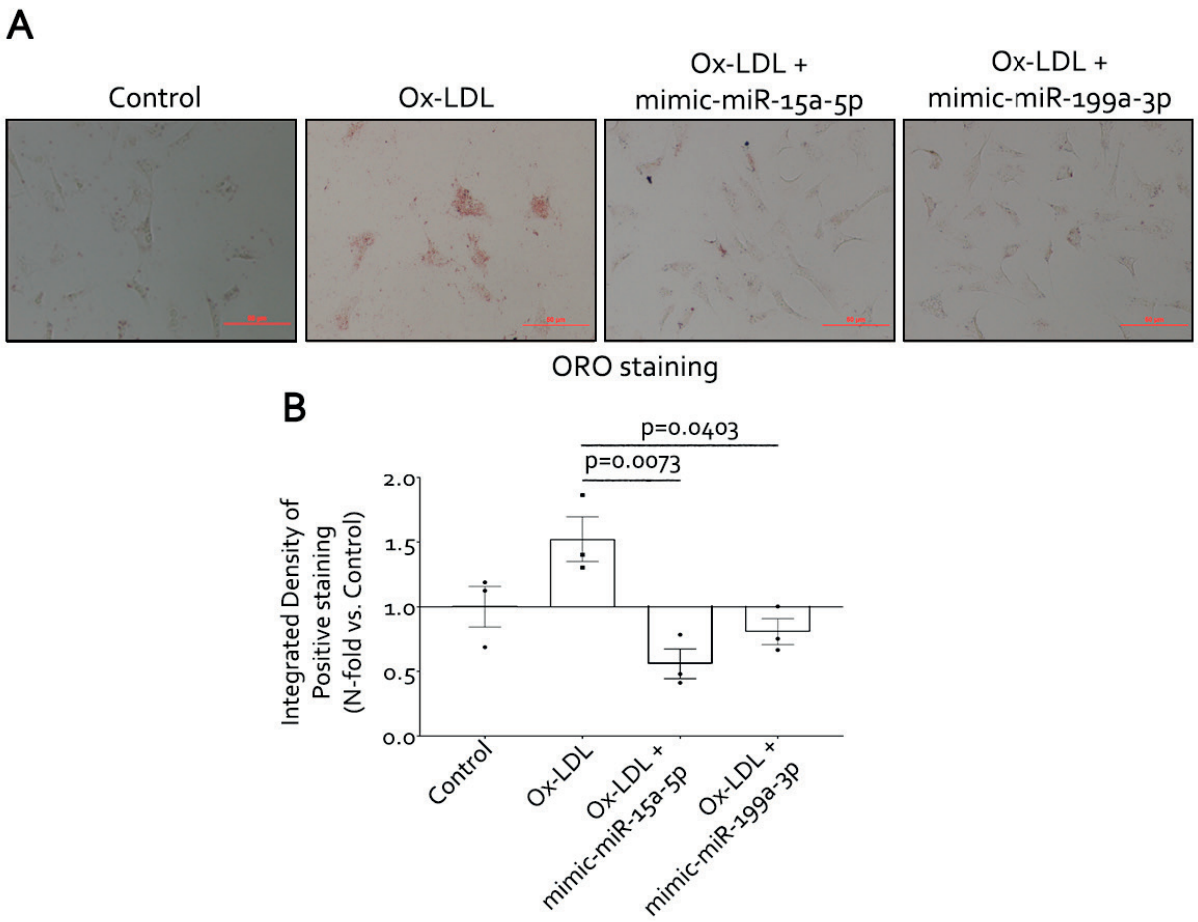

Figure 45. miR-15a-5p and miR-199a-3p overexpression reduced ox-LDL uptake in VSMCs. VSMCs were transfected with mimic-miR-15a-5p or mimic-miR-199a-3p for 48h and the increase in miRNA expression was measured by RT-qPCR. In the last 24h of transfection, the cells were treated with ox-LDL (100 µg/mL) and then stained with Oil Red O. **(A)** Representative images from Oil Red O staining, from which it was measured the uptake of ox-LDLs **(B)**. VSMCs= vascular smooth muscle cells; Ox-LDL= oxidized low-density lipoprotein; ORO= Oil Red O. All the *in vitro* experiments were performed at least in triplicate.

5.6. miRNAs are also altered in the carotids and immune cells from a mouse model of atherosclerosis transgenic for the human *APOB100* gene

5.6.1. Characterization of the Hu*APOB100*-tg *Ldlr*$^{-/-}$ model

We used the Hu*APOB100*-tg *Ldlr*$^{-/-}$ mice (HuBL) from Anton Gisterå's lab in the Karolinska Institutet, this is a Ldlr knockout mice that is also transgenic for the human *apolipoprotein B 100* gene. With this transgene, mice develop atherosclerotic injuries faster than the *Ldlr* knockout mice, and their lipoprotein profile is more similar to the human one compared with other mouse models.

Table 4. Table with the characteristics regarding the BW (g), cholesterol (mg/dL) and triglycerides (mg/dL) of the HuBL mice.

	11-weeks	46-weeks	11-weeks vs. 46-weeks
BW (g)	21.9 ± 0.9	24.4 ± 2.2	p=n.s.
Cholesterol (mg/dL)	96.1 ± 3.5	102.7 ± 8.7	p=n.s.
Triglycerides (mg/dL)	72.6 ±5.1	60.4 ± 3.3	p=n.s.

In this specific case, we wanted to focus on the possible miRNA alteration in the mice carotids and CD_3 cells during disease severity with age, comparing initial atherosclerosis and/or advanced atherosclerosis. To do so, we used 11-weeks female mice, as young mice and 46-weeks female mice, as middle-aged mice, both groups were fed a standard chow diet and showed no difference in body weight and plasma cholesterol and triglycerides (Table 4). After those weeks, we harvested the heart and aortic roots for histological analysis; and the carotids (common carotids and carotid bifurcation) and CD_3 cells from the spleen for the miRNA isolation (Figure XIV).

To characterize the severity of the atherosclerotic injury in these mice, we performed an Oil Red O staining in the aortic roots from the 11-weeks and 46-weeks groups (Figure 46A) to quantify the lipid deposition in the area. We observed a significant increase in this parameter in the aortic roots from 46-weeks mice compared with the young mice (Figure 46B). In addition, we were able to assess that the 46-weeks mice showed an advanced atherosclerosis, while the 11-weeks mice showed initial injuries development, therefore by comparing middle-age and young mice, we are also comparing initial and advanced atherosclerosis.

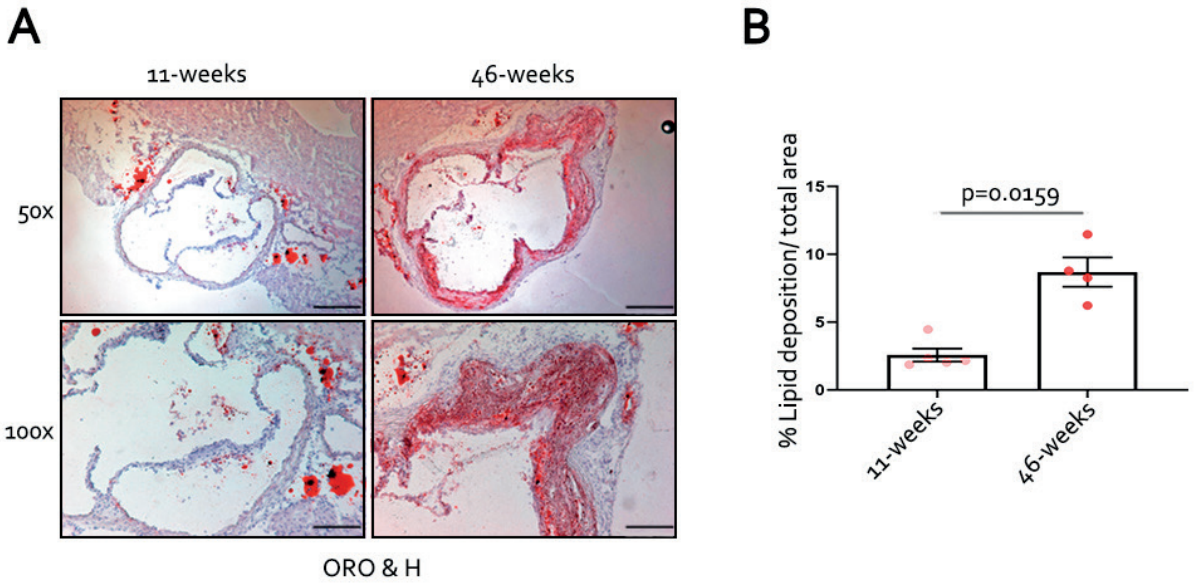

Figure 46. Characterization of the atherosclerotic injury in the Hu*APOB100*-tg *Ldlr*$^{-/-}$ mice. (A) Representative images of the Oil Red O staining from the aortic roots. Magnification 50x (scale bar = 200 µm); magnification 100x (scale bar = 100 µm). Quantification of the percentage of lipid accumulation of the aortic root from the mouse model **(B).** ORO= Oil Red O; H= hematoxylin. 11-weeks (n=6); 46-weeks (n=4).

5.6.2. miR-143-3p and miR-155-5p are altered in mice carotids

Once we harvested the carotid bifurcation and the common carotids from the mice, we began by isolating miRNAs and total RNA, to study the levels of miR-143-3p, miR-155-5p, miR-15a-5p and miR-199a-3p. First, we assessed the miRNA alteration in the carotid bifurcation from the 11-weeks compared to 46-weeks mice.

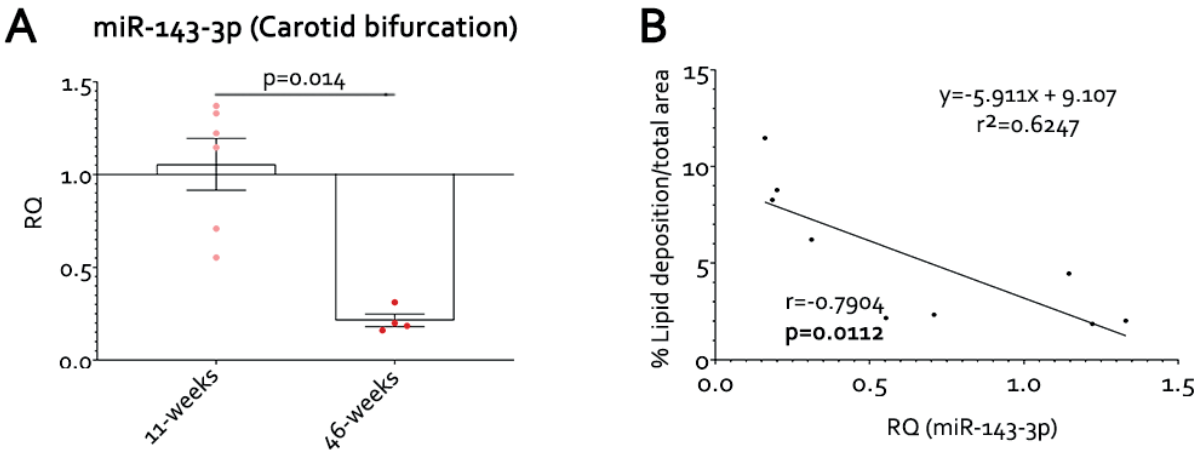

Figure 47. miR-143-3p is downregulated in the carotid bifurcation and correlates with atherosclerosis severity in mice with advanced carotid atherosclerosis. (A) The expression of miR-143-3p was analyzed in the carotid bifurcation of young and middle-aged mice by RT-qPCR. **(B)** By Pearson's correlation, we set the correlation between miR-143-3p in the carotid bifurcation and the % of lipid deposition RQ = relative quantification. 11-weeks (n=6); 46-weeks (n=4). Correlation between miR-143-3p and atherosclerosis (n=10).

The carotid bifurcation is an area that develops atherosclerosis easier than the common carotid or the aorta. When studying the four miRNAs in these mice, only miR-143-3p was statistically downregulated in the carotid bifurcation of mice with advanced atherosclerosis compared with mice with initial atherosclerosis (Figure 47A) and correlates with the disease severity (Figure 47B).

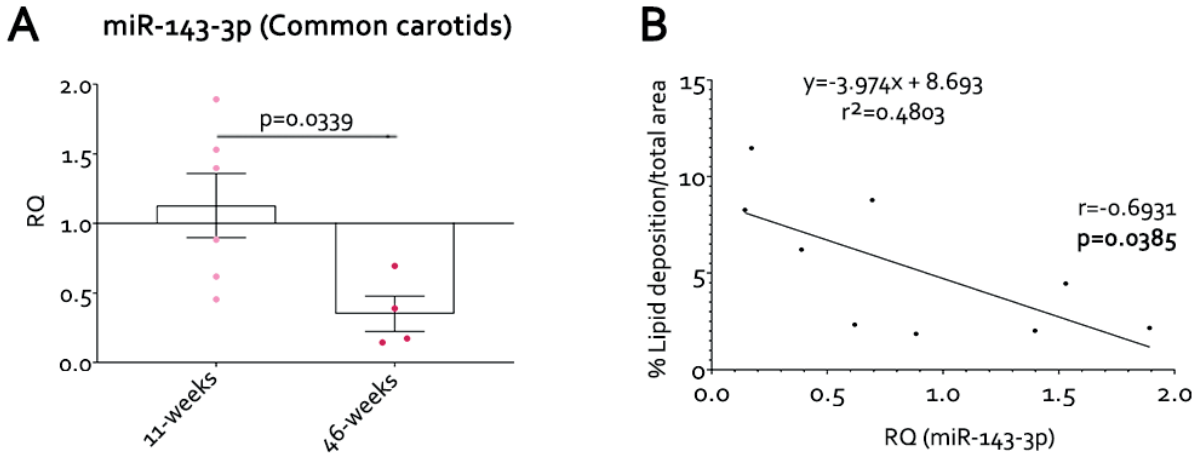

Figure 48. miR-143-3p is downregulated in the common carotids and correlates with atherosclerosis severity in mice with advanced carotid atherosclerosis. (A) The expression of miR-143-3p was analyzed in the common carotids of young and middle-aged mice by RT-qPCR. (B) By Pearson's correlation, we set the correlation between miR-143-3p in the common carotids and the % of lipid deposition. RQ = relative quantification. 11-weeks (n=6); 46-weeks (n=4). Correlation between miR-143-3p and atherosclerosis (n=10).

Then we compared the miRNA expression in common carotids of 11-weeks and 46-weeks mice, where miR-143-3p was downregulated (Figure 48A), and miR-155-5p (Figure 49A) was overexpressed, and in both cases these miRNAs were correlated with the disease progression (Figure 48B and 49B).

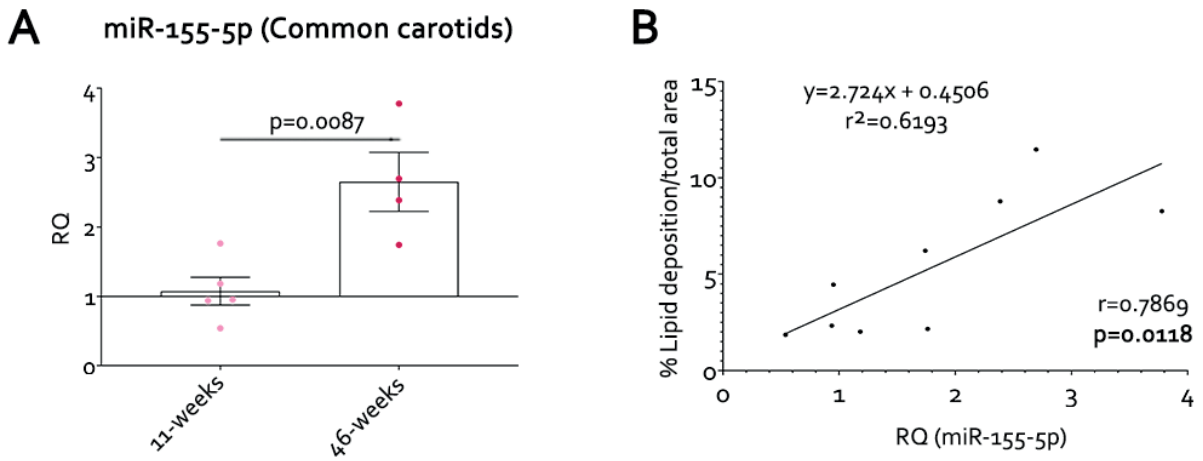

Figure 49. miR-155-5p is upregulated in the common carotids and correlates with atherosclerosis severity in mice with advanced carotid atherosclerosis. (A) The expression of miR-155-5p was studied in the common carotids of young and middle-aged mice by RT-qPCR. **(B)** By Pearson's correlation, we set the correlation between miR-155-5p levels in the common carotids and the % of lipid deposition. RQ = relative quantification. 11-weeks (n=6); 46-weeks (n=4). Correlation between miR-155-5p and atherosclerosis (n=10).

In addition, we also wanted to assess if other genes that participate in atherosclerosis development were altered, like *Ccl2*, *Il1β*; *Serpine*, *Vcam1*, *Cd68*, *Arg1*, and *Nos2*. In the carotid bifurcation, there was no significant change; but in the common carotids there was a significant increase in *Ccl2* (Figure 50A), *Vcam1* (Figure 50D) and *Il1β* (Figure 50G) levels in the 46-weeks mice. To further delve in the possible relationship between miR-143-3p, miR-155-5p and those genes, we performed a Pearson's correlation amongst them. *Ccl2* and *Vcam1* correlated with miR-143-3p levels (Figure 50B, E) and miR-155-5p levels (Figure 50C, F), in addition *Il1β* expression was also related to miR-155-5p (Figure 50H).

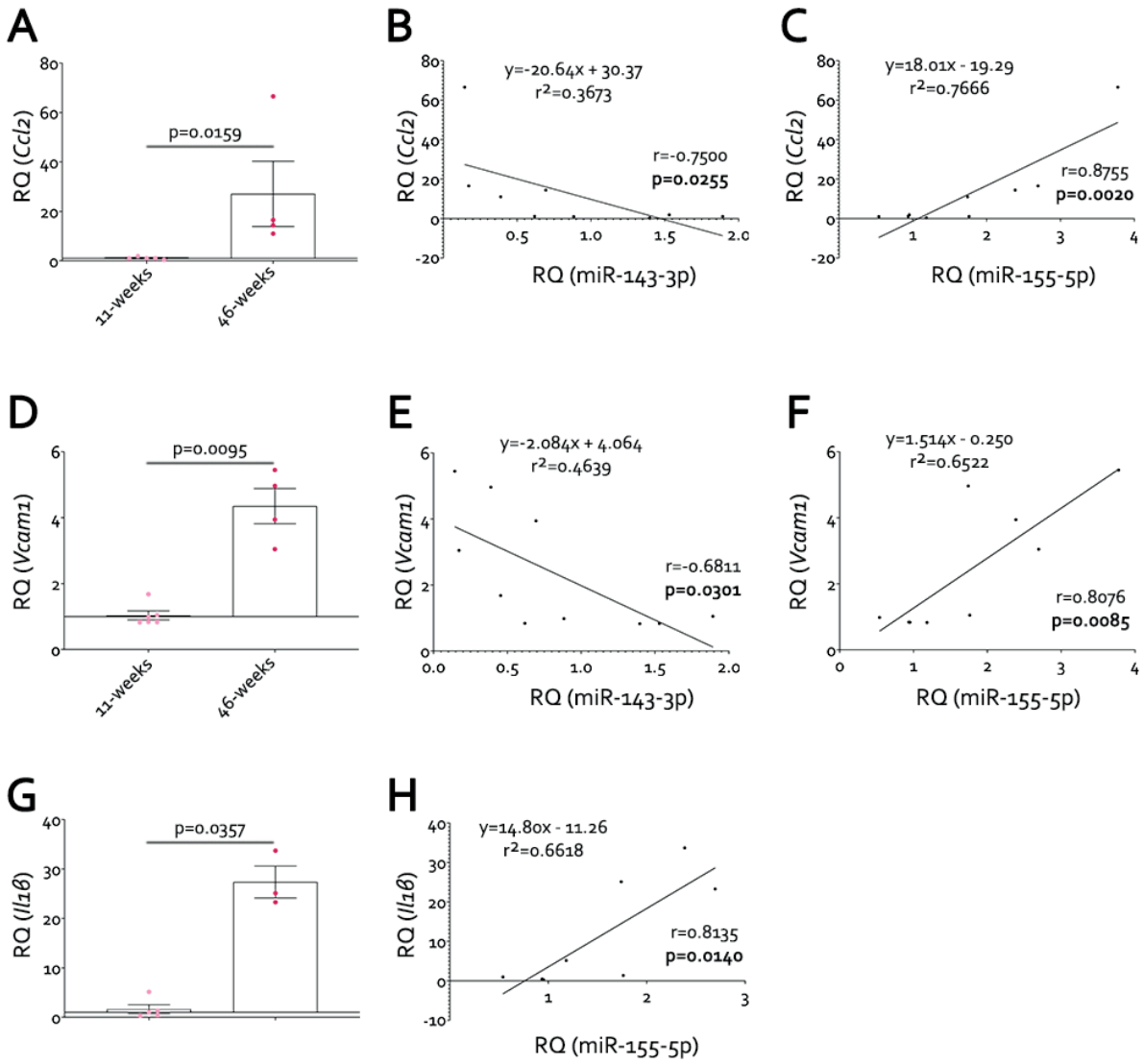

Figure 50. *Ccl2*, *Vcam1* and *Il1β* are overexpressed in advanced atherosclerosis and correlate with miR-143-3p and miR-155-5p levels. The expression of *Ccl2* **(A)**, *Vcam1* **(D)** and *Il1β* **(G)** were analysed in the common carotids of young and middle-age female mice by RT-qPCR. By a Pearson's correlation, the expression of *Ccl2*, *Vcam1* and *Il1β* was correlated to miR-143-3p levels **(B, E)** and miR-155-5p levels **(C, F and H)**, respectively. RQ= relative quantification; *Ccl2*= gene encoding the monocyte chemoattractant protein-1; *Vcam1*= gene encoding the vascular cell adhesion molecule-1; *Il1β*= gene encoding the interleukin-1 beta. 11-weeks (n=6); 46-weeks (n=4). Correlations between miRNAs and mRNA (n=10).

5.6.3. miR-143-3p, miR-155-5p, miR-15a-5p and miR-199a-3p are altered in the carotid bifurcation of mice with initial atherosclerosis

After confirming that some miRNAs were altered with age and disease severity in the carotid bifurcation and common carotids in mice (Figure 47-49). We wanted to compare if there were site-specific differences between the common carotid and the carotid bifurcation in young mice.

As a result, miR-155-5p (Figure 51B) was overexpressed and miR-143-3p (Figure 51A), miR-15a-5p (Figure 51C) and miR-199a-3p (Figure 51D) were downregulated in a site specific manner in the 11-weeks group. Surprisingly, when assessing the expression of the before mentioned genes, only *Ccl2* was statistically overexpressed in the carotid bifurcation (Figure 52A) correlating with miR-155-5p levels (Figure 52B) and miR-199a-3p levels (Figure 52C).

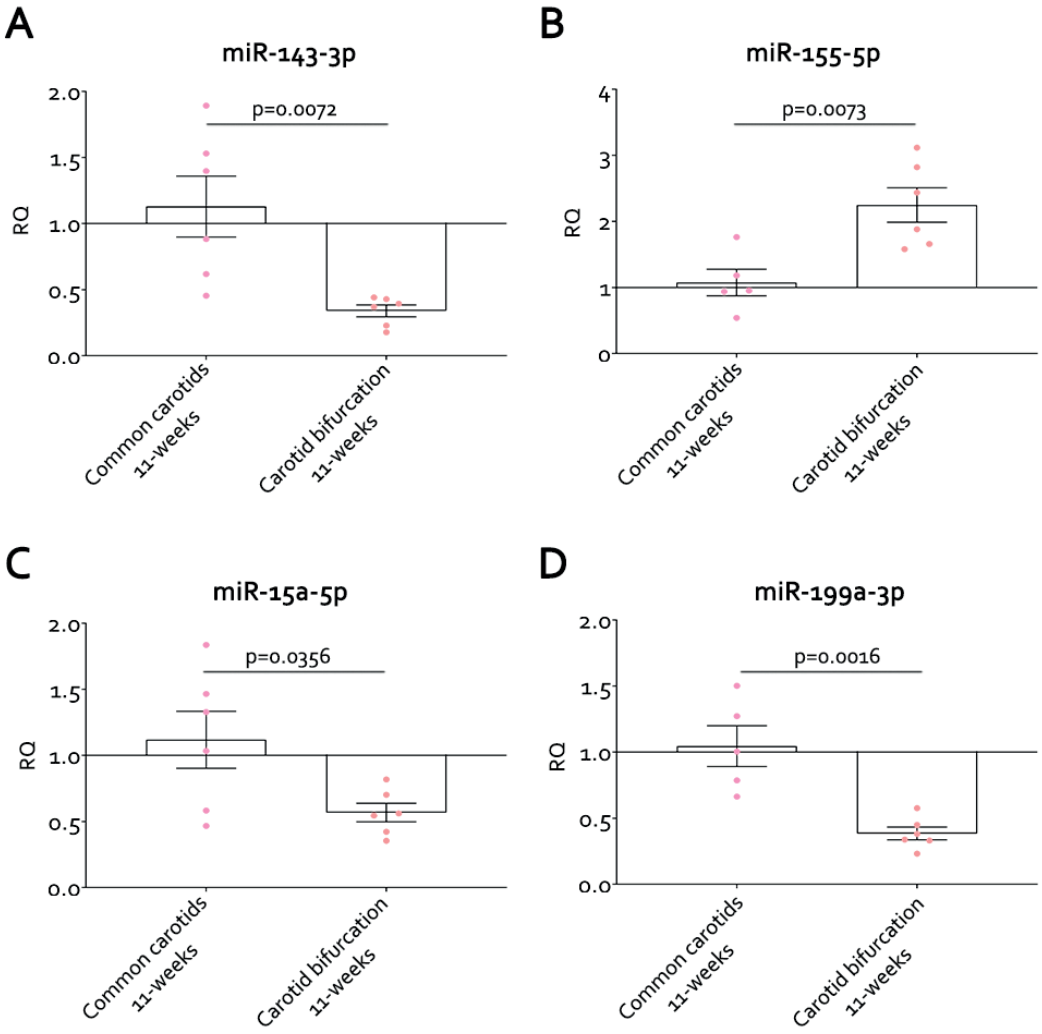

Figure 51. miR-143-3p, miR-155-5p, miR-15a-5p and miR-199a-3p levels are altered in the carotid bifurcation of mice with initial atherosclerosis. The expression of miR-143-3p **(A)**, miR-155-5p **(B)**, miR-15a-5p **(C)** and miR-199a-3p **(D)** was assessed in the common carotids and carotid bifurcation of the 11-weeks mice by RT-qPCR. RQ = relative quantification 11-weeks (n=6).

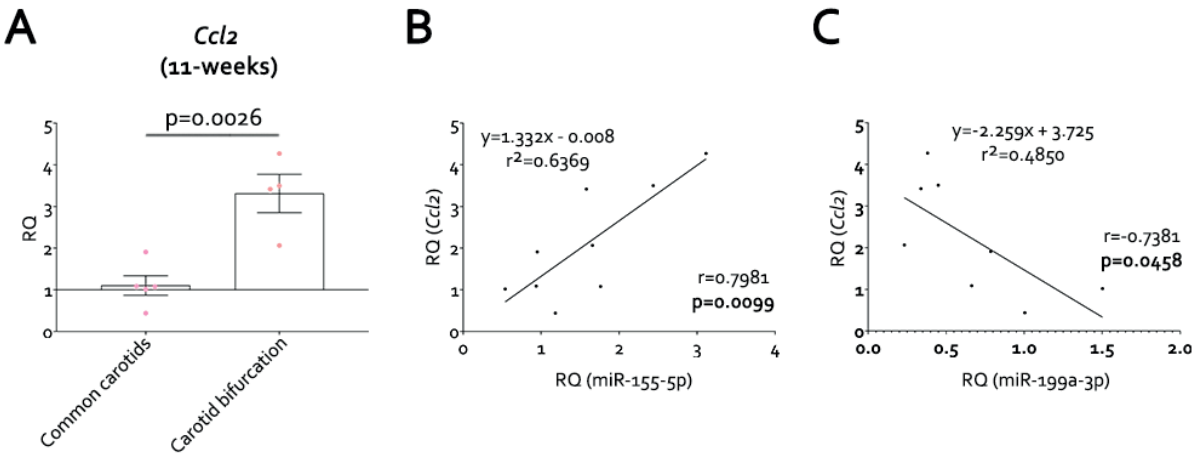

Figure 52. *Ccl2* is overexpressed in the carotid bifurcation of mice with initial atherosclerosis and correlates with the expression of miR-155-5p and miR-199a-3p. The expression of *Ccl2* **(A)** was assessed by RT-qPCR in the common carotids and carotid bifurcation of mice with an initial atherosclerosis. By a Pearson's correlation the expression of *Ccl2* was correlated with miR-155-5p **(B)** and miR-199a-3p **(C)**. *Ccl2*= gene encoding the monocyte chemoattractant protein 1. RQ= relative quantification. 11-weeks (n=6). Correlation between Ccl2 and miRNAs (n=10).

5.6.4. miR-143-3p, miR-155-5p, miR-15a-5p and miR-199a-3p are altered in CD3 cells in the spleen of mice with advanced atherosclerosis

Anton Gisterå's lab is an expert in the immunological side of atherosclerosis, so we wanted to dig deeper into how the miRNAs could modulate the inflammatory cells in an atherosclerotic process. To do so, we harvested the spleen from the 11- and 46-weeks mice and isolated CD3- cells (non-mature T cells) and CD3+ cells (mature T cells).

For the first analysis, we wanted to compare the expression of our miRNAs of interest in CD3+ cells from 11- and 46-weeks mice, which showed that miR-143-3p was the only one overexpressed in advanced atherosclerosis (Figure 53), and the expression of miR-199a-3p was undetectable in these cells via RT-qPCR.

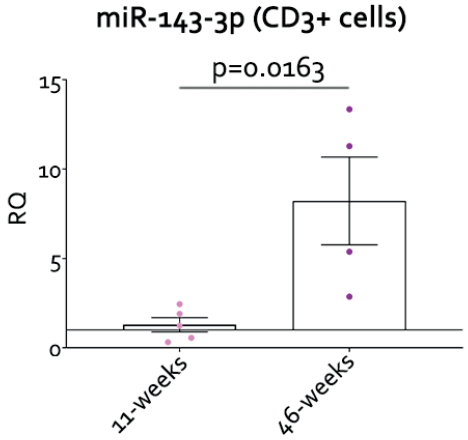

Figure 53. miR-143-3p is overexpressed in the CD3+ cells from the spleen of mice with advanced atherosclerosis. The expression of miR-143-3p was studied in the CD3+ cells from the spleen of 11- and 46-weeks old mice by RT-qPCR. RQ= relative quantification. 11-weeks (n=6); 46-weeks (n=4).

In addition, we wanted to analyse the levels of mRNA for different genes related to T cell (CD3+ positive cells) phenotype: *Il21* (Figure 54A), *Ifng* (Figure 54B), *Foxp3* (Figure 54C) and *Pdcd1* (Figure 54D). All of them were upregulated in the CD3+ cells from 46-weeks mice compared to 11-weeks mice. Like in other cases, when performing a correlation among gene-miRNAs, *Pdcd1* was directly correlated to miR-143-3p in the CD3+ cells.

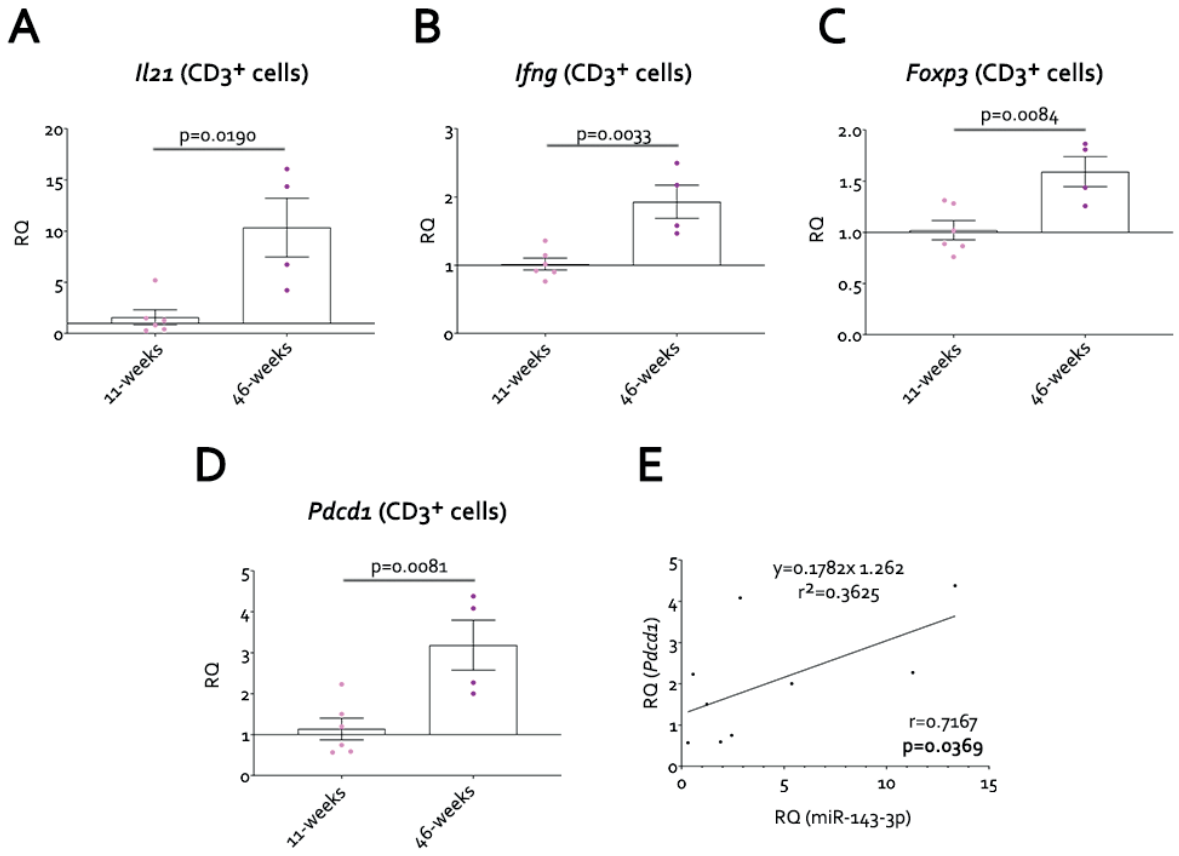

Figure 54. *Il21*, *Ifng*, *Foxp3* and *Pdcd1* levels are increased in CD3+ cells in mice with advanced atherosclerosis, and the last one correlates with miR-143-3p levels. The expression of *Il21* **(A)**, *Ifng* **(B)**, *Foxp3* **(C)** and *Pdcd1* **(D)** was studied in CD3+ cells from the spleen of mice with initial or advanced atherosclerosis by RT-qPCR. **(E)** We compared by Pearson's correlation the expression of those genes and miR-143-3p and only *Pdcd1* showed a significant correlation. RQ= relative quantification; *Il21*= gene encoding the interleukin 21; *Ifng*= gene encoding the interferon gamma; *Foxp3*= gene encoding the transcription factor Foxp3; *Pdcd1*= gene encoding the programmed cell death protein 1. 11-weeks (n=6); 46-weeks (n=4). Correlation between *Pdcd1* and miR 143-3p (n=10).

Then we also wanted to compare the expression of our miRNAs of interest in CD3- cells from our mice groups. In this case, miR-143-3p (Figure 55A), and miR-199a-3p levels were overexpressed (Figure 55B) in advanced atherosclerosis.

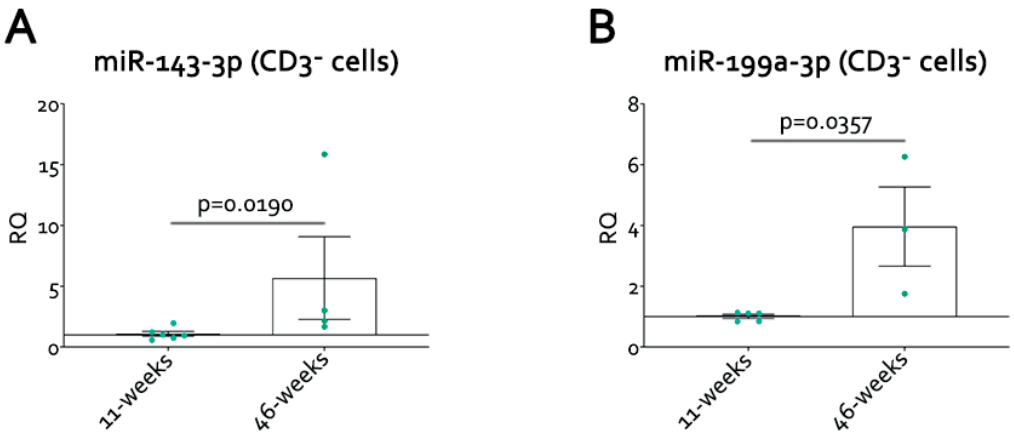

Figure 55. miR-143-3p and miR-199a-3p are overexpressed in CD3- cells from the spleen of mice with advanced atherosclerosis. The expression of miR-143-3p **(A)** and miR-199a-3p **(B)** was analysed in the CD3- cells from the spleen of mice with initial or advanced atherosclerosis by RT-qPCR. RQ= relative quantification. 11-weeks (n=6); 46-weeks (n=4).

Like with the carotids, we wanted to compare the expression of the miRNAs between $CD3^-$ and $CD3^+$ cells in initial atherosclerosis. This resulted in miR-155-5p (Figure 56A) and miR-15a-5p (Figure 56B) being overexpressed in $CD3^+$ cells compared with $CD3^-$ cells in young mice with initial atherosclerosis.

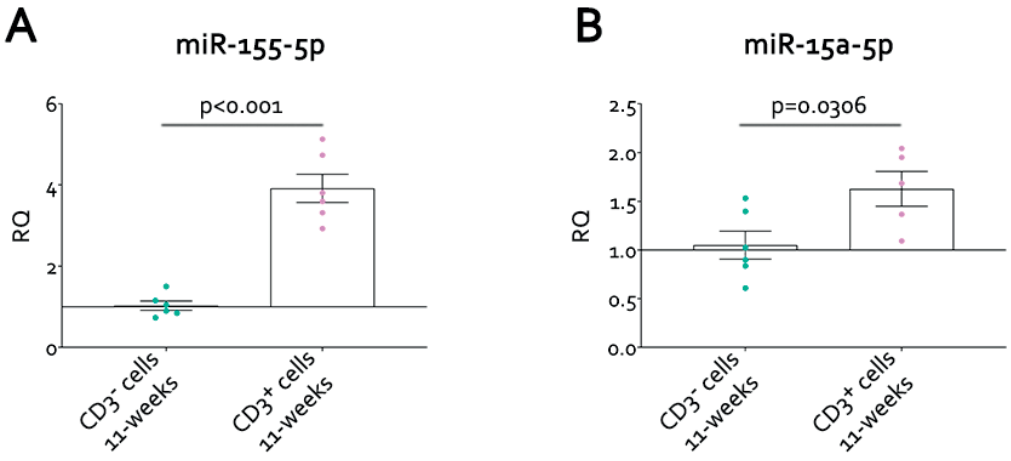

Figure 56. miR-155-5p and miR-15a-5p are overexpressed in $CD3^+$ cells from the spleen of mice with initial atherosclerosis. The expression of miR-155-5p **(A)** and miR-15a-5p **(B)** was analysed in the $CD3^+$ and $CD3^-$ cells from the spleen of mice with initial atherosclerosis by RT-qPCR. RQ= relative quantification.11-weeks (n=6).

Finally, we wanted to assess if there might be some kind of correlation between miRNAs levels in the inflammatory cells, the carotids, and atherosclerosis progression. For it, we calculated RQ values of miR-143-3p from 46-weeks mice referred to 11-weeks mice. miR-143-3p levels in $CD3^+$ (Figure 57A, left) or $CD3^-$ (Figure 57A, right) cells of carotid bifurcation show an inverse correlation with atherosclerosis progression. However, miR-155-5p levels in the common carotid and carotid bifurcation in initial atherosclerosis are correlated with the expression of $CD3^-$ and $CD3^+$ cells in mice with initial atherosclerosis (Figure 57B).

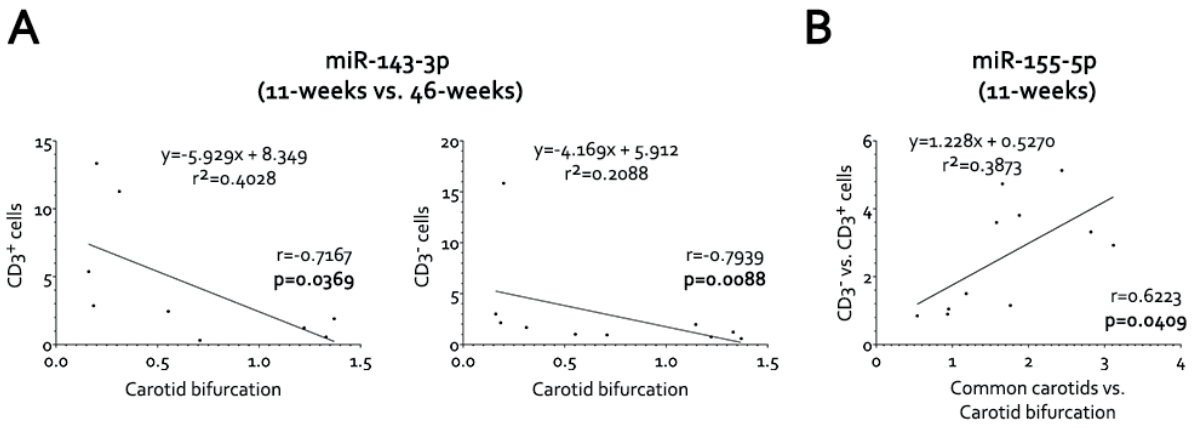

Figure 57. The expression of miR-143-3p and miR-155-p is correlated between $CD3$ cells and the carotids during atherosclerosis development. The expression of miR-143-3p was correlated by Pearson's correlation between the carotid bifurcation, $CD3^+$ cells **(A**, left) and $CD3^-$ cells **(A**, right) in mice with initial or advanced atherosclerosis. **(B)** The expression of miR-155-5p was correlated by Pearson's correlation between the common carotid vs. carotid bifurcation, and $CD3^-$ vs. $CD3^+$ cells in mice with initial atherosclerosis. 11-weeks (n=6); 46-weeks (n=4). Correlation between cells and carotids (n=10).

After finding these correlations, we wanted to study if the effects in the tissue may be because there was an increase in T cells (CD_3+ cells) in the actual atherosclerotic injuries. To answer that question, we performed an immunofluorescence against CD_4+, CD8+ and CD_3+ (Figure 58A), but there was no difference in the deposition of T cells between 11- or 46-week-old mice. However, there were more CD8+ cells in the 46-weeks group if compared with CD_4+ cells in the 11-weeks one (Figure 58B and C). However, thanks to the DAPI staining in the aortic root, we were able to identify a fibrotic cap in the advanced atherosclerotic injuries combined with a necrotic core.

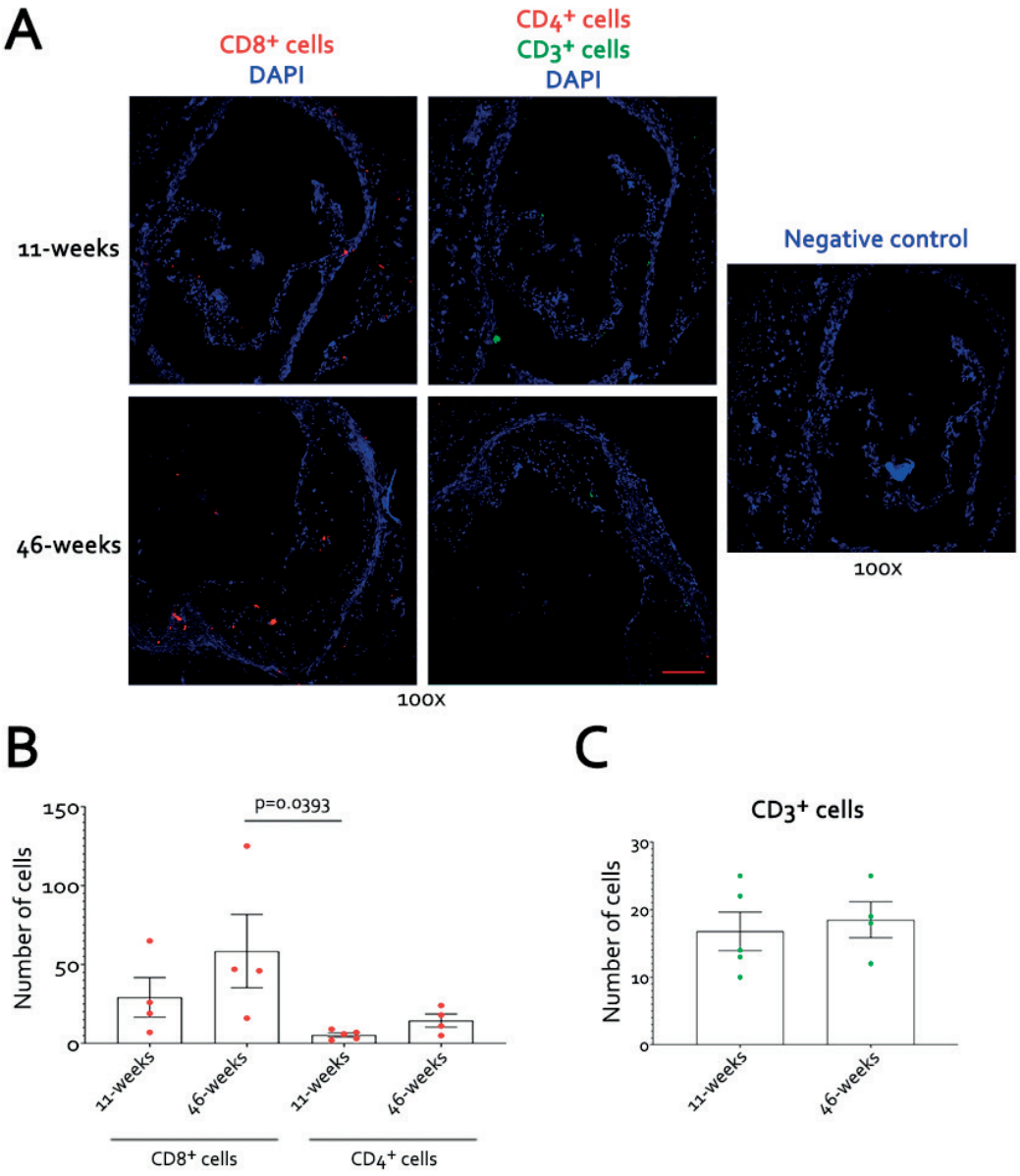

Figure 58. There are T cells in the atherosclerotic injury in the aortic roots in initial and advanced atherosclerosis. (A) To assess the T cell infiltration in the atherosclerotic injury, an immunofluorescence for CD8+, CD_4+, and CD_3+ cells were done in the aortic root of 11 and 46-weeks mice. Representative images of the immunofluorescence are shown. The CD8+ cells and CD_4+ cells **(B)** and CD_3+ cells **(C)** were counted in the initial and advanced atherosclerosis groups. 11-weeks (n=6); 46-weeks (n=4).

5.7. Identification of miRNAs as potential non-invasive biomarkers for advanced atherosclerosis

5.7.1. Profile of miRNAs in the plasma of the mouse model of atherosclerosis

miRNAs are soluble in the blood where they are mobilized inside exosomes. We wanted to study if the expression of our miRNAs of interest was altered in the mouse model of atherosclerosis, so we took the plasma from three groups of 18 weeks of diet and isolate miRNAs from them.

We first precipitated extracellular vesicles from the plasma and to assess if the vesicles were enriched in exosomes, we performed a Western blot of specific markers from the exosome's extracellular membrane like CD63 antigen and CD81 antigen and the absence of Golgi subfamily A member 2 (GM130), a specific marker from the surface of vesicles from the endoplasmic reticulum (Figure 59). We also used a cellular control from hepatocytes lines (Huh7 lysate) that is enriched in GM130 while poor in CD63 and CD81 (Figure 59).

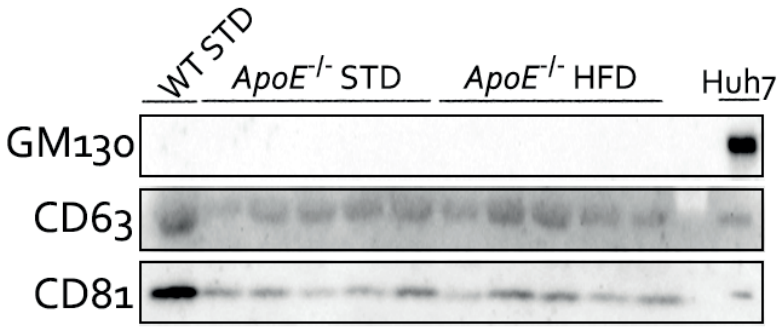

Figure 59. The plasma extracellular vesicles from our mice groups are enriched in exosomes. Representative images from the Western blot of exosomal positive markers like CD63 and CD81, and the negative marker GM130. All were compared to a control sample that is positive for GM130 and poor in exosomal markers. WT= wild-type; STD= standard type diet; *ApoE*$^{-/-}$= apolipoprotein E deficient mice; HFD= high-fat diet. WT STD (n=1); *ApoE*$^{-/-}$ STD (n=5); *ApoE*$^{-/-}$ HFD (n=5).

After confirming that the extracellular vesicles isolated were enriched in exosomes, we isolated the miRNAs and quantified the expression of miR-143-3p (Figure 60A), miR-155-5p (Figure 60B), miR-15a-5p (Figure 60C) and miR-199a-3p (Figure 60D), but there was no alteration in the levels of the miRNAs between the groups.

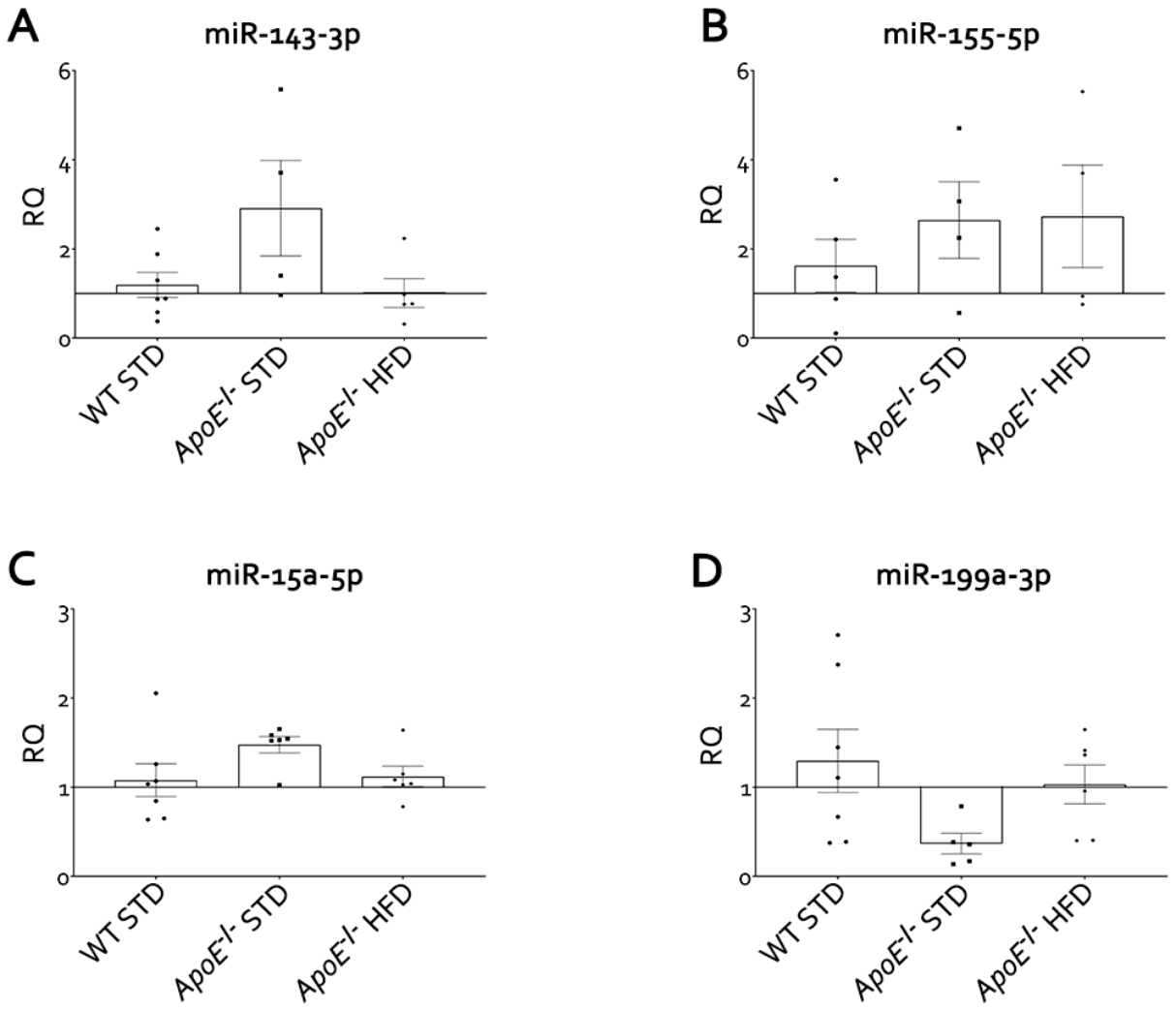

Figure 60. Study of miRNAs expression in the plasma of the experimental model of atherosclerosis. The exosomes from the plasma of three groups of 18 weeks of diet were precipitated and miRNAs were isolated from them. The expression of miR-143-3p **(A)**, miR-155-5p (B), miR-15a-5p **(C)** and miR-199a-3p **(D)** was analyzed by RT-qPCR. WT= wild-type; STD = standard type diet; *ApoE*$^{-/-}$= apolipoprotein E deficient mice; HFD= high-fat diet; RQ= relative quantification. WT STD (n=7); *ApoE*$^{-/-}$ STD (n=6); *ApoE*$^{-/-}$ HFD (n=6).

5.7.2. miR-143-3p, miR-15a-5p and miR-199a-3p are potential biomarkers for advanced carotid atherosclerosis

Even though the miRNAs studied were not altered in the plasma from our mouse model of atherosclerosis, we were interested in studying if they were altered in human atherosclerosis and might be potential diagnostic biomarkers for advanced atherosclerosis. We isolated miRNAs from plasma extracellular vesicles (EVs) from patients with ACA and Controls without atherosclerosis (Table 5).

Table 5. Clinical characteristics of patients bearing advanced carotid atherosclerosis (ACA).

	ACA Patients (Exosomes) (n=29)
Age, years	67 ± 10
Biological sex (male/female), %	72.4% / 27.6 %
BMI (Kg/m²)	28.8 ± 4.8
Diabetes mellitus, %	34.5 %
Hypertension, %	75.8 %
Coronary artery disease, %	100 %
Current smoking, %	27.6 %

To confirm whether the isolated EVs from plasma were enriched in exosomes, we analysed the presence of the exosome markers CD63 antigen and CD81 antigen and the absence of GM130. We did not find GM130 in the isolated EVs compared to positive controls (HUVECs lysate or Huh7 lysate) but we did find CD63 and CD81 expression (Figure 61A and B). In addition, we obtained that the diameter of the isolated EVs measured by DLS was between 10 and 106 nm, most exosomes having a diameter of 21.04–50.8 nm (Figure 62).

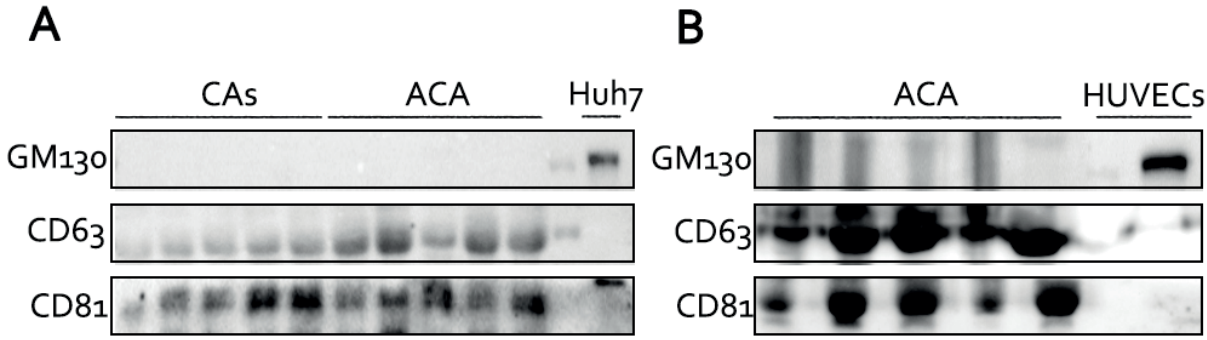

Figure 61. The isolated plasma extracellular vesicles are enriched in exosomes. Representative images from the Western blot of exosomal positive markers like CD63 and CD81, and the negative marker GM130. All were compared to a cellular control (Huh7 **(A)** or HUVECs **(B)** lysates) that is positive for GM130 and lacks exosomal markers **(A-B)**. CAs= control aortas; ACA= advanced carotid atherosclerosis; HUVECs= human umbilical vein endotelial cells. CAs (n=5); ACA (n=10).

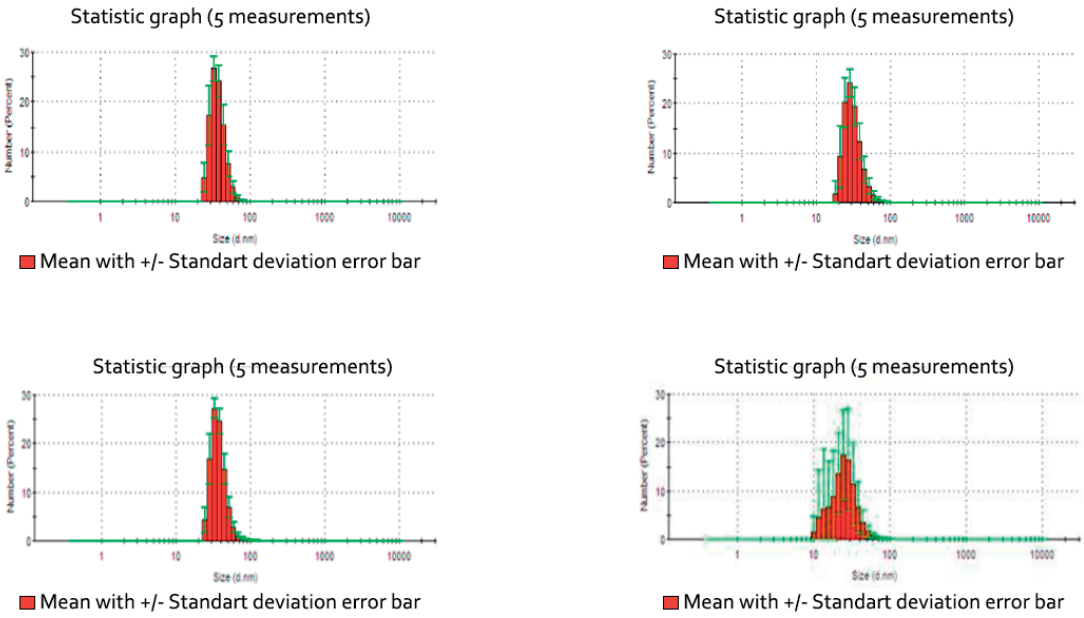

Figure 62. Characterization of size of extracellular vesicles isolated from plasma from patients with advanced carotid atherosclerosis. The size from the extracellular vesicles precipitated from the plasma of patients with ACA have mostly the size of exosomes. To further confirm that our extracellular vesicles were enriched in exosomes, we performed a dynamic light scattering analysis of each sample, here we represent the graphs from the size of the particles. These graphs represent the mean of 5 measurements of each sample.

After that, we isolated the miRNAs from EVs in control as well as in ACA patients. By RT-qPCR, we analyzed the expression of miR-143-3p, miR-155-5p, miR-15a-5p and miR-199a-3p. The levels of miR-143-3p were downregulated in the plasma from ACA patients (Figure 63A). In contrast, the levels of miR-15a-5p (Figure 63C) and miR-199a-3p (Figure 63D) were upregulated, while miR-155-5p showed no differences (Figure 63B).

Lastly, a receiver operating characteristic analysis curve (ROC) was performed to propose the altered miRNAs as possible non invasive biomarkers of advanced atherosclerosis (Figure 64). During this analysis different parameters were studied like the area under the curve (A.U.C.), that has a value between 0.0 and 1.1, and the closer this value is from 1, the better the proposed biomarker is; there are also two percentages: sensitivity, is the number of patients with ACA that you are able to discriminate as such, and the specificity is the number of healthy subjects that you are able to discriminate as such with accuracy depending on the variable that you are analysing, in this case depending on the expression of miRNA in CAs vs. ACA patients.

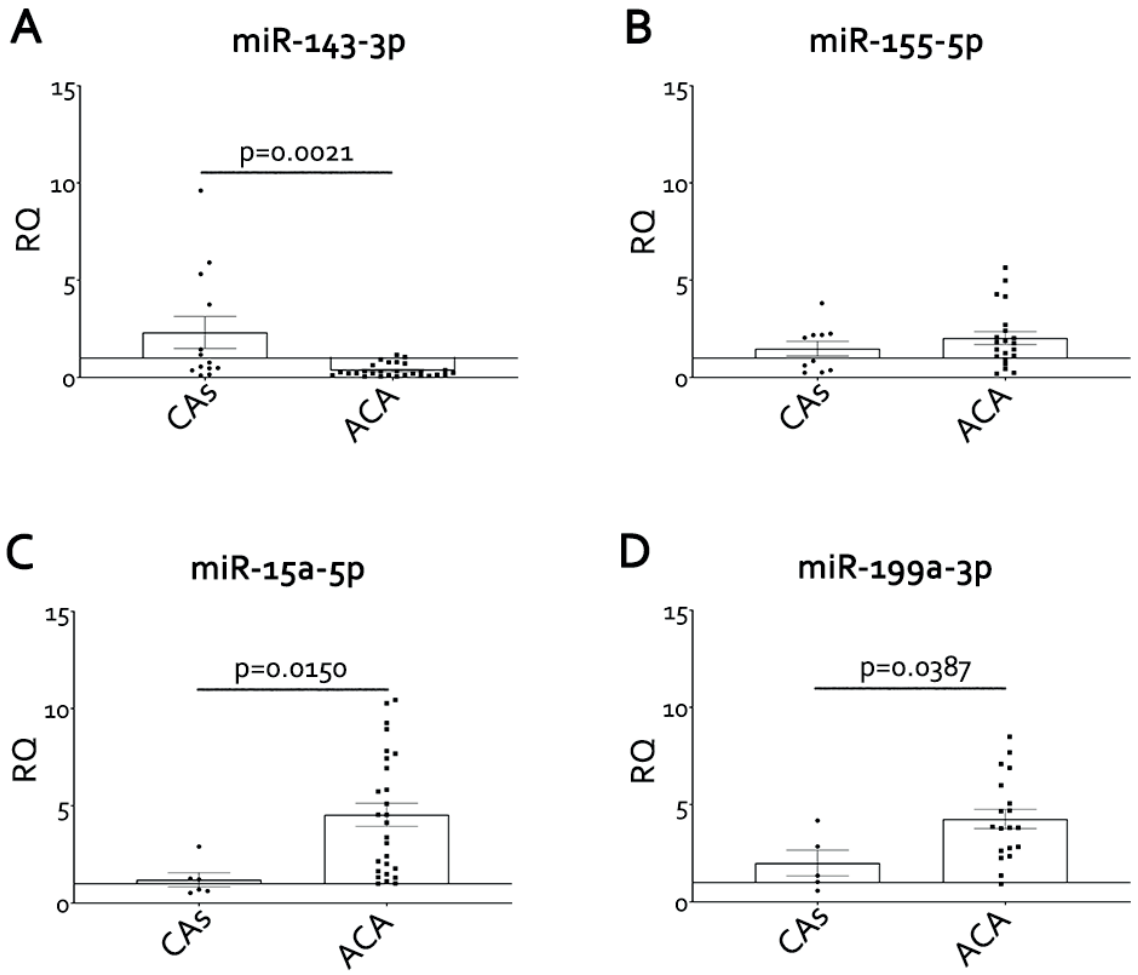

Figure 63. Study of miR-143-3p, miR-155-5p, miR-15a-5p and miR-199a-3p expression in the plasma of ACA patients. The exosomal expression of miR-143-3p **(A)**, miR-155-5p **(B)**, miR-15a-5p **(C)** and miR-199a-3p **(D)** was assessed by RT-qPCR. CAs= control aortas; ACA= advanced carotid atherosclerosis; RQ=relative quantification. CAs (n=6-13); ACA (n=28).

This study showed that all the altered miRNAs (miR-143-3p, miR-15a-5p and miR-199a-3p) could be potential biomarkers of the disease, having a significant difference in expression between control and ACA patients (Figure 64).

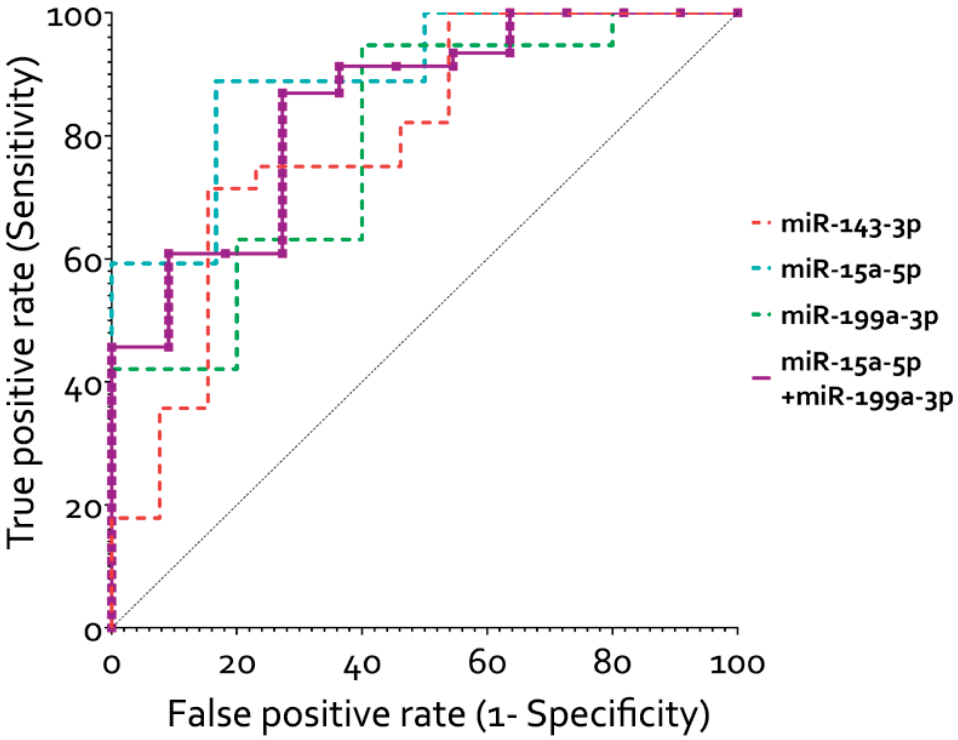

Figure 64. ROC curve representation of the different miRNAs from the plasma of the patients. Here we combined all the ROC curves that resulted from the analysis of the plasmatic miRNAs as biomarkers. The curve for individual miRNAs is represented by dashed lines and the combination of miRNAs by normal lines with symbols. The curve for miR-143-3p is coloured in red; miR-15a-5p is coloured in blue, miR-199a-3p is coloured in green; the combination of miR-15a-5p and miR-199a-3p is coloured in purple with square symbols.

In the case of miR-15a-5p and miR-199a-3p, that are overexpressed in ACA patients, we studied if the combination of the miRNAs would be better than individually, so we performed ROC analysis for miR-15a-5p and miR-199a-3p. Interestingly, the combination of the two miRNAs had a slight worst A.U.C. than individually, (Table 6), even though this combination had a more significant p value.

Table 6. Results from the ROC analysis of the differentially expressed miRNAs in ACA patient's plasma. In this table all the ROC analysis parameters are shown, area under the curve (A.U.C.) with the 95% confident interval (95% CI), the sensitivity (Sens %) and specificity (Spec %) percentages, the high-low limit (H-L) which informs the value of expression of the miRNA that can discriminate between the most CAs and ACA patients, and the p value.

Model	A.U.C. (95% CI)	Sens %	Spec %	H-L	p value
miR-143-3p	**0.7940** (0.64, 0.95)	71.43	84.62	<0.343	**0.0027**
miR-15a-5p	**0.8951** (0.72, 0.96)	88.89	83.33	>1.278	**0.0028**
miR-199a-3p	**0.7895** (0.57, 0.92)	78.95	60.00	>2.485	0.0506
miR-15a-5p + miR-199a-3p	**0.8458** (0.74,0.94)	86.96	72.73	>1.351	**0.0004**

Once confirmed as potential non-invasive biomarkers of advanced atherosclerosis, we performed different assessments of the circulating levels of miRNAs and clinical characteristics. As we had previously obtained that miR-155-5p levels in carotid plaque is higher in diabetic patients, we also evaluated this relationship in the circulating levels of the four miRNAs studied. The expression of miR-143-3p was decreased in both diabetic or non-diabetic ACA patients compared to control (Figure 65A); miR-155-5p (Figure 65B) and miR 199a 3p (Figure 65D) showed no difference among diabetic or non-diabetic ACA patients; and lastly, the levels of miR-15a-5p (Figure 65C) were only increased in non-diabetic patients compared with the CAs.

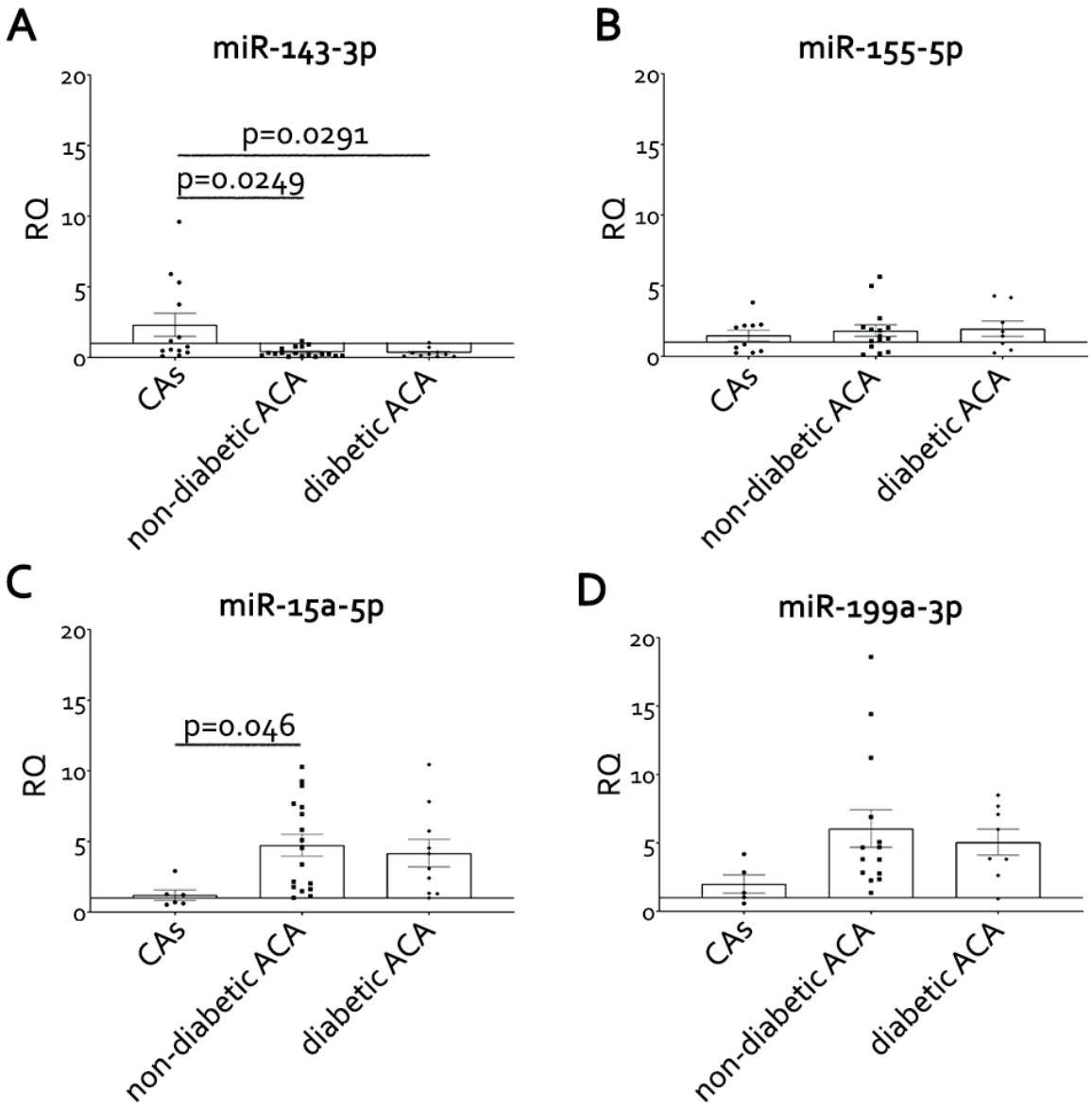

Figure 65. Analysis of circulating miRNAs expression in ACA patients with or without diabetes. Patients with ACA were separated in diabetic and non-diabetic according to their clinical information and **(A)** miR-143-3p, **(B)** miR-155-5p, **(C)** miR-15a-5p and **(D)** miR-199a-3p expression was quantified using RT-qPCR in plasma samples. CAs= control aortas; ACA= advanced carotid atherosclerosis; RQ = relative quantification. CAs (n=13); ACA (non-diabetic (n=17); ACA diabetic (n=10).

Finally, the ACA patients were grouped by their biological sex, but only miR-15a-5p and miR-199a-3p showed some kind of differential profile. The expression of miR-15a-5p was increased in women with advanced carotid atherosclerosis when compared to controls (Figure 66A); while miR-199a-3p was increased in women if compared with controls and men patients (Figure 66B).

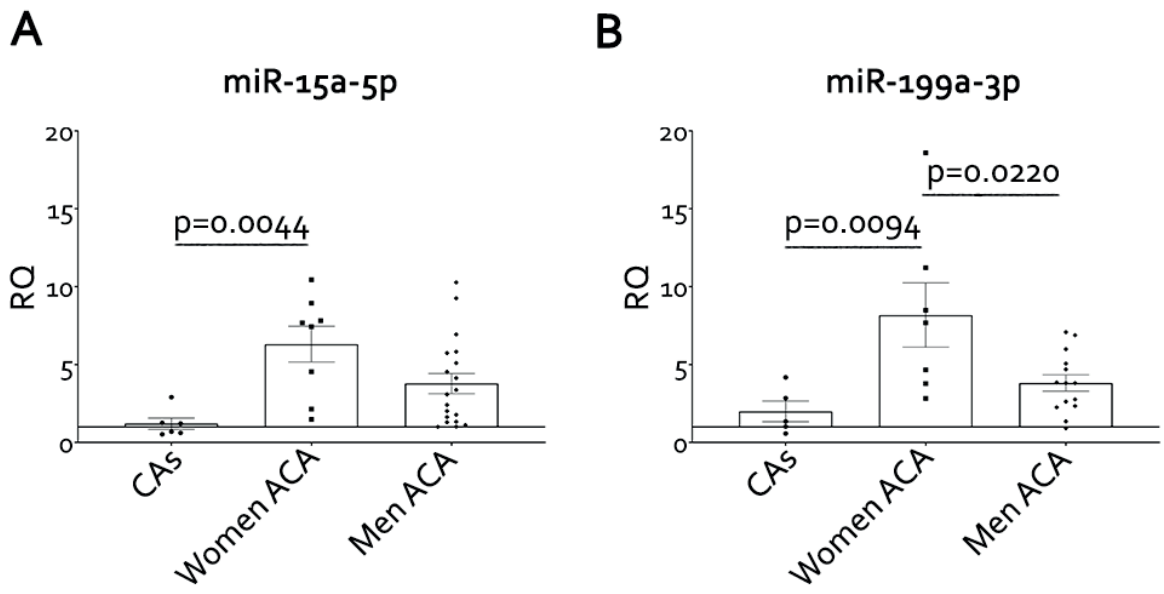

Figure 66. Analysis of miR-15a-5p and miR-199a-3p in the plasma of the patients with advanced atherosclerosis according to their biological sex. The patients with ACA were grouped by their biological sex, and the expression of miR-15a-5p **(A)** and miR-199a-3p **(B)** was assessed by RT-qPCR. CAs=control aortas; ACA= advanced carotid atherosclerosis; RQ= relative quantification. CAs (n=6); ACA (women (n=8)); ACA (men (n=19)).

"Para algunos, la vida es galopar
por un camino empedrado
de horas, minutos y segundos,
yo, que más humilde soy,
solo quiero que la ola que surge
del último suspiro de un segundo,
me transporte mecido
hasta el siguiente"

-Salir, Extremoduro

6. Discussion

6. DISCUSSION

The underlying pathology behind many cardiovascular diseases is atherosclerosis, a pathological process affecting large and medium-sized arteries with many contributing factors: endothelial dysfunction, VSMCs and macrophage phenotype-switching, lymphocyte infiltration, inflammation, oxidative stress, cell apoptosis, cell proliferation, and miRNA dysregulation, are all examples of factors that can promote atherosclerosis progression and the development of disease manifestations such as stroke or myocardial infarction (163,170–173). In our studies, we confirmed that several miRNAs were altered during atherosclerosis progression in early and advanced experimental atherosclerosis as well as in humans with advanced carotid atherosclerosis. This led us to a focused interest in miR-143-3p, miR-155-5p, miR-15a-5p, and miR-199a-3p.

6.1. miR-143-3p is dysregulated during atherosclerosis progression

At atherosclerosis-prone sites in the vasculature, apoptosis of endothelial and VSMCs can promote the progression of the disease (174). In line with this, miRNAs levels can be altered, not only as a consequence of the disease but can be causative in modulating pro-atherosclerotic mechanisms like apoptosis (175). In our work, we propose that the dysregulation of miR-143-3p during atherosclerosis may increase apoptosis of vascular cells leading to the progression of the disease.

miR-143-3p is dysregulated in different diseases like cancer, e.g. downregulation of the miRNA in hepatocellular carcinoma cells modulates their growth and apoptosis by targeting the fibroblast growth factor 1 (176); Alzheimer's disease, where miR-143-3p is downregulated promoting Tau protein phosphorylation by targeting the death-associated protein kinase 1 (177); and acute myocardial infarction, where miR 143-3p is also downregulated and its expression can be restored by skeletal myoblast transplantation treatment (178).

When discussing the available scientific literature on miR-143-3p in atherosclerosis, a large part of the bibliography is contradictory regarding the cluster formed by miR-143/miR-145, or only miR-143. Many references do not specify if it is the 3p or 5p sequence. It is known that the miR-143/miR-145 cluster is crucial for the correct function and phenotype of VSMCs. Several publications state that increased expression of both miR-143/miR-145 promotes the contractile phenotype of VSMCs while decreases the proliferative phenotype (179,180). In this direction, some authors state that the ablation of miR-143/miR-145 increases atherosclerotic injuries in several mouse models (181). However, other studies have given a protective role to the miR-143/miR-145 cluster, *Ldlr*$^{-/-}$ mice also deficient in the miR-143/miR-145 cluster, showed less atherosclerosis (182). In addition, other authors have shown that miR-143 seems to be increased in human atherosclerotic injuries and endothelial cell dysfunction altering endothelial glycolysis (183). In our case, we show a decreased expression of miR-143-3p throughout our experimental and human atherosclerosis studies. Taken together, this is indicative that miR-143 confers protection for the malady.

Another point that is important in the atherosclerosis development is the age and the location of the plaque. Age is indeed the most prominent risk factor for having larger plaques (184). Regarding the location in the vasculature, low-shear stress areas with a turbulent flow, like the carotid bifurcation or the lesser curvature of the aorta, develop atherosclerosis faster than other areas with high-shear stress and laminar flow like the internal mammary arteries, or the common carotids. Most of the studies done in humans investigate carotid atherosclerosis while in mice it is more common to investigate atherosclerosis in the aorta, specifically in aortic roots where they develop the maximum lesion (185). We found that miR-143-3p was downregulated in the whole aorta and carotid bifurcation of young mice with initial atherosclerosis development, as well as in the carotid bifurcation and common carotids of "middle-aged" HuBL mice with 46-weeks-of-age that showed advanced atherosclerosis. In addition, miR-143-3p was downregulated in the carotid plaques of patients with advanced atherosclerosis as

compared with subjects without atherosclerosis or with early aortic atherosclerosis. We compared the miRNA expression in the aorta and carotids because even though the aorta and the carotids are very different anatomically and size-wise, the miRNA expression between the thoracic aorta and the carotids is very similar and comparable, only showing differences with the femoral aorta (186). In our case, we were able to correlate the expression of miR-143-3p in the aorta and carotids of our mouse models and the severity of the atherosclerotic injury. Similarly, the expression of other miRNAs such as miR-33a and miR-33b has also been related to atherosclerosis progression (187).

Next, we used miRNA-target interaction databases to select targets of miR-143-3p that may be promoting atherosclerosis. We selected the IGF-IIR since this protein has been confirmed as a target of miR-143-3p in the metabolic syndrome (188), but not atherosclerosis. In our experimental model of atherosclerosis, HFD-fed *ApoE*$^{-/-}$ mice showed lower miR-143-3p expression and a consequent increase in IGF-IIR expression (although the difference observed in the IGF-IIR was not statistically significant). In the same way, we obtained a significant decrease of the IGF-IIR in HUVECs and VSMCs after overexpressing the miR-143-3p using mimics. In addition, previous results from our group showed that IGF-IIR was overexpressed in the shoulder area of carotid plaques from patients with advanced atherosclerosis (141). For a long time, IGF-IIR only served as a plasmatic and tissue regulator of IGF-II, that participated in tissue growth (22). In this line, we found that there was an increase in the plasmatic expression of IGF-IIR that correlated with a decrease in IGF-II after 18 weeks of HFD in our *ApoE*$^{-/-}$ mouse model, but more investigation is needed to assess how this is related to atherosclerosis.

Nowadays, it is confirmed that IGF-IIR has a G protein activity when IGF-II is coupled to the receptor (132), but the pathway and effects of this activation need to be fully elucidated. It is confirmed that IGF-IIR decreases cardiomyocyte viability by activating the ERK1/2 cascade and increasing mitophagy and Bcl-2 phosphorylation (189). Other studies performed in cardiomyocytes confirm IGF-IIR as a promoter of apoptosis. Ang-II via the activation of jun kinase 1, promotes the degradation of sirtuin-1 and the heat-shock transcription factor 1 that in normal conditions impairs the transcription of IGF-IIR, protecting the cardiomyocytes; but an increase in IGF-IIR augments the caspase-3 activity and apoptosis in those cells (133). In agreement with those results, previous studies from our group demonstrated that the upregulation of IGF-IIR in atherosclerotic lesions could contribute to plaque instability by two potential mechanisms: reducing IGF-II bioavailability and thereby less effect on cell survival, or increasing apoptosis of plaque-resident cells (141). Moreover, miR-143-3p has been shown to modulate apoptosis not only in cardiomyocytes but in astrocytes, and bladder carcinoma cells (190–192). Taking all this data into consideration, we wanted to assess if an increase in miR-143-3p may protect HUVECs and VSMCs from apoptosis. Our results show that miR-143-3p overexpression reduced the apoptosis in both cell types in the presence of pro-apoptotic signals. For these reasons, we propose a protective role of miR-143-3p in atherosclerosis progression by modulating IGF-IIR and apoptosis, but the exact pathway remains to be elucidated (Figure XIV).

The atherosclerosis process in experimental models has been associated with the development of germinal centres in the spleen, and the foundation of T-cell-dependent humoral responses leading to the production of high-affinity antibodies (193,194). Since the systemic implications of miRNA dysregulation in atherosclerosis are not thoroughly explored, we wanted to study if miR-143-3p was altered in the spleen of mice during atherosclerosis progression. To do so, we sorted $CD3^+$ cells (mature T cells) and $CD3^-$ cells (B cells, and others) from the spleen of the HuBL mice. This revealed that miR-143-3p was overexpressed in $CD3^+$ cells and $CD3^-$ cells from the spleen of mice with advanced atherosclerosis as compared to controls. There are very few publications about the expression of miR-143 3p in $CD3^+$ or $CD3^-$ cells and the effects of this miRNA in these cells. One study has shown that miR-143-3p is downregulated in $CD3^+$ cytokine-induced killer cells that upregulate TNFα and IFNγ in oncogenic mouse models (195).

Due to the lack of literature on this topic, we wanted to delve into the phenotype of the $CD3^+$ cells from mice with advanced atherosclerosis and observe correlations to miR-143-3p. The splenic $CD3^+$ T cells showed an increase in the mRNA of *Il21*, *Ifng*, *Foxp3*, and *Pdcd1*. Interestingly, only *Pdcd1* levels, encoding PD-1 (programmed cell death protein-1), positively correlated with miR-143-3p. IFNγ (encoded by *Ifng*) is the hallmark cytokine of Th1 responses that may lead to plaque rupture and instability (78), while *Foxp3* is expressed in Treg cells that are atheroprotective. PD-1 is an immune checkpoint molecule and is considered a T cell exhaustion marker in chronic infections. It is also expressed in activated $CD8^+$ T cells in atherosclerosis and blocking PD-1 could increase the production of pro-atherogenic cytokines (196). Our transcriptional profiling of the $CD3^+$ cells in mice with advanced atherosclerosis indicates that these T cells are more atherogenic and shows an increase in miR-143-3p levels, however, to assess the implications in atherosclerosis development, further functional investigations are needed.

Surprisingly, we were able to inversely correlate the expression of miR-143-3p during atherosclerosis progression in the carotid bifurcation of HuBL mice with the expression of the miRNA in both $CD3^+$ and $CD3^-$ cells. This indicates that these processes are intertwined or commonly regulated by organ crosstalk. Pro-inflammatory molecules like MCP-1 and adhesion molecules like VCAM-1 that promote lymphocyte infiltration in the vessel wall are upregulated during atherosclerosis development (197,198). In line with this, we found that the mRNAs for *Ccl2* (encoding MCP-1) and *Vcam1* (encoding VCAM-1) were increased in the common carotids of 46-week HuBL mice with advanced atherosclerosis. The expression of these miRNAs was inversely correlated with the expression of miR-143-3p. This reaffirms their opposing roles in atherosclerosis, known from the literature. Taken together, further investigations into how the expression of miR-143-3p in immune effector cells and the carotids affects the progression of the disease are warranted.

Even if MCP-1 and VCAM-1 do not appear as possible targets in any miRNA-target databases, a recent report by Xiong *et al.* showed that an increase of miR-143-3p levels in cardiomyocytes protects against apoptosis, and an increase in VCAM-1 and ICAM-1 expression by modulating the neuropeptide Y and the circular RNA mmu_circ_0000021 expression (199). Zhou *et al.* also stated that an increase in miR-143-3p decreased the expression of MCP 1 via the modulation of GLUT9, a target of miR-143-3p in renal tubular epithelial cells (200). This indicates that a decrease in miR-143-3p may indirectly increase *Ccl2* and *Vcam1* in the carotids, but a proper investigation in VSMCs and endothelial cells is still needed to confirm this. To assess T cell infiltration in the atherosclerotic plaques, we performed an IF for the T cell markers CD8, $CD4$, and $CD3$, finding no obvious increase in lymphocyte infiltration between initial and advanced atherosclerosis. A small sample size and technical issues obstructed further conclusions regarding these data. Consistent with previous reports, there was a high infiltration of $CD8^+$ cells in the plaques as compared to $CD4^+$ cells (13). Nonetheless, the effect of $CD4^+$ cells might be more prominent (201) compared to $CD8^+$ cells in the atherosclerotic plaques of HuBL mice (202).

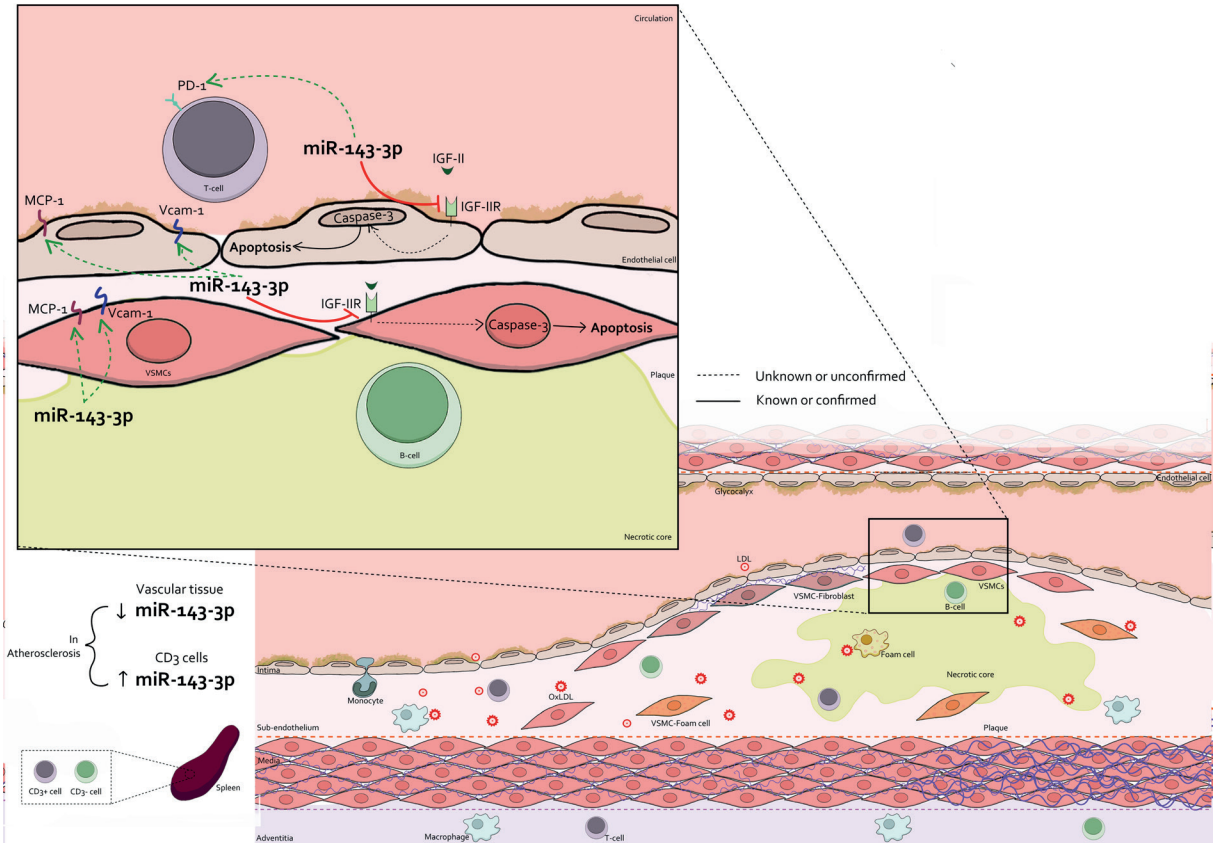

Figure XIV. Representation of miR-143-3p dysregulation in atherosclerosis. Atherosclerosis progression is represented with VSMCs migration; monocytes, macrophage, T and B-cell infiltration; the infiltration and oxidation of LDL, VSMCs phenotype switching, the formation of foam cells and necrotic core. In addition, the zoomed-in area represents the effect of miR-143-3p in VSMCs and endothelial cell apoptosis, where it acts by diminishing the expression of IGF-IIR that decreases caspase-3 activation and therefore apoptosis; also, other proteins like MCP 1, and VCAM-1 are indirectly correlated with the expression of the miRNA; the illustration also shows the increase in PD-1 in T-cells that correlates with the expression of miR-143-3p. Dashed lines represent unknown or unconfirmed molecular effects, while continued lines represent known or confirmed effects from one molecule to the other. Red lines represent inhibition and green lines activation by the miR-143-3p. Black lines represent the direction of the signalling pathway. IGF-II= insulin-like growth factor type-2, IGF-IIR= IGF-II receptor, LDL= low-density lipoprotein, Ox-LDL= oxidized LDL, PD-1= programmed cell death protein 1, MCP-1= monocyte chemoattractant protein-1, VCAM-1= vascular cell adhesion molecule-1, VSMCs= vascular smooth muscle cells.

6.2. miR-155-5p is increased during atherosclerosis development

Metabolic syndrome is a cluster of conditions that occur together, increasing the risk of cardiovascular diseases and type 2 diabetes. Its components, obesity, hypertension, dyslipidemia, and elevated blood glucose are considered risk factors for atherosclerosis (203). However, the exact relation between glucose levels, insulin resistance, and atherosclerosis remains unknown (140). In this sense, miRNAs could potentially be a link between the vasculature that directly modulates targets in the insulin pathway. This is why we wanted to assess how the dysregulation of miR-155-5p may affect insulin resistance and related pathways in an atherosclerotic context.

miR-155-5p seems to play a controversial role in atherosclerosis and the most plausible explanation might be that the function of miR-155-5p depends on the phase of atherosclerosis. Thus, miR-155-5p could delay atherosclerosis development in the early phases, while it could promote its progression in advanced stages (204,205). Some reports suggest that this miRNA is increased in patients with advanced carotid atherosclerosis (206) while others suggest that is downregulated (207). In addition, some authors indicate that a decrease in miR-155-5p expression can be protective to restore endothelial function by inhibiting lipid uptake and inflammation in macrophages (208,209), while others propose that a decrease in miR-155-5p could be protective by limiting foam cell formation by targeting proteins like the scavenger receptor CD36 or by decreasing cell proliferation of HUVECs and VSMCs (207,210). Moreover, studies using macrophages as a model for advanced atherosclerosis, demonstrated that a treatment using antagomiR-155 attenuated atherosclerosis development and progression (211). Similarly, lower plaque sizes were observed in *ApoE*$^{-/-}$ mice with a leukocyte specific miR-155 deficiency (212) or in *ApoE*$^{-/-}$ *miR-155*$^{-/-}$ double knockout mice (213). However, there is indeed more bibliography that proposes miR-155-5p to be a promoter of atherosclerosis rather than a protector. Our results are more in tune with the first option since we found that miR-155-5p was overexpressed in the whole aorta and carotid bifurcation of mice with early atherosclerosis as well as the common carotids of 46-week-old mice with advanced atherosclerosis. Moreover, an upregulation was also observed in the carotid plaques of patients with advanced atherosclerosis; and the expression of miR-155-5p positively correlated with atherosclerosis progression in *ApoE*$^{-/-}$ and HuBL mice.

After screening miRNA-target databases we decided to study: AKT, eNOS, and p85α. AKT and p85α are confirmed targets of miR-155-5p (207,214). We also obtained a decrease in AKT and p85α expression after induction of miR-155-5p in VSMCs. However, the direct interaction between NOS3 (encoding eNOS) and miR-155-5p is not confirmed yet via dual luciferase assays, even though it is confirmed that eNOS protein levels are regulated by miR-155-5p (215,216). In line with this, we observed a decrease in AKT and eNOS protein levels after the induction of miR-155-5p expression in HUVECs.

Prior to the *in vitro* assays, we could show that AKT was decreased in the whole aorta of *ApoE*$^{-/-}$ mice after 18 weeks of high fat diet as well as in the patients with advanced carotid atherosclerosis when compared with control arteries. AKT protein levels were negatively correlated with the levels of miR-155-5p. AKT promotes proliferation and survival of VSMCs and ECs during atherosclerosis (207,217,218). AKT levels were higher in fibro-lipidic plaques, representing an early stage of the disease, as compared to advanced carotid atherosclerosis. In initial plaque formation, there is more VSMCs proliferation and migration, and AKT is generally increased during these processes (207). In contrast, in more advanced plaque stages there is an increase in vascular cell apoptosis where AKT is decreased (219). AKT is not only involved in cell survival and apoptosis but it is also crucial for other pathways like the insulin response pathway (21). We studied insulin responses in the aorta from 18-weeks mice and only the mice fed a HFD showed a lack of insulin response measured by phosphorylation of AKT in S473. Measuring the phosphorylation of this residue is one of the main ways to assess insulin signalling and the approach has been validated by different authors (220–222). In our case, we confirmed that the increased expression of miR-155-5p in VSMCs decreased AKT levels and phosphorylated-S473 after insulin stimulation. We propose that the increase of miR-155-5p could be inducing vascular insulin resistance in atherosclerosis by decreasing AKT.

miR-155-5p is widely known as a modulator of inflammation and cellular lipid accumulation. As it has been previously shown, miR-155-5p promotes white adipocyte differentiation and inhibits brown/beige phenotypes. Therefore, a decrease of this miRNA has been proposed as a protective mechanism against obesity (223). In addition, the accumulation of white adipose tissue in patients is related to an impairment in the PI3K/AKT pathway and the risk of the development of type 2 diabetes and CVDs that correlates with the increase in BMI (224,225). We studied associations with BMI in miR-155-5p and AKT expression in human vascular samples and we could show an increase in miR-155-5p expression and a decrease in AKT expression that correlated with BMI. In addition, we wanted to study if the expression of the miRNA was related to other clinical characteristics of the patients with advanced carotid atherosclerosis, such as symptomatology and type 2 diabetes. In both cases, patients with type 2 diabetes and symptomatic plaques showed higher expression of miR-155-5p. Taking into account that the transcription of miR-155-5p is driven by inflammation (215) and that symptomatic plaques (226), diabetic (227) and obese (225) patients have higher inflammation, this could be a likely explanation for the increase in miR-155-5p expression, but further experiments are needed to confirm this (Figure XV).

Lastly, we obtained an increase in miR-155-5p in the common carotids of HuBL mice with advanced atherosclerosis that positively correlated with an increase in *Ccl2, Vcam1,* and *Il1β* mRNA levels. As previously stated, *Ccl2* and *Vcam1* are increased in advanced atherosclerosis which is also the case for *Il1β* (228). These miRNAs do not appear to be targeted by miR-155-5p, but there is an increase in *Ccl2* (encoding MCP-1), *Vcam1, Il1β*, and miR-155-5p in response to NF-κB (229), and this inflammatory pathway is increased in atherosclerosis (230–232). Therefore, this increase in miR-155-5p, *Ccl2, Vcam1,* and *Il1β* in advanced atherosclerosis may be due to an increase in NF-κB. In this sense, it has been reported that NF-κB-p65 interacts with the promoter site of miR-155, and thus NF-κB activation promotes miR-155 transcription (233). In this regard, the overexpression of miR-155-5p observed in advanced atherosclerosis could be induced by NF-κB activation itself since some groups have described a significant NF-κB activation in advanced carotid atherosclerosis (234,235) as well as in aortic root from *ApoE*$^{-/-}$ mice under HFD (236), both similar to the samples used by us.

Nevertheless, increased *Ccl2* and *Vcam1* promote the infiltration of leukocytes in the vascular wall (146), so we studied the expression of miR-155-5p in the $CD3^+$ and $CD3^-$ cell populations from the spleen of the HuBL mice, this miRNA was increased in the $CD3^+$ cells from mice with initial atherosclerosis compared with $CD3^-$ cells, and the expression positively correlated with the expression of miR-155-5p in the carotid bifurcation compared with the common carotids. miRNAs also serve as signals between cell types in different diseases (237). Specifically, miR-155-5p has been studied as an exosomal signal from different types of T cells. Th17-derived miR-155-5p increases inflammation and aggravates systemic sclerosis (238). miR-155-5p could also activate $CD8^+$ cells to decrease tumor growth in ovarian cancer (239) and promote macrophage polarization to an M1-like phenotype (240). Hence, the increase in miR-155-5p in the carotid bifurcation could be due to miR-155-5p-enriched exosomes

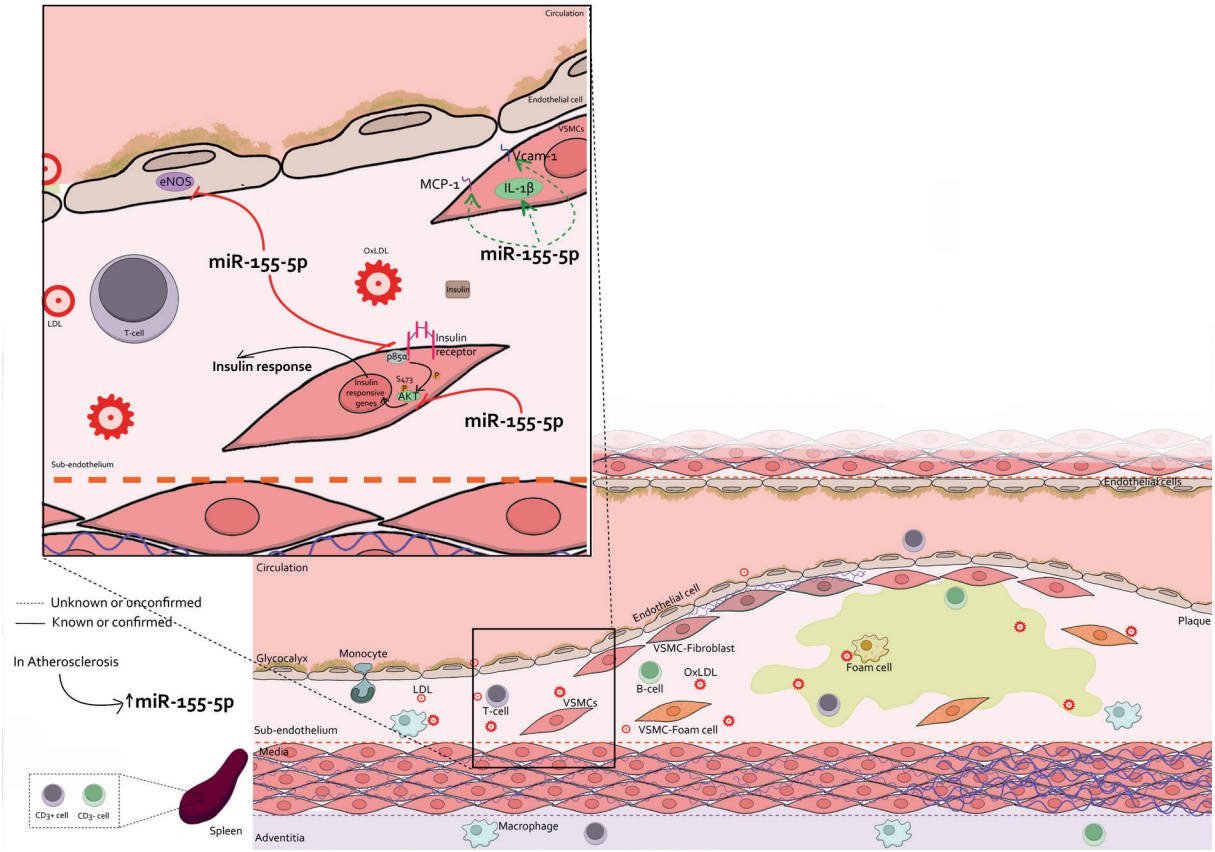

Figure XV. Representation of miR-155-5p dysregulation in atherosclerosis. The first steps in atherosclerosis are represented by VSMCs migration; monocytes, macrophage, T- and B-cell infiltration; the oxidation of LDL, and VSMCs phenotype switching. In addition, the zoomed-in area represents the effect of miR-155-5p in VSMCs, where it acts by diminishing the expression of AKT and p85α to decrease insulin response; also, other proteins like MCP-1, IL-1β, and VCAM-1 are directly correlated with the expression of the miRNA; and in HUVECs where miR-155-5p also diminishes eNOS. Dashed lines represent unknown or unconfirmed relationships between molecules, and continued lines known or confirmed effects between molecules. Red lines represent inhibition and green lines activation by miR-155-5p. Black lines represent the direction of the signalling pathway. AKT= protein kinase B, p85α= phosphoinositide-3-Kinase Regulatory Subunit 1, LDL= low-density lipoprotein, Ox-LDL= oxidized LDL, eNOS= endothelial nitric oxide synthase, MCP-1= monocyte chemoattractant protein-1, VCAM-1= vascular cell adhesion molecule-1, IL-1β= interleukin-1 beta, VSMCs= vascular smooth muscle cells, S473= serine 473.

6.3. miR-15a-5p and miR-199a-3p downregulation and the promotion of atherosclerosis

The redefinition of atherosclerosis as an inflammatory disease at the end of the last century challenged the old paradigm of it being solely a lipid dysfunction-driven disease (241). Lifestyle choices such as diet, stress, smoking, etc. have been proposed as modulators of inflammation (242,243). On a molecular scale, miRNAs have been postulated as important modulators of inflammation and atherosclerosis (160). Here we propose the downregulation of miR-15a-5p and miR-199a-3p in vascular tissues during atherosclerosis as a potential cause for increased inflammation and atherosclerosis progression.

Most of the investigation regarding miR-15a-5p (244,245) and miR-199a-3p (246,247) has been done in different types of cancer. We observed a decrease in miR-15a-5p and miR-199a-3p expression in the aorta and carotid bifurcation of *ApoE*$^{-/-}$ and HuBL mice with initial atherosclerotic injuries, respectively; we also found that both miRNAs were downregulated in patients with advanced carotid atherosclerosis. There is little known about how miR-15a-5p directly affects atherosclerosis and the few reports contain conflicting information. It has been proposed to inhibit chemokine (C X3 C motif) unique ligand 1- increasing inflammation in endothelial cells (248), and also to promote VSMCs proliferation and migration by inhibiting Bcl-2 and increasing MCP-1 and MMP-9. There are a few more reports on miR-199a-3p and atherosclerosis but they contain somewhat conflicting data as well. miR-199a-3p was decreased in *ApoE*$^{-/-}$ mice after 12 weeks of HFD and seems to protect against foam cell formation in macrophages and VSMCs proliferation and migration (249,250), but in the endothelium, an increase in miR-199a-3p levels seem to promote endothelial dysfunction by decreasing NO availability (251). The mediated effects seem to be cell and context dependent.

Similar to our previous approach, we searched in miRNA-target databases to select potential or confirmed targets for miR-15a-5p and miR-199a-3p that could modulate atherosclerosis. We selected targets related to inflammation, cell survival, and/or lipid uptake. For miR-15a-5p we chose IKKα, IKKβ, mTOR and LOX-1; and for miR-199a-3p, IKKβ, p65 and mTOR. In this case, we focused on studying these targets related to inflammation in the experimental model and the human samples. In mice, IKKα, IKKβ, and p65 were increased in the aorta, and the latter two were also increased in the endothelial cells and VSMCs from the aortic root of the mice submitted to 18-weeks of HFD, while IκBα was decreased. Similarly in humans, IKKα, IKKβ, and p65 were increased in the carotid samples from patients with advanced carotid atherosclerosis, and the expression was inversely correlated with miR-15a-5p expression. In the literature, IKKα has been confirmed as a target of miR-15a-5p (252); while IKKβ (253,254) and mTOR (255) are confirmed targets for miR-199a-3p. In line with this, increased miR-15a-5p levels decreased IKKβ and p65 expression in HUVECs and VSMCs, IKKα in HUVECs, and mTOR and LOX-1 in VSMCs. Increasing miR-199a-3p levels correlated with decreased IKKβ expression in HUVECs and VSMCs, p65 and IκBα in HUVECs, and mTOR in VSMCs. To further confirm this miRNA-mRNA interaction, dual-luciferase assays were performed and confirmed IKKα as a target of miR-15a-5p, IKKβ as a target for miR-15a-5p and miR-199a-3p, but not p65 as a target for miR-199a-3p. Nonetheless, Zeng *et al.* have previously shown that p65 could modulate the expression of miR-199a-3p (256).

As IKKα, IKKβ, and p65 are part of the NF-κB pathway, we wanted to assess how miR-15a-5p and miR-199a-3p may modulate this pathway in HUVECs and VSMCs. Different studies have already defined miR-15a-5p as a modulator of the NF-κB pathway. Decreased miR-15a-5p increases NF-κB activation in macrophages (257); hippocampal neurons (258); retina (using a specific deletion of miR-15a/miR-16 in vascular endothelial cells) (259); and chondrocytes (260). Similar effects are seen with miR-199a-3p, a decrease in this miRNA has been shown to promote NF-κB signalling in kidney cells (254), cervical epithelial cells (261), and bovine mammary epithelial cells (262). In line with these results, we obtained a decrease in IKKα/β activity and NF-κB activation in HUVECs when miR-15a-5p or miR-199a-3p were overexpressed, and in VSMCs when miR-15a-5p was overexpressed. Therefore, we can conclude that

miR-15a-5p, by targeting IKKα and IKKβ, and miR-199a-3p, by targeting IKKβ, modulate the NF-κB pathway during the progression of atherosclerosis.

In addition to the inflammatory targets, we also studied mTOR, which is a confirmed target for miR-199a-3p (255). However, there is no confirmation in the literature for miR-15a-5p to target mTOR. For that reason, confirmation experiments need to be done. Our last target was LOX-1 for miR-15a-5p. Initially, we found elevated LOX-1 protein levels in atherosclerotic carotid plaques from patients with advanced carotid atherosclerosis, and that ECs and VSMCs expressed LOX-1 in human and experimental samples. LOX-1 is a scavenger receptor expressed in macrophages, endothelial cells, and VSMCs. LOX-1 protein is increased in atherosclerosis and can modulate the proliferation and migration of VSMCs (92,263) and the foaming of VSMCs and macrophages (97,264). Furthermore, miRNAs like miR-98 (265), miR-186-5p (266) and let-7g (267) target LOX-1 and protect against atherosclerosis. In our case, we propose miR-15a-5p as the modulator of LOX-1 expression in VSMCs, and we obtained a significant decrease of the protein by increasing this miRNA in those cells. CD36, another scavenger receptor, is a potential target for miR-199a-3p, however, to confirm it as target, luciferase assays are needed. Our next step was to study if an overexpression of miR-15a-5p or miR-199a-3p would decrease lipid uptake in VSMCs and, as a consequence, the foaming of those cells. In this sense, Liu *et al.* confirmed that Ox-LDL decreased the expression of miR-199a-3p increasing foam cell formation in macrophages by targeting the runt-related transcription factor 1 (249); and Wu *et al.* also confirmed that Ox-LDL decreased the expression of miR-15a-5p in endothelial cells promoting cell proliferation, apoptosis and endothelial-to-mesenchymal transition by targeting the epidermal growth factor receptor (268). We also obtained a decrease in lipid uptake in VSMCs when miR-15a-5p and miR-199a-3p where overexpressed. We demonstrated that miR-15a-5p overexpression downregulate LOX-1 protein levels (but the direct interaction between them, needs to be confirmed) and in consequence VSMCs could uptake lower Ox-LDL, having both miRNAs an anti-foaming role in VSMCs (Figure XVI).

Lastly, we also studied the expression of miR-15a-3p and miR-199a-3p in $CD3^+$ and $CD3^-$ cell populations from the spleen of HuBL mice. Regarding inflammatory cells, miR-15a-5p is known for activating: the $CD8^+$ and natural killers by targeting PD-1 (269,270), the pro inflammatory Th1 response, and usually the pro-atherogenic response from $CD4^+$ cells (271). Moreover, miR-199a-3p was upregulated in $CD4^+$ cells from systemic lupus erythematosus patients (272), but Haralambieva *et al.* showed that both, miR-199a-3p and miR-15a-5p, were specific for B cells (273). We found expression of miR-15a-5p in $CD3^+$ cells, that was in fact, increased if compared with the expression in $CD3^-$ cells in initial atherosclerosis, which contradicts the results shown by Haralambieva *et al*. However, miR-199a-3p was only expressed in $CD3^-$ cells, where it was increased in mice with advanced atherosclerosis. To delve into how $CD3^-$ cell specific miR-199a-3p may be involved in advanced atherosclerosis, or how miR-15a-5p may be involved in initial atherosclerosis, more experiments need to be carried out.

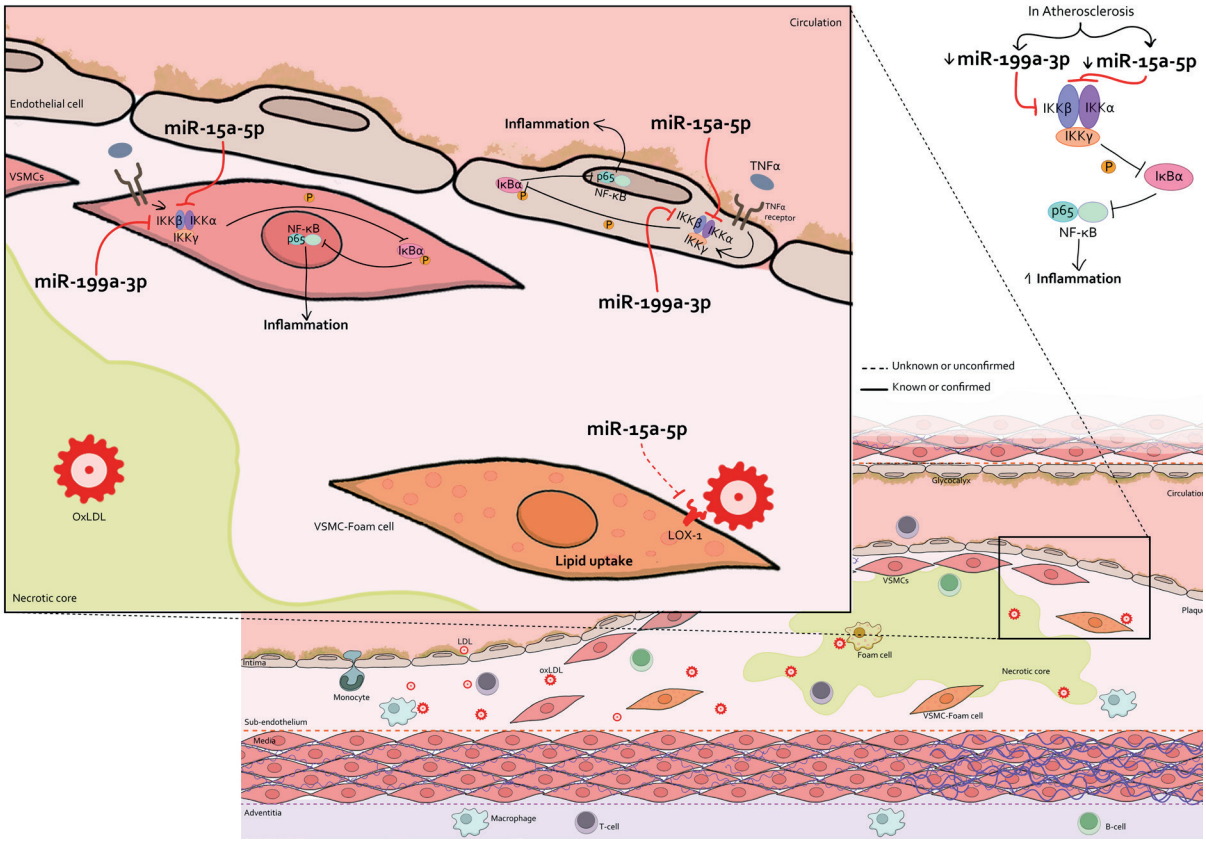

Figure XVI. Representation of miR-15a-5p and miR-199a-3p dysregulation in atherosclerosis. Atherosclerosis progression is represented with VSMCs migrating; monocytes, macrophage, LDL T and B-cell infiltration; the oxidation of LDL, VSMCs phenotype switching, the formation of foam cells and the necrotic core. In addition, there is a zoom that represents the effect of miR-15a-5p and miR-199a-3p in VSMCs and endothelial cell NF-κB inflammatory pathway, where they act by diminishing the expression of IKKα and IKKβ that decreases NF-κB activation by increasing the inhibitory protein IκBα; and therefore inflammation; moreover, the scheme shows the effect of miR-15a5p in VSMCs phenotype switch to foam cells by decreasing lipid uptake via the modulation of LOX-1. Dashed lines represent unknown or unconfirmed effect from molecules, and continued lines known or confirmed effects from one molecule to the other. Red lines represent inhibition and green light activation by the miRNAs. Black lines represent the direction of the signalling pathway. NF-κB= Nuclear factor kappa B, IκBα= NF-κB inhibitor alpha, IKK= IκBα kinase, IKKα= IKK alpha, IKKβ= IKK beta, IKKγ= IKK gamma, p65= NF κB p65 subunit, LOX-1= lectin-like oxidized low-density lipoprotein receptor, LDL= low-density lipoprotein, Ox-LDL= oxidized LDL, VSMCs= vascular smooth muscle cells.

6.4. miR-143-3p, miR-15a-5p and miR-199a-3p might be useful as potential biomarkers in advanced carotid atherosclerosis

In recent years it has been confirmed that miRNAs not only act as intracellular signals for modulating the expression of target proteins, but also as extracellular signals between cells; in order to do this, the cells vehicle the miRNAs inside extracellular vesicles, mainly in exosomes (237). We precipitated extracellular vesicles from the plasma of healthy donors and patients with atherosclerosis, then, we purified exosomes and isolated miRNAs, proposing circulating miR-143-3p and miR-15a-5p individually, and the combination of circulating miR-15a-5p and miR-199a-3p as potential biomarkers for advanced carotid atherosclerosis.

There are different evidences in the bibliography of how the exosomes derived from a specific cell type can affect other. This cellular communication of exosomal miRNAs (exo-miRNAs) has been seen in various diseases like cancer (269), pulmonary hypertension (274) or atherosclerosis (275,276). Exosomes enriched in miR-143-3p from pulmonary arteries smooth muscle cells are captured by pulmonary artery endothelial cells increasing pulmonary hypertension; miR-155-5p is increased in the exosomes from glioma-stem cells, and when captured by glioma cells promotes proliferation and tumor growth (277); exosomes from cancer cells that are enriched in miR-15a-5p are detected by $CD8^+$ cells and activate them by inhibiting PD-1 (269); and exosomes containing miR-199a-3p from endothelial progenitor cells (275) or adipocyte-progenitor cells (276) can be captured by endothelial cells promoting atherosclerosis.

These exo-miRNAs are also released into the blood, and therefore, have been proposed as biomarkers of several diseases. In this sense, the identification of new miRNAs or panels of new miRNAs could make possible to detect the change from stable to unstable plaques and the consequent increase in cardiovascular risk. In this way, we validated whether the four miRNAs studied could be useful as potential biomarkers of advanced atherosclerosis and compared them with other published studies. The first of them, miR-143-3p, its elevated levels have been found in clinical heart failure (278), and are proposed as a biomarker of acute ischemic stroke (279); but decreased miR-143-3p has been proposed as a biomarker for pulmonary hypertension (280) and atherosclerosis, being even lower in patients with vulnerable plaques (281). In line with these results, miR-143-3p was also significantly lower in our patients with advanced atherosclerosis than in the subjects without atherosclerosis.

Other potential biomarker studied was miR-155-5p, its elevated levels have also been proposed as a biomarker of rheumatoid arthritis (282) and unstable coronary artery disease (206), in the studied cohort, we did not find any difference in the plasmatic levels of miR-155-5p in advanced carotid atherosclerosis patients compared with subjects without atherosclerosis, contrary to what we found in our vascular samples where patients with an unstable carotid atherosclerosis had an increased miR-155-5p expression. The third miRNA studied was miR-15a-5p, its elevated levels have been proposed as a biomarker of rheumatoid arthritis (282) and coronary artery disease where is related to the necrotic core and decreases after exercise (243), our results also propose that elevated miR-15a-5p can be a biomarker of advanced carotid atherosclerosis. Finally, the last miRNA studied was miR-199a-3p, and its decreased expression has been proposed as a biomarker of atherosclerotic patients after heart failure (283), and is also related to the necrotic core size (243), our results showed elevated levels of miR-199a-3p in the plasma of patients with advanced carotid atherosclerosis, but did not reach enough significance to be considered a potential biomarker. Furthermore, we also wanted to relate other clinical characteristics like diabetes or biological sex, to the levels of the exo-miRNAs in patients with advanced atherosclerosis, but even finding some differences like between biological women and man in the expression of miR-199a-3p, the main driver of miRNA dysregulation seems to be the advanced atherosclerosis.

Taking all this in consideration, we propose miR-143-3p and miR-15a-5p as potential biomarkers of advanced atherosclerosis, and miR-199a-3p only if combined with miR-15a-5p (Figure XVII).

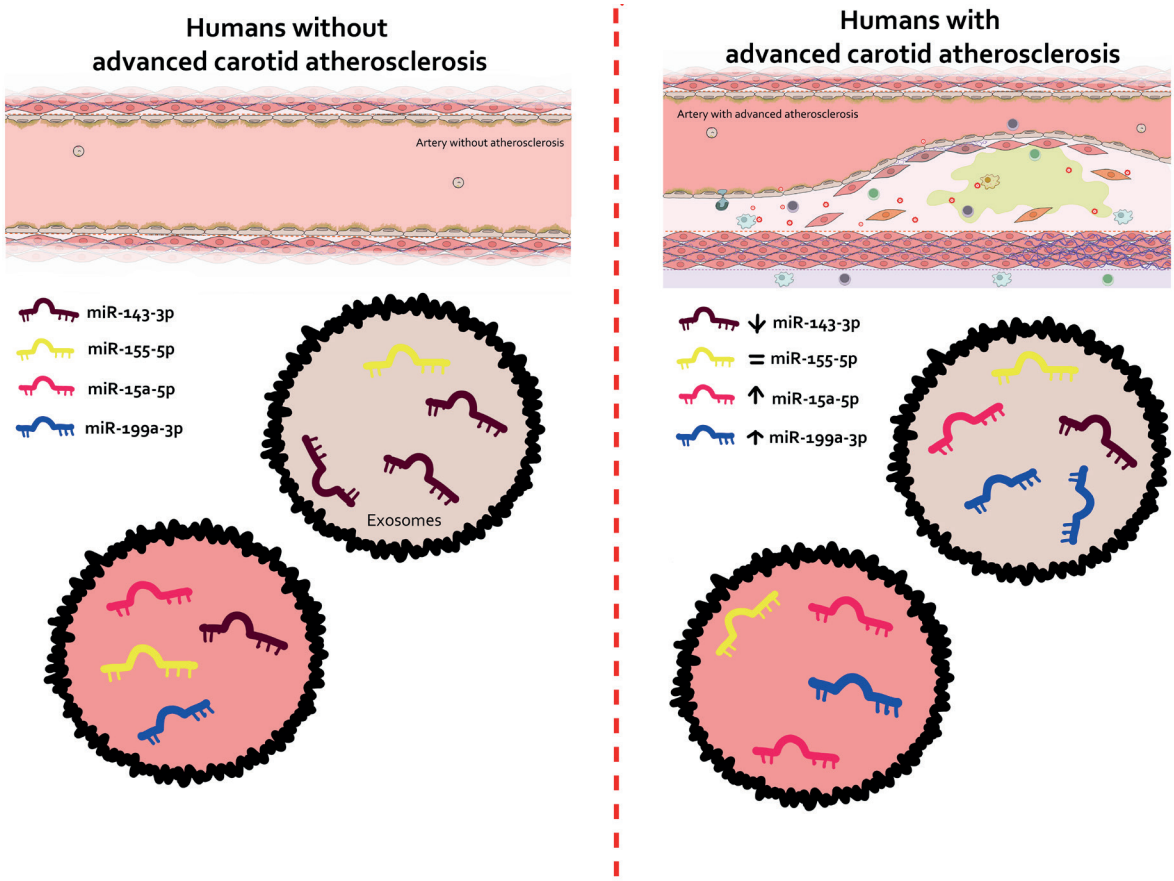

Figure XVII. Representation of circulating miRNA dysregulation in advanced atherosclerosis. The scheme represents the differences in miRNA expression in the plasma from subjects without atherosclerosis and patients with advanced carotid atherosclerosis.

“Fundieron plomo y cobre,
pusieron sal en sobres,
Alerta, hay un testigo,
nos han dejado vivos.
Fue un atraco perfecto,
excepto por esto,
Nos queda garganta, puño y
pies.
No fue un golpe maestro,
dejaron un rastro,
ya pueden correr, ya vuelve la
sed”

-Golpe Maestro, Vetusta Morla

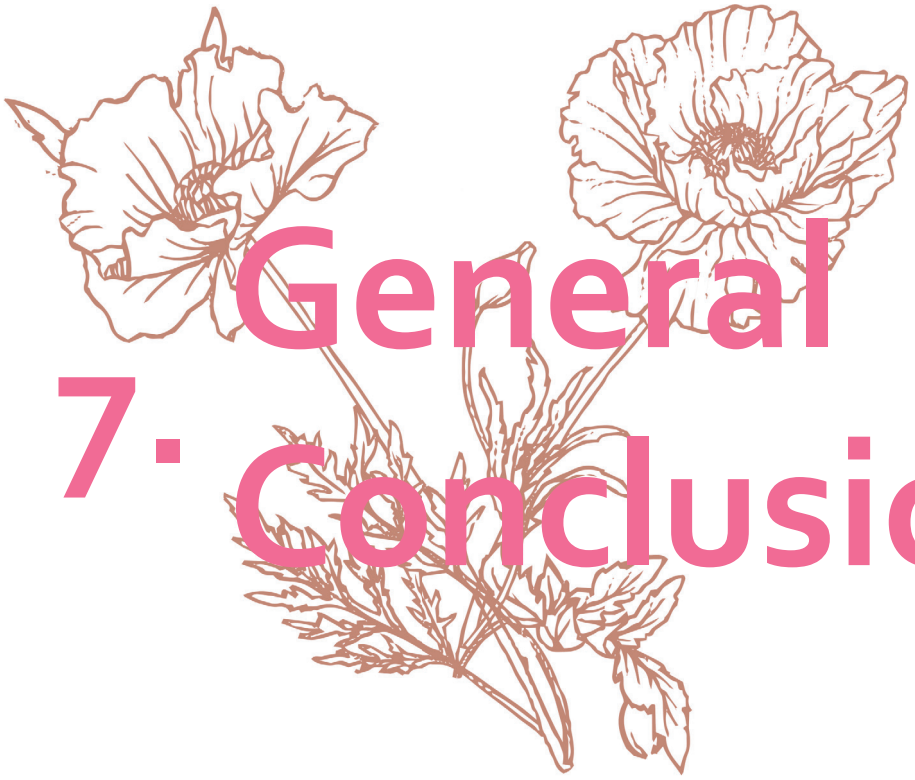

7. General Conclusions

7. GENERAL CONCLUSIONS

Based on the performed studies and the obtained results in the current Doctoral Thesis, we can reach the following conclusions:

1. **The downregulation of miR-143-3p promotes vascular cell apoptosis and plaque instability by targeting IGF-IIR.**

2. **Increased levels of miR-155-5p induces vascular insulin resistance in experimental and human atherosclerosis by targeting AKT.**

3. **The decrease in miR-15a-5p and miR-199a-3p induces the upregulation of IKKα, IKKβ, p65 and LOX-1 favouring inflammation and lipid uptake in atherosclerosis.**

4. **The downregulation of miR-15a-5p and miR-199a-3p occurs in early experimental atherosclerosis, while increased miR-155-5p and decreased miR-143-3p is observed in both early and advanced carotid atherosclerosis.**

5. **miR-143-3p, miR-15a-5p and the combination of miR-15a-5p and miR-199a-3p are potential non-invasive biomarkers of human advanced carotid atherosclerosis**.

"...Hay un mundo por descubrir y
una vida que arrancar,
de brazos del guión final.
A veces siento al despertar,
que el sueño es la realidad.
Bebe, canta, sueña, siente que
el viento ha sido hecho para ti,
vive, escucha y habla, usando,
para ello el corazon,
Siente que la lluvia besa tu cara,
cuando haces el amor.
Grita con el alma, grita tan alto,
que de tu vida tú seas, amigo, el
único actor "

-Molinos de viento, Mägo de Oz

8. Final Conclusion

8. FINAL CONCLUSION

Our results show that altered levels of miR-143-3p (i), miR-155-5p (ii), miR-15a-5p (iii,iv) and miR-199a-3p (iii,iv) in vascular lesions are involved in the progression of experimental and human atherosclerosis promoting: (i) apoptosis of endothelial and vascular smooth muscle cells and plaque instability, (ii) vascular insulin resistance, (iii) inflammation and (iv) lipid uptake in vascular smooth muscle cells. Finally, regarding human diagnosis, circulating miR-143-3p and miR-15a-5p could serve as potential biomarkers of advanced atherosclerosis (Figure XVIII).

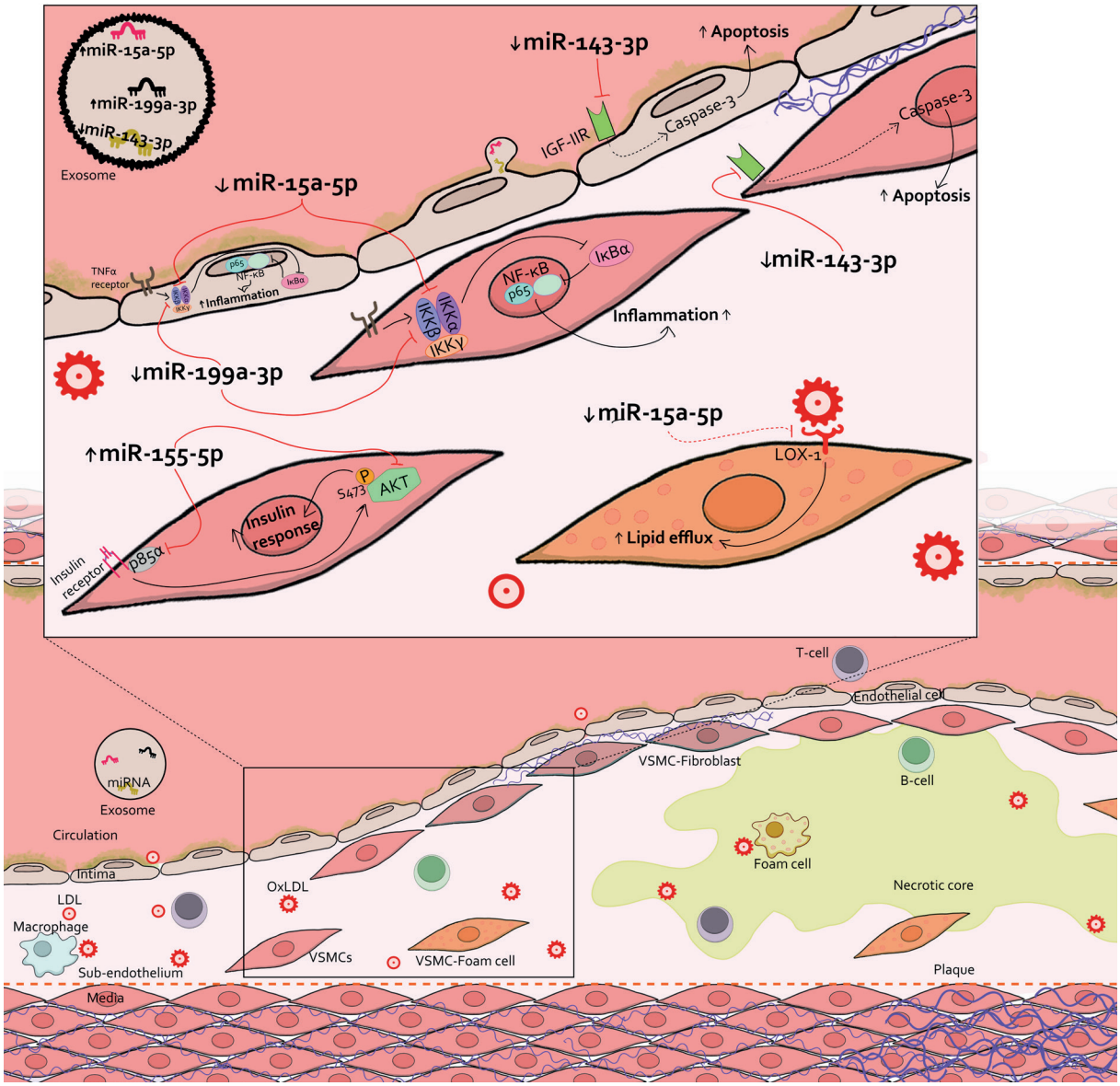

Figure XVIII. Summary of the effects of miR-143-3p, miR-155-5p, miR-15a-5p and miR-199a-3p in experimental and human atherosclerosis. Atherosclerosis progression is represented with VSMCs migrating; monocytes, macrophage, LDL, T and B-cell infiltration; the oxidation of LDL, VSMCs phenotype switching, the formation of foam cells and the necrotic core. There is a zoom-in area that represents the effect of miR-143-3p in endothelial cells and VSMCs apoptosis by modulating IGF-IIR; miR-155-5p effect in insulin response in VSMCs by decreasing AKT activation and p85 α expression; miR-15a-5p and miR-199a-3p role in VSMCs and endothelial cell NF κB inflammatory pathway, where they act by diminishing the expression of IKKα and IKKβ, moreover, the scheme shows the effect of miR-15a-5p in VSMCs phenotype switch to foam cells by decreasing lipid uptake via the modulation of LOX-1; and the dysregulation of miR-143-3p, miR-15a-5p and miR-199a-3p in the plasma of patients with advanced carotid atherosclerosis. Dashed lines represent unknown or unconfirmed effects from molecules, and continued lines known or confirmed effects from one molecule to the other. Red lines represent inhibition by the miRNAs. Black lines represent the direction of the signalling pathway. IGF-IIR= IGF-II receptor, AKT= protein kinase B, p85α= phosphoinositide-3-Kinase Regulatory Subunit 1, NF-κB = Nuclear factor kappa B, IκB α = NF-κB inhibitor alpha, IKK= IκB α kinase, IKKα= IKK apha, IKKβ= IKK beta, IKKγ= IKK gamma, p65= NF-κB p65 subunit, LOX-1= lectin-like oxidized low-density lipoprotein receptor, LDL= low-density lipoprotein, Ox-LDL= oxidized LDL, VSMCs= vascular smooth muscle cells.

"...Fuiste la niña de azul,
ahora eres la vieja verde,
como se porta la vida,
cuando vales lo que tienes.
Las vueltas que da la vida,
el destino se burla de ti,
Dónde vas, bala perdida,
dónde vas, triste de ti"

-Dolores se llamaba Lola, Los Suaves

7. Conclusiones Generales

7. CONCLUSIONES GENERALES

Basándonos en los estudios realizados y los resultados obtenidos en la presente Tesis Doctoral, podemos llegar a las siguientes conclusiones:

1. **La disminución de miR-143-3p induce un aumento en la expresión de IGF-IIR que promueve la apoptosis de las células vasculares y la inestabilidad de las placas de ateroma.**

2. **Niveles elevados de miR-155-5p inducen resistencia a la insulina vascular en la aterosclerosis experimental y humana mediante la inhibición de la expresión de AKT.**

3. **La disminución de miR-15a-5p y miR-199a-3p induce la sobreexpresión de IKKα, IKKβ, p65 y LOX-1, favoreciendo la inflamación vascular y la captación de lípidos durante la progresión de la aterosclerosis.**

4. **La disminución de miR-15a-5p y miR-199a-3p se observa en la aterosclerosis carotidea experimental temprana, así como el aumento de miR-155-5p y la disminución de miR-143-3p, se observa tanto en la aterosclerosis carotídea temprana como avanzada.**

5. **miR-143-3p, miR-15a-5p y la combinación de miR-15a-5p y miR-199a-3p son potenciales biomarcadores no invasivos de aterosclerosis carotídea avanzada en humanos.**

"...Como las frases que ya no te escribo,
pa' que vuelvas otra vez.
Y ahora que, voy más solo que la luna,
negociando gasolina para este amanecer,
ya ves, voy buscando en la basura,
unos labios que me digan:
`esta noche quedate´"

-Buscando en la basura, La Fuga

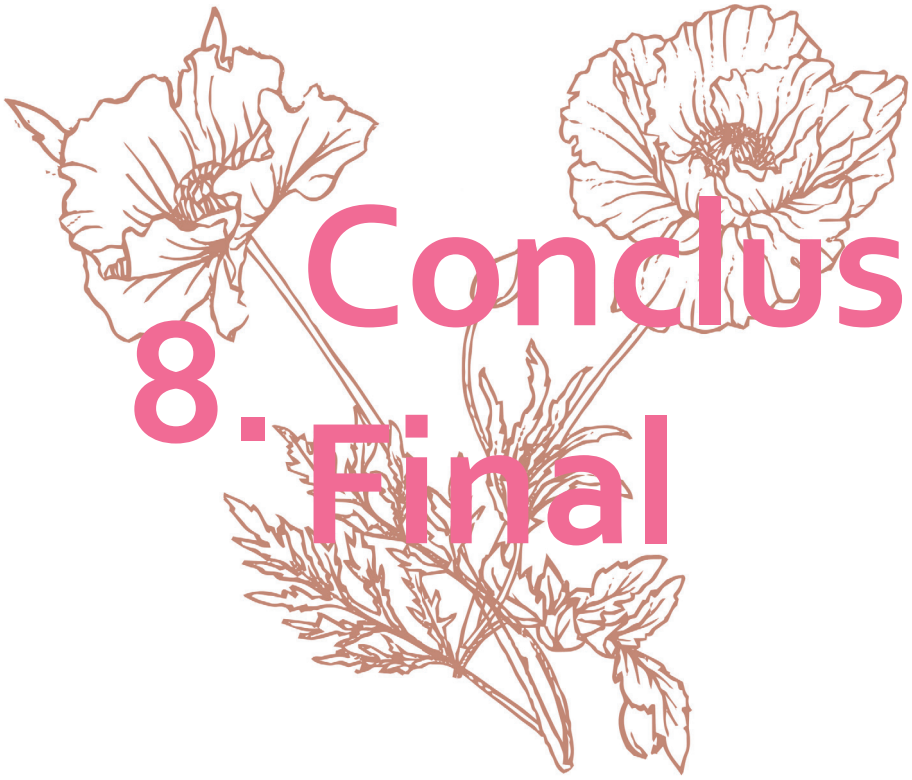

8. Conclusión Final

8. CONCLUSIÓN FINAL

Nuestros resultados muestran que los niveles alterados de los miR-143-3p (i), miR-155-5p (ii), miR-15a-5p (iii,iv) y miR-199a-3p (iii,iv) en lesiones vasculares están involucrados en la progresión de la aterosclerosis experimental y humana, promoviendo: (i) la apoptosis de las células endoteliales y de músculo liso vascular y la inestabilidad de las placas, (ii) la resistencia a la insulina vascular, (iii) la inflamación y (iv) la captación de lípidos en las células de músculo liso vascular. Finalmente, en cuanto al diagnóstico en humanos, los miR-143-3p y miR-15a-5p circulantes podrían servir como potenciales biomarcadores de la aterosclerosis avanzada (Figura XIX).

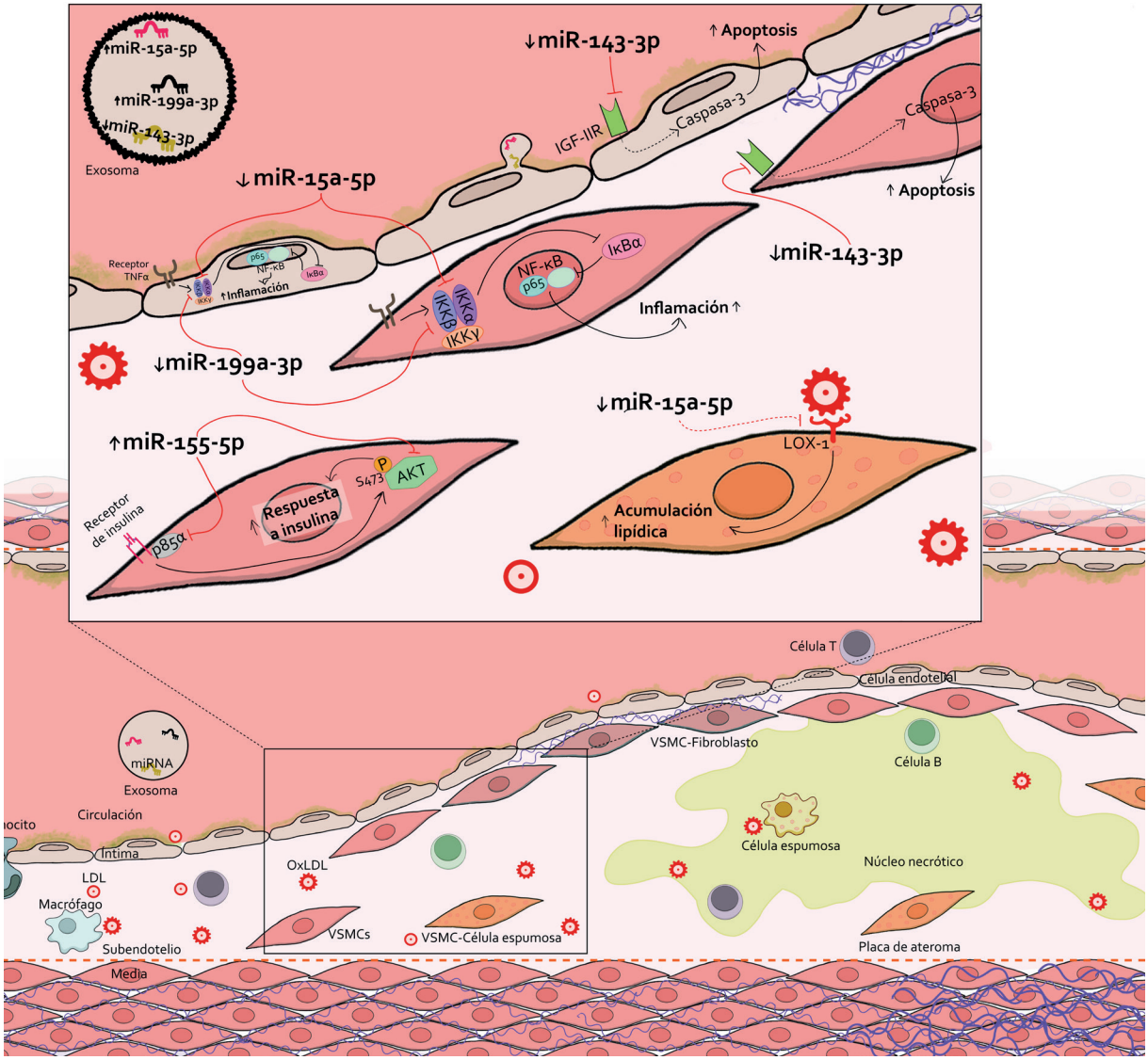

Figura XIX. Resumen de los efectos de los miR-143-3p, miR-155-5p, miR-15a-5p y miR-199a-3p en la aterosclerosis. La progresión de la aterosclerosis se representa con la migración de las células de músculo liso vascular; la infiltración de monocitos, macrófagos, LDL, células T y B; la oxidación de LDL; el cambio de fenotipo de las VSMCs; la formación de células espumosas y el núcleo necrótico. Hay una zona de aumento que representa el efecto del miR-143-3p en la apoptosis de las células endoteliales y las VSMCs al modular el IGF-IIR; el efecto de miR-155-5p en la respuesta a la insulina en las VSMCs al disminuir la activación de AKT y la expresión de p85α; el papel de miR-15a-5p y miR-199a-3p en la vía inflamatoria NF-κB, donde actúan disminuyendo la expresión de IKKα e IKKβ, además, el esquema muestra el efecto de miR-15a-5p en el cambio de fenotipo de las VSMCs a células espumosas a través de la modulación de LOX-1; y la desregulación de miR-143-3p, miR 15a-5p y miR-199a-3p en el plasma de pacientes con aterosclerosis carotídea avanzada. Las líneas discontinuas representan efectos desconocidos o no confirmados de las moléculas, y las líneas continuas representan efectos conocidos o confirmados de una molécula a otra. Las líneas rojas representan inhibición por parte de los miRNAs. Las líneas negras representan la dirección de la vía de señalización. IGF-IIR = receptor de IGF-II, AKT = proteína quinasa B, p85α = subunidad reguladora de fosfoinositida-3-cinasa 1, NF-κB = factor nuclear kappa B, IκB α = inhibidor alfa de NF-κB, IKK = quinasa IκBα, IKKα = IκBα, IKKβ = IκBβ, IKKγ = IκB γ, p65 = subunidad p65 de NF-κB, LOX-1 = receptor de lipoproteínas de baja densidad oxidadas de tipo lectina-1, LDL = lipoproteína de baja densidad, Ox-LDL = LDL oxidada, VSMCs = células de músculo liso vascular.

"Vivir más con menos,
Quiero, ser necesario,
quiero, encontrar el norte,
quiero, risas y abrazos,
gente con valores"

-Quiero, quiero y quiero, Arnau Griso

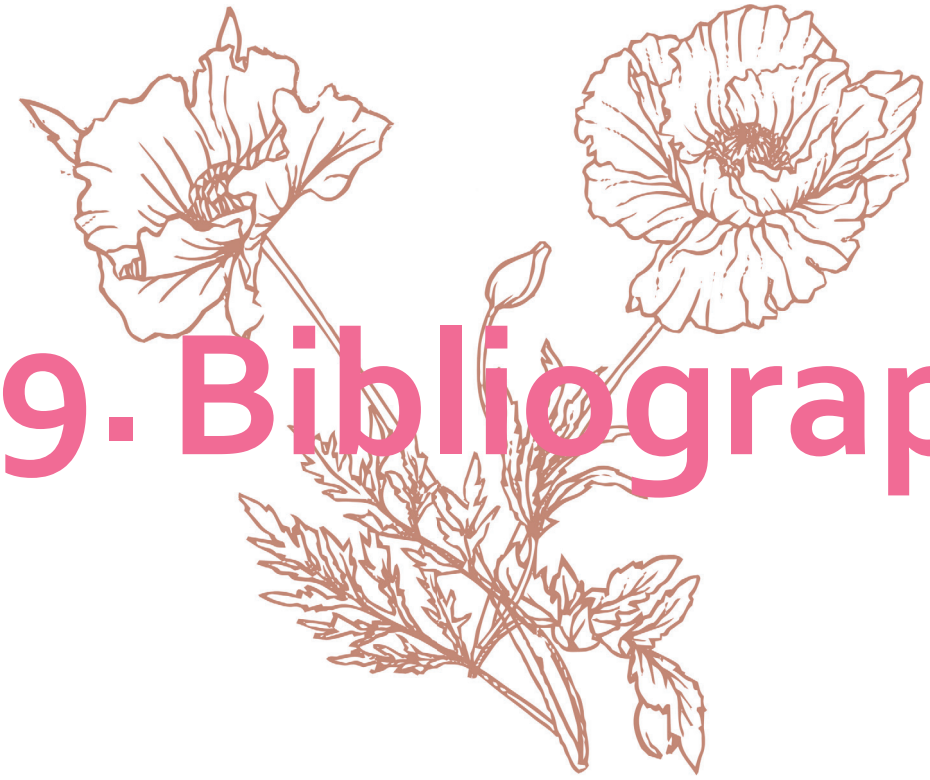

9. Bibliography

9. BIBLIOGRAPHY

1. Libby P. The changing landscape of atherosclerosis. Nature [Internet]. 2021;592(7855):524–33. Available from: http://dx.doi.org/10.1038/s41586-021-03392-8

2. Fan J, Watanabe T. Atherosclerosis: Known and unknown. Pathol Int. 2022;72(3):151–60.

3. Milutinović A, Šuput D, Zorc-Pleskovič R. Pathogenesis of atherosclerosis in the tunica intima, media, and adventitia of coronary arteries: An updated review. Bosn J Basic Med Sci. 2020;20(1):21–30.

4. Tellides G, Pober JS. Inflammatory and immune responses in the arterial media. Circ Res. 2015;116(2):312–22.

5. Stenmark KR, Yeager ME, El Kasmi KC, Nozik-Grayck E, Gerasimovskaya E V., Li M, et al. The Adventitia: Essential Regulator of Vascular Wall Structure and Function. Annu Rev Physiol [Internet]. 2013 Feb 10;75(1):23–47. Available from: https://www.annualreviews.org/doi/10.1146/annurev-physiol-030212-183802

6. Deanfield JE, Halcox JP, Rabelink TJ. Endothelial function and dysfunction: Testing and clinical relevance. Circulation. 2007;115(10):1285–95.

7. Incalza MA, D'Oria R, Natalicchio A, Perrini S, Laviola L, Giorgino F. Oxidative stress and reactive oxygen species in endothelial dysfunction associated with cardiovascular and metabolic diseases. Vascul Pharmacol [Internet]. 2018;100:1–19. Available from: http://dx.doi.org/10.1016/j.vph.2017.05.005

8. Michael A. GJ, Guillermo GC. Endothelial cell dysfunction and the pathobiology of atherosclerosis. Circ Res. 2016;176(1):139–48.

9. Tacke F, Alvarez D, Kaplan TJ, Jakubzick C, Spanbroek R, Llodra J, et al. Monocyte subsets differentially employ CCR2, CCR5, and CX3CR1 to accumulate within atherosclerotic plaques. J Clin Invest. 2007;117(1):185–94.

10. Moore KJ, Sheedy FJ, Fisher EA. Macrophages in atherosclerosis: A dynamic balance. Nat Rev Immunol. 2013;13(10):709–21.

11. Maguire EM, Pearce SWA, Xiao Q. Foam cell formation: A new target for fighting atherosclerosis and cardiovascular disease. Vascul Pharmacol. 2019;112(July 2018):54–71.

12. Chen J, Xiang X, Nie L, Guo X, Zhang F, Wen C, et al. The emerging role of Th1 cells in atherosclerosis and its implications for therapy. Front Immunol. 2023;13(January):1–12.

13. Schäfer S, Zernecke A. CD8+ T cells in atherosclerosis. Cells. 2021;10(1):1–16.

14. Sharma M, Schlegel MP, Afonso MS, Brown EJ, Rahman K, Weinstock A, et al. Regulatory T Cells License Macrophage Pro-Resolving Functions During Atherosclerosis Regression. Circ Res [Internet]. 2020 Jul 17;127(3):335–53. Available from: http://europepmc.org/backend/ptpmcrender.fcgi?accid=PMC5604322&blobtype=pdf

15. Deroissart J, Binder CJ. Mapping the functions of IgM antibodies in atherosclerotic cardiovascular disease. Nat Rev Cardiol. 2023;

16. Liu T, Shi N, Zhang S, Silverman GJ, Duan XW, Zhang S, et al. Systemic lupus erythematosus aggravates atherosclerosis by promoting IgG deposition and inflammatory cell imbalance. Lupus. 2020;29(3):273–82.

17. Zhang X, Li J, Luo S, Wang M, Huang Q, Deng Z, et al. IgE Contributes to Atherosclerosis and Obesity by Affecting Macrophage Polarization, Macrophage Protein Network, and Foam Cell Formation. Arterioscler Thromb Vasc Biol [Internet]. 2020 Mar;40(3):597–610. Available from: https://www.ahajournals.org/doi/10.1161/ATVBAHA.119.313744

18. Shi J, Yang Y, Cheng A, Xu G, He F. Metabolism of vascular smooth muscle cells in vascular diseases. Am J Physiol - Hear Circ Physiol. 2020;319(3):H613–31.

19. Zhang F, Guo X, Xia Y, Mao L. An update on the phenotypic switching of vascular smooth muscle cells in the pathogenesis of atherosclerosis. Cell Mol Life Sci [Internet]. 2022;79(1):1–19. Available from: https://doi.org/10.1007/s00018-021-04079-z

20. Santoleri D, Titchenell PM. Resolving the Paradox of Hepatic Insulin Resistance. Cmgh [Internet]. 2019;7(2):447–56. Available from: https://doi.org/10.1016/j.jcmgh.2018.10.016

21. James DE, Stöckli J, Birnbaum MJ. The aetiology and molecular landscape of insulin resistance. Nat Rev Mol Cell Biol [Internet]. 2021;22(11):751–71. Available from: http://dx.doi.org/10.1038/s41580-021-00390-6

22. LeRoith D, Holly JMP, Forbes BE. Insulin-like growth factors: Ligands, binding proteins, and receptors. Mol Metab [Internet]. 2021;52(May):101245. Available from: https://doi.org/10.1016/j.molmet.2021.101245

23. Feng L, Li B, Xi Y, Cai M, Tian Z. Aerobic exercise and resistance exercise alleviate skeletal muscle atrophy through IGF-1/IGF-1R-PI3K/Akt pathway in mice with myocardial infarction. Am J Physiol - Cell Physiol. 2022;322(2):C164–76.

24. Sélénou C, Brioude F, Giabicani E, Sobrier ML, Netchine I. IGF2: Development, Genetic and Epigenetic Abnormalities. Cells. 2022;11(12).

25. Karunakaran D, Nguyen MA, Geoffrion M, Vreeken D, Lister Z, Cheng HS, et al. RIPK1 Expression Associates With Inflammation in Early Atherosclerosis in Humans and Can Be Therapeutically Silenced to Reduce NF-κB Activation and Atherogenesis in Mice. Circulation. 2021;143(2):163–77.

26. Lawrence T. The nuclear factor NF-kappaB pathway in inflammation. Cold Spring Harb Perspect Biol. 2009;1(6):1–10.

27. Mitchell S, Vargas J, Hoffmann A. Signaling via the NFκB system. WIREs Syst Biol Med [Internet]. 2016 May 16;8(3):227–41. Available from: https://onlinelibrary.wiley.com/doi/10.1002/wsbm.1331

28. Yu H, Lin L, Zhang Z, Zhang H, Hu H. Targeting NF-κB pathway for the therapy of diseases: mechanism and clinical study. Signal Transduct Target Ther [Internet]. 2020;5(1). Available from: http://dx.doi.org/10.1038/s41392-020-00312-6

29. Meng Q, Pu L, Lu Q, Wang B, Li S, Liu B, et al. Morin hydrate inhibits atherosclerosis and LPS-induced endothelial cells inflammatory responses by modulating the NFκB signaling-mediated autophagy. Int Immunopharmacol. 2021;100.

30. Ben J, Jiang B, Wang D, Liu Q, Zhang Y, Qi Y, et al. Major vault protein suppresses obesity and atherosclerosis through inhibiting IKK–NF-κB signaling mediated inflammation. Nat Commun. 2019;10(1).

31. Catalanotto C, Cogoni C, Zardo G. MicroRNA in control of gene expression: An overview of nuclear functions. Int J Mol Sci. 2016;17(10).

32. Matsuyama H, Suzuki HI. Systems and synthetic microRNA biology: From biogenesis to disease pathogenesis. Int J Mol Sci. 2020;21(1):1–23.

33. Baldán Á, Fernández-Hernando C. Truths and controversies concerning the role of miRNAs in atherosclerosis and lipid metabolism. Curr Opin Lipidol. 2016;27(6):623–9.

34. Meng Q, Liang C, Hua J, Zhang B, Liu J, Zhang Y, et al. A miR-146a-5p/TRAF6/NF-kB p65 axis regulates pancreatic cancer chemoresistance: Functional validation and clinical significance. Theranostics. 2020;10(9):3967–79.

35. Chen ML, Hong CG, Yue T, Li HM, Duan R, Hu WB, et al. Inhibition of miR-331-3p and miR-9-5p ameliorates Alzheimer's disease by enhancing autophagy. Theranostics. 2021;11(5):2395–409.

36. De Yébenes VG, Briones AM, Martos-Folgado I, Mur SM, Oller J, Bilal F, et al. Aging-Associated miR-217 Aggravates Atherosclerosis and Promotes Cardiovascular Dysfunction. Arterioscler Thromb Vasc Biol. 2020;40(10):2408–24.

37. Carosi JA, Eskin SG, McIntire L V. Cyclical strain effects on production of vasoactive materials in cultured endothelial cells. J Cell Physiol. 1992;151(1):29–36.

38. Ballermann BJ, Dardik A, Eng E, Liu A. Shear stress and the endothelium. Kidney Int Suppl. 1998;54(67):100–8.

39. Li Y, Zheng J, Bird IM, Magness RR. Effects of pulsatile shear stress on nitric oxide production and endothelial cell nitric oxide synthase expression by ovine fetoplacental artery endothelial cells. Biol Reprod. 2003;69(3):1053–9.

40. Qi YX, Jiang J, Jiang XH, Wang XD, Ji SY, Han Y, et al. PDGF-BB and TGF-β1 on cross-talk between endothelial and smooth muscle cells in vascular remodeling induced by low shear stress. Proc Natl Acad Sci U S A. 2011;108(5):1908–13.

41. Godo S, Shimokawa H. Endothelial Functions. Arterioscler Thromb Vasc Biol. 2017;37(9):e108–14.

42. Bates DO, Harper SJ. Regulation of vascular permeability by vascular endothelial growth factors. Vascul Pharmacol. 2002;39(4–5):225–37.

43. Mohindra R, Agrawal DK, Thankam FG. Altered Vascular Extracellular Matrix in the Pathogenesis of Atherosclerosis. J Cardiovasc Transl Res. 2021;14(4):647–60.

44. Reitsma S, Slaaf DW, Vink H, Van Zandvoort MAMJ, Oude Egbrink MGA. The endothelial glycocalyx: Composition, functions, and visualization. Pflugers Arch Eur J Physiol. 2007;454(3):345–59.

45. Foote CA, Soares RN, Ramirez-Perez FI, Ghiarone T, Aroor A, Manrique-Acevedo C, et al. Endothelial Glycocalyx. Compr Physiol. 2022;12(4):3781–811.

46. Dogné S, Flamion B. Endothelial Glycocalyx Impairment in Disease: Focus on Hyaluronan Shedding. Am J Pathol [Internet]. 2020;190(4):768–80. Available from: https://doi.org/10.1016/j.ajpath.2019.11.016

47. Wolf D, Ley K. Immunity and inflammation in atherosclerosis. Herz. 2019;44(2):107–20.

48. Kong P, Cui ZY, Huang XF, Zhang DD, Guo RJ, Han M. Inflammation and atherosclerosis: signaling pathways and therapeutic intervention. Signal Transduct Target Ther. 2022;7(1).

49. Beutler B. Innate immunity: An overview. Mol Immunol. 2004;40(12):845–59.

50. Mantovani A, Garlanda C. Humoral Innate Immunity and Acute-Phase Proteins. N Engl J Med. 2023;388(5):439–52.

51. Gil-Pulido J, Zernecke A. Antigen-presenting dendritic cells in atherosclerosis. Eur J Pharmacol [Internet]. 2017;816(August):25–31. Available from: https://doi.org/10.1016/j.ejphar.2017.08.016

52. Josefs T, Barrett TJ, Brown EJ, Quezada A, Wu X, Voisin M, et al. Neutrophil extracellular traps promote macrophage inflammation and impair atherosclerosis resolution in diabetic mice. JCI Insight. 2020;5(7):1–10.

53. Knight JS, Luo W, O'Dell AA, Yalavarthi S, Zhao W, Subramanian V, et al. Peptidylarginine deiminase inhibition reduces vascular damage and modulates innate immune responses in murine models of atherosclerosis. Circ Res. 2014;114(6):947–56.

54. Huang SUS, O'Sullivan KM. The Expanding Role of Extracellular Traps in Inflammation and Autoimmunity: The New Players in Casting Dark Webs. Int J Mol Sci. 2022;23(7).

55. Porsch F, Mallat Z, Binder CJ. Humoral immunity in atherosclerosis and myocardial infarction: From B cells to antibodies. Cardiovasc Res. 2021;117(13):2544–62.

56. Staub HL, Franck M, Ranzolin A, Norman GL, Iverson GM, von Mühlen CA. IgA antibodies to beta2-glycoprotein I and atherosclerosis. Autoimmun Rev. 2006;6(2):104–6.

57. Pattarabanjird T, Li C, McNamara C. B Cells in Atherosclerosis: Mechanisms and Potential Clinical Applications. JACC Basic to Transl Sci [Internet]. 2021;6(6):546–63. Available from: https://doi.org/10.1016/j.jacbts.2021.01.006

58. Saigusa R, Winkels H, Ley K. T cell subsets and functions in atherosclerosis. Nat Rev Cardiol [Internet]. 2020 Jul 16;17(7):387–401. Available from: http://www.nature.com/articles/s41569-020-0352-5

59. Tse K, Tse H, Sidney J, Sette A, Ley K. T cells in atherosclerosis. Int Immunol. 2013;25(11):615–22.

60. Li Q, Ming T, Wang Y, Ding S, Hu C, Zhang C, et al. Increased Th9 cells and IL-9 levels accelerate disease progression in experimental atherosclerosis. Am J Transl Res. 2017;9(3):1335–43.

61. Wang Q, Wang Y, Xu D. Research progress on Th17 and T regulatory cells and their cytokines in regulating atherosclerosis. Front Cardiovasc Med. 2022;9(5).

62. Shi L, Ji Q, Liu L, Shi Y, Lu Z, Ye J, et al. IL-22 produced by Th22 cells aggravates atherosclerosis development in ApoE−/− mice by enhancing DC-induced Th17 cell proliferation. J Cell Mol Med. 2020;24(5):3064–78.

63. Douna H, de Mol J, Amersfoort J, Schaftenaar FH, Kiss MG, Suur BE, et al. IFNγ-Stimulated B Cells Inhibit T Follicular Helper Cells and Protect Against Atherosclerosis. Front Cardiovasc Med. 2022;9(February):1–11.

64. Förstermann U, Xia N, Li H. Roles of vascular oxidative stress and nitric oxide in the pathogenesis of atherosclerosis. Circ Res. 2017;120(4):713–35.

65. Kimura Y, Tsukui D, Kono H. Uric acid in inflammation and the pathogenesis of atherosclerosis. Int J Mol Sci. 2021;22(22).

66. Wu X, Zhang H, Qi W, Zhang Y, Li J, Li Z, et al. Nicotine promotes atherosclerosis via ROS-NLRP3-mediated endothelial cell pyroptosis. Cell Death Dis [Internet]. 2018;9(2):0–11. Available from: http://dx.doi.org/10.1038/s41419-017-0257-3

67. Zhao M, Wang Y, Li L, Liu S, Wang C, Yuan Y, et al. Mitochondrial ROS promote mitochondrial dysfunction and inflammation in ischemic acute kidney injury by disrupting TFAM-mediated mtDNA maintenance. Theranostics. 2021;11(4):1845–63.

68. Balkwill FR, Burke F. The cytokine network. Immunol Today [Internet]. 1989 Sep;10(9):299–304. Available from: https://linkinghub.elsevier.com/retrieve/pii/0167569989900856

69. Tedgui A, Mallat Z. Cytokines in atherosclerosis: Pathogenic and regulatory pathways. Physiol Rev. 2006;86(2):515–81
.
70. González L, Rivera K, Andia ME, Martínez Rodriguez G. The IL-1 Family and Its Role in Atherosclerosis. Int J Mol Sci. 2023;24(1):1–25.

71. Orecchioni M, Kobiyama K, Winkels H, Ghosheh Y, McArdle S, Mikulski Z, et al. Olfactory receptor 2 in vascular macrophages drives atherosclerosis by NLRP3-dependent IL-1 production. Science (80-). 2022;375(6577):214–21.

72. Grebe A, Hoss F, Latz E. NLRP3 inflammasome and the IL-1 pathway in atherosclerosis. Circ Res. 2018;122(12):1722–40.

73. Altara R, Ghali R, Mallat Z, Cataliotti A, Booz GW, Zouein FA. Conflicting vascular andmetabolic impact of the IL-33/sST2 axis. Cardiovasc Res. 2018;114(12):1578–94.

74. Kasahara K, Sasaki N, Yamashita T, Kita T, Yodoi K, Sasaki Y, et al. CD3 antibody and IL-2 complex combination therapy inhibits atherosclerosis by augmenting a regulatory immune response. J Am Heart Assoc. 2014;3(2):1–12.

75. Shi H, Guo J, Yu Q, Hou X, Liu L, Gao M, et al. CRISPR/Cas9 based blockade of IL-10 signaling impairs lipid and tissue homeostasis to accelerate atherosclerosis. Front Immunol. 2022;13(August):1–19.

76. Luo P, Wang Y, Zhao C, Guo J, Shi W, Ma H, et al. Bazedoxifene exhibits anti-inflammation and anti-atherosclerotic effects via inhibition of IL-6/IL-6R/STAT3 signaling. Eur J Pharmacol [Internet]. 2021;893(December 2020):173822. Available from: https://doi.org/10.1016/j.ejphar.2020.173822

77. Zheng Y, Li Y, Ran X, Wang D, Zheng X, Zhang M, et al. Mettl14 mediates the inflammatory response of macrophages in atherosclerosis through the NF-κB/IL-6 signaling pathway. Cell Mol Life Sci. 2022;79(6):1–18.

78. Benagiano M, Borghi MO, Romagnoli J, Mahler M, Bella C Della, Grassi A, et al. Interleukin-17/Interleukin-21 and Interferon-γ producing T cells specific for β2 Glycoprotein I in atherosclerosis inflammation of systemic lupus erythematosus patients with antiphospholipid syndrome. Haematologica. 2019;104(12):2519–27.

79. Li Q, Liu Y, Xia X, Sun H, Gao J, Ren Q, et al. Activation of macrophage TBK1-HIF-1α-mediated IL-17/IL-10 signaling by hyperglycemia aggravates the complexity of coronary atherosclerosis: An in vivo and in vitro study. FASEB J. 2021;35(5):1–12.

80. Borriello F, Galdiero MR, Varricchi G, Loffredo S, Spadaro G, Marone G. Innate immune modulation by GM-CSF and IL-3 in health and disease. Int J Mol Sci. 2019;20(4):1–17.

81. van der Does AM, Beekhuizen H, Ravensbergen B, Vos T, Ottenhoff THM, van Dissel JT, et al. LL-37 Directs Macrophage Differentiation toward Macrophages with a Proinflammatory Signature. J Immunol. 2010;185(3):1442–9.

82. Singhal A, Subramanian M. Colony stimulating factors (CSFs): Complex roles in atherosclerosis. Cytokine [Internet]. 2019;122(October 2017):154190. Available from: https://doi.org/10.1016/j.cyto.2017.10.012

83. De Villiers WJS, Fraser IP, Hughes DA, Doyle AG, Gordon S. Macrophage-colony-stimulating factor selectively enhances macrophage scavenger receptor expression and function. J Exp Med. 1994;180(2):705–9.

84. Wang JM, Griffin JD, Rambaldi A, Chen ZG, Mantovani A. Induction of monocyte migration by recombinant macrophage colony-stimulating factor. J Immunol. 1988;141(2):575–9.

85. Chen P yu, Qin L, Li G, Wang Z, Dahlman JE, Malagon-Lopez J, et al. Endothelial TGF-β signalling drives vascular inflammation and atherosclerosis. Nat Metab [Internet]. 2019 Aug 26;1(9):912–26. Available from: https://www.nature.com/articles/s42255-019-0102-3

86. Gao W, Liu H, Yuan J, Wu C, Huang D, Ma Y, et al. Exosomes derived from mature dendritic cells increase endothelial inflammation and atherosclerosis via membrane TNF-α mediated NF-κB pathway. J Cell Mol Med. 2016;20(12):2318–27.

87. Jia X, Bai X, Yang X, Wang L, Lu Y, Zhu L, et al. VCAM-1-binding peptide targeted cationic liposomes containing NLRP3 siRNA to modulate LDL transcytosis as a novel therapy for experimental atherosclerosis. Metabolism [Internet]. 2022;135(February):155274. Available from: https://doi.org/10.1016/j.metabol.2022.155274

88. Basurto L, Gregory MA, Hernández SB, Sánchez-Huerta L, Martínez AD, Manuel-Apolinar L, et al. Monocyte chemoattractant protein-1 (MCP-1) and fibroblast growth factor-21 (FGF-21) as biomarkers of subclinical atherosclerosis in women. Exp Gerontol [Internet]. 2019;124(May):110624. Available from: https://doi.org/10.1016/j.exger.2019.05.013

89. Chen W, Zheng W, Liu S, Su Q, Ding K, Zhang Z, et al. SRC-3 deficiency prevents atherosclerosis development by decreasing endothelial ICAM-1 expression to attenuate macrophage recruitment. Int J Biol Sci. 2022;18(15):5978–93.

90. Ahmed MMU. Age and sex differences in the structure of the tunica media of the coronary arteries in chinese subjects. Cells Tissues Organs. 1969;73(3):431–41.

91. Bačáková L, Kuneš J. Gender differences in growth of vascular smooth muscle cells isolated from hypertensive and normotensive rats. Clin Exp Hypertens. 2000;22(1):33–44.

92. Li H, Zhuang W, Xiong T, Park WS, Zhang S, Zha Y, et al. Nrf2 deficiency attenuates atherosclerosis by reducing LOX-1-mediated proliferation and migration of vascular smooth muscle cells. Atherosclerosis [Internet]. 2022;347(March):1–16. Available from: https://doi.org/10.1016/j.atherosclerosis.2022.02.025

93. Tan X, Feng L, Huang X, Yang Y, Yang C, Gao Y. Histone deacetylase inhibitors promote eNOS expression in vascular smooth muscle cells and suppress hypoxia-induced cell growth. J Cell Mol Med. 2017;21(9):2022–35.

94. Huang C, Huang W, Wang R, He Y. Ulinastatin inhibits the proliferation, invasion and phenotypic switching of PDGF-BB-induced vsmcs via Akt/eNOS/NO/cGMP signaling pathway. Drug Des Devel Ther. 2020;14:5505–14.

95. Bennett MR, Sinha S, Owens GK. Vascular Smooth Muscle Cells in Atherosclerosis. Circ Res [Internet]. 2016 Feb 19;118(4):692–702. Available from: https://linkinghub.elsevier.com/retrieve/pii/S001650851634954X

96. Orr AW, Lee MY, Lemmon JA, Yurdagul A, Gomez MF, Schoppee Bortz PD, et al. Molecular mechanisms of collagen isotype-specific modulation of smooth muscle cell phenotype. Arterioscler Thromb Vasc Biol. 2009;29(2):225–31.

97. Pi S, Mao L, Chen J, Shi H, Liu Y, Guo X, et al. The P2RY12 receptor promotes VSMC-derived foam cell formation by inhibiting autophagy in advanced atherosclerosis. Autophagy. 2021;17(4):980–1000.

98. Miao G, Zhao X, Chan SL, Zhang L, Li Y, Zhang Y, et al. Vascular smooth muscle cell c-Fos is critical for foam cell formation and atherosclerosis. Metabolism [Internet]. 2022;132(January):155213. Available from: https://doi.org/10.1016/j.metabol.2022.155213

99. Zhang DD, Song Y, Kong P, Xu X, Gao YK, Dou YQ, et al. Smooth muscle 22 alpha protein inhibits VSMC foam cell formation by supporting normal LXRα signaling, ameliorating atherosclerosis. Cell Death Dis. 2021;12(11).

100. Wang PW, Pang Q, Zhou T, Song XY, Pan YJ, Jia LP, et al. Irisin alleviates vascular calcification by inhibiting VSMC osteoblastic transformation and mitochondria dysfunction via AMPK/Drp1 signaling pathway in chronic kidney disease. Atherosclerosis [Internet]. 2022;346(February):36–45. Available from: https://doi.org/10.1016/j.atherosclerosis.2022.02.007

101. Dai X, Liu S, Cheng L, Huang T, Guo H, Wang D, et al. Epigenetic Upregulation of H19 and AMPK Inhibition Concurrently Contribute to S-Adenosylhomocysteine Hydrolase Deficiency-Promoted Atherosclerotic Calcification. Circ Res. 2022;130(10):1565–82.

102. Chen P yu, Qin L, Li G, Malagon-Lopez J, Wang Z, Bergaya S, et al. Smooth Muscle Cell Reprogramming in Aortic Aneurysms. Cell Stem Cell [Internet]. 2020 Apr;26(4):542-557.e11. Available from: https://linkinghub.elsevier.com/retrieve/pii/S1934590920300667

103. Zou F, Li Y, Zhang S, Zhang J. DP1 (Prostaglandin D2Receptor 1) Activation Protects Against Vascular Remodeling and Vascular Smooth Muscle Cell Transition to Myofibroblasts in Angiotensin II-Induced Hypertension in Mice. Hypertension. 2022;79(6):1203–15.

104. Guo Y, Tang Z, Yan B, Yin H, Tai S, Peng J, et al. PCSK9 (Proprotein Convertase Subtilisin/Kexin Type 9) Triggers Vascular Smooth Muscle Cell Senescence and Apoptosis: Implication of Its Direct Role in Degenerative Vascular Disease. Arterioscler Thromb Vasc Biol. 2022;42(1):67–86.

105. Newman AAC, Serbulea V, Baylis RA, Shankman LS, Bradley X, Alencar GF, et al. Multiple cell types contribute to the atherosclerotic lesion fibrous cap by PDGFRβ and bioenergetic mechanisms. Nat Metab [Internet]. 2021 Feb 22;3(2):166–81. Available from: https://www.nature.com/articles/s42255-020-00338-8

106. Fishbein MC. The vulnerable and unstable atherosclerotic plaque. Cardiovasc Pathol [Internet]. 2010;19(1):6–11. Available from: http://dx.doi.org/10.1016/j.carpath.2008.08.004

107. Wang N, Zhang X, Ma Z, Niu J, Ma S, Wenjie W, et al. Combination of tanshinone IIA and astragaloside IV attenuate atherosclerotic plaque vulnerability in ApoE(-/-) mice by activating PI3K/AKT signaling and suppressing TRL4/NF-κB signaling. Biomed Pharmacother [Internet]. 2020;123(November 2019):109729. Available from: https://doi.org/10.1016/j.biopha.2019.109729

108. Bos D, Arshi B, van den Bouwhuijsen QJA, Ikram MK, Selwaness M, Vernooij MW, et al. Atherosclerotic Carotid Plaque Composition and Incident Stroke and Coronary Events. J Am Coll Cardiol. 2021;77(11):1426–35.

109. Guo M, Cai Y, Yao X, Li Z. Mathematical modeling of atherosclerotic plaque destabilization: Role of neovascularization and intraplaque hemorrhage. J Theor Biol [Internet]. 2018;450:53–65. Available from: https://doi.org/10.1016/j.jtbi.2018.04.031

110. John Chapman M, Preston Mason R. Cholesterol crystals and atherosclerotic plaque instability: Therapeutic potential of Eicosapentaenoic acid. Pharmacol Ther [Internet]. 2022;240:108237. Available from: https://doi.org/10.1016/j.pharmthera.2022.108237

111. Koelwyn GJ, Corr EM, Erbay E, Moore KJ. Regulation of macrophage immunometabolism in atherosclerosis. Nat Immunol [Internet]. 2018 Jun 18;19(6):526–37. Available from: https://www.nature.com/articles/s41590-018-0113-3

112. Ruggio A, Pedicino D, Flego D, Vergallo R, Severino A, Lucci C, et al. Correlation between CD4 + CD28 null T lymphocytes, regulatory T cells and plaque rupture: An Optical Coherence Tomography study in Acute Coronary Syndromes. Int J Cardiol [Internet]. 2019;276:289–92. Available from: https://doi.org/10.1016/j.ijcard.2018.08.101

113. Xu J, Chen C, Yang Y. Identification and Validation of Candidate Gene Module Along With Immune Cells Infiltration Patterns in Atherosclerosis Progression to Plaque Rupture via Transcriptome Analysis. Front Cardiovasc Med. 2022;9(June):1–14.

114. Bessueille L, Kawtharany L, Quillard T, Goettsch C, Briolay A, Taraconat N, et al. Inhibition of alkaline phosphatase impairs dyslipidemia and protects mice from atherosclerosis. Transl Res. 2023;251(March 2022):2–13.

115. Penz S, Reininger AJ, Brandl R, Goyal P, Rabie T, Bernlochner I, et al. Human atheromatous plaques stimulate thrombus formation by activating platelet glycoprotein VI. FASEB J. 2005;19(8):898–909.

116. Badimon L, Vilahur G. Thrombosis formation on atherosclerotic lesions and plaque rupture. J Intern Med. 2014;276(6):618–32.

117. Badimon JJ, Lettino M, Toschi V, Fuster V, Berrozpe M, Chesebro JH, et al. Local inhibition of tissue factor reduces the thrombogenicity of disrupted human atherosclerotic plaques. Effects of tissue factor pathway inhibitor on plaque thrombogenicity under flow conditions. Circulation. 1999;99(14):1780–7.

118. Ignatowski A. Über die Wirkung des tierischen Eiweißes auf die Aorta und die parenchymatösen Organe der Kaninchen. Virchows Arch Pathol Anat Physiol Klin Med. 1909;198(2):248–70.

119. Gisterå A, Ketelhuth DFJ, Malin SG, Hansson GK. Animal Models of Atherosclerosis-Supportive Notes and Tricks of the Trade. Circ Res. 2022;130(12):1869–87.

120. Stoletov K, Fang L, Choi SH, Hartvigsen K, Hansen LF, Hall C, et al. Vascular lipid accumulation, lipoprotein oxidation, and macrophage lipid uptake in hypercholesterolemic zebrafish. Circ Res. 2009;104(8):952–60.

121. Griggs TR, Bauman RW, Reddick RL, Read MS, Koch GG, Lamb MA. Development of coronary atherosclerosis in swine with severe hypercholesterolemia. Lack of influence of von Willebrand factor or acute intimal injury. Arteriosclerosis. 1986;6(2):155–65.

122. Bond MG, Bullock BC, Bellinger DA, Hamm TE. Myocardial infarction in a large colony of nonhuman primates with coronary artery atherosclerosis. Am J Pathol. 1980;101(3):675–92.

123. Zhang SH, Reddick RL, Piedrahita JA, Maeda N. Spontaneous hypercholesterolemia and arterial lesions in mice lacking apolipoprotein E. Science (80-). 1992;258(5081):468–71.

124. Ishibashi S, Brown MS, Goldstein JL, Gerard RD, Hammer RE, Herz J. Hypercholesterolemia in low density lipoprotein receptor knockout mice and its reversal by adenovirus-mediated gene delivery. J Clin Invest. 1993;92(2):883–93.

125. Ishibashi S, Goldstein JL, Brown MS, Herz J, Burns DK. Massive Xanthomatosis and Atherosclerosis. J Clin Invest. 1994;93:1885–93.

126. Roche-Molina M, Sanz-Rosa D, Cruz FM, García-Prieto J, López S, Abia R, et al. Induction of sustained hypercholesterolemia by single adeno-associated virus-mediated gene transfer of mutant hPCSK9. Arterioscler Thromb Vasc Biol. 2015;35(1):50–9.

127. Sanan DA, Newland DL, Tao R, Marcovina S, Wang J, Mooser V, et al. Low density lipoprotein receptor-negative mice expressing human apolipoprotein B-100 develop complex atherosclerotic lesions on a chow diet: No accentuation by apolipoprotein(a). Proc Natl Acad Sci U S A. 1998;95(8):4544–9.

128. Lewis GF, Brubaker PL. The discovery of insulin revisited: Lessons for the modern era. J Clin Invest. 2021;131(1):1–9.

129. Lee. Jongsoon PPF. The insulin receptor: structure, function, and signaling. Am Physiol Soc. 1994;

130. Saltiel AR. Insulin signaling in health and disease. J Clin Invest [Internet]. 2021 Jan 4;131(1):1–12. Available from: https://doi.org/10.1172/JCI142241.

131. Hawkes C, Kar S. The insulin-like growth factor-II/mannose-6-phosphate receptor: Structure, distribution and function in the central nervous system. Brain Res Rev. 2004;44(2–3):117–40.

132. Okamoto T, Nishimoto I, Murayama Y, Ohkuni Y, Ogata E. Insulin-like Growth Factor-II/Mannose 6-Phosphate receptor is incapable of activating GTP-binding proteins in response to manose-6-Phosphate, but capable in response to insulin-like growth factor II. Biochem Biophys Res Commun. 1990;168(3):1201–10.

133. Huang C y, Kuo W w, Yeh Y l, Ho T j, Lin J y, Lin D y, et al. ANG II promotes IGF-IIR expression and cardiomyocyte apoptosis by inhibiting HSF1 via JNK activation and SIRT1 degradation. 2014;1262–74.

134. Lee SH, Park SY, Choi CS. Insulin Resistance: From Mechanisms to Therapeutic Strategies. Diabetes Metab J. 2022;46(1):15–37.

135. Guo X, Sun W, Luo G, Wu L, Xu G, Hou D, et al. Panax notoginseng saponins alleviate skeletal muscle insulin resistance by regulating the IRS1–PI3K–AKT signaling pathway and GLUT4 expression. FEBS Open Bio. 2019;9(5):1008–19.

136. Yan J, Wang C, Jin Y, Meng Q, Liu Q, Liu Z, et al. Catalpol ameliorates hepatic insulin resistance in type 2 diabetes through acting on AMPK/NOX4/PI3K/AKT pathway. Pharmacol Res [Internet]. 2018;130:466–80. Available from: http://dx.doi.org/10.1016/j.phrs.2017.12.026

137. Li BY, Guo YY, Xiao G, Guo L, Tang QQ. SERPINA3C ameliorates adipose tissue inflammation through the Cathepsin G/Integrin/AKT pathway. Mol Metab [Internet]. 2022;61(April):101500. Available from: https://doi.org/10.1016/j.molmet.2022.101500

138. Gong XM, Li YF, Luo J, Wang JQ, Wei J, Wang JQ, et al. Gpnmb secreted from liver promotes lipogenesis in white adipose tissue and aggravates obesity and insulin resistance. Nat Metab [Internet]. 2019;1(5):570–83. Available from: http://dx.doi.org/10.1038/s42255-019-0065-4

139. Petersen MC, Shulman GI. Mechanisms of insulin action and insulin resistance. Physiol Rev. 2018;98(4):2133–223.

140. Di Pino A, Defronzo RA. Insulin Resistance and Atherosclerosis: Implications for Insulin-Sensitizing Agents. Endocr Rev. 2019;40(6):1447–67.

141. Beneit N, Luis J, Ventura M, Longás CR, Escribano Ó, Gómez GG, et al. Potential role of insulin receptor isoforms and IGF receptors in plaque instability of human and experimental atherosclerosis. Cardiovasc Diabetol [Internet]. 2018;1–14. Available from: https://doi.org/10.1186/s12933-018-0675-2

142. Fang S, Wan X, Zou X, Sun S, Hao X, Liang C, et al. Arsenic trioxide induces macrophage autophagy and atheroprotection by regulating ROS-dependent TFEB nuclear translocation and AKT/mTOR pathway. Cell Death Dis. 2021;12(1):1–18.

143. Jin QS, Huang LJ, Zhao TT, Yao XY, Lin LY, Teng YQ, et al. HOXA11-AS regulates diabetic arteriosclerosis-related inflammation via PI3K/AKT pathway. Eur Rev Med Pharmacol Sci. 2018;22(20):6912–21.

144. Shao-Cong Sun. The non-canonical NF-κB pathway in immunity and inflammation. Nat Rev Immunol. 2017;17(9):545–58.

145. Lee K, Yim JH, Lee HK, Pyo S. Inhibition of VCAM-1 expression on mouse vascular smooth muscle cells by lobastin via downregulation of p38, ERK 1/2 and NF-κB signaling pathways. Arch Pharm Res. 2016;39(1):83–93.

146. Feng X, Du M, Li S, Zhang Y, Ding J, Wang J, et al. Hydroxysafflor yellow A regulates lymphangiogenesis and inflammation via the inhibition of PI3K on regulating AKT/mTOR and NF-κB pathway in macrophages to reduce atherosclerosis in ApoE-/- mice. Phytomedicine [Internet]. 2023;112:154684. Available from: https://doi.org/10.1016/j.phymed.2023.154684

147. Feinbaum R, Ambros V, Lee R. The C. elegans Heterochronic Gene lin-4 Encodes Small RNAs with Antisense Complementarity to lin-14. Cell. 1993;116(116):843–54.

148. Han J, Lee Y, Yeom KH, Nam JW, Heo I, Rhee JK, et al. Molecular Basis for the Recognition of Primary microRNAs by the Drosha-DGCR8 Complex. Cell. 2006;125(5):887–901.

149. Alarcón CR, Lee H, Goodarzi H, Halberg N, Tavazoie SF. N6-methyladenosine marks primary microRNAs for processing. Nature [Internet]. 2015 Mar 18;519(7544):482–5. Available from: https://www.nature.com/articles/nature14281

150. Gu S, Jin L, Zhang Y, Huang Y, Zhang F, Valdmanis PN, et al. The Loop Position of shRNAs and Pre-miRNAs Is Critical for the Accuracy of Dicer Processing In Vivo. Cell [Internet]. 2012 Nov;151(4):900–11. Available from: https://linkinghub.elsevier.com/retrieve/pii/S0092867412012457

151. Medley JC, Panzade G, Zinovyeva AY. microRNA strand selection: Unwinding the rules. Wiley Interdiscip Rev RNA. 2021;12(3):1–22.

152. McGeary SE, Lin KS, Shi CY, Pham TM, Bisaria N, Kelley GM, et al. The biochemical basis of microRNA targeting efficacy. Science (80-). 2019;366(6472).

153. Hausser J, Syed AP, Bilen B, Zavolan M. Analysis of CDS-located miRNA target sites suggests that they can effectively inhibit translation. Genome Res. 2013;23(4):604–15.

154. Li G, Wu X, Qian W, Cai H, Sun X, Zhang W, et al. CCAR1 5′ UTR as a natural miRancer of miR-1254 overrides tamoxifen resistance. Cell Res. 2016;26(6):655–73.

155. Collado A, Gan L, Tengbom J, Kontidou E, Pernow J, Zhou Z. Extracellular vesicles and their non-coding RNA cargos: Emerging players in cardiovascular disease. J Physiol. 2022;0:1–21.

156. Peng M, Sun R, Hong Y, Wang J, Xie Y, Zhang X, et al. Extracellular vesicles carrying proinflammatory factors may spread atherosclerosis to remote locations. Cell Mol Life Sci [Internet]. 2022;79(8):1–20. Available from: https://doi.org/10.1007/s00018-022-04464-2

157. Ying W, Gao H, Dos Reis FCG, Bandyopadhyay G, Ofrecio JM, Luo Z, et al. MiR-690, an exosomal-derived miRNA from M2-polarized macrophages, improves insulin sensitivity in obese mice. Cell Metab [Internet]. 2021 Apr;33(4):781-790.e5. Available from: https://linkinghub.elsevier.com/retrieve/pii/S1550413120307178

158. Long JK, Dai W, Zheng YW, Zhao SP. MiR-122 promotes hepatic lipogenesis via inhibiting the LKB1/AMPK pathway by targeting Sirt1 in non-alcoholic fatty liver disease. Mol Med. 2019;25(1):1–13.

159. Wu X, Yu T, Ji N, Huang Y, Gao L, Shi W, et al. IL6R inhibits viability and apoptosis of pancreatic beta-cells in type 2 diabetes mellitus via regulation by miR-22 of the JAK/STAT signaling pathway. Diabetes, Metab Syndr Obes. 2019;12:1645–57.

160. Wei Q, Tu Y, Zuo L, Zhao J, Chang Z, Zou Y, et al. MiR-345-3p attenuates apoptosis and inflammation caused by oxidized low-density lipoprotein by targeting TRAF6 via TAK1/p38/NF-kB signaling in endothelial cells. Life Sci [Internet]. 2020;241:117142. Available from: https://doi.org/10.1016/j.lfs.2019.117142

161. Feng S, Gao L, Zhang D, Tian X, Kong L, Shi H, et al. Mir-93 regulates vascular smooth muscle cell proliferation, and neointimal formation through targeting Mfn2. Int J Biol Sci. 2019;15(12):2615–26.

162. Chin DD, Poon C, Wang J, Joo J, Ong V, Jiang Z, et al. miR-145 micelles mitigate atherosclerosis by modulating vascular smooth muscle cell phenotype. Biomaterials [Internet]. 2021 Jun;273(4):120810. Available from: https://www.ncbi.nlm.nih.gov/pmc/articles/PMC5958625/pdf/nihms960157.pdf

163. Farina FM, Hall IF, Serio S, Zani S, Climent M, Salvarani N, et al. MiR-128-3p Is a Novel Regulator of Vascular Smooth Muscle Cell Phenotypic Switch and Vascular Diseases. Circ Res. 2020;126(12):e120–35.

164. Goettsch C, Rauner M, Pacyna N, Hempel U, Bornstein SR, Hofbauer LC. MiR-125b regulates calcification of vascular smooth muscle cells. Am J Pathol [Internet]. 2011;179(4):1594–600. Available from: http://dx.doi.org/10.1016/j.ajpath.2011.06.016

165. Wu YT, Li JB, Lin HQ, Zhang GX, Hong CM, Li M, et al. Inhibition of miR-200b-3p alleviates lipid accumulation and promotes cholesterol efflux by targeting ABCA1 in macrophage-derived foam cells. Exp Ther Med. 2021;22(2):1–9.

166. Stary HC. Composition and classification of human atherosclerotic lesions. Virchows Arch A Pathol Anat Histopathol. 1992;421(4):277–90.

167. Stary H, Chandler A, Glagov S, Jr G, Insull W, Rosenfeld MJ, et al. AHA Medical / Scientific Statement Special Report A Definition of Initial , Fatty Streak , and Intermediate Lesions of Atherosclerosis. Circulation. 1994;89:2462–78.

168. Skålén K, Gustafsson M, Knutsen Rydberg E, Hultén LM, Wiklund O, Innerarity TL, et al. Subendothelial retention of atherogenic lipoproteins in early atherosclerosis. Nature. 2002;417(6890):750–4.

169. Gómez-Hernández A, Escribano Ó, Perdomo L, Otero YF, García-Gómez G, Fernández S, et al. Implication of insulin receptor A isoform and IRA/IGF-IR hybrid receptors in the aortic vascular smooth muscle cell proliferation: Role of TNF-α and IGF-II. Endocrinology. 2013;154(7):2352–64.

170. Falk E. Pathogenesis of Atherosclerosis. J Am Coll Cardiol. 2006;47(8 SUPPL.):0–5.

171. Bentzon JF, Otsuka F, Virmani R, Falk E. Mechanisms of plaque formation and rupture. Circ Res. 2014;114(12):1852–66.

172. Kang DH, Choi M, Chang S, Lee MY, Lee DJ, Choi K, et al. Vascular proteomics reveal novel proteins involved in SMC phenotypic change: OLR1 as a SMC receptor regulating proliferation and inflammatory response. PLoS One. 2015;10(8):1–23.

173. Wang X, Li H, Zhang Y, Liu Q, Sun X, He X, et al. Suppression of miR-4463 promotes phenotypic switching in VSMCs treated with Ox-LDL. Cell Tissue Res. 2021;383(3):1155–65.

174. Shan R, Liu N, Yan Y, Liu B. Apoptosis, autophagy and atherosclerosis: Relationships and the role of Hsp27. Pharmacol Res [Internet]. 2021;166:105169. Available from: https://doi.org/10.1016/j.phrs.2020.105169

175. Jovanovic M, Hengartner MO. miRNAs and apoptosis: RNAs to die for. Oncogene. 2006;25(46):6176–87.

176. Peng J, Wu HJ, Zhang HF, Fang SQ, Zeng R. miR-143-3p inhibits proliferation and invasion of hepatocellular carcinoma cells by regulating its target gene FGF1. Clin Transl Oncol. 2021;23(3):468–80.

177. Wang L, Shui X, Mei Y, Xia Y, Lan G, Hu L, et al. miR-143-3p Inhibits Aberrant Tau Phosphorylation and Amyloidogenic Processing of APP by Directly Targeting DAPK1 in Alzheimer's Disease. Int J Mol Sci. 2022;23(14).

178. Liu Q, Du GQ, Zhu ZT, Zhang C, Sun XW, Liu JJ, et al. Identification of apoptosis - related microRNAs and their target genes in myocardial infarction post - transplantation with skeletal myoblasts. J Transl Med. 2015;1–11.

179. Boucher JM, Peterson SM, Urs S, Zhang C, Liaw L. The miR-143/145 cluster is a novel transcriptional target of Jagged-1/Notch signaling in vascular smooth muscle cells. J Biol Chem. 2011;286(32):28312–21.

180. Zhang HP, Wang YH, Cao CJ, Yang XM, Ma SC, Han XB, et al. A regulatory circuit involving miR-143 and DNMT3a mediates vascular smooth muscle cell proliferation induced by homocysteine. Mol Med Rep. 2016;13(1):483–90.

181. Vacante F, Rodor J, Lalwani MK, Mahmoud AD, Bennett M, De Pace AL, et al. CARMN Loss Regulates Smooth Muscle Cells and Accelerates Atherosclerosis in Mice. Circ Res. 2021;128(9):1258–75.

182. Sala F, Aranda JF, Rotllan N, Ramírez CM, Aryal B, Elia L, et al. MiR-143/145 deficiency attenuates the progression of atherosclerosis in Ldlr-/- mice. Thromb Haemost. 2014;112(4):796–802.

183. Xu RH, Liu B, Wu JD, Yan YY, Wang JN. MIR-143 is involved in endothelial cell dysfunction through suppression of glycolysis and correlated with atherosclerotic plaques formation. Eur Rev Med Pharmacol Sci. 2016;20(19):4063–71.

184. Head T, Daunert S, Goldschmidt-Clermont PJ. The aging risk and atherosclerosis: A fresh look at arterial homeostasis. Front Genet. 2017;8(DEC):1–11.

185. Morbiducci U, Kok AM, Kwak BR, Stone PH, Steinman DA, Wentzel JJ. Atherosclerosis at arterial bifurcations: Evidence for the role of haemodynamics and geometry. Thromb Haemost. 2016;115(3):484–92.

186. Collura S, Ciavarella C, Morsiani C, Motta I, Valente S, Gallitto E, et al. MicroRNA profiles of human peripheral arteries and abdominal aorta in normal conditions: MicroRNAs-27a-5p, -139-5p and -155-5p emerge and in atheroma too. Mech Ageing Dev [Internet]. 2021;198(April):111547. Available from: https://doi.org/10.1016/j.mad.2021.111547

187. Koyama S, Horie T, Nishino T, Baba O, Sowa N, Miyasaka Y, et al. Identification of differential roles of microRNA-33a and -33b during atherosclerosis progression with genetically modified mice. J Am Heart Assoc. 2019;8(13).

188. Xihua LIN, Shengjie T, Weiwei GUI, Matro E, Tingting TAO, Lin LI, et al. Circulating miR-143-3p inhibition protects against insulin resistance in Metabolic Syndrome via targeting of the insulin-like growth factor 2 receptor. Transl Res [Internet]. 2018;205:33–43. Available from: https://doi.org/10.1016/j.trsl.2018.09.006

189. Huang CY, Lai CH, Kuo CH, Chiang SF, Pai PY, Lin JY, et al. Inhibition of ERK-Drp1 signaling and mitochondria fragmentation alleviates IGF-IIR-induced mitochondria dysfunction during heart failure. J Mol Cell Cardiol [Internet]. 2018;122(April):58–68. Available from: https://doi.org/10.1016/j.yjmcc.2018.08.006

190. Zhou D, Huang Z, Zhu X, Hong T, Zhao Y. Circular RNA 0025984 Ameliorates Ischemic Stroke Injury and Protects Astrocytes Through miR-143-3p/TET1/ORP150 Pathway. Mol Neurobiol. 2021;58(11):5937–53.

191. Ma W ya, Song R jie, Xu B bin, Xu Y, Wang X xiu, Sun H yue, et al. Melatonin promotes cardiomyocyte proliferation and heart repair in mice with myocardial infarction via miR-143-3p/Yap/Ctnnd1 signaling pathway. Acta Pharmacol Sin [Internet]. 2021;42(6):921–31. Available from: http://dx.doi.org/10.1038/s41401-020-0495-2

192. Dong LM, Zhang XL, Mao MH, Li YP, Zhang XY, Xue DW, et al. LINC00511/miRNA-143-3p Modulates Apoptosis and Malignant Phenotype of Bladder Carcinoma Cells via PCMT1. Front Cell Dev Biol. 2021;9(April):1–12.

193. Shao Y, Yang WY, Saaoud F, Drummer C, Sun Y, Xu K, et al. IL-35 promotes CD4+Foxp3+ Tregs and inhibits atherosclerosis via maintaining CCR5-amplified Treg-suppressive mechanisms. JCI Insight. 2021;6(19).

194. Xu W, Zhu R, Zhu Z, Yu K, Wang Y, Ding Y, et al. Interleukin-27 Ameliorates Atherosclerosis in ApoE-/-Mice through Regulatory T Cell Augmentation and Dendritic Cell Tolerance. Mediators Inflamm. 2022;2022.

195. Wang W, Li R, Meng M, Wei C, Xie Y, Zhang Y, et al. MicroRNA profiling of CD3+ CD56+ cytokine-induced killer cells. Sci Rep. 2015;5.

196. Qiu MK, Wang SC, Dai YX, Wang SQ, Ou JM, Quan ZW. PD-1 and Tim-3 pathways regulate CD8+ T cells function in atherosclerosis. PLoS One. 2015;10(6):1–11.

197. Vogel ME, Idelman G, Konaniah ES, Zucker SD. Bilirubin prevents atherosclerotic lesion formation in low-density lipoprotein receptor-deficient mice by inhibiting endothelial VCAM-1 and ICAM-1 signaling. J Am Heart Assoc. 2017;6(4):1–18.

198. Nasiri-Ansari N, Dimitriadis GK, Agrogiannis G, Perrea D, Kostakis ID, Kaltsas G, et al. Canagliflozin attenuates the progression of atherosclerosis and inflammation process in APOE knockout mice. Cardiovasc Diabetol [Internet]. 2018;17(1):1–12. Available from: https://doi.org/10.1186/s12933-018-0749-1

199. Xiong J, Hu Y, Liu Y, Zeng X. CircRNA mmu_circ_0000021 regulates microvascular function via the miR-143-3p/NPY axis and intracellular calcium following ischemia/reperfusion injury. Cell Death Discov. 2022;8(1):1–13.

200. Zhou Z, Dong Y, Zhou H, Liu J, Zhao W. MiR-143-3p directly targets GLUT9 to reduce uric acid reabsorption and inflammatory response of renal tubular epithelial cells. Biochem Biophys Res Commun [Internet]. 2019;517(3):413–20. Available from: https://doi.org/10.1016/j.bbrc.2019.07.114

201. Gisterå A, Klement ML, Polyzos KA, Mailer RKW, Duhlin A, Karlsson MCI, et al. Low-Density Lipoprotein-Reactive T Cells Regulate Plasma Cholesterol Levels and Development of Atherosclerosis in Humanized Hypercholesterolemic Mice. Circulation. 2018;138(22):2513–26.

202. Schaftenaar FH, Amersfoort J, Douna H, Kröner MJ, Foks AC, Bot I, et al. Induction of HLA-A2 restricted CD8 T cell responses against ApoB100 peptides does not affect atherosclerosis in a humanized mouse model. Sci Rep. 2019;9(1):1–11.

203. Francula-Zaninovic S, Nola IA. Management of Measurable Variable Cardiovascular Disease' Risk Factors. Curr Cardiol Rev. 2018;14(3):153–63.

204. Bruen R, Fitzsimons S, Belton O. MiR-155 in the resolution of atherosclerosis. Front Pharmacol. 2019;10(MAY).

205. Zhu J, Chen T, Yang L, Li Z, Wong MM, Zheng X, et al. Regulation of MicroRNA-155 in Atherosclerotic Inflammatory Responses by Targeting MAP3K10. PLoS One. 2012;7(11).

206. Singh S, de Ronde MWJ, Kok MGM, Beijk MA, De Winter RJ, van der Wal AC, et al. MiR-223-3p and miR-122-5p as circulating biomarkers for plaque instability. Open Hear. 2020;7(1):e001223.

207. Chen L, Zheng SY, Yang CQ, Ma BM, Jiang D. MiR-155-5p inhibits the proliferation and migration of VSMCs and HUVECs in atherosclerosis by targeting AKT1. Eur Rev Med Pharmacol Sci. 2019;23(5):2223–33.

208. Maucher D, Schmidt B, Schumann J. Loss of endothelial barrier function in the inflammatory setting: Indication for a cytokine-mediated post-transcriptional mechanism by virtue of upregulation of mirnas mir-29a-3p, mir-29b-3p, and mir-155-5p. Cells. 2021;10(11).

209. Wang G, Chen JJ, Deng WY, Ren K, Yin SH, Yu XH. CTRP12 ameliorates atherosclerosis by promoting cholesterol efflux and inhibiting inflammatory response via the miR-155-5p/LXRα pathway. Cell Death Dis. 2021;12(3).

210. Rachmawati E, Sargowo D, Rohman MS, Widodo N, Kalsum U. miR-155–5p predictive role to decelerate foam cell atherosclerosis through CD36, VAV3, and SOCS1 pathway. Non-coding RNA Res [Internet]. 2021;6(2):59–69. Available from: https://doi.org/10.1016/j.ncrna.2021.02.003

211. Zhu GF, Yang LX, Guo RW, Liu H, Shi YK, Wang H, et al. MiR-155 inhibits oxidized low-density lipoprotein-induced apoptosis of RAW264.7 cells. Mol Cell Biochem. 2013;382(1–2):253–61.

212. Nazari-Jahantigh M, Wei Y, Noels H, Akhtar S, Zhou Z, Koenen RR, et al. MicroRNA-155 promotes atherosclerosis by repressing Bcl6 in macrophages. J Clin Invest. 2012;122(11):4190–202.

213. Du F, Yu F, Wang Y, Hui Y, Carnevale K, Fu M, et al. MicroRNA-155 Deficiency Results in Decreased Macrophage Inflammation and Attenuated Atherogenesis in Apolipoprotein E–Deficient Mice. Arterioscler Thromb Vasc Biol [Internet]. 2014 Apr;34(4):759–67. Available from: https://www.ahajournals.org/doi/10.1161/ATVBAHA.113.302701

214. Huang X, Shen Y, Liu M, Bi C, Jiang C, Iqbal J, et al. Quantitative proteomics reveals that miR-155 regulates the PI3K-AKT pathway in diffuse large B-cell lymphoma. Am J Pathol. 2012;181(1):26–33.

215. Choi S, Kim J, Kim JH, Lee DK, Park W, Park M, et al. Carbon monoxide prevents TNF-α-induced eNOS downregulation by inhibiting NF-κB-responsive miR-155-5p biogenesis. Exp Mol Med [Internet]. 2017;49(11). Available from: http://dx.doi.org/10.1038/emm.2017.193

216. Kim TH, Kim JY, Bae J, Kim YM, Won MH, Ha KS, et al. Korean Red ginseng prevents endothelial senescence by downregulating the HO-1/NF-κB/miRNA-155-5p/eNOS pathway. J Ginseng Res [Internet]. 2021;45(2):344–53. Available from: https://doi.org/10.1016/j.jgr.2020.08.002

217. Zegeye MM, Lindkvist M, Fälker K, Kumawat AK, Paramel G, Grenegård M, et al. Activation of the JAK/STAT3 and PI3K/AKT pathways are crucial for IL-6 trans-signaling-mediated pro-inflammatory response in human vascular endothelial cells. Cell Commun Signal. 2018;16(1):1–10.

218. Yao X, Yan C, Zhang L, Li Y, Wan Q. LncRNA ENST00113 promotes proliferation, survival, and migration by activating PI3K/Akt/mTOR signaling pathway in atherosclerosis. Med (United States). 2018;97(16).

219. Stoneman VEA, Bennett MR. Role of apoptosis in atherosclerosis and its therapeutic implications. Clin Sci. 2004;107(4):343–54.

220. Li S, Huang Q, Zhang L, Qiao X, Zhang Y, Tang F, et al. Effect of CAPE-pNO2 against type 2 diabetes mellitus via the AMPK/GLUT4/ GSK3β/PPARα pathway in HFD/STZ-induced diabetic mice. Eur J Pharmacol. 2019;853(December 2018):1–10.

221. Zhang H, Ge Z, Ang S, Meng R, Bi Y, Zhu D. Erythropoietin ameliorates PA-induced insulin resistance through the IRS/AKT/FOXO1 and GSK-3β signaling pathway, and inhibits the inflammatory response in HepG2 cells. Mol Med Rep. 2017;16(2):2295–301.

222. Li L, Yao Y, Zhao J, Cao J, Ma H. Dehydroepiandrosterone protects against hepatic glycolipid metabolic disorder and insulin resistance induced by high fat via activation of AMPK-PGC-1α-NRF-1 and IRS1-AKT-GLUT2 signaling pathways. Int J Obes [Internet]. 2020;44(5):1075–86. Available from: http://dx.doi.org/10.1038/s41366-019-0508-8

223. Gaudet AD, Fonken LK, Gushchina L V., Aubrecht TG, Maurya SK, Periasamy M, et al. MIR-155 deletion in female mice prevents diet-induced obesity. Sci Rep [Internet]. 2016;6(February):1–13. Available from: http://dx.doi.org/10.1038/srep22862

224. Savova MS, Mihaylova L V., Tews D, Wabitsch M, Georgiev MI. Targeting PI3K/AKT signaling pathway in obesity. Biomed Pharmacother [Internet]. 2023;159:114244. Available from: https://doi.org/10.1016/j.biopha.2023.114244

225. Piché ME, Tchernof A, Després JP. Obesity Phenotypes, Diabetes, and Cardiovascular Diseases. Circ Res. 2020;126(11):1477–500.

226. Wang J, Kang Z, Liu Y, Li Z, Liu Y, Liu J. Identification of immune cell infiltration and diagnostic biomarkers in unstable atherosclerotic plaques by integrated bioinformatics analysis and machine learning. Front Immunol. 2022;13(September):1–18.

227. Mahjabeen W, Khan DA, Mirza SA. Role of resveratrol supplementation in regulation of glucose hemostasis, inflammation and oxidative stress in patients with diabetes mellitus type 2: A randomized, placebo-controlled trial. Complement Ther Med [Internet]. 2022;66(June 2020):102819. Available from: https://doi.org/10.1016/j.ctim.2022.102819

228. Nau F, Yu B, Martin D, Nichols CD. Serotonin 5-HT2A Receptor Activation Blocks TNF-α Mediated Inflammation In Vivo. PLoS One. 2013;8(10):2–9.

229. Scoditti E, Carpi S, Massaro M, Pellegrino M, Polini B, Carluccio MA, et al. Hydroxytyrosol modulates adipocyte gene and mirna expression under inflammatory condition. Nutrients. 2019;11(10):1–29.

230. Zhang Q, Liu J, Duan H, Li R, Peng W, Wu C. Activation of Nrf2/HO-1 signaling: An important molecular mechanism of herbal medicine in the treatment of atherosclerosis via the protection of vascular endothelial cells from oxidative stress. J Adv Res [Internet]. 2021;34:43–63. Available from: https://doi.org/10.1016/j.jare.2021.06.023

231. Pan JX. LncRNA H19 promotes atherosclerosis by regulating MAPK and NF-kB signaling pathway. Eur Rev Med Pharmacol Sci. 2017;21(2):322–8.

232. Patil NP, Gómez-Hernández A, Zhang F, Cancel L, Feng X, Yan L, et al. Rhamnan sulfate reduces atherosclerotic plaque formation and vascular inflammation. Biomaterials. 2022;291(December 2021).

233. Subedi A, Park PH. Autocrine and paracrine modulation of microRNA-155 expression by globular adiponectin in RAW 264.7 macrophages: Involvement of MAPK/NF-κB pathway. Cytokine [Internet]. 2013;64(3):638–41. Available from: http://dx.doi.org/10.1016/j.cyto.2013.09.011

234. Martín-Ventura JL, Blanco-Colio LM, Muñoz-García B, Gómez-Hernández A, Arribas A, Ortega L, et al. NF-κB Activation and Fas Ligand Overexpression in Blood and Plaques of Patients with Carotid Atherosclerosis: Potential Implication in Plaque Instability. Stroke. 2004;35(2):458–63.

235. Gómez-Hernández A, Martín-Ventura JL, Sánchez-Galán E, Vidal C, Ortego M, Blanco-Colio LM, et al. Overexpression of COX-2, Prostaglandin E Synthase-1 and Prostaglandin E Receptors in blood mononuclear cells and plaque of patients with carotid atherosclerosis: Regulation by nuclear factor-κB. Atherosclerosis. 2006;187(1):139–49.

236. López-Franco O, Hernández-Vargas P, Ortiz-Muñoz G, Sanjuán G, Suzuki Y, Ortega L, et al. Parthenolide modulates the NF-κB-mediated inflammatory responses in experimental atherosclerosis. Arterioscler Thromb Vasc Biol. 2006;26(8):1864–70.

237. Zhang J, Li S, Li L, Li M, Guo C, Yao J, et al. Exosome and exosomal microRNA: Trafficking, sorting, and function. Genomics, Proteomics Bioinforma. 2015;13(1):17–24.

238. Han L, Lv Q, Guo K, Li L, Zhang H, Bian H. Th17 cell-derived miR-155-5p modulates interleukin-17 and suppressor of cytokines signaling 1 expression during the progression of systemic sclerosis. J Clin Lab Anal. 2022;36(6):1–10.

239. Li X, Wang S, Mu W, Barry J, Han A, Carpenter RL, et al. Reactive oxygen species reprogram macrophages to suppress antitumor immune response through the exosomal miR-155-5p/PD-L1 pathway. J Exp Clin Cancer Res [Internet]. 2022;41(1):1–19. Available from: https://doi.org/10.1186/s13046-022-02244-1

240. Bi J, Liu J, Chen X, Shi N, Wu H, Tang H, et al. MiR-155-5p-SOCS1/JAK1/STAT1 participates in hepatic lymphangiogenesis in liver fibrosis and cirrhosis by regulating M1 macrophage polarization. Hum Exp Toxicol. 2023;42:1–13.

241. Libby P, Ridker PM, Maseri A. Inflammation and atherosclerosis. Circulation. 2002;105(9):1135–43.

242. Malekmohammad K, Sewell RDE, Rafieian-Kopaei M. Antioxidants and atherosclerosis: Mechanistic aspects. Biomolecules. 2019;9(8):1–19.

243. Taraldsen MD, Wiseth R, Videm V, Bye A, Madssen E. Associations between circulating microRNAs and coronary plaque characteristics: Potential impact from physical exercise. Physiol Genomics. 2022;54(4):129–40.

244. Wang H, Yang Q, Li J, Chen W, Jin X, Wang Y. MicroRNA-15a-5p inhibits endometrial carcinoma proliferation, invasion and migration via downregulation of VEGFA and inhibition of the Wnt/β-catenin signaling pathway. Oncol Lett. 2021;21(4):1–10.

245. Guo Y, Gao X, An S, Li X, Pan L, Liu H, et al. Deletion of miR-15a inhibited glioma development via targeting Smad7 and inhibiting EMT pathway. Aging (Albany NY). 2021;13(21):24339–48.

246. Liu W, zheng L, Zhang R, Hou P, Wang J, Wu L, et al. Circ-ZEB1 promotes PIK3CA expression by silencing miR-199a-3p and affects the proliferation and apoptosis of hepatocellular carcinoma. Mol Cancer [Internet]. 2022;21(1):1–15. Available from: https://doi.org/10.1186/s12943-022-01529-5

247. Phatak P, Burrows WM, Chesnick IE, Tulapurkar ME, Rao JN, Turner DJ, et al. MiR-199a-3p decreases esophageal cancer cell proliferation by targeting p21 activated kinase 4. Oncotarget. 2018;9(47):28391–407.

248. Li H, Zhang HM, Fan LJ, Li HH, Peng ZT, Li JP, et al. STAT3/MIR-15A-5P/CX3CL1 loop regulates proliferation and migration of vascular endothelial cells in atherosclerosis. Int J Med Sci. 2021;18(4):964–74.

249. Liu M, Cao Y, Hu Y, Zhang Z, Ji S, Shi L, et al. MiR-199a-3p Restrains Foaming and Inflammation by Regulating RUNX1 in Macrophages. Mol Biotechnol. 2022;64(10):1130–42.

250. Sun X, Zhang Y, Liu Z, Li S, Wang L. MicroRNA-199a-3p Exhibits Beneficial Effects in Asymptomatic Atherosclerosis by Inhibiting Vascular Smooth Muscle Cell Proliferation and Migration. Mol Biotechnol [Internet]. 2021;63(7):595–604. Available from: https://doi.org/10.1007/s12033-021-00323-w

251. Joris V, Leon Gomez E, Menchi L, Lobysheva I, Di Mauro V, Esfahani H, et al. MicroRNA-199a-3p and MicroRNA-199a-5p Take Part to a Redundant Network of Regulation of the NOS (NO Synthase)/NO Pathway in the Endothelium. Arterioscler Thromb Vasc Biol. 2018;38(10):2345–57.

252. Li T, Morgan MJ, Choksi S, Zhang Y, Kim YS, Liu ZG. MicroRNAs modulate the noncanonical NF-κB pathway by regulating IKKα expression during macrophage differentiation HHS Public Access. Nat Immunol [Internet]. 2010;11(9):799–805. Available from: http://www.nature.com/authors/editorial_policies/license.html#terms

253. Bardin P, Marchal-Duval E, Sonneville F, Blouquit-Laye S, Rousselet N, Le Rouzic P, et al. Small RNA and transcriptome sequencing reveal the role of miR-199a-3p in inflammatory processes in cystic fibrosis airways. J Pathol. 2018;245(4):410–20.

254. Zhang R, Qin L, Shi J. MicroRNA-199a-3p suppresses high glucose-induced apoptosis and inflammation by regulating the IKKβ/NF-κB signaling pathway in renal tubular epithelial cells. Int J Mol Med. 2020;46(6):2161–71.

255. Gu X, Weng R, Hou J, Liu S. Endothelial miR-199a-3p regulating cell adhesion molecules by targeting mTOR signaling during inflammation. Eur J Pharmacol [Internet]. 2022;925(63):174984. Available from: https://doi.org/10.1016/j.ejphar.2022.174984

256. Zeng N, Huang YQ, Yan YM, Hu ZQ, Zhang Z, Feng JX, et al. Diverging targets mediate the pathological roleof miR-199a-5p and miR-199a-3p by promoting cardiac hypertrophy and fibrosis. Mol Ther - Nucleic Acids [Internet]. 2021;26(December):1035–50. Available from: https://doi.org/10.1016/j.omtn.2021.10.013

257. Lou Y, Huang Z. microRNA-15a-5p participates in sepsis by regulating the inflammatory response of macrophages and targeting TNIP2. Exp Ther Med. 2020;3060–8.

258. Wang Z, Na Z, Cui Y, Wei C, Wang S. LncRNA ZFAS1 regulates the hippocampal neurons injury in epilepsy through the miR-15a-5p/OXSR1/NF-κB pathway. Metab Brain Dis [Internet]. 2022;37(7):2277–90. Available from: https://doi.org/10.1007/s11011-022-01013-5

259. Ye EA, Liu L, Jiang Y, Jan J, Gaddipati S, Suvas S, et al. miR-15a/16 reduces retinal leukostasis through decreased pro-inflammatory signaling. J Neuroinflammation [Internet]. 2016;13(1):1–9. Available from: http://dx.doi.org/10.1186/s12974-016-0771-8

260. Zhang G, Zhang Q, Zhu J, Tang J, Nie M. LncRNA ARFRP1 knockdown inhibits LPS-induced the injury of chondrocytes by regulation of NF-κB pathway through modulating miR-15a-5p/TLR4 axis. Life Sci [Internet]. 2020;261(438):118429. Available from: https://doi.org/10.1016/j.lfs.2020.118429

261. Peng J, Jiang J, Wang H, Feng X, Dong X. miR-199a-3p suppresses cervical epithelial cell inflammation by inhibiting the HMGB1/TLR4/NF-KB pathway in preterm birth. Mol Med Rep. 2020;22(2):926–38.

262. Li Y, Ren Q, Wang X, Luoreng Z, Wei D. Bta-miR-199a-3p Inhibits LPS-Induced Inflammation in Bovine Mammary Epithelial Cells via the PI3K/AKT/NF-κB Signaling Pathway. Cells. 2022;11(21).

263. Kattoor AJ, Goel A, Mehta JL. LOX-1: Regulation, signaling and its role in atherosclerosis. Antioxidants. 2019;8(7):1–15.

264. Dai Y, Cao Y, Zhang Z, Vallurupalli S, Mehta JL. Xanthine Oxidase Induces Foam Cell Formation through LOX-1 and NLRP3 Activation. Cardiovasc Drugs Ther. 2017;31(1):19–27.

265. Chen Z, Wang M, He Q, Li Z, Zhao Y, Wang W, et al. Microrna-98 rescues proliferation and alleviates ox-LDL-induced apoptosis in HUVECs by targeting LOX-1. Exp Ther Med. 2017;13(5):1702–10.

266. Ding J, Li H, Liu W, Wang X, Feng Y, Guan H, et al. miR-186-5p Dysregulation in Serum Exosomes from Patients with AMI Aggravates Atherosclerosis via Targeting LOX-1. Int J Nanomedicine. 2022;17(December):6301–16.

267. Liu M, Tao G, Liu Q, Liu K, Yang X. MicroRNA let-7g alleviates atherosclerosis via the targeting of LOX-1 in vitro and in vivo. Int J Mol Med. 2017;40(1):57–64.

268. Wu S, Yang S, Qu H. Circ_chfr regulates ox-ldl-mediated cell proliferation, apoptosis, and endomt by mir-15a-5p/egfr axis in human brain microvessel endothelial cells. Open Life Sci. 2021;16(1):1053–63.

269. Zhang HY, Liang HX, Wu SH, Jiang HQ, Wang Q, Yu ZJ. Overexpressed Tumor Suppressor Exosomal miR-15a-5p in Cancer Cells Inhibits PD1 Expression in CD8+T Cells and Suppresses the Hepatocellular Carcinoma Progression. Front Oncol. 2021;11(March):1–9.

270. Pathania AS, Prathipati P, Olwenyi OA, Chava S, Smith O V., Gupta SC, et al. miR-15a and miR-15b modulate natural killer and CD8+T-cell activation and anti-tumor immune response by targeting PD-L1 in neuroblastoma. Mol Ther - Oncolytics [Internet]. 2022;25(June):308–29. Available from: https://doi.org/10.1016/j.omto.2022.03.010

271. Wei Y, Han B, Dai W, Guo S, Zhang C, Zhao L, et al. Exposure to ozone impacted Th1/Th2 imbalance of CD 4+ T cells and apoptosis of ASMCs underlying asthmatic progression by activating lncRNA PVT1-miR-15a-5p/miR-29c-3p signaling. Aging (Albany NY). 2020;12(24):25230–55.

272. Wang H, Geng G, Zhang D, Han F, Ye S. Analysis of microRNA-199a-3p expression in CD4+ T cells of systemic lupus erythematosus. Clin Rheumatol [Internet]. 2023;42(6):1683–94. Available from: https://doi.org/10.1007/s10067-023-06534-7

273. Haralambieva IH, Kennedy RB, Simon WL, Goergen KM, Grill DE, Ovsyannikova IG, et al. Differential miRNA expression in B cells is associated with inter-individual differences in humoral immune response to measles vaccination. PLoS One. 2018;13(1):1–12.

274. Deng L, Blanco FJ, Stevens H, Lu R, Caudrillier A, McBride M, et al. MicroRNA-143 Activation Regulates Smooth Muscle and Endothelial Cell Crosstalk in Pulmonary Arterial Hypertension. Circ Res [Internet]. 2015 Oct 23;117(10):870–83. Available from: https://www.ahajournals.org/doi/10.1161/CIRCRESAHA.115.306806

275. Li L, Wang H, Zhang J, Chen X, Zhang Z, Li Q. Effect of endothelial progenitor cell-derived extracellular vesicles on endothelial cell ferroptosis and atherosclerotic vascular endothelial injury. Cell Death Discov [Internet]. 2021;7(1):1–11. Available from: http://dx.doi.org/10.1038/s41420-021-00610-0

276. Du L, Li G, Yang Y, Yang G, Wan J, Ma Z, et al. Exosomes from adipose-derived stem cells promote proliferation and migration of endothelial tip cells by downregulation of semaphorin 3A. 2018;11(10):4879–88.

277. Bao Z, Zhang N, Niu W, Mu M, Zhang X, Hu S, et al. Exosomal miR-155-5p derived from glioma stem-like cells promotes mesenchymal transition via targeting ACOT12. Cell Death Dis. 2022;13(8).

278. Wang J, Tong KS, Wong LL, Liew OW, Raghuram D, Richards AM, et al. MicroRNA-143 modulates the expression of Natriuretic Peptide Receptor 3 in cardiac cells. Sci Rep. 2018;8(1):1–11.

279. Tiedt S, Prestel M, Malik R, Schieferdecker N, Duering M, Kautzky V, et al. RNA-seq identifies circulating MIR-125a-5p, MIR-125b-5p, and MIR-143-3p as potential biomarkers for acute ischemic stroke. Circ Res. 2017;121(8):970–80.

280. Düzgün Z, Kayikçioğlu M, Aktan Ç, Bara B, Eroğlu Z, Yağmur B, et al. Decreased circulating microRNA-21 and microRNA-143 are associated to pulmonary hypertension. Turkish J Med Sci. 2023;53(1):130–41.

281. Rozhkov AN, Shchekochikhin DY, Ashikhmin YI, Mitina YO, Evgrafova V V., Zhelankin A V., et al. The Profile of Circulating Blood microRNAs in Outpatients with Vulnerable and Stable Atherosclerotic Plaques: Associations with Cardiovascular Risks. Non-coding RNA. 2022;8(4).

282. Ormseth MJ, Solus JF, Vickers KC, Oeser AM, Raggi P, Stein CM. Utility of Select Plasma MicroRNA for Disease and Cardiovascular Risk Assessment in Patients with Rheumatoid Arthritis. J Rheumatol [Internet]. 2015 Oct;42(10):1746–51. Available from: http://www.jrheum.org/lookup/doi/10.3899/jrheum.150232

283. Vegter EL, Ovchinnikova ES, van Veldhuisen DJ, Jaarsma T, Berezikov E, van der Meer P, et al. Low circulating microRNA levels in heart failure patients are associated with atherosclerotic disease and cardiovascular-related rehospitalizations. Clin Res Cardiol. 2017;106(8):598–609.

"I tried to be perfect,
It just wasn't worth it,
Nothing could ever be so wrong,
It's hard to believe me,
It never gets easy,
I guess I knew that all along"

-Pieces, Sum 41

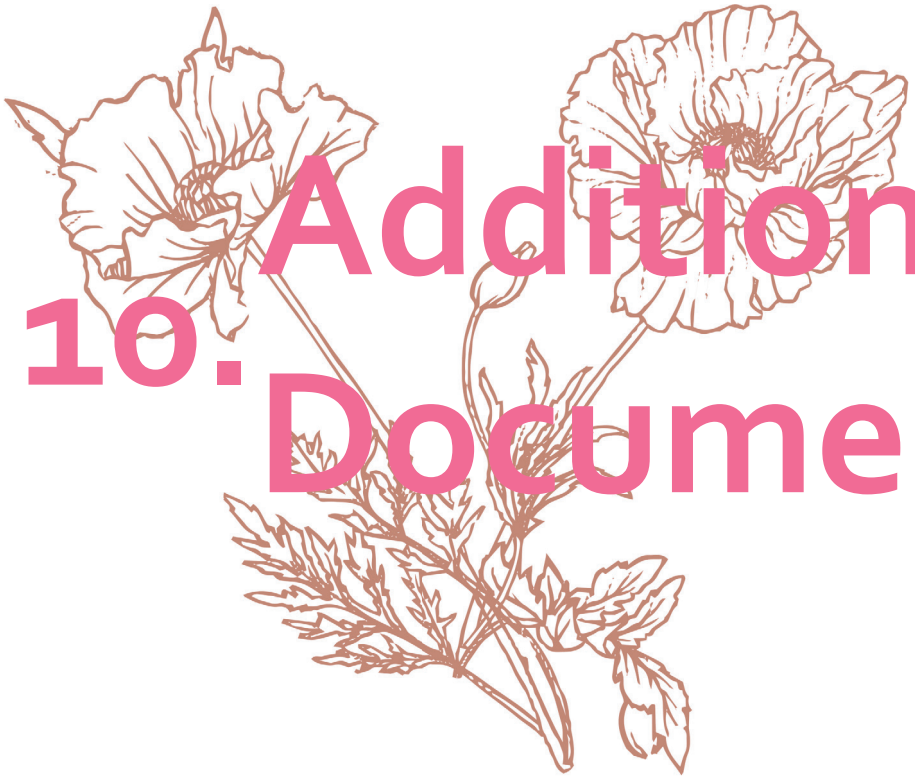

10. Additional Documents

10. ADDITIONAL DOCUMENTS

International Journal of *Molecular Sciences*

MDPI

Article

Implication of miR-155-5p and miR-143-3p in the Vascular Insulin Resistance and Instability of Human and Experimental Atherosclerotic Plaque

Paula González-López [1], Carla Ares-Carral [1], Andrea R. López-Pastor [1], Jorge Infante-Menéndez [1], Tamara González Illaness [1], Melina Vega de Ceniga [2,3], Leticia Esparza [2,3], Nuria Beneit [1], José Luis Martín-Ventura [4,5], Óscar Escribano [1,*,†] and Almudena Gómez-Hernández [1,*,†]

1 Hepatic and Vascular Diseases Laboratory, Biochemistry and Molecular Biology Department, School of Pharmacy, Complutense University of Madrid, 28040 Madrid, Spain
2 Department of Angiology and Vascular Surgery, Hospital de Galdakao-Usansolo, 48960 Galdakao, Spain
3 Biocruces Bizkaia Health Research Institute, 48903 Barakaldo, Spain
4 IIS-Fundation Jimenez-Diaz, Autonoma University of Madrid, 28040 Madrid, Spain
5 Centro de Investigación Biomédica en Red de Enfermedades Cardiovasculares (CIBERCV), 28029 Madrid, Spain
* Correspondence: oescriba@ucm.es (Ó.E.); algomezh@ucm.es (A.G.-H.); Tel.: +34-91-3941853 (Ó.E. & A.G.-H.)
† These authors contributed equally to this work.

check for updates

Citation: González-López, P.; Ares-Carral, C.; López-Pastor, A.R.; Infante-Menéndez, J.; González Illaness, T.; Vega de Ceniga, M.; Esparza, L.; Beneit, N.; Martín-Ventura, J.L.; Escribano, Ó.; et al. Implication of miR-155-5p and miR-143-3p in the Vascular Insulin Resistance and Instability of Human and Experimental Atherosclerotic Plaque. *Int. J. Mol. Sci.* **2022**, *23*, 10253. https://doi.org/10.3390/ijms231810253

Academic Editor: Wan Lee

Received: 7 June 2022
Accepted: 2 September 2022
Published: 6 September 2022

Publisher's Note: MDPI stays neutral with regard to jurisdictional claims in published maps and institutional affiliations.

Abstract: (1) Background: Cardiovascular diseases (CVDs) are the main cause of death in developed countries, being atherosclerosis, a recurring process underlying their apparition. MicroRNAs (miRNAs) modulate the expression of their targets and have emerged as key players in CVDs; (2) Methods: 18 miRNAs were selected (Pubmed and GEO database) for their possible role in promoting atherosclerosis and were analysed by RT-qPCR in the aorta from apolipoprotein E-deficient ($ApoE^{-/-}$) mice. Afterwards, the altered miRNAs in the aorta from 18 weeks-$ApoE^{-/-}$ mice were studied in human aortic and carotid samples; (3) Results: miR-155-5p was overexpressed and miR-143-3p was downregulated in mouse and human atherosclerotic lesions. In addition, a significant decrease in protein kinase B (AKT), target of miR-155-5p, and an increase in insulin-like growth factor type II receptor (IGF-IIR), target of miR-143-3p, were noted in aortic roots from $ApoE^{-/-}$ mice and in carotid plaques from patients with advanced carotid atherosclerosis (ACA). Finally, the overexpression of miR-155-5p reduced AKT levels and its phosphorylation in vascular smooth muscle cells, while miR-143-3p overexpression decreased IGF-IIR reducing apoptosis in vascular cells; (4) Conclusions: Our results suggest that miR-155-5p and miR-143-3p may be implicated in insulin resistance and plaque instability by the modulation of their targets AKT and IGF-IIR, contributing to the progression of atherosclerosis.

Keywords: atherosclerosis; miR-155-5p; miR-143-3p; unstable plaque; apoptosis; AKT; IGF-IIR

1. Introduction

Cardiovascular diseases are the main cause of premature death in developed countries and usually progress with an asymptomatic period [1]. Atherosclerosis is usually the underlying cause of cardiovascular diseases like coronary artery disease or myocardial infarction [2–4].

Insulin-resistant states are associated with metabolic abnormalities that include glucotoxicity, lipotoxicity and inflammation, and which also lead to endothelial dysfunction. Therefore, hyperglycaemia, hyperlipidemia and proinflammatory cytokines are known to selectively impair the phosphoinositide 3-kinase (PI3K)/AKT/ endothelial nitric oxide synthase (eNOS) pathway, increase oxidative stress and enhance the release of endothelin 1 (ET-1) from the endothelium [5]. Different manifestations associated with insulin resistance, including dyslipidemia, hyperglycaemia, inflammation and obesity,

may be intermediary mediators along with insulin resistance to generate endothelial dysfunction [6,7].

MicroRNAs (miRNA) are small non-coding RNAs conserved between species that regulate the expression of genes. Since their discovery, hundreds of these transcripts have been described unravelling the role they play in development or disease [8]. In this sense, both inhibition and overexpression of miRNAs that participate in the establishment and progression of CVDs have been described. For instance, miR-145 and miR-143 regulate vascular smooth muscle cell (VSMC) fate and plasticity [9], whereas miR-24-3p has been described as an important regulator in VSMCs proliferation and apoptosis [10]. Moreover, miR-27b, -130a and -210, which are involved in the maintenance of endothelial cell homeostasis, are increased in patients with peripheral arterial disease [11] and downregulated in T2DM patients after treatment with liraglutide [12].

The effect of miR-155-5p in several diseases is controversial. Some studies demonstrated that this miRNA protects against the progression of diseases such as cervical cancer by targeting phosphoinositide-dependent protein kinase 1 (PDK1) [13] or type-2-diabetes by targeting the transcription factor MafB (Mafb) [14]. During atherosclerosis progression, miR-155-5p overexpression promotes inflammation [15] and oxidized low-density lipoprotein uptake in macrophages [16].

The miR-143-3p is well studied in the progress and development of different types of cancer like adenocarcinoma [17] or ovarian cancer [18]. In recent years, miR-143-3p has emerged as a possible regulator of myocardial infarction [19,20]. In contrast, the role of this miRNA plays in atherosclerosis remains mostly unknown.

For these reasons, 18 miRNAs were selected by searching in PubMed and GEO database for their possible role in promoting atherosclerosis and analyzed by RT-qPCR in the aorta from *ApoE*$^{-/-}$ and wild-type mice. To carry out this objective, we have used a classic experimental model of atherosclerosis, *ApoE*$^{-/-}$ mice under a standard diet (STD) or a high-fat diet (HFD) for 8 and 18 weeks. Then, the altered miRNAs in the aorta from *ApoE*$^{-/-}$ mice fed with the corresponding diets for 18 weeks were studied in human aortic and carotid samples, using vascular samples from control subjects (CAs), subjects with fibrolipidic plaques (FAs) or patients with advanced carotid atherosclerosis (ACA). Finally, we focused on the role of miR-155-5p and miR-143-3p and their targets (AKT and IGF-IIR, respectively) in the progression of experimental and human atherosclerosis, as well as its implication in vascular insulin resistance. To unravel the molecular mechanism by which these miRNAs promote atherosclerosis, we performed in vitro overexpression experiments in human vein endothelial cells (HUVECs) and vascular smooth muscle cells (VSMCs).

2. Results

2.1. miR-143-3p and miR-155-5p Levels Are Altered in Aorta from ApoE$^{-/-}$ *Mice*

ApoE$^{-/-}$ mice under HFD were used as an animal model of atherosclerosis. Firstly, we confirmed that *ApoE*$^{-/-}$ mice had a significant increase in body weight and weight gain in addition to hypercholesterolemia and hypertriglyceridemia (Supplemental Table S1), being significantly higher in *ApoE*$^{-/-}$ fed with HFD for 18 weeks.

After that, we analysed vascular damage by Oil Red O (ORO) staining of aortic roots (Figure 1A). A significant increase in lipid depot, lesion area and % of stenosis was noted in aortic roots from *ApoE*$^{-/-}$ HFD 18 wks in comparison with the other groups (Figure 1B). Similarly, *en face* analysis of ORO-stained whole aorta showed a significant increase in lesion area in *ApoE*$^{-/-}$ under HFD for 18 weeks vs. Control STD and *ApoE*$^{-/-}$ STD of the same age (Supplementary Figure S1).

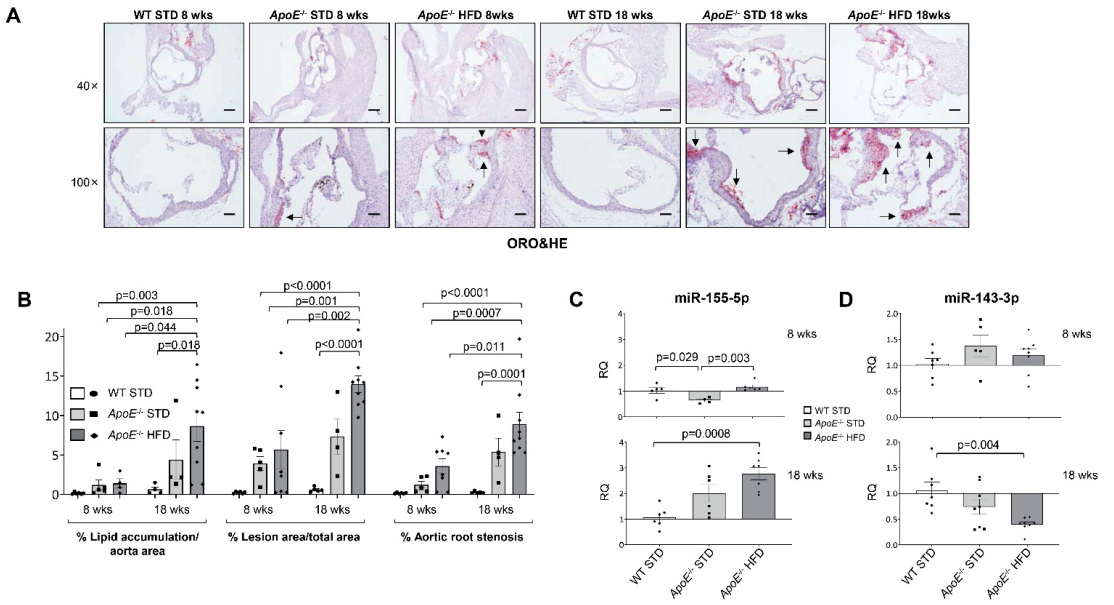

Figure 1. miR-155-5p and miR-143-3p expression in the aorta of the mouse model of atherosclerosis. (**A**) Representative images of the Oil Red O staining from the aortic roots of the six groups of experimental mouse model of atherosclerosis. Magnification 40× (scale bar = 200 μm); magnification 100× (scale bar = 100 μm). The black arrows point out the lipid depots in the aortic roots. (**B**) Quantification of the percentage of lipid accumulation, lesion area and stenosis of aortic root from the mouse model. WT STD 8 wks (n = 6); *ApoE*$^{-/-}$ STD 8 wks (n = 5); *ApoE*$^{-/-}$ HFD 8 wks (n = 4); WT STD 18 wks (n = 4); *ApoE*$^{-/-}$ STD 18 wks (n = 4); *ApoE*$^{-/-}$ HFD 18 wks (n = 9). Relative expression of miR-155-5p (**C**) and miR-143-3p (**D**) in the aorta of the three experimental groups at 8 (**upper** graphics) and 18 weeks (**lower** graphics) of diet was measured by qPCR. Amplification of miR-191-5p was used in the same reaction of all samples as an internal control. WT = Wild type group; STD = standard type diet; *ApoE*$^{-/-}$ = *ApoE* deficient mice; HFD = high-fat diet; wks = weeks. qPCR miR-155-5p: WT STD 8 wks (n = 5); *ApoE*$^{-/-}$ STD 8 wks (n = 4); *ApoE*$^{-/-}$ HFD 8 wks (n = 6); WT STD 18 wks (n = 6); *ApoE*$^{-/-}$ STD 18 wks (n = 6); *ApoE*$^{-/-}$ HFD 18 wks (n = 7). qPCR miR-143-3p: WT STD 8 wks (n = 7); *ApoE*$^{-/-}$ STD 8 wks (n = 5); *ApoE*$^{-/-}$ HFD 8 wks (n = 8); WT STD 18 wks (n = 7); *ApoE*$^{-/-}$ STD 18 wks (n = 8); *ApoE*$^{-/-}$ HFD 18 wks (n = 8).

PubMed and GEO Databases were used to perform a search of miRNAs that could play a role in atherosclerosis. After the search, a screening of the selected miRNAs was performed in the aorta of all groups of mice (Supplemental Figure S2 and Table S2). We observed that miR-155-5p was significantly overexpressed in *ApoE*$^{-/-}$ mice after 18 weeks of HFD compared with WT STD mice (Figure 1C); while miR-143-3p was significantly downregulated in *ApoE*$^{-/-}$ mice after 18 weeks of HFD vs. WT mice (Figure 1D).

Moreover, we have established correlations between miR-155-5p or miR-143-3p and atherosclerosis progression (% lipid accumulation/aorta area, % lesion area/total area or % aortic root stenosis) showed that miR-155-5p levels significantly and positively correlate with % stenosis and lesion area (Supplemental Figure S3A,B, respectively). On the other hand, we found a significant and inverse correlation between miR-143-3p levels and % lipid accumulation or lesion area (Supplemental Figure S3C,D, respectively).

2.2. miR-143-3p and miR-155-5p Levels Are Also Altered in Human Atherosclerotic Carotid Plaque

To confirm whether the levels of the studied miRNAs in the murine model of atherosclerosis might have a clinical relevance in human atherosclerosis, we analyzed the levels of different miRNAs in vascular samples from control subjects (CAs), subjects with fibrolipidic plaque (FAs) and patients with human advanced atherosclerosis undergoing carotid endarterectomy (ACA) (Supplemental Table S2). Firstly, we performed H&E stainings, and we could differentiate regions as media in samples from CAs and FAs and media, fibrous and shoulders in samples from ACA (Figure 2A). Histological analysis revealed that complicated plaques from ACA contained an intraplaque hemorrhage and/or a certain degree of calcification with a higher percentage of inflammatory cells. The adjacent non-complicated regions were composed of fibrous thickening with a variable content of VSMCs (Figure 2A).

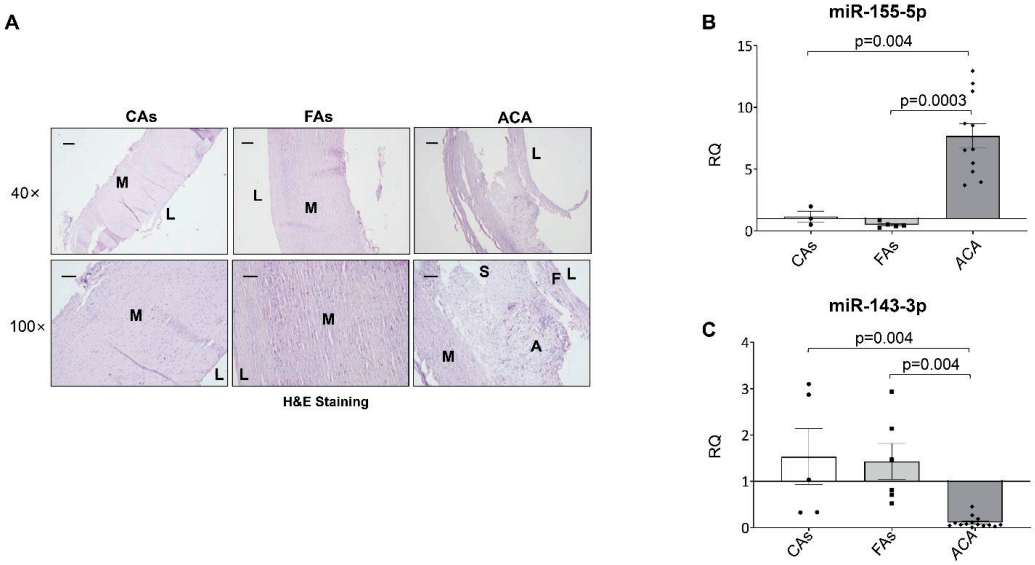

Figure 2. Characterization of the atherosclerotic plaques and miRNA expression of the human vascular samples. (**A**) Representative images of the Hematoxylin and Eosin staining from the aorta of control subjects (CAs) and subjects with fibrolipidic lesions (FAs) and the carotid artery from ACA patients (ACA). Magnification 40× (scale bar = 200 μm) and 100× (scale bar = 100 μm). Relative quantification of the levels of the miR-155-5p (**B**) and miR-143-3p (**C**) by qPCR. FAs= fibrolipidic plaque; ACA = advanced carotid atherosclerotic plaque; M = media; F = fibrous; S = shoulder; A = atheroma; L = lumen. qPCR miR-155-5p: Control subjects (n = 3); FAs (n = 5); ACA patients (n = 11). qPCR miR-143-3p: Control subjects (n = 5); fibrolipidic patients (n = 6); ACA patients (n = 14).

In serial sections of samples used for histological characterization, we isolated miRNAs and analyzed the levels of miR-155-5p (Figure 2B) and miR-143-3p (Figure 2C) by qPCR, showing that miR-155-5p expression was significantly upregulated (Figure 2B) and miR-143-3p downregulated (Figure 2C) in the ACA patients compared with the other two groups.

2.3. AKT Expression Is Modulated by miR-155-5p Levels in Atherosclerosis and Non-Alcoholic Fatty Liver Disease

To study the effect of miR-155-5p overexpression in vascular insulin resistance, HUVECs and VSMCs were transfected with a specific precursor for miR-155-5p. After 72 h of transfection, miR-155-5p was overexpressed in both vascular cell lines (Figure 3A). Following an extensive search in different databases, AKT, eNOS and p85α were the most relevant predicted miR-155-5p targets in atherosclerosis (Supplemental Figure S4A,B).

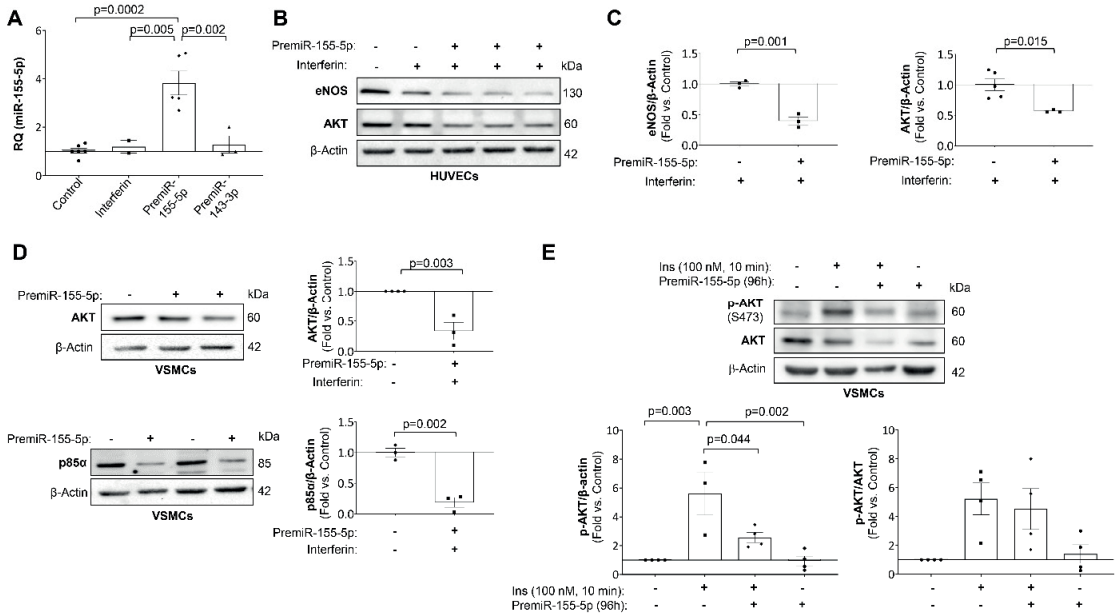

Figure 3. miR-155-5p reduced AKT expression and its activation in vascular cells. (**A**) Relative quantification of the expression levels of miR-155-5p in transfected HUVECs. (**B**) Representative Western blot images of AKT and eNOS expression and (**C**) their quantification in transfected HUVECs. (**D**) Representative Western blot images of the expression of p85α and AKT (**left**) and their quantification (**right**) in transfected HUVECs. (**E**) Representative Western blot images of AKT phosphorylation in response to insulin stimulation in transfected VSMCs (**upper**) and their quantification (**lower**). HUVECs = human umbilical vein endothelial cells; VSMCs = vascular smooth muscle cells; eNOS = endothelial nitric oxide synthase; AKT = protein kinase B; p85α= phosphoinositide-3-kinase regulatory subunit 1; Ins = insulin. All the in vitro experiments were performed in triplicate.

After 96 h of transfection with the miR-155-5p precursor, eNOS and AKT were significantly downregulated in HUVECs (Figure 3B,C). Similarly, the expression of AKT and p85α significantly decreased in transfected VSMCs (Figure 3D). Furthermore, AKT expression was also significantly downregulated in the aorta of the 18 weeks-fed *ApoE*$^{-/-}$ mice (Figure 4A) and in the carotid from patients with advanced carotid atherosclerosis (Figure 4B). Moreover, in the carotid of patients with atherosclerosis, miR-155-5p levels negatively correlated with the expression of its target, AKT (Figure 4C).

Next, we assessed whether the downregulation of AKT induced by miR-155-5p could impair its phosphorylation. In fact, VSMCs overexpressing miR-155-5p showed a significant reduction in AKT phosphorylation induced by 100 nM insulin for 10 min (Figure 3E). Regarding in vivo insulin signaling, insulin administration did not induce AKT phosphorylation in the aorta from *ApoE*$^{-/-}$ HFD 18 wks, which had high levels of miR-155-5p. Conversely, it induced a significant increase in AKT phosphorylation in WT STD and *ApoE*$^{-/-}$ STD mice (Figure 4D).

Moreover, when patients were classified by their body mass index (BMI) following the criteria established by the World Health Organization (lean, overweight and obese), we observed a significant increase in miR-155-5p expression (Figure 5A), as well as a progressive decrease in AKT (Figure 5B), as the BMI increased. This was supported by a significant and positive correlation between the BMI and both miR-155-5p (Figure 5C, left) and a significant and inverse correlation between the BMI and AKT levels (Figure 5C, right). In addition,

we also separated the patients into diabetic and non-diabetic, which revealed a high and significant increase in miR-155-5p in diabetic patients with ACA (Supplemental Figure S5).

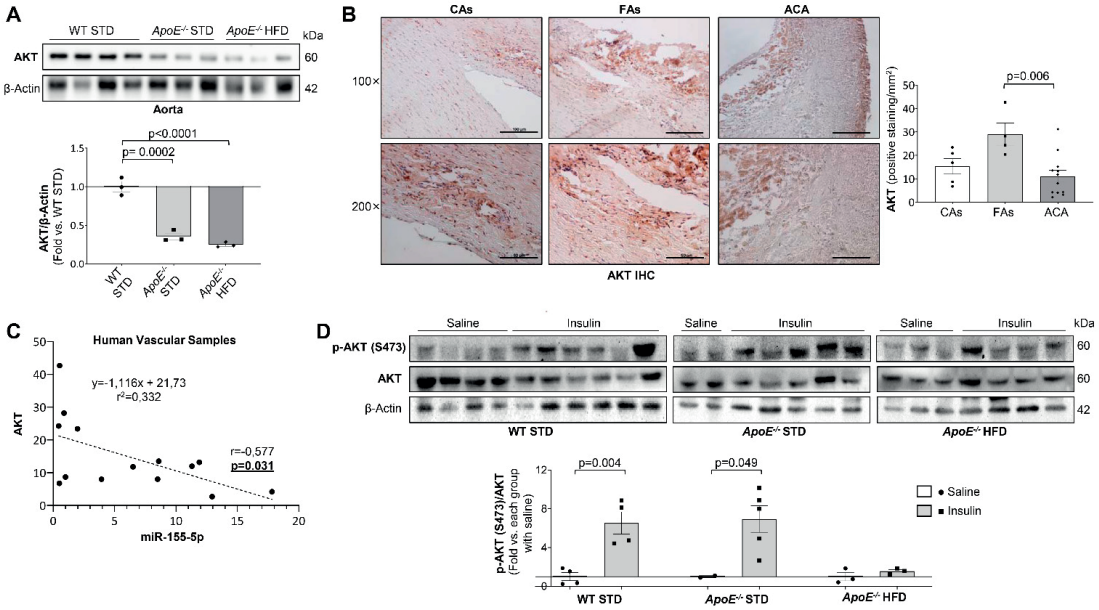

Figure 4. AKT levels are downregulated in the human samples and the mouse model where its activity is also impaired. (**A**) Representative Western blot images of the expression of AKT (**upper**) and their quantification (**lower**) in murine aorta samples. (**B**) Representative images of AKT levels measured by immunohistochemistry in the aorta and carotid human samples (**left**) and their quantification (**right**) expressed as % positive staining/mm^2. Magnification 100× (scale bar = 100 µm); magnification 200× (scale bar = 50 µm). (**C**) Scatter plot and Spearman's r correlation between the expression of miR-155-5p and AKT expression in human samples. (**D**) Representative Western Blot images of AKT phosphorylation (**upper**) and their quantification (**lower**) in aortas from mice subjected to in vivo insulin signaling studies. WT = Wild type group; STD = standard type diet; *ApoE*$^{-/-}$ = *ApoE* deficient mice; HFD = high fat diet; AKT = protein kinase B; FAs = fibrolipidic plaque; ACA = advanced carotid atherosclerotic plaque. Mouse model AKT Western blot: WT STD 18 wks (n = 3); *ApoE*$^{-/-}$ STD 18 wks (n = 3); *ApoE*$^{-/-}$ HFD 18 wks (n = 3); AKT immunohistochemistry: Control subjects (n = 5); FAs (n = 4); ACA (n = 12). miR-155-5p-AKT correlation (n = 14). In vivo signalling experiments: WT STD 18 wks saline (n = 4); WT STD 18 wks insulin (n = 4); *ApoE*$^{-/-}$ STD 18 wks saline (n = 2); *ApoE*$^{-/-}$ STD 18 wks insulin (n = 5); *ApoE*$^{-/-}$ HFD 18 wks saline (n = 3); *ApoE*$^{-/-}$ HFD 18 wks insulin (n = 3).

Since the *ApoE*$^{-/-}$ mice also showed hepatic steatosis after 18 weeks of diet (Figure 6A), the expression of miR-155-5p was analysed in the liver by qPCR. Hepatic expression of miR-155-5p was significantly higher in both *ApoE*$^{-/-}$ mice groups (Figure 6B), which correlated with a downregulation in liver AKT expression in *ApoE*$^{-/-}$ HFD mice (Figure 6C). Moreover, a significant and positive correlation was observed between miR-155-5p hepatic levels and hepatic steatosis (Figure 6D).

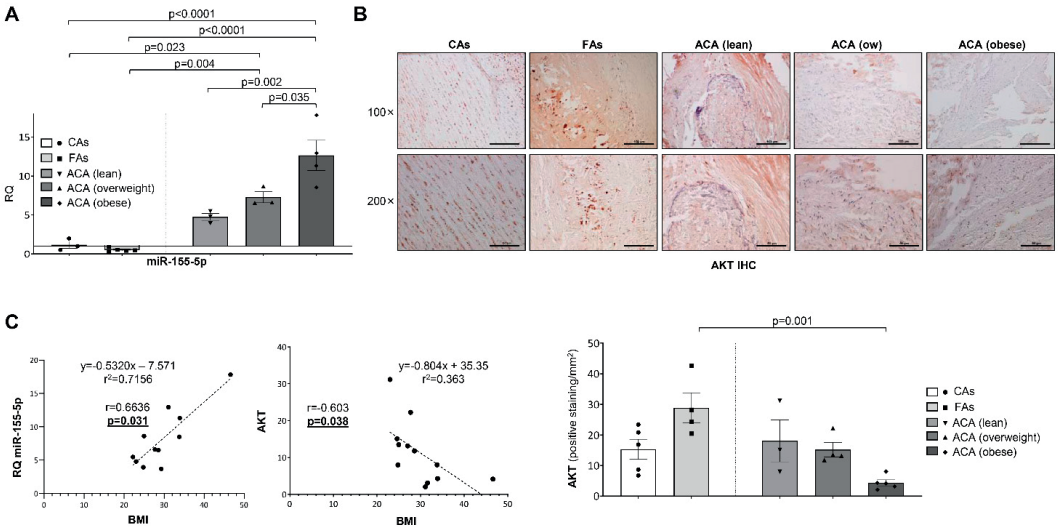

Figure 5. miR-155-5p and AKT expression correlated with the body mass index in human samples. (**A**) Expression levels of miR-155-5p in human carotid samples of patients stratified according to the Body Mass Index criteria of the World Health Organization. (**B**) Representative images of AKT immunohistochemistry (**upper**) and their quantification (**lower**) in human samples of patients stratified according to the Body Mass Index criteria of the World Health Organization. Magnification 100× (scale bar = 100 µm); magnification 200× (scale bar = 50 µm). (**C**) Scatter plots and Spearman's r correlations between the Body Mass Index and miR-155-5p expression (**left**) or AKT expression (**right**). AKT = protein kinase B; FAs = fibrolipidic plaque; ACA = advanced carotid atherosclerotic plaque; ow = overweight; IHC = immunohistochemistry; BMI = body mass index. miR-155-5p qPCR: CAs (n = 3); FAs (n = 5); ACA (lean) (n = 3); ACA (overweight) (n = 3); ACA (obese) (n = 4). AKT immunohistochemistry: CAs (n = 5); FAs (n = 4); ACA (lean) (n = 3); ACA (overweight) (n = 4); ACA (obese) (n = 5). Correlation between miR-155-5p and BMI (n = 11) and between AKT and BMI (n = 12).

2.4. IGF-IIR Expression Is Modulated by miR-143-3p

To study the role of miR-143-3p in the mechanisms involved in atherosclerosis progression, HUVECs and VSMCs were transfected with a specific miRNA precursor to increase miR-143-3p expression. After 72h of transfection, miR-143-3p expression was significantly increased in both HUVECs and VSMCs (Figure 7A). Among its targets, IGF-IIR was selected due to its role in the progression of atherosclerosis (Supplemental Figure S4C,D).

After 96 h of transfection with the miRNA mimic, IGF-IIR expression was significantly downregulated in HUVECs and VSMCs (Figure 7B). In the same way, HFD-fed *ApoE*$^{-/-}$ mice showed lower miR-143-3p expression and a consequent increase in IGF-IIR expression (Figures 1C and 7C, respectively). Moreover, miR-143-3p was downregulated, and in the shoulder regions IGF-IIR was significantly overexpressed in carotid plaque from ACA patients (Figures 2C and 7D).

Since IGF-IIR has been implicated in the instability of advanced atherosclerotic plaques, we performed new experiments to elucidate the relationship between miR-143-3p, IGF-IIR and apoptosis. For that, we induced the activation of caspase 3 by FBS starvation for 6 h in HUVECs or 100 nM thapsigargin treatment for 2 h in VSMCs (Figure 7E). More importantly, when HUVECs and VSMCs were pre-treated with pre-miR-143-3p for 96h the levels of active caspase 3 was significantly reduced in basal conditions or in HUVECs with FBS starvation for 6h (HUVECs) or in VSMCs stimulated with thapsigargin (Figure 7E).

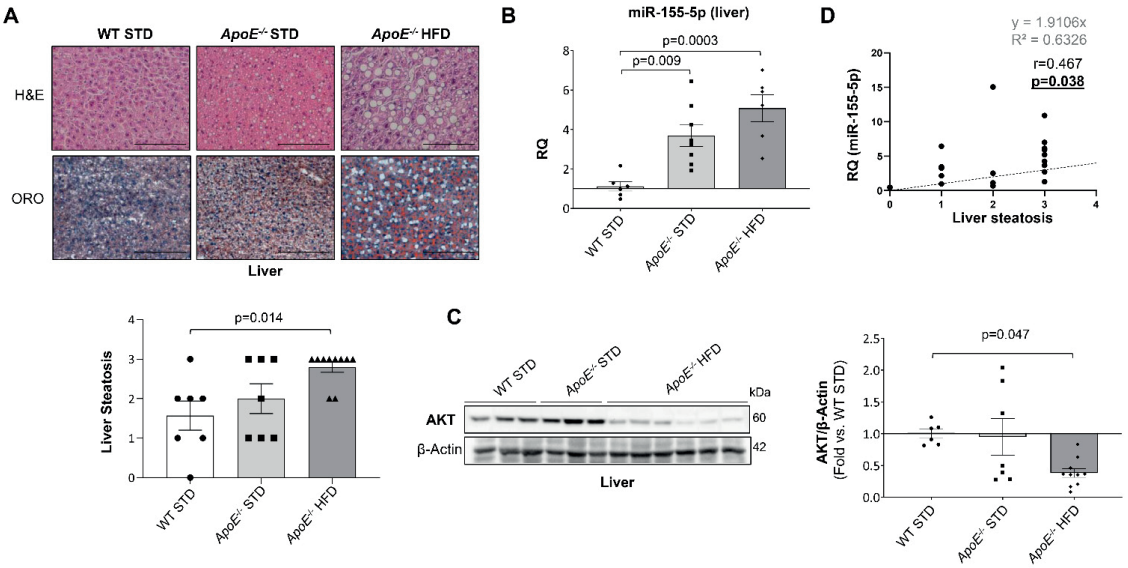

Figure 6. miR-155-5p is overexpressed and AKT downregulated in the liver of the mouse model after 18 weeks of high-fat diet. miR-155-5p is overexpressed and AKT downregulated in the liver of the mouse model after 18 weeks of high-fat diet. (**A**) Representative images of H&E staining to perform liver histological analysis (**upper**) and of Oil Red O staining (**lower**) to evaluate hepatic-specific lipid content. Magnification 200× (scale bar = 25 μm). Below, its corresponding graph that show the quantification of liver steatosis. (**B**) Relative expression of miR-155-5p in murine liver samples measured by qPCR. (**C**) Representative Western blot images of AKT expression (**left**) and their quantification (**right**) in liver samples from the mouse groups. (**D**) Scatter plots and Spearman's r correlations between liver steatosis and hepatic miR-155-5p expression. WT= Wild type group; STD = standard type diet; *ApoE*$^{-/-}$ = *ApoE* deficient mice; HFD = high-fat diet; AKT = protein kinase B. Image and its quantification steatosis liver: WT STD 18 wks (n = 7), *ApoE*$^{-/-}$ STD 18 wks (n = 7) and *ApoE*$^{-/-}$ HFD (n = 10) mice after 18 weeks on the diet. miR-155-5p qPCR liver: WT STD 18 wks (n = 6); *ApoE*$^{-/-}$ STD 18 wks (n = 8); *ApoE*$^{-/-}$ HFD 18 wks (n = 6). Western blot of AKT liver: WT STD 18 wks (n = 6); *ApoE*$^{-/-}$ STD 18 wks (n = 7); *ApoE*$^{-/-}$ HFD 18 wks (n = 10).

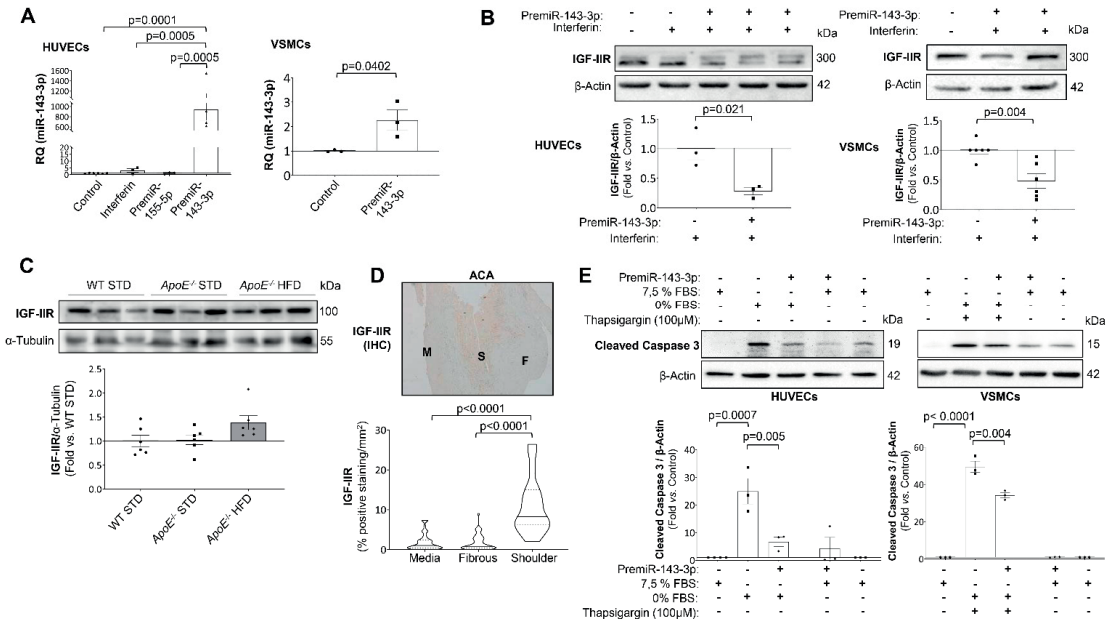

Figure 7. miR-143-3p protects against apoptosis in endothelial and vascular smooth muscle cells by targeting IGF-IIR. (**A**) Relative quantification of the expression levels of miR-143-3p in transfected HUVECs (**left**) and VSMCs (**right**). (**B**) Representative Western blot images of IGF-IIR expression (**upper**) and their quantification (**lower**) in transfected HUVECs (**left** panels) and VSMCs (**right** panels). (**C**) Representative Western blot images of IGF-IIR expression (**upper**) and their quantification (**lower**) in murine aorta samples. (**D**) Representative immunohistochemical analysis of IGF-IIR expression in advanced carotid atherosclerosis patients (**upper**) and its quantification (**lower**) expressed in %positive staining/mm^2 in the different areas of the atherosclerotic plaque. Magnification 40× (scale bar = 200 μm). (**E**) Representative Western blot images of active caspase 3 (**upper**) and their quantification (**lower**) in transfected HUVECs following serum deprivation (**left**) and transfected VSMCs following thapsigargin exposure (**right**). HUVECs = human umbilical vein endothelial cells; VSMCs = vascular smooth muscle cells; IGF-IIR= insulin-like growth factor type 2 receptor; WT = Wild type group; STD = standard type diet; *ApoE*$^{-/-}$ = *ApoE* deficient mice; HFD = high fat diet; IHC = immunohistochemistry; M = media; F = fibrous; S = shoulder; FBS = foetal bovine serum. All the in vitro experiments have been performed at least 3 times (n = 3). Western blot of IGF-IIR: WT STD 18 wks (n = 6); *ApoE*$^{-/-}$ STD 18 wks (n = 6); *ApoE*$^{-/-}$ HFD 18 wks (n = 6). Immunohistochemistry of IGF-IIR: Media (n = 44); Fibrous (n = 49); Shoulder (n = 19).

3. Discussion

Atherosclerosis has been a silent and asymptomatic disease for decades in which various factors can contribute to the progression and rupture of vulnerable plaques and, consequently, trigger the acute event such as acute myocardial infarction or stroke [21]. In this regard, not only could the study of miRNAs panels help in the future to identify the presence of vulnerable plaques, but also to avoid the progression process. In this study, we have analyzed 18 miRNAs and have finally identified two miRNAs, miR-155-5p and miR-143-3p, with altered levels in both an experimental atherosclerosis model in mice and in patients with advanced carotid atherosclerosis. In this paper, we present a novel role of miR-155-5p and miR-143-3p in the insulin resistance and apoptosis of vascular resident cells, respectively, being both key processes in the progression and instability of atherosclerotic plaque.

Clearly miR-155 is one of the most dynamically regulated and multifunctional miRNAs, which has been associated with the regulation of immune-related processes, with an impact on cancer [8,13] and atherosclerosis [21]. Diverse studies about the role of miR-155-5p in atherosclerosis have obtained contradictory results and the most plausible explanation might be that the function of miR-155-5p depends on the phase of atherosclerosis. Thus, miR-155-5p could suppress atherosclerosis in the early phases, while promoting its progression in advanced stages [22,23]. For instance, in a model of early atherosclerosis, low-density lipoprotein receptor deficient mice transplanted with miR-155-deficient bone marrow had increased atherosclerotic plaques, elevated levels of pro-inflammatory monocytes, and decreased interleukin (IL)-10 production [24]. However, several studies using *ApoE*$^{-/-}$ mice as a model for an advanced phase of atherosclerosis demonstrated that a treatment using antagomiR-155 attenuated atherosclerosis development and progression in *ApoE*$^{-/-}$ mice [25]. Similarly, lower plaque sizes were observed in *ApoE*$^{-/-}$ mice with a leukocyte specific miR-155 deficiency [26] or in *ApoE*$^{-/-}$ miR-155$^{-/-}$ double knockout mice [27]. In accordance with these findings, we observed that miR-155-5p expression significantly increased in aortic roots from *ApoE*$^{-/-}$ fed with HFD, a model of advanced atherosclerosis, as well as in carotid biopsies from patients with advanced atherosclerosis. In contrast, subjects with fibrolipidic plaques, an early phase of atherosclerosis, showed lower miR-155-5p levels than healthy subjects. In this regard, previous studies have described that miR-155-5p might be a possible biomarker of plaque instability in the plasma of coronary artery disease (CAD) patients [28] and overexpressed in macrophages during atherosclerosis progression [29], consistent with our findings reporting a noteworthy miR-155-5p overexpression in diabetic patients with advanced carotid atherosclerosis. The miR-155 has also been described to promote inflammatory activation of macrophages by repressing B-cell leukemia/lymphoma (BCL-6), a negative regulator of nuclear factor-kappa B (NF-κB) signaling, thus promoting atherosclerosis [26].

Since the role of miR-155-5p in vascular insulin resistance has not been elucidated yet and AKT is a confirmed target of this miRNA [30] that promotes proliferation and survival of VSMCs and ECs during atherosclerosis [30–32], we explored whether miR-155-5p could contribute to the development of insulin resistance. We demonstrated that AKT was decreased in the aorta from HFD-fed *ApoE*$^{-/-}$ mice and in carotid samples from ACA patients, which correlate with an overexpression of miR-155-5p. However, patients with early atherosclerosis presented a significant increase in AKT protein levels. We also established a significant inverse correlation between miR-155-5p and AKT in human carotid artery. Moreover, in VSMCs and HUVECs a significant decrease in AKT protein levels was noted after miR-155-5p overexpression, and in consequence a strong decrease in AKT phosphorylation and function. Moreover, miR-155-5p also regulates p85α as we observed in VSMCs, which could contribute to the significant decrease in AKT phosphorylation.

We have also found a significant and robust correlation between BMI and both miR-155-5p and AKT expression. Recently, several miRNAs have emerged as key agents involved in pathways related to obesity such as adipokine expression, glucose and lipid metabolism, insulin signaling, oxidative stress, and inflammation [33,34]. Both the adipose tissue and circulating miRNAs are deregulated in human obesity [35]. Previous studies have described that the expression of miR-155-5p, miR-34a and let-7c might be altered in response to tumor necrosis factor-α (TNF-α) in human adipocytes, and that miR-155-5p is closely associated with NF-κB signalling [36,37]. It has been reported that NF-κB-p65 interacts with the promoter site of miR-155, and thus NF-κB activation promotes miR-155 transcription [38]. In this regard, the overexpression of miR-155-5p observed in advanced atherosclerosis could be induced by NF-κB activation itself since some groups have described a significant NF-κB activation in carotid advanced atherosclerosis [39,40] as well as in aortic root from *ApoE*$^{-/-}$ mice under HFD [41], both similar to the samples used by us.

In this regard, modulation of this inflammation-related miR-155-5p in both adipocytes and their exosomes would improve adipocyte dysfunction and would have an impact on distant organs, such as liver or vascular tissues [42]. Indeed, the deletion of miR-155 in

mice prevented diet-induced obesity, improved insulin sensitivity, and abrogated adipocyte hypertrophy and adipose tissue inflammation [43]. Moreover, the reduction in miR-155 increases the expression of genes involved in brown adipogenesis, lipolysis, and energy release, which could synergize to improve fat metabolism [44–47]. Our results suggest that miR-155-5p might promote the simultaneous development of several pathophysiological processes in different organs, such as vascular and hepatic insulin resistance. Other reports have already described that hepatic miR-155-5p is upregulated in HFD-induced non-alcoholic fatty liver disease (NAFLD) in rats [47] and in non-alcoholic steatohepatitis (NASH) mouse models [48]. Furthermore, miR-155 plays a key role in hepatic lipid metabolism and its deficiency reduces steatosis and fibrosis [49]. Therefore, miR-155-5p coordinately affects various pathways that may elicit adiposity and obesity as well as vascular and hepatic alterations.

The other miRNA candidate that we have studied has been miR-143-3p, which modulates the expression of several genes relevant to cardiovascular biology and function. This miRNA plays a protective role in myocardial infarction by targeting ciclooxygenase-2 [20] or apoptosis-related genes [50]. So, the action of miR-143-3p might be inducing cell migration and inhibiting apoptosis. In this regard, miR-143-3p plays a key role in VSMCs differentiation through the downregulation of its target, Ets-like gene 1, a transcriptional coactivator that is crucial in the regulation of the VSMC phenotype [9]. In our experimental model of advanced atherosclerosis and in patients with ACA, we observed a significant decrease in miR-143-3p whereas in *ApoE*$^{-/-}$ mice after only 8 weeks of HFD and in subjects with fibrolipidic plaques, both with early atherosclerosis, miR-143-3p levels did not significantly differ from their respective controls.

On the other hand, we have also attributed a role to miR-143-3p in the progression of atherosclerosis through the regulation of IGF-IIR. Xihua L et al. confirmed IGF-IIR as a target for miR-143-3p, giving a protective role against atherosclerosis to this miRNA in patients with metabolic syndrome [51]. IGF-IIR is a fetal promoter of cell growth, survival and differentiation [52]. During atherosclerosis, IGF-IIR overexpression may have a protective role in macrophages and a detrimental role in VSMCs or unstable atherosclerotic plaques [53,54]. Moreover, IGF-IIR activates caspase 3 in cardiomyocytes, promoting apoptosis [55]. In our work, we associated a decrease in miR-143-3p with an increase in IGF-IIR expression both in human advanced atherosclerotic plaques and in aortic roots from *ApoE*$^{-/-}$ mice fed with HFD. Therefore, miR-143-3p downregulation might have a pro-apoptotic effect in HUVECs and VSMCs. However, further studies are needed to determine the mechanism by which IGF-IIR activates caspase 3 in atherosclerosis.

In summary, this study demonstrates a novel role for miR-155-5p and miR-143-3p in atherosclerosis progression. Our results suggest that miR-155-5p overexpression may be involved in vascular insulin resistance by targeting AKT, whereas miR-143-3p downregulation could be a pro-apoptotic mechanism by increasing IGF-IIR during plaque progression (Graphical Abstract).

4. Materials and Methods

4.1. Human Samples

We used two cohorts of patients. In the first of them, human aortas were consecutively collected from deceased organ donors from 2010 to 2013 under the authorization of the French Biomedicine Agency (PFS 09-007). After macroscopic examination, the aortas were classified according to Stary classification [56] into two groups: control aortas (CAs, $n = 7$), and aortas with fibrolipidic initial plaques [fibroatheromas (FAs), $n = 7$]. A small portion of tissue from each sample was fixed in 3.7% paraformaldehyde for classical histology and immunochemistry assessments. For the CA samples, it was practically and virtually impossible to separate and independently process the tunica intima. For these samples, the adventitia was carefully removed, and only the results obtained from the tunica media are presented. There were no significant differences in terms of age and gender. The investigation conforms to the principles outlined in the Declaration of Helsinki.

The second cohort corresponds to patients with advanced carotid atherosclerosis. Forty atherosclerotic plaques from patients with carotid stenosis > 70% undergoing carotid endarterectomy at IIS-Fundación Jiménez Díaz (Supplemental Table S3). The plaques showed an increase in inflammatory cells (Stary stages V–VI), whereas adjacent areas were mainly composed of VSMCs and lipid deposits (Stary stage III). The study was approved by the Hospital's Ethics Committee (IIS-Fundación Jiménez Díaz) with the reference number PI1442016 according to the institutional and the Good Clinical Practice guidelines, which was performed in accordance with the Declaration of Helsinki. All participants gave written informed consent.

4.2. Animal Model

Male C57Bl/6 Wild type (WT) and *ApoE* knockout ($ApoE^{-/-}$) mice were maintained under standard light (12 h long light/dark cycles), temperature (23.3 °C), and humidity (65.1%) conditions, and ad libitum diet from their weaning, up to their sacrifice. The WT mice (n = 7) were fed a standard type diet ([STD] 3% of the kcal are provided by fat, Envigo, USA) for 8 or 18 weeks, while the $ApoE^{-/-}$ mice were separated in two groups: one was fed the STD (n = 7), and the other a HFD (n = 10) (60% of the kcal are provided by fat, Envigo, Indianapolis, IN, USA) for 8 or 18 weeks before sacrifice. After 8 or 18 weeks fed with the corresponding diet, animals were sacrificed following fasting for 16 h. All animal experimentation was conducted in accordance with the accepted standards of animal use approved by the Complutense University of Madrid Ethics Committee, Autonomic Community of Madrid (PROEX188/88) and the guidelines from Directive 2010/63/EU of the European Parliament on the protection of animals used for scientific purposes. The microbiological and health state of the mice was controlled by the FELASA (Federation of European Laboratory Animal Science Associations) criteria and showed no pathogenic infection.

For euthanasia, the mice were anesthetized with Ketamine (50 ng/mL, Ketalar® [Pfizer, New York, NY, USA]) and Xylazine (200 mg/mL Rompun® [Bayer, Barmen, Germany]) intraperitoneal injection on a 50:5 dose per Kg. The aorta and the liver were harvested and stored at −80 °C, while the aortic root was washed with saline and then included in Tissue-Tek® O.C.T. Compound ([O.C.T.], VWR BDH Chemicals®, Radnor, PA, USA) and stored at −80 °C for further analysis. Both tissues were extracted under sterile conditions. Blood was extracted from the jugular vein and mixed with 0.4% p/v Citrate (Merck, Darmstadt, Germany), then the plasma was recovered after a 1200× g centrifuge for 15 min at 4 °C for subsequent analysis. Before the injection, the animals were weighted, and plasma glucose was measured using an Accu-Chek® glucometer (Aviva Roche, Basilea, Switzerland). Finally, cholesterol and triglycerides were tested in plasma samples from fasted mice (Spinreact, Girona, Spain).

In order to study the vascular insulin signaling in physiological conditions, in vivo insulin signaling assays were performed. Fasted mice were intraperitoneally (i.p.) injected with 1 U/kg BW of insulin glulisine (Apidra SoloStar, Sanofi, Paris, France) or an equivalent volume of 0,9% p/v saline solution (n = 5 per group). After 10 min, mice were sacrificed, and harvested tissues were immediately frozen in liquid nitrogen. Insulin signaling was assessed by Western blot against phospho-AKT (Ser473) in homogenates of aorta artery.

4.3. Cell Culture

HUVECs were purchased from PromoCell. They were grown in MCDB-131 culture medium (Life Technologies, Carlsbad, CA, USA) enriched with L-glutamine 2mM (Gibco™, Fisher Scientific, Hampton, NH, USA), foetal bovine serum 7.5% v/v (Gibco™, Fisher Scientific, Hampton, NH, USA), Penicillin/Streptomycin 100 U/mL (Gibco™, Fisher Scientific, Hampton, NH, USA) and endothelial growth factor 1X (R&D systems®, Minneapolis, MN, USA). Cells were received at passage 2 and were grown until passage 8. All cells were grown at 37 °C in a humified 5% CO_2 incubator (Fisher Scientific, Hampton, NH, USA).

Generation of immortalized WT VSMCs lines was previously described [57]. Cell lines were cultured to subconfluence (70–80%) with 10% foetal bovine serum (FBS)-DMEM for in vitro experiments.

4.4. Histological Tissue Samples

Paraffin-embedded human carotids and livers from an experimental model were cut into 5 µm sections and stained with hematoxylin and eosin purchased from PanReac Appli Chem ITW Reagents. AKT and IGF-IIR were detected by immunoperoxidase with rabbit anti-AKT (#9272, Cell Signalling Technology Inc.®, Danvers, MA, USA) and anti-IGF-IIR (sc-25462, Santa Cruz Biotechnology, Dallas, TX, USA) polyclonal antibodies. After an overnight incubation with each primary antibody, sections were incubated with a peroxidase-conjugated secondary antibody for 1 h at 1:100 dilution. The sections were stained for 10 min at room temperature with 3,3-diaminobenzidine and then counterstained with hematoxylin and mounted in DPX mounting medium (255,254.1610, PanReac AppliChem ITW Reagent, Sigma-Aldrich, Saint Louis, MO, USA). In each experiment, negative controls without the primary antibody were included to check for nonspecific staining.

The immunohistochemistry images were quantified using the "count and measure objects" tool in the Image-Pro Plus software IPWin (v4.5, Media Cybernetics, Rockville, USA). The color considered as positive staining for the same protein was manually selected, and the value corresponding to the sum of all stained areas was obtained. The results were expressed as the percentage of the stained area with respect to the total area analyzed in each sample.

Hepatic H&E staining was performed in paraffin-embedded sections (4 µm thick) that were evaluated by a single-blinded highly qualified hepatopathologist from Santa Cristina Hospital (Madrid, Spain). The score range was set between 0 and 3. Steatosis score was assessed, grading percentage involvement by steatotic hepatocytes as follows: grade 0, 0–5%; grade 1, >5–33%; grade 2, >33–66%; grade 3, >66%.

Aortic root and a section of liver samples was included in Tissue-Tek® optimum cutting temperature (OCT) compound (Sakura Finetek, Alphen aan den Rijn, The Netherlands), and later in liquid nitrogen for freezing. The O.C.T. embedded aortic root or liver samples from the experimental model were cut into 5 µm sections using a cryostat (CM1510 S; Leica, Wetzlar, Germany). Cut sections were stained with Oil Red O and hematoxylin to assess lipid depot. Individual lesion area in aortic roots was determined by averaging the maximal values. A stock Oil Red O (Sigma-Aldrich, USA) solution was made with 3 mg/mL Oil Red O in 99% isopropanol. The stock was diluted in a 3:2 ratio in ultrapure water. Frozen cryosections were air dried, fixed in 10% formalin, stained with Oil Red O and counterstained with Mayer's hematoxylin (Electron Microscopy Sciences, Hatfield, PA, USA). The sections were mounted with aqueous mounting medium for imaging (Vector Labs, Newark, CA, USA). Images of sections were acquired using an inverted Eclipse TE300 microscope coupled to a Digital Sight DS-U2 camera (Nikon, Tokyo, Japan). Quantifications for images of Oil Red O staining in aortic roots were performed using IP Win32 v4.5 software (Acromag, Wixom, MI, USA). Finally, % stenosis and % lesion area/total area was analyzed using Image J (v1.52a, Wayne Rasband, National Institute of Health, Stapleton, NY, USA).

4.5. En Face Imaging of Aorta

Atherosclerotic lesions were quantified by *en face* analysis of the whole aorta. For *en face* preparations, the aorta was opened longitudinally, while still attached to the heart and major branching arteries in the body. The aorta from the heart to the iliac bifurcation was then removed and was pinned out on a white wax surface in a dissecting pan using stainless steel pins 0.2 mm in diameter. After overnight fixation with 4% paraformaldehyde and PBS rinsing, the aortas were stained for 6 min in a filtered solution containing 0.5% Oil Red-O, 35% ethanol and 50% acetone, and then destained in 80% ethanol. The Oil

Red-O-stained aortas were photographed, and the atherosclerotic lesions were quantified using IP Win32 v4.5 software.

4.6. miRNA Extraction from the Aorta, Liver, Vascular Cell Lines and Paraffin-Embedded Carotid Tissue

The miRNA content from the aorta, the liver and the cells were extracted following the mirVana^{TM} miRNA Isolation Kit (Invitrogen^{TM}, Thermo Fisher Scientific, Waltham, MA, USA). The miRNA content from paraffin-embedded carotids was extracted using the RNeasy FFPE kit (Qiagen, Hilden, Germany). All the extractions were made following the protocol handled by the manufacturers. In all cases, miRNAs and long RNAs were obtained in separate fractions. The miRNA sample concentration was then determined using a NanoDrop^{TM} 2000 and the NanoDrop 2000/2000c Operating Software (Thermo Scientific, Waltham, MA, USA).

4.7. Cell Transfection with miRNA Precursors

Precursors of miR-155-5p and miR-143-3p were purchased from Sigma-Aldrich. Approximately 5×10^4 cells were seeded in P60 culture plates (353002, Falcon^{TM}, Thermo Fisher Scientific, Waltham, MA, USA) and transfected with 10–20 nM of MISSION® miRNA mimic hsa-miR143-3p or hsa-miR-155-5p (HMI0221 or HMN0254, Sigma-Aldrich, Saint Louis, MO, USA). As specified in the manufacturer's protocol (#409-10, Polyplus transfection®, Strasbourg, France), miRNA expression in transfected cells was assessed 72 h after transfection, whereas protein downregulation was analysed 96 h following transfection. To evaluate insulin signaling in cells transfected with pre-miR-155-5p, they were deprived in 0% FBS medium for 6h and then stimulated with 100 nM insulin (Sigma-Aldrich, Saint Louis, MO, USA) for 10 min. To study the effect of the pre-miR-143-3p on cell apoptosis, HUVECs were deprived of FBS for 6 h or VSMCs were deprived of FBS for 2 h followed by a treatment with thapsigargin for 2 h (100 nM, Santa Cruz Biotechnology, Dallas, TX, USA).

4.8. RT-qPCR Analysis

Complementary DNA (cDNA) was synthesized by a High-Capacity cDNA Reverse Transcription Kit (Applied Biosystems, Foster City, CA, USA) for mRNA analysis. Quantitative polymerase chain reaction (qPCR) was done using cDNA as template and the TaqMan® Fast Advanced Master Mix (Thermo Scientific, Waltham, MA, USA). The genes were detected using TaqMan® (Thermo Scientific, Waltham, MA, USA) probes for hsa-miR-143-3p (477912_mir, mature miRNA sequence: UGAGAUGAAGCACUGUAGCUC), mmu-miR-155-5p (mmu480953_mir, mature miRNA sequence: UUAAUGCUAAUUGUGAUAGGGGU) and mmu-miR-191-5p (mmu481584_mir, mature miRNA sequence: CAACGGAAUCCCAAAAGCAGCUG) used as endogenous gene. The references of other Taq-Man® probes used are indicated in the Supplemental Table S2. All the probes detect both mouse and human target genes. All RT-qPCR experiments were performed in an ABI Prism 7900HT Thermal Cycler (Applied Biosystems, Foster City, CA, USA).

The relative abundance of mRNA targets, normalized with the endogenous gene and relative to the control, is calculated as follow a: Relative Quantification (RQ) = $2^{-\Delta\Delta Ct}$; ΔCt (cycle threshold) = Ct (miRNA target) − Ct (miR-191-5p); ΔΔCt = ΔCt for any sample − ΔCt for the control]. Amplification of miR-191-5p was used in the same reaction of all samples as an internal control.

4.9. Western Blot Analysis

Proteins from cell lysates (20–60 μg), and tissue samples (20–70 μg) were separated on a 10% or 10–20% gradient acrylamide gel and then transferred to a 0.45 μM pore PVDF membrane (Merck, Darmstadt, Germany) as previously described [57]. The primary antibodies used are shown in Supplemental Table S4 and all of them were diluted in TTBS. Rabbit and mouse primary antibodies were immunodetected using horseradish peroxidase-

conjugated anti-rabbit IgG (NA931V; 1:4000 in TTBS) or anti-mouse IgG secondary antibody (NA934V; 1:5000 in TTBS) (GE Healthcare, Buckinghamshire, UK), respectively. When possible, phospho-proteins and their total expression were detected in the same gel, using Restore™ Western Blot Stripping Buffer (Thermo Fisher Scientific) as per the manufacturer's instructions, blocking the membrane again before the incubation with the next antibody. Loading was normalized by β-actin or α-tubulin. Protein bands were visualized using the Clarity Western Blot Analysis ECL (BioRad®, Hercules, CA, USA). Band densitometry was analysed using ImageJ Software (v1.52a, Wayne Rasband, National Institute of Health, Stapleton, NY, USA).

4.10. Database Search to Find miRNAs and Their Possible Targets

The miRNAs analyzed in the study were identified by an exhaustive search for keywords (miRNAs, atherosclerosis, insulin resistance, inflammation, and fatty liver) and different publications in PubMed. Once the miRNAs of interest were selected, the interaction between them and their mRNA targets was evaluated in miRNA-Target Interaction databases such as GEO Database, TargetScan, miRWalk, miRDB, DIANA and miRTarBase. The data collected from these databases were analyzed, and only those targets that appeared in two or more databases were considered as possible targets. A diagram showing the proposed regulatory axes during atherosclerosis progression is supplied in the Supplemental Figure S4B,D. These representations were made using Cytoscape software (v.3.8.2. on Java 11.0.6. by AdoptOpenJDK, Darmstadt, Germany).

4.11. Statistical Analysis

The data from the experimental groups were analyzed using GraphPad Prism (v8, JPM ®, New York, USA). Normality and Lognormality tests were performed to confirm that the data followed a normal distribution. Statistical significance of the differences between groups was assessed by Student's t tests when comparing two groups, or with ANOVA tests followed by a Bonferroni *post-hoc* test when comparing more than two groups. Correlation between variables was assessed by two-tailed Spearman's r correlation analyses. The exact p value is indicated in each figure when it reached statistically significance ($p < 0.05$).

Supplementary Materials: The following supporting information can be downloaded at: https://www.mdpi.com/article/10.3390/ijms231810253/s1.

Author Contributions: P.G.-L.: Conceptualization; Investigation; Methodology; Data curation; Writing: original draft, review and editing. C.A.-C.: Conceptualization; Investigation; Methodology; Data curation. A.R.L.-P.: Investigation; Methodology; Data curation. J.I.-M.: Investigation; Methodology; Data curation; Writing: review and editing. T.G.I.: Investigation; Methodology; Data curation. M.V.d.C. and L.E.: Conceptualization; Investigation; Resources. N.B.: Investigation; Methodology; Data curation. J.L.M.-V.: Investigation; Methodology; Writing: review and editing. Ó.E. and A.G.-H.: Conceptualization; Data curation; Formal analysis; Funding acquisition; Investigation; Methodology; Project administration; Supervision; original draft, Writing: review and editing. All authors have read and agreed to the published version of the manuscript.

Funding: This research was funded by grants RTI-2018-095098-B100 and PID2021-123076OB-I00 from Ministerio de Ciencia e Innovación y Universidades, Santander-UCM PR75/18-21572, UCM AENC1/22-29754 given to A. Gómez-Hernández and Ó. Escribano. Jorge Infante-Menéndez and Paula González-López were funded by Programa Operativo de Empleo Juvenil from Comunidad de Madrid.

Institutional Review Board Statement: Each of the samples (controls without vascular lesion or with fibrolipidic plaques) was harvested from a different donor after organ transplantation with the authorization of the French Biomedicine Agency (authorization number PFS09-007). Samples from patients with advanced carotid atherosclerosis were collected and approved by the hospital's Ethics Committee (IIS-Fundación Jiménez Díaz) with the reference number PI1442016 according to the institutional and the Good Clinical Practice guidelines, which was performed in accordance with the Declaration of Helsinki. All participants gave written informed consent. All the procedures of

mouse model were handled according to the rules set by the ethical committee from the Universidad Complutense de Madrid (PROEX188/88).

Informed Consent Statement: All participants gave written informed consent.

Data Availability Statement: The datasets used and/or analyzed during the current study are available from the corresponding authors (algomezh@ucm.es or oescriba@ucm.es) on reasonable request.

Acknowledgments: We want to thank Jean-Baptiste Michel for the transfer of human infradiaphragmatic aortic segments from control subjects and subjects with fibrolipidic lesions. Each of them was harvested from a different donor after organ transplantation with the authorization of the French Biomedicine Agency.

Conflicts of Interest: The authors declare no conflict of interest.

References

1. Francula-Zaninovic, S.; Nola, I.A. Management of Measurable Variable Cardiovascular Disease' Risk Factors. *Curr. Cardiol. Rev.* **2018**, *14*, 153–163. [CrossRef] [PubMed]
2. Saigusa, R.; Winkels, H.; Ley, K. T cell subsets and functions in atherosclerosis. *Nat. Rev. Cardiol.* **2020**, *17*, 387–401. [CrossRef] [PubMed]
3. Wolf, D.; Ley, K. Immunity and inflammation in atherosclerosis. *Herz* **2019**, *44*, 107–120. [CrossRef] [PubMed]
4. Poller, W.C.; Nahrendorf, M.; Swirski, F.K. Hematopoiesis and cardiovascular disease. *Circ. Res.* **2020**, *126*, 1061–1085. [CrossRef] [PubMed]
5. Muniyappa, R.; Montagnani, M.; Koh, K.K.; Quon, M.J. Cardiovascular Actions of Insulin. *Endocr Rev.* **2007**, *28*, 463–491. [CrossRef]
6. Muris, D.M.J.; Houben, A.J.H.M.; Schram, M.T.; Stehouwer, C.D.A. Microvascular dysfunction is associated with a higher incidence of type 2 diabetes mellitus: A systematic review and meta-analysis. *Arterioscler. Thromb. Vasc. Biol.* **2012**, *32*, 3082–3094. [CrossRef]
7. Gómez-Hernández, A.; de las Heras, N.; López-Pastor, A.R.; García-Gómez, G.; Infante-Menéndez, J.; González-López, P.; González-Illanes, T.; Lahera, V.; Benito, M.; Escribano, O. Severe hepatic insulin resistance induces vascular dysfunction: Improvement by liver-specific insulin receptor isoform a gene therapy in a murine diabetic model. *Cells* **2021**, *10*, 2035. [CrossRef]
8. Bartel, D.P. Metazoan MicroRNAs. *Cell* **2018**, *173*, 20–51. [CrossRef]
9. Cordes, K.R.; Sheehy, N.T.; White, M.P.; Berry, E.C.; Morton, S.U.; Muth, A.N.; Lee, T.H.; Miano, J.M.; Ivey, K.N.; Srivastava, D. miR-145 and miR-143 regulate smooth muscle cell fate and plasticity. *Nature* **2009**, *460*, 705–710. [CrossRef]
10. Zhang, H.; Xue, S.; Feng, Y.; Shen, J.; Zhao, J. MicroRNA-24-3p inhibition prevents cell growth of vascular smooth muscle cells by targeting Bcl-2-like protein 11. *Exp. Ther. Med.* **2020**, *19*, 2467–2474. [CrossRef]
11. Signorelli, S.S.; Volsi, G.L.; Pitruzzella, A.; Fiore, V.; Mangiafico, M.; Vanella, L.; Parenti, R.; Rizzo, M.; Volti, G.L. Circulating miR-130a, miR-27b, and miR-210 in Patients with Peripheral Artery Disease and Their Potential Relationship with Oxidative Stress. *Angiology* **2016**, *67*, 945–950. [CrossRef] [PubMed]
12. Giglio, R.V.; Nikolic, D.; Volti, G.L.; Stoian, A.P.; Banerjee, Y.; Magan-Fernandez, A.; Castellino, G.; Patti, A.M.; Chianetta, R.; Castracani, C.C.; et al. Liraglutide Increases Serum Levels of MicroRNA-27b, -130a and -210 in Patients with Type 2 Diabetes Mellitus: A Novel Epigenetic Effect. *Metabolites* **2020**, *10*, 391. [CrossRef] [PubMed]
13. Wang, F.; Shan, S.; Huo, Y.; Xie, Z.; Fang, Y.; Qi, Z.; Chen, F.; Li, Y.; Sun, B. MiR-155-5p inhibits PDK1 and promotes autophagy via the mTOR pathway in cervical cancer. *Int. J. Biochem. Cell Biol.* **2018**, *99*, 91–99. [CrossRef] [PubMed]
14. Zhu, M.; Wei, Y.; Geißler, C.; Abschlag, K.; Campos, J.C.; Hristov, M.; Möllman, J.; Lehrke, M.; Karshovska, E.; Schober, A. Hyperlipidemia-induced MicroRNA-155-5p improves β-cell function by targeting Mafb. *Diabetes* **2017**, *66*, 3072–3084. [CrossRef] [PubMed]
15. Jiang, K.; Hu, J.; Luo, G.; Song, D.; Zhang, P.; Zhu, J.; Sun, F. MiR-155-5p Promotes Oxalate- And Calcium-Induced Kidney Oxidative Stress Injury by Suppressing MGP Expression. *Oxid. Med. Cell Longev.* **2020**, *2020*, 5863617. [CrossRef] [PubMed]
16. Wang, G.; Chen, J.J.; Deng, W.Y.; Ren, K.; Yin, S.H.; Yu, X.H. CTRP12 ameliorates atherosclerosis by promoting cholesterol efflux and inhibiting inflammatory response via the miR-155-5p/LXRα pathway. *Cell Death Dis.* **2021**, *12*, 254. [CrossRef]
17. Xie, F.; Li, C.; Zhang, X.; Peng, W.; Wen, T. MiR-143-3p suppresses tumorigenesis in pancreatic ductal adenocarcinoma by targeting KRAS. *Biomed. Pharmacother.* **2019**, *119*, 109424. [CrossRef] [PubMed]
18. Shi, H.; Shen, H.; Xu, J.; Zhao, S.; Yao, S.Z.; Jiang, N. MiR-143-3p suppresses the progression of ovarian cancer. *Am. J. Transl. Res.* **2018**, *10*, 866–874.
19. Ma, W.Y.; Song, R.J.; Xu, B.B.; Xu, Y.; Wang, X.X.; Sun, H.Y.; Liu, S.Z.; Yu, M.X.; Yang, F.; Ye, D.Y.; et al. Melatonin promotes cardiomyocyte proliferation and heart repair in mice with myocardial infarction via miR-143-3p/Yap/Ctnnd1 signaling pathway. *Acta Pharmacol. Sin.* **2021**, *42*, 21–31. [CrossRef] [PubMed]
20. Liu, K.; Zhao, D.; Wang, D. LINC00528 regulates myocardial infarction by targeting the miR-143-3p/COX-2 axis. *Bioengineered* **2020**, *11*, 11–18. [CrossRef]
21. Stefanadis, C.; Antoniou, C.K.; Tsiachris, D.; Pietri, P. Coronary atherosclerotic vulnerable plaque: Current perspectives. *J. Am. Heart Assoc.* **2017**, *6*, 1–18. [CrossRef]
22. Zhu, J.; Chen, T.; Yang, L.; Li, Z.; Wong, M.M.; Zheng, X.; Pan, X.; Zhang, L.; Yan, H. Regulation of MicroRNA-155 in Atherosclerotic Inflammatory Responses by Targeting MAP3K10. *PLoS ONE* **2012**, *7*, e46551. [CrossRef]
23. Bruen, R.; Fitzsimons, S.; Belton, O. MiR-155 in the resolution of atherosclerosis. *Front. Pharmacol.* **2019**, *10*, 463. [CrossRef] [PubMed]

24. Donners, M.M.P.C.; Wolfs, I.M.J.; Stöger, L.J.; van der Vorst, E.P.C.; Pöttgens, C.C.H.; Heymans, S.; Schroen, B.; Gijbels, M.J.J.; Winther, M.P.J. Hematopoietic miR155 deficiency enhances atherosclerosis and decreases plaque stability in hyperlipidemic mice. *PLoS ONE* **2012**, *7*, 4–12. [CrossRef]
25. Zhu, G.F.; Yang, L.X.; Guo, R.W.; Liu, H.; Shi, Y.K.; Wang, H.; Ye, J.S.; Yang, Z.H.; Liang, X. MiR-155 inhibits oxidized low-density lipoprotein-induced apoptosis of RAW264.7 cells. *Mol. Cell Biochem.* **2013**, *382*, 253–261. [CrossRef] [PubMed]
26. Nazari-Jahantigh, M.; Wei, Y.; Noels, H.; Akhtar, S.; Zhou, Z.; Koenen, R.R.; Heyll, K.; Gremse, F.; Kiessling, F.; Grommes, J.; et al. MicroRNA-155 promotes atherosclerosis by repressing Bcl6 in macrophages. *J. Clin. Investig.* **2012**, *122*, 4190–4202. [CrossRef] [PubMed]
27. Du, F.; Yu, F.; Wang, Y.; Hui, Y.; Carnevale, K.; Fu, M.; Lu, H.; Fan, D. MicroRNA-155 Deficiency Results in Decreased Macrophage Inflammation and Attenuated Atherogenesis in Apolipoprotein E–Deficient Mice. *Arterioscler. Thromb. Vasc. Biol.* **2014**, *34*, 759–767. [CrossRef]
28. Singh, S.; de Ronde, M.W.J.; Kok, M.G.M.; Beijk, M.A.; De Winter, R.J.; van der Wal, A.C.; Sondermeijer, B.M.; Meijers, J.C.M.; Creemers, E.E.; Pinto-Sietsma, S.J. MiR-223-3p and miR-122-5p as circulating biomarkers for plaque instability. *Open Heart* **2020**, *7*, e001223. [CrossRef]
29. Fitzsimons, S.; Oggero, S.; Bruen, R.; McCarthy, C.; Strowitzki, M.J.; Mahon, N.G.; Ryan, N.; Brennan, E.P.; Barry, M.; Perretti, M.; et al. microRNA-155 Is Decreased During Atherosclerosis Regression and Is Increased in Urinary Extracellular Vesicles During Atherosclerosis Progression. *Front. Immunol.* **2020**, *11*, 1–18. [CrossRef]
30. Chen, L.; Zheng, S.Y.; Yang, C.Q.; Ma, B.M.; Jiang, D. MiR-155-5p inhibits the proliferation and migration of VSMCs and HUVECs in atherosclerosis by targeting AKT1. *Eur. Rev. Med. Pharmacol. Sci.* **2019**, *23*, 2223–2233. [CrossRef]
31. Zegeye, M.M.; Lindkvist, M.; Fälker, K.; Kumawat, A.K.; Paramel, G.; Grenegård, M.; Sirsjö, A.; Ljungberg, L. Activation of the JAK/STAT3 and PI3K/AKT pathways are crucial for IL-6 trans-signaling-mediated pro-inflammatory response in human vascular endothelial cells. *Cell Commun. Signal* **2018**, *16*, 1–10. [CrossRef] [PubMed]
32. Yao, X.; Yan, C.; Zhang, L.; Li, Y.; Wan, Q. LncRNA ENST00113 promotes proliferation, survival, and migration by activating PI3K/Akt/mTOR signaling pathway in atherosclerosis. *Medicine* **2018**, *97*, e0473. [CrossRef] [PubMed]
33. Arner, P.; Kulyté, A. MicroRNA regulatory networks in human adipose tissue and obesity. *Nat. Rev. Endocrinol* **2015**, *11*, 276–288. [CrossRef]
34. Ortega, F.J.; Moreno, M.; Mercader, J.M.; Moreno-Navarrete, J.M.; Fuentes-Batllevell, N.; Sabater, M.; Ricart, W.; Fernández-Real, J.M. Inflammation triggers specific microRNA profiles in human adipocytes and macrophages and in their supernatants. *Clin. Epigenetics* **2015**, *7*, 1–10. [CrossRef] [PubMed]
35. Ortega, F.J.; Moreno-Navarrete, J.M.; Pardo, G.; Sabater, M.; Hummel, M.; Ferrer, A.; Rodriguez-Hermosa, J.I.; Ruiz, B.; Ricart, W.; Peral, B.; et al. MiRNA expression profile of human subcutaneous adipose and during adipocyte differentiation. *PLoS ONE* **2010**, *5*, e9022. [CrossRef]
36. Ma, X.; Becker Buscaglia, L.E.; Barker, J.R.; Li, Y. MicroRNAs in NF-κB signaling. *J. Mol. Cell Biol* **2011**, *3*, 159–166. [CrossRef] [PubMed]
37. Carpi, S.; Scoditti, E.; Massaro, M.; Polini, B.; Manera, C.; Digiacomo, M.; Salsano, J.E.; Poli, G.; Tuccinardi, T.; Doccini, S.; et al. The Extra-Virgin Olive Oil Polyphenols Oleocanthal and Oleacein Counteract Inflammation-Related Gene and miRNA Expression in Adipocytes by Attenuating NF-κB Activation. *Nutrients* **2019**, *11*, 2855. [CrossRef]
38. Subedi, A.; Park, P.H. Autocrine and paracrine modulation of microRNA-155 expression by globular adiponectin in RAW 264.7 macrophages: Involvement of MAPK/NF-κB pathway. *Cytokine* **2013**, *64*, 638–641. [CrossRef]
39. Martín-Ventura, J.L.; Blanco-Colio, L.M.; Muñoz-García, B.; Gómez-Hernández, A.; Arribas, A.; Ortega, L.; Tuñón, J.; Egido, J. NF-κB Activation and Fas Ligand Overexpression in Blood and Plaques of Patients with Carotid Atherosclerosis: Potential Implication in Plaque Instability. *Stroke* **2004**, *35*, 458–463. [CrossRef]
40. Gómez-Hernández, A.; Martín-Ventura, J.L.; Sánchez-Galán, E.; Vidal, C.; Ortego, M.; Blanco-Colio, L.M.; Ortega, L.; Tuñón, J.; Egido, J. Overexpression of COX-2, Prostaglandin E Synthase-1 and Prostaglandin E Receptors in blood mononuclear cells and plaque of patients with carotid atherosclerosis: Regulation by nuclear factor-κB. *Atherosclerosis* **2006**, *187*, 139–149. [CrossRef]
41. López-Franco, O.; Hernández-Vargas, P.; Ortiz-Muñoz, G.; Sanjuán, G.; Suzuki, Y.; Ortega, L.; Blanco, J.; Egido, J.; Gómez-Guerrero, C. Parthenolide modulates the NF-κB-mediated inflammatory responses in experimental atherosclerosis. *Arterioscler. Thromb. Vasc. Biol.* **2006**, *26*, 1864–1870. [CrossRef]
42. Scoditti, E.; Carpi, S.; Massaro, M.; Pellegrino, M.; Polini, B.; Carluccio, M.A.; Wabitsch, M.; Verri, T.; Nieri, P.; Caterina, R. Hydroxytyrosol modulates adipocyte gene and mirna expression under inflammatory condition. *Nutrients* **2019**, *11*, 2493. [CrossRef] [PubMed]
43. Gaudet, A.D.; Fonken, L.K.; Gushchina, L.V.; Aubrecht, T.G.; Maurya, S.K.; Periasamy, M.; Nelson, R.J.; Popovich, P.G. MIR-155 deletion in female mice prevents diet-induced obesity. *Sci. Rep.* **2016**, *6*, 22862. [CrossRef] [PubMed]
44. Kajimura, S.; Seale, P.; Kubota, K.; Lunsford, E.; Frangioni, J.V.; Gygi, S.P.; Spiegelman, B.M. Initiation of myoblast to brown fat switch by a PRDM16–C/EBP-β transcriptional complex. *Nature* **2009**, *460*, 1154–1158. [CrossRef] [PubMed]
45. Huijsman, E.; Van De Par, C.; Economou, C.; Van Der Poel, C.; Lynch, G.S.; Schoiswohl, G.; Haemmerle, G.; Zechner, R.; Watt, M.J. Adipose triacylglycerol lipase deletion alters whole body energy metabolism and impairs exercise performance in mice. *Am. J. Physiol. Endocrinol. Metab.* **2009**, *297*, 505–513. [CrossRef]
46. Li, Y.; Fromme, T.; Schweizer, S.; Schöttl, T.; Klingenspor, M. Taking control over intracellular fatty acid levels is essential for the analysis of thermogenic function in cultured primary brown and brite/beige adipocytes. *EMBO Rep.* **2014**, *15*, 1069–1076. [CrossRef]

47. Pan, M.; Deng, Y.; Zheng, C.; Nie, H.; Tang, K.; Zhang, Y.; Yang, Q. Chinese Herbal Medicine Formula Shenling Baizhu San Ameliorates High-Fat Diet-Induced NAFLD in Rats by Modulating Hepatic MicroRNA Expression Profiles. *Evid. Based Complement. Alternat. Med.* **2019**, *2019*, 8479680. [CrossRef]
48. Miller, A.M.; Gilchrist, D.S.; Nijjar, J.; Araldi, E.; Ramirez, C.M.; Lavery, C.A.; Fernández-Hernando, C.; Mclnnes, I.B.; Kurowska-Stolarska, M. MiR-155 Has a Protective Role in the Development of Non-Alcoholic Hepatosteatosis in Mice. *PLoS ONE* **2013**, *8*, e72324. [CrossRef]
49. Csak, T.; Bala, S.; Lippai, D.; Kodys, K.; Catalano, D.; Iracheta-Vellve, A.; Szabo, G. MicroRNA-155 Deficiency Attenuates Liver Steatosis and Fibrosis without Reducing Inflammation in a Mouse Model of Steatohepatitis. *PLoS ONE* **2015**, *10*, 1–21. [CrossRef]
50. Liu, Q.; Du, G.Q.; Zhu, Z.T.; Zhang, C.; Sun, X.W.; Liu, J.J.; Li, X.; Wang, Y.S.; Du, W.J. Identification of apoptosis—Related microRNAs and their target genes in myocardial infarction post—Transplantation with skeletal myoblasts. *J. Transl. Med.* **2015**, *13*, 1–11. [CrossRef]
51. Xihua, L.I.N.; Shengjie, T.; Weiwei, G.U.I.; Matro, E.; Tingting, T.A.O.; Lin, L.I.; Fang, W.; Jiaqiang, Z.; Fenping, Z.; Hong, L. Circulating miR-143-3p inhibition protects against insulin resistance in Metabolic Syndrome via targeting of the insulin-like growth factor 2 receptor. *Transl. Res.* **2019**, *205*, 33–43. [CrossRef] [PubMed]
52. Ghosh, P.; Dahms, N.M.; Kornfeld, S. Mannose 6-phosphate receptors: New twists in the tale. *Nat. Rev. Mol. Cell Biol.* **2003**, *4*, 202–212. [CrossRef]
53. Zaina, S.; Nilsson, J. Insulin-like growth factor II and its receptors in atherosclerosis and in conditions predisposing to atherosclerosis. *Curr. Opin. Lipidol.* **2003**, *14*, 483–489. [CrossRef]
54. Beneit, N.; Luis, J.; Ventura, M.; Longás, C.R.; Escribano, Ó.; Gómez-García, G.; Fernández, S.; Sesti, G.; Hribal, M.L.; Egido, J.; et al. Potential role of insulin receptor isoforms and IGF receptors in plaque instability of human and experimental atherosclerosis. *Cardiovasc. Diabetol.* **2018**, *17*, 1–14. [CrossRef]
55. Huang, C.Y.; Kuo, W.W.; Yeh, Y.L.; Ho, T.J.; Lin, J.Y.; Lin, D.Y.; Chu, C.H.; Tsai, F.J.; Tsai, C.H.; Huang, C.Y. ANG II promotes IGF-IIR expression and cardiomyocyte apoptosis by inhibiting HSF1 via JNK activation and SIRT1 degradation. *Cell Death Differ.* **2014**, *21*, 1262–1274. [CrossRef] [PubMed]
56. Stary, H.C.; Chandler, A.B.; Glagov, S.; Guyton, J.R.; Insull, W., Jr.; Rosenfeld, M.E.; Schaffer, S.A.; Schwartz, C.J.; Wagner, W.D.; Wissler, R.W. A definition of initial, fatty streak, and intermediate lesions of atherosclerosis. A report from the Committee on Vascular Lesions of the Council on Arteriosclerosis, American Heart Association. *Circulation* **1994**, *89*, 2462–2478. [CrossRef] [PubMed]
57. Gómez-Hernández, A.; Escribano, Ó.; Perdomo, L.; Otero, Y.F.; García-Gómez, G.; Fernández, S.; Beneit, N.; Benito, M. Implication of insulin receptor A isoform and IRA/IGF-IR hybrid receptors in the aortic vascular smooth muscle cell proliferation: Role of TNF-α and IGF-II. *Endocrinology* **2013**, *154*, 2352–2364. [CrossRef] [PubMed]

Received: 7 March 2023 | Revised: 26 July 2023 | Accepted: 5 August 2023

DOI: 10.1002/ctm2.1363

CLINICAL AND TRANSLATIONAL MEDICINE Open Access WILEY

RESEARCH ARTICLE

Role of miR-15a-5p and miR-199a-3p in the inflammatory pathway regulated by NF-κB in experimental and human atherosclerosis

Paula González-López[1] | **Marta Álvarez-Villarreal**[1] | **Rubén Ruiz-Simón**[1] | **Andrea R. López-Pastor**[1] | **Melina Vega de Ceniga**[2,3] | **Leticia Esparza**[2,3] | **José L. Martín-Ventura**[4] | **Óscar Escribano**[1] | **Almudena Gómez-Hernández**[1]

[1]Hepatic and Vascular Diseases Laboratory. Biochemistry and Molecular Biology Department, School of Pharmacy, Complutense University of Madrid, Madrid, Spain

[2]Department of Angiology and Vascular Surgery, Hospital of Galdakao-Usansolo, Galdakao, Bizkaia, Spain

[3]Biocruces Bizkaia Health Research Institute, Barakaldo, Bizkaia, Spain

[4]IIS-Fundation Jimenez-Diaz, Autonoma University of Madrid and CIBERCV, Madrid, Spain

Correspondence
Óscar Escribano and Almudena Gómez-Hernández, Hepatic and Vascular Diseases Laboratory. Biochemistry and Molecular Biology Department, School of Pharmacy, Complutense University of Madrid, Madrid, Spain.
Email: oescriba@ucm.es; algomezh@ucm.es

Graphical Abstract

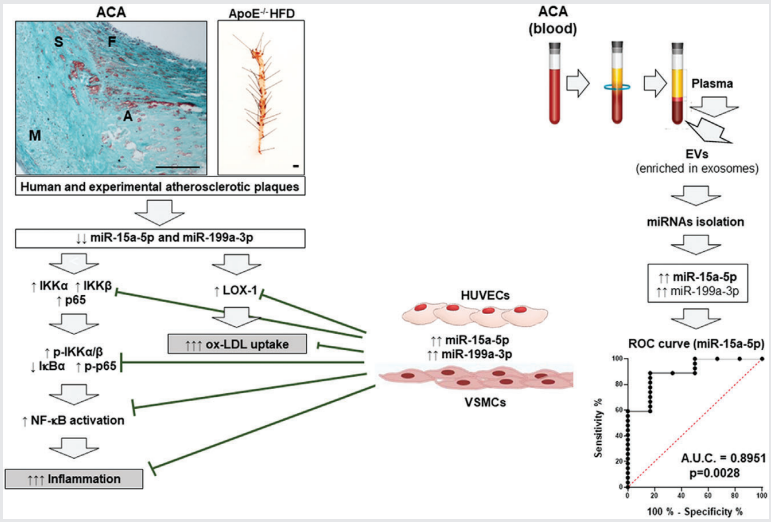

This study demonstrates a novel role for miR-15a-5p and miR-199a-3p in atherosclerosis progression. Both miRNAs have an anti-inflammatory role due to the regulation of their targets involved NF-kappa B pathway, in addition, they have an anti-foaming role in vascular smooth muscle cells. Finally, miR-15a-5p might be useful for diagnosis of advanced carotid atherosclerosis.

Received: 7 March 2023 | Revised: 26 July 2023 | Accepted: 5 August 2023

DOI: 10.1002/ctm2.1363

RESEARCH ARTICLE

CLINICAL AND TRANSLATIONAL MEDICINE Open Access WILEY

Role of miR-15a-5p and miR-199a-3p in the inflammatory pathway regulated by NF-κB in experimental and human atherosclerosis

Paula González-López[1] | **Marta Álvarez-Villarreal**[1] | **Rubén Ruiz-Simón**[1] | **Andrea R. López-Pastor**[1] | **Melina Vega de Ceniga**[2,3] | **Leticia Esparza**[2,3] | **José L. Martín-Ventura**[4] | **Óscar Escribano**[1] | **Almudena Gómez-Hernández**[1]

[1]Hepatic and Vascular Diseases Laboratory. Biochemistry and Molecular Biology Department, School of Pharmacy, Complutense University of Madrid, Madrid, Spain

[2]Department of Angiology and Vascular Surgery, Hospital of Galdakao-Usansolo, Galdakao, Bizkaia, Spain

[3]Biocruces Bizkaia Health Research Institute, Barakaldo, Bizkaia, Spain

[4]IIS-Fundation Jimenez-Diaz, Autonoma University of Madrid and CIBERCV, Madrid, Spain

Correspondence
Óscar Escribano and Almudena Gómez-Hernández, Hepatic and Vascular Diseases Laboratory. Biochemistry and Molecular Biology Department, School of Pharmacy, Complutense University of Madrid, Madrid, Spain.
Email: oescriba@ucm.es; algomezh@ucm.es

Funding information
Grants RTI-2018-095098-B100 and PID2021-123076OB-I00 from Ministerio de Ciencia e Innovacion y Universidades, Santander-UCM PR75/18-21572 and UCM AENC1/22-29754 were given to Almudena Gomez-Hernandez and Oscar Escribano. Paula Gonzalez-Lopez was funded by Programa Operativo de Empleo Juvenil from Comunidad de Madrid.

Óscar Escribano and Almudena Gómez-Hernández are co-senior authors.

Trial Registration: authorization numbers PFS09-007 and PI1442016

Abstract

Background: Cardiovascular diseases (CVDs) prevalence has significantly increased in the last decade and atherosclerosis development is the main trigger. MicroRNAs (miRNAs) are non-coding RNAs that negatively regulate gene expression of their target and their levels are frequently altered in CVDs.

Methods: By RT-qPCR, we analysed miR-9-5p, miR-15a-5p, miR-16-5p and miR-199a-3p levels in aorta from apolipoprotein knockout (*ApoE*$^{-/-}$) mice, an experimental model of hyperlipidemia-induced atherosclerosis, and in human aortic and carotid atherosclerotic samples. By in silico studies, Western blot analysis and immunofluorescence studies, we detected the targets of the altered miRNAs.

Results: Our results show that miR-15a-5p and miR-199a-3p are significantly decreased in carotid and aortic samples from patients and mice with atherosclerosis. In addition, we found an increased expression in targets of both miRNAs that participate in the inflammatory pathway of nuclear factor kappa B (NF-κB), such as IKKα, IKKβ and p65. In human vein endothelial cells (HUVECs) and vascular smooth muscle cells (VSMCs), the overexpression of miR-15a-5p or miR-199a-3p decreased IKKα, IKKβ and p65 protein levels as well as NF-κB activation. On the other hand, miR-15a-5p and miR-199a-3p overexpression reduced ox-LDL uptake and the inflammation regulated by NF-κB in VSMCs. Moreover, although miR-15a-5p and miR-199a-3p were significantly increased in exosomes

from patients with advanced carotid atherosclerosis, only in the ROC analyses for miR-15a-5p, the area under the curve was 0.8951 with a *p* value of .0028.

Conclusions: Our results suggest that the decrease of miR-199a-3p and miR-15a-5p in vascular samples from human and experimental atherosclerosis could be involved in the NF-κB activation pathway, as well as in ox-LDL uptake by VSMCs, contributing to inflammation and progression atherosclerosis. Finally, miR-15a-5p could be used as a novel diagnostic biomarker for advanced atherosclerosis.

KEYWORDS
atherosclerosis, inflammation, miRNAs, NF-κB

1 | INTRODUCTION

Cardiovascular diseases (CVDs) and cancer are the dominant causes of death in the world.[1] Atherosclerosis is the main cause of CVDs including heart failure, stroke, myocardial infarction and peripheral arterial disease.[2] Atherosclerosis is located in the intima of many middle sized and large arteries, especially in the locations with geometrically complex vessels.[2] Laminar and unidirectional flow induces an increase in transcription factors such as Kruppel-like factors (KLF2 and KLF4) and nuclear factor erythroid 2-related factor 2 (Nrf2) that will favour an atheroprotective phenotype.[3] However, non-uniform, turbulent, multidirectional or oscillatory flow regions, as in the bifurcation of the carotid artery produces an increase of inflammatory transcription factors and degradation of endothelial glycocalyx, leading to atherosclerotic phenotype.[3,4]

Inflammation is a key factor in the progression of atherosclerosis and in the rupture of advanced atherosclerotic plaques.[5] The dysfunctional and activated endothelium increases the secretion of chemokines, such as monocyte chemoattractant protein-1 (MCP-1), which favours the recruitment and diapedesis of monocytes and the different lymphocytes, as well as adhesion molecules and selectins that favour rolling, and transmigration in the subendothelial space. These monocytes in the subendothelial space will differentiate into macrophages. Mainly, there have been identified two populations of macrophages, M1 and M2, being the first one highly expressed in symptomatic patients with advanced carotid atherosclerosis (ACA).[6] Moreover, other immune-inflammatory cells as dendritic cells or lymphocytes T and B also participate in the development of atherosclerosis.[5] In addition, many of the proinflammatory mediators, enzymes, chemokines and cytokines involved in atherogenesis could be regulated by different transcription factors, among them the nuclear factor kappa B (NF-κB).[7]

NF-κB is formed by p50 and p65, and IκB subunits in the cytosol. The phosphorylation of inhibitory subunit, IκB, by IKK complex (IKKα/IKKβ/IKKγ), its polyubiquitination, and finally, degradation by proteasome, permit the p50/p65 heterodimer nucleus translocation,[7] which activates the transcription of genes involved in the inflammatory, immune or acute-phase response. Increased NF-κB activation has been found in peripheral blood mononuclear cells (PBMCs) from patients with unstable angina[8] or acute coronary syndrome.[9] Moreover, patients with ACA also showed a significant increase of active NF-κB in atherosclerotic lesions and in PBMCs.[10,11]

MicroRNAs (miRNAs) are small endogenous noncoding RNAs that negatively regulate the translation of mRNAs. miRNAs play a role in development, metabolism, cell proliferation, growth, differentiation and death.[12] However, it has been described that the alteration in the expression profile of miRNAs might be related to human diseases, such as atherosclerosis. For instance, miR-145 and miR-143 regulate vascular smooth muscle cells (VSMCs) fate and plasticity,[13] whereas miR-24-3p has been described as an important regulator in VSMCs proliferation and apoptosis.[14]

Atherosclerosis is an asymptomatic disease for long periods in which several factors can contribute to the progression and rupture of vulnerable plaques and, consequently, provoke the acute event such as stroke or acute myocardial infarction.[15] In this regard, to identify new biomarkers, miRNAs or miRNA panels will help in the future to detect the presence of vulnerable plaques, but also to avoid the progression process. After a screening of 20 miRNAs involved in inflammation and metabolic diseases such as NAFLD and atherosclerosis, in this manuscript, we have deepened the study of two miRNAs (miR-15a-5p and miR-199a-3p) that showed a similar behaviour in vascular samples from human and experimental atherosclerosis. We have analysed the expression of these miRNAs by RT-qPCR in human atherosclerotic samples, using aortic samples from control subjects (CAs) and subjects with

fibrolipidic plaques (FAs) or carotid samples from patients with ACA. Then, these miRNAs were also studied in the aorta from $ApoE^{-/-}$ mice (a classical experimental model of atherosclerosis) under a standard diet (STD) or a high-fat diet (HFD) for 8 and 18 weeks and wild-type mice. So, we focused on the role of miR-15a-5p and miR-199a-3p and their targets (IKKα, IKKβ and p65) in the progression of experimental and human atherosclerosis, as well as their implication in inflammation and NF-κB activation. To further characterize the role of these miRNAs in atherosclerosis progression, we performed overexpression experiments in human vein endothelial cell (HUVECs) and VSMCs. Finally, we analysed the utility of circulating miR-15a-5p and/or miR-199a-3p levels as diagnostic biomarkers of human advanced atherosclerosis.

2 | METHODS

2.1 | Human samples

Two cohorts of patients were analysed in this study. In the first cohort, under the authorization of the French Biomedicine Agency (PFS 09-007) human aortas were collected from deceased organ donors from 2010 to 2013. After macroscopic evaluation, the aortas were classified following the Stary classification[15] into two groups: control aortas (CAs, $n = 7$), and aortas with initial fibrolipidic plaques (fibroatheromas [FAs], $n = 7$) as previously described.[16] The investigation conforms to the principles outlined in the Declaration of Helsinki.

The second cohort includes patients with ACA. Patients with carotid stenosis >70% underwent carotid endarterectomy at IIS-Fundación Jiménez Díaz (Table S1) and the atherosclerotic plaques ($n = 40$) were collected for further analysis. The plaques showed higher inflammatory cells infiltration (Stary stages V–VI), however, the adjacent areas showed mainly lipid depots and VSMCs (Stary stage III). In the same study, plasma was collected from 29 patients to obtain extracellular vesicles and analyse miRNAs levels (Table S1). The study was approved by the Hospital's Ethics Committee (IIS-Fundación Jiménez Díaz) with reference number PI1442016 according to the institutional and the Good Clinical Practice guidelines, which was performed in accordance with the Declaration of Helsinki. All participants gave written informed consent.

2.2 | Animal model

Male C57Bl/6 wild type (WT) and ApoE deficient ($ApoE^{-/-}$) mice were maintained under standard light (12 h long light/dark cycles), temperature (23.3°C) and humidity (65.1%) conditions, and ad libitum diet from their weaning, up to their sacrifice. The WT mice ($n = 7$) were fed a standard type diet (STD; 3% of the kcal are provided by fat, Envigo, USA) for 8 or 18 weeks, while the $ApoE^{-/-}$ mice were separated into two groups: one was fed the STD ($n = 7$) and the other a HFD ($n = 10$) for 8 or 18 weeks before sacrifice. The formula of HFD (TD06414, Envigo, USA) is composed of casein (265.0 g/kg), L-cystine (4.0 g/kg), maltodextrin (60.0 g/kg), sucrose (90.0 g/kg), lard (310.0 g/kg), soybean oil (30.0 g/kg), cellulose (65.5 g/kg), mineral mix (AIN-93G-MX (94046), 48.0 g/kg), calcium phosphate dibasic (3.4 g/kg), vitamin mix (AIN-93-VX (94047), 21.0 g/kg) and choline bitartrate (3.0 g/kg). The percentage of kcal supported by protein (18.3%), carbohydrate (27.3%) and fat (60.3%). Fatty acid profile (percentage of total fat): 36% saturated, 41% monounsaturated and 23% polyunsaturated.

Mice were sacrificed at 8 or 18 weeks of feeding with STD or HFD, after 16 h of fasting. All animal experimentations were conducted in accordance with Complutense University of Madrid Ethics Committee, Autonomic Community of Madrid (PROEX133/19) and the guidelines from Directive 2010/63/EU of the European Parliament regarding the protection of animals used for scientific purposes. The microbiological and health state of the mice was controlled by the Federation of European Laboratory Animal Science Associations (FELASA) criteria and showed no pathogenic infection.

For euthanasia, the mice were anesthetized with ketamine (50 ng/mL, Ketalar® [Pfizer, New York, USA]) and xylazine (200 mg/mL Rompun® [Bayer, Barmen, Germany]) intraperitoneal injection on a 50:5 dose per Kg. The aorta was harvested and stored at −80°C, while the aortic root was washed with saline and then included in Tissue-Tek® O.C.T. Compound ([O.C.T.], VWR BDH Chemicals®, Radnor, PA, USA) and stored at −80°C for further analysis. Both tissues were extracted under sterile conditions. Blood was extracted from the jugular vein and mixed with 0.4% p/v citrate (Merck, Darmstadt, Germany), then the plasma was recovered after a 1200 × g centrifuge for 15 min at 4°C for subsequent analysis. Before the injection, the animals were weighted, and plasma glucose was measured using an Accu-Chek® glucometer (Aviva Roche, Basel, Switzerland). Finally, cholesterol and triglycerides were tested in plasma samples from fasted mice (Spinreact, Girona, Spain).

2.3 | Cell culture

HUVECs were purchased from PromoCell. They were grown in MCDB-131 culture medium (Life Technologies,

Carlsbad, CA, USA) enriched with L-glutamine 2 mM (GibcoTM, Fisher Scientific, Hampton, NH, USA), foetal bovine serum (FBS) 7.5% v/v (GibcoTM, Fisher Scientific, Hampton, NH, USA), Penicillin/Streptomycin 100 U/mL (GibcoTM, Fisher Scientific, Hampton, NH, USA) and endothelial growth factor 1X (R&D systems®, Minneapolis, MN, USA). Cells were received at passage 2 and were grown until passage 5. All cells were grown at 37°C in a humidified 5% CO_2 incubator (Fisher Scientific, Hampton, NH, USA).

Generation of immortalized WT VSMCs lines was previously described.[17] Cell lines were cultured to subconfluence (70%–80%) with 10% FBS-DMEM for in vitro experiments.

2.4 | Histological tissue samples

Paraffin-embedded human carotids were cut into 5 μm sections and stained with Masson trichrome and contrasted with haematoxylin and eosin purchased from PanReac Appli-Chem ITW Reagents (PanReac Appli-Chem ITW Reagents, Darmstadt, Germany). IKKα, IKKβ, p65 and LOX-1 were detected by immunoperoxidase with rabbit anti-IKKα (sc-7606, Santa Cruz Biotechnology, Dallas, TX, USA), anti-IKKβ (#2678, Cell Signalling Technology Inc.®, Danvers, MA, USA), anti-LOX-1 (#PA5-102452, Invitrogen, Waltham, MA, USA) and anti-p65 (#PA1-186, Invitrogen, Waltham, MA, USA) polyclonal antibodies (see Table S2). After an overnight incubation with each primary antibody, sections were incubated with a peroxidase-conjugated secondary antibody for 1 h at 1:100 dilution or biotin-conjugated secondary antibody (1:200) (Table S2). When we used peroxidase-conjugated secondary antibodies, the slides were incubated with peroxidase substrate DAB (416424, Palex, Barcelona, Spain) for 30 min. For the IKKα and LOX-1, an incubation of 30 min with Vectastain Elite ABC-HRP Kit (416411, Palex, Barcelona, Spain) at room temperature was carried out after the secondary antibody incubation and before the DAB incubation. The sections were stained for 10 min with DAB at room temperature and then counterstained with haematoxylin and mounted in DPX mounting medium (255,254.1610, PanReac Appli-Chem ITW Reagents, Darmstadt, Germany). In each experiment, we included negative controls without the primary antibody to check for non-specific staining.

The immunohistochemistry images were quantified using the "count and measure objects" tool in the Image-Pro Plus software IPWin (v4.5, Media Cybernetics, Rockville, USA) (IPWin v4.5 software). The colour considered as positive staining for the same protein was manually selected and all samples quantified with the same parameters, and the value corresponding to the sum of all stained areas was obtained. The results were expressed as the percentage of the stained area with respect to the total area analysed in each sample.

2.5 | En face imaging of aorta

We quantified the atherosclerotic lesions of the whole aorta were quantified by en face analysis. For *it*, the aorta was opened longitudinally, while still attached to the heart and major branching arteries in the body. The aorta from the heart to the iliac bifurcation was then removed and was pinned out on a white wax surface in a dissecting pan using stainless steel pins 0.2 mm in diameter. After overnight fixation with 4% paraformaldehyde and PBS rinsing, the aortas were stained for 6 min in a filtered solution containing 0.5% Oil Red O, 35% ethanol and 50% acetone, and then destained in 80% ethanol. The Oil Red O stained aortas were photographed, and the atherosclerotic lesions were quantified using IP Win32 v4.5 software.

2.6 | miRNA extraction from the aorta, vascular cell lines and paraffin-embedded carotid tissue

The miRNA content from the aorta and the cells were extracted following the mirVanaTM miRNA Isolation Kit (InvitrogenTM, Thermo Fisher Scientific, Waltham, MA, USA). The miRNA content from paraffin-embedded carotids was extracted using the RNeasy FFPE kit (Qiagen, Hilden, Germany). All the extractions were made following the protocol handled by the manufacturers. The mirVana™ kit allows the isolation of miRNAs and long RNAs in separate fractions by differential precipitation. The miRNA sample concentration was determined using a NanoDropTM 2000 and the NanoDrop 2000/2000c Operating Software (Thermo Scientific, Waltham, MA, USA).

2.7 | Cell transfection with miRNA precursors

Precursors of miR-15a-5p and miR-199a-3p were purchased from Sigma-Aldrich. Approximately 5×10^4 cells were seeded in P60 culture plates (353002, FalconTM, Thermo Fisher Scientific, Waltham, MA, USA) and transfected with 10–20 nM of MISSION® miRNA mimic hsa-miR15a-5p or 50 nM hsa-miR-199a-3p (HMI0256 or HMI0340, Sigma-Aldrich, St. Louis, MO, USA). As specified in the manufacturer's protocol (#409-10, Polyplus transfection®, Strasbourg, France), miRNA expression in HUVECs was

assessed 72 h after transfection, whereas protein down-regulation was analysed 96 h following transfection. In VSMCs, the effect of the transfection in both miRNA and protein levels was assessed after 48 h transfection with Lipofectamine®2000 RNAiMAX. To evaluate the effect in NF-κB pathway in cells transfected with pre-miR-15a-5p or/and miR-199a-3p, they were deprived in 0% FBS medium for 1 h and then stimulated with 10 ng/mL TNF-α (Sigma-Aldrich, St. Louis, MO, USA) for 10 min. To study the effect of the pre-miR-15a-5p and miR-199a-3p on inflammation, VSMCs were treated with low density lipoprotein from human plasma, oxidized (ox-LDL) (L34357, Thermo Fisher Scientific, Waltham, MA, USA) and some of them were transfected with the pre-miRNAs and analysed whether there was a less LDL uptake, reduced NF-κB activation as well as gene target regulated by above nuclear transcription factor.

On the other hand, we have also used hsa-antagomiR15a-5p (MSTUD0211, Sigma-Aldrich, St. Louis, MO, USA) and hsa-antagomiR-199a-3p (MSTUD0113, Sigma-Aldrich, St. Louis, MO, USA) to demonstrate the effect of the decrease of miR-15a-5p or miR-199a-3p levels on NF-κB activation. The effects of the transfection in both, miRNAs and protein levels, were assessed after 48 h of transfection with Lipofectamine®2000 RNAiMAX. To evaluate the effect in NF-κB pathway in cells transfected with hsa-antagomiR-15a-5p (20 nM) or hsa-antagomiR-199a-3p (20 nM), they were deprived in 0% FBS medium for 1 h and then stimulated with 10 ng/mL TNF-α (Sigma-Aldrich, St. Louis, MO, USA) for 10 min.

2.8 | Oil Red O staining of vascular smooth muscle cells

After the 100 μg/mL ox-LDL treatment in the last 24 h of transfection with the pre-miR-15a-5p and pre-miR-199a-3p, the cells were carefully washed two times with PBS 1X and put on ice. To fix the cells, they were incubated for 20 min with 10% formalin. The formalin was removed with PBS 1X. The cells were quickly washed with 65% isopropanol before the 15-min incubation with Oil Red O stock solution (0.5 g of Oil Red in 100 mL of 99% of 2-propanol, then we added 40 mL of water). We wait for 10−15 min before filtering and then washed with 65% isopropanol again. Finally, the cells were washed with distilled water to remove the excess colouring. The pictures were taken with a Nikon TE300 Inverted Phase Contrast DIC Fluorescence Microscope using a Nikon digital sight camera and the Nikon NIS-Elements F software (v 5.22.00 64-bit). The LDL uptake was quantified using ImageJ-win 64 software. All the pictures were open at the same time and the image type was changed to 8-bit, then the same threshold was asset for all the pictures to detect lipid deposition, and the selected staining from the images was measured at the same time.

2.9 | RT-qPCR analysis

Complementary DNA (cDNA) was synthesized by a High-Capacity cDNA Reverse Transcription Kit (Applied Biosystems, Foster City, CA, USA) for mRNA analysis. Quantitative polymerase chain reaction (qPCR) was done using cDNA as template and the TaqMan® Fast Advanced Master Mix (Thermo Scientific, Waltham, MA, USA). The genes were detected using TaqMan® (Thermo Scientific, Waltham, MA, USA) probes for mmu-miR-15a-5p (mmu482962_mir, mature miRNA sequence: UAGCAGCACAUAAUGGUUUGUG), hsa-miR-199-3p (477961_mir, mature miRNA sequence: ACAGUAGUCUGCACAUUGGUUA), mmu-miR-9a-5p (mmu481285_mir, mature miRNA sequence: UCUUUGGUUAUCUAGCUGUAUGA) and mmu-miR-16-5p (mmu482960_mir, mature miRNA sequence: UAGCAGCACGUAAAUAUUGGCG) was used as an endogenous gene in plasma samples, and mmu-miR-191-5p (mmu481584_mir, mature miRNA sequence: CAACGGAAUCCCAAAAGCAGCUG) used as endogenous gene in the other analysis. All the probes detect both mouse and human target genes. All RT-qPCR experiments were performed in an ABI Prism 7900HT Thermal Cycler (Applied Biosystems, Foster City, CA, USA).

The relative abundance of mRNA targets, normalized with the endogenous gene and relative to the control, is calculated as follows: Relative quantification (RQ) = 2−ΔΔCt; ΔCt (cycle threshold) = Ct (miRNA target) − Ct (miR-191-5p); ΔΔCt = [ΔCt (for any sample) − ΔCt (for the control)]. Amplification of miR-191-5p was used in the same reaction of all samples as an internal control.

2.10 | Western blot analysis

Proteins from cell lysates (20–40 μg), and tissue samples (60 μg) were separated on a 10% or 10%−20% gradient acrylamide gel and then transferred to a 0.45 μM pore PVDF membrane (Merck, Darmstadt, Germany) as previously described.[16,17] The primary antibodies used are shown in Table S2 and all of them were diluted in TTBS. Rabbit and mouse primary antibodies were immunodetected using horseradish peroxidase-conjugated anti-rabbit IgG (NA931V; 1:4000 in TTBS) or anti-mouse IgG secondary antibody (NA934V; 1:5000 in TTBS) (GE Healthcare, Buckinghamshire, UK), respectively. When

possible, phosphoproteins and their total expression were detected in the same gel, using Restore™ Western Blot Stripping Buffer (Thermo Fisher Scientific) as per the manufacturer's instructions, blocking the membrane again before the incubation with the next antibody. Loading was normalized by β-actin or α-tubulin. Protein bands were visualized using the SuperSignal™ West Pico PLUS Chemiluminescent Substrate (34580, Thermo Fisher Scientific®, Hercules, CA, USA). Band densitometry was analysed using ImageJ Software (v1.52a, Wayne Rasband, National Institute of Health, Stapleton, USA).

2.11 | Immunofluorescence

The coverslips were pretreated with 0.2% gelatin for 30 min at room temperature and rinsed twice with PBS 1X in a 24-well culture plate, then 15×10^3 HUVECs were seeded for transfection. After the 96 h transfection with pre-miR-15a-5p or/and pre-miR-199a-3p followed by a 1 h deprivation and the stimulation with 10 ng/mL TNF-α, the cells were rinsed twice with PBS 1X and fixed with 4% paraformaldehyde (252931.1214, PanReac AppliChem, ITW Reagents, Glenview, IL, USA) for 20 min, then the cells were rinsed twice with PBS 1X again and permeabilized with Triton X-100 0.5% and SDS 0.1% for 5 min each. Afterwards the cells were blocked with PBS 1X—4% BSA (A6588,0100, PanReac AppliChem, ITW Reagents, Glenview, IL, USA)—1.5% normal goat serum (1000 C, Invitrogen, Waltham, MA, USA) for 30 min at room temperature, then the p65 NF-κB primary antibody was diluted at 1:200 of the blocking buffer and was incubated at 4°C overnight. After the primary antibody incubation, the cells were rinsed three times with PBS 1X, and were then incubated with the secondary antibody 555 goat anti-rabbit (A32732, Invitrogen, Waltham, MA, USA) diluted at 1:500 and DAPI (A4099, Sigma-Aldrich, Darmstadt, Germany) at 1:1000 of the blocking buffer, for 1 h at room temperature. Finally, the cells were rinsed twice with PBS 1X and once with distilled water and the coverslips were mounted with ProLong™ Gold antifade reagent mounting medium (P36930, Invitrogen, Waltham, MA, USA) and inverted onto glass slides. The pictures were taken with a Nikon TE300 Inverted Phase Contrast DIC Fluorescence Microscope using a Nikon HB-10101AF super high pressure mercury lamp power supply and a Nikon digital sight camera and the Nikon NIS-elements F software (v 5.22.00 64-bit) and Fluorescence microscopy (Leica SP-2 AOBS). The co-localization of p65/DAPI and DAPI/p65 was calculated with the JaCoP plugin from the Image J-win64 Software to calculate the M1, M2 and Pearson's coefficients.

2.12 | Nuclear fractionation and extraction of proteins

HUVECs were maintained in MCDB-131 medium with 0.5% FBS for at least 18 h, then stimulated with TNF-α (10 ng/mL) for 10–40 min. Lysates of endothelial cells were resuspended in a buffer, which consisted of 10 mM HEPES (pH 7.8), 15 mM KCl, 2 mM $MgCl_2$, 0.1 mM EDTA, 1 mM dithiothreitol (DTT) and 1 mM phenylmethylsulfonyl fluoride. After 10 min on ice, the lysates were pelleted and resuspended in 2 volume of the buffer. Then, 3 M KCl was added dropwise to reach a 0.39 M KCl concentration. We extracted the nuclei from the cells with incubation for 1 h at 4°C followed by centrifugation at 12,000 × *g* for 1 h. The supernatants were then dialyzed in a buffer containing 50 mM HEPES (pH 7.8), 50 mM KCl, 0.1 mM EDTA, 1 mM DTT and 1 mM phenylmethylsulfonyl fluoride with 10% (v/v) glycerol. The samples were then cleared by centrifugation and stored at −80°C until further use. Total protein concentration was determined by the Bradford method (Thermo Fisher Scientific). We analysed the levels and phosphorylation of IκBα, IKKα and IKKβ in cytosolic fractions by Western blotting as described above. We measured p65 in the nuclear and cytosol fractions by Western blot studies. We used β-actin and histone H3 as control for total protein in cytosolic and nuclear fractions, respectively.

2.13 | Luciferase reporter assays

For reporter assays, a region of wild-type 3′-untranslated region (3′UTR) from *IKBKB* (miR-15a-5p), the 3′UTR from mutated *IKBKB* (miR-15a-5p), the wild-type 3′UTR from *IKBKB* (miR-199a-3p), the 3′UTR from mutated *IKBKB* (miR-199a-3p), the wild-type 3′UTR from *CHUK* (miR-15a-5p), the 3′UTR from mutated *CHUK* (miR-15a-5p), the wild-type 3′UTR from *RELA* (miR-199a-3p) and the 3′UTR from mutated *RELA* (miR-199a-3p) were constructed annealing the following primers:

3′UTR-*IKBKB* (miR-15a-5p) F: 5′-TCGAGACTGACCTCTTTTTATTTCACTGCTG CTATATTAAAAGGAGTATGC-3′ and 3′UTR-*IKBKB* (miR-15a-5p) R: 5′-GGCCGCA TACTCCTTTTAATATAGCAGCAGTGAAATAA AAAGAGGTCAGTC-3′; 3′UTR-*IKBKB* (miR-15a-5p) mutated. F: 5′-TCGAGACTGACCTCTTTTTATTTCACCCCTTTGCTATTAAA AGGAGTATGC-3′ and 3′UTR-*IKBKB* (miR-15a-5p) mutated. R: 5′-GGCCGC ATACTCCTTTTAATAGCAAAGGGGTGAAATAAAAAGAGGTCAGTC-3′.

3′UTR-*IKBKB* (miR-199a-3p) F: 5′-TCGAGACTGACCGCCTTGTCTGCACACTGGAGG TCCTCCATTTAT

TAAAAGGAGTATGC-3′ and 3′UTR-*IKBKB* (miR-199a-3p) R: 5′-GGCCGCATACTCCTTTTAATAAATGGAGGACCTCCAGTGTGCAGACAAGGCGGTCAGTC-3′; and 3′UTR-*IKBKB* (miR-199a-3p) mutated F: 5′-TCGAGACTGACCGGC GCCTTGTCTGCGAGGACCATATTAAAAGGAGTATGC-3′ and 3′UTR-*IKBKB* (miR-199a-3p) mutated R: 5′-GGCCGCATACTCCTTTTAATATGGTCCTCGCAGACAAGGCGCC GGTCAGTC-3′.

3′UTR-*CHUK* (miR-15a-5p) F: 5′-TCGAGACTGACGAATATTCCTTTATTTTGCTGCT TATTAAAAGGAGTATGC-3′ and 3′UTR-*CHUK* (miR-15a-5p) R: 5′-GGCCGCATA CTCCTTTTAATAAGCAGCAAAATAAAGGAATATTCGTCAGTC-3′; and 3′UTR-*CHUK* (miR-15a-5p) mutated F: 5′-TCGAGACTGACGAATATTCCTTTATTTCTGTAAGTAT TAAAAGGAGTATGC-3′ and 3′UTR-*CHUK* (miR-15a-5p) mutated R: 5′-GGCCGCATACT CCTTTTAATACTTACAGAAATAAAGGAATATTCGTCAGTC-3′.

3′UTR-*RELA* (miR-199a-3p) F: 5′-TCGAGACTGACAGGTGACAGTGCGGGACC CATCAGTATTAAAAGGAGTATGC-3′ and 3′UTR-*RELA* (miR-199a-3p) R: 5′-GGCCGCATACTCCTTTTAATACTGATGGGTCCCGC ACTGTCACCTGTCAGTC-3′; and 3′UTR-*RELA* (miR-199a-3p) mutated F: 5′-TCGAGACTGACAGGTGACAGTGCGG GACCAGGCCATATTAAAAGGAGTATGC-3′ and 3′UTR-*RELA* (miR-199a-3p) mutated R: 5′-GGCCGCATACTCCTTTTAATATGGCCTGGTCCCGCACTGTCACCTGTCAGTC-3′.

Annealing was conducted by incubating both primers for 4 min at 95°C and for 10 min at 70°C in annealing buffer (100 mM potassium acetate, 30 mM HEPES, pH 7.4 and 2 mM magnesium acetate). Primers were then phosphorylated and cloned into the psiCHECK2 vector from Promega digested with *Xho*I and *Not*I.

Thirty thousand HEK293 cells were plated in DMEM containing 10% FBS. Twenty-four hours later, cells were transfected with the psiCHECK2 vectors either with pre-miR control, pre-miR-15a-5p or pre-miR-199a-5p using lipofectamine (Invitrogen) following the manufacturer's instructions. The luciferase reporter assay was performed 72 h after transfection using the Dual-Glo Luciferase Kit (Promega, Madison, WI, USA).

The ratio between the firefly and the *Renilla* luciferase allows the normalization of luciferase values. Ratios were normalized against the ratio of the corresponding plasmid transfected with the miR-Control. Statistical differences were determined using unpaired *t*-test.

2.14 | Extraction of exosomes of plasma from patients with ACA and controls

To precipitate the exosomes from the plasma samples the total exosome RNA and protein isolation kit (from plasma) (4478545, Thermo Fisher Scientific, Waltham, MA, USA), were used following the protocol recommended by the manufacturer. First, the plasma was clarified with one centrifugation at 2000 × *g* for 20 min, and a second centrifugation at 10,000 × *g* for 20 min, in both cases the supernatant was collected, and the pellet was discharged. When the plasma was ready, we added 0.5 volume of PBS 1X and 0.2 volume of the Exosome Precipitation Reagent (from plasma) (4484451, Thermo Fisher Scientific, Waltham, MA, USA) mixing until the sample becomes cloudy, at this point the mix was incubated for 30 min on ice followed by a centrifugation at 10,000 × *g* for 30 min at room temperature. The pellet containing the exosomes was used to extract the miRNAs following the mirVanaTM miRNA Isolation Kit. To confirm the pellet was enriched in exosomes a diffuse light scattering analysis and Western blot analysis of CD81, CD63 and GM130 markers were performed.

2.15 | Database search to find miRNAs and their possible targets

The miRNAs analysed in the study were identified by an extensive search in PubMed by using the terms (miRNAs, atherosclerosis and inflammation, NF-κB) and GEO Database. Once the miRNAs of interest were selected, the possible mRNA targets were evaluated in predictive miRNA-target interaction databases such as, TargetScan, miRWalk, miRDB and the experimentally validated miRNA-target interaction database: miRTarBase. The data collected from these databases were analysed, and only those targets that appeared in two or more of the predictive databases or just in miTarBase were considered as possible targets. A diagram showing the proposed regulatory axes during atherosclerosis progression is supplied in Figure S5. These representations were made using Cytoscape 3.8.2. software (v.3.8.2. on Java 11.0.6. by AdoptOpenJDK, Darmstadt, Germany) and the online tool http://www.interactivenn.net/ was used to generate the Venn diagram with the target results of each database.

2.16 | Statistical analysis

The data from the experimental groups were analysed using the GraphPad Prism v8.2.1 software (GraphPad Software, San Diego, CA, USA). Normality and lognormality tests were performed to confirm that the data followed a normal distribution. Statistical significance of the differences between groups was assessed by Student's *t*-tests when comparing two groups, or with ANOVA tests followed by a Bonferroni post hoc test when comparing

more than two groups. Correlation between variables was assessed by two-tailed Spearman's *r* correlation analyses. The exact *p* value is indicated in each figure when it reached statistically significance ($p < .05$).

Receiver operating characteristic (ROC) analyses were performed to test the diagnostic accuracy of the evaluated miRNAs. All statistical procedures were performed using the GraphPad Prism v8.2.1 software (GraphPad Software, San Diego, CA, USA).

3 | RESULTS

3.1 | miR-15a-5p and miR-199a-3p levels are decreased in human atherosclerotic carotid plaque

We aimed to identify miRNAs involved in human atherosclerosis progression. For that purpose, we collected vascular samples from control subjects (CAs), subjects with fibrolipidic plaque (FAs) and patients with human advanced atherosclerosis undergoing carotid endarterectomy (ACA) (Table S1). First, we performed Masson trichrome staining, and we could distinguish the media region in aortas from CAs and FAs and media, fibrous and shoulders in carotid from ACA (Figure S1). The histological analysis showed that complicated plaques from ACA contained an intraplaque haemorrhage with a higher percentage of inflammatory cells and/or a certain degree of calcification. The adjacent non-complicated regions showed a variable content of VSMCs and fibrous thickening (Figure S1).

PubMed and GEO Databases were used to perform a search of miRNAs that could play a role in the inflammation during atherosclerosis progression. We selected and analysed 20 miRNAs involved in inflammation and metabolic diseases such as NAFLD and atherosclerosis, from that screening we selected and further study four miRNAs, miR-9-5p, miR-15a-5p, miR-16-5p and miR-199a-3p that were involved in NF-κB pathway. Finally, we deepened in the study of miR-15a-5p and miR-199a-3p because both showed a similar behaviour in vascular samples from human and experimental atherosclerosis. In serial sections of samples used for histological characterization, we isolated and analysed miRNAs levels showing that miR-15a-5p expression was significantly downregulated in ACA patients compared with the other two groups, miR-16-5p and miR-199a-3p expressions were significantly decreased in ACA patients in relation to FAs subjects (Figure 1A). In contrast, miR-9-5p expression was upregulated in ACA patients compared with Controls and FAs, but without reaching statistical significance.

3.2 | miR-15a-5p and miR-199a-3p levels are downregulated in aorta from *ApoE*$^{-/-}$ mice

We further analysed the levels of the four miRNAs studied in human atherosclerosis in the hyperlipidemic model of atherosclerosis of *ApoE*$^{-/-}$ mice under HFD. The first step was to confirm that *ApoE*$^{-/-}$ mice gained body weight, showed increased visceral and subcutaneous adiposity in addition to hypertriglyceridemia and hypercholesterolemia (Figure S2A–C) in comparison with Control STD, being significantly higher in *ApoE*$^{-/-}$ mice fed with HFD for 18 weeks. Moreover, we observed a significant increase in lesion area in *ApoE*$^{-/-}$ mice under HFD for 18 weeks versus Control STD and *ApoE*$^{-/-}$ STD of the same age by en face analysis of ORO-stained whole aorta (Figure S2D).

A screening of four miRNAs was performed in the aorta of all the experimental groups (Figure 1B and Figure S3). We observed that miR-15a-5p and miR-199a-3p levels were significantly decreased in *ApoE*$^{-/-}$ mice after 18 weeks of HFD or STD compared with WT STD mice (Figure 1B); showing a higher decrease in aorta from *ApoE*$^{-/-}$ HFD 18 wks. Moreover, a significant decrease of miR-16-5p was also noted in *ApoE*$^{-/-}$ HFD in relation to WT STD (Figure 1B). However, we did not observe any significant change in miR-9-5p levels at 18 weeks (Figure 1B) as well as in those miRNAs studied in aorta of the three groups at 8 weeks of diet (Figure S3).

In addition, we established correlations between atherosclerosis progression (percentage lipid accumulation/aorta area or percentage lesion area/total area) and miR-15a-5p or miR-199-3p levels. We observed a significant and negative correlation between miR-15a-5p or miR-199a-3p levels and percentage lesion area or percentage lipid accumulation (Figures S4A, S4B, S4C and S4D, respectively).

Since miR-15a-3p and miR-199a-3p were altered in the same way in human and murine atherosclerosis, we focused on the study of both miRNAs and their targets in vivo and in vitro (Figure S5).

3.3 | IKKα, IKKβ and p65 expression is modulated by both miRNAs

First, in PubMed and GEO Databases we studied the possible targets of both miRNAs regarding the inflammation, concisely, proteins involved in NF-κB pathway (Figure S5C,D). We found as possible candidates: IKKα,[18] IKKβ[18] and p65.[18–20]

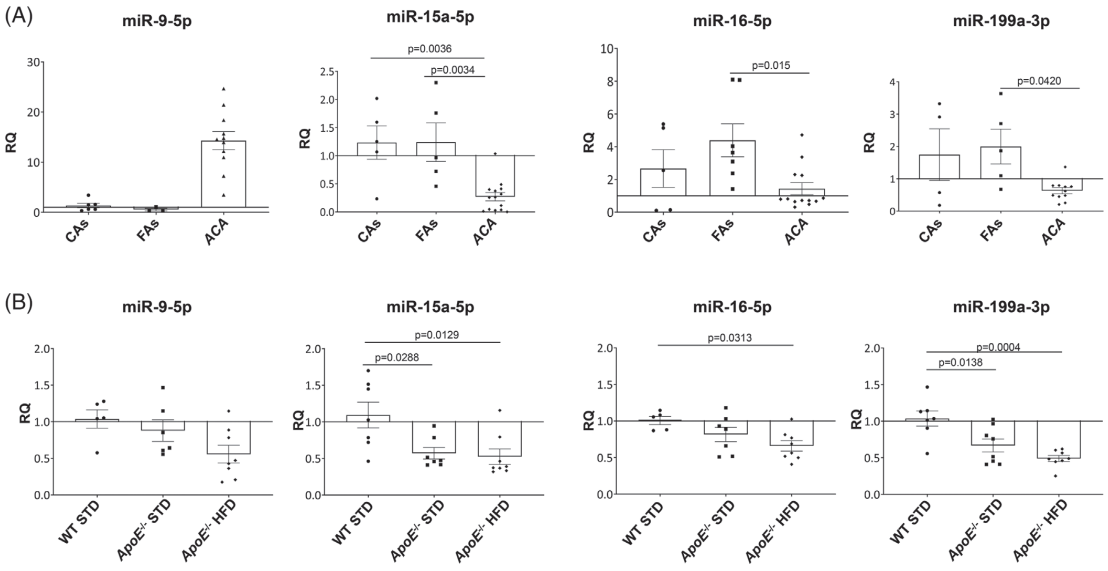

FIGURE 1 The expression of miR-9-5p, miR-15a-5p, miR-16-5p and miR-199a-3p is altered in human and experimental atherosclerosis. Relative expression of miR-9-5p (left), miR-15a-5p (middle left), miR-16-5p (middle right) and miR-199a-3p (right) in vascular human samples (A) and in the aorta of the experimental groups submitted to 18 weeks of diet (B) was measured by qPCR. Amplification of miR-191-5p was used in the same reaction of all samples as an internal control. ACA, advanced carotid atherosclerotic plaque patients; *ApoE*$^{-/-}$, *ApoE* deficient mice; CAs, control subjects; FAs, fibrolipidic plaque subjects; HFD, high-fat diet; STD, standard type diet; WT, wild-type group. qPCR miR-9-5p: WT STD ($n = 5$); *ApoE*$^{-/-}$ STD ($n = 6$); *ApoE*$^{-/-}$ HFD ($n = 8$); CAs ($n = 6$); FAs ($n = 3$); ACA ($n = 11$). qPCR miR-15a-5p: WT STD ($n = 7$); *ApoE*$^{-/-}$ STD ($n = 7$); *ApoE*$^{-/-}$ HFD ($n = 8$); CAs ($n = 5$); FAs ($n = 5$); ACA ($n = 14$). qPCR miR-16-5p: WT STD ($n = 5$); *ApoE*$^{-/-}$ STD ($n = 7$); *ApoE*$^{-/-}$ HFD ($n = 8$); CAs ($n = 5$); FAs ($n = 7$); ACA ($n = 13$). qPCR miR-199a-3p: WT STD ($n = 7$); *ApoE*$^{-/-}$ STD ($n = 8$); *ApoE*$^{-/-}$ HFD 18 weeks ($n = 8$); CAs ($n = 4$); FAs ($n = 5$); ACA ($n = 11$).

Second, we checked whether their targets expression was altered in human and experimental atherosclerosis. Then, by immunohistochemistry we analysed the protein levels of IKKβ, IKKα and p65 in human vascular samples (Figure 2) and confirmed a significant increase of IKKα, IKKβ and p65 in vascular samples from ACA in relation to CAs or subjects with early atherosclerosis (Figures 2A, 2B, 2C and 2D, respectively). Moreover, we established a significant and inverse correlation between miR-15a-5p and its three targets (IKKα, IKKβ and p65) (Figure 2E).

After that, by Western blot analysis, we demonstrated a significant increase in IKKα and p65 in aorta from *ApoE*$^{-/-}$ HFD mice and consequently a decrease of IκBα (Figure 3A,B). Moreover, by immunohistochemistry a significant increase of IKKβ was noted in aorta from both *ApoE*$^{-/-}$ mice, being clearly higher in *ApoE*$^{-/-}$ under HFD (Figure 3C,D). In Western blot studies the increase of IKKβ did not reach statistical significance (Figure 2A,B).

Moreover, we have demonstrated that p65 is expressed by endothelial cells and VSMCs in aortic roots, mainly in *ApoE*$^{-/-}$ HFD mice (Figures S6 and S7). More importantly, there is a strong increase of p65 in the nucleus, indicating NF-κB activation. For these reasons, we have focused and deepened into the role of both miRNAs and its modulation in inflammation, specifically regarding NF-κB activation through different in vitro experiments in HUVECs and VSMCs.

3.4 | Overexpression of miR-15a-5p and miR-199a-3p reduced NF-κB activation in endothelial cells

To explore whether the overexpression of miR-15a-5p and/or miR-199a-3p might reduce NF-κB activation and consequently the inflammation present in the atherosclerotic process, HUVECs were transfected with the pre-miR-15a-5p or pre-miR-199a-3p. First, we confirmed that when HUVECs were transfected with pre-miR-15a-5p or pre-miR-199a-3p for 72 h, we obtained the overexpression of miR-15a-5p (Figure 4A) or miR-199a-3p (Figure 4C), respectively. After that, when we transfected with pre-miR-15a-5p for 96 h, we observed a significant decrease in the protein levels of IKKα, IKKβ and p65 (Figure 4B). In

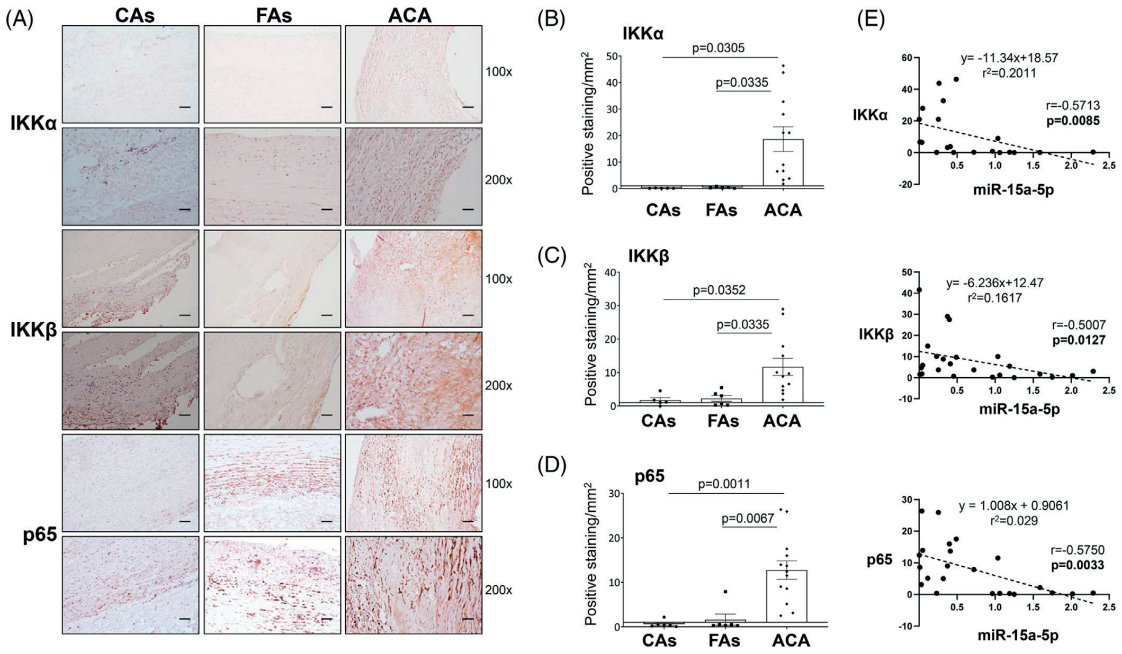

FIGURE 2 The expression of IKKα, IKKβ and p65 is upregulated in human aorta. (A) Representative images from the immunohistochemistry of IKKα (upper panels), IKKβ (middle panels) and p65 (lower panels). Magnification 100× (scale bar = 100 μm); magnification 200× (scale bar = 50 μm). The expression of IKKα (B, left), IKKβ (C, left) and p65 (D, left) was measured and the relation with miR-15a-5p expression (B, C and D, right) was tested by a Spearman's correlation. ACA, advanced carotid atherosclerotic plaque patients; CAs, control subjects; FAs, fibrolipidic plaque subjects; IKKα, inhibitor of nuclear factor kappa-B kinase subunit alpha; IKKβ, inhibitor of nuclear factor kappa-B kinase subunit beta; p65, transcription factor p65. Measurement of IKKα: CAs (n = 5); FAs (n = 5); ACA (n = 12). Measurement of IKKβ: CAs (n = 4); FAs (n = 6); ACA (n = 12). Measurement of p65: CAs (n = 6); FAs (n = 6); ACA (n = 13). Correlation between IKKα and miR-15a-5p (n = 20), between IKKβ and miR-15a-5p (n = 24) and between p65 and miR-15a-5p (n = 23).

the same way, when HUVECs were transfected with pre-miR-199a-3p for 96 h, a significant reduction of IKKβ, p65 and IκBα was noted (Figure 4D). By immunofluorescence, overexpression of miR-15a-5p or miR-199a-3p significantly reduced p65 expression in HUVECs (Figure 5A,B).

Next, we analysed whether the overexpression of miR-15a-5p or miR-199a-3p was able to reduce NF-κB activation. One of the mechanisms implicated in the activation of NF-κB is the IKK complex activation by phosphorylation of IKKα and IKKβ. TNF-α is widely used as an inductor of NF-κB activation. For this reason, HUVECs were stimulated with 10 ng/mL TNF-α at different times (10 to 40 min, see Figure S8) and we analysed the phosphorylation of IKK complex as well as the phosphorylation and translocation to the nucleus of p65 and the degradation of IκBα. So, we checked that 10 ng/mL TNF-α for 10 min provoked the phosphorylation of IKKα/β (Figure S8A), a decrease of IκBα levels (Figure S8C,D), the phosphorylation and the translocation into the nucleus of p65 (Figure S8B,D). First, we confirmed that miR-15a-5p or miR-199a-3p overexpression significantly reduced the phosphorylation and the activation of IKKα/β induced by 10 ng/mL TNF-α (Figure S9). After that, by immunofluorescence we also observed that miR-15a-5p or miR-199a-3p overexpression significantly decreased the translocation of p65 into the nucleus due to a lesser M1 and M2 Mander's coefficient (Figure 5A,C,D) as well as Pearson's Correlation (Figure 5A,E).

3.5 | Overexpression of miR-15a-5p and miR-199a-3p reduced ox-LDL uptake and NF-κB activation in vascular smooth muscle cells

The next objective was to study whether the overexpression of miR-15a-5p or miR-199a-3p might interfere in LDL uptake and inflammation in VSMCs. For this aim, VSMCs were transfected for 72 h with pre-miR-15a-5p or pre-miR-199a-3p and we observed a significant increase of

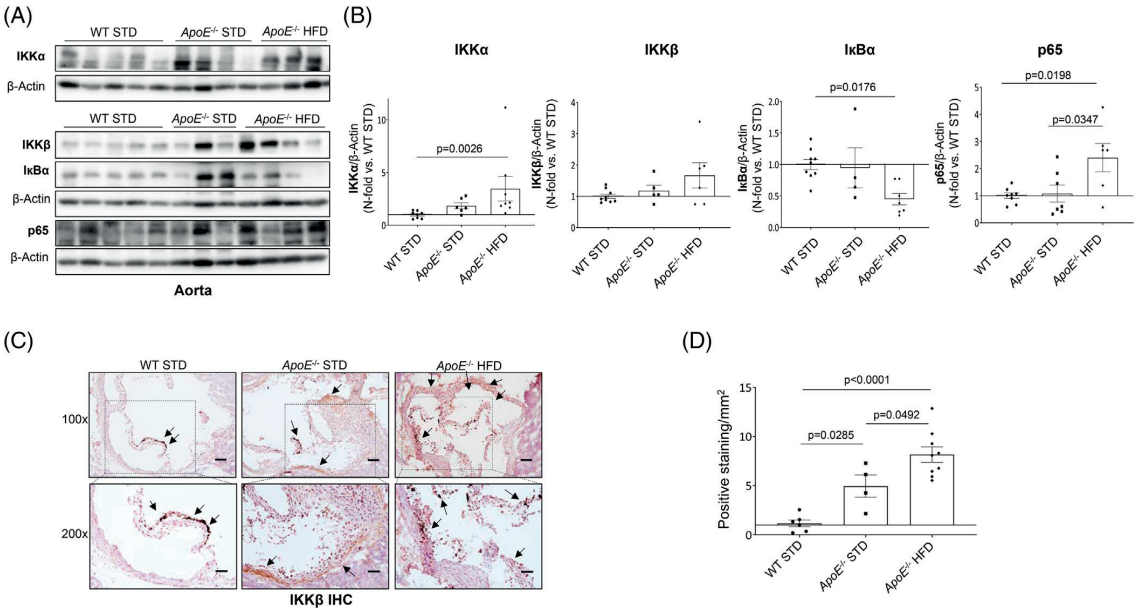

FIGURE 3 The expression of IKKα, IKKβ and p65 is upregulated in the aorta from *ApoE*$^{-/-}$ mice by HFD. (A) Representative Western blot images from the aorta of the three groups. (B) Measurement of the levels of IKKα, IKKβ, IκBα and p65 by Western blot in the aorta of the experimental groups submitted to 18 weeks of diet. (C) Representative images from the immunohistochemistry of IKKβ in the aortic root of the experimental groups. Magnification 100× (scale bar = 100 μm); magnification 200× (scale bar = 50 μm). (D) IKKβ expression was measured by immunohistochemistry. *ApoE*$^{-/-}$, *ApoE* deficient mice; HFD, high-fat diet; IHC, immunohistochemistry; IκBα, nuclear factor kappa-B kinase inhibitor alpha; IKKα, inhibitor of kappa-B kinase subunit alpha; IKKβ, inhibitor of kappa-B kinase subunit beta; p65, transcription factor p65; STD, standard type diet; WT, wild-type group. Measurement of IKKα: WT STD ($n = 8$); *ApoE*$^{-/-}$ STD ($n = 6$); *ApoE*$^{-/-}$ HFD ($n = 7$). Measurement of IKKβ by Western blot: WT STD ($n = 9$); *ApoE*$^{-/-}$ STD ($n = 5$); *ApoE*$^{-/-}$ HFD ($n = 6$). Measurement of IκBα: WT STD ($n = 9$); *ApoE*$^{-/-}$ STD ($n = 4$); *ApoE*$^{-/-}$ HFD ($n = 7$). Measurement of p65: WT STD ($n = 8$); *ApoE*$^{-/-}$ STD ($n = 7$); *ApoE*$^{-/-}$ HFD ($n = 6$). Measurement of IKKβ by IHC: WT STD ($n = 6$); *ApoE*$^{-/-}$ STD ($n = 4$); *ApoE*$^{-/-}$ HFD ($n = 9$).

miR-15a-5p or miR-199a-3p by qRT-PCR (Figures 6A and 6B, respectively). After that, we demonstrated that the overexpression of miR-15a-5p or miR-199a-3p reduced ox-LDL uptake by VSMCs (Figure 6C). One of the mechanisms that might explain this result could be that miR-15a-5p or miR-199a-3p regulate LOX-1 that is involved in ox-LDL uptake by VSMCs. In this sense, we have shown a significant increase of LOX-1 protein levels in ACA plaques (Figure S10A). Moreover, we found that LOX-1 was expressed by VSMCs in human plaques and in aortic roots mainly from *ApoE*$^{-/-}$ HFD mice (Figures S10B and S11A, respectively). And finally, we demonstrate that miR-15a-5p overexpression significantly reduces LOX-1 protein levels (Figure S11B).

Moreover, as occurs in HUVECs, we also confirmed in VSMCs that the overexpression of miR-15a-5p or miR-199a-3p reduced IKKβ and p65 protein levels (Figure 7A,B). In this sense, we found that the overexpression of miR-15a-5p significantly reduced the NF-κB activation induced by TNF-α (Figure 7C).

3.6 | Regulation of IKBKB and CHUK expression through the direct interaction of miR-15a-5p or miR-199a-3p with their 3′UTR sequence

We performed experiments based on luciferase constructs to demonstrate the direct interaction of miR-15a-5p and miR-199a-3p with the 3′UTRs of p65, IKKβ and IKKα mRNAs (Figure S12). Our results demonstrate a direct and specific interaction of miR-15a-5p with the 3′UTR of IKBKB (IKKβ) and CHUK (IKKα) mRNAs and miR-199a-3p with the 3′UTR of IKBKB (IKKβ) mRNA. However, we did not find any change regarding the interaction of miR-199a-3p with the 3′UTR of RELA mRNA.

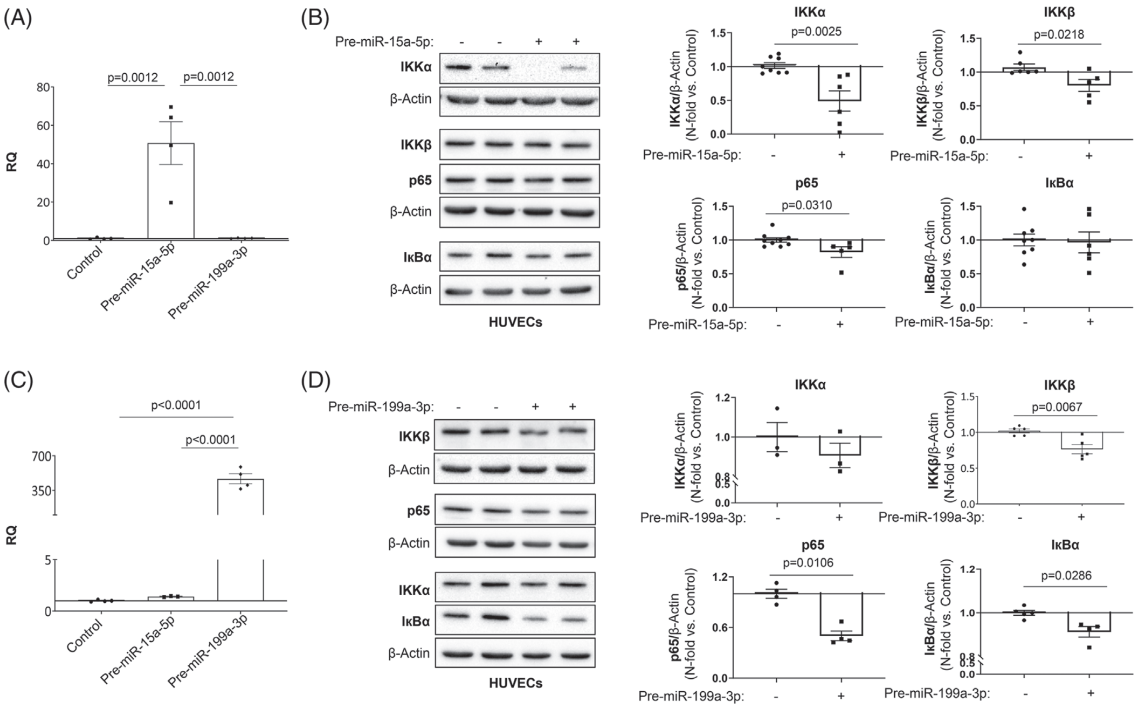

FIGURE 4 miR-15a-5p and miR-199a-3p overexpression reduced IKKα, IKKβ and p65 expression in endothelial cells. HUVECs were transfected with miR-15a-5p (A) or miR-199a-3p (C) precursors for 72 h. The increase in miRNA expression was measured by qPCR. The silencing effect miR-15a-5p or miR-199a-3p has on their targets IKKα (upper left) and IKKβ (upper right), as well as p65 (lower left) and IκBα (lower right), was analysed by Western blot 96 h after transfection (B and D, respectively). All the in vitro experiments were performed at least in triplicate. HUVECs, human umbilical vascular endothelial cells; IκBα, nuclear factor kappa-B kinase inhibitor alpha; IKKα, inhibitor of nuclear factor kappa-B kinase subunit alpha; IKKβ, inhibitor of nuclear factor kappa-B kinase subunit beta; p65, transcription factor p65. qPCR miR-15a-5p: Control ($n = 4$); Pre-miR-15a-5p ($n = 4$); Pre-miR-199a-3p ($n = 4$). qPCR miR-199a-3p: Control ($n = 4$); Pre-miR15a-5p ($n = 4$); Pre-miR-199a-3p ($n = 4$). Measurement of miR-15a-5p effect on IKKα: Control ($n = 8$), Pre-miR-15a-5p ($n = 6$); effect on IKKβ: Control ($n = 5$), Pre-miR-15a-5p ($n = 5$); effect on p65: control ($n = 9$); Pre-miR-15a-5p ($n = 5$); effect on IκBα: control ($n = 8$); Pre-miR-15a-5p ($n = 6$). Measurement of miR-199a-3p effect on IKKα: Control ($n = 3$), Pre-miR-199a-3p ($n = 3$); effect on IKKβ: Control ($n = 5$), Pre-miR-199a-3p ($n = 5$); effect on p65: Control ($n = 4$); pre-miR-199a-3p ($n = 4$); effect on IκBα: Control ($n = 5$); pre-miR-199a-3p ($n = 4$).

3.7 | miR-15a-5p and miR-199a-3p as biomarkers of advanced atherosclerosis

Finally, trying to find novel miRNAs as possible diagnostic biomarkers for advanced atherosclerosis, we isolated miRNAs from plasma extracellular vesicles (EVs) from patients with ACA and Controls without atherosclerosis (see Table S1). To confirm whether the isolated EVs from plasma could be enriched in exosomes, we analysed the presence of the exosome markers CD63 antigen and CD81 antigen and the absence of Golgi subfamily A member 2 (GM130), a Golgi vesicle marker. We did not find GM130 in the isolated EVs compared to a positive control (HUVECs lysate) but we did find CD63 and CD81 expression (Figure 8A). In addition, we obtained that the diameter of the isolated EVs measured by DLS was between 10 and 106 nm, most exosomes having a diameter of 21.04–50.8 nm (Figure 8B). These findings support that the isolated EVs were enriched in exosomes.

Regarding circulating miRNA expression, we observed a significant increase of miR-15a-5p and miR-199a-3p (Figure 8C) in patients with ACA in relation to CAs. To evaluate their putative role as a diagnostic biomarker in advanced atherosclerosis, we performed ROC analyses (Figure 8D). For miR-15a-5p, the area under the curve was 0.8951 with a p value of 0.0028. The optimal cut-off value for advanced atherosclerosis diagnosis was an RQ of 1.278 or higher, with a sensitivity of 88.89% and a specificity of 83.33% (Figure 8C). For miR-199a-3p, the area under the curve was 0.7895 with a p value of .0506 (Figure 8D).

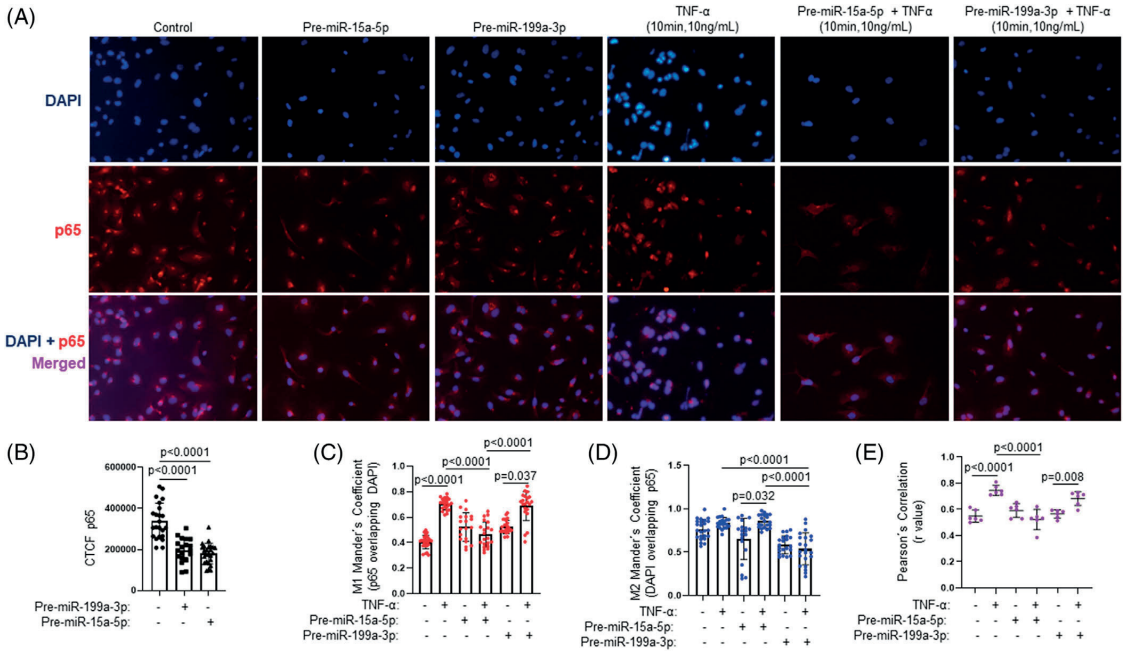

FIGURE 5 miR-15a-5p and miR-199a-3p reduced the activation of p65 in endothelial cells. HUVECs were stimulated with TNFα with or without pre-miR-15a-5p, pre-miR-199a-3p or both, and the activation of p65 was measured by immunofluorescence. (A) Representative images from the immunofluorescence of p65 (red) contrasted with DAPI (blue) and merged (purple). (B) The intensity of fluorescence of p65 was measured in all the conditions. Since p65 is active in the nucleus, the JaCoP plugin from Fiji was used to quantify the co-localization of p65 and DAPI by three values: the M1 (C) and M2 (D) Mander's coefficient, and the Pearson's correlation (E) of each picture. In all cases, the closer the value is to 1, the more co-localization. All the in vitro experiments were performed at least in triplicate. CTCF, corrected total cell fluorescence; p65, transcription factor p65; TNFα, tumour necrosis factor alpha. Measurement of p65 CTCF: Control ($n = 23$), Pre-miR-199a-3p ($n = 25$); Pre-miR-15a-5p ($n = 19$). Measurement of M1 Mander's coefficient: Control ($n = 26$), TNFα ($n = 22$), Pre-miR-199a-3p ($n = 24$); Pre-miR-199a-3p + TNFα ($n = 21$), Pre-miR-15a-5p ($n = 19$); Pre-miR-15a-5p + TNFα ($n = 21$). Measurement of M2 Mander's coefficient: Control ($n = 24$), TNFα ($n = 21$), Pre-miR-199a-3p ($n = 21$); Pre-miR-199a-3p + TNFα ($n = 22$), Pre-miR-15a-5p ($n = 20$); Pre-miR-15a-5p + TNFα ($n = 21$). Measurement of Pearson's correlation: Control ($n = 6$), TNFα ($n = 6$), Pre-miR-199a-3p ($n = 6$); Pre-miR-199a-3p + TNFα ($n = 6$), Pre-miR-15a-5p ($n = 6$); Pre-miR-15a-5p + TNFα ($n = 6$).

Finally, when we performed ROC analysis with both miRNAs simultaneously, the p value improved ($p = .0004$), although the sensitivity and the specificity were similar as compared with ROC analysis with only miR-15a-5p (Figure 8D).

4 | DISCUSSION

Atherosclerosis is a disease that develops over several decades of life in an asymptomatic way, but when it progresses, it becomes one of the main causes of cardiovascular mortality, causing acute coronary syndrome or stroke.[21] The development of acute events is mostly produced not by the complete stenosis of the vessel but because stable atherosclerotic plaques become unstable, favouring their rupture and the formation of a thrombus that can be occlusive and generate ischemia in that artery.[22]

For these reasons, it is of great interest to develop new strategies that allow the clinician to identify the presence of vulnerable plaques. More importantly, the identification of new markers or panels of new markers could make it possible to detect the change from stable to unstable plaques and the consequent increase in cardiovascular risk. In this context, the identification of miRNAs as disease mediators and new biomarkers are being widely studied in different metabolic diseases and could also be very useful in CVDs.[23,24] In this work, we have focused on four miRNAs, miR-9-5p, miR-15a-5p, miR-16-5p and miR-199a-3p, which we have considered of special relevance due to their involvement in inflammation,[18] being one of the key events in the progression and instability of the atherosclerotic plaques. An increased presence of inflammatory cells,

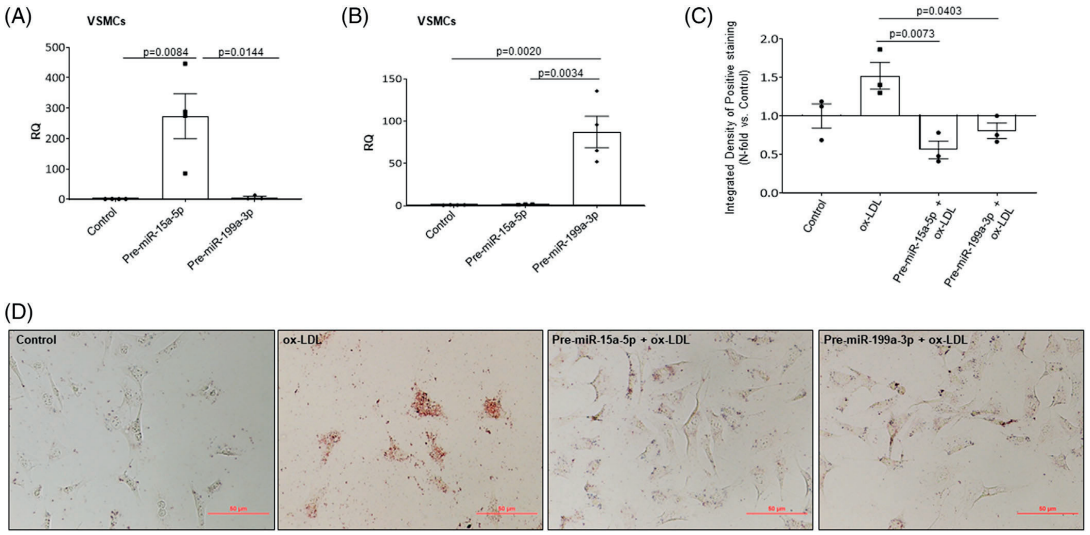

FIGURE 6 miR-15a-5p and miR-199a-3p overexpression reduced ox-LDL uptake in VSMCs. VSMCs were transfected with miR-15a-5p (A) and miR199a-3p (B) precursors for 48 h and the increase in miRNA expression was measured by qPCR. In the last 24 h of transfection, the cells were treated with ox-LDL and then stained with Oil Red O. Quantification of measured the uptake of ox-LDLs by VSMCs (C) and representative images from Oil Red O staining (D). All the in vitro experiments were performed at least in triplicate. ox-LDL, oxidized low-density lipoprotein; VSMCs, vascular smooth muscle cells. qPCR miR-15a-5p: Control ($n = 4$); Pre-miR-15a-5p ($n = 4$); Pre-miR-199a-3p ($n = 3$). qPCR miR-199a-3p: Control ($n = 4$); Pre-miR-15a-5p ($n = 3$); Pre-miR-199a-3p ($n = 4$). Measurement of ox-LDL uptake: Control ($n = 3$), ox-LDL ($n = 3$); Pre-miR-15a-5p + ox-LDL ($n = 3$); Pre-miR-199a-3p + ox-LDL ($n = 3$).

such as M1 macrophages, T lymphocytes, dendritic cells and eosinophils, has been found in symptomatic patients and in the vulnerable shoulder area of human carotid plaques.[25,26]

From the four miRNAs studied, the most consistent results between human and mice atherosclerosis were for miR-15a-5p and miR-199a-3p. In human atherosclerosis, significant decreases of miR-15a-5p and miR-199a-3p were observed in advanced human atherosclerotic carotid plaques. Similarly, other authors had previously demonstrated a downregulation of miR-199a/b-3p in human atherosclerotic coronary arteries.[27] In the experimental atherosclerosis model, we also found reduced levels of miR-15a-5p and miR-199a-3p in the aorta of $ApoE^{-/-}$ STD or HFD. In this sense, other study revealed that the levels of miR-199a-3p were diminished in aortas from mice with atherosclerosis.[28] It should be noted that both miR-15a-5p and miR-199a-3p decreases were significantly higher as the disease progressed. Thus, the greatest decreases were found in the carotids from patients with advanced atherosclerosis and in the aorta from $ApoE^{-/-}$ mice subjected to HFD for 18 weeks. Moreover, in the experimental model we established a significant and inverse correlation between the levels of both miRNAs and percentage of lesion area and percentage of lipid depot in aortic roots. These results suggest the involvement of both miRNAs in the progression of atherosclerosis. In this sense, it has been described that serum levels of miR-199a-3p negatively correlated with the carotid intima-media thickness and C reactive protein in patients with atherosclerosis.[29] In addition, miR-199a-3p levels were decreased in the peripheral blood of T2DM patients and were associated with the progression of the disease.[30]

There is a vast number of potential target genes regulated by miR-15a-5p or/and miR-199a-3p, which are involved in atherosclerosis, lipid metabolism and inflammation, including mTOR,[31] ET-1,[27] YAP,[32] CXCL11,[33] CD44,[34] MAP3K4,[35] p65,[36] IKKα/β,[37] ICAM-1[38] and p85α.[39] In addition to review of the literature, we performed in silico studies to determine possible targets of both miRNAs related to the inflammation, specifically, with proteins involved in NF-κB pathway. We found as possible candidates: IKKα, IKKβ and p65. First, we confirmed elevated levels of IKKα, IKKβ and p65 in the aorta from $ApoE^{-/-}$ HFD 18 weeks and in carotids from patients with ACA. In VSMCs and HUVECs, we confirmed that overexpression of miR-15a-5p and/or miR-199a-3p reduced the protein levels of IKKα, IKKβ and p65 as well as NF-κB activation, evaluated as lower degradation of IκBα and translocation of p65 to the nucleus. Similar to our

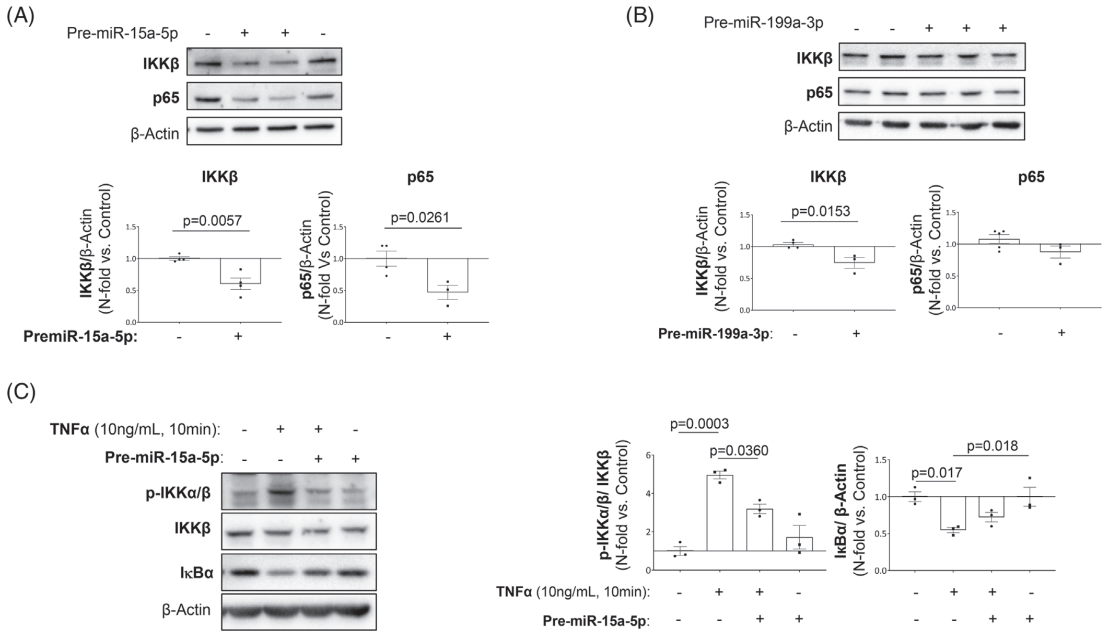

FIGURE 7 Effect of miR-15a-5p and miR-199a-3p overexpression in the expression of their targets in VSMCs. miR-15a-5p reduced IKKβ and p65 expression and IKKα and IKKβ activity while increasing IκBα, and miR-199a-3p reduced IKKβ expression in VSMCs. The silencing effect miR-15a-5p has on their targets (A) IKKβ (lower left), as well as p65 (lower right) was analysed by Western blot 48 h after transfection. The silencing effect miR-199a-3p has on their targets (B) IKKβ (lower left) and p65 (lower right) was analysed by Western blot 48 h after transfection. To test the effect on IKKα and IKKβ activity the VSMCs were pretreated with 0% FBS culture medium after the 48 h transfection and stimulated with TNFα for 10 min. (C) The activation of the proteins was analysed by the Western blot of their phosphorylated forms (left graph), and the expression of IκBα (right graph) was also analysed by Western blot. All the in vitro experiments were performed at least in triplicate. IκBα, nuclear factor kappa-B kinase inhibitor alpha; IKKα, inhibitor of nuclear factor kappa-B kinase subunit alpha; IKKβ, inhibitor of nuclear factor kappa-B kinase subunit beta; p65, transcription factor p65; TNFα, tumour necrosis factor alpha. Measurement of miR-15a-5p effect on IKKβ: Control ($n = 4$), PremiR-15a-5p ($n = 4$), effect on p65: Control ($n = 4$); Pre-miR-15a-5p ($n = 3$). Measurement of miR-199a-3p effect on IKKβ: Control ($n = 4$), Pre-miR-199a-3p ($n = 3$). Measurement of miR-199a-3p effect on p65: Control ($n = 5$); Pre-miR-199a-3p ($n = 3$). Measurement of miR-15a-5p effect on IKKβ and IKKα activity: Control ($n = 3$), TNFα ($n = 3$); Pre-miR-15a-5p + TNFα ($n = 3$); Pre-miR-15a-5p ($n = 3$). Measurement of miR-15a-5p effect on IκBα expression: Control ($n = 3$), TNFα ($n = 3$); Pre-miR-15a-5p + TNFα ($n = 3$); Pre-miR-15a-5p ($n = 3$).

results, other authors have found that overexpression of miR-199a-3p suppresses NF-κB signalling in cervical epithelial cells[40] increasing the migration, proliferation and autophagy of HUVECs, potentially through the regulation of PI3K/AKT/NF-κB pathway.[30] On the other hand, the miR-199a-3p restrained inflammation by downregulating RUNX1 in macrophages[18] and deactivated STAT3 signalling in macrophages under ox-LDL treatment.[41] All these results point to and reinforce the idea that miR-199a-3p could have a protective role in the vascular endothelium and in the reduction of inflammation in the progression of atherosclerosis. In addition, our results also demonstrate that miR-15a-5p could have a new atheroprotective role by decreasing NF-κB activation (Figure 9).

Continuing with the idea of the protective role of miR-199a-3p in the development of atherosclerosis, there are other authors who describe the regulation of other targets that could be involved in the vascular dysfunction and angiogenesis. So, in human atherosclerotic coronary arteries other authors observed a significant upregulation of ET-1 and downregulation of miR-199a/b-3p.[27] Neovascularization as angiogenesis in atherosclerotic lesions is a key factor in plaque growth and instability.[42] Therefore, in atherosclerotic regions, hypoxia and local inflammation may induce intraplaque angiogenesis through growth and angiogenic factors, lipoproteins, MMPs and oxidized lipids.[43,44] In this context, miR-199a-3p has been described as a hypoxia-related miRNA and can induce angiogenesis.[45] Moreover, miR-199a-3p was related with

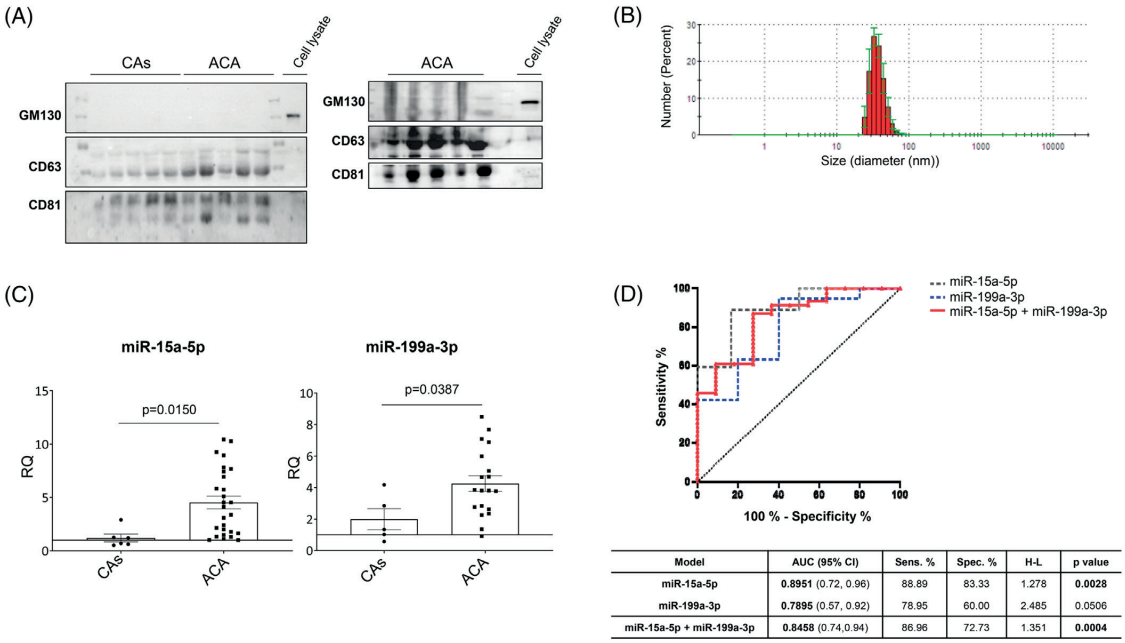

Model	AUC (95% CI)	Sens. %	Spec. %	H-L	p value
miR-15a-5p	**0.8951** (0.72, 0.96)	88.89	83.33	1.278	**0.0028**
miR-199a-3p	**0.7895** (0.57, 0.92)	78.95	60.00	2.485	0.0506
miR-15a-5p + miR-199a-3p	**0.8458** (0.74,0.94)	86.96	72.73	1.351	**0.0004**

FIGURE 8 miR-15a-5p and miR-199a-3p are overexpressed in the plasmatic EVs of advance carotid atherosclerotic patients, and miR-15-5p may be a potential biomarker of the disease. To test whether miR-15a-5p and miR-199a-3p could be biomarkers of advanced atherosclerosis, we precipitated EVs from the plasma of healthy donors and advanced carotid atherosclerosis patients. Once the EVs were precipitated from the plasma, and in order to confirm that the pellet was enriched in exosomes, we performed the (A) Western blot of a negative exosomal biomarker, the Golgi membrane protein GM-130; and two common markers from the exosomal membrane: CD63 and CD81, with a cell lysate as a control; and we also performed a DLS analysis of the samples (B) to confirm that the EVs were in the correct size range of exosomes. Afterwards the miRNAs were isolated from the exosomes and then the levels of miR-15a-5p and miR-199a-3p (C) were analysed by qPCR. The validity of the miR-15a-5p and miR-199a-3p (D) was confirmed by a ROC curve. ACA, advanced carotid atherosclerotic plaque patients; CAs, control subjects; ROC, receiver operating characteristic. qPCR of miR-15a-5p: CAs ($n = 6$), ACA ($n = 27$). qPCR of miR-199a-3p: CAs ($n = 5$); ACA ($n = 19$). ROC curve miR-15a-5p ($n = 34$) and ROC curve miR-199a-3p ($n = 25$).

markers of angiogenesis including neuropilin-1, angiogenin and galectin-3.[46]

We also demonstrated that both miRNAs regulate the function of VSMCs. Thus, we observed a differential expression of miR-15a-5p or miR-199a-3p in patients with initial or advanced atherosclerosis. In fibrolipidic plaques, the levels of both miRNAs were very similar or slightly higher than controls whereas in advanced atherosclerosis, there was a significant decrease of both miRNAs. This would fit with the protective role of both miRNAs. In early stages, miRNAs could be overexpressed as an atheroprotective mechanism, regulating different targets involved in the migration and proliferation of VSMCs to reduce vessel stenosis. Thus, it has been described that miR-199a-3p overexpression inhibited VSMCs migration and proliferation mediated by its target, SP1.[29] In the current manuscript, we have demonstrated that miR-15a-5p or miR-199a-3p overexpression reduces the levels of theirs targets, IKKβ and p65 as well as NF-κB activation contributing to a significant reduction of the inflammation produced by VSMCs. Moreover, an important percentage of foam cells could come from VSMCs that have lost specific markers of their contractile function and have gained membrane receptors, having a phenotype similar to macrophages, which allows them to capture modified LDL.[47] In this sense, it has been described that VSMCs contain LOX-1 as an endogenous ox-LDL receptor that mediates the NF-κB activation.[48] According to this, we have also found elevated LOX-1 protein levels in atherosclerotic carotid plaques from patients with ACA and in the aortic roots from *ApoE*$^{-/-}$ HFD mice and even, a higher number of VSMCs expressed LOX-1 in both samples.

In in silico studies, we have obtained that one of the targets of miR-15a-5p is LOX-1 and on the other hand, miR-15a-5p or miR-199a-3p overexpression reduced ox-LDL uptake in VSMCs. Therefore, we demonstrated that miR-15a-5p overexpression downregulate LOX-1 protein levels and in consequence VSMCs could uptake lower

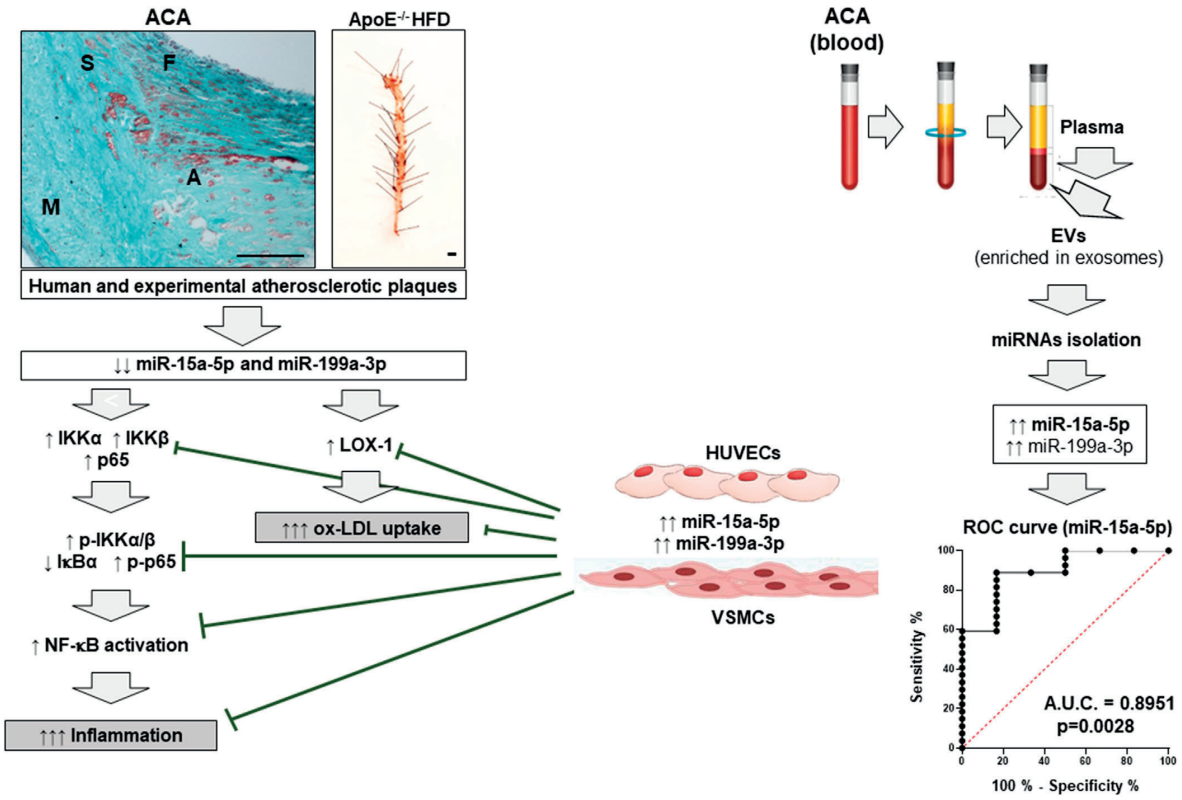

FIGURE 9 Role of miR-15a-5p and miR-199a-3p in the human and experimental atherosclerosis. The levels of miR-15a-5p and miR-199a-3p were significantly increased in carotid from patients with advanced atherosclerosis (ACA) and in the aortas from *ApoE*$^{-/-}$ HFD. These decreases of both miRNAs provoke a significant increase of their potential targets' expression, such as: IKKα, IKKβ and p65 as well as their phosphorylation in consequence a higher IκBα degradation and NF-κB activation, contributing to the inflammation present in advanced atherosclerosis. On the other hand, the decrease of miR-15a-5p and miR-199a-3p produce a significant increase of LOX-1 that might favour ox-LDL uptake in VSMCs. More importantly, in vascular cell lines, HUVECs and VSMCs, we demonstrated that miR-15a-5p or miR-199a-3p overexpression reduced protein levels of their studied targets in consequence the decline of NF-κB activation and ox-LDL uptake. Moreover, we isolated miRNAs from EVs (enriched exosomes) of patients with advanced atherosclerosis and healthy controls and a significant increase of both miRNAs in EVs from ACA was noted, whereas only miR-15a-5p might be useful as biomarker of advanced atherosclerosis.

ox-LDL, having both miRNAs an anti-foaming role in VSMCs. In the case of miR-199a-3p might be by the down-regulation of other endogenous ox-LDL receptors but this anti-foaming role of miR-199a-3p have previously been described in macrophages.[28]

Our results indicate that circulating miR-15a-5p levels are higher in patients with ACA, and ROC analyses suggesting a potential role for advanced atherosclerosis non-invasive diagnosis. In this sense, a previous study also showed high miR-15a-5p levels in plasma from patients with stable coronary artery disease (CAD) compared with controls.[49] More importantly, other authors have established a positive correlation between miR-15a-5p and coronary necrotic core as marker of plaque vulnerability in plaques from patients with CAD, while the exercise intervention induced a regression of coronary plaque burden and normalized miR-15a-5p levels.[50] Other authors have also demonstrated that elevated circulating levels of miR-15a-5p along with miR-34a-5p and miR-374-5p in patients with aneurysmal subarachnoid haemorrhage, are potential biomarkers in aneurysmal rupture.[51] There are more studies in the literature that support that miR-15a-5p might also be a biomarker of coronary heart disease (CHD).[52,53] In one of them, the authors used direct S-Poly(T)Plus method for CHD diagnosis and determined that miR-15a-5p and miR-199a-3p together to other 10 miRNAs could be used for diagnosis of CHD.[52] In this sense, Vegter et al.[46] demonstrated that miR-199a-3p levels are related to angiogenesis markers in patients with heart failure. Moreover, there was a correlation between miR-199a-3p and galectin-3 in patients with acute heart failure that might be due to the importance of cardiac remodelling and fibrosis in heart

failure.[54] In the current work, we also obtained a significantly higher level of miR-199a-3p in patients with ACA in relation to controls, being the *p* value of ROC curve close to statistical significance, potentially related to the small number of human samples included in this analysis.

5 | CONCLUSIONS

In summary, our results demonstrate a novel role for miR-15a-5p and miR-199a-3p in atherosclerosis progression. Both miRNAs have anti-inflammatory role due to regulation of their targets involved NF-κB pathway in addition of anti-foaming role in VSMCs. Finally, miR-15a-5p might be useful for diagnosis of ACA.

ACKNOWLEDGEMENTS

This research was funded by grants RTI-2018-095098-B100 and PID2021-123076OB-I00 from Ministerio de Ciencia e Innovación y Universidades, Santander-UCM PR75/18-21572, UCM AENC1/22-29754 given to Almudena Gómez-Hernández and Óscar Escribano. Paula González-López was funded by Programa Operativo de Empleo Juvenil from Comunidad de Madrid. We want to thank Dr. Jean-Baptiste Michel for the transfer of human infradiaphragmatic aortic segments from control subjects and subjects with fibrolipidic lesions. Each of them was harvested from a different donor after organ transplantation with the authorization of the French Biomedicine Agency. We also thank to Alba Cebrecos for her technical assistance.

CONFLICT OF INTEREST STATEMENT

The authors declare no conflicts of interest.

ORCID

Óscar Escribano https://orcid.org/0000-0002-8249-1645
Almudena Gómez-Hernández https://orcid.org/0000-0002-2742-4298

REFERENCES

1. Roth GA, Mensah GA, Fuster V. The global burden of cardiovascular diseases and risks: a compass for global action. *J Am Coll Cardiol*. 2020;76(25):2980-2981. doi:10.1016/j.jacc.2020.11.021
2. Hetherington I, Totary-Jain H. Anti-atherosclerotic therapies: milestones, challenges, and emerging innovations. *Mol Ther*. 2022;30(10):3106-3117. doi:10.1016/j.ymthe.2022.08.024
3. Gimbrone MA Jr, García-Cardeña G. Endothelial cell dysfunction and the pathobiology of atherosclerosis. *Circ Res*. 2016;118(4):620-636. doi:10.1161/CIRCRESAHA.115.306301
4. Mitra R, O'Neil GL, Harding IC, Cheng MJ, Mensah SA, Ebong EE. Glycocalyx in atherosclerosis-relevant endothelium function and as a therapeutic target. *Curr Atheroscler Rep*. 2017;19(12):63. doi:10.1007/s11883-017-0691-9
5. Chiorescu RM, Mocan M, Inceu AI, Buda AP, Blendea D, Vlaicu SI. Vulnerable atherosclerotic plaque: is there a molecular signature? *Int J Mol Sci*. 2022;23(21):13638. doi:10.3390/ijms232113638
6. Cho KY, Miyoshi H, Kuroda S, et al. The phenotype of infiltrating macrophages influences arteriosclerotic plaque vulnerability in the carotid artery. *J Stroke Cerebrovasc Dis*. 2013;22(7):910-918. doi:10.1016/j.jstrokecerebrovasdis.2012.11.020
7. Henkel T, Machleidt T, Alkalay I, Krönke M, Ben-Neriah Y, Baeuerle PA. Rapid proteolysis of I kappa B-alpha is necessary for activation of transcription factor NF-kappa B. *Nature*. 1993;365(6442):182-185. doi:10.1038/365182a0
8. Ritchie ME. Nuclear factor-kappaB is selectively and markedly activated in humans with unstable angina pectoris. *Circulation*. 1998;98(17):1707-1713. doi:10.1161/01.cir.98.17.1707
9. Gómez-Hernández A, Sánchez-Galán E, Ortego M, et al. Effect of intensive atorvastatin therapy on prostaglandin E2 levels and metalloproteinase-9 activity in the plasma of patients with non-ST-elevation acute coronary syndrome. *Am J Cardiol*. 2008;102(1):12-18. doi:10.1016/j.amjcard.2008.02.090
10. Martín-Ventura JL, Blanco-Colio LM, Muñoz-García B, et al. NF-kappaB activation and Fas ligand overexpression in blood and plaques of patients with carotid atherosclerosis: potential implication in plaque instability. *Stroke*. 2004;35(2):458-463. doi:10.1161/01.STR.0000114876.51656.7A
11. Martín-Ventura JL, Blanco-Colio LM, Gómez-Hernández A, et al. Intensive treatment with atorvastatin reduces inflammation in mononuclear cells and human atherosclerotic lesions in one month. *Stroke*. 2005;36(8):1796-1800. doi:10.1161/01.STR.0000174289.34110.b0
12. Bartel DP. Metazoan MicroRNAs. *Cell*. 2018;173(1):20-51. doi:10.1016/j.cell.2018.03.006
13. Cordes KR, Sheehy NT, White MP, et al. miR-145 and miR-143 regulate smooth muscle cell fate and plasticity. *Nature*. 2009;460(7256):705-710. doi:10.1038/nature08195
14. Zhang H, Xue S, Feng Y, Shen J, Zhao J. MicroRNA-24-3p inhibition prevents cell growth of vascular smooth muscle cells by targeting Bcl-2-like protein 11. *Exp Ther Med*. 2020;19(4):2467-2474. doi:10.3892/etm.2020.8517
15. Stary HC, Chandler AB, Glagov S, et al. A definition of initial, fatty streak, and intermediate lesions of atherosclerosis. A report from the Committee on Vascular Lesions of the Council on Arteriosclerosis, American Heart Association. *Circulation*. 1994;89(5):2462-2478. doi:10.1161/01.cir.89.5.2462
16. González-López P, Ares-Carral C, López-Pastor AR, et al. Implication of miR-155-5p and miR-143-3p in the vascular insulin resistance and instability of human and experimental atherosclerotic plaque. *Int J Mol Sci*. 2022;23(18):10253. doi:10.3390/ijms231810253
17. Gómez-Hernández A, Escribano Ó, Perdomo L, et al. Implication of insulin receptor A isoform and IRA/IGF-IR hybrid receptors in the aortic vascular smooth muscle cell proliferation: role of TNF-α and IGF-II. *Endocrinology*. 2013;154(7):2352-2364. doi:10.1210/en.2012-2161
18. Ma X, Buscaglia LEB, Barker JR, Li Y. MicroRNAs in NF-kappaB signaling. *J Mol Cell Biol*. 2011;3(3):159-166. doi:10.1093/jmcb/mjr007
19. Liu Z, Tao B, Li L, Liu P, Xia K, Zhong C. LINC00511 knockdown suppresses glioma cell malignant progression through

miR-15a-5p/AEBP1 axis. *Brain Res Bull*. 2021;173:82-96. doi:10.1016/j.brainresbull.2021.05.010

20. Zeng N, Huang YQ, Yan YM, et al. Diverging targets mediate the pathological roleof miR-199a-5p and miR-199a-3p by promoting cardiac hypertrophy and fibrosis. *Mol Ther Nucleic Acids*. 2021;26:1035-1050. doi:10.1016/j.omtn.2021.10.013
21. Stefanadis C, Antoniou CK, Tsiachris D, Pietri P. Coronary atherosclerotic vulnerable plaque: current perspectives. *J Am Heart Assoc*. 2017;6(3):1-18. doi:10.1161/JAHA.117.005543
22. Silvain J, Collet JP, Nagaswami C, et al. Composition of coronary thrombus in acute myocardial infarction. *J Am Coll Cardiol*. 2011;57(12):1359-1367. doi:10.1016/j.jacc.2010.09.077
23. Brandão-Lima PN, Carvalho GB, Payolla TB, Sarti FM, Rogero MM. Circulating microRNA related to cardiometabolic risk factors for metabolic syndrome: a systematic review. *Metabolites*. 2022;12(11):1044. doi:10.3390/metabo12111044
24. López-Pastor AR, Infante-Menéndez J, Escribano Ó, Gómez-Hernández A. miRNA dysregulation in the development of non-alcoholic fatty liver disease and the related disorders type 2 diabetes mellitus and cardiovascular disease. *Front Med*. 2020;7:527059. doi:10.3389/fmed.2020.527059
25. Galkina E, Ley K. Immune and inflammatory mechanisms of atherosclerosis (*). *Annu Rev Immunol*. 2009;27:165-197. doi:10.1146/annurev.immunol.021908.132620
26. Erbel C, Sato K, Meyer FB, et al. Functional profile of activated dendritic cells in unstable atherosclerotic plaque. *Basic Res Cardiol*. 2007;102(2):123-132. doi:10.1007/s00395-006-0636-x
27. Hao L, Wang XG, Cheng JD, et al. The up-regulation of endothelin-1 and down-regulation of miRNA-125a-5p, -155, and -199a/b-3p in human atherosclerotic coronary artery. *Cardiovasc Pathol*. 2014;23(4):217-223. doi:10.1016/j.carpath.2014.03.009
28. Liu M, Cao Y, Hu Y, et al. MiR-199a-3p restrains foaming and inflammation by regulating RUNX1 in macrophages. *Mol Biotechnol*. 2022;64(10):1130-1142. doi:10.1007/s12033-022-00484-2
29. Sun X, Zhang Y, Liu Z, Li S, Wang L. MicroRNA-199a-3p exhibits beneficial effects in asymptomatic atherosclerosis by inhibiting vascular smooth muscle cell proliferation and migration. *Mol Biotechnol*. 2021;63(7):595-604. doi:10.1007/s12033-021-00323-w
30. Wang H, Wang Z, Tang Q. Reduced expression of microRNA-199a-3p is associated with vascular endothelial cell injury induced by type 2 diabetes mellitus. *Exp Ther Med*. 2018;16(4):3639-3645. doi:10.3892/etm.2018.6655
31. Kurdi A, De Meyer GR, Martinet W. Potential therapeutic effects of mTOR inhibition in atherosclerosis. *Br J Clin Pharmacol*. 2016;82(5):1267-1279. doi:10.1111/bcp.12820
32. Liu M, Yan M, Lv H, et al. Macrophage K63-linked ubiquitination of YAP promotes its nuclear localization and exacerbates atherosclerosis. *Cell Rep*. 2020;32(5):107990. doi:10.1016/j.celrep.2020.107990
33. Kameda M, Otsuka M, Chiba H, et al. CXCL9, CXCL10, and CXCL11; biomarkers of pulmonary inflammation associated with autoimmunity in patients with collagen vascular diseases-associated interstitial lung disease and interstitial pneumonia with autoimmune features. *PLoS One*. 2020;15(11):e0241719. doi:10.1371/journal.pone.0241719
34. Krolikoski M, Monslow J, Puré E. The CD44-HA axis and inflammation in atherosclerosis: a temporal perspective. *Matrix Biol*. 2019;78-79:201-218. doi:10.1016/j.matbio.2018.05.007
35. Zhou H, Simion V, Pierce JB, Haemmig S, Chen AF, Feinberg MW. LncRNA-MAP3K4 regulates vascular inflammation through the p38 MAPK signaling pathway and cis-modulation of MAP3K4. *FASEB J*. 2021;35(1):e21133. doi:10.1096/fj.202001654RR
36. Mallavia B, Recio C, Oguiza A, et al. Peptide inhibitor of NF-κB translocation ameliorates experimental atherosclerosis. *Am J Pathol*. 2013;182(5):1910-1921. doi:10.1016/j.ajpath.2013.01.022
37. Ortego M, Gómez-Hernández A, Vidal C, et al. HMG-CoA reductase inhibitors reduce I kappa B kinase activity induced by oxidative stress in monocytes and vascular smooth muscle cells. *J Cardiovasc Pharmacol*. 2005;45(5):468-475. doi:10.1097/01.fjc.0000159042.50488.e5
38. Peng M, Sun R, Hong Y, et al. Extracellular vesicles carrying proinflammatory factors may spread atherosclerosis to remote locations. *Cell Mol Life Sci*. 2022;79(8):430. doi:10.1007/s00018-022-04464-2
39. Ruan Z, Chu T, Wu L, et al. miR-155 inhibits oxidized low-density lipoprotein-induced apoptosis in different cell models by targeting the p85α/AKT pathway. *J Physiol Biochem*. 2020;76(2):329-343. doi:10.1007/s13105-020-00738-0
40. Peng J, Jiang J, Wang H, Feng X, Dong X. miR199a3p suppresses cervical epithelial cell inflammation by inhibiting the HMGB1/TLR4/NFκB pathway in preterm birth. *Mol Med Rep*. 2020;22(2):926-938. doi:10.3892/mmr.2020.11184
41. Vasamsetti SB, Karnewar S, Kanugula AK, Thatipalli AR, Kumar JM, Kotamraju S. Metformin inhibits monocyte-to-macrophage differentiation via AMPK-mediated inhibition of STAT3 activation: potential role in atherosclerosis. *Diabetes*. 2015;64(6):2028-2041. doi:10.2337/db14-1225
42. Camaré C, Pucelle M, Nègre-Salvayre A, Salvayre R. Angiogenesis in the atherosclerotic plaque. *Redox Biol*. 2017;12:18-34. doi:10.1016/j.redox.2017.01.007
43. Carmeliet P, Jain RK. Molecular mechanisms and clinical applications of angiogenesis. *Nature*. 2011;473(7347):298-307. doi:10.1038/nature10144
44. Ho-Tin-Noé B, Michel JB. Initiation of angiogenesis in atherosclerosis: smooth muscle cells as mediators of the angiogenic response to atheroma formation. *Trends Cardiovasc Med*. 2011;21(7):183-187. doi:10.1016/j.tcm.2012.05.007
45. Pencheva N, Tran H, Buss C, et al. Convergent multi-miRNA targeting of ApoE drives LRP1/LRP8-dependent melanoma metastasis and angiogenesis. *Cell*. 2012;151(5):1068-1082. doi:10.1016/j.cell.2012.10.028
46. Vegter EL, Ovchinnikova ES, van Veldhuisen DJ, et al. Low circulating microRNA levels in heart failure patients are associated with atherosclerotic disease and cardiovascular-related rehospitalizations. *Clin Res Cardiol*. 2017;106(8):598-609. doi:10.1007/s00392-017-1096-z
47. Durham AL, Speer MY, Scatena M, Giachelli CM, Shanahan CM. Role of smooth muscle cells in vascular calcification: implications in atherosclerosis and arterial stiffness. *Cardiovasc Res*. 2018;114(4):590-600. doi:10.1093/cvr/cvy010
48. Kang DH, Choi M, Chang S, et al. Vascular proteomics reveal novel proteins involved in SMC phenotypic change: oLR1 as a SMC receptor regulating proliferation and inflammatory response. *PLoS One*. 2015;10(8):e0133845. doi:10.1371/journal.pone.0133845

49. Sullivan JF, Neylon A, McGorrian C, Blake GJ. miRNA-93-5p and other miRNAs as predictors of coronary artery disease and STEMI. *Int J Cardiol*. 2016;224:310-316. doi:10.1016/j.ijcard.2016.09.016
50. Taraldsen MD, Wiseth R, Videm V, Bye A, Madssen E. Associations between circulating microRNAs and coronary plaque characteristics: potential impact from physical exercise. *Physiol Genomics*. 2022;54(4):129-140. doi:10.1152/physiolgenomics.00071.2021
51. Kang D, Supriya M, Christopher R, Devi BI, Bhat DI, Shukla D. Circulating microRNAs as potential molecular biomarkers for intracranial aneurysmal rupture. *Mol Diagn Ther*. 2020;24(3):351-364. doi:10.1007/s40291-020-00465-8
52. Su M, Niu Y, Dang Q, et al. Circulating microRNA profiles based on direct S-Poly(T)Plus assay for detection of coronary heart disease. *J Cell Mol Med*. 2020;24(11):5984-5997. doi:10.1111/jcmm.15001
53. Zhu Y, Yang T, Duan J, Mu N, Zhang T. MALAT1/miR-15b-5p/MAPK1 mediates endothelial progenitor cells autophagy and affects coronary atherosclerotic heart disease via mTOR signaling pathway. *Aging*. 2019;11(4):1089-1109. doi:10.18632/aging.101766
54. Vegter EL, Schmitter D, Hagemeijer Y, et al. Use of biomarkers to establish potential role and function of circulating microRNAs in acute heart failure. *Int J Cardiol*. 2016;224:231-239. doi:10.1016/j.ijcard.2016.09.010

SUPPORTING INFORMATION

Additional supporting information can be found online in the Supporting Information section at the end of this article.

How to cite this article: González-López P, Álvarez-Villarreal M, Ruiz-Simón R, et al. Role of miR-15a-5p and miR-199a-3p in the inflammatory pathway regulated by NF-κB in experimental and human atherosclerosis. *Clin Transl Med*. 2023;13:e1363. https://doi.org/10.1002/ctm2.1363

Dear Dr Gisterå:

I am pleased to inform you that your manuscript, Dysregulation of micro-RNA 143-3p as a biomarker of carotid atherosclerosis and the associated immune reactions during disease progression, has been accepted for publication in the Journal of Cardiovascular Translational Research. For queries regarding your accepted paper, please contact Mr. David Seidenfeld at [mailto:david.seidenfeld@springer.com].

Please include your manuscript number, CATR-D-23-00514R1, whenever inquiring about your manuscript.

Thank you for your time and effort in writing for JCTR.

Respectfully,

Enrique Lara-Pezzi Ph.D.

Editor-in-Chief, JCTR

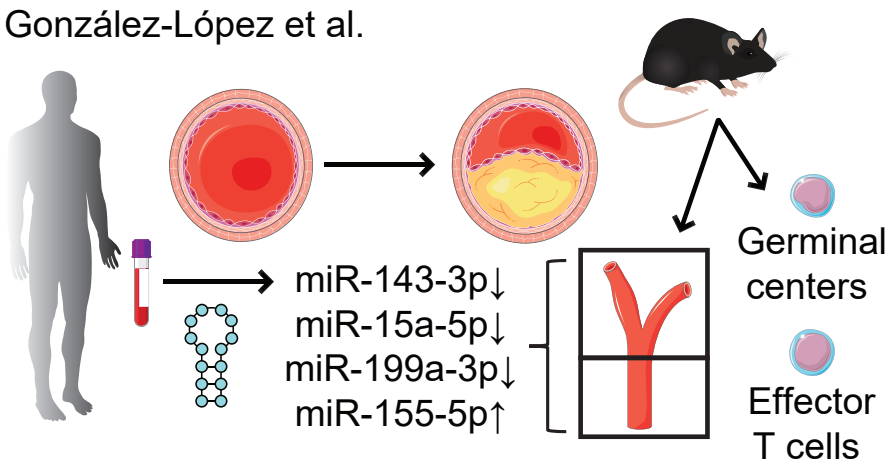

MicroRNAs in plasma extracellular vesicles can serve as biomarkers for atherosclerosis in humans. In mice, low levels of miR-143-3p are an early indicator of carotid disease and dysregulation of microRNAs is closely linked to the immune reactions associated with atherosclerosis.

Dysregulation of micro-RNA 143-3p as a biomarker of carotid atherosclerosis and the associated immune reactions during disease progression

Paula González-López MSc[1], Yinda Yu MSc[2], Shiying Lin MSc[2], Óscar Escribano PhD[1,3], Almudena Gómez-Hernández PhD[1], Anton Gisterå MD PhD[2†]

[1]Department of Biochemistry and Molecular Biology, Faculty of Pharmacy, Complutense University of Madrid, Madrid, Spain

[2]Department of Medicine Solna, Center for Molecular Medicine, Karolinska University Hospital, Karolinska Institutet, Stockholm, Sweden

[3]Centro de Investigación Biomédica en Red de Diabetes y Enfermedades Metabólicas Asociadas (CIBERdem), Instituto de Salud Carlos III, Madrid, Spain

[†]**Corresponding author**: Anton Gisterå, Bioclinicum J8:20, Karolinska University Hospital, Visionsgatan 4, SE-17164 Solna, Stockholm, Sweden, anton.gistera@ki.se, +46705378678

Short title: miR-143-3p in atheroprogression

Type: Original Article, 5 figures

Word count: 5981 (including references, figures, and references)

Abbreviations

HuBL = human *APOB100*-transgenic *Ldlr*$^{-/-}$

miRNA = micro ribonucleic acids

PD1 = programmed cell death protein 1

RQ = relative quantification

T_{EM} cells = T effector/memory cells

Abstract

Atherosclerosis commonly remains undiagnosed until disease manifestations occur. The disease is associated with dysregulated micro(mi)RNAs, but how this is linked to atherosclerosis-related immune reactions is largely unknown. A mouse model of carotid atherosclerosis, human *APOB100*-transgenic *Ldlr*$^{-/-}$ (HuBL), was used to study the spatiotemporal dysregulation of a set of miRNAs. Middle-aged HuBL mice with established atherosclerosis had decreased levels of miR-143-3p in their carotid arteries. In young HuBL mice, early atherosclerosis was observed in the carotid bifurcation, which had lower levels of miR-15a-5p, miR-143-3p, and miR-199a-3p, and higher levels of miR-155-5p. The dysregulation of these miRNAs was reflected by specific immune responses during atheroprogression. Finally, levels of miR-143-3p were 70.6% lower in extracellular vesicles isolated from the plasma of patients with carotid stenosis compared to healthy controls. Since miR-143-3p levels progressively decrease when transitioning between early and late experimental carotid atherosclerosis, we propose it as a biomarker for atherosclerosis.

Keywords: Atherosclerosis, micro-RNA, carotid stenosis, dyslipidemia, T-lymphocytes

Introduction

Immune-vascular interactions drive the atherosclerotic process, along with hemodynamic turbulence at predilection sites such as the carotid bifurcation [1, 2]. This leads to the buildup of plaque in the carotid arteries, which is a major risk factor for ischemic stroke that causes morbidity and neurological sequelae. As atherosclerosis is increasingly asymptomatic [3], there is a demand for early non-invasive biomarkers to initiate and motivate lifestyle improvements. Early diagnosis and monitoring of treatment responses using biomarkers could become even more important when novel therapeutic approaches are introduced.

The dysregulation of miR-143-3p has been implicated in carotid atherosclerosis and related vascular diseases [4-9]. miR-143-3p is a small, non-coding RNA molecule that plays a crucial role in the regulation of a broad range of target genes, such as *Elk1* mRNA [10]. In individuals with carotid artery plaques, the expression of miR-143-3p is downregulated [6, 8] but conflicting results regarding its effects and regulation exist from experimental models and observational studies [11-15]. Due to proximity, miR-143 is co-transcribed with miR-145, and these are among the highest expressed miRNAs in the medial layer of the vessel wall [4]. Laminar flow induces the expression of miR-143 in endothelial cells and upstream regulators are serum response factor, homeobox protein Nkx-2.5, myocardin, and transforming growth factor-β signaling [10, 16]. miR-143-3p can be packaged and released extracellularly in microvesicles and exert atheroprotective effects in vascular cells or be secreted in the circulation [16]. Injections of extracellular vesicles containing miR-143-3p may reduce the progression of atherosclerosis in mice [17]. In smooth muscle cells, miR-143-3p represses proliferation and maintains cellular contractility by suppressing transcriptional regulators important for de-differentiation to a synthetic cell state [5, 10]. However, the regulation of miR-143 in immune cells during atheroprogression has not been explored. Further

knowledge of this regulation is important since local and systemic shifts in miRNA levels occurring during atheroprogression have broad regulatory consequences.

In this regard, miRNAs have been proposed not only as modulators of the disease but also as potential early- or late-stage biomarkers of atherosclerosis. Therefore, we wanted to study the alteration of miR-15a-5p, miR-143-3p, miR-155-5p, and miR-199a-3p in mouse carotids and immune cells; and as a proof-of-principle, investigate if miR-143-3p is a potential biomarker of late-stage human carotid atherosclerosis. Our previous studies showed that miR-155-5p was upregulated, while miR-15a-5p, miR-143-3p, and miR-199a-3p were downregulated in human and experimental atherosclerosis and have proposed miR-15a-5p and miR-199a-3p as biomarkers of advanced human carotid atherosclerosis [8, 18]. In the present study, we propose the downregulation of miR-143-3p as a potential non-invasive biomarker of the disease. A mouse model of carotid atherosclerosis sheds further light upon the dysregulation of the above-mentioned set of miRNAs in carotid atherosclerosis and their associations with immune reactions. The data indicate that miR-143-3p reflects early atherosclerosis as well as atheroprogression and that its expression is associated with immune processes not limited to the vessel wall.

Material and Methods

Human samples

Plasma samples from healthy donors (n=13) and patients with advanced carotid atherosclerosis (n=28) were analyzed. Sample collection and extracellular vesicle isolation were previously described [18], and the use of this cohort was extended by analyzing miR-143-3p levels. Patients were 67 ±10 years old (see Table S1 for more details).

Mouse experiments

Human *APOB100*-transgenic *Ldlr*^{tm1Her} (HuBL) and *Ldlr*^{tm1Her} mice, both on C57BL/6J background, were used. Mice were fed a standard chow diet (2018 Teklad global 18% protein rodent diet, Envigo) and water ad libitum, and were maintained in conventional light, humidity, and heat conditions. Female mice were sacrificed at 11 and 46 weeks of age and male mice were sacrificed at 52 weeks of age. Spectral flow cytometry was performed using fluorophore-conjugated antibodies (Table S2). RNA was analyzed using real-time PCR (Table S3). See the Supplemental Material and Methods for more details.

Statistics

Data are presented with scatter dot plots with mean and standard deviation. The Mann-Whitney test was used for the comparison of two groups. Data normality was assessed using the Shapiro-Wilk test. Calculations were performed in GraphPad Prism 9.5.1.

Results

Decreased miR-143-3p in advanced carotid atherosclerosis

miRNAs in extracellular vesicles were isolated from plasma samples of patients with advanced carotid atherosclerosis and donors without manifested atherosclerosis to assess the relative levels of miR-143-3p by real-time PCR. Median miR-143-3p levels were 70.6% lower in the plasma of patients with carotid stenosis (Fig. 1a). No significant difference was observed in terms of sex and diabetes (Fig. S1). A receiver operating characteristic curve analysis showed an area under the curve of 0.79 (p=.0027) and a cut-off value <0.34 produced a sensitivity of 71.4% and a specificity

of 84.6% for advanced disease (Fig. 1b). This confirms that miR-143-3p could be a potential biomarker of carotid stenosis and atherosclerosis in humans.

Altered miRNAs with age and atherosclerosis severity in mice

By comparing young (11 weeks) and middle-aged (46 weeks) female HuBL mice we were able to assess atheroprogression (Fig. 2a). The median atherosclerotic burden in the en-face-prepared aortic arches was 28.4 times higher in the 46-week group (Fig. 2b). Oil Red O staining of the aortic root showed 3.9 times higher lipid-stained lesions in the 46-week group (Fig. 2c). Body weight, spleen weight, splenocyte count, and blood leukocytes were not significantly altered with age in this cohort of mice (Table S4).

The carotid bifurcation and common carotids were microdissected as displayed in a set of Sudan-IV-stained arteries (Fig. 2d). Initial lesion formation was observed in the carotid bifurcation at 11 weeks (Fig. 2e). Relative levels of miR-15a-5p, miR-143-3p, miR-155-5p, and miR-199a-3p were assessed but only the expression of miR-143-3p was significantly downregulated in the carotid bifurcation of the middle-aged HuBL mice (Fig. 2f). In the common carotids, miR-155-5p levels were significantly increased with age in addition to the downregulated miR-143-3p (Fig. 2g). Further supporting these changes, carotid miR-143-3p levels showed a negative association with disease progression as measured by Oil Red O staining in the aortic roots, and miR-155-5p levels in the common carotids showed a positive association with disease progression (Fig. 2h). The age difference between the two groups did not significantly impact plasma cholesterol and triglyceride levels (Fig. 2i). This would indicate that the disease process itself, and not hypercholesterolemia, drives these local miRNA changes at predilection sites in the vasculature.

To assess whether there was site-specific miRNA dysregulation in either early or advanced atherosclerosis, we compared the carotids separately for the 11- and 46-week age groups (Fig. 3a-b). The most striking changes were observed when comparing miRNA levels between the common carotids and the carotid bifurcation in early atherosclerosis: miR-15a-5p, miR-143-3p, and miR-199a-3p were significantly downregulated, and miR-155-5p was upregulated (Fig. 3a). In advanced atherosclerosis, there was no significant difference in miRNA expression between the carotid bifurcation and common carotids (Fig. 3b), likely due to the extension of the disease to the common carotids at this time point.

mRNA levels for a handful of genes related to atherosclerosis progression were investigated in a site-specific manner in the carotids. In early atherosclerosis, only *Ccl2* mRNA, encoding monocyte chemoattractant protein 1, was overexpressed in the carotid bifurcation compared with the common carotid (Fig. 3c). *Ccl2* mRNA showed a strong positive relationship with miR-155-5p expression and was inversely correlated with miR-199a-3p levels (Fig. 3d). In advanced atherosclerosis, *Vcam1* mRNA, encoding vascular cell adhesion molecule 1, was increased in the common carotids and *Cd68*, a highly expressed mRNA in macrophages, was increased in the carotid bifurcation (Fig. 3e), indicating that these sites were in different phases of atheroprogression. *Cd68* mRNA levels were negatively associated with miR-143-3p whereas *Vcam1* mRNA levels were positively associated with miR-143-3p (Fig. 3f). Although these associations were very weak, they support the notion that miR-143-3p is dysregulated in advanced atherosclerosis.

Since there was a site-specific alteration of mRNA levels, we wanted to assess whether the expression was altered by disease severity. When comparing the mRNA levels of the selected genes of interest in the carotid bifurcation of 11 *vs*. 46-week mice, *Nos2* mRNA, encoding inducible nitric oxide synthase, and *Ccl2* mRNA were found to be increased (Fig. S2a). However, these transcript

levels did not correlate with any of the measured miRNAs. In the common carotids, there was an increase in mRNA levels of *Vcam1*, *Ccl2*, and *Il1b*, the latter encoding the interleukin-1β cytokine precursor, in middle-aged mice (Fig. S2b). The expression of these three transcripts showed a positive relationship with miR-155-5p levels (Fig. S2c). At the same time, *Ccl2* and *Vcam1* mRNA were inversely correlated with miR-143-3p expression (Fig. S2d). This further denotes the differential expression of miR-143-3p and miR-155-5p in the common carotids, which is a vascular site that typically has laminar blood flow and is affected late in the atherosclerotic process.

Altered miRNAs in immune cells of atherosclerotic mice

We investigated whether the selected miRNAs were altered in immune cells during early and advanced carotid atherosclerosis since previous studies mainly focused on their role in resident vascular cells. $CD3^+$ T cells and $CD3^-$ non-T cells were isolated from the spleen of young and middle-aged mice (Fig. 4a-b). When studying the miRNA expression in the splenic $CD3^+$ T cells, miR-143-3p was selectively increased in mice with advanced atherosclerosis, and miR-199a-3p was non-detectable in those cells (Fig. 4c). A handful of transcripts related to the T-cell phenotype were analyzed. In mice with advanced atherosclerosis, *Foxp3*, *Ifng*, *Il21*, and *Pdcd1* mRNA levels were increased in the splenic $CD3^+$ cells indicating that atheroprogression drives T-cell activation and regulatory transcriptional programs (Fig. 4d). *Pdcd1* mRNA, encoding the immune checkpoint programmed cell death protein 1 (PD1), and *Tbx21* mRNA, encoding the T-box transcription factor expressed in T-helper type 1 cells, were positively correlated with miR-143-3p expression in those cells, implicating this miRNA in the context of immune regulation (Fig. 4e).

When analyzing the relative expression of miRNAs in the $CD3^-$ cells, only miR-199a-3p was increased during atheroprogression (Fig. 4f). A few transcripts involved in inflammatory pathways

were analyzed, and mRNA from the MHC class II encoding gene *H2ab1* was found to be significantly decreased in the non-T cell fraction (Fig. 4g), indicating that antigen presentation could be differentially regulated during atheroprogression in the spleen. To observe specific enrichments in the immune cell compartment during atheroprogression, we compared if there was an alteration in miRNAs between splenic $CD3^-$ and $CD3^+$ cells in early and advanced atherosclerosis. In early atherosclerosis, significant enrichments of miR-15a-5p and miR-155-5p were found in $CD3^+$ cells (Fig. 4h), while this enrichment was subdued in advanced atherosclerosis (Fig. 4i).

Specifically, cellularity in the aorta-associated mediastinal and renal lymph nodes was increased, while cellularity remained at a similar level in the spleen (Fig. S3a-b and Table S4). An expansion of germinal center B cells and plasma cells was observed in the mediastinal and renal lymph nodes as analyzed by flow cytometry (Fig. 4j and S3c-f). The expansion of plasma cells was, at this time point and location, limited to the absolute cell counts (Fig. S3d-e). As miR-199a-3p is known to be upregulated in germinal center B cells [19], this miRNA correlated with the germinal center reactions (Fig. 4k, Fig. S3n).

Blood lymphocytes as well as total T cell number in the mediastinal and renal lymph nodes were not significantly different between groups (Fig. S3g-h and Table S4). However, there was an increase in the total and relative number of T effector/memory (T_{EM}) cells (Fig. S3i-j). Confirming the upregulated *Pdcd1* mRNA levels, $PD1^{high}$ T_{EM} cells were found to accumulate in the aorta-associated lymph nodes during atheroprogression (Fig. 4l and S3l). Speculatively, persistent presentation of atherosclerosis-associated antigens may be driving these effects. The T_{EM} cell with intermediate PD1 expression remained unaltered (Fig. S3k-m). Expression of miR-143-3p in T cells correlated with the number of $PD1^{high}$ T_{EM} cells (Fig. 4m). Since the correlation to *Tbx21*

mRNA was stronger, this might reflect an upregulation in activated T cells or Th1 cells more specifically. However, this could not be distinguished using our experimental design.

Altered miRNAs in middle-aged mice

Finally, we investigated whether the dysregulation of miRNAs occurs during atheroprogression without the influence of age differences. Age-matched one-year-old male *Ldlr*$^{-/-}$ and HuBL mice fed a standard chow diet were used for this purpose (Fig. 5a). The atherosclerotic burden was 7.0-fold increased in the aorta of HuBL mice as driven by more severe hypercholesterolemia induced by transgenic overproduction of *APOB100* (Fig. 5b-c). No difference in body weight was recorded but HuBL mice had higher blood counts of lymphocytes, monocytes, and granulocytes (Table S5) as well as plasma cholesterol and triglyceride levels (Fig. 5c). To analyze miRNA levels, the iliac lymph nodes in proximity to the aorta were used. Levels of miR-15a-5p, miR-143-3p, and miR-199a-3p were lower in HuBL compared to *Ldlr*$^{-/-}$ mice (Fig. 5d). This is similar to our findings in the vasculature of female HuBL mice at different ages but in the iliac lymph nodes of those mice, only miR-143-3p was found to be significantly decreased (Fig. S4).

miR-15a-5p showed a negative association with plasma lipid levels, indicating its inverse association with hypercholesterolemia (Fig. 5e). A weaker association was observed between miR-199a-3p and plasma cholesterol (Fig. 5f). miR-143-3p did not correlate with hypercholesterolemia levels, indicating that its dysregulation is more associated with disease progression than dyslipidemia. However, atheroprogression is tightly linked to hypercholesterolemia in these mice, and separating these entities is challenging.

A few selected transcripts related to T-cell phenotype were analyzed. *Gata3* mRNA, encoding a transcription factor involved in T-helper type 2 responses, *Ifng* mRNA, encoding interferon-γ, *Il21*

mRNA, encoding the T follicular helper-related cytokine interleukin-21, *Rorc* mRNA, encoding retinoic acid receptor-related orphan receptor C associated with T-helper 17 cells, and *Pdcd1* mRNA were all observed to be lower in the HuBL mice (Fig. 5g). *Pdcd1* and *Ifng* correlated with miR-15a-5p expression (Fig. 5h). Taken together, severe dyslipidemia was identified as a contributing mediator of dysregulation of miR-15a-5p and, to a lesser extent, miR-143-3p.

Discussion

We show that the dysregulation of miR-143-3p in carotid atherosclerosis reflects the progression of the disease and that it potentially could be used as a screening tool for atherosclerosis or for non-invasive disease staging. In our mouse model, we found that miR-143-3p was decreased in early and advanced atherosclerosis, as well as in the carotid bifurcation and common carotids. Downregulation of miR-143-3p has been observed in both human carotid plaques and animal models of atherosclerosis before [8]. The novel aspect of this study is the mapping of the dysregulation of miR-143-3p to different parts of the carotid arteries in mice, and that we show an upregulation of miR-143-3p in T cells during atheroprogression. Notably, miR-143-3p is transmitted by the endothelium to the circulation in extracellular vesicles and to vascular smooth muscle cells to keep them in a contractile state. T cells also release extracellular vesicles constitutively [20], which opens the possibility that T cells can communicate with and affect gene expression in vascular resident cells through miR-143-3p. However, whether miR-143-3p is a cargo of extracellular vesicles from T cells and whether they could reach vascular smooth muscle cells remains to be investigated.

The differential regulation of miR-143-3p between the vasculature and the immune cell compartment might explain some conflicting observations in the field [12-15]. miR-143-3p

downregulation has previously been observed in *Apoe*$^{-/-}$ and *Ldlr*$^{-/-}$ mouse aortas when comparing mice on a high-fat diet with controls fed a chow diet [8, 21]. This finding is corroborated by our data showing that miR-143-3p is continuously decreased with age and atheroprogression. We therefore propose that it could be used as a marker for atheroprogression. Experiments of balloon-injured carotid arteries in rats provide further support for this notion [22]. However, several miRNAs are downregulated in atherosclerosis and further comparisons are needed to select the most selective and sensitive markers for vascular dysfunction. PCR-based extracellular vesicle testing is not a clinically convenient methodology but can be multiplexed, adding together a set of markers to increase specificity.

miRNAs exert their effects through binding complementary sequences in mRNA molecules and, due to their versatile effects, are not unanimously considered promising novel therapeutic targets anymore. Our bulk tissue analysis of carotids found miR-143-3p to be associated with *Cd68*, *Vcam1*, and *Ccl2* mRNA. miR-143-3p is not known to bind those targets directly but has been shown to be an indirect modulator of *Vcam1* [23] and *Ccl2* [24] mRNA. Its effects are challenging to distinguish from the cotranscribed miR-145 and *Carmn* non-coding RNA, which are in proximity to the miR-143 locus. However, detailed mapping of this intricate coregulatory network is not critical if miR-143-3p is viewed as a strict biomarker.

Immune-vascular interactions are drivers of atherosclerosis progression but how miRNAs are involved in these processes is less explored. We made a simple comparison of miRNA levels in splenic T cells and non-T cells during atheroprogression. Surprisingly, this revealed that miR-143-3p was overexpressed in T cells in mice with advanced atherosclerosis. To further characterize the T cells, we studied genes related to their phenotype, showing an increase in mRNA levels of *Il21*, *Ifng*, *Foxp3*, and *Pdcd1*. Interestingly, only *Pdcd1*, encoding PD1, correlated with miR-143-3p.

Additionally, this miRNA also correlated with the PD1^{high} T-helper cells found in the aorta-associated lymph nodes. PD1 is highly expressed on activated and exhausted T cells and is commonly targeted with immune checkpoint inhibitors in cancer treatment to increase T-cell reactivity. Blocking PD1 could at the same time increase the production of pro-atherogenic cytokines in iliac lymph nodes [25]. One prior report corroborates our finding that miR-143-3p is expressed in T cells [26]. Wang et al. studied cytokine-induced killer cells, which include cytotoxic T cells, and report that miR-143-3p is involved in regulating T-cell activation and proliferation. Whether miR-143-3p is involved in T-cell activation in our model and how this is related to pathological processes in the vascular wall remains to be investigated.

Another miRNA we measured in our atheroprogression model was miR-15a-5p, which is widely studied in the cancer field. Tumor tissue often has downregulated miR-15a-5p levels, which leads to less regulated gene expression that, in turn, could facilitate tumor growth and carcinogenesis [27]. In atherosclerosis, we found a similar effect with downregulated miR-15a-5p in early atherogenesis and iliac lymph nodes in older mice. A few reports have studied the mechanistic implications of miR-15a-5p in a vascular context and have shown that it could reduce inflammatory changes in the endothelium [28] and promote smooth muscle cell migration [29], i.e., effects that could be interpreted as beneficial for atherosclerosis and plaque stability, respectively. We found that miR-15a-5p levels were higher in splenic T cells compared to non-T cells during early atherogenesis. With disease progression, this difference was eliminated. miR-15a-5p has been associated with activated cytotoxic T cells in a tumor microenvironment [30] and its downregulation could boost T-helper cell responses in asthmatic airways [31]. Moreover, the expression of miR-15a-5p in B cells has been associated with vaccination responses [32]. We did not observe a significant difference in miR-15a-5p levels in splenic cells that could indicate a

similar effect during atheroprogression. As relative miRNA levels were measured, further controls are required to understand whether levels increased or decreased in certain lymphocyte subsets. Nonetheless, the observed lower levels in the iliac lymph nodes of HuBL mice could implicate its involvement in reduced cellular antigen responsiveness during hypercholesterolemia. Moreover, in the age-matched mice with more advanced atherosclerosis due to severe dyslipidemia, miR-15a-5p correlated positively with *Pdcd1* and *Ifng* mRNA and inversely with plasma cholesterol and triglyceride levels. *Pdcd1* mRNA is a confirmed target of miR-15a-5p [33], and our data are seemingly at odds with this effect. However, the positive association with *Ifng* mRNA was stronger according to our data, and interferon-γ is an upstream modulator that increases miR-15a-5p expression [34]. Taken together, our study design is more suited to detect commonly regulated pathways in atherosclerosis and not to detect miRNA-targeted effects. Mechanistic studies are needed to unravel how dyslipidemia could cause dysregulation of miR-15a-5p and whether it is mediated through interferon signaling.

miR-155-5p is, in a cardiovascular context, the most studied of the four miRNAs we measured. Previous reports have found it to be both increased [35] and decreased [36] in plasma samples from patients with advanced atherosclerosis. Functionally, it has been associated with increased cholesterol efflux from macrophages and reverse cholesterol transport [37, 38]. In our mouse model, we found that miR-155-5p was increased in carotid bifurcations with early atherosclerosis and in common carotids during disease progression. In the latter, it correlated positively with *Ccl2*, *Vcam1*, and *Il1b* mRNA. These mRNAs are not predicted to be targets of miR-155-5p but are under transcriptional control by the nuclear factor-κB pathway [39], which is activated in atherosclerosis. Levels of miR-155-5p were higher in splenic $CD3^+$ cells compared to $CD3^-$ cells in mice with initial atherosclerosis. In the literature, miR-155-5p has been studied as an exosomal signal from different

types of T cells, *e.g.*, miR-155-5p could increase activation of cytotoxic T cells, which decreases tumor growth in an ovarian cancer model [40]. Possibly, a similar effect on T cells would play only a minor role in atheroprogression since the miR-155-5p elevation in T cells was not observed in middle-aged mice with more pronounced disease.

Finally, we found that miR-199a-3p is downregulated in early carotid atherosclerosis in mice. A similar downregulation of miR-199a-3p was observed in iliac lymph nodes in 1-year-old HuBL mice compared to *Ldlr*$^{-/-}$ mice. Previously, miR-199a-3p has been reported to be involved in endothelial dysfunction [41] and the inhibition of vascular smooth muscle cell migration [42]. The most striking data for this miRNA in our study was the upregulation in non-T splenocytes and its association with germinal center B-cell responses. During atheroprogression, germinal centers expand in the aorta-associated lymph nodes. Such reactions are central to the generation of affinity-matured B cells in response to T-dependent antigens, leading to the maturation of long-lived plasma cells, the generation of memory B cells, and the production of high-affinity antibodies. Our results are consistent with previous studies focusing on miRNAs in B-cell responses and germinal centers [19, 32]. Supporting our observation, we found that splenic miR-199a-3p levels correlate with PD1^{high} effector T cells, which could interact with germinal center B cells.

There are limitations to the present study. It is a translational research study with a small sample size and large effect sizes. Biologically relevant effects of smaller magnitude and sex-specific effects could be missed. The findings are mainly correlative since it is a biomarker study, but as discussed, have generated hypotheses that could be explored mechanistically. The broadly targeted effects of miRNAs limit their therapeutic use but do not influence their potential as biomarkers. Replication of the results in other cohorts has partly been performed previously [4-6, 8, 9]. However, larger sample sizes with matched controls and adjustments for confounders would be

needed, and the validation of miR-143-3p dysregulation as a biomarker for early atherosclerosis in humans is still pending. The development of extracellular vesicle extraction coupled with real-time PCR as diagnostic tests would also be required to enable clinical use.

In conclusion, the downregulation of miR-143-3p is a sensitive marker for carotid atherosclerosis in mice, and it has the potential to serve as a non-invasive biomarker for atherosclerosis in humans when measured in plasma extracellular vesicles. Furthermore, since miR-143-3p levels progressively decrease in experimental carotid atherosclerosis, it could be utilized to grade the severity of the disease.

Sources of funding

This work was supported by grants from the Swedish Heart-Lung Foundation (20210469 and 20230391), Åke Wibergs Stiftelse, Jeanssons Stiftelse, Gun och Bertil Stohnes Stiftelse, Foundation for Geriatric Diseases at Karolinska Institutet, Karolinska Institutet Research Foundation, Stiftelsen för Gamla Tjänarinnor, and Spanish Ministry of Science and Innovation (PID2021-123076OB-I00). PGL was supported by a grant from The European Federation of Immunological Societies.

Disclosures

The authors declare no conflict of interest. Illustrations were partly generated using Servier Medical Art, licensed under a Creative Commons Attribution 3.0 unported license.

Ethics declarations

The study was ethically approved (IIS-Fundación Jiménez Díaz, reference number PI1442016) and followed the Declaration of Helsinki. All participants gave written informed consent. All institutional and national guidelines for the care and use of laboratory animals were followed and approved by the Stockholm Regional Board for Animal Ethics.

References

1. Gisterå A, Hansson GK. The immunology of atherosclerosis. Nat Rev Nephrol. 2017;13(6):368-80. doi: 10.1038/nrneph.2017.51.
2. Chèvre R, González-Granado JM, Megens RT, Sreeramkumar V, Silvestre-Roig C, Molina-Sánchez P, et al. High-resolution imaging of intravascular atherogenic inflammation in live mice. Circ Res. 2014;114(5):770-9. doi: 10.1161/circresaha.114.302590.
3. Libby P. The changing landscape of atherosclerosis. Nature. 2021;592(7855):524-33. doi: 10.1038/s41586-021-03392-8.
4. Ji R, Cheng Y, Yue J, Yang J, Liu X, Chen H, et al. MicroRNA expression signature and antisense-mediated depletion reveal an essential role of MicroRNA in vascular neointimal lesion formation. Circ Res. 2007;100(11):1579-88. doi: 10.1161/circresaha.106.141986.
5. Elia L, Quintavalle M, Zhang J, Contu R, Cossu L, Latronico MV, et al. The knockout of miR-143 and -145 alters smooth muscle cell maintenance and vascular homeostasis in mice: correlates with human disease. Cell Death Differ. 2009;16(12):1590-8. doi: 10.1038/cdd.2009.153.
6. Liu K, Xuekelati S, Zhang Y, Yin Y, Li Y, Chai R, et al. Expression levels of atherosclerosis-associated miR-143 and miR-145 in the plasma of patients with hyperhomocysteinaemia. BMC Cardiovasc Disord. 2017;17(1):163. doi: 10.1186/s12872-017-0596-0.
7. Gao J, Yang S, Wang K, Zhong Q, Ma A, Pan X. Plasma miR-126 and miR-143 as Potential Novel Biomarkers for Cerebral Atherosclerosis. J Stroke Cerebrovasc Dis. 2019;28(1):38-43. doi: 10.1016/j.jstrokecerebrovasdis.2018.09.008.
8. González-López P, Ares-Carral C, López-Pastor AR, Infante-Menéndez J, González Illaness T, Vega de Ceniga M, et al. Implication of miR-155-5p and miR-143-3p in the Vascular Insulin Resistance and Instability of Human and Experimental Atherosclerotic Plaque. Int J Mol Sci. 2022;23(18). doi: 10.3390/ijms231810253.
9. Rozhkov AN, Shchekochikhin DY, Ashikhmin YI, Mitina YO, Evgrafova VV, Zhelankin AV, et al. The Profile of Circulating Blood microRNAs in Outpatients with Vulnerable and Stable Atherosclerotic Plaques: Associations with Cardiovascular Risks. Noncoding RNA. 2022;8(4). doi: 10.3390/ncrna8040047.
10. Cordes KR, Sheehy NT, White MP, Berry EC, Morton SU, Muth AN, et al. miR-145 and miR-143 regulate smooth muscle cell fate and plasticity. Nature. 2009;460(7256):705-10. doi: 10.1038/nature08195.
11. Sala F, Aranda JF, Rotllan N, Ramírez CM, Aryal B, Elia L, et al. MiR-143/145 deficiency attenuates the progression of atherosclerosis in Ldlr-/-mice. Thromb Haemost. 2014;112(4):796-802. doi: 10.1160/th13-11-0905.
12. Fichtlscherer S, De Rosa S, Fox H, Schwietz T, Fischer A, Liebetrau C, et al. Circulating microRNAs in patients with coronary artery disease. Circ Res. 2010;107(5):677-84. doi: 10.1161/circresaha.109.215566.

13. Ekedi A, Rozhkov AN, Shchekochikhin DY, Novikova NA, Kopylov PY, Bestavashvili AA, et al. Evaluation of microRNA Expression Features in Patients with Various Types of Arterial Damage: Thoracic Aortic Aneurysm and Coronary Atherosclerosis. J Pers Med. 2023;13(7). doi: 10.3390/jpm13071161.
14. Grosse GM, Derda AA, Stauss RD, Neubert L, Jonigk DD, Kühnel MP, et al. Circulating microRNAs in Symptomatic and Asymptomatic Carotid Stenosis. Front Neurol. 2021;12:755827. doi: 10.3389/fneur.2021.755827.
15. Markus B, Grote K, Worsch M, Parviz B, Boening A, Schieffer B, et al. Differential Expression of MicroRNAs in Endarterectomy Specimens Taken from Patients with Asymptomatic and Symptomatic Carotid Plaques. PLoS One. 2016;11(9):e0161632. doi: 10.1371/journal.pone.0161632.
16. Climent M, Quintavalle M, Miragoli M, Chen J, Condorelli G, Elia L. TGFβ Triggers miR-143/145 Transfer From Smooth Muscle Cells to Endothelial Cells, Thereby Modulating Vessel Stabilization. Circ Res. 2015;116(11):1753-64. doi: 10.1161/circresaha.116.305178.
17. Hergenreider E, Heydt S, Tréguer K, Boettger T, Horrevoets AJ, Zeiher AM, et al. Atheroprotective communication between endothelial cells and smooth muscle cells through miRNAs. Nat Cell Biol. 2012;14(3):249-56. doi: 10.1038/ncb2441.
18. González-López P, Álvarez-Villarreal M, Ruiz-Simón R, López-Pastor AR, de Ceniga MV, Esparza L, et al. Role of miR-15a-5p and miR-199a-3p in the inflammatory pathway regulated by NF-κB in experimental and human atherosclerosis. Clin Transl Med. 2023;13(8):e1363. doi: 10.1002/ctm2.1363.
19. Basso K, Sumazin P, Morozov P, Schneider C, Maute RL, Kitagawa Y, et al. Identification of the human mature B cell miRNome. Immunity. 2009;30(5):744-52. doi: 10.1016/j.immuni.2009.03.017.
20. Gutiérrez-Vázquez C, Villarroya-Beltri C, Mittelbrunn M, Sánchez-Madrid F. Transfer of extracellular vesicles during immune cell-cell interactions. Immunol Rev. 2013;251(1):125-42. doi: 10.1111/imr.12013.
21. Vacante F, Rodor J, Lalwani MK, Mahmoud AD, Bennett M, De Pace AL, et al. CARMN Loss Regulates Smooth Muscle Cells and Accelerates Atherosclerosis in Mice. Circ Res. 2021;128(9):1258-75. doi: 10.1161/circresaha.120.318688.
22. Liu X, Cheng Y, Yang J, Qin S, Chen X, Tang X, et al. Flank sequences of miR-145/143 and their aberrant expression in vascular disease: mechanism and therapeutic application. J Am Heart Assoc. 2013;2(6):e000407. doi: 10.1161/jaha.113.000407.
23. Xiong J, Hu Y, Liu Y, Zeng X. CircRNA mmu_circ_0000021 regulates microvascular function via the miR-143-3p/NPY axis and intracellular calcium following ischemia/reperfusion injury. Cell Death Discov. 2022;8(1):315. doi: 10.1038/s41420-022-01108-z.
24. Zhou Z, Dong Y, Zhou H, Liu J, Zhao W. MiR-143-3p directly targets GLUT9 to reduce uric acid reabsorption and inflammatory response of renal tubular epithelial cells. Biochem Biophys Res Commun. 2019;517(3):413-20. doi: 10.1016/j.bbrc.2019.07.114.
25. Bu DX, Tarrio M, Maganto-Garcia E, Stavrakis G, Tajima G, Lederer J, et al. Impairment of the programmed cell death-1 pathway increases atherosclerotic lesion development and inflammation. Arterioscler Thromb Vasc Biol. 2011;31(5):1100-7. doi: 10.1161/atvbaha.111.224709.
26. Wang W, Li R, Meng M, Wei C, Xie Y, Zhang Y, et al. MicroRNA profiling of CD3+ CD56+ cytokine-induced killer cells. Sci Rep. 2015;5:9571. doi: 10.1038/srep09571.

27. Wang H, Yang Q, Li J, Chen W, Jin X, Wang Y. MicroRNA-15a-5p inhibits endometrial carcinoma proliferation, invasion and migration via downregulation of VEGFA and inhibition of the Wnt/β-catenin signaling pathway. Oncol Lett. 2021;21(4):310. doi: 10.3892/ol.2021.12570.
28. Li H, Zhang HM, Fan LJ, Li HH, Peng ZT, Li JP, et al. STAT3/miR-15a-5p/CX3CL1 Loop Regulates Proliferation and Migration of Vascular Endothelial Cells in Atherosclerosis. Int J Med Sci. 2021;18(4):964-74. doi: 10.7150/ijms.49460.
29. Peng H, Wang J, Li S. MiR-15a-5p accelerated vascular smooth muscle cells viabilities and migratory abilities via targeting Bcl-2. Physiol Res. 2022;71(5):667-75. doi: 10.33549/physiolres.934914.
30. Pathania AS, Prathipati P, Olwenyi OA, Chava S, Smith OV, Gupta SC, et al. miR-15a and miR-15b modulate natural killer and CD8(+)T-cell activation and anti-tumor immune response by targeting PD-L1 in neuroblastoma. Mol Ther Oncolytics. 2022;25:308-29. doi: 10.1016/j.omto.2022.03.010.
31. Wei Y, Han B, Dai W, Guo S, Zhang C, Zhao L, et al. Exposure to ozone impacted Th1/Th2 imbalance of CD(4+) T cells and apoptosis of ASMCs underlying asthmatic progression by activating lncRNA PVT1-miR-15a-5p/miR-29c-3p signaling. Aging (Albany NY). 2020;12(24):25229-55. doi: 10.18632/aging.104124.
32. Haralambieva IH, Kennedy RB, Simon WL, Goergen KM, Grill DE, Ovsyannikova IG, et al. Differential miRNA expression in B cells is associated with inter-individual differences in humoral immune response to measles vaccination. PLoS One. 2018;13(1):e0191812. doi: 10.1371/journal.pone.0191812.
33. Zhang HY, Liang HX, Wu SH, Jiang HQ, Wang Q, Yu ZJ. Overexpressed Tumor Suppressor Exosomal miR-15a-5p in Cancer Cells Inhibits PD1 Expression in CD8+T Cells and Suppresses the Hepatocellular Carcinoma Progression. Front Oncol. 2021;11:622263. doi: 10.3389/fonc.2021.622263.
34. Zhu QJ, Wang J, Li Y, Bai ZJ, Guo XB, Pan T. PRKCA Promotes Mitophagy through the miR-15a-5p/PDK4 Axis to Relieve Sepsis-Induced Acute Lung Injury. Infect Immun. 2023;91(1):e0046522. doi: 10.1128/iai.00465-22.
35. Singh S, de Ronde MWJ, Kok MGM, Beijk MA, De Winter RJ, van der Wal AC, et al. MiR-223-3p and miR-122-5p as circulating biomarkers for plaque instability. Open Heart. 2020;7(1). doi: 10.1136/openhrt-2019-001223.
36. Chen L, Zheng SY, Yang CQ, Ma BM, Jiang D. MiR-155-5p inhibits the proliferation and migration of VSMCs and HUVECs in atherosclerosis by targeting AKT1. Eur Rev Med Pharmacol Sci. 2019;23(5):2223-33. doi: 10.26355/eurrev_201903_17270.
37. Wang G, Chen JJ, Deng WY, Ren K, Yin SH, Yu XH. CTRP12 ameliorates atherosclerosis by promoting cholesterol efflux and inhibiting inflammatory response via the miR-155-5p/LXRα pathway. Cell Death Dis. 2021;12(3):254. doi: 10.1038/s41419-021-03544-8.
38. Rachmawati E, Sargowo D, Rohman MS, Widodo N, Kalsum U. miR-155-5p predictive role to decelerate foam cell atherosclerosis through CD36, VAV3, and SOCS1 pathway. Noncoding RNA Res. 2021;6(2):59-69. doi: 10.1016/j.ncrna.2021.02.003.
39. Scoditti E, Carpi S, Massaro M, Pellegrino M, Polini B, Carluccio MA, et al. Hydroxytyrosol Modulates Adipocyte Gene and miRNA Expression Under Inflammatory Condition. Nutrients. 2019;11(10). doi: 10.3390/nu11102493.
40. Li X, Wang S, Mu W, Barry J, Han A, Carpenter RL, et al. Reactive oxygen species reprogram macrophages to suppress antitumor immune response through the exosomal miR-155-5p/PD-L1 pathway. J Exp Clin Cancer Res. 2022;41(1):41. doi: 10.1186/s13046-022-02244-1.

41. Joris V, Gomez EL, Menchi L, Lobysheva I, Di Mauro V, Esfahani H, et al. MicroRNA-199a-3p and MicroRNA-199a-5p Take Part to a Redundant Network of Regulation of the NOS (NO Synthase)/NO Pathway in the Endothelium. Arterioscler Thromb Vasc Biol. 2018;38(10):2345-57. doi: 10.1161/atvbaha.118.311145.
42. Sun X, Zhang Y, Liu Z, Li S, Wang L. MicroRNA-199a-3p Exhibits Beneficial Effects in Asymptomatic Atherosclerosis by Inhibiting Vascular Smooth Muscle Cell Proliferation and Migration. Mol Biotechnol. 2021;63(7):595-604. doi: 10.1007/s12033-021-00323-w.

Figure Captions

Fig. 1 Plasma detection of miR-143-3p in carotid stenosis patients. **(a)** miRNAs in extracellular vesicles were isolated from the plasma of patients with advanced atherosclerosis and the plasma from healthy donors without manifest atherosclerosis. The relative expression of miR-143-3p was measured by real-time PCR (Mann-Whitney test, healthy donors n=13, carotid stenosis n=28, log_2-scaled *y*-axis) **(b)** A receiver operating characteristic curve analysis illustrates how miR-143-3p can be used as a biomarker for carotid atherosclerosis.

Fig. 2 Dysregulation of a set of miRNAs in mouse carotid arteries. **(a)** Experimental setup comparing atheroprogression in HuBL mice. **(b)** Micrographs of Sudan-IV-stained aortic arches with a 2 mm scale bar and quantification of the atherosclerotic plaques (orange color) divided by total aortic arch area. **(c)** Micrographs of Oil Red O-stained sections 300 µm from the aortic root with a 500 µm scale bar. Mean aortic root lipids were quantified (red color) and divided by aortic cross-section area. **(d)** Sudan-IV stained aortic arches with branches to depict microdissection of common carotids and carotid bifurcation. **(e)** Micrograph of a carotid artery from an 11-week-old HuBL mouse, the arrow indicates Sudan-IV^+ plaque in the carotid bifurcation. **(f-g)** Relative quantification of miRNAs in the carotid bifurcation (bright colors) and common carotids (pale colors) from the 11-week (pink colors, n=6) and 46-week (purple colors, n=4) old female HuBL

mice. **(h)** Linear regression between lipid deposition in the aortic root and the levels of miR-143-3p in the carotid bifurcation and between lipid deposition in the aortic root and the levels of miR-155-5p and miR-143-3p in the common carotids. **(i)** Plasma concentration of cholesterol and triglycerides.

Fig. 3 Site-specific miRNA level changes in early and late carotid atherosclerosis. **(a-b)** Relative quantification of miRNAs in the common carotids (pale colors) and carotid bifurcation (bright colors) from the 11-week (pink colors, n=6) and 46-week (purple colors, n=4) old female HuBL mice. **(c)** mRNA levels for genes of interest in 11-week-old mice. **(d)** Linear regression between *Ccl2* mRNA and miR-155-5p (left) and miR-199a-3p (right) in carotids with early atherosclerosis. **(e)** mRNA levels for genes of interest in 46-week-old mice. **(f)** Linear regression between *Cd68* mRNA (left) and *Vcam1* mRNA (right), respectively, and miR-143-3p in carotids with advanced atherosclerosis.

Fig. 4 miRNA levels in splenic immune cells during atheroprogression. **(a)** Experimental setup of $CD3^+$ and $CD3^-$ cell isolation. **(b)** Cell fractions before and after isolation of $CD3^+$ cells from the spleen. **(c)** miRNA levels in $CD3^+$ cells from the 11-week (pink, n=6) and 46-week (purple, n=4) old female HuBL mice. **(d)** mRNA levels for genes of interest in $CD3^+$ cells. **(e)** Linear regression between miR-143-3p in $CD3^+$ cells and *Pdcd1* and *Tbx21* mRNA. **(f)** miRNA levels in $CD3^-$ cells. **(g)** mRNA levels in $CD3^-$ cells. **(h-i)** miRNA levels in the $CD3^+$ and $CD3^-$ cells from the 11- and 46-week groups. **(j-k)** Germinal center B cells as quantified using flow cytometry from the mediastinal and renal lymph nodes and their correlation to miR-199a-3p in splenic $CD3^-$ cells. **(l-m)** $PD1^{high}$ T_{EM} cells in the mediastinal and renal lymph nodes and their correlation to miR-143-3p in splenic $CD3^+$ cells.

Fig. 5 Dysregulated transcripts in iliac lymph nodes of middle-aged mice. **(a)** Experimental setup. **(b)** Micrographs of Sudan-IV-stained aortas with a 4 mm scale bar. **(c)** Total plasma cholesterol and triglycerides concentrations. **(d)** Relative quantification of miRNAs in the iliac lymph nodes from male *Ldlr*$^{-/-}$ (pink color, n=8) and HuBL mice (purple color, n=8). **(e-f)** Linear regression between miR-15a-5p and miR-199-3p with plasma cholesterol and triglycerides. **(g)** mRNA levels for genes of interest in the iliac lymph nodes. **(h)** Linear regression between *Pdcd1* and *Ifng* mRNA, respectively, and miR-15a-5p levels in the iliac lymph nodes.

Figure 1.

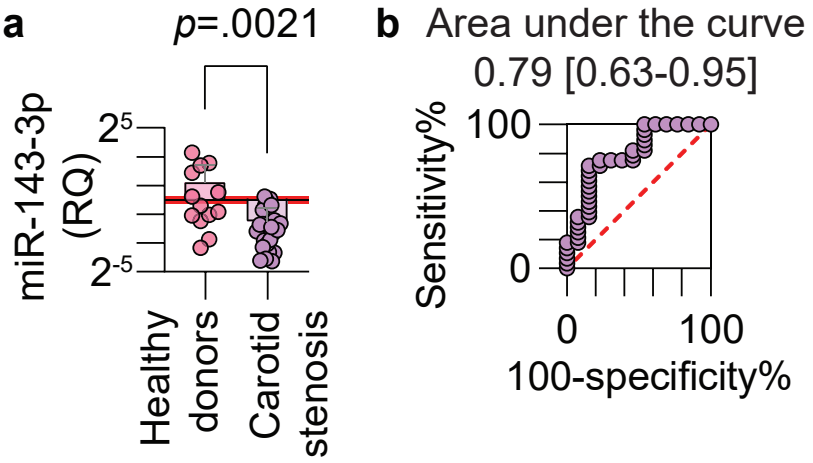

Figure 2.

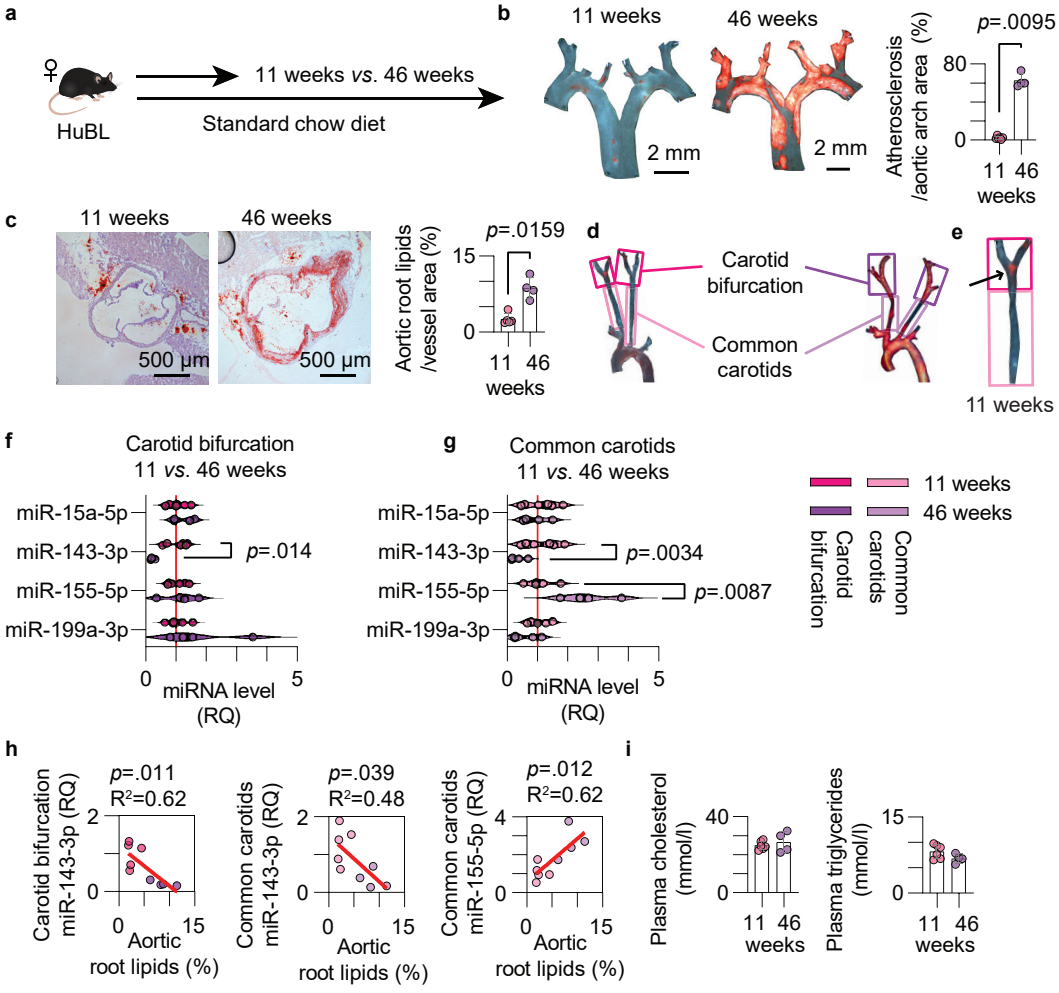

Figure 3.

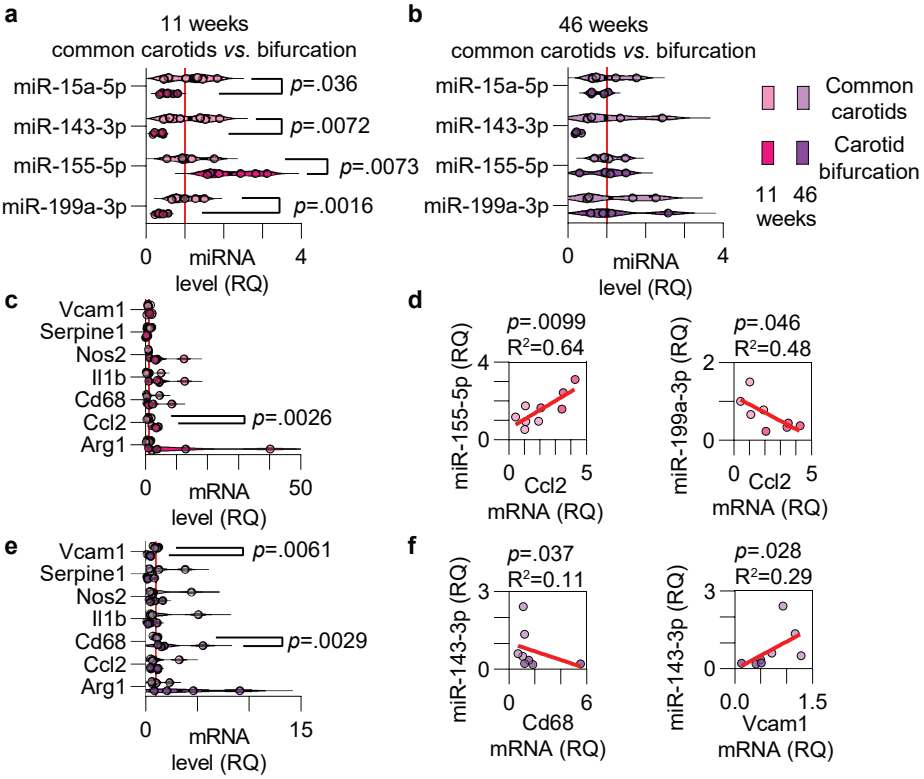
a
11 weeks
common carotids vs. bifurcation
miR-15a-5p
miR-143-3p
miR-155-5p
miR-199a-3p
p=.036
p=.0072
p=.0073
p=.0016
0
miRNA level (RQ)
4
b
46 weeks
common carotids vs. bifurcation
Common carotids
Carotid bifurcation
11 46 weeks
c
Vcam1
Serpine1
Nos2
Il1b
Cd68
Ccl2
Arg1
p=.0026
0
mRNA level (RQ)
50
d
p=.0099
R²=0.64
miR-155-5p (RQ)
Ccl2 mRNA (RQ)
p=.046
R²=0.48
miR-199a-3p (RQ)
e
p=.0061
p=.0029
15
f
p=.037
R²=0.11
miR-143-3p (RQ)
Cd68 mRNA (RQ)
p=.028
R²=0.29
Vcam1 mRNA (RQ)

Figure 4.

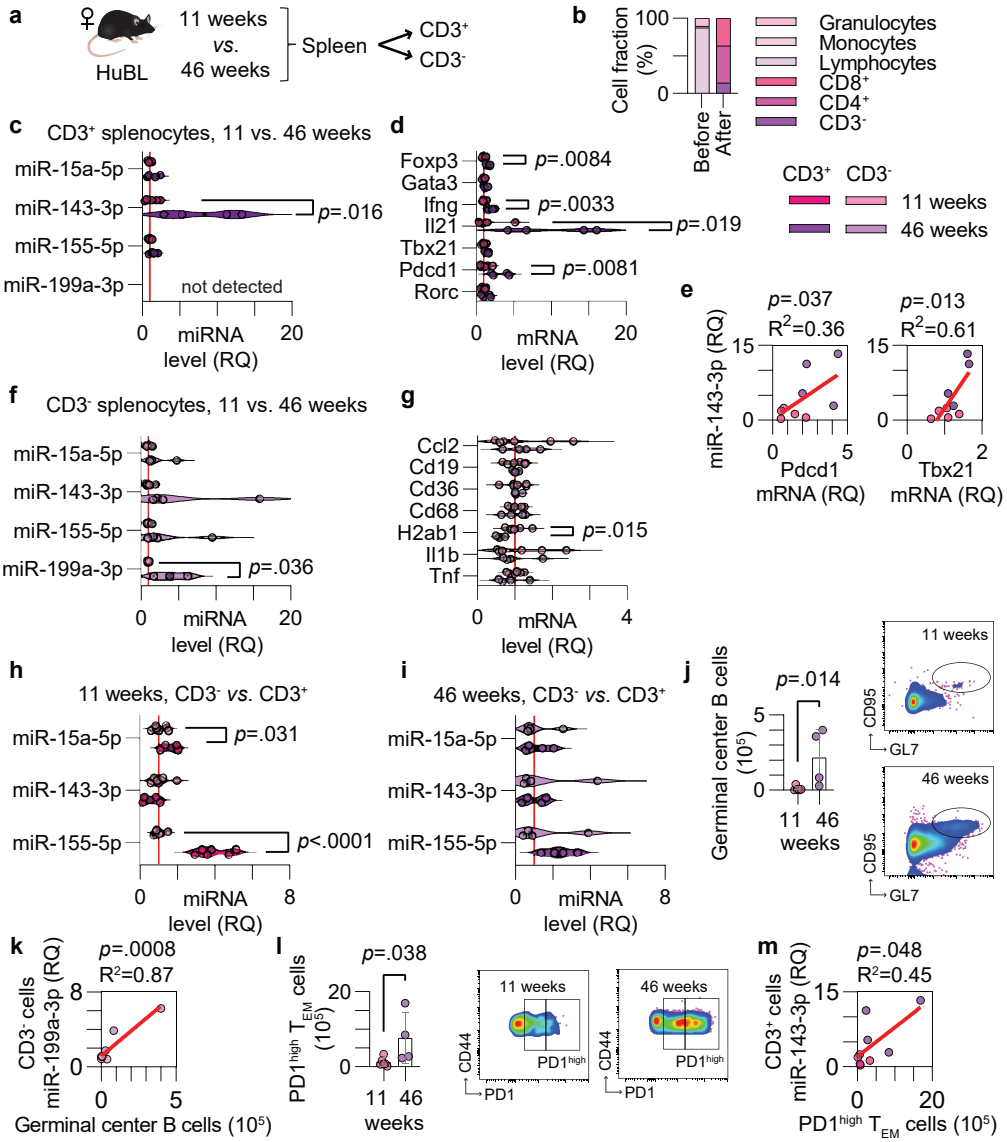
a
HuBL
11 weeks
vs.
46 weeks
Spleen
CD3+
CD3-
b
Cell fraction (%)
100
0
Before
After
Granulocytes
Monocytes
Lymphocytes
CD8+
CD4+
CD3-
c
CD3+ splenocytes, 11 vs. 46 weeks
miR-15a-5p
miR-143-3p
miR-155-5p
miR-199a-3p
p=.016
not detected
0
miRNA level (RQ)
20
d
Foxp3
Gata3
Ifng
Il21
Tbx21
Pdcd1
Rorc
p=.0084
p=.0033
p=.019
p=.0081
0
mRNA level (RQ)
20
CD3+ CD3-
11 weeks
46 weeks
e
p=.037
R2=0.36
p=.013
R2=0.61
miR-143-3p (RQ)
15
0
0
5
Pdcd1 mRNA (RQ)
0
2
Tbx21 mRNA (RQ)
f
CD3- splenocytes, 11 vs. 46 weeks
miR-15a-5p
miR-143-3p
miR-155-5p
miR-199a-3p
p=.036
0
miRNA level (RQ)
20
g
Ccl2
Cd19
Cd36
Cd68
H2ab1
Il1b
Tnf
p=.015
0
mRNA level (RQ)
4
h
11 weeks, CD3- vs. CD3+
miR-15a-5p
miR-143-3p
miR-155-5p
p=.031
p<.0001
0
miRNA level (RQ)
8
i
46 weeks, CD3- vs. CD3+
miR-15a-5p
miR-143-3p
miR-155-5p
0
miRNA level (RQ)
8
j
p=.014
Germinal center B cells (10^5)
5
0
11
46
weeks
11 weeks
CD95
GL7
46 weeks
CD95
GL7
k
p=.0008
R2=0.87
CD3- cells miR-199a-3p (RQ)
8
0
0
5
Germinal center B cells (10^5)
l
p=.038
PD1high TEM cells (10^5)
20
0
11
46
weeks
11 weeks
CD44
PD1
PD1high
46 weeks
CD44
PD1
PD1high
m
p=.048
R2=0.45
CD3+ cells miR-143-3p (RQ)
15
0
0
20
PD1high TEM cells (10^5)

Figure 5.

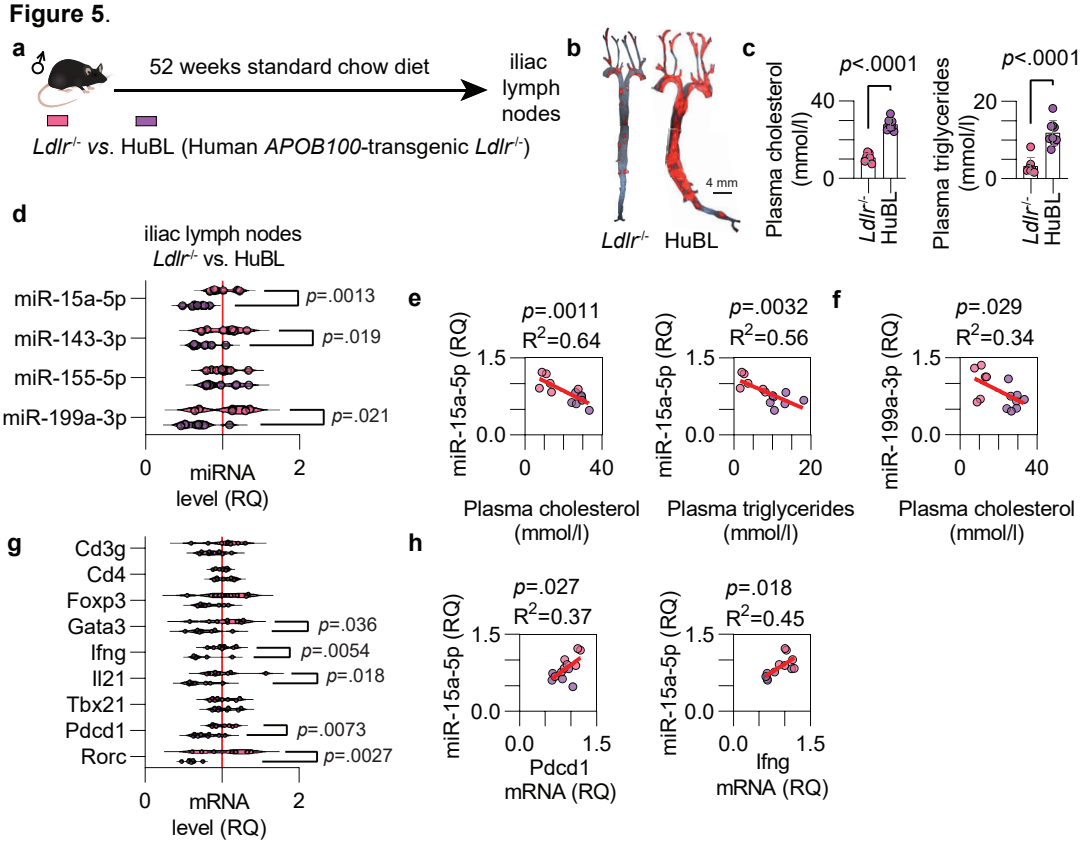
a
52 weeks standard chow diet
iliac lymph nodes
Ldlr-/- vs. HuBL (Human APOB100-transgenic Ldlr-/-)
b
4 mm
Ldlr-/-
HuBL
c
Plasma cholesterol (mmol/l)
p<.0001
Plasma triglycerides (mmol/l)
p<.0001
d
iliac lymph nodes
Ldlr-/- vs. HuBL
miR-15a-5p
miR-143-3p
miR-155-5p
miR-199a-3p
p=.0013
p=.019
p=.021
miRNA level (RQ)
e
p=.0011
R2=0.64
p=.0032
R2=0.56
Plasma cholesterol (mmol/l)
Plasma triglycerides (mmol/l)
f
p=.029
R2=0.34
miR-199a-3p (RQ)
Plasma cholesterol (mmol/l)
g
Cd3g
Cd4
Foxp3
Gata3
Ifng
Il21
Tbx21
Pdcd1
Rorc
p=.036
p=.0054
p=.018
p=.0073
p=.0027
mRNA level (RQ)
h
p=.027
R2=0.37
p=.018
R2=0.45
Pdcd1 mRNA (RQ)
Ifng mRNA (RQ)